AVIAN PHOTORECEPTORS

Nathan Scott Hart

School of Biological Sciences

University of Bristol

A dissertation submitted to the University of Bristol in accordance with the requirements of the degree of Doctor of Philosophy in the Faculty of Science.

November 1998

ABSTRACT

Vision is a major sensory modality in virtually all birds, and neognathus species have among the most complex retinae of any vertebrate. The widespread occurrence of visual mimics and of cryptically or aposematically coloured prey indicate the importance of vision in prey detection, just as the extensive use of visual displays confirms its role in communication. Until recently, most hypotheses regarding the role of colour in avian behavioural ecology have relied on human assessment of colour rather than the perceptual system of the natural receivers of the signals. Such oversights on the part of evolutionary and behavioural biologists are partly due to the paucity of relevant physiological data.

A microspectrophotometric study was conducted on the retinal photoreceptors of the European starling (*Sturnus vulgaris*), blackbird (*Turdus merula*), blue tit (*Parus caeruleus*), Indian blue-shouldered peacock (*Pavo cristatus*) and domestic turkey (*Meleagris gallopavo*). In addition to a single class of medium wavelength-sensitive rod visual pigment (wavelength of maximum absorbance, λ_{max}, 503 to 505 nm), the retinae of each species contained four cone visual pigments maximally sensitive to long (LWS, λ_{max} 557 to 566 nm), medium (MWS, λ_{max} 503 to 505 nm), short (SWS, λ_{max} 449 to 459 nm) and either violet (VS, λ_{max} 420 to 421 nm) or ultraviolet (UVS, λ_{max} 368 to 376 nm) wavelengths. The LWS, MWS, SWS and VS / UVS visual pigments found in the single cones were associated with oil droplets designated as R-type (cut-off wavelength, λ_{cut}, 517 to 572 nm), Y-type (λ_{cut} 490 to 515 nm), C-type (λ_{cut} 399 to 450 nm) and T-type (transparent) respectively. The LWS cone visual pigment was also found in both the principal and accessory members of the double cone, associated with P-type (λ_{cut} 407 to 500 nm) and, occasionally, A-type (λ_{cut} 479 to 490 nm) oil droplets respectively.

Absorption of short wavelengths by the P-type oil droplets found in the starling, blackbird, blue tit and peacock gradually increased from the dorsal to the ventral retina. The adaptive significance of this feature is discussed. The oil droplets found in the single cones did not vary in their spectral absorption characteristics according to retinal location. However, systematic variations in the topographical distribution of different cone types were observed in the starling, blackbird and peacock. In all species, double cones were less abundant in the posterior dorsal (PD) retina than in the remaining retinal area. Whilst in the blackbird and peacock all classes of single cone were relatively more abundant in the PD retina, the same region in the starling eye was characterised by a relative deficiency of LWS single cones and a relative abundance of SWS and UVS single cones. The study of the spatial distribution of cone types in the starling is the most comprehensive so far published. As well as spatial heterogeneity, left-right asymmetries were found, but no sex differences. The relationship of this retinal asymmetry to behaviour and neural asymmetries is discussed.

Estimates of the relative abundance of the different types of single cone photoreceptor were used in conjunction with the microspectrophotometric data, and measurements of the spectral transmission of the dioptric apparatus, to predict the photopic spectral sensitivity functions of the starling, blackbird, blue tit and peacock.

Dedicated to the memory of Charles Hart

ACKNOWLEDGEMENTS

The author wishes to thank Julian Partridge and Innes Cuthill for supervising the work described in this thesis. Their help, advice and encouragement were second only to their desire to destroy mind and body by enforcing long hours in small, dark rooms and gruelling runs on Lundy Island!

Sue Wilkie and David Hunt of the Institute of Ophthalmology, London, are gratefully acknowledged for demonstrating the technique of *in situ* hybridisation on the starling retina. I would also like to express my gratitude to Daniel Osorio and Misha Vorobyev for patiently explaining their spectral sensitivity model to a non-mathematician! The visual pigment analysis macros were modified from those written by Jeremy Kent who, along with Andrew Hope, introduced me to the Bristol MSPs. Thanks guys.

Birds were obtained with the help of Arthur Goldsmith, Andrew Bennett, Mike Burke (the pig farmer), Chris Sherwin and Peter Lewis. Linda Teagle and Paul Chappell assisted with a number of technical applications and Ron Douglas kindly lent us his SPEX spectrometer. The project was funded by the Biotechnology and Biological Sciences Research Council.

Finally, I would especially like to thank my parents, for emotional and financial support, my grandparents, for their boundless encouragement, and Julia, for her love.

"What is harder than rock, or softer than water? Yet soft water hollows out hard rock. Persevere."

Ovid (43 BC to AD 18)

AUTHOR'S DECLARATION

I declare that the work in this dissertation was conducted in accordance with the Regulations of the University of Bristol. The work is original, except where indicated by special reference in the text, and no part of the dissertation has been submitted for any other degree. Any views expressed in the dissertation are those of the author and in no way represent those of the University of Bristol. The dissertation has not been presented to any other University for examination, either in the United Kingdom or overseas.

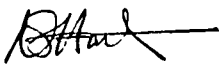

Nathan Scott Hart

November 1998

TABLE OF CONTENTS

ABBREVIATIONS AND SYMBOLS

A-type	accessory-type oil droplet
AD	anterior dorsal
Asn	asparagine
AP	alkaline phosphatase
ATP	adenosine triphosphate
AV	anterior ventral
BCPIP	5-bromo-4-chloro-3-indoyl phosphate
BHz	frequency output of the V / F converter for the baseline signal
BUT	British union turkey
c	velocity of electromagnetic radiation in a vacuum (2.988×10^8 m s^{-1})
C-type	colourless-type oil droplet
ca^{2+}	calcium ion (divalent cation)
CCTV	closed circuit television
cDNA	complementary DNA
cGMP	guanosine 3′5′-cyclic-monophosphate
CIE	Commission Internationale de l'Eclairage
Cys	cysteine
D	absorbance
DC	direct current
DIG	digoxygenin
DNA	deoxyribose nucleic acid
DPBS	dextran in phosphate buffered saline
E	electric
exp	exponential
ERG	electroretinogram
ERP	early receptor potential
FWHM	full width at half maximum (bandwidth)
GDP	guanosine 5′-diphosphate
Gln	glutamine
Glu	glutamic acid
GPBS	glycerol in phosphate buffered saline
GTP	guanosine 5′-triphosphate
His	histidine
I_i	intensity of incident light
I_t	intensity of transmitted light
HT	high tension voltage
INL	inner nuclear layer
ION	isthmo-optic nucleus
K	photosensitivity
$\log_{10}$	logarithm to the base 10
LWS	long wavelength-sensitive
Lys	lysine
λ	wavelength
λ_{cut}	cut-off wavelength
λ_{max}	wavelength of maximum absorbance
λ_{mid}	wavelength of 50 % maximum measured transmission
$\lambda_{T50\,\%}$	wavelength at which transmission is 50 %
mAb	monoclonal antibody
mg^{2+}	magnesium ion (divalent cation)
mosmol	milliosmole
mRNA	messenger ribonucleic acid
MM	Mansfield-MacNichol transform
MSP	microspectrophotometer
MWS	medium wavelength-sensitive
n	number (observations or degrees of freedom)

N	noise
na^+	sodium ion (monovalent cation)
NA	numerical aperture
NaCl	sodium chloride
NaOH	sodium hydroxide
NBT	nitroblue tetrazolium chloride
NRO	N-retinylidene-opsin
OffHz	frequency output of the V / F converter at zero light
OPL	outer plexiform layer
P-type	principal-type oil droplet
PAO	polyclonal anti-opsin antibody
PBS	phosphate-buffered saline
PD	posterior dorsal
PDE	phosphodiesterase
PE	pigmented epithelium
PMT	photomultiplier tube
PV	posterior ventral
r	radius
R-type	red-type oil droplet
RI	refractive index
RMM	relative molecular mass
RMS	root-mean squared
RNA	ribonucleic acid
RPM	revolutions per minute
S	signal
s.d.	standard deviation
SDS	sodium dodecyl sulphate
SHz	frequency output of the V / F converter for the sample signal
S / N	signal-to-noise ratio
SSC	standard sodium citrate
SWS	short wavelength-sensitive
T	transmission
T-type	transparent-type oil droplet
Trp	tryptophan
UV	ultraviolet
UVS	ultraviolet-sensitive
v	frequency of electromagnetic radiation
v_{max}	frequency at the λ_{max}
$\bar{v}$	wavenumber
V / F	voltage to frequency converter
VS	violet-sensitive
w/v	weight-to-volume ratio
Y-type	yellow-type oil droplet

CHAPTER ONE

AN INTRODUCTION TO THE AVIAN EYE

1. An introduction to the avian eye

The avian eye comprises an optical system, which produces real images of the objects and surfaces of a three-dimensional world, and a sensory system, or retina, which functions as a two-dimensional detector array to extract visual information from those images (Martin, 1985).

1.1 Optical system

The structure of the eye and its optical system are responsible for forming the image on the retina which is transduced by the nervous system.

1.1.1 Eye shape and size

The large absolute size of the avian eye is suggestive of the importance of vision to birds (Meyer, 1977). The mass of both eyes in some species (e.g. eave swallow, *Chelidon erythrogaster*) is greater than the mass of their brain (Slonaker, 1918). By comparison, the human brain is approximately 51 times heavier then the combined mass of our eyes (Vierordt, 1893 cited in Slonaker, 1918).

Generally, nocturnal predators possess the largest eyes, whereas water and swamp birds the smallest (Martin, 1985). However, absolute eye size *per se* is no particular indication of light gathering ability. Rather, it is the F-number (or relative aperture number), which is the ratio of the focal length of the eye to its aperture (pupil diameter). The F-number is reduced in the eyes of nocturnally adapted species to enhance retinal illuminance (Pettigrew, 1983).

Walls (1942) classified avian eyes into three morphological types: flat, globose and tubular. Allegedly the most common shape, the flat eye has an axial (anterior-posterior) diameter which is smaller than its radial (equatorial) diameter (e.g. swan, *Cygnus olor*; black-capped chickadee, *Parus atricapillus*). It is thought that their shape is adaptive to fitting them laterally into a narrow head to maximise the visual field (Suthers, 1978).

Globose eyes, in which axial and radial diameters are of similar magnitude, are characteristic of many passerines (e.g. European starling, *Sturnus vulgaris*; Martin, 1986) and diurnal birds of prey (e.g. eagle, *Aquila chrysaetos*; broad-winged hawk, *Buteo platypterus*; Walls, 1942). It is proposed that this shape of eye, with its

increased focal length relative to the flat form, provides high resolution at great distances, although this will also depend on properties of the dioptric apparatus and the retina.

Tubular eyes, in which the axial diameter exceeds the radial diameter, occur in most owls (e.g. great horned owl, *Bubo virginianus*) and some eagles (Walls, 1942; Martin, 1985). The increase in axial length has been implicated as an adaptation for more precise accommodation. Furthermore, the large focal length of these eyes, which increases the size of the retinal image, and flexible retinal neural integration allows the eye to function over a wider range of luminance levels, with greater visual acuity, as more photoreceptors are illuminated per visual angle (Martin, 1982). Such an eye is adaptive for species which are active both day and night rather than strictly nocturnal (Martin, 1985). In each case, the anterior portion of the eye is supported by a ring of bones, the scleral ossicles. In small eyes, the ossicles consist of compact bone, but in larger eyes the plates are hollow, as is much of the avian skeleton. By preventing the globe from changing shape, the scleral ossicles may facilitate accommodative distortion of the lens and cornea (Sillman, 1973).

Typically the avian eye is not a symmetrical structure, and in particular displays marked nasal-temporal asymmetry in the distance between the corneoscleral junction and the equator (Martin, 1985; Martin, 1986). This 'nasad asymmetry' (Walls, 1942) results in the retina being arranged asymmetrically about the bulbar axis, and is thought to maximise the width of the cyclopean (panoramic) visual field (Martin, 1985). Generally, there is little asymmetry about the dorso-ventral axis. Nasad-asymmetry in the European starling is thought to provide a mechanism of static accommodation by creating a 'ramp retina' (Martin, 1986) which, as discussed in chapter three, may also be correlated with the topographical distribution of the different cone photoreceptor types.

1.1.2 Dioptric apparatus

The principal refractive components of the avian eye are a biconvex lens and a convexo-concavo cornea. The combined refractive power of these two tissues differs greatly between species, as does the relative contribution of each component (Martin, 1985).

The cornea is a 'transparent' section of the sclera, the fibrous tunic which forms the outer casing of all vertebrate eyes (Walls, 1942). The cornea generally has a smaller radius of curvature than the sclera and, in the European starling, has a uniform thickness of approximately 0.16 mm and a refractive index relative to air of 1.376 (Martin, 1986). In the pigeon (*Columba livia*) the refractive power of the cornea is over twice that of the lens, whereas in the tawny owl (*Strix aluco*) the total refractive power of the eye is divided approximately evenly between the two lenses (Martin, 1982; Martin, 1985).

The anterior chamber between the cornea and lens contains the aqueous humour. Because the refractive index of this 'transparent' fluid (1.337 in the European starling; Martin, 1986) is similar to that of the cornea, the posterior surface of the cornea has a much lower refractive power than the anterior surface.

The avian lens, which is typically very soft and pliable, consists of a central body of concentrically graded refractive index surrounded by an annular pad (Martin, 1985). The annular pad, which is a feature unique to avian and reptilian lenses, is thought not to have an optical role since it is always shielded by the iris. Instead, it may function either as part of the accommodative mechanism (Walls, 1942) or as a source of nutrients for the lens (Slonaker, 1918). The average refractive index of the lens in the European starling is 1.523 (Martin, 1986), compared to values of 1.408 in the pigeon, 1.470 in the tawny owl and 1.508 in the penguin, *Spheniscus humboldti*, (Martin, 1982; Martin and Young, 1984; Martin, 1985). Lens size and shape varies markedly between different avian species, presumably reflecting differences in refractive power, accommodative range and visual fields of the eye. Avian lenses (and corneas) are generally transparent to near-ultraviolet wavelengths (320 to 400 nm), transmitting well down to about 320 nm (Govardovskii and Zeuva, 1977; Emmerton *et al.*, 1980; Goldsmith, 1990).

The large chamber behind the lens contains a fluid, the vitreous humour, rendered gelatinous by retinal secretion of proteins during development (Martin, 1985). The refractive index of the vitreous is similar to that of the aqueous humour (1.337 in the European starling), conferring considerable refractive power to both the anterior and posterior surfaces of the lens (Martin, 1986). The combined pressures of the aqueous and vitreous humours distend the fibrous tunic to the point of rigidity.

Intraocular pressure is maintained partly by the continual secretion of aqueous humour, and partly by external pressure exerted by the extraocular muscles (Martin, 1985).

Absorption of light by the dioptric apparatus determines the short wavelength limit of photoreception (Rodieck, 1973). Consequently, the spectral transmission of the pre-retinal tissues and media must be considered when predicting the spectral sensitivity of an organism from the spectral absorptance characteristics of its photoreceptors (chapter four).

1.1.3 Pupil and Iris

Pupil diameter is controlled by the iris, a heavily pigmented, vascularised diaphragm immediately anterior to the lens. Its two major muscles, the pupil sphincter and the pupil dilator, are responsible for the rapidity of the pupillary response, which is notably high in birds (Martin, 1985).

Iris pigmentation serves no optical function except to render it opaque. However, sexual, seasonal and age-dependent variations in iris colour, as well as dietary influences, have been reported. Female European starlings, for example, have a characteristic light brown ring around the outer margin of the iris which is absent in the male (Feare, 1984). The brewer's blackbird, *Euphagus cyanocephalus*, also varies in iridial colour depending on sex and age-class (Hudon and Muir, 1996). In both cases, iridial opacity is enhanced by guanine-based reflective organelles in the anterior pigment epithelium (Hudon and Oliphant, 1995; Hudon and Muir, 1996).

A pupil of varying aperture may perform several functions within the avian eye (Martin, 1985). Firstly, the iris can control the brightness of the retinal image by expanding or contracting as appropriate. The difference between minimum and maximum pupil size in vertebrate eyes with circular pupils produces only a relatively small change in image brightness (approximately 1.2 $\log_{10}$ units; Martin and Young, 1984) compared to the range of luminance levels which may be encountered in natural environments (approximately 11.8 $\log_{10}$ units; Martin, 1985). Nevertheless, variation in pupil diameter is probably sufficient to equalise retinal illuminance within a particular habitat when natural luminance levels are changing relatively slowly and over a more limited range.

Secondly, the pupil may protect the retina from photic or thermal damage by reducing retinal image brightness. Whilst most avian pupils are spherical, ellipsoidal and even vertical slit pupils have been observed (Martin, 1985). Slit pupils are found in several vertebrate taxa (Walls, 1942) and are thought to protect the retina of nocturnal or crepuscular species when exposed to bright sunlight by closing to a smaller aperture than a circular pupil is able to (Martin, 1985).

Thirdly, the pupil may form part of the dioptric apparatus to improve retinal image quality. By restricting the pupil aperture, rays which would otherwise pass peripherally through the dioptric system, and would thus be susceptible to most of the aberrations from which optical systems suffer, are removed. In addition, the pupil may serve as a stenopaic aperture to improve the depth of focus of the eye (Walls, 1942; Martin, 1985).

Lastly, the pupil of certain species may work in conjunction with the lens to achieve accommodation. This phenomenon is discussed in the following section.

1.1.4 Accommodation

Generally, the relaxed avian eye provides a sharply focused image on the retina of objects at optical infinity (an 'emmetropic' eye; Martin, 1985). Objects closer than infinity will remain unfocused unless accommodation occurs to increase the optical power of the eye (Glasser and Howland, 1996). The diversity of avian visual ecology has led to specialisation and differentiation of the avian eye with regard to accommodative ability, as with so many other aspects of its functional morphology. Special mechanisms for rapid accommodation, involving both the cornea and lens, are particularly well developed in diurnal species (Suthers, 1978). However, good accommodative ability is by no means universal in birds. Many nocturnal birds, the eyes of which are well adapted for low-light conditions, show little or no accommodation (Glasser and Howland, 1996).

Usually, accommodation is achieved by two mechanisms: i) corneal curvature is increased by contraction of Crampton's muscle, which extends from the sclera to the edge of the cornea, and ii) contraction of Brucke's muscle increases the refractive power of the lens by actively pressing the ciliary body against its margin. Humans, incidentally, accommodate using only their lens (Glasser and Howland, 1996).

Birds which pursue their prey underwater show morphological adaptations to compensate for the loss in refractive power of the cornea when immersed (Pumphrey, 1948). Piscivorous species, such as cormorants (*Phalacrocorax carbo* and *P. auritus*), dippers (*Cinclus mexicanus*), black guillemots (*Cepphus grylle*), hooded mergansers (*Mergus cucullatus*) and redhead duck (*Aythya americana*), accommodate underwater using an ingenious iris control mechanism. A hypertrophied ciliary body squeezes the anterior surface of the malleable lens against the iris sphincter muscle. The central lens bulges through the pupil, changing the refractive power of the dioptric apparatus by up to 80 dioptres (Sivak *et al.*, 1977; Katzir, 1993). Crampton's muscle is degenerate or absent in these species (Pumphrey, 1948).

Some diving ducks are thought to combine this technique with a window in their nictitating membrane of high refractive index (Suthers, 1978). Penguins (e.g. *Spheniscus demersus*), on the other hand, have addressed the problems of amphibious vision by evolving a relatively flat cornea. This minimises the loss of corneal refractive power on entering the water and thus reduces the amount of accommodation required (Sivak, 1976). Plunge divers, like the brown pelican (*Pelecanus occidentalis*), which locate their prey prior to entering the water, do not need good underwater vision and similar adaptations to compensate for the loss of corneal refraction in water are absent (Sivak *et al.*, 1977).

1.2 Sensory system

The image analysing system consists of the sensory retina and the ancillary structures which support its metabolism.

1.2.1 Retina

A great deal of our knowledge regarding avian retinal structure is derived from the pioneering studies of S. Ramon y Cajal, which were collated in his "La rétine des vertébrés", first published in 1893 (Rodieck, 1973). Cajal's observations were a major source of information for the excellent reviews of Rodieck (1973) and Martin (1985), which are summarised below.

The avian retina, which is relatively thick, avascular and lines the fundus, can be divided into two principal layers, the outer pigmented layer and the inner neural

layers. The outer pigmented layer, which separates the neural retina from the choroid, comprises the pigmented epithelium (PE), a thin layer of polygonal cells held together by junctional complexes. The PE has a number of important visual functions, including the transfer of nutrients from the choroidal circulation to the neural retina. PE cells are well adapted for this function, containing a profusion of mitochondria and endoplasmic reticulum. Furthermore, extensive infolding of their basal surface, adjacent to the choroid, greatly increases the surface area for metabolic exchange, and long apical processes, extending between the photoreceptors for as much as two-thirds of the length of the inner segments, facilitate transfer to the neural retina. Other metabolic functions of the PE include the active, phagocytotic breakdown of membrane disks shed continually from photoreceptor outer segments, and the regeneration of bleached visual pigment.

The PE contains light-absorbing melanin pigment granules which, being situated between the outer segments, are able to prevent optical coupling between neighbouring photoreceptors, or even directly reduce the amount of light absorbed by the outer segments. In fish, amphibians, reptiles and birds, a change from darkness to light causes the migration of pigment granules into the apical processes, shielding the more sensitive rods from bright light. In this state, the spindle-like granules lie end-to-end with their long axis parallel to the outer segment.

In the European starling, pigment migration is considered to be very rapid and, as in other species, is thought to be associated with photomechanical changes which draw cones towards the light and extend rods away from it (Dalland, 1958; Adler and Dalland, 1959). Studies of teleost retinomotor movements suggest that light adaptive cone contraction is triggered by light absorption in rods (Kirsch *et al.*, 1989). During dark adaptation, the pigment granules migrate out of the apical processes, exposing the rod outer segments.

The inner neural retina can be subdivided into seven layers, although it is perhaps more instructive to describe the cells involved by their function rather than their absolute position. The neuroepithelial layer, which lies adjacent to the PE, contains the photoreceptors. The avian retina, as is true of most vertebrates, is duplex in nature, containing both rods, which are responsible for dim light (scotopic)

vision, and cones, which are responsible for bright light (photopic) vision and mediate colour discrimination.

Photoreceptor axons synapse with bipolar cell dendrites in the outer plexiform region of the bipolar layer. It is at this point that processing of the neural visual signal begins. Several rods will synapse with a single bipolar cell (summation), thus sacrificing spatial acuity for sensitivity. Each cone, on the other hand, usually synapse with a single bipolar cell, promoting high visual acuity at the expense of sensitivity. Accordingly, the cone-dominated retinae of diurnal birds have a thicker inner nuclear layer (INL), which contains the nuclei of the bipolar cells, than nocturnal birds whose photoreceptors are mostly rods.

In the diurnal retina, three concentric strata may be distinguished in the outer plexiform layer (OPL). Following an initial suggestion by Cajal (1893, cited in Rodieck, 1973), Mariani and Leure-DuPree (1978) found that this stratification was due to the distribution at three levels of the synaptic bodies of three groups of photoreceptors: i) rods and double cones; ii) upright (straight) single cones, and iii) oblique single cones. Stratification of the OPL is absent in nocturnal species, presumably as rods greatly outnumber the other receptor types (e.g. Braekevelt, 1993a).

Bipolar cells synapse in the inner plexiform region of the bipolar layer with proximally located ganglion cells, whose axons leave the globe as the optic nerve. Ganglion cells are morphologically heterogeneous, varying in size, configuration and the location of their dendrites in the inner plexiform layer. They are also functionally heterogeneous, and respond to specific visual stimuli. Ganglion cells responding to brightness contrast, verticality, horizontality, different shaped edges, movement and colour have all been described in the pigeon. Some ganglion cells are 'displaced' to the bipolar layer, but their function is unknown.

Also contained within the INL are the nuclei of horizontal, amacrine and Müller cells. Müller cells form the scaffolding of the retina, their processes occupying the extracellular spaces of the neural layers. Horizontal and amacrine cells have modified axons which interconnect with other retinal neurones. These 'association' cells are involved in signal integration. Their relative abundance in birds not only explains the thickness of the avian retina, but also suggests that many

of the complex functions of the visual system (e.g. movement detection) that are delegated to higher centres of the mammalian nervous system are performed at the retinal level in birds (Sillman, 1973).

Amacrine, and possibly 'displaced' ganglion cells, also synapse with efferents of the centrifugal system, which arise from cell bodies in the isthmo-optic nucleus (ION) of the mid-brain. Once thought to be a unique feature of the avian visual system, centrifugal projections to the retina have been described in all classes of vertebrate (Repérant *et al.*, 1989). Centrifugal fibres are thought to modulate the output of amacrine cells (Meyer, 1977) and have been shown to enhance the temporal response properties of ganglion cells (Uchiyama and Barlow, 1994), thus providing localised control of retinal function. The precise role of the centrifugal system in behaviour is unclear, but there is evidence to suggest that it may be involved in visual attention switching between different regions of the retina (Clarke *et al.*, 1996).

1.2.1.1 Photoreceptors

Vertebrate photoreceptors, which are distinguished from other retinal neurons by their proliferation of specialised membranes, can be classified as either rods or cones (Fein and Szuts, 1982). Both consist of a cell body which synapses with the neural retina, a central 'inner' segment and an 'outer' segment which contains the photosensitive visual pigment molecules. Outer segments are modified non-motile cilia that are outgrowths from the inner segment. Traditionally, the terms 'rod' and 'cone' described the appearance, under the light microscope, of the geometrical shape of the outer segment, which in rods were considered to be oblong, but in cones tapered from their base at the inner segment towards the distal (scleral) tip. However, there is considerable intraretinal and interspecific variation in photoreceptor morphology, and shape alone is no indication of cell type. Instead, rods and cones are often differentiated on the basis of functional properties, including photosensitivity and spatial and temporal resolution.

Nevertheless, the rods and cones of avian retinae are easily distinguished by their morphology. Rods have relatively large, cylindrical outer segments. Cones display a much thinner, tapering outer segment and usually display a large oil droplet in their inner segment. In general, the avian retina contains a single class of medium wavelength-sensitive rod, four different types of single cone maximally sensitive to

long (LWS), medium (MWS), short (SWS) and violet (VS) / ultraviolet (UVS) wavelengths, and a single class of LWS double cone (Bowmaker *et al.*, 1997).

The structure and spectral absorption characteristics of the photoreceptors determine the efficiency with which a given species can acquire visual information from the retinal image provided by the dioptric apparatus. Some of the important considerations in photoreceptor design are discussed below.

1.2.1.1.1 Outer segment

The outer segment is the primary site of phototransduction, where light energy is converted into a signal involving the movement of ions. Outer segments are characterised by a stack of lamellar membranes oriented perpendicular to the photoreceptor long axis. These pigmented membranes, or *disks*, are infoldings of the plasma membrane (Rodieck, 1973; Fein and Szuts, 1982). An important distinction between rods and cones is apparent with regard to membrane topology. In cones, the disks remain as infoldings of the plasma membrane for the entire length of the outer segment and, accordingly, their internal space is filled with extracellular fluid. In rods, with the exception of a few basal disks nearest to the ciliary junction with the inner segment, disks are pinched off from the plasma membrane, with each disk forming a closed, intracellular vesicle. However, the disks are not free-floating and remain attached to the enveloping plasma membrane by as yet unidentified ligatures.

To provide reasonable photosensitivity, photoreceptors must contain a large number of visual pigment molecules. Because these molecules are integral membrane proteins, the membranes containing them must have a large surface area. The primary achievement of the laminated structure is to provide an extensive membrane area whilst maintaining a relatively compact volume: a more dense array of photoreceptors increases the spatial information which can be gleaned from the retinal image (Rodieck, 1973).

Rod saccules, which occur as a single column within the limiting membrane, display several shallow incisures at their periphery, giving them a 'scalloped' appearance in horizontal section (Braekevelt, 1990; Braekevelt, 1993a; Braekevelt, 1993b; Braekevelt, 1994a; Braekevelt, 1994b; Braekevelt *et al.*, 1996). Each incisure branches into a network of fimbriae which may speed the diffusion of substances to and from the saccule membrane (Rodieck, 1973). In avian cones, the lamellar

structure usually takes the form of a single column of infoldings that originate in a line opposite the connecting cilium. However, Cohen (1963) reported infoldings at more than one site in pigeon cones, resulting in two or even three columns. In horizontal section, cone disks are characterised by their lack of peripheral incisures.

Much of the ultrastructural organisation of the lamellar membranes has been determined using X-ray diffraction. Briefly, a specimen is irradiated with an intense, collimated beam of X-rays. Rays scattered by its atoms and molecules, usually by Fraunhofer diffraction (Born and Wolf, 1970), are detected by a photographic plate placed some distance behind the specimen. With regard to outer segments, X-ray diffraction has been used to measure the distance between disks, and the size and arrangement of visual pigment molecules within the membrane (Rodieck, 1973; Fein and Szuts, 1982). By orienting the X-ray beam perpendicular to the photoreceptor long axis, the observed saccule to saccule period in vertebrate rods has been determined at approximately 30 nm. Diffraction patterns obtained with the beam orientated perpendicular to the surface of the saccule membranes suggest that visual pigment units 4 to 5 nm in diameter form a liquid-like (unordered) array across the membrane.

Visual pigment molecules are oriented such that the long axis of the chromophore is parallel to the surface of the saccule membrane (Knowles and Dartnall, 1977). Furthermore, each visual pigment unit is free to rotate about an axis normal to the disk surface, facilitated by the fluidity of the lamellar membranes. Spinning results from random Brownian movements caused by intermolecular collisions, and is known as rotational diffusion (Fein and Szuts, 1982). For any absorbing molecule, the transition moment vector giving rise to a specific absorption band has a fixed orientation with respect to the molecule's three-dimensional structure. The principal (α-band) transition moment for the visual pigment chromophore is roughly parallel to its polyene chain. Light absorption by an individual molecule is maximal when the electric field vector (e-vector) of the incident light, which oscillates perpendicularly to its direction of propagation, is parallel to the transition moment, and minimal when it is perpendicular to it. Unequal absorption of linearly polarised light about two orthogonal axes is known as linear dichroism. Due to the orientation of visual pigment molecules, photoreceptor

outer segments are dichroic when illuminated from the side: preferential absorption occurs when the e-vector is parallel to the plane of the disks (perpendicular to the long axis). The value obtained by dividing the absorption of the outer segment when the e-vector is parallel to the plane of the disks by the absorption when it is perpendicular is termed the dichroic ratio.

Accurate measurement of the dichroic ratio involves the use of a microspectrophotometer (see chapter two). Furthermore, the dichroic ratio is dependent on the spectral location of the wavelength of maximum sensitivity (λ_{max}) and the degree of collimation of the light beam used to measure it (Hárosi and Malerba, 1975). Nevertheless, the dichroic ratio determined for frog outer segments (approximately 4 to 5, Hárosi and MacNichol, 1974; Hárosi, 1975) suggests that the transition moment vector of the chromophore is directed at a small constant angle (about 17°) relative to the lamellar surface.

Dichroic absorption by photoreceptor outer segments has led the use of linearly polarised light in visual pigment microspectrophotometry, as it compensates for the relatively short pathlength of measurements made transversely through the outer segment rather than axially (Partridge, 1986). Because of rotational diffusion, the chromophores are orientated randomly within the plane of the lamellar membrane and as such no dichroism is observed for linearly polarised light travelling axially along the outer segment, i.e. in the 'natural' direction of the rays impinging on the retina. The specific absorbance of the outer segment to axial illumination will be half of the maximum possible value regardless of whether the light is linearly polarised or not (Hárosi, 1971). When the outer segment is illuminated transversely, the specific absorbance will also be half the maximum possible value if the light is linearly polarised with the e-vector parallel to the plane of the disks (perpendicular to the long axis) (Hárosi, 1971). It is therefore reasonable to use specific absorbances measured transversely to predict the specific absorbance of the outer segment to axial illumination (chapter four).

1.2.1.1.2 Connecting cilium and calycal processes

A short, slender, eccentrically located ciliary stalk, arising from one of the centrioles at the distal end of the inner segment, connects the inner and outer

segments (Fein and Szuts, 1982). In cross section, the stalk consists of nine pairs of tubules (filaments) arranged in a circle, but lacks the central pair characteristic of motile cilia (Rodieck, 1973). Filaments of the ciliary stalk extend partially into the outer segment, creating a narrow region free of lamellar membranes (Morris and Shorey, 1967). It is *via* the connecting cilium that newly synthesised visual pigment molecules pass into the outer segment, to replace those lost through membrane turnover. Mammalian photoreceptors also possess a cytoplasmic bridge between the inner and outer segments, separated by a channel of extracellular space from the connecting cilium.

Slender, finger-like outgrowths from the apex of the inner segment, known as calycal processes, pass alongside the outer segment for approximately one third of its length. It is possible that these peculiar structures have a supportive role, or prevent the outer segment from rotating about the connecting cilium (Rodieck, 1973).

1.2.1.1.3 Inner segment

The inner segment consists of two main regions, the ellipsoid and myoid (Fein and Szuts, 1982). The ellipsoid is characterised by an agglomeration of mitochondria, which provide the cell's metabolic energy. The ellipsoids of most birds, and a variety of other vertebrate taxa , also contain a large oil droplet which is often pigmented. On absorption of a photon of light, the photoreceptor undergoes a burst of respiration, for which the ellipsoid mitochondria are largely responsible. Production of adenosine triphosphate (ATP) by the mitochondria, which is used as an energy source for a variety of reactions, involves the oxidation of succinate to fumarate in the citric acid cycle. This conversion is mediated by the enzyme succinic dehydrogenase which is located in the mitochondria. Enoch (1963; 1964) demonstrated that if nitroblue tetrazolium chloride (NBT), a soluble yellow compound, was present during this reaction, it was reduced to an insoluble blue precipitate (diformazan). Furthermore, the quantity of diformazan produced was proportional to the amount of light incident upon the photoreceptor. This not only confirmed the involvement of ellipsoid mitochondria in phototransduction, but also provided a technique by which different spectral classes of photoreceptor could be localised within the retina (Marc and Sperling, 1976; 1977; Levine *et al.*, 1979).

This technique was adapted for use with avian retinae in the present thesis, as described in chapter three.

Located immediately proximal to the ellipsoid in rods and the accessory member of the double cone pair is an accumulation of granular inclusions, known as the paraboloid (sometimes referred to as the hyperboloid in rods) (Morris and Shorey, 1967). The paraboloid contains smooth endoplasmic reticulum and glycogen granules, which are thought to serve the metabolic activity of the myoid region (Rodieck, 1973).

The myoid region of the inner segment, lying between the ellipsoid (or paraboloid) and the cell body, is characterised by the organelles normally associated with protein synthesis: free ribosomes, rough endoplasmic reticulum and Golgi apparatus (Fein and Szuts, 1982). As its name implies, the myoid (literally 'muscle-like') of some fish, amphibians and birds is contractile, and responsible for the light-dependent photomechanical movements observed in these taxa. Recent electron microscopic studies have suggested that there is considerable interspecific variation in the range of retinomotor movement exhibited by avian photoreceptors (Braekevelt, 1990; Braekevelt, 1993a; Braekevelt, 1993b; Braekevelt, 1994a; Braekevelt, 1994b; Braekevelt *et al.*, 1996). Elongation of the myoid towards the PE may serve to shield outer segments from the light, and thus have an effect equivalent to the movement of pigment granules in the PE (Rodieck, 1973).

1.2.1.1.4 Synaptic terminations

Like fish and mammals (Rodieck, 1973), the synaptic terminations of avian rods and cones differ in both shape and size (e.g. Braekevelt *et al.*, 1996). Cones have a flat conical 'foot', called a pedicle, the base of which display numerous invaginated (ribbon associated) synaptic sites in addition to several of the more conventional synapses. The pedicles of single cones are identical to those of the principal and accessory members of the double cone pair. Rods, however, terminate in a round swelling called a spherule, which has fewer of both the ribbon associated and conventional synaptic sites. Each ribbon synapse of the cone pedicle makes contact with three postsynaptic processes. In rod terminals, four or more processes are observed per ribbon (Fein and Szuts, 1982). In both types of photoreceptor, the processes lying deepest in the invaginations are horizontal cell processes, with

bipolar cell dendrites contacting more superficially. Less prominent contacts occur at the conventional synaptic sites.

The neural signal induced by absorption of light, in the form of an electrical hyperpolarisation of the cell membrane caused by the movement of ions in the photoreceptor, influences higher-order neurons by modulating the rate of neurotransmitter (glutamate) release from the synaptic terminal of the photoreceptor (Yau, 1994). This release is high in the dark and reduced in a graded fashion by light. The response of the postsynaptic neurons to light can be a membrane hyperpolarisation or depolarisation, depending on whether a particular synapse is 'sign-preserving' or 'sign-inverting'. In addition to these chemical synapses, photoreceptors interact with second-order neurons using electrical synapses, known as gap junctions (Fein and Szuts, 1982).

1.2.1.1.5 Light funnelling and photoreceptor waveguides

Rays focused onto the retina by the dioptric apparatus are funnelled into 'waveguides' containing visual pigments, the outer segments (van Hateren, 1989). The refractive index of photoreceptor inner and outer segments is higher than that of the interstitial medium (Sidman, 1957), mostly due to the high lipid content of the outer segment lamellar membranes, and the mitochondria of the inner segment (Johnston and Hudson, 1974; Knabe *et al.*, 1997). Consequently, rays entering the photoreceptor at a shallow angle will be confined within the cell by total internal reflection. Light entering the cell at a more obtuse angle will be lost through refraction at the photoreceptor membrane, the reduction in intensity depending on both the incident angle and the difference in refractive index between the inside of the photoreceptor and the external medium (Snyder, 1975). Because inner segments are usually wider, it is possible that they funnel light into the outer segment, thereby increasing its geometric light-capture area. As cones generally have larger inner segments than rods, they have a greater potential for funnelling light into the outer segment (Rodieck, 1973).

Rather than entering the photoreceptors as rays, however, incident plane waves are diffracted by the lens, and the resulting (Airy) diffraction pattern produces 'modes' in the waveguide (van Hateren, 1989). A mode is a stable pattern of electromagnetic energy distribution, produced when rays of different phase interfere

constructively and destructively. The number of modes which can propagate within a waveguide depend on the wavelength, the diameter and the refractive index. Whilst geometric (ray-optical) models can predict much of light guiding behaviour of larger photoreceptors (outer segment diameter greater than about 1 μm), the axial propagation of light along narrow outer segments, the diameter of which approaches the wavelength of the incident rays, is better explained by electromagnetic (wave-optical) models (Snyder, 1975).

A fundamental property of modes is that only a fraction of their total light energy is transmitted within the waveguide. The remaining portion is transmitted along, but outside, the photoreceptor. The internal component is attenuated by visual pigment absorption as it propagates along the waveguide, whereas the external component is not, or only weakly, attenuated. Consequently, during transmission, light energy flows from the surrounding medium into the waveguide where it is absorbed. This funnelling behaviour endows the outer segment with a light-capture area that is larger than its geometric cross-section (Röhler and Fischer, 1971; Snyder and Hamer, 1972).

Pigment migration in the apical processes of the pigmented epithelium may alter the funnelling properties of waveguides. Movement of melanin granules towards the waveguide in response to bright light will result in more rapid attenuation of the external mode component, thus improving spatial acuity (Snyder, 1975; van Hateren, 1989).

Photon catch by a funnelling receptor would be no greater than that of a wider cell in the absence of funnelling, but a broader outer segment would have a larger volume and would thus require more visual pigment to maintain the same absorbance. Because, the rate of spontaneous, thermally generated, false signals is proportional to the total amount of visual pigment (Barlow *et al.*, 1993), one possible advantage of funnelling could be to reduce the amount of visual pigment required for a given photon catch and therefore improve the signal-to-noise ratio of the photoreceptors.

1.2.1.1.6 Photoreceptor membrane turnover

Photoreceptors are not static structures and continually undergo a process of renewal known as membrane turnover (Rodieck, 1973; Fein and Szuts, 1982). This

phenomenon was demonstrated in frog rods by injecting radioactively-labelled amino acids into the vitreous and observing their passage through the cells of the eye using autoradiography (Young, 1976). Labelled amino acids were sequestered by the retina and eventually accumulated in the myoid region of the inner segment, the primary site of protein synthesis in photoreceptors. Once converted into visual pigment, and other cellular proteins, they were transferred through the cell, mainly *via* Golgi complex where they were modified by the addition of carbohydrates. Some of the labelled proteins (mostly visual pigment) migrated through the connecting cilium to form a narrow band of radioactivity at the base of the outer segment. Over a period of weeks, depending on ambient temperature, the band of labelled proteins travelled as a discrete unit towards the distal end of the rod, where it was eventually shed and incorporated into a phagosome of the pigment epithelium. Because the rod stayed a constant length during this process, it was concluded that the loss and destruction of disks from the distal end was balanced with disk synthesis at the base. The pigment epithelium is essential in disk destruction and if it becomes incapable of phagocytizing the shed disks, the rod cells eventually die off (Rodieck, 1973).

1.2.1.2 Avian photoreceptors

Cajal (1893, translated in Rodieck, 1973) described four morphologically distinct types of photoreceptor in the greenfinch (*Fringilla chloris*) retina: rods, upright (straight) cones, oblique cones and double (unequal twin) cones. Upright and oblique single cones were distinguished by the fact that the inner segment of the oblique type was displaced laterally. Upright single cones were subdivided into two further classes depending on the location of the synaptic terminal in the outer plexiform layer (OPL). However, Cajal gave no description of the oil droplet contained within each of the different cone types.

In a study of the photoreceptors of the pigeon, Mariani and Leure-DuPree (1978) described the same five morphological types and indicated the strata in the OPL in which their synapses were located. They also described the colour of the oil droplets observed in each of the different cone types. The two upright single cones contained either a red or orange oil droplet, which we now know correspond to the LWS and MWS cone types (Bowmaker, 1977; Bowmaker *et al.*, 1997). The oblique single cone contained a yellow-green droplet, which was most likely the SWS cone

class. Furthermore, the stratification of oil droplets in the neuroepithelial layer observed in radial section reflected the stratification of the synaptic terminals in the outer plexiform layer (OPL). Yellow oil droplets (double cones) were located at the most sclerad level, yellow-green droplets at the most vitread level (oblique singles) and orange and red droplets (upright single cones) were located at level intermediate between the yellow and yellow-green.

Morris and Shorey (1967) described rods, double cones and two types of single cone on the chicken, but did not distinguish between upright and oblique types. A third type of single cone in the chicken was later distinguished on the basis of oil droplet electron density (Morris, 1970).

Subsequent *in situ* microspectrophotometric measurements (Bowmaker and Knowles, 1977; Bowmaker, 1977; Bowmaker *et al.*, 1997), immunocytochemical assays (Cserháti *et al.*, 1989) and chromatography of retinal pigment extracts (Fager and Fager, 1981; Fager and Fager, 1982; Yen and Fager, 1984; Yoshizawa and Fukada, 1993) have revealed the existence of four spectrally distinct cone visual pigments in these two species, in addition to the rod pigment. From the results of the microspectrophotometric and immunocytochemical investigations, these are known to be localised within a specific type of cone and paired with a particular type of oil droplet.

Microspectrophotometry has also revealed the existence of five different visual pigments in the retina of a number of other avian species (Jane and Bowmaker, 1988; Maier and Bowmaker, 1993; Bowmaker *et al.*, 1997; Das, 1997). The spectral absorption characteristics of the avian visual pigments and oil droplets discovered to date, are detailed in the next sections.

Avian rod outer segments are generally much larger then cone outer segments, typically 1.5 to 6 μm in diameter and 10 to 20 μm in length (Morris and Shorey, 1967; Braekevelt, 1990; Braekevelt, 1993a; Braekevelt, 1993b; Braekevelt, 1994a; Braekevelt, 1994b; Braekevelt *et al.*, 1996). Avian rods do not contain an oil droplet, and only one spectral class of rod photoreceptor has been discovered in the avian retina.

Cone outer segments are generally shorter and narrower than rod outer segments, typically 8 to 10 μm long with a diameter tapering from 1 to 3 μm at the

junction with the inner segment to about 1 μm at the apex. An exception is the chicken, in which the outer segments of the single cones and the accessory member of the double cone are up to 19 μm long, compared to a length of approximately 16 μm for the rods and the principle member of the double cones (Morris and Shorey, 1967). The size of the oil droplets in each of the single cones varies, but all are generally smaller than the droplet in the principal member of the double cones (Goldsmith *et al.*, 1984b). The accessory member of the double cone occasionally displays a very small oil droplet in its inner segment, e.g. chicken (Meyer and May, 1973; Bowmaker and Knowles, 1977) and pigeon (Mariani and Leure-DuPree, 1978). When no properly formed droplet is evident, carotenoid pigment, which would normally be contained within such a droplet, is often detected at low concentrations within the ellipsoid, e.g. duck, *Anas platyrhynchos domesticus* (Jane and Bowmaker, 1988), budgerigar, *Melopsittacus undulatus,* and zebra finch, *Taeniopygia guttata*, (Bowmaker *et al.*, 1997).

One of the most intriguing features of the avian retina is the abundance of double cones, which occupy approximately four times the area of a single cone and constitute roughly half of the photoreceptor population in diurnal species (Meyer, 1977). Double cones account for 82 % of the retinal area in the great tit (*Parus major*) and form a square mosaic, each single cone surrounded by four doubles (Engström, 1958). Double cones are composed of two disparate, but always related, receptor cells, separated as a pair from other photoreceptors by the processes of Müller cells. The principal member is relatively long and thin and has a large oil droplet in the ellipsoid. The accessory member is relatively short and broad, contains a small, essentially degenerate, oil droplet and has a large paraboloid in its inner segment (Martin, 1985). Although the outer segments of the principal and accessory cones are optically isolated as a pair from other cone outer segments, by pigment granules in the apical processes of the pigment epithelium, they are not optically isolated from each other. Thus, the possibility of optical 'cross-talk' between the two members exists. Furthermore, gap junctions located at the level of the myoid of the principal cone and the perikaryon of the accessory cone suggest that the two members are also electrically coupled (Smith *et al.*, 1985).

The function of double cones is unclear. A recent behavioural measure of photopic spectral sensitivity appeared to show no involvement of the double cones, only peaks in sensitivity corresponding to the corrected spectral sensitivities[1] of the four single cone types (Maier and Bowmaker, 1993). Nevertheless, electroretinographically determined photopic spectral sensitivity functions are dominated by a broad peak at approximately 570 nm (e.g. Blough, 1972; Chen and Goldsmith, 1986), which corresponds to the peak effective spectral sensitivity of the double cones. This mismatch suggests that the neural signal from the double cones is not involved in colour discrimination, at least under the conditions used for the behavioural test of photopic spectral sensitivity.

It has been suggested that double cones may be involved in the detection of polarised light, which may be used by both vertebrates and invertebrates for orientation and navigation (Brines and Gould, 1982). However, recent studies in the pigeon (Vos Hzn *et al.*, 1995; Coemans *et al.*, 1994) have cast doubt on the original investigation which inferred polarisation sensitivity in birds (Kreithen and Keeton, 1974).

The biophysical basis of polarisation sensitivity in invertebrates is an intrinsic dichroism due to alignment of chromophores along the photoreceptor microvilli (Cameron and Pugh, 1991). Vertebrate photoreceptors, however, have no such dichroism to axially propagating light as chromophores are free to rotate in the plane of the outer segment disk membranes. Nevertheless, outer segment membranes are dichroic to transverse illumination (Hárosi, 1975; Hárosi, 1985).

The absence of screening pigment between the two members of the double cone pair (Morris and Shorey, 1967; Mariani and Leure-DuPree, 1978) led Young and Martin (1984) to suggest that light scattered by the oil droplet in the principal cone, which would consist of two components polarised parallel and perpendicular to the scattering plane, might enter the accessory cone outer segment transversely and constitute a mechanism for detecting the plane of polarisation of the incident light. Further circumstantial evidence for the involvement of double cones in polarisation

---

[1] The corrected spectral sensitivity of a photoreceptor is a function of the photosensitivity spectrum and specific absorbance of the visual pigment, the pathlength of the outer segment, and the effects of spectral filtering by the pre-retinal media (lens, cornea, etc.) and the oil droplet through which much of the incident light must pass to reach the outer segment.

detection came from the greater relative abundance of double cones in the yellow (anterior ventral) field of the pigeon's eye (Waelchli, 1883; Bowmaker, 1977). This region of the retina views the celestial hemisphere, from which polarisation cues of use in navigation are assumed to originate (Brines and Gould, 1982). Such a mechanism would require an additional intensity signal so that intensity modulation was not confused with a change in polarisation. This could be provided by the principal member or adjacent cones (Young and Martin, 1984). However, it is not clear how axial and transverse stimulation of the accessory cone would be distinguished by the nervous system, especially as the principal and accessory members are though to be electrically coupled (Smith *et al.*, 1985).

An alternative mechanism for polarisation sensitivity based on the waveguide properties of double cone inner segments has been proposed, which obviates some of the problems encountered in the oil droplet model. Cameron and Pugh (1991) suggest that the double cone inner segments act as a birefringent, polarisation-sensitive dielectric waveguide. Because the two members of the double cone are contiguous, it is assumed that they act as a unitary waveguide. Furthermore, the roughly elliptical cross-section of the double cone pair may endow the waveguide with some degree of geometrical birefringence, i.e. capable of trapping and propagating light of one polarisation more efficiently than others to the outer segments. By comparing the signals from double cones whose axes of symmetry were, for example, locally orthogonal, as in the square patterned tetradic mosaics observed in many teleost fish (Boehlert, 1978), and also the great tit (Engström, 1958), a 'polarisation contrast' neural image could be generated, with a 90° periodicity in polarisation sensitivity. Cameron and Pugh provided experimental data, from heart rate conditioning experiments, that the green sunfish (*Lepomis cyanellus*) did indeed respond with a 90° periodicity in polarisation sensitivity and possessed such a double cone mosaic. However, recent optical and electrophysiological experiments have failed to support polarisation detection in sunfishes (Novales Flamarique and Hawryshyn, 1997).

A third hypothesis is that the partition between the two members acts as a dielectric 'mirror' which provides the optical anisotropy necessary for polarisation discrimination by comparing signals from orthogonal cells in paired cone mosaics

(Novales Flamarique and Hawryshyn, 1998). Polarisation detection mediated by UVS cones in salmonids (e.g. Hawryshyn *et al.*, 1990) could arise indirectly from polarisation-dependent reflection and light scattering at the double cone partition onto the UVS cones. It is known that UVS cones face the partition of adjacent double cones in brown trout, *Salmo trutta* (Bowmaker and Kunz, 1987) and yellow perch, *Perca flavescens* (Loew and Wahl, 1991). Furthermore, UVS cone inner segments are shorter than double cones, placing their outer segments nearer to the double cone ellipsoid where the reflective interface would be larger. The importance of an orthogonal mosaic is emphasised by the lack of polarisation sensitivity in fish which display a random orientation of double and UVS cones (Novales Flamarique and Hawryshyn, 1998).

This theory is attractive as it is applicable to taxa which possess cones that lack oil droplets. Furthermore, it could account for differences in the spectral sensitivity of polarisation detection simply on the basis of the spectral sensitivity of the cone types which receives the reflected light from the double cone partition. SWS rhodopsins (λ_{max} about 450 nm) are thought to maximise detection efficiency under high polarisation whereas UVS (λ_{max} about 350 nm) rhodopsins maximise signal-to-noise ratios for the detection of plane polarised light under low polarisation (Seliger *et al.*, 1994). Interestingly, a large number of fish species have SWS single cones arranged in orthogonal double cone mosaics in an similar fashion to the salmonids (Levine and MacNichol, 1982).

Examination of avian cone mosaics, which to date have received surprisingly little attention, and a rigorous empirical investigation of polarisation sensitivity is now needed to assess the possibility of a polarisation detection mechanism in birds and the potential involvement of double cones. On the basis of the studies in fish, however, one would predict that the likelihood of discovering avian polarisation sensitivity would be greater in the great tit, with its regular square double cone mosaic (Engström, 1958), than in the chicken, where the receptor mosaic forms an irregular, but non-random, hexagonal lattice (Morris, 1970). A well-developed mosaic of single and double cones in fish has been correlated with improved movement detection (Boehlert, 1978), and it is possible that double cones subserve this function in birds (see chapter three).

1.2.1.3 Oil droplets

1.2.1.3.1 Description

Retinal oil droplets are highly refractile spherical organelles located at the distal end (ellipsoid) of the inner segments of retinal photoreceptors, and occupy the entire diameter of the inner segment at this site (Walls, 1942; Meyer *et al.*, 1965). This geometric relationship implies that at least some of the light reaching the visual pigment in the outer segment must have been transmitted by the oil droplet (see section 1.2.1.3.6.5). Consequently, the effective spectral sensitivity of the photoreceptor will be determined jointly by the product of the spectral transmittance of the oil droplet (and other pre-retinal filters, e.g. cornea and lens) and the absorptance (1-transmittance) of the visual pigment (Fujimoto *et al.*, 1957; Bowmaker, 1977; Varela *et al.*, 1993).

1.2.1.3.2 Phylogeny

Retinal oil droplets occur in all vertebrate classes and are generally found only in cone photoreceptors. Rods containing oil droplets have only been observed in the retinae of a few species: the African lungfish *Protopterus aethiopicus*, the 'primitive' reptile *Sphenodon punctatum* and the gecko *Coleonyx variegatus* (Walls, 1942). Walls (1942) speculated that oil droplet-bearing rods, especially those found in secondarily nocturnal geckos, might be 'transmutated' cones. However, as discussed by Goldsmith (1990), this theory depends partially on the criteria used to differentiate between photoreceptor types.

Anuran amphibians possess colourless or pale yellow oil droplets in single cones and the principal member of their double cones (Walls, 1942). These cone oil droplets should not be confused with the yellow droplets found in the pigment epithelium (Hailman, 1976), which are thought to act as a store of retinol for use by the adjacent outer segments (Rodieck, 1973).

Whilst oil droplets do not occur in eutherian (placental) mammals, an unidentified photostable pigment absorbing maximally at around 420 nm has been observed in the cone ellipsoid of some primates, including humans (Bowmaker *et al.*, 1991). Of the metatherians, 'colourless' oil droplets have been reported in marsupials (O'Day, 1935) and some monotremes (the duck-billed platypus,

Ornithorhynchus paradoxus, but not the echidna, *Tachyglossus aculeatus*, Young and Pettigrew, 1991).

'Colourless' oil droplets have been observed in the photoreceptors of some 'primitive' fish[2]: the sturgeon, *Acipenser fulvescens* (order Acipensiformes) and three species of lungfish (infraclass Dipnoi), *Protopterus aethiopicus*, *Lepidosiren paradoxa* and *Neoceratodus forsteri*, but are absent from subclass Neopterygii, which comprises the 'holosteans' and teleosts (Walls, 1942). However, the retinal cones of several teleost fish contain dense, spherical structures called elliposomes which superficially resemble oil droplets and are similarly located in the inner segment (MacNichol *et al.*, 1978; Avery and Bowmaker, 1982). Elliposomes do not stain with oil-soluble dyes, display an organised internal structure and contain a cytochrome-based chromophore rather than carotenoid pigments, thus differentiating them from oil droplets, although both are thought to have arisen from mitochondria (Pedler and Tansley, 1963; MacNichol *et al.*, 1978). Cytochromes absorb strongly below about 450 nm and elliposomes are assumed to share many of the spectral functions ascribed to retinal oil droplets.

Brightly coloured (i.e. red, orange and bright yellow) retinal oil droplets are found only in turtles and birds, particularly those that display a strongly diurnal habit (Walls, 1942). The similarity between avian and chelonian retinae is striking. The spectral sensitivity of the visual pigments, and the types of carotenoids responsible for oil droplet pigmentation, appear to be remarkably conserved in these taxa (Liebman and Granda, 1971; Liebman and Granda, 1975; Goldsmith *et al.*, 1984b; Lipetz, 1984b). The only notable difference is that some fresh water turtles (*Pseudemys scripta*) have 3-dehydroretinal-based visual pigments (porphyropsins), whereas sea turtles (*Chelonia mydas*) have retinal-based chromophores (rhodopsins) as do birds, and indeed all truly terrestrial vertebrates studied to date with the exception of some lizards (Provencio *et al.*, 1992).

Unsurprisingly, nocturnality appears to obviate the need for brightly coloured oil droplets which could significantly reduce cone sensitivity. Lizards, geckos and the 'primitive' reptile *Sphenodon*, which are largely nocturnal or fossorial in habit, possess only colourless or yellow droplets (Walls, 1942). Crocodilians and snakes

[2] Classification given by Nelson (1994)

have none. Nocturnal birds such as the tawny owl (*Strix aluco*), great horned owl (*Bubo virginianus*), barred owl (*Strix varia*), Ural owl (*Strix uralensis*) and the snowy owl (*Nyctea scandiaca*) retain spectrally distinct types of droplet, but these lack the dense pigmentation of their diurnal relatives (Bowmaker and Martin, 1978; Braekevelt, 1993a; Gondo and Ando, 1995; Braekevelt *et al.*, 1996).

1.2.1.3.3 Classification and terminology

Whilst it is relatively easy to distinguish some of the oil droplets occurring in the avian retina with the use of a light microscope, several ambiguities arise due to the subjective nature of the human visual system. Different types of oil droplet may appear the same either because we cannot distinguish between very similar colours, or because we are not sensitive to wavelengths that the droplets absorb.

Microspectrophotometry (see chapter two) has provided an objective method for determining the spectral absorption characteristics of oil droplets (Fujimoto *et al.*, 1957; Strother and Wolken, 1960; Strother, 1963; Liebman and Granda, 1975; Goldsmith *et al.*, 1984b; Partridge, 1989) and correlating oil droplet absorptance with the spectral sensitivity of the visual pigment with which it is associated (Bowmaker and Knowles, 1977; Bowmaker, 1977). However, absorption spectra recorded microspectrophotometrically must be interpreted carefully. In any spectrophotometric measurement, the light that is scattered, or by-passes the sample, will distort the measured absorption spectrum. With samples of low absorbance, such as photoreceptor outer segments, this effect can be minimised by the appropriate selection of optical components. However, due to the high concentration of coloured pigments they often contain, retinal oil droplets generally have very high absorbances, which may exceed 20 or even 30 in the red oil droplets of some birds (Goldsmith *et al.*, 1984b). In such cases, light that is not transmitted, but by-passes the oil droplet, can be a high fraction of that measured.

When measuring small samples, microspectrophotometers can only make reliable measurements over a limited range of low absorbances. The upper limit is reached when the amount of light scattered around the sample becomes comparable to that passing through it. This threshold is frequently exceeded with the microspectrophotometry of retinal oil droplets in which high absorbances are combined with very small size (typically 1 to 4 μm in diameter). Consequently, the

true absorption spectra of intact oil droplets cannot be measured directly and the optical behaviour of these organelles must be inferred from artefactual measurements (Partridge, 1986).

Highly pigmented oil droplets act as long-pass cut-off filters, blocking wavelengths towards the short wavelength end of the spectrum (Roaf, 1929; Fujimoto *et al.*, 1957; Strother and Wolken, 1960; Strother, 1963; King-Smith, 1969). Traditionally, the transmission properties of such droplets have been classified according to the wavelength ($\lambda_{T50\,\%}$) at which measured transmission is 50 % (equivalent to an absorbance of 0.301, Bowmaker and Knowles, 1977; Bowmaker, 1977; Bowmaker and Martin, 1978; Bowmaker and Martin, 1985). However, measurements of intact oil droplets by microspectrophotometry do not provide exactly correct values for $\lambda_{T50\,\%}$ because by-passing light will increase the apparent transmission (by a significant proportion at high absorbances) and hence shift the apparent $\lambda_{T50\,\%}$ to a shorter wavelength than the true value. Furthermore, the error in $\lambda_{T50\,\%}$ will be difficult to quantify as it depends on the shape of the true absorption spectrum and the magnitude of the by-passing light (which depends in part on the design of the MSP used to make the measurements).

A solution to this problem was proposed by Lipetz (1984a). He defined a parameter, termed the cut-off wavelength (λ_{cut}), which corresponded to the intercept with the value of maximum apparent absorptance by the tangent to the absorptance spectrum at the wavelength corresponding to half maximum measured absorptance (λ_{mid}). Both λ_{cut} and λ_{mid} were shown to be unaffected by the presence of by-passing light in the MSP. Furthermore, λ_{cut} was directly useful in that it described the wavelength below which there was no significant transmission by the oil droplet and could be related to peak absorbance. Although this method assumes that by-passing light in the MSP is constant at all wavelengths, which may not be the case, it has been adopted as the standard nomenclature for describing the spectral absorption properties of avian oil droplets (Jane and Bowmaker, 1988; Partridge, 1989; Bowmaker *et al.*, 1993; Maier, 1994; Bowmaker *et al.*, 1997).

For some purposes, however, categorisations using such spectral parameters are meaningless in the absence of knowledge regarding the nature of the visual pigments with which the oil droplets are associated. The spectral sensitivity of a

cone is dependent upon both the transmission of the oil droplet and the absorption of the visual pigment. Accordingly, a descriptive terminology has arisen which classifies oil droplets according to their λ_{cut} and the wavelength of maximum absorbance (λ_{max}) of the visual pigment with which they are associated (Table 1.1).

Orange oil droplets are uncommon in birds (Goldsmith *et al.*, 1984b; Partridge, 1989). In a large study on a number of waterfowl, Partridge (1989) also measured the oil droplets of the Japanese quail (*Coturnix coturnix japonica*). These were found to have orange oil droplets (mean λ_{cut} 545 nm) but no red droplets. A later study on the effect of carotenoid deprivation on the cone photoreceptors of this species reported that the LWS single cones in normal birds contained red oil droplets (mean λ_{cut} 568 nm) instead of orange (Bowmaker *et al.*, 1993). This suggests that the occurrence of orange oil droplets in some species may simply be a physiological artefact arising from dietary deficiencies or the effects of captivity, and emphasises the importance of studying fresh retinae from healthy, wild caught birds. The occurrence of orange droplets in the gannet (*Sula bassana*), Caribbean flamingo (*Phoenicoparus ruber*) and southern pochard (*Netta erythophalma*), however, is also accompanied by a separate type of droplet which can truly be classified as a red oil droplet (mean λ_{cut} 558-577 nm, Partridge, 1989), suggesting that these orange droplets (mean λ_{cut} 528-538 nm) are highly pigmented versions of Y-type droplets associated with the MWS visual pigment in single cones.

Oil droplet nomenclature	Oil droplet appearance	Range of oil droplet λ_{cut} (nm)	Range of visual pigment λ_{max} (nm)	Cone nomenclature
Single cones				
R-type	Red	560-570	543-570[1]	LWS
Y-type	Yellow	500-510	497-509	MWS
C-type	Colourless to pale yellow	420-440	430-463	SWS
T-type	Transparent	<350	355-426	UVS or VS
Double cones				
P-type	Colourless to yellow	480-485	[2]	Principal
A-type	Colourless	Triple-peaked (low pigment densities)	[2]	Accessory

Table 1.1 Classification scheme for avian retinal oil droplets. The cut-off wavelength, λ_{cut}, is defined according to Lipetz (1984a). Terminology is that given by Bowmaker (1991) and Das (1997) and combines several approaches to oil droplet nomenclature (Bowmaker, 1977; Liebman and Granda, 1975; Goldsmith *et al.*, 1984b; Partridge, 1989). The range of λ_{cut} given for some classes of droplet may be too restrictive, particularly in the case of the P-type droplet of the double cones. Transparent oil droplets show no detectable absorptance over the range of wavelengths investigated. [1] Oil droplets associated with the LWS pigments of the penguin and tawny owl (λ_{max} 543 and 555 nm respectively) had very low carotenoid concentrations and no λ_{cut} values are available. [2] Both members of the double cone are reported to contain the same visual pigment as the LWS single cones. Sources of λ_{max} values are those used to compile **Table 1.3**.

1.2.1.3.4 Composition

Retinal oil droplets are composed almost entirely of neutral lipids (cholesterol, cholesterol ester, mono-, di-, and triacylglycerols, Johnston and Hudson, 1974; Johnston and Hudson, 1976) and carotenoids (Wald and Zussman, 1937; Meyer *et al.*, 1965; Goldsmith *et al.*, 1984b). Carotenoids are a class of hydrocarbons (carotenes) and their oxygenated derivatives (xanthophylls). Their basic structure consists of eight isoprenoid units in aliphatic or alicyclic configuration. A series of conjugated double bonds constitutes the characteristic chromophore which can be modified by cleavage of the polyene tail, hydrogenation, dehydrogenation, cyclization or oxidation (Meyer *et al.*, 1965; Isler, 1971; Davies, 1976). The fatty acyl-containing neutral lipids are greatly enriched in polyunsaturated fatty acids, which enhance their ability to act as solvents for the unsaturated carotenoid structure (Johnston and Hudson, 1976). Coloured oil droplets contain high concentrations of carotenoid pigment. Calculated absorbances for red oil droplets may exceed 20 in birds (Goldsmith *et al.*, 1984b) and be as high 90 in turtles, which corresponds to a concentration of approximately 1 M (Liebman and Granda, 1975). The accumulation of such high concentrations is facilitated by the mixture of lipid solvents which provide much greater solubility for certain xanthophyllic carotenoids when compared to only limited solubility observed in the separate solvents of which the mixture is composed (Johnston and Hudson, 1976).

The spectral transmission of each oil droplet is largely determined by the carotenoid pigment(s) that it contains. Japanese quail develop transparent oil droplets when raised on a carotenoid-free diet (Meyer, 1971; Meyer *et al.*, 1971; Duecker and Schultz, 1977; Wallman, 1979; Bowmaker *et al.*, 1993). A number of different carotenoid pigments have been identified in retinal oil droplets (Wald and Zussman, 1937; Strother and Wolken, 1960; Meyer *et al.*, 1965; Liebman and Granda, 1975; Davies, 1976; Davies, 1979; Goldsmith *et al.*, 1984b). Orange and red oil droplets almost certainly derive their coloration by the inclusion of the carotenoid astaxanthin, regardless of whether the oil droplet is found in the single cone photoreceptors of a turtle or a bird. There is some evidence to suggest that red oil droplets in the Japanese quail may also contain a second carotenoid in addition to astaxanthin (Bowmaker *et al.*, 1993), as do the orange oil droplets of the mourning

dove, *Zeneida macroura* (Goldsmith *et al.*, 1984b). Examination of the absorption spectra from which these deductions have been made suggest that the secondary carotenoid functions to increase absorption of short wavelengths. This may be important where the λ_{cut} occurs at shorter wavelengths, as in orange or developing red oil droplets in which the lower concentration of astaxanthin might fail to absorb sufficiently at short wavelengths.

The bright golden-yellow oil droplets observed in single cones are more variable in their carotenoid composition and probably contain either lutein or zeaxanthin, or a mixture of both. Interestingly, both of these chromophores are also responsible for the yellow pigmentation of the *macula lutea* in primate retinae, and are found, along with other short-wavelength absorbing pigments, in the human lens (Bone and Landrum, 1992; Handelman *et al.*, 1992; Yeum *et al.*, 1995).

The P-type oil droplets found in the principal member of the double cones contain a variable amount of short wavelength-absorbing carotenoid in addition to galloxanthin, which accounts for the variability in λ_{cut} observed both within the retina and between species (Bowmaker *et al.*, 1997). These oil droplets can appear colourless, green or yellow under the microscope and in some instances their λ_{cut} values can differ by only a few nanometres from some of the other droplet types. The identity of the secondary carotenoid is unknown. Liebman and Granda (1975) noted the similarity with ε-carotene, which is known to occur in avian retinae (Davies, 1985), but Goldsmith *et al.* (1984b) were more cautious, observing that the unidentified chromophore had a peak absorption at longer wavelengths.

Whilst the 'colourless' or C-type oil droplets appear transparent to the human eye, they contain a carotenoid which absorbs maximally at 385 nm. Goldsmith *et al.* (1984b) gave this compound the trivial name of fringillixanthin and postulated that it was similar in structure to galloxanthin, but with the conjugated chain shorter by one double bond. Naturally occurring transparent oil droplets, which show no detectable absorption between 320-750 nm, presumably contain only lipid and no carotenoid pigment. It is unclear whether the droplets described in older studies (e.g. Walls, 1942) as 'colourless' were equivalent to the C-type droplets of birds and turtles, in containing carotenoid pigment but that which is undetectable to the human eye, or whether they were truly transparent.

1.2.1.3.5 Ontogeny

The majority of avian cones contain a single, spherical, membrane-bound oil droplet (e.g. Morris and Shorey, 1967). However, multiple red 'microdroplets' (< 0.5 μm diameter) occur in addition to the large single red oil droplet in the inner segments of LWS single cone photoreceptors in the red field (posterior dorsal quadrant) of the pigeon retina (Pedler and Boyle, 1969; Bowmaker, 1977). Furthermore, Japanese quail are reported to display yellowish-green teardrop-shaped inclusions in the dorsal retina, in addition to the other types of oil droplet (Budnik *et al.*, 1984), and multiple droplets in the accessory member of the double cone (Hazlett *et al.*, 1974) although this was not noted in subsequent studies (Partridge, 1989; Bowmaker *et al.*, 1993).

Their intimate association in the inner segment has led to the theory that oil droplets arise from, or are generated by, mitochondria (Pedler and Tansley, 1963; Berger, 1966; Armengol *et al.*, 1981). The observation in the diurnal gecko, *Phelsuma inunguis*, that there was no membrane separating the contents of the oil droplet from the adjacent mitochondrion, and that the oil penetrated between the cristae, may explain how carotenoids have been detected in the ellipsoid region of the accessory members of avian double cones despite the absence of a formed droplet (Bowmaker *et al.*, 1997). It may also explain the presence of multiple microdroplets in the inner segments of some cones if mitochondria were to accumulate carotenoid before forming, or fusing with, a single large droplet.

Animals cannot synthesise carotenoids *de novo*, and instead must obtain them through their diet (Davies, 1979). Nevertheless, some metabolic transformations are possible. Zeaxanthin, a constituent carotenoid of many avian tissues and readily obtained in the diet, is a likely precursor for lutein, astaxanthin, galloxanthin and ε-carotene (Davies, 1985; Schiedt *et al.*, 1991). The development of retinal oil droplets in the domestic chicken (*Gallus gallus domesticus*) embryo is reviewed by Meyer *et al.* (1965) and, although there is some dispute over the exact time of origin of each colour, it is generally agreed that the first droplets to appear *in embryo* are colourless. Seventeen days after fertilisation, however, all adult colours are discernible (Meyer *et al.*, 1965), and these must have arisen solely from carotenoids stored in the egg yolk, i.e. zeaxanthin and lutein (Davies, 1985).

1.2.1.3.6 Possible functions

The effect of these optical filters on the visual system, and their adaptive significance, has been the subject of much debate since their discovery. The principal contending hypotheses, some of which are mentioned in historical context only, are discussed briefly in the following sections. In view of the distribution of retinal oil droplets throughout the other vertebrate classes, particularly turtles, caution must be exercised in ascribing any theory regarding the function of retinal oil droplets exclusively to the Aves.

1.2.1.3.6.1 The monopigment hypothesis

Krause (1863, cited in Walls, 1942) suggested that colour vision in birds was mediated by a single cone visual pigment in conjunction with different coloured oil droplets. In transmitting only specific wavelengths of light to their respective outer segments, he proposed that oil droplet absorption alone could differentiate cones into several spectral types. Whilst the gamut of oil droplet colours observed in these original investigations were largely artefacts of chromatic aberrations in microscope objectives, the theory is still plausible. A failure to prove the existence of more than one class of cone visual pigment in birds by either extraction techniques (Wald *et al.*, 1955; Bridges, 1962; Crescitelli *et al.*, 1964; Sillman, 1969; Knowles, 1976) or microspectrophotometry (Liebman, 1972) ensured the theory retained its adherents for over a century. For example, Donner (1958) and King-Smith (1969) both attempted to explain wavelength discrimination by the pigeon (Hamilton and Coleman, 1933) on the basis of three cone types each containing the same visual pigment but different colours of oil droplet.

However, cone visual pigments are now known to be readily denatured by most detergents used for extraction (Yoshizawa and Fukada, 1993) and are 'bleached' at pH values and temperatures that do not affect rod pigment (Fager and Fager, 1982). Although multiple cone visual pigments can now be separated chromatographically from retinal extracts (Fager and Fager, 1981; Fager and Fager, 1982; Yen and Fager, 1984; Yoshizawa and Fukada, 1993), it was results from microspectrophotometric studies which first provided the evidence invalidating Krause's monopigment hypothesis. In 1977, multiple cone visual pigments were measured in both the chicken and pigeon (Bowmaker and Knowles, 1977;

Bowmaker, 1977). These findings were confirmed by electrophysiological evidence which suggested that these species possessed four cone pigments with absorption maxima near 413, 467, 507 and 562 nm (Govardovskii and Zeuva, 1977). Furthermore, it was demonstrated that Japanese quail raised on a carotenoid-free diet, and therefore possessing only colourless oil droplets, retained colour vision (Meyer, 1971; Meyer *et al.*, 1971; Duecker and Schultz, 1977; Wallman, 1979). Liebman's failure to identify more than one cone pigment using microspectrophotometry was probably due to difficulties in measuring the absorption spectra of avian cone outer segments, which are very small (typically 2 μm in diameter) and often remain attached to the pigmented epithelium (PE) when the retina is removed from the eyecup (Bowmaker, 1984). Despite this, he had already demonstrated the existence of three spectrally distinct cone visual pigments in the turtle retina, another species in which cone photoreceptors are characterised by the presence of brightly coloured oil droplets, and thus predicted the presence of multiple cone visual pigments in birds (Liebman and Granda, 1971). Microspectrophotometry has now demonstrated the presence of up to four cone visual pigments in bird retinae (Jane and Bowmaker, 1988; Bowmaker *et al.*, 1993; Bowmaker *et al.*, 1997; Maier and Bowmaker, 1993).

Nevertheless, Krause's hypothesis was partially correct in that LWS single cones and both members of the double cone pair contain a visual pigment with the same λ_{max} but different types of oil droplet. These cells will undoubtedly have different spectral sensitivities which are directly attributable to the absorption characteristics of their respective oil droplets, although it is not known whether the double cones are involved in colour vision.

1.2.1.3.6.2 Effect on spectral sensitivity and colour discrimination

The prediction that pigmented oil droplets act as long-pass cut-off filters (Roaf, 1929) has been confirmed experimentally in lizards, turtles and birds by comparing the electroretinographic (ERG) response of isolated retinae when illuminated normally and from behind. The gross spectral sensitivity curve obtained when the retina was illuminated normally was narrower and had its maximum displaced towards longer wavelengths (Orlov and Maximova, 1964 cited in Muntz, 1972; Pautler, 1967; Kawamuro *et al.*, 1997).

Bowmaker (1977) modelled the effect of oil droplets on the spectral sensitivity of individual cones and concluded that:

> "As a general rule, the effect of an oil droplet in a given cone is to displace the effective maximum sensitivity of the cone to a wavelength longer than the λ_{max} of the visual pigment, to reduce the bandwidth of the spectral sensitivity of the visual pigment by cutting off the shorter wavelengths, and to reduce the absolute sensitivity of the cone at its λ_{max} from that of the visual pigment λ_{max}."

Accordingly, the maxima of the effective spectral sensitivities of the MWS and LWS single cones in the pigeon are shifted by approximately 40 nm to longer wavelengths than their respective visual pigment λ_{max} values.

Excessive overlap between different spectral types of photoreceptor will cause a loss of spectral discrimination between narrow-band stimuli. It has been suggested that the narrowing of cone spectral sensitivities with oil droplets will reduce overlap and thus increase perceived colour contrast (Govardovskii, 1983). This is analogous to opponent interactions between the primary signals of different cone types that occur in the neural retina (Bowmaker and Knowles, 1977). Indeed, Barlow (1982) proposed that any advantage of tetrachromacy over trichromatic colour vision would be dependent on such an adaptation.

More recently, the effect of oil droplets on the spectral discrimination ability of birds has been investigated with regard to plumage coloration by modelling the performance of tetrachromatic visual systems with and without cone oil droplets (Vorobyev *et al.*, submitted). It appears that discriminability is improved, as is colour constancy under a variety of illumination conditions, by the presence of oil droplets. These results are consistent with those of Wallman (1979) who showed that carotenoid deprived birds with colourless oil droplets still discriminated between spectrally broadband red and green stimuli, but that their vision was more influenced by luminance differences than were normal birds. This is attributable to the increased overlap of cone sensitivities which means that signals tend to be more correlated (Osorio and Vorobyev, 1996) and hence chromatic signals are small.

Absorption of wavelengths below 300 nm by the pre-retinal tissues precludes a visual function for the gamma (γ) absorbance band of the visual pigment (section 1.2.1.4.1), which is also thought to be capable of initiating the phototransduction

cascade (section 1.2.1.4.3) in the same way as the alpha (α) and beta (β) bands (Palacios *et al.*, 1996).

However, the ocular media of most birds studied to date have good transmission of near-ultraviolet wavelengths (Govardovskii and Zeuva, 1977; Emmerton *et al.*, 1980; Jane and Bowmaker, 1988) and thus the potential for photostimulation of the β-band exists if some of the shorter wavelengths by-pass the oil droplets *in vivo*. This increases the probability that a long wavelength sensitive visual pigment will generate a visual signal due to absorption of short wavelengths by the β-band, thus confounding hue discrimination. Wolbarsht (1976) suggested that the function of pigmented oil droplets was to prevent absorption by the β-band of MWS and LWS visual pigments without reducing the sensitivity of SWS (or VS / UVS) visual pigments by use of a yellow lens or cornea. Because the spectral location of the β-band is proportional to the spectral location of the α-band λ_{max} (Palacios *et al.*, 1996 and see chapter four), β-band absorption by UVS / VS and SWS visual pigments would prevented by the ocular media.

1.2.1.3.6.3 Protection against ultraviolet (UV) radiation

In collecting light for the purposes of vision, the eye is also vulnerable to photochemical damage (Kirschfeld, 1982). As well as being absorbed by the visual pigments, light will interact with other chromophores, e.g. mitochondrial porphyrins which are abundant in the retina. Thus, photo-oxidative processes may be sensitised and result in the generation of free radicals and excited molecules, such as singlet oxygen, which can induce extensive cellular damage.

In mammals, retinal damage increases rapidly at wavelengths below 500 nm and is particularly severe in the ultraviolet (UV) (Ham *et al.*, 1976). It is thought that, in addition to simply absorbing the most harmful actinic wavelengths, retinal carotenoids such as the macular pigment might protect the retina by quenching singlet oxygen and scavenging free radicals (Miki, 1991). A similar function has been ascribed to the corneal and lenticular pigments of some species.

However, it would be undesirable to absorb all short wavelengths if they provided useful visual information. The ocular media of most birds is relatively transparent to near-UV wavelengths (Govardovskii and Zeuva, 1977; Emmerton *et*

al., 1980; Jane and Bowmaker, 1988; Goldsmith, 1990; Das, 1997; this study, see chapter four) and it is proposed that retinal oil droplets protect receptors individually, allowing short wavelength vision in only specialised cones with transparent droplets. By contrast, the incorporation of short wavelength-absorbing pigments into the mammalian lens, and *macula lutea* in primates, seems to be a relatively coarse adaptive solution to needs for short wavelength filtering (Goldsmith, 1990).

Whilst this theory does not explain the occurrence of more than one type of oil droplet, or the lack of a protective pigment associated with avian rods, there is some evidence for a protective role of UV-absorbing compounds. The macular region in primates is less prone to phototoxic damage than the unprotected periphery (Ham *et al.*, 1978) and squirrels which had their highly pigmented lens removed suffer considerable retinal damage following exposure to UV wavelengths (Collier *et al.*, 1989).

1.2.1.3.6.4 Improvement of visual acuity

Walls and Judd (1933) presented a unified view of the function of yellow ocular filters which has been reviewed on numerous occasions (Walls, 1942; Muntz, 1972; Meyer, 1977; Kirschfeld, 1982). Retinal oil droplets were assumed to have the same function as yellow lenses and corneas which might act to improve visual acuity by absorbing short wavelengths.

Chromatic aberrations induced by the dioptric apparatus can be considerable, especially in larger eyes, and result in a blurred retinal image. Furthermore, short wavelengths are affected more by changes in refractive index as light traverses the pre-retinal tissues. By absorbing short wavelengths, yellow and red long-pass filters would restrict the spectral range used for vision, thus improving spatial resolution.

Such coloured filters might also improve visual acuity by absorbing scattered light. Rayleigh scattering in the atmosphere occurs when the interfering particles are much smaller than the wavelength of light (Born and Wolf, 1970). The wavelength dependent nature of this optical phenomenon (proportional to $1/\lambda^4$) suggests that the use of yellow filters to block short wavelengths would improve the discrimination of distant objects, although this is thought to be of little practical advantage for distances less than about 1000 m (Muntz, 1972).

Oil droplets might also be employed to block short wavelengths scattered within the eye by the ocular media and neural retina. Measurements on the rabbit cornea suggest that the amount of scattering is wavelength dependent and proportional to $1/\lambda^3$ (Farrel *et al.*, 1973 cited in Lythgoe, 1979).

1.2.1.3.6.5 Oil droplets as secondary lenses

Roaf (1929) suggested that oil droplets, in their natural position at the junction of inner and outer segments of the cones, might have a lens like action in concentrating light in the outer segment. Due to their high refractive index relative to the surrounding tissues, oil droplets may well induce specific optical phenomena that are unrelated to any effect on the spectral composition of the light they transmit.

Using immersion refractive index (RI) matching techniques, the RI of colourless, yellow, orange and red oil droplets in the turtle *Pseudemys scripta elegans* were measured as 1.48, 1.51, 1.55 and 1.69 respectively (Ives *et al.*, 1982; Ives *et al.*, 1983). Similar values were calculated for avian oil droplets (Young and Martin, 1984). These figures are much higher than those determined for the cone myoid, outer segment and extracellular space (1.34 to 1.386).

This mismatch suggests that there is likely to be significant diffraction around droplets at all wavelengths, in addition to refractile behaviour where the droplets have negligible absorptance. Because of their small size, refraction of light by oil droplets cannot be accurately described using geometrical optics. For objects with dimensions approaching the wavelength of the incident light, electromagnetic (or wave optical) models must be applied. Rayleigh scattering occurs when the object intercepting the incident light is much smaller than the latter's wavelength, and scatter occurs equally in all directions. As the radius of the object increases, however, more light is scattered forward of the object that backwards in the direction of the light source. This is Mie scattering and the phenomenon is described by its own theory which has been derived specifically for predicting the energy distribution around spherical objects and incorporates the effects of refraction, reflection, absorption and diffraction (Born and Wolf, 1970).

Mie scattering theory predicts that oil droplets act as converging lenses and focus the incident light into the outer segment, thus increasing photon capture by the visual pigment (Ives *et al.*, 1982; Ives *et al.*, 1983; Young and Martin, 1984).

Furthermore, energy considerations suggest that oil droplets may enhance light intensity in the outer segment by a factor of between 1 and 4, thereby improving cone sensitivity. These calculations also suggested that a large proportion of the incident light is diffracted around the oil droplet without being transmitted through it.

Consequently, Ives *et al.* (1983) predicted that the effective photosensitivity of turtle cone photoreceptors containing yellow and red oil droplets would be much higher at short wavelengths than would be calculated if the oil droplets act as long-pass cut-off filters. However, electrophysiological studies on turtle photoreceptors have suggested that pigmented oil droplets do reduce sensitivity to short wavelengths considerably (Baylor and Hodgkin, 1973) and it appears that diffraction around droplets *in vivo* is greatly reduced, perhaps due to absorption by the pigmented epithelium (PE) which, at least in birds, extends between photoreceptors to the level of the oil droplets (e.g. Morris and Shorey, 1967; Braekevelt, 1994).

Nevertheless, oil droplets may still act as secondary lenses by refraction of wavelengths above the λ_{cut}, and a similar function has been proposed for the highly refractile 'megamitochondria' found in the ellipsoid of the tree shrew, *Tupaia belangeri* (Knabe *et al.*, 1997), which may also contain a short wavelength-absorbing pigment similar to that found in ellipsoid region of primate cones (Bowmaker *et al.*, 1991). This theory is appealing in that it justifies the retention of transparent oil droplets in sauropsid retinae. Furthermore, a dioptric function could explain the occurrence of oil droplets, or similar refractile organelles, in species in which a colour vision system, if any, is of fewer chromatic dimensions than birds or turtles, or which are mainly nocturnal. The incorporation of short wavelength-absorbing pigments, and thus the development of a spectral tuning function, may have been a secondary event.

1.2.1.3.6.6 Detection of magnetic field

The precise mechanisms underlying magnetoreception in birds is unclear, although two main hypotheses are currently discussed (Wiltschko *et al.*, 1993; Munro *et al.*, 1997). The first is based on light-dependent processes associated with the visual system. The second involves endogenous magnetic crystals (magnetite).

The effect of illuminating wavelength on the magnetic orientation of birds, newts and fruit flies (Phillips and Borland, 1992; Phillips and Sayeed, 1993;

Wiltschko *et al.*, 1993) suggests a significant role for the visual system. Initially, a physicochemical method involving magnetic field-dependent resonance of rhodopsin molecules was proposed by Leask (1977).

However, a simpler model applicable to avian oil droplets, which combines both theories, has also been suggested (Edmonds, 1996). Carotenoids are long chain molecules which only absorb light when its electric field direction is along the long axis of the chromophore. If carotenoids were arranged in a regular, liquid crystal formation in certain oil droplets and associated with small magnetic crystals, light of wavelengths that are absorbed resonantly by the carotenoid would only reach the visual pigment when the cone axis was parallel or antiparallel to the direction of the earth's magnetic field. As yet, no oil droplet has been demonstrated to possess a regular internal structure or magnetite crystals. However, P-type oil droplets in the mallard were shown to be more heterogeneous than those found in the single cones and contained granular or membranous material (Braekevelt, 1990).

1.2.1.4 Visual pigments

1.2.1.4.1 Structure and spectral absorption

The acquisition of visual information from the environment is mediated by photosensitive molecules, known as visual pigments, packaged within the retinal photoreceptor cells. The structure and chemistry of visual pigments have been reviewed many times (e.g. Knowles and Dartnall, 1977; Fein and Szuts, 1982; Applebury and Hargrave, 1986; Saibil, 1986; Stryer, 1987; Bowmaker, 1991; Yau, 1994). The most salient points are summarised in the following paragraphs.

All vertebrate visual pigments consist of a large protein moiety, opsin, bound covalently to an aldehyde of vitamin A, the chromophore (Bownds, 1967; Nakanishi, 1991). With the exception of some lizards, *Anolis carolinensis* and *Podarcis sicula* (Provencio *et al.*, 1992), the chromophore of most terrestrial vertebrates is 11-*cis* retinal, the aldehyde of vitamin A_1. Visual pigments containing 11-*cis* retinal are called rhodopsins to distinguish them from visual pigments based on 3-dehydroretinal, the aldehyde of vitamin A_2, which are known as porphyropsins. Porphyropsins are mainly restricted to some teleost fish, amphibians and some aquatic reptiles (Bowmaker, 1991).

Opsin molecules are single polypeptide chains, containing approximately 350 amino acid residues, embedded in the lamellar membranes of the photoreceptor outer segment (Bowmaker, 1991). The three-dimensional structure of opsin consists of a palisade of seven alpha-helices traversing the lipid bilayer, each of which are composed of 24-28 largely nonpolar amino acids, connected by short, non-helical segments rich in polar amino acids (Applebury and Hargrave, 1986; Stryer, 1987).

The opsin molecules of all vertebrate visual pigment share a number of important features. Where specific amino acids are referred to by numbers, these correspond to their analogous positions in bovine rod opsin. The carboxyl or C-terminal of the protein (protruding on the cytoplasmic side of the membrane) is characterised by numerous hydroxy-amino acids (serine and threonine) which are the sites of phosphorylation by rhodopsin kinase (Thompson and Findlay, 1984; Applebury and Hargrave, 1986). It is thought that only bleached pigments become phosphorylated, and that the phosphate is lost upon regeneration (Knowles and Dartnall, 1977). Phosphorylation of photoisomerised rhodopsin causes it to be recognised by a cytoplasmic protein, arrestin, which eventually replaces the rhodopsin kinase and quenches the activated visual pigment molecule (Rodieck, 1998). Similar phosphorylation sites (serine) on the cytoplasmic loop connecting the fifth and sixth helices are thought to act directly with cytoplasmic proteins, including transducin, which form part of the phototransduction cascade (Applebury and Hargrave, 1986).

The amino or N-terminal of the protein (located on the extracellular side of the membrane, or in rods the inside of the disks) contains one to two asparagine residues which form glycosylation sites (Applebury and Hargrave, 1986).

Opsin contains a number of proline residues, each of which is capable of creating a 20° 'kink' in the helix (Applebury and Hargrave, 1986). The presence of proline in five of the seven helices of bovine rhodopsin has been suggested to produce helices with slight bends that may be important in accommodating the bound chromophore (Dratz and Hargrave, 1983). Other ubiquitous amino acids include two cysteine residues, located in the extracellular loops linking the second and third (Cys-110) and fourth and fifth (Cys-187) helices, which form a disulphide 'bridge' essential for the formation of the correct structure of rhodopsin (Karnik *et al.*, 1988).

Furthermore, at least in bovine rod opsin, two adjacent cysteine residues (Cys-322 and Cys-323) are palmitoylated, anchoring the C-terminal to the membrane (Ovchinnikov *et al.*, 1988).

Retinal's covalent bond to opsin is formed by a condensation reaction between the aldehyde group on the chromophore and the ε-amino group of a lysine residue (Lys-296) located approximately midway in the seventh transmembrane helix (Bownds, 1967; Wang *et al.*, 1980). This spontaneous reaction creates a carbon-nitrogen double-bond linkage known as an 'aldimide' or 'Schiff's base' bond. With the possible exception of UVS visual pigments (Hárosi and Sandorfy, 1995), the Schiff's base is usually protonated (Wang *et al.*, 1980). As it is energetically costly to bury charges which are not ion-paired in a hydrophobic environment, a 'counterion' must balance the Schiff's base. This has been identified as a glutamic acid residue (Glu-113) towards the extracellular end of the third helix (Sakmar *et al.*, 1989). A tryptophan (Trp-265) residue may also be involved in binding the β-ionone ring of the chromophore (Nakayama and Khorana, 1990).

Opsin absorbs maximally below 300 nm whereas 11-*cis* retinal has a maximum absorption at about 375 nm (Knowles and Dartnall, 1977; Nakanishi, 1991). The broad, asymmetrical, bell-shaped absorption spectrum characteristic of visual pigments is formed when the chromophore binds with opsin (Bowmaker, 1991). This phenomenon is called the bathochromic shift and represents a decrease in the energy required for absorption (Rodieck, 1973).

The absorption spectra of retinal-based visual pigments display four distinct peaks as follows: a) a broad peak between about 345 and 570 nm (alpha peak, α) due to the main absorption band (α-band) of the chromophore and dependent on the type of opsin with which it is conjugated; b) a low broad peak (beta peak, β), which in bovine rod opsin occurs at about 340 nm but has a spectral location that varies and is probably related to the position of the alpha peak λ_{max} (Palacios *et al.*, 1996; Palacios *et al.*, 1998), due to absorption by the *cis*-band of the chromophore; c) a narrow peak at about 278 nm (gamma peak, γ) which is due to certain aromatic amino acids (tyrosine and tryptophan) in the opsin, and d) a peak at 231 nm (delta peak, δ) due to a variety of organic bonds (Rodieck, 1973). 3-Dehydroretinal-based visual pigments (porphyropsins) also display four similar absorption peaks. However, an extra

double bond in the chromophore dictates that, for a given opsin, the α-band absorbance[3] spectrum will have its wavelength of maximum absorbance (λ_{max}) at longer (lower energy) wavelengths, and a broader full-width at half maximum absorbance (FWHM) bandwidth, than when conjugated with retinal (Knowles and Dartnall, 1977).

A model retinylidene Schiff base linkage has a λ_{max} at 440 nm (Nakanishi, 1991). The hypsochromic or bathochromic shift necessary to account for the wide range of λ_{max} observed, from about 345 to 570 nm in rhodopsin pigments (Knowles and Dartnall, 1977), is called the 'opsin shift' (Applebury and Hargrave, 1986). The degree of opsin shift is determined by the genetically-controlled amino acid sequence of the opsin, and its electric effects on the embedded chromophore. In particular, charged amino acids buried within the protein's chromophore binding cavity are thought to affect the conformational structure of retinal (Applebury and Hargrave, 1986; Nakanishi, 1991).

By comparing the amino acid sequences of different opsins, it is possible to identify particular residues which represent spectral tuning sites. However, only a few opsin sequences are available for avian visual pigments, and comparisons must be made with other taxa (e.g. Okano *et al.*, 1992; Yokoyama *et al.*, 1998).

Birds typically have four retinal-based cone pigments maximally sensitive to long (λ_{max} 543 to 570 nm), medium (λ_{max} 497 to 509 nm), short (λ_{max} 430 to 463) and violet/near ultraviolet (λ_{max} approximately 355 to 426 nm) wavelengths, plus a single type of MWS (λ_{max} 501 to 509 nm) rod pigment (Table 1.3, and references therein). Only in the chicken (Takao *et al.*, 1988; Okano *et al.*, 1992; Wang *et al.*, 1992a; Wang *et al.*, 1992b) and the canary, *Serinus canaria* (Das, 1997), have the amino acid sequences for all visual pigments been obtained.

Phylogenetic comparison of vertebrate visual pigments on the basis of amino acid identity (sequence homology) suggests that an ancestral visual pigment evolved first into four groups of cone pigments, each of which includes one of the chicken

---

[3] Absorbance is a logarithmic measure of absorption, which means that absorbances are additive: doubling the pathlength doubles the absorbance but, when normalised, the shape of the absorbance spectrum remains unchanged. Absorbance is defined as the $\log_{10}$ of the ratio of the intensity of the light incident upon a sample to the intensity of the light transmitted by the sample, or $-\log_{10}(T)$ where T is transmittance (1-absorptance).

and canary cone pigments, and that rod opsins diverged from the group of MWS cone opsins later (Okano *et al.*, 1992). The UVS cone pigment of the budgerigar, *Melopsittacus undulatus*, (Wilkie *et al.*, 1998), and the VS cone pigment of the pigeon (Yokoyama *et al.*, 1998) fall into the same group which contains the VS pigment of the chicken and the UVS pigment of the canary (Das, 1997).

Divergence of rod opsin has bought about a change in the net charge of the pigment. Thus, rod and cone pigments in vertebrates are negatively and positively charged, respectively, at neutral environmental pH. The difference in charge may or may not affect their relative photoresponses. Sequences for the rod and MWS cone pigments of both budgerigar and mallard duck (*Anas platyrhynchos*) confirm the similarity of these two pigments, but reveal a consistent difference between the two opsins at site 122 (Heath *et al.*, 1997). Site 122 has been shown to be important in the formation and stabilisation of metarhodopsin II forms of bovine rod opsin (Weitz and Nathans, 1993). Furthermore, site-directed mutagenesis studies have shown that replacement of the charged glutamic acid (Glu-122) residue at site 122 with an uncharged asparagine (Asn-122) transforms the rate of regeneration and metarhodopsin II decay from rod-like to cone-like (Imai *et al.*, 1997). In both budgerigar and duck Glu-122 is present in rod opsin but replaced by Asn-122 in the MWS cone opsin (Heath *et al.*, 1997). In the MWS cone pigment of the chicken (Okano *et al.*, 1992) and canary (Das, 1997), Glu-122 is replaced by glutamine (Gln-122), which is an uncharged (polar) amino acid just like asparagine, and it is known that chicken MWS cone pigment bleaches and regenerates faster than rod pigment (Shichida *et al.*, 1994).

However, substitution of the Glu-122 by Asn-122 in human and bovine rhodopsin results in a 15 to 20 nm hypsochromic shift in λ_{max} (Sakmar *et al.*, 1989; Nakayama and Khorana, 1990). From microspectrophotometric studies of visual pigments *in situ* it is known that the λ_{max} of avian rod and MWS cone pigments are almost identical within a given species, and show minimal variation between species (Table 1.3). Consequently, the loss of a charged residue from site 122 must be compensated for by a substitution which induces a bathochromic shift in spectral absorption (Heath *et al.*, 1997). Hydroxyl-bearing amino acids (e.g. serine, tyrosine, threonine) are known to cause bathochromic spectral shifts when introduced to

bovine rod opsin (Chan *et al.*, 1992). Only two sites (222 and 299) which face in to the retinal binding pocket, and are therefore in a position to interact with the chromophore, differ between the rod and MWS cone opsins of duck, chicken, budgerigar and canary with regard to charge change or the gain/loss of a hydroxyl group (Das, 1997; Heath *et al.*, 1997). Both sites exhibit the gain of a hydroxyl-bearing amino acid (serine) in the MWS cone opsin. Thus, the amino acid sequence of an opsin affects both the biochemistry and spectral absorption characteristics of the visual pigment.

It has been known for some time that certain LWS visual pigments are affected by the availability of chloride ions. Chicken LWS cone visual pigment extracted into solution displayed a hypsochromic shift in λ_{max} to 520 nm in the absence of chloride ions, but shifted back to 562 nm upon the addition of chloride (Knowles, 1976; Shichida *et al.*, 1990). However, chicken SWS (λ_{max} 449 nm) and VS (λ_{max} 417 nm) cone pigments extracted using digitonin were shown to be chloride insensitive (Fager and Fager, 1981). Similar experiments in the Tokay gecko, *Gecko gecko*, reported a 10 to 15 nm hypsochromic shift only in the more long wavelength-sensitive of the two pigments extracted from the retina (native λ_{max} 467 and 521 nm) (Crescitelli, 1977; Crescitelli, 1991). Confirming that this phenomenon was not an artefact of the unnatural environment into which the visual pigments were extracted, Kleinschmidt and Hárosi (1992) demonstrated the chloride sensitivity of LWS cone visual pigments *in situ*.

Wang *et al.* (1993) identified two charged amino acid residues (histidine, His-197 and Lysine, Lys-200, which correspond to positions 181 and 184 respectively in the bovine rod opsin numbering scheme) in the chloride binding site of human 'red' and 'green' cone pigments. These amino acids are strictly conserved at this location in LWS visual pigments but absent from rod and SWS cone opsins. His-181 is located close to the highly conserved Cys-187, which forms the disulphide bond with Cys-110 that is essential in creating the correct structure of opsin (Karnik *et al.*, 1988). In addition, Cys-110, and therefore His-181, is very close to Glu-113, the counterion for the Schiff's base linkage of the chromophore and a crucial residue in determining the spectral absorption properties of rhodopsin (Sakmar *et al.*, 1989). It seems likely that the spectral shifts might result from an indirect perturbation of the

protein structure, although chloride may also have a direct effect by stabilising the binding of the chromophore in the protein (Yoshizawa *et al.*, 1991). Wang *et al.* (1993) speculated that the evolutionary branch of the LWS pigments was established when an ancestral pigment acquired the ability to bind chloride ions and, as a result, shift the λ_{max} to longer wavelengths.

Avian VS opsins are thought to be closely related evolutionarily to UVS opsins (Yokoyama *et al.*, 1998), even though the λ_{max} of the two pigments they create can be separated by more than 40 nm. In an attempt to identify potential spectral tuning sites responsible for the difference in λ_{max}, Wilkie *et al.* (1998) sequenced the UVS opsin gene of the budgerigar and compared it with the sequence for chicken VS opsin (Okano *et al.*, 1992). Assuming that only non-conservative amino acid changes (i.e. involving either a change in charge or the gain/loss of a hydroxyl group) were responsible for opsin shifts, five sites where non-conservative substitution had occurred between chicken VS and budgerigar UVS opsins sequences were identified: 81, 88, 113, 114 and 293 (corresponding to 86, 93, 118, 119 and 298 using bovine opsin numbering). Site 114 (119) was eliminated as a potential tuning site as it was not situated on the inner face of the chromophore-binding pocket. Sites 81, 88 and 113 (86, 93 and 118), however, were all located near to the Schiff's base counterion (Glu108 in budgerigar). If, as has been suggested, the Schiff's base in UVS pigments is unprotonated (Hárosi and Sandorfy, 1995), the counterion effect of Glu108 would need to be neutralised by electrostatic interactions with nearby residues.

1.2.1.4.2 Bleaching, regeneration and the visual cycle

Following photoactivation of the chromophore, the visual pigment molecule spontaneously and rapidly progresses through a series of transient states ('bleaching sequence') without the need of further enzymatic or metabolic energy, followed by a series of energy-consuming regenerative reactions (Fein and Szuts, 1982). This process has been termed the 'visual cycle' (Wald, 1935).

Opsin-bound 11-*cis*-retinal is isomerised to the all-*trans* configuration by the absorption of a single photon, with a probability of approximately 0.67 (Knowles and Dartnall, 1977). This conformational change, which takes only a few picoseconds (10^{-12} s) to complete, results in the formation of the first intermediate of the

bleaching sequence, bathorhodopsin (Nakanishi, 1991). The ensuing changes to the visual pigment molecule induced by the chromophore, during which bathorhodopsin decays through a series of intermediates (lumirhodopsin, metarhodopsin I, II and III and N-retinylidene-opsin) of lower energy state (Knowles and Dartnall, 1977), are thermal (Bowmaker, 1991). The conformation adopted by the intermediate metarhodopsin II triggers the phototransduction cascade (section 1.2.1.4.3) by exposing the binding site for transducin (Nakanishi, 1991). The end-point of the bleaching sequence is the hydrolysis of the visual pigment molecule. Whilst the opsin protein remains embedded in the lamellar membranes, free all-*trans* retinal is liberated from its binding site. This represents the end of the spontaneous reactions and the beginning of the regeneration step of the visual cycle. Because opsin proteins and the free chromophore absorb only weakly in the human-visible spectrum, the pigment is referred to as having been 'bleached' (Nakanishi, 1991).

Before the visual pigment can be used again, opsin and 11-*cis* retinal must recombine, and a number of different biochemical pathways are involved in reisomerising all-*trans* retinal (Rodieck, 1973). Within the outer segment, all-*trans* retinal can either be isomerised directly into 11-*cis* retinal by the enzyme retinal isomerase, and is then free to bind spontaneously with opsin, or reduced to all-*trans* retinol by retinal dehydrogenase (Rodieck, 1998). Both of these mechanisms prevent the potentially toxic accumulation of free retinal. Furthermore, excess all-*trans* retinol may be converted into retinal ester by microsomes in the inner segment (Rodieck, 1973).

Visual pigment regeneration is substantially reduced, or even absent, if the sensory retina is separated from the pigment epithelium (Rodieck, 1973). All-*trans* retinol migrates from the outer segments to the pigment epithelium within the hydrophobic 'pockets' of specific transport proteins known as all-*trans* retinol binding proteins (Fein and Szuts, 1982; Rodieck, 1998). An enzyme, retinyl-ester isomerase, converts all-*trans* retinol to 11-*cis* retinol. Another enzyme, 11-*cis* retinol dehydrogenase, uses metabolic energy to convert 11-*cis* retinol back to 11-*cis* retinal, which is subsequently conveyed to the outer segment via an 11-*cis* retinal binding protein where it recombines with opsin (Rodieck, 1998).

1.2.1.4.3 Phototransduction cascade

When the 11-*cis*-retinal chromophore of a vertebrate visual pigment absorbs a photon of light, the energy transferred isomerises the molecule into the all-*trans* configuration (Knowles and Dartnall, 1977). This in turn leads to a conformational change in the opsin which triggers its enzymatic activity by exposing a binding site for transducin (Applebury and Hargrave, 1986). Transducin is a guanosine 5′-triphosphate (GTP) binding regulatory protein complex, or G-protein, with multiple enzymatic functions. As a consequence of light-induced binding of G-protein to the opsin, one of its protein subunits (the nucleotide-binding or *N*-protein) converts the guanosine 5′-diphosphate (GDP) to which it is bound into GTP (Saibil, 1986). The *N*-protein-GTP complex subsequently dissociates from the opsin binding site and activates guanosine 3′5′-cyclic-monophosphate (cGMP) phosphodiesterase which hydrolyses cytoplasmic cGMP. In the dark, Na^+, Ca^{2+} and Mg^{2+} ions flow from the inner to the outer segment of the photoreceptor *via* an extracellular route. This 'dark current' maintains the photoreceptor resting potential at around -40 mV, a mild depolarisation which maintains a high steady rate of neurotransmitter release (Yau, 1994). Cell membrane channel proteins which permit this current are activated by conjugation with cGMP in the dark (Stryer, 1987). The reduction in cytoplasmic cGMP following phototransduction restricts cation ingress and the outer segment hyperpolarises in an intensity-dependent manner up to a maximum receptor potential of -80 mV (Stryer, 1987). The receptor potential then spreads electrotonically through the cell to the site of synaptic output and reduces the rate of neurotransmitter (glutamate) release at the receptor terminal (Shepherd, 1988; Yau, 1994).

The absorption of a single photon of light by a molecule of rhodopsin results in the liberation of approximately 500 *N*-proteins, each of which activates a single cGMP phosphodiesterase (PDE). PDE can hydrolyse 4,200 molecules of cGMP per second, thus preventing the influx of millions of cations. This cascade of enzymatic reactions enables a single photochemical event to have a large effect on the electric potential of the photoreceptor.

The reduction of Ca^{2+} influx into the outer segment results in a negative feedback mechanism which is thought to mediate light adaptation (Yau, 1994). Divalent calcium ions inhibit guanylate cyclase, the cGMP-synthesizing enzyme.

When light triggers the hydrolysis of cGMP, the ensuing fall in intracellular Ca^{2+} concentration disinhibits the cyclase and results in increased cGMP synthesis. This production antagonises the light-induced increase in cGMP hydrolysis and, by allowing more cation channels to open, down-regulates the sensitivity of the photoreceptor to light.

Cones are approximately 25 to 100 times less sensitive than rods, but their electrical responses are several times faster. These differences in rod and cone physiology are thought to arise from quantitative differences in the transduction cascade, although the nature of these differences is unclear (Yau, 1994).

1.2.1.5 Avian visual pigments

A variety of techniques have been employed to determine or infer the spectral absorption properties of avian visual pigments.

1.2.1.5.1 Extraction

Chemical extraction of visual pigments from the retina into solution, which are then subject to conventional photometric techniques (spectroscopy), is the oldest method used in the investigation of visual pigments. The first spectrophotometric analysis of a visual pigment extracted from a bird retina was performed by Köttgen and Abelsdorff in 1896 (cited in Sillman, 1973), who established that the difference spectrum λ_{max} of the rod pigment of the barn owl, *Tyto alba*, occurred at about 500 nm. A number of studies since have illustrated that the spectral location of the avian rod pigment varies little between species (see Table 1.2).

Despite recent advances, particularly with respect to separation of the different visual pigment types using column chromatography (Fager and Fager, 1981; Fager and Fager, 1982; Yen and Fager, 1984; Okano *et al.*, 1989; Yoshizawa and Fukada, 1993), visual pigment extracts are subject to a number of problems.

Firstly, because visual pigments are water insoluble, extraction relies on the use of solvents or detergents to separate them from the lamellar membranes. It has been known for some time that avian LWS cone pigment is more labile than rod opsin (Bliss, 1946), and it appears that cone pigments in general are more difficult to extract chemically (Knowles and Dartnall, 1977; Yoshizawa and Fukada, 1993).

Another problem, which applies even to suspensions of outer segments which have not been extracted, is the ionic composition of the interstitial medium. The effects of chloride ions on the spectral absorption characteristics of LWS pigments have already been discussed (section 1.2.1.4.1) and are now common knowledge. However, chloride sensitivity was unrecognised when Bridges (1962) attempted to isolate visual pigments from the pigeon retina, and the putative LWS cone pigment he characterised (difference spectrum λ_{max} 544 nm, see Table 1.2), in addition to rod opsin, probably represents a chloride-deficient λ_{max} 567 nm pigment (Bowmaker, 1977; Bowmaker *et al.*, 1997).

Visual pigment extracts are usually analysed by 'partial bleaching' (Knowles and Dartnall, 1977). The procedure involves partially bleaching an extract with monochromatic (or narrow band) lights from suitably chosen regions of the spectrum, so as to bleach one spectral type of pigment more than another. Because the photosensitivity of all visual pigment extends further on the short wavelength side of its λ_{max} (due to absorption by the β- and γ-bands) than on the long wavelength side, partial bleaching usually begins with long wavelengths. Subsequent bleaches are made with monochromatic light of shorter and shorter wavelength.

Legend to **Table 1.2** (overleaf) Wavelengths of maximum absorbance change (difference spectrum λ_{max}) for visual pigments extracted from the retinae of several avian species. The system of classification used for the listed species is that given by Sibley and Monroe (1990) and is based on recent results from DNA-DNA hybridisation. [1] Bridges (1962); [2] Sillman (1969); [3] Crescitelli (1958); [4] Bliss (1946); [5] Wald (1937); [6] Wald *et al.* (1955); [7] Fager and Fager (1982); [8] Fager and Fager (1981); [9] Okano *et al.* (1989); [10] Crescitelli *et al.* (1964); [11] Köttgen and Abelsdorff (cited in Sillman, 1973); [12] Shichida *et al.* (1990).

Order	Specific name	English name	Visual pigment λ_{max} (nm)				
			VS	SWS	MWS	LWS	Rod
Anseriformes	*Anas playrhynchos domesticus*	Aylesbury duck					502[1]
Caprimulgiformes	*Phalaenoptilus nuttallii*	Poorwill					506[2]
Ciconiiformes	*Larus occidentalis*	Western gull					503[3]
	Buteo magnirostris	Roadside hawk					500[2]
Columbiformes	*Columba livia*	Feral pigeon				544[1,2]	502[1,2]
	Streptopelia risoria	Ring dove					502[2]
	Zenaida macroura	Mourning dove					502[2]
Galliformes	*Gallus gallus domesticus*	Domestic chicken	417[7,8]	449[7,8]	508[9]	560[7]	500[7]
		"	425[9]	455[9]		562[4,5,6,12]	502[4,5,6]
		"				571[9]	503[9]
		"					504[3]
	Meleagris gallopavo	Domestic turkey				562[10]	504[10]
	Colinus virginianus	Bobwhite quail					500[2]
	Lophortyx californicus	California quail					500[2]

Table 1.2 Avian visual pigment spectral sensitivities determined by extraction methods (continued over).

Order	Specific name	English name	Visual pigment λ_{max} (nm)				
			VS	SWS	MWS	LWS	Rod
Passeriformes	*Lonchura striata*	Bengalese finch					502[2]
	Molothrus ater	Brown-headed cowbird					501[2]
	Carpodacus mexicanus	House finch					502[2]
	Pipilo fuscus	Brown towhee					500[2]
	Zonotrichia leucophrys	White-crowned sparrow					502[2]
	Taeniopygia guttata	Zebra finch					502[2]
	Plocepasser mahali	White-browed sparrow-weaver					504[2]
	Estrilda troglodytes	Black-rumped waxbill					502[2]
	Lonchura malabarica	Common silverbill					502[2]
	Lonchura malacca	Chestnut mannikin					503[2]
Pelicaniformes	*Pelecanus occidentalis*	Brown pelican					502[3]
Psittaciformes	*Melopsittacus undulatus*	Budgerigar					505[2]
Strigiformes	*Tyto alba*	Barn owl					500[11]
	Bubo virginianus	Great horned owl					502[3]
	Otus asio	Screech owl					505[3]
	Speotyto aluco	Burrowing owl					503[2]

Table 1.2 (continued).

The difference spectra thus created should indicate the presence of more than one pigment, and reveal the wavelength at which there was the greatest change in absorbance between the pre- and post-bleach scans (the difference spectrum λ_{max}). The success of this technique is dependent upon the relative proportions and λ_{max} separation of the component pigments, and on the wavelengths, intensities and durations of the bleaching lights used (Knowles and Dartnall, 1977).

Even when only one visual pigment is present in an extract, its spectral absorbance must be inferred from a difference spectrum, i.e. the absorbance of the extract before and after full or partial bleaching of the pigment. This is necessary because other light-stable impurities contained within the extract, such as melanin from the pigment epithelium, haemoglobin and oil droplet carotenoid, would distort the pre-bleach absorption spectrum.

However, depending on the pH of the extract, significant absorption of 'visible' wavelengths by the stable products of photobleaching will affect the apparent λ_{max} of the difference spectra obtained, especially for pigments with λ_{max} at or below 500 nm (Knowles and Dartnall, 1977). In neutral pH extracts, the principal stable photoproduct is all-*trans* retinal, liberated by hydrolysis of the isomerised visual pigment molecule. All-*trans* retinal has a peak absorbance at 380 nm (Rodieck, 1973). At alkaline pH (pH > 8), the visual pigment does not dissociate and all-*trans* retinal remains bonded to opsin *via* a Schiff's base linkage. This final intermediate in the bleaching sequence is called N-retinylidene-opsin (NRO). Alkaline NRO has a peak absorbance at about 365 nm (Knowles and Dartnall, 1977). However, under acidic conditions (pH < 5.5), NRO has a λ_{max} at 440 nm, which will have a large effect on the shape of the visual pigment difference spectrum. Another stable photoproduct, metarhodopsin III, absorbs maximally at 470 nm in acidic solutions. Whilst the λ_{max} values of both of these photoproducts are shifted hypsochromically by the use of alkaline conditions, metarhodopsin III will still absorb appreciably above 500 nm (Knowles and Dartnall, 1977).

Hydroxylamine can be added to visual pigment extracts to scavenge 11-*trans* retinal, thus preventing its build-up in solution and denaturing metarhodopsin III and NRO. The 'retinal-oxime' produced in this reaction has a λ_{max} at 367 nm. Knowles and Dartnall (1977) have calculated that the shift in apparent difference spectrum

λ_{max} towards longer wavelengths induced by retinal-oxime is less than 1 nm for visual pigments with λ_{max} greater than about 460 nm. However, whilst hydroxylamine is a useful tool in the spectroscopic study of most rod visual pigment extracts, it readily denatures cone visual pigments, and avian rhodopsins are no exception (Wald *et al.*, 1955; Fager and Fager, 1981; Okano *et al.*, 1989). The increased susceptibility of cone pigments to hydroxylamine attack probably reflects a greater accessibility in cone than in rod pigments of the retinal binding pocket (Wang *et al.*, 1992b), a hypothesis which would also explain the greater speed of cone pigment regeneration (Wald *et al.*, 1955)

Consequently, determination of the absorbance spectra of avian cone visual pigments from extracts relies on the interpretation of potentially artefactual difference spectra. Photoproduct absorption is thought to account for the discrepancy between the λ_{max} estimate (425 nm) obtained for chicken VS cone pigment by Okano *et al.* (1989) and that determined microspectrophotometrically (λ_{max} 418 nm, Bowmaker *et al.*, 1997).

Even when absorption by photoproducts is accounted for, both the absorbance and difference spectra of the visual pigment in the intact retina are shifted bathochromically with respect to the visual pigment in solution. It is thought that this represents an effect of the different physiological environment of the visual pigment under these two conditions (Bowmaker, 1973).

1.2.1.5.2 Electrophysiology

The most common electrophysiological technique used in the investigation of avian visual pigments is the electroretinogram (ERG). The ERG represents the gross electrical response of the eye to illumination, and comprises a variety of extracellular field potentials (Rodieck, 1973). Generally, the component field potentials sum across the retina so that, although the ERG is an epiphenomenon which plays no direct role in vision, the size of the ERG potential is related to the intensity of the illumination and the spectral sensitivity of the retina.

ERGs can be measured in live, anaesthetised birds with a corneal electrode (e.g. van Norren, 1975), or in opened eyecups (e.g. Chen and Goldsmith, 1986). The technique is combined either with flicker photometry, where a flickering stimulus

light exploits the slower regeneration of rod visual pigment to isolate cone mechanisms, or a criterion response method, which uses bright flashes of light to stimulate cone systems with slower temporal characteristics whilst saturating the rods with a white background illuminant.

By far the most popular subject for studies of avian vision has been the pigeon. In 1965, Ikeda used single flashes and flicker photometry to determine the scotopic and photopic spectral sensitivities of this species, which had peak responses at 502 and 547 nm respectively. These maxima in sensitivity corresponded well with absorbance maxima of pigeon rod and LWS cone pigment extracted by Bridges (1962), although microspectrophotometry has failed to confirm the existence of a λ_{max} 544 nm (Bowmaker, 1977; Bowmaker *et al.*, 1997). By selective adaptation with 547 nm light, a further photopic mechanism was isolated with a peak sensitivity at around 605 nm, which would approximate well to a LWS (λ_{max} 567 nm) visual pigment filtered by a red oil droplet with a cut-off wavelength at about 570 nm.

Like Ikeda (1965), Blough *et al.* (1972) also measured a broad photopic spectral sensitivity using flicker photometry ERG, but they observed a peak sensitivity at around 560 to 580 nm, which was more consistent with a cone pigment absorbing maximally at about 562 nm (Wald, 1937; Wald *et al.*, 1955). Numerous psychophysical studies have confirmed this shape for the pigeon's photopic sensitivity function (Graf, 1969; Romeskie and Yager, 1976a; Romeskie and Yager, 1976b; Kreithen and Eisner, 1978; Martin and Muntz, 1978; Delius and Emmerton, 1979; Kreithen, 1979; Martin and Muntz, 1979; Vos Hzn *et al.*, 1994). In all of these studies it is assumed that a LWS visual pigment dominates the cone population, and double cones, which are the most common cone type in the pigeon retina (Waelchli, 1883), contain a λ_{max} 567 nm pigment (Bowmaker, 1977; Bowmaker *et al.*, 1997). Unlike the LWS single cones, which also contains the λ_{max} 567 nm visual pigment, absorption by the P-type and A-type oil droplets associated with the double cones is unlikely to shift their peak sensitivity to longer wavelengths, and these measures of photopic spectral sensitivity probably reflect the effective spectral sensitivity of the double cones.

Further evidence for the dominance of double cones in the photopic spectral sensitivity function comes from behavioural (Martin and Muntz, 1979) and

electrophysiological (Wortel *et al.*, 1984) studies in the pigeon. In both cases, the photopic sensitivity of the red field between about 450 and 550 nm was found to be much lower than that of the yellow field, although the peak sensitivity was almost identical. P-type oil droplets in the double cones of the red field have a greater absorption (λ_{cut} at longer wavelengths) in this spectral region than those in the yellow field (Bowmaker, 1977).

Interestingly, both ERG (Chen *et al.*, 1984; Wortel *et al.*, 1984; Chen and Goldsmith, 1986; Vos Hzn *et al.*, 1994) and behavioural measures of photopic spectral sensitivity (Kreithen and Eisner, 1978) in the pigeon have also revealed a second peak with maximum sensitivity at around 340 to 380 nm. The peak absorbance of the β-band of a visual pigment with a λ_{max} of 567 nm is at approximately 364 nm, and it is known that, at least in fish, absorption by the β-band can lead to photoisomerisation with a high quantal efficiency (Palacios *et al.*, 1996). Thus, the possibility emerges that the peak in sensitivity in the near-ultraviolet is not the result of a dedicated UVS cone pigment, but absorption by the β-band of the abundant LWS double cone pigment.

Microspectrophotometric measurements have revealed the presence of four cone pigments in the pigeon, with λ_{max} at 409 (VS), 453, 507 and 567 nm (Bowmaker *et al.*, 1997). However, the existence of a further UVS pigment with a λ_{max} at 370 nm in the pigeon retina is controversial. Spectrophotometry of pigeon VS pigment, regenerated by adding 11-*cis* retinal to the purified expression products of vector cells transfected with the VS opsin gene, revealed a λ_{max} at 393 nm (Yokoyama *et al.*, 1998). Unpublished work cited by the authors of the same study suggests that, having screened the pigeon's genomic DNA library, there are only four types of cone pigment gene present.

The ERG data are not helpful in resolving this discrepancy. Graf and vanNorren (1974) employed criterion response ERG to record the photopic spectral sensitivity of the pigeon. Selective chromatic adaptation with long wavelength light (> 530 nm) reduced the broad sensitivity peak at about 560 nm and revealed a narrow, independent sensitivity peak at 400 nm, consistent with the VS pigment determined microspectrophotometrically. Using a similar experimental paradigm, vanNorren (1975) isolated two short wavelength-sensitive mechanisms in

experiments on the chicken, pigeon and jackdaw (*Corvus monedula*), with peak sensitivities at 400-420 nm and 480 nm. In all three species, sensitivity dropped rapidly between 400 nm and the short wavelength limits of the spectral range investigated (360 nm). The peak in sensitivity at around 400 nm might well be attributable to a VS pigment associated with a transparent oil droplet with insignificant absorption above 350 nm. Similarly, the 480 nm peak would perhaps be expected by the pairing of the SWS pigment and an oil droplet which absorbed strongly below 450 nm. A peak at about 460 nm was also observed electroretinographically in the pigeon by Wortel and Nuboer (1986), after selective chromatic adaptation with a combination of violet (404 nm) and long wavelength (> 610 nm) lights, and attributed to a similar pigment and oil droplet pairing.

Of the ERG studies which reported a sensitivity peak at 370 nm, only Chen *et al.* (1984) and Chen and Goldsmith (1986) performed the ERGs after selective chromatic adaptation with long wavelength (530 and 590 nm) light. Their results suggested that UV sensitivity in a number of species, including the pigeon, did not decline significantly in response to adaptation of the LWS pigment, which would be expected if β-band sensitivity was the cause of the 370 nm sensitivity peak. However, apart from a peak at 570 nm, the same study failed to isolate in pigeon ERGs the peaks in sensitivity at 450 and 480 or 510 nm noted in the majority of other species, or any other peaks which might have corresponded to photoreceptor sensitivity.

In addition to a broad peak at around 600 nm, VosHzn *et al.* (1994) observed two peaks in sensitivity at about 370 nm and 404 nm. As already discussed, the peak at 600 nm is consistent with the LWS pigment filtered by a red oil droplet, and the peak at 404 nm a reflection of the VS pigment and transparent droplet pairing. The photopic sensitivity function obtained also displayed a distinct dip in sensitivity between 450 and 500 nm, but this would perhaps be expected if the sensitivity of the SWS and MWS pigments was reduced significantly by oil droplet absorption (Bowmaker, 1977).

In an ERG study in the chicken, Wortel *et al.* (1987) revealed peaks in sensitivity at about 365 nm and 560 nm, but a distinct dip in sensitivity between 400 and 450 nm. The chicken is known to have a VS pigment with a λ_{max} of around

419 nm from microspectrophotometric studies (Bowmaker *et al.*, 1997) visual pigment extraction (Fager and Fager, 1981; Fager and Fager, 1982) and recordings of the early receptor potential (Govardovskii and Zeuva, 1977; see below). The presence of a peak in sensitivity at 365 nm instead, suggests that either chicken and pigeon have both UVS and VS pigments, or that the 365 nm peak is the β-band of the LWS pigment.

Chen *et al.* (1984) used sodium aspartate to block synaptic transmission between photoreceptors and retinal interneurons to confirm that higher order neural interactions were not responsible for the 370 nm peak in sensitivity. Furthermore, intracellular recordings of horizontal cells in chelonian retinae (*Pseudemys scripta elegans* and *Mauremys caspica*), which have a similar retinal organisation to birds (Bowmaker, 1991), have revealed that, in addition to yellow / blue chromaticity-type horizontal cells which received excitatory input from presumptive UVS cones, red / green chromaticity-type and luminosity-type horizontal cells displayed a UV sensitivity derived from the β-band of the MWS and LWS visual pigments respectively (Ammermüller *et al.*, 1998).

Behaviourally-determined wavelength discrimination functions describe the minimum wavelength differences that an animal can usefully distinguish. Such a function has been measured for the pigeon on a number of occasions (Hamilton and Coleman, 1933; Blough, 1972; Wright, 1972). Two of the more recent studies (Delius and Emmerton, 1979; Emmerton and Delius, 1980) have suggested that, in addition to regions of heightened wavelength discrimination ability at 460, 530 and 595 nm, a fourth minimum is located at around 365 to 385. Such an observation is suggestive of a pentachromatic visual system. Furthermore, colour mixing experiments in the pigeon have suggested that colour vision involves five primary mechanisms (Palacios and Varela, 1992). Nevertheless, UV sensitivity provided by β-band absorption could just as easily be integrated into these two psychophysical measures as the signal from a dedicated UVS photoreceptor.

The biggest anomaly to reconcile in proposing that the 370 nm peak in the pigeon and chicken ERG is derived from β-band photosensitivity is absorption of short wavelengths by the oil droplets associated with LWS pigment. However, as in microspectrophotometric measurements of oil droplet absorption spectra *in vitro* (see

chapter two), 'leakage' of the incident light around the droplet may also occur *in vivo*, permitting absorption by the β-band. Short wavelength-absorbing filters do not necessarily preclude UV sensitivity. The diurnal gecko, *Gonatodes albogularis*, has a dedicated UVS visual pigment (λ_{max} 362) but a 'yellow' lens which absorbs strongly below 450 nm (Ellingson *et al.*, 1995). Spectral sensitivity measurements reveal considerable UV sensitivity in this species, and the absorbance of the lens (1.3) is presumably optimised to permit UV vision whilst protecting the retina from excessive levels of short wavelength radiation. Alternatively, β-band photosensitivity could arise from the LWS visual pigment in the accessory member of the double cone, which, although sometimes displays a small, discrete oil droplet (Jane and Bowmaker, 1988), often contains only a very low concentration of diffuse carotenoid in the ellipsoid (Bowmaker, 1997).

Even if oil droplets do act as cut-off filters, UV photosensitivity of the LWS double cone visual pigment could be mediated by fluorescence of the P-type droplet when stimulated with ultraviolet light. As described in chapter three, irradiation of the retina with near-ultraviolet wavelengths (334 and 365 nm) resulted in appreciable autofluorescence by the C-type droplets of the SWS single cones, and particularly the P-type droplets of the double cones. This phenomenon has been described in a number of other bird species (Goldsmith *et al.*, 1984b) and even in turtles (Ohtsuka, 1984; Ohtsuka, 1985).

The purpose of this necessarily long and convoluted argument has been to review the evidence regarding the possibility of a fifth cone pigment in the avian retina. It is the author's opinion that, on the basis of the available information, this is unlikely. However, this need not preclude the occurrence of pentachromatic colour vision, and should not deter the rigorous investigation of all avian retinae to discover additional pigments.

The ERG study by Chen *et al.* (1984) and Chen and Goldsmith (1986) discovered sensitivity maxima at around 370, 450, either 480 or 510, and 570 in a number of species from several different families, although not all peaks were observed in every species. These four peaks approximate to UVS, SWS, MWS and LWS pigments filtered by their respective oil droplets in the UVS, SWS and MWS single cones and the double cone respectively (see Table 1.1 and Table 1.3).

Curiously, these authors did not selectively adapt the retinae with short and medium wavelength light to isolate a LWS single cone mechanism which, through the combination of LWS pigment and red oil droplet, should peak at around 600 nm.

Other notable results include the determination, by flicker photometry ERG, of a putative 555 nm λ_{max} cone pigment dominant in the great horned owl, *Bubo virginianus* (Jacobs *et al.*, 1987). This is identical to the LWS pigment of the tawny owl, *Strix aluco* as measured microspectrophotometrically by Bowmaker and Martin (1978), and is of interest with regard to the microspectrophotometric results obtained for the LWS pigment of the blackbird, *Turdus merula*, in this study.

An alternative electrophysiological technique is the measurement of the early receptor potential (ERP). The ERP is a rapid potential change recorded across the retina or eye in response to an intense but brief flash of light (Rodieck, 1973). This potential, which has a positive and negative component (biphasic), results from charge displacements in the visual pigment molecule that accompany the sequence of bleaching intermediates (Fein and Szuts, 1982).

The ERP can be recorded extracellularly, across the retina or eye, or intracellularly. Intracellular recordings have the opposite polarity and a signal approximately 20 times greater in amplitude (Falk and Fatt, 1972). The advantage of the ERP over the electroretinogram is that it represents responses of the visual pigment molecules only and not interactions with higher order neurons. In addition, due to structural differences in their respective outer segments, the ERP is derived predominantly from cone photoreceptors rather than rods (Rodieck, 1973).

Visual pigment molecules are distributed symmetrically on either side of the lamellar disks. Thus in rod outer segments, where the disks are present as saccules isolated from the external medium, any potential produced by visual pigment molecules in the upper membrane of the saccule will be cancelled by an equal and opposite potential from the lower membrane. Rod ERP is therefore restricted to the very few disks which remain as infoldings of the plasma membrane at the base of the outer segment. However, the interior of the disks in cone outer segments, which remain as infoldings of the plasma membrane for the length of the outer segment, are in contact with the extracellular medium, enabling an external potential across the outer segment plasma membrane to be measured.

Recording ERPs before and after selective photobleaching of isolated retinae allowed Govardovskii and Zueva (1977) to isolate four spectral classes of cone in the pigeon and chicken. The response maxima of the pigments identified were similar for both species, 413, 467, 507 and 562 nm, and are very close to the λ_{max} estimates determined microspectrophotometrically (see Table 1.3, Bowmaker and Knowles, 1977; Bowmaker, 1977; Bowmaker *et al.*, 1997). No difference in ERP response was evident between the central and peripheral areas of the chicken retina, or between the red and yellow fields of the pigeon. Because the retinae were illuminated from the receptor side, the response maxima displayed no shift in spectral sensitivity towards longer wavelengths due to the filtering effect of the oil droplets.

1.2.1.5.3 Psychophysical determination

The use of psychophysical and psychometric tests to investigate avian visual capabilities was mentioned briefly in the previous section. Whilst such tests are useful in defining the visual capabilities of particular species under a given set of test or task conditions, they are even more subject to higher order neural processing than ERG recordings and can be highly specific to the test conditions (Jacobs, 1981). Consequently, it is difficult to infer the sensitivity of the cone mechanisms underlying visual ability, although there are some notable exceptions.

In addition to investigating the ability of various species to detect just ultraviolet wavelengths (Huth and Burkhardt, 1972; Goldsmith, 1980; Parrish *et al.*, 1981; Parrish *et al.*, 1984), operant experiments have been used to create photopic spectral sensitivity functions. Kreithen and Eisner (1978) employed a cardiac conditioning paradigm to reveal two peaks in sensitivity at 350 and 540 nm in the pigeon. Subjects were conditioned to expect a mild electric shock following the presentation of a monochromatic stimulus, and the intensity of this stimulus was varied to obtain a sensitivity function.

Graf (1969), Romeskie and Yager (1976a) and Martin and Muntz (1978), used increment threshold operant techniques to reveal the same broad peak in photopic spectral sensitivity at around 570 to 600 nm and a secondary rise in sensitivity below 400 nm in the pigeon. Martin and Gordon (1974) used a similar protocol to measure a broad 580 nm peak in the photopic spectral sensitivity of the tawny owl, *Strix aluco*. Graf (1979) extended his studies in pigeon to include

selective chromatic adaptation with background illuminants, and predicted that four cone mechanisms, with sensitivity maxima at around 400, 480, 560 and 615 nm, subserved photopic vision.

The most successful determination of photopic spectral sensitivity by operant methods was that performed by Maier (1992; 1994). He determined four peaks in sensitivity at 370, 460, 530 and 620 nm in the red-billed leothrix (pekin robin), *Leothrix lutea*. These peaks were subsequently shown to correspond well to the four single cone pigments screened by their respective oil droplets (Maier and Bowmaker, 1993).

Of relevance to this study are the results of Adler and Dalland (1959) and Dalland (1958), who determined, by operant techniques, the spectral sensitivity of the European starling to peak at 510 and 550 nm under scotopic and photopic conditions respectively.

1.2.1.5.4 Microspectrophotometry

The technique and practise of microspectrophotometry is described in detail in chapter two. It is the only method by which the absorbance spectra of visual pigments can be measured *in situ* in individual outer segments, and as such has obvious advantages over the other methods described above.

The first MSP measurements of avian visual pigments, carried out in the late 1960's, were reported by Liebman (1972). Rod outer segments of chickens, pigeons and laughing gulls (*Larus atricilla*) were shown to contain a visual pigment which absorbed maximally at around 500 nm. Cones, on the other hand, appeared to contain a pigment maximally sensitive to longer wavelengths (λ_{max} 560 to 575 nm). Whilst the absorption spectra of cone oil droplets were easily determined (Roaf, 1929; Fujimoto *et al.*, 1957; Strother and Wolken, 1959; Strother and Wolken, 1960; Strother, 1963) the optical problems encountered in the measurement of such tiny outer segments (approximately 1 to 2 μm in diameter), not to mention their physical fragility, complicated the study of avian cone visual pigments.

In fact, further measurements of avian cone visual pigments were not published until 1977 when Bowmaker finally established the multiple visual pigment nature of the chicken and pigeon retina (Bowmaker, 1977; Bowmaker and Knowles,

1977). To date, the visual pigments of only seventeen species of bird have been measured microspectrophotometrically (Table 1.3). Of these, 8 species have been shown to possess four spectrally distinct types of cone visual pigment in addition to a single type of MWS rod visual pigment. Whilst the absence of one or more cone pigments reported for some species may very well reflect the true condition of their retinae, a more likely explanation is that they have been overlooked due to the limitations of sampling, the small size of the cone outer segments, and the difficulty in obtaining intact cones (Bowmaker, 1984).

Subclass	Order	Specific name	English Name	Visual pigment λ_{max} (nm)				
				UVS/VS	**SWS**	**MWS**	**LWS**	**Rod**
Neognathae								
	Anseriformes	*Anas platyrhynchos*	Mallard duck[1]	415	452	506	567	505
		Anas playrhynchos domesticus	Aylesbury duck[1]	415	449	501	570	504
		Anas playrhynchos domesticus	Khaki Campbell duck[1]	426	456	501	570	505
	Ciconiiformes	*Puffinus puffinus*	Manx shearwater[2]	402	452			505
		Larus atricilla	Laughing gull[3]				560-575	508
		Buteo jamaicensis	Red-tailed Hawk[4]					501
		Spheniscus humboldti	Humboldt penguin[5]	403	450		543	504
	Columbiformes	*Columba livia*	Feral pigeon[2]	409	453	507	567	506
	Galliformes	*Gallus gallus domesticus*	Domestic chicken[2]	419	455	508	570	506
		Coturnix coturnix japonica	Japanese quail[6]	418	450	505	567	505
	Passeriformes	*Leothrix lutea*	Pekin robin[7] (red-billed leothrix)	*ca.* 355	453	501	567	501
		Taeniopygia guttata	Zebra finch[2]	360-380	430	503	567	507
		Serinus canaria	Canary[8]	369	444	500	571	506
		Corvus frugilegus	Rook[9]			497	565	504
	Psittaciformes	*Melopsittacus undulatus*	Budgerigar[2]	371	444	509	564	509

Table 1.3 Summary of avian visual pigments determined from microspectrophotometry (continued over).

Subclass	Order	Specific name	English Name	Visual pigment λ_{max} (nm)				
				UVS/VS	SWS	MWS	LWS	Rod
Neognathae								
	Strigiformes	*Strix aluco*	Tawny owl[10]		463	503	555	503
Palaeognathae								
	Struthioniformes	*Dromiceius novae-hollandiae*	Emu[4]				567	502
	Tinamiformes	*Nothoprocta cinerascens cinerascens*	Brushland tinamou[4]			?498	564	504
		Nothoprocta perdicaria sanborni	Chilean tinamou[4]				566	501

Table 1.3 (continued) Summary of avian visual pigments determined from microspectrophotometry. λ_{max}, wavelength of maximum absorbance of the alpha band. The system of classification of avian species is that given by Sibley and Monroe (1990) and is based on recent results from DNA-DNA hybridisation. [1] Jane and Bowmaker (1988); [2] Bowmaker *et al.* (1997); [3] Liebman (1972); [4] Sillman *et al.* (1981); [5] Bowmaker and Martin (1985); [6] Bowmaker *et al.* (1993); [7] Maier and Bowmaker (1993); [8] Das (1997); [9] Bowmaker (1979); [10] Bowmaker and Martin (1978).

As detailed in Table 1.1, avian cone visual pigments are reliably associated with specific spectral types of oil droplet. In the case of the pigeon, chicken, mallard duck, Japanese quail, pekin robin, zebra finch, budgerigar and canary, the organisation of the cone photoreceptors is as follows:

- R-type oil droplets with cut-off wavelengths (λ_{cut}) between 560 and 580 nm, which appear red to the human eye, are paired with a LWS visual pigment of λ_{max} 564 to 571 nm in one class of single cone.

- Y-type oil droplets with λ_{cut} between 500 and 540 nm, which appear yellow or orange to the human eye, are paired with a MWS visual pigment of λ_{max} 500 to 509 nm in another class of single cone. There is evidence to suggest that in the pigeon, the Y-type droplets in the dorsal retina (red field) have a consistently longer λ_{cut} (by approximately 20 nm) than those found in the ventral retina (yellow field).

- C-type oil droplets, which appear 'colourless' or pale yellow to the human eye, are always associated with a SWS visual pigment of λ_{max} 430 to 456 nm in a third class of single cone. However, the nature of the C-type droplet appears to depend on whether the retina also contains either a VS or UVS visual pigment. In the mallard, chicken, quail and pigeon, the fourth type of single cone contains a VS visual pigment. The C-type droplets in these species have higher measured absorbances (0.28 to 0.5) and a range of λ_{cut} from approximately 435 to 450 nm. The budgerigar, zebra finch, pekin robin and canary all possess a UVS visual pigment, and the C-type droplets in these species have lower measured absorbances (0.1 to 0.15) and λ_{cut} values at shorter wavelengths (approximately 400 to 415 nm). Due to their low apparent absorbance it is unlikely that the C-type droplets in the latter group act as true 'cut-off' filters.

- T-type oil droplets, which are truly transparent, contain no detectable carotenoid and show no significant absorption over the range of wavelengths scanned, are found in the fourth known class of single cone. In the mallard,

chicken and quail, this type of droplet is associated with a VS visual pigment of λ_{max} 415 to 426 nm. In the pigeon, the associated visual pigment has a shorter λ_{max} at 409 nm, but is still classed as a VS visual pigment. In the budgerigar, canary, zebra finch and pekin robin, T-type droplets are paired with a 'true' UVS visual pigment of λ_{max} approximately 355 to 380 nm. It should be noted, however, that avian VS and UVS pigments have probably arisen from the same evolutionary branch of UVS opsin gene (Okano *et al.*, 1992; Yokoyama *et al.*, 1998).

- Both members of the double cone contain the LWS visual pigment recorded in the LWS single cones. The P-type droplet in the principal member has a variable cut-off between 410 and 500 nm, and occasionally displays a distinct 'shoulder' in the absorbance spectrum at about 480 nm. The A-type droplet in the accessory member, or carotenoid pigment located at the distal tip of the inner segment when a droplet is not apparent, has a low absorbance (typically approximately 0.1) and a characteristic triple-peaked spectrum with absorbance maxima at about 430, 450 and 480 nm.

Microspectrophotometric examination of the emu (*Dromiceius novae-holandiae*) and two species of tinamou (*Nothoprocta cinerascens cinerascens* and *N. perdicaria sanborni*) by Sillman *et al.* (1981) largely revealed only one cone pigment (LWS) in addition to the rod pigment. The LWS pigment had a λ_{max} at 567 nm and was found in cones without oil droplets, and in cones with oil droplets with quoted λ_{T50} at about 508 and 568 nm. These cells probably represent the typical accessory, principal and LWS single cones respectively. The outer segment of one cone-like cell in the brushland tinamou had a peak absorbance close to 498 nm, although the inner segment contained no oil droplet. No further oil droplet types were observed. The same authors studied a neognathus species, the red-tailed hawk (*Buteo jamaicensis*) for comparison, and observed four spectral types of oil droplet. Hawk cone outer segments were deemed to small to measure. Because the hawk retina was subjected to the same fixation and preparation techniques, it is tempting to believe that the palaeognathus species genuinely contain fewer cone types. Only further

study, perhaps using immunocytochemical or *in situ* hybridisation techniques, will help to resolve this potentially interesting story.

Microspectrophotometric examination of the tawny owl (*Strix aluco*) revealed three types of cone visual pigment with λ_{max} at 463, 503 and 555 nm and four types of oil droplet, in addition to a 503 nm λ_{max} rod pigment (Bowmaker and Martin, 1978). However, all of the oil droplets had very low absorbances, as would perhaps be expected of nocturnal or crepuscular species which operate in photon-limited environments, and did not resemble the characteristic droplet types described above. Interestingly, the specimens used in the microspectrophotometric investigation had been in captivity for 5 years, and it is possible that the concentration of carotenoid pigment in the oil droplets was much less than would be found in a freshly caught wild bird, as was noted in the present thesis for the domestic turkey, *Meleagris gallopavo* (see chapter two). The 463 nm λ_{max} cone pigment (SWS) was paired with a 'pale yellow' droplet (C-type) and accounted for approximately 5 % of the cone population. The 503 nm λ_{max} cone pigment (MWS) was paired with 'darker yellow' oil droplet (Y-type) and accounted for a about 5 to 10 % of the cone population. The 555 nm λ_{max} cone pigment (LWS) was paired with 'pale yellow' droplets (P-type) distinct from the C-type droplets of the SWS cones. This pairing, which represented 80 to 90 % of the cone population, was almost certainly the principal member of the double cones. No outer segments attached to the reddish brown (R-type) droplets were measured. Because of the relative lack of cones in the rod-dominated owl retina, it would not be surprising if a fourth UVS or VS cone class was overlooked.

The retina of the Humboldt penguin, *Spheniscus humboldti*, was also found to contain only three cone pigments (Bowmaker and Martin, 1984). A 403 nm λ_{max} cone pigment (VS) was generally associated with a transparent (T-type) droplet with no detectable absorbance above 400 nm. A 'pale' droplet absorbing maximally at about 405 nm (C-type) was associated with a 450 nm λ_{max} cone pigment (SWS). The third type of cone pigment (λ_{max} 543 nm) was associated with 'pale' droplets resembling the C-type droplet of the SWS single cones, and 'yellow' droplets with a quoted λ_{T50} of 525 nm. Whilst these 'yellow' droplets most closely resemble the Y-type droplets, the fact that the 543 nm λ_{max} pigment is found in another class of cone

which has a pale oil droplet and probably represents the principal member of the double cone pair, suggests they are in fact less pigmented R-type droplets. Like the tawny owls, the penguins used had been kept in captivity for at least a year prior to examination and oil droplet carotenoid concentration may have been depleted. Consequently, the 543 nm λ_{max} pigment is probably equivalent to the LWS pigment in other species, and it is the MWS cone which was absent or overlooked. A shorter cut-off wavelength in the R-type droplet would be necessary if the λ_{max} of the LWS pigment was shifted hypsochromically. A λ_{cut} at around 560 or 570 nm would reduce the sensitivity of the LWS pigment too much.

A consistent theme in all of the species for which data are available is that the λ_{max} values of the rod and MWS cone pigments are very close, often within a few nanometres of each other. Furthermore, these two pigments show the least variation of all the pigment types between species.

1.2.2 Pecten

A notable feature of the avian fundus is the pecten (*Pecten oculi*), a vascular structure projecting from the retina into the vitreal body at the point of exit of the optic nerve (Martin, 1985). The structure and potential functions of the pecten have been reviewed at length elsewhere (Walls, 1942; Meyer, 1977). The most salient points are discussed below.

The pecten exhibits marked interspecific variation in size and form. Three morphological types have been distinguished: conical, vaned and pleated. A conical pecten occurs only in the retinae of the flightless kiwi (*Apteryx australis mantelli*) and was considered by Walls (1942) to be as degenerate as the rest of the eye in this species. The conical pecten is heavily pigmented, without vanes or pleats and extends from a circular optic disk almost as far as the lens. A vaned pecten is found in the remaining species of palaeognathus birds (e.g. ostrich, *Struthio camelus*, and greater rhea, *Rhea americana*). It consists of a central vertical lamina from which arises a series of lateral vanes (Martin, 1985). All neognathus species studied display a pleated pecten. Arising from a linear optic disk as a simple 'accordion-pleated' lamina, its pleats are held in formation at the free (vitreal) end by a heavily pigmented bridge of tissue, the *pons pectinis*.

The pecten has a well developed arterial supply, separate from that of the choroid. Each pleat contains a single arteriole which branches into an extensive capillary network. The absence of muscular and nervous tissue in the pecten, in addition to the pleated structure which greatly increases its surface area, has led most workers to consider its primary function to be that of a supplementary nutritive device for the sensory retina (Walls, 1942). Whilst choroidal circulation is assumed to be the primary nutritive source for the avascular retina, in particular the photoreceptor layer, it is thought that the pecten might serve to nourish the inner neural layers when choroidal supply is limited by high levels of metabolic activity in cone-rich retinae. In support of this theory are observations that active, diurnal species have more pecten folds than nocturnal species (Walls, 1942; Meyer, 1977; Pettigrew, 1983).

Several other functions for the pecten have been proposed, including its role as an heat exchanger or a regulator of intraocular pH, and as a device to compensate for changes in vitreal pressure when the eye accommodates. Various other hypotheses involving the shadow cast by the pecten onto the fundus have been suggested, including the improvement of visual acuity and enhanced movement detection, a role as an intraocular shade against glare from the sun and a 'sextant' to measure the angle of elevation of the sun. However, critics maintain that, under normal viewing conditions, the pecten shadow falls mainly on its own base and slightly to each side (Walls, 1942).

Structures resembling the avian pecten are observed in many other taxa. The *conus papillaris*, which is thought to be analogous, if not homologous, to the conical pecten, is widespread in lizards, and even some mammals (e.g. golden hamster, *Cricetus auratus*). Interestingly, turtles, which display a similar retinal morphology to birds, lack any similar structure. It is thought that, despite a cone-dominated retina, their metabolic rates are generally lower than most birds and the choroidal circulation may be adequate for retinal nutrition.

1.3 Species used in this study

1.3.1 European starling *Sturnus vulgaris* (Linnaeus, 1758)

The European starling, *Sturnus vulgaris*, is a 'medium-sized' passerine approximately 20 cm long and weighs 75-100 g (Feare, 1984). With a global population of around 600 million (Martin, 1987) and a vast geographic distribution, the starling is one of the most successful bird species. It has a varied, omnivorous diet but displays particular morphological adaptations for probing the soil in search of small invertebrate prey. When foraging on the ground, *S. vulgaris* pokes its head into the grass mat and spreads its bill with considerable force to pry apart the turf. The eyes are then turned forwards towards the sagittal mid-line to scan the feeding area thus revealed (Beecher, 1978). Beecher (1978) noted that the skull of *S. vulgaris* was narrower than non-prying (fruit-eating) starlings, e.g. *Spreo superbus* and displayed an unusually deep 'groove' extending from the base of the upper mandible to the eye, and proposed that this anatomical adaptation facilitated forward vision. Furthermore, in an investigation of eye movements and visual fields in *S. vulgaris*, Martin (1986) showed that, when the bill is open, the binocular field width is maximal between the mandibles.

The plumage coloration of *S. vulgaris* is sexually dimorphic both in the 'human visible' (approximately 400 to 700 nm) and near-ultraviolet regions of the spectrum (Cuthill *et al.*, in press), and it is evident that near-ultraviolet wavelengths reflected from male plumage are used by females in mate selection (Bennett *et al.*, 1997).

1.3.2 Blackbird *Turdus merula* (Linnaeus, 1758)

The blackbird, *Turdus merula*, is another medium-sized passerine, approximately 25 cm in length and weighing 80-100 g (Perrins, 1987). Blackbirds occupy a wide range of habitats with trees and bushes from deep forest to inner cities (Ehrlich *et al.*, 1994). They feed on insects, molluscs and earthworms which they obtain by turning over leaf litter or probing the soil, and will also take berries and fruit from trees (Hillstead, 1944). Blackbird plumage is sexually dimorphic, males being almost exclusively matt black with a conspicuous yellow-orange bill whereas females are usually deep brown (Hillstead, 1944).

1.3.3 Blue tit *Parus caeruleus* (Linnaeus, 1758)

The blue tit, *Parus caeruleus*, is a common inhabitant of broad-leaved temperate woodland, but is also found among scattered trees in hedgerows, orchards, town parks and gardens. It is one of the smaller passerine species, approximately 11.5 cm long and weighing 9-12 g (Perrins, 1987), and eats a range of insects and spiders taken from foliage and seeds in winter (Ehrlich *et al.*, 1994). The blue tits plumage is sexually dimorphic in the near-ultraviolet (Andersson *et al.*, 1998; Hunt *et al.*, 1998) and, as with *S. vulgaris*, near-ultraviolet plumage reflectance probably plays a role in the assessment of potential mates (Andersson *et al.*, 1998; Hunt *et al.*, 1998).

1.3.4 Domestic turkey *Meleagris gallopavo* (Linnaeus, 1758)

The turkey, *Meleagris gallopavo*, is a North American galliform, formerly distributed east of the Rocky mountains from Mexico to southern Canada. The species was domesticated in Mexico and south west USA and imported to Europe from the 16th century onwards (Snow and Perrins, 1998a). The wild turkey is characterised by a bright blue head, red legs and a general copper bronze plumage (Baird *et al.*, 1875). The domesticated British Union Turkeys (BUT strain 8) used in this study were white. Adult turkeys weigh between 7-16 kg, are approximately 120 cm in length and, in the wild, feed on a variety of nuts, seeds, berries, fruits and insects. Their natural habitat is mostly woodland and mountain hillsides, but also the damp and swampy lands alongside larger streams (Bendire, 1892).

Commercially reared turkeys are often kept under very low light intensities to reduce injurious pecking (Sherwin, 1998). However, severe light deprivation may result in changes in ocular morphology that can cause blindness (Siopes *et al.*, 1984). Like the domestic chicken, *Gallus gallus* (Prayitno *et al.*, 1994; Prayitno and Phillips, 1997), turkeys show preferences for both the wavelength and intensity of the ambient illumination (Smith *et al.*, 1989; Sherwin, 1998). In the interests of improving the welfare of commercially farmed turkeys, by optimising the spectral composition and intensity of the ambient illumination, the spectral absorption properties of the retinal photoreceptors of the turkey were determined microspectrophotometrically to predict the range of wavelengths to which this species might be sensitive.

1.3.5 Peacock *Pavo cristatus* (Linnaeus, 1766)

The peacock is the male peafowl, *Pavo cristatus*, a relatively large galliform weighing 4-5 kg and measuring 100-120 cm in length from the head to the base of the tail (200-230 cm from the head to the end of the train). Characterised by its unmistakable blue and green plumage, it is found wild from India to Sri Lanka at altitudes of up to 1300 m. Living in thick jungle, its diet consists predominately of vegetable matter, grain seeds and some insects, molluscs and larvae of all kinds (Whistler, 1935).

Because of the striking sexual dimorphism in plumage coloration between the peahen and the peacock, and the elaborate train of the male bird, the peafowl has become a model species in the study of avian sexual selection. Peacocks with the most elaborate trains have the highest mating success (Petrie *et al.*, 1996) and their offspring grow and survive better (Petrie, 1994). Receiver psychology is an important evolutionary force on the design of animal signals (Goldsmith and Dawkins, 1991), and the detectivity and discriminability of a given visual signal will be largely dependent on the receiver's visual system.

CHAPTER TWO

MICROSPECTROPHOTOMETRY OF AVIAN RETINAL PHOTORECEPTORS

2 Microspectrophotometry of avian retinal photoreceptors

2.1 Introduction to the technique of microspectrophotometry

Developed to examine and measure nucleic acids in the cell nucleus (Caspersson, 1940 cited in Wolken *et al.*, 1968) microspectrophotometry has become an invaluable tool for the vision researcher. It is the only method by which the spectral absorption properties of visual pigments can be measured *in situ* in individual photoreceptors.

The technique is an adaptation of standard spectrophotometric procedures to microscopic samples. Single-cell microspectrophotometry involves passing a very narrow beam of light through the cell under investigation and measuring the transmission at each wavelength. However, whilst conceptually simple, the practice of microspectrophotometry is complicated greatly by both the wave and quantal behaviour of electromagnetic radiation (see sections 2.2.6 and 2.2.7).

The first measurements of visual pigments in individual photoreceptors were made by Hanaoka and Fujimoto (1957) in carp, *Cyprinus carpio*. At the same time they attempted to obtain absorption spectra of avian photoreceptors, but were thwarted by the small size of the cone outer segments and succeeded only in recording the spectral transmission of the cone oil droplets (Fujimoto *et al.*, 1957). Soon after, Brown (1961) obtained better records from frog rod outer segments using a modified commercial spectrophotometer.

Whilst these spectra were recorded by devices employing separate sample and reference beams, the construction of the first 'dual-beam' microspectrophotometer (MSP) is credited to Chance *et al.* (1959), the fundamental difference being that both beams were passed through the specimen preparation and were separated spatially by only 12 μm. This design allows the reference beam to provide a more accurate control of feedback circuits which adjust signal amplification at each wavelength. Inevitably, this machine was soon modified for the study of photosensitive pigments in rods (Liebman, 1962) and cones (Liebman and Entine, 1964; Liebman and Entine, 1968). Other dual-beam machines also were constructed and used for the measurement of single photoreceptors in fish, amphibians and primates (e.g. Marks *et al.*, 1964; Marks, 1965; Wolken *et al.*, 1968).

In the dual-beam design, light from a monochromator is split into sample and reference beams by either a reciprocal or James chopper. Both beams are then demagnified by an inverted objective lens and superimposed onto the specimen plane of a conventional high magnification microscope. One beam passes through the sample, the other is directed into a cell free area of the preparation. Whilst the monochromator scans through the spectrum, a photomultiplier (PMT) measures the relative intensities of the two beams, the ratio of which, in principle, gives a measure of the transmission (and hence the absorbance) of the sample. The reference beam is also used to control PMT high tension voltage (HT), *via* a negative feedback loop, such that signal amplification was increased when photon flux is low. Because only one PMT is used in the design, the beams are separated temporally as well as spatially, the photocurrents induced by each beam being recorded alternately at every wavelength.

However, the design of the dual-beam machine is such that sample and reference beams are not identical. Originating from different points on the lamp filament or arc, they traverse disparate regions of the optics and arrive at different locations on the photocathode. For these reasons, a separate baseline recording must be made, with both beams passing through cell-free areas, and deducted from the sample scans. Attempts to reduce baseline anomalies due to differing sensitivity functions for different points on the photocathode include the use of a supplementary Bertrand-Amici lens to reduce beam divergence and image the back focal plane of the collector objective onto the same region of the PMT (e.g. Liebman and Entine, 1964; MacNichol, 1978).

Further developments led to the construction of a single-beam, photon-counting design of MSP (PMSP, Hárosi and MacNichol, 1974; Hárosi, 1975; Hárosi and Malerba, 1975; Hárosi, 1976; MacNichol, 1978) which was used to investigate the dichroic absorption properties of visual cells in addition to their wavelengths of maximum sensitivity (λ_{max}). Because there is only one beam, which can be aligned axially through the objectives, this design has potentially fewer optical aberrations (see section 2.2.6) and the same point on the photocathode is used for both baseline and sample measurements. Instead of a reference beam to adjust PMT HT, the baseline is 'flattened' initially to give a relatively constant output voltage at each

wavelength for a given size and photon flux density of measuring beam. The reference file calculated in this way by a microcomputer adjusts the signal amplification, or gain, automatically during fast scanning of the sample and baseline. Gain control can be achieved by variation in PMT HT, but this is intrinsically slow and to increase scan speeds HT needs to be kept constant and gain variation achieved by the control of the analogue amplifier. Assuming that fluctuations in the intensity of the light source and the behaviour of the electronic circuitry are insignificant (or that their effects are detectable so that all records subject to anomalous drift may be discarded) the single beam design is capable of measuring very low absorbances in small specimens with equal or greater accuracy than a dual beam instrument (Hárosi and MacNichol, 1974). This achievement is, however, critically dependent on high temporal stability in all components.

All measurements in the course of this study were made with the receptor long axis perpendicular to the direction of propagation of the measuring beam. Despite the difficulties of the preparation, end-on measurements were attempted by several workers (Marks *et al.*, 1964; Liebman, 1972). In addition to being the 'natural' direction of light penetration into a photoreceptor cell, end-on measurements maximise the pathlength of light through the outer segment, giving the highest possible absorbance, and utilise any inherent focusing properties of the ellipsoid region or outer segment (Snyder and Hamer, 1972). However, such measurements suffered from severe wavelength-dependent light scattering of the measuring beam by the adjoining neural layers of the retina (Liebman, 1972) and, in larger photoreceptors, anomalous dispersion due to differences in refractive index of the outer segment at different wavelengths (Snyder and Richmond, 1972; Jagger and Liebman, 1976). With regards to microspectrophotometry of avian photoreceptors, transverse measurement is the only way to distinguish absorption by cone visual pigments from that of their associated oil droplets.

2.2 The Bristol microspectrophotometer

2.2.1 Description

The microspectrophotometer (MSP) used in this thesis to measure both visual pigment and oil droplet absorption spectra is a single-beam, wavelength-scanning,

computer-controlled instrument developed from the machine described in detail by Partridge *et al.* (1992). A diagrammatic view of the MSP is shown in Figure 2.1.

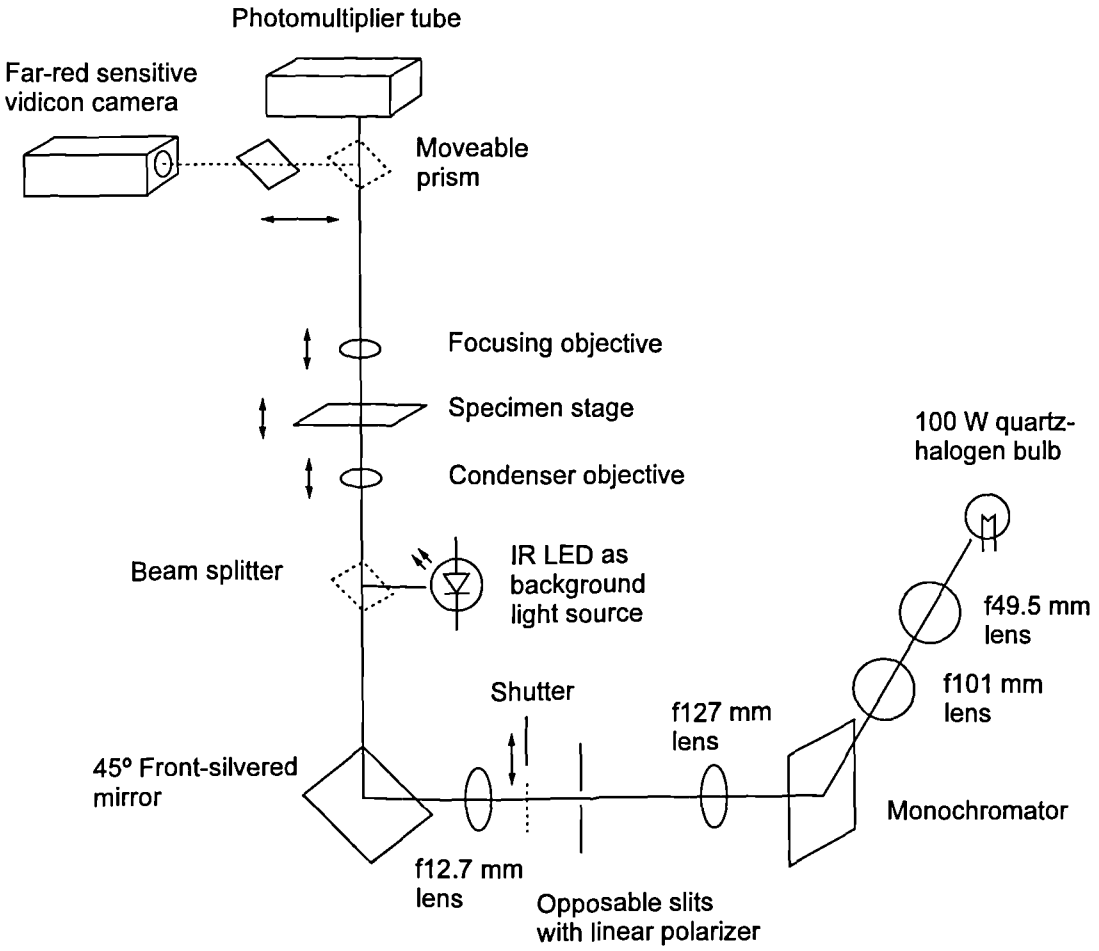

Figure 2.1 Diagrammatic view of the microspectrophotometer (MSP) used in the present study. All lenses are ultraviolet-transmitting, fused silica. Focusing of the specimen by the focusing objective is achieved by moving the specimen stage vertically with the microscope's conventional coarse and fine focus controls. The focus of the condenser objective can also be adjusted manually, but is usually controlled by a computer-driven piezo-electric translator (PIFOC P-720.00, Physik Instrumente, Germany).

The MSP measuring beam is derived from light produced by a 100 W quartz-halogen bulb powered by a stabilised 12 V DC power supply (Oriel model 60,000 Q series convective lamp housing, Oriel Corporation, USA). The filament of the bulb is focused onto the entrance slit (1 mm width × 5 mm height) of a Jobin Yvon H-1061 UV-VIS grating monochromator (Instruments SA Ltd., Middlesex, UK), the output of which (8 nm full width half maximum, FWHM, bandwidth) illuminates an adjustable aperture. This consists of two sets of opposable slits which control the vertical and horizontal dimensions of the beam in the plane of the specimen. The aperture housing also contains a calcite crystal which linearly polarises the light passing through the aperture, a feature that enables the dichroic absorption properties of rod outer segments to be exploited (Hárosi and MacNichol, 1974; Hárosi and Malerba, 1975). Outer segment dichroism, which, as explained in chapter one, arises from the orientation of visual pigment molecules embedded in the outer segment disk membranes, ensures that pigment absorption is four to five times greater for light linearly polarised with its electric vector perpendicular to the long axis of the outer segment than for light polarised parallel to that axis (Jagger and Liebman, 1976). This optical phenomenon helps to compensate for the reduced pathlength resulting from transverse measurement.

The measuring beam is directed into the plane of the specimen on a microscope stage and demagnified by a Zeiss Ultrafluar × 32 objective used as a condenser lens (NA 0.4). Above the stage, an Olympus × 100 DApo 100UV objective (set to a NA of 1.3) focuses the beam either onto a small area of the photocathode of a Hamamatsu C1556-51 photomultiplier (Hamamatsu photonics, UK) or, by use of a sliding prism, towards a far-red-sensitive video camera (75 series miniature CCTV camera; Insight Vision Systems Ltd., Malvern, UK) which is connected to a monochrome video monitor for viewing the specimen. Background illumination is provided by an infra-red LED, the light from which is introduced to the light path by a thin glass beam-splitter positioned below the condenser lens. The passage of the measuring beam can be interrupted before reaching the specimen by an electric shutter controlled either manually or automatically *via* the computer.

Light hitting the PMT photocathode induces a nA current in the photomultiplier which is converted to a voltage in the headstage amplifier. This

voltage is amplified and fed into an analogue multiplier together with the voltage from a digital to analogue converter, which receives a variable digital signal from the computer to control the gain of an analogue multiplier and give an approximately constant voltage at all wavelengths. The signal is then amplified, inverted and low-pass filtered with a variable low-pass Butterworth two-stage active filter, and fed to a 2 MHz voltage to frequency (V / F) converter. After a short delay at each wavelength to allow the filtered signal to settle, the frequency output at each odd integer wavelength on the downward, long wavelength to short wavelength, spectral pass, and each even integer wavelength on the upward, short wavelength to long wavelength, spectral pass is integrated over 10 ms using a CTM-05 counter/timer board (MetraByte Co., Taunton, MA, USA) in the computer.

2.2.2 Measurement protocol

In use, the photoreceptor outer segment or oil droplet was first focused using the microscope's conventional coarse and fine focus controls which moved the specimen stage vertically. The measuring beam, typically 1-2 μm square, was then focused (usually at 730 or 750 nm) in an area adjacent to the photoreceptor, the infra-red LED background illumination extinguished, and the light path directed to the photomultiplier.

Prior to any measurements, the baseline was 'flattened'. This was necessary due to wavelength-dependent variations in the photon flux of the measuring beam. The microcomputer gain signal, or 'gainbyte', which was converted by the digital to analogue converter into a gain-controlling voltage, was chosen such that the baseline signal recorded by the computer was approximately 500 kHz at each wavelength. The gainbyte for each wavelength was stored in a computer file for reference during baseline and sample scans. By removing the variation in photon flux density at each wavelength, the full range of the V / F converter could be used to detect differences between the baseline and sample scans.

A baseline scan was recorded as the computer-controlled stepper motor drove the monochromator from 750 to 330 nm (or, in earlier work, 730 to 350 nm) and back again. Two long wavelength to short wavelength, short wavelength to long wavelength spectral passes were performed during each scan. A scan took

approximately 25 seconds to complete and, like all other automated procedures, was controlled by a Microsoft QuickBASIC version 4.5 program.

Having recorded a baseline scan, the photoreceptor outer segment or oil droplet was moved into the measuring beam and a sample scan made in the same way. A further scan was made with the shutter shut to record any residual dark current (although this was also nulled by a manually adjusted offset voltage to one of the amplifiers). This dark current scan was deducted from both the sample and baseline scans which were recorded, along with summary file information, as comma-delimited text files. When measuring visual pigments, another baseline scan was made and combined with the sample scan to obtain a second record of the photoreceptor without further bleaching of the visual pigment. Averaging together two scans has the same purpose as making two spectral passes in that the signal to noise (S / N) ratio of the measurements is increased by $\sqrt{2}$. Although in this study only the baseline scans were repeated, and so the signal to noise ratio for the combined sample and baseline scans was increased by less than $\sqrt{2}$, the effect, an increase in S / N ratio of 1.225 $\left(\sqrt{3}/\sqrt{2}\right)$, was still appreciable in such noisy data. Only one sample scan of each outer segment was made in attempt to reduce distortions in visual pigment absorbance spectra due to progressive 'in-scan' bleaching, and the resultant accumulation of stable photoproducts absorbing light over the range of wavelengths scanned, which might be evident in subsequent sample scans. Outer segments containing putative ultraviolet-sensitive pigments were an exception, however, and up to three sample scans, which were subsequently averaged together, were made from the same region of the outer segment. This was necessary due to the relatively low signal to noise ratio of measurements made from this class of cone. The low photon flux density of the measuring beam at short wavelengths precluded excessive in-scan bleaching of this pigment type.

Outer segments containing visual pigments were bleached for 10 minutes using monochromatic (8 nm FWHM bandwidth) light from the monochromator at a wavelength corresponding approximately to the λ_{max} of the pigment measured. Because of the reduced light flux from the monochromator light source at ultraviolet wavelengths, putative ultraviolet-sensitive visual pigments were bleached with a 10 minute exposure to white light emitted by the monochromator at its blaze angle.

Two post-bleach scans were then made in order to create difference spectra and confirm photolability. Consistency in the number of scans made of each outer segment, both before and after bleaching, is essential for ensuring that the data are weighted equally during subsequent averaging and calculation of difference spectra.

2.2.3 Accuracy of transmission measurements

Accuracy is defined as the difference between the values recorded (averaged to reduce the effects of noise) and their true values. To test the linearity and transmission accuracy of the MSP used in this study, the transmissions of a range of neutral density filters (four identical filters of each transmission value from 1.64×10^{-2} to 0.88 in 20 unequal steps) were determined using a Shimadzu UV-2101PC UV-VIS scanning spectrophotometer (Shimadzu scientific instruments, Inc., Columbia, USA). From the manufacturer's specifications, the latter is known to be linear up to an absorbance of 5 with a transmission accuracy of ± 0.3 % and a repeatability of ± 0.1 %. Variation in transmission measurement by the Shimadzu spectrophotometer is thus assumed to be negligible compared to the MSP.

The transmission of each filter at 550 nm as measured by the MSP was then plotted against the transmission measured using the Shimadzu (Figure 2.2). Polynomial regression was performed on the data to test for a departure from linearity, but the squared term was found to be non-significant ($t_{76} = 0.08$; $p = 0.933$). The linear regression line calculated gave a gradient of 0.930, an intercept of 5.9×10^{-4}, and accounted for 99.6 % of the observed variation. The gradient of the regression line was significantly different from unity ($t_{78} = 10.53$; $p < 0.001$), but the value of the intercept was not significantly different from zero ($t_{78} = 0.20$; $p = 0.843$).

Whilst linear over the range of transmittance values investigated, the MSP appears to systematically underestimate transmission (mean difference 8.2 % $\pm$ standard deviation of 4.6 % of transmission as measured by the Shimadzu spectrophotometer) and the magnitude of this underestimation is proportional to the relative transmission value of the filter.

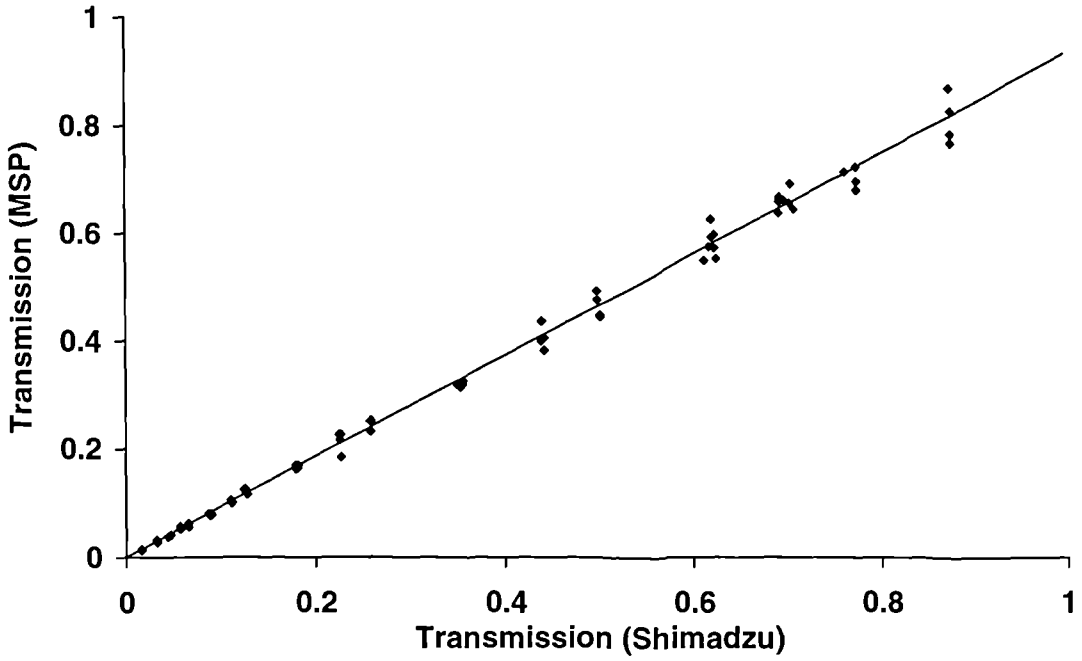

Figure 2.2 Linearity of the MSP used in this study. The transmission at 550 nm of a series of neutral density filters was measured by both the MSP and a Shimadzu UV-2101PC UV-VIS scanning spectrophotometer. The Shimadzu was known to be linear over the transmittance range investigated and the linear response of the MSP was confirmed by polynomial regression (squared term non-significant: $t_{76} = 0.08$; $p = 0.933$). The linear regression line has a gradient of 0.930, which is significantly different from unity ($t_{78} = 10.53$; $p < 0.001$), and an intercept of 5.9×10^{-4}, which is not significantly different from zero ($t_{78} = 0.20$; $p = 0.843$).

This discrepancy may have arisen through differences in the optical arrangements of the two machines used to measure the filters. Alternatively, the error may have occurred as a result of incorrect calculation of the transmission from the microspectrophotometric data. Transmission is calculated from MSP sample and baseline measurements by comparing the output of the V / F converter, which receives the filtered and amplified signal from the PMT, thus:

$$T_\lambda = \frac{\text{Light transmitted}}{\text{Light incident}} = \frac{\text{OffHz} - \text{SHz}_\lambda}{\text{OffHz} - \text{BHz}_\lambda} \qquad \textbf{Equation 1}$$

where SHz_λ is the sample scan frequency, BHz_λ is the baseline scan frequency, OffHz is the calculated frequency when there is no signal from the PMT and λ is wavelength. Estimates of sample transmission are therefore potentially sensitive to errors in estimating OffHz. Such an error might have arisen through the use of an adjustable 'gain' in the signal interface circuit which was incorporated in order to utilise the whole dynamic range of the V / F converter with samples of different maximum absorbance.

In an attempt to isolate likely sources of error in estimating sample transmission, a further experiment was conducted. The MSP electronics contain a calibration circuit which can be used to mimic the signal from the photomultiplier tube (PMT). Thus a calibration voltage of between 0 and 1 V can be fed into the signal processing circuitry, and onwards to the microcomputer, to identify non-linearities or signal-dependent errors inherent in the instrument's electronics. The signal from the PMT headstage, or the calibration circuit, passes through four amplifiers and a V / F converter before reaching the microcomputer, and these components are all potential sources of error.

The MSP was set up as for normal use, thus incorporating all sources of extrinsic noise. The signal source was switched from the PMT headstage to the calibration circuit, the input voltage set at 0.8 V, and the baseline flattened. A baseline and sample scan were then made with the signal set at 0.8 V. Subsequent measurements were then made with the baseline signal set at 0.8 V, but the sample signal at regular, decreasing increments. The 'real' transmission values imitated using this procedure were calculated by dividing the voltage of the signal by that of the baseline. After the baseline and sample signals had been amplified, inverted,

low-pass filtered and converted into a frequency as recorded by the microcomputer, transmission was calculated from the MSP data files using the method described in equation 1 (page 84).

With transmission determined by the ratio of sample and baseline signal voltages as the independent variable, and the calculated transmission from the MSP data file as the dependent variable, a polynomial regression was performed on the data to test for a departure from linearity. The squared term, however, was found to be non-significant ($t_{12} = 0.25$; $p = 0.808$). The linear regression line calculated subsequently had a gradient of 1.007, an intercept of -2.44×10^{-3} and accounted for 100 % of the variation (Figure 2.3). The gradient of the regression line was significantly different from unity ($t_{13} = 3.75$; $p < 0.005$), although the intercept was not significantly different from zero ($t_{13} = 2.00$; $p = 0.07$). However, the associated error is small (mean difference in calculated transmission was 0.04 % ± standard deviation of 0.9 %), which suggests that the signal processing electronics downstream of the analogue multiplier, and the determination of OffHz frequency, are not responsible for the discrepancy in measured transmission observed in the original experiment. The PMT was always operated within the range of high tension (HT) voltage specified by the manufacturer to result in a linear performance. The error in transmission measurement observed in the original experiment was, therefore, assumed to be a consequence of the test method employed. Specifically, transmission can only be properly assessed if samples are introduced into the light path where the light is collimated. This was not the case with the insertion of neutral density filters into the MSP light path.

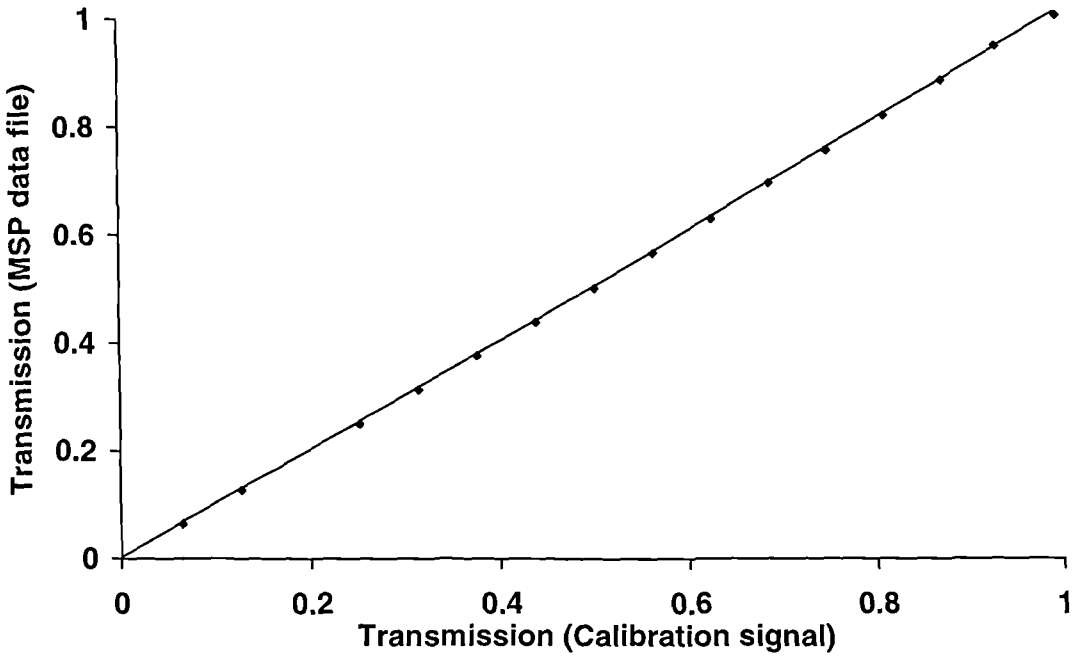

Figure 2.3 Linearity and transmission accuracy of the signal processing electronics employed in the MSP. Abscissa: transmission determined by the ratio of the sample and baseline calibration signal voltages. Ordinate: transmission calculated from baseline and sample frequencies recorded by the microcomputer as MSP data files. A linear relationship was established by polynomial regression (squared term non-significant: $t_{12} = 0.25$; $p = 0.808$). The linear regression line has a gradient of 1.007 and an intercept of -2.44×10^{-3}. The gradient of the regression line is significantly different from unity ($t_{13} = 3.75$; $p < 0.005$), but the intercept is not significantly different from zero ($t_{13} = 2.00$; $p = 0.07$).

Visual pigment specific absorbances were not calculated in this study. Deterioration of cone outer segments, which had a tendency to become flattened and fold over upon themselves following enucleation, prevented accurate determination of measured pathlengths. Furthermore, this deterioration masked the orientation of the long axis of the outer segment. Alignment of the measuring beam in the outer segment such that the electric vector of the beam is perpendicular to its long axis is essential in exploiting the dichroic arrangement of the visual pigment molecules and is conditional for estimating longitudinal specific absorbance from transverse measurements (Hárosi, 1975). Instead, the absorbance at the λ_{max} of the difference spectrum for each visual pigment is given. However, whilst it is desirable to measure transmission as accurately as possible, the shape of the normalized absorbance spectrum will be unaffected, provided the MSP is linear over the range of transmittance measured.

2.2.4 Precision of transmission measurements

The precision of the transmission measurements obtained with the MSP can be regarded as the repeatability of a given measurement, and is therefore dependent on noise in the signal. Closer inspection of Figure 2.2 reveals the heteroscedastic nature of the data. As filter transmission increases, so does the magnitude of the variance. To ascertain that this heteroscedascity was not due to transmission-dependent irregularities in the filters used, a nonparametric statistical analysis was performed as follows.

Firstly, the mean transmission of each quartet as measured using the Shimadzu spectrophotometer was deducted from it's four component individual transmission values to remove all between-quartet variation. The association of the within-quartet variation and the variance observed in the MSP transmission values was then found to be non-significant by determining Spearman's rank correlation coefficient ($r_s = -0.1742$; $n = 80$; $p = 0.122$). Thus, it appears that the precision of the MSP deteriorates as sample transmission increases, although, when expressed as a proportion of filter transmission, the magnitude of the variance (a mean standard deviation of ± 4.15 % of measured transmission) is independent of transmission (linear regression: $t_{18} = 0.41$; $p = 0.685$). This phenomenon emphasises the

importance of averaging a number of visual pigment absorbance measurements in order to obtain a reliable estimate for the λ_{max}.

2.2.5 Wavelength accuracy and precision

The accuracy of the wavelengths as recorded by the MSP is determined by the wavelength accuracy of the monochromator used. Manufacturer's specifications for the Jobin Yvon H-1061 VIS grating monochromator report an accuracy of $\pm$ 0.5 nm. Such tolerance, however, is only approached if the backlash is taken up (i.e. the slack in the toothed belt between the monochromator and the stepper motor which drives it, and in the lead-screw within the monochromator). The modifications to ensure this, both mechanical and in the controlling software, have been discussed elsewhere (Kent, 1997). The wavelength precision of the MSP was controlled by the software because each wavelength reached by the monochromator was referenced to a wavelength calibration file, and it was the latter value which was recorded along with the absorbance.

A didymium filter was used to test the wavelength accuracy and precision (repeatability) of the MSP. This glass filter is a mixture of the rare earth elements Neodymium, Praseodymium and Samarium (Wyszecki and Stiles, 1967). It's spectral transmission shows a number of distinct minima and maxima at wavelengths characteristic of the filter. Nevertheless, specific manufacturing conditions and ageing can affect the exact position of these absorbance bands and the filter was calibrated by measuring it with a Shimadzu UV-2101PC UV-VIS scanning spectrophotometer. This machine is self-calibrating and has a wavelength accuracy of $\pm$ 0.3 nm and a precision of $\pm$ 0.1 nm.

Because some of the absorbance bands of the didymium filter are narrow and close together, the wavelengths of maximum absorbance will, to some degree, depend on the spectral bandwidth of the spectrophotometer. Accordingly, scans made by the Shimadzu with a 1 nm FWHM bandwidth were numerically converted to represent a scan made with an 8 nm FWHM bandwidth so as to be directly comparable to that of the MSP. This was achieved by passing a weighted (delta function) running average through the Shimadzu data. When comparing the scans made by the Shimadzu and the MSP (Figure 2.4) all discrepancies were found to be

within ± 1 nm (mean + 0.7 nm; standard deviation ± 0.5 nm; n = 7). Thus the accuracy of the MSP used in this study is approximately ± 1 nm.

2.2.6 Limitations imposed by the wave behaviour of electromagnetic radiation

Wave behaviour reduces the ability of any optical system to direct light onto a very small area. The design of the single-beam MSP ensures that many lens aberrations (e.g. astigmatism and lateral chromatic aberration) are irrelevant, as long as the measuring beam is aligned axially in the optical pathway. Chromatic and spherical aberrations of component lenses, however, are potentially problematic, especially in the measurement of small cells.

The refractive index (RI) of glass varies according to the wavelength of light. Thus, light originating from an axial point will not come to a common focus, a phenomenon known as axial chromatic aberration. Instead, shorter wavelengths will be focused at a point nearer to the lens than longer wavelengths. Axial chromatic aberration of the measuring beam by the Zeiss Ultrafluar × 32 condenser objective used in this study exceeded 9 μm between 440 and 800 nm Figure 2.5.

It follows that the MSP measuring beam would be brought to a focus in different planes depending on the wavelength and, if left uncorrected, would result in unacceptable levels of light leakage around photoreceptor outer segments or oil droplets which are generally less than 4 μm in diameter. Whilst it is possible to partially correct axial chromatic aberrations optically, apochromatic objectives usually display poor transmission of ultraviolet wavelengths due to the incorporation of extra lenses, and achromatic lenses, such as the Zeiss Ultrafluar used in this study, are preferred. Consequently, this optical constraint was circumvented by automatically adjusting the focus of the condenser objective during each scan. A computer-driven piezo-electric translator (PIFOC P-720.00, Physik Instrumente, Germany) beneath the condenser objective moved the lens rapidly, with a resolution of approximately 10 nm, to maintain the plane of focus during a scan.

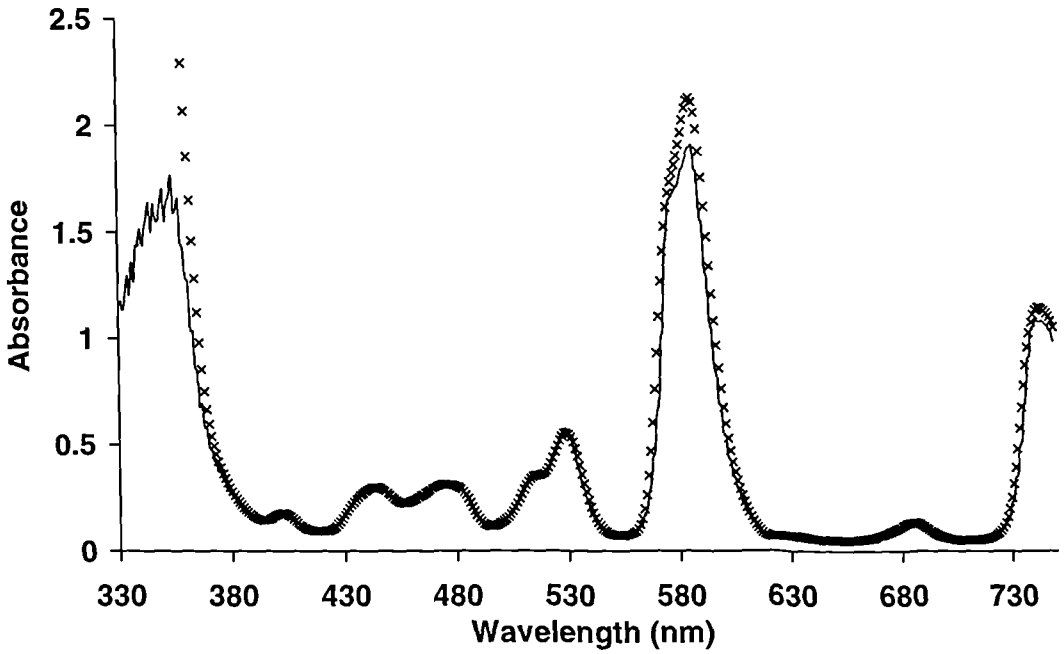

Figure 2.4 Wavelength accuracy of the MSP used in this study. The absorbance spectrum of a didymium filter was measured using a Shimadzu UV-2101PC UV-VIS scanning spectrophotometer with a 1 nm FWHM bandwidth. This scan was numerically converted to represent a scan (symbols) with an 8 nm FWHM bandwidth (i.e. equivalent to that of the MSP). Such a scan was frequently compared to scans made by the MSP (line) to check wavelength accuracy and precision. The discrepancy between the two scans at high absorbance values is due to limitations of the MSP, which is designed to measure absorbances less than one, and because the didymium filter could only be introduced into the MSP light path at a point at which the light was uncollimated.

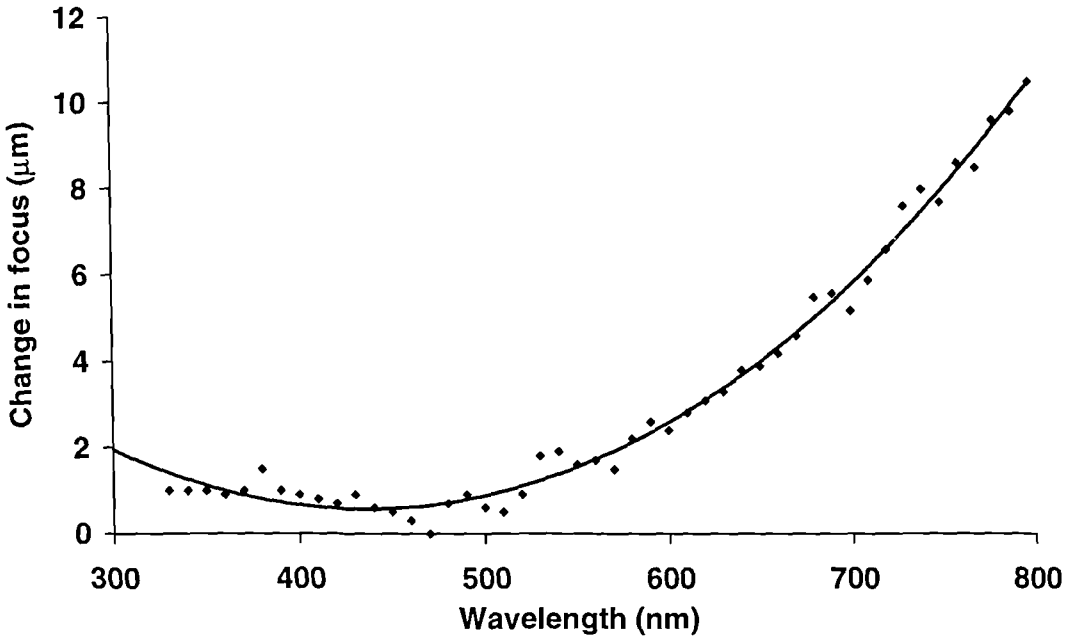

Figure 2.5 Chromatic aberration of the Zeiss Ultrafluar × 32 condenser objective used in the present study. The line shown represents a quadratic function, of the form:

$$y = a + bx + cx^2$$

where $a = 14.7523$, $b = -0.0651$ and $c = 7.4716 \times 10^{-5}$, fitted to data (symbols) obtained at 10 nm intervals (330 to 800 nm inclusive) using a non-linear regression software package (CurveExpert 1.2). The difference in focus between 440 and 800 nm is 9.9 μm.

Spherical aberration arises from the curvature of lens surfaces. Rays passing through marginal zones of a lens are refracted more than those passing through zones closer to the optic axis. Consequently, rather than a point of sharp focus, there is a 'zone of confusion' along the optical axis (Bradbury, 1989). Spherical aberration in the MSP used in this study was minimised by careful selection of lenses with low spherical aberration.

Lenses that are well corrected for axial chromatic aberration may still suffer from lateral chromatic aberration, resulting from lens combinations which cause the focal length of peripheral rays to be different for short and long wavelengths (Bradbury, 1989). The single beam design of microspectrophotometer, as used in this study, facilitates axial alignment of the measuring beam and thus minimises this form of aberration.

Even given perfect optics, diffraction effects ultimately restrict the ability of lenses to concentrate light to a focal point. Fraunhofer diffraction causes a point source of light to be transformed by a lens into a series of concentric rings of decreasing brightness, known as an Airy diffraction pattern (Born and Wolf, 1970). The resolution of a microscope objective is equal to the radius, r, of the first dark ring of the Airy pattern, which is given by:

$$r = \frac{0.61\lambda}{NA}$$ **Equation 2.**

Whilst resolution is usually considered with respect to a magnified image, the concept is equally applicable to demagnification of the measuring beam by an inverted microscope, such as in the MSP. Paradoxically, this inverse relationship between resolution and NA suggests that a condenser objective of high NA should be used in order to maximise the precision with which the measuring beam can be superimposed on a single photoreceptor. However, in addition to reducing spherical aberration, restricting objective NA improves the collimation of the transilluminating beam. This is desirable for all spectroscopy and is especially important where measurement of receptor dichroism is required (Hárosi and Malerba, 1975).

Furthermore, it is empirically evident that, whilst condenser NA should be low, collector objective NA should be comparatively high in order to catch as much of the light scattered off-axis by the sample. Failure to ensure this results in a

wavelength dependent distortion of visual pigment absorption spectra, manifested as an increase in apparent absorbance at short wavelengths (Hárosi, 1971 cited in Partridge, 1986). In this study, a Zeiss Ultrafluar × 32 objective (NA 0.4) was used as the condenser and an Olympus × 100 DApo 100UV objective (set to an NA of 1.3) was employed as the collector objective. Both lenses have relatively high transmission to ultraviolet wavelengths and satisfy the above criteria regarding NA.

2.2.7 Limitations imposed by the quantal behaviour of electromagnetic radiation

By far the greatest complication in modifying the technique of microspectrophotometry for the measurement of visual pigments is their photolabile nature. High light intensities bleach away the pigment before it can be measured, but low light intensities limit the precision of the measurements due to the stochastic nature of the photon flux.

In his treatise on the emergent technology of single cell microspectrophotometry, Liebman (1972) expounded the theoretical basis for the detection of photosensitive substances. The most salient points are discussed below with reference to the device used in this study.

To detect a substance by virtue of its spectral absorption, the difference between the mean number of photons transmitted by the sample (I_t) and the mean number of photons incident (I_i) upon the sample (the signal, S, equation 3) must exceed by a sufficient magnitude all random fluctuations in the combined measuring and measured system (the noise, N).

$$S = I_i - I_t \qquad \textbf{Equation 3.}$$

At the low flux densities employed in microspectrophotometry of visual pigments, the relative contribution of the signal-induced noise must be greater than all extrinsic noise.

2.2.7.1 Intrinsic or signal-induced noise

Signal-induced noise, otherwise known as photoelectron shot noise, is the noise present in the signal from the photomultiplier. Primarily, this is due to

quantum behaviour of electromagnetic radiation, which sets the irreducible intrinsic limit to any photoelectric measurement (Liebman, 1972).

The random nature of photon emission from an incandescent source also leads to stochastic modulation of the signal. Various light sources have been utilised in microspectrophotometry. However, their selection has undoubtedly addressed the desire to extend the measuring range of the machine into the ultraviolet, for example by using a Xenon arc lamp, rather than the attainment of shot noise limited performance. Tungsten filament lamps, operated from a constant current regulated DC power supply, provide by far the most stable quantum flux, having no unstable arc and considerable thermal inertia in the filament.

2.2.7.2 Extrinsic noise

Noise arising from sources that are independent of the stochastic behaviour of electromagnetic radiation must be eliminated or suppressed as much as possible. Photomultiplier noise and drift, amplifier noise, exogenous and endogenous electrical noise, mechanical vibration and the movement of the retinal preparation are all likely sources of extrinsic noise.

The photomultiplier, PMT, is the heart of the MSP detection system. PMT noise is due to current pulses generated within the PMT which are not caused by the signal and have various origins. These have been discussed extensively elsewhere (Partridge, 1986) and it is sufficient to stress the importance of utilising a PMT with low noise and high quantum efficiency (Liebman, 1972). The Hamamatsu C1556-51 PMT used in the Bristol MSP satisfies these criteria. Furthermore, as in this study, a differential amplifier which allows the MSP operator to 'zero' the PMT dark noise (the current produced when the PMT photocathode is shielded from light), in addition to routine subtraction of the residual measured 'dark current' from MSP baseline and sample scans, helps to reduce the effect of PMT noise and drift.

Extrinsic noise inherent in signal amplification circuits was reduced by the selection of low noise components. Furthermore, digital components were isolated from analogue circuitry by the use of separate power supplies and optoelectronic couplers. Although a potential source of extrinsic noise in itself, the electronic reduction of noise can increase signal-to-noise ratios and thus improve microspectrophotometric measurements. The MSP used in this study employs a

Butterworth two-stage active low-pass filter which removes spurious high frequencies generated by various extrinsic factors and, more importantly, ensures, by elimination of high frequency transients, that voltages do not exceed the input voltage of the V / F converter.

A reduction in mechanical vibrations due to people or machinery in the vicinity of the MSP is essential. This was achieved by mounting the optical section on a steel sheet (approximately 1.5 cm thick) which was isolated from the supporting bench by a layer of foam-backed carpet and three small motorcycle inner tubes inflated to a very low pressure. In addition, the stepper-motor which was used to drive the monochromator was mounted on a bracket attached to the supporting bench rather than the steel sheet.

Movement of cells in the preparation by convection currents, Brownian motion or even motile bacteria or protists can be reduced by increasing the viscosity of the mountant. Gelatine at a concentration of 8 % (Liebman and Granda, 1971), 5 or 7.5 % dextran (Partridge, 1986 and this study), 2 % methyl cellulose (Loew, personal communication, cited in Partridge, 1986) and glycerol in various concentrations (this study) have all been successfully employed. The selection of tissue mountants for use in microspectrophotometric preparations is discussed further in section 2.4.4. Cell movement due to mountant evaporation was prevented by sealing the edge of the top coverslip with acrylic nail varnish. Silicone grease and paraffin wax have also been used for this purpose (Das, 1997; Kent, 1997). Cell movements induced by focusing changes can be reduced by eliminating as much excess mountant from the preparation as possible. Compression of the preparation for this purpose must be traded off with cellular damage, but is of particular increased importance with the introduction of dynamic focus adjustment during scanning (see section 2.2.6).

2.2.7.3 Intrinsic *versus* extrinsic noise

For the low light intensities routinely employed in the microspectrophotometry of visual pigments, intrinsic photoelectron shot-noise should, ideally, be larger than noise due to all extrinsic sources. According to Liebman (1972), if an MSP is photoelectron shot-noise limited any change in signal

level, S, should be accompanied by a square-root change in signal to noise ratio, S / N, i.e.

$$\frac{S}{N} \propto \sqrt{S} \qquad \textbf{Equation 4}$$

or

$$\log_{10}\left(\frac{S}{N}\right) \propto 0.5 \log_{10}(S) \qquad \textbf{Equation 5.}$$

To test this relationship with the MSP used in this study, the S / N ratio was measured for different values of the signal. With the instrument set up as for normal use, the monochromator was stepped to an output of 550 nm and disconnected from the computer. At this wavelength, photon flux density was relatively high and, accordingly, a relatively low amplification of the signal from the PMT was required. Utilising the software which normally controlled and recorded the scanning process, a file was created storing the successive output from the V / F converter at each wavelength step which, as the monochromator was disconnected, corresponded to a series of discrete recordings at 550 nm. Each of these discrete recordings were converted to a value for the signal (OffHz-SHz) and averaged to give the mean signal for the scan. The standard deviation of these signal values was used as a measure of the noise in the signal. The signal was then reduced by introducing neutral density filters into the MSP light path. The filters used had a range of transmission values from 1.64×10^{-2} to 0.88 in 20 unequal steps. Four identical filters of each transmission value, henceforth known as a quartet, were scanned.

With the linearity of the MSP confirmed (see section 2.2.3) the inherent noise of the instrument was investigated by plotting the $\log_{10}$ S / N ratios against the $\log_{10}$ S (Figure 2.6). A polynomial regression was performed on the log-transformed data, and the squared term was found to be significant ($t_{81} = 3.47$; $p = 0.001$). Whilst this suggests that the relationship between $\log_{10}$ S / N and $\log_{10}$ S is non-linear, a linear regression line, with an intercept of -0.695 and a gradient of 0.517, accounted for 98.8 % of the variation. The gradient of this line is different from that predicted by Liebman (1972; equation 5), which suggests that noise in the MSP is a function of the signal other than that predicted by shot-noise performance. The

components of the MSP most likely to affect the noise in a signal-dependent manner are the PMT and the Butterworth two-stage active low-pass filter. Because the PMT was operated well within the range of HT voltages specified by the manufacturer to result in a linear performance, the active filter is implicated. If the gradient was less than 0.5, the MSP would not be operating as a shot-noise limited device and extrinsic noise, rather than intrinsic signal-induced noise, would be limiting the machine's precision. As the gradient is greater than 0.5, however, the MSP may be operating as a shot noise device but, because active noise filtering increases as the signal increases, it is not possible to tell.

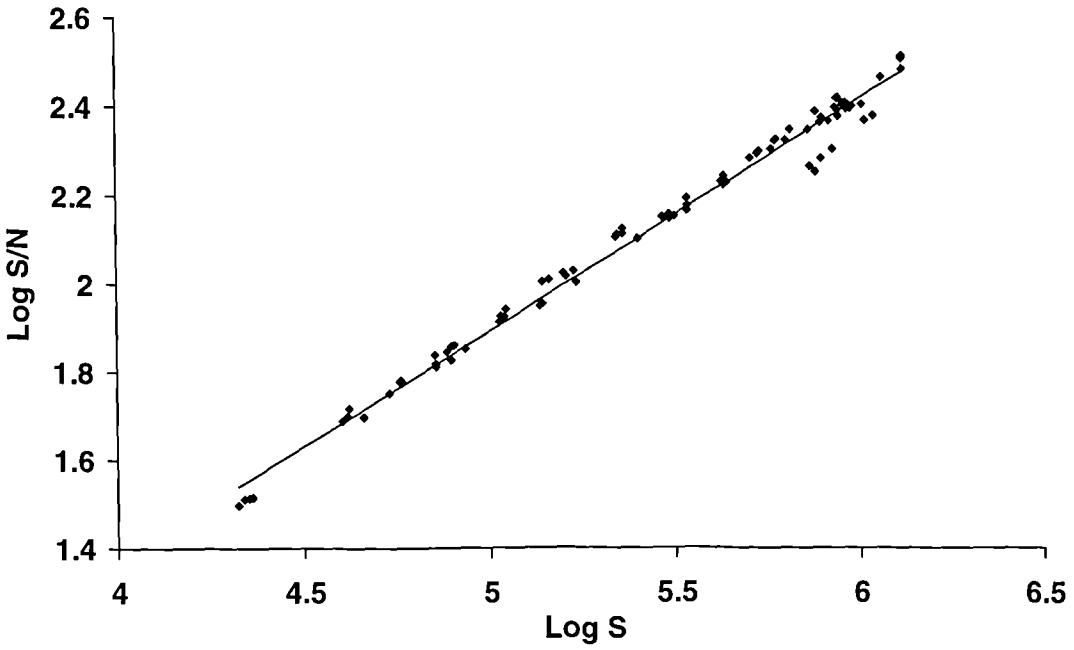

Figure 2.6 The relationship between signal to noise ratio and signal for the MSP used in this study. As the signal increases (here expressed as $\log_{10}$ S) the signal to noise ratio (here expressed as $\log_{10}$ S / N) also increases. Whilst the squared term in a polynomial regression of the data was significant ($t_{81} = 3.47$; $p = 0.001$), suggesting that the relationship was non-linear, a linear regression accounted for 98.8 % of the variation. The gradient of the linear regression line displayed was 0.517, suggesting that, whilst the MSP may be operating as a shot noise limited device, there is also some signal dependent filtering of the noise.

2.3 Experimental animals

Microspectrophotometric measurements were conducted on the retinal photoreceptors of European starlings (*Sturnus vulgaris*), blue tits (*Parus caeruleus*), blackbirds (*Turdus merula*), domestic turkeys (*Meleagris gallopavo*) and Indian blue-shouldered peacocks (*Pavo cristatus*). The starlings used were either reproductively inactive adult birds, which had been held in captivity for approximately eighteen months, or freshly caught adult birds, which were analysed within one month of the capture date. Adult blue tits and blackbirds caught from the wild were kept for a maximum of 2 months prior to use. All species taken from the wild were caught under English Nature Licences 19970164 and 19970165. Starlings were housed in environmentally-controlled conditions under artificial light (Phillips TLD 58W / 35 white light fluorescent tubes) and allowed water and food, in the form of 404 Gold Start crumbs ACS (Dalgety Agriculture Ltd., Bristol, UK), *ad libitum*. Blue tits and blackbirds were kept in unheated outdoor aviaries with natural skylight partially filtered by translucent perspex roofing. Their diet consisted of mealworms (the larvae of *Tenebrio molitor*) and a proprietary insect-based feed (Orlux soft bill, Belgium).

One year old peacocks were obtained from a commercial supplier (Quinton Spratt, Norwich, Norfolk, UK) and used immediately. Five and twenty four week old male British Union Turkeys (strain BUT 8) were obtained from the University of Bristol Department of Animal Health and Husbandry at Langford, Bristol, with the kind assistance of Drs. Chris Sherwin and Peter Lewis. Prior to examination, birds were held in darkness for a minimum of two hours, usually overnight, and killed by approved humane methods.

2.4 Preparation of retinal tissue

2.4.1 Enucleation

Eyes were removed under infra-red light (Kodak Wratten filter No. 87C over a standard 6 V tungsten source) with the aid of an infra-red image converter (FJW Industries, USA) attached to one ocular of a low power stereo microscope. Subsequent dissections of the eyes and retinae were performed under dim red light

from a head torch (3.8 V tungsten lamp filtered by double thickness Lee No. 182 filter; wavelength at 50 % transmission, $\lambda_{T50\%}$, 677 nm). Illumination with red light, and associated photobleaching of the retinae, was undesirable, but some manipulations required a depth perception not provided by monocular operation of the stereo microscope. Wherever possible, exposure of the retinae to light was kept to a minimum. One eye was used immediately, the other being stored, intact, overnight on ice.

2.4.2 Osmolality of physiological media

Initial difficulties in obtaining sufficient outer segments for measurement with the MSP raised concerns that the osmolality of the dissection and mountant media used might be incorrect. Osmolality is the molality (concentration in mol kg^{-1}) of an ideal solution that exerts the same osmotic pressure as the solution being considered. Measured osmolalities of avian plasma range from 337 to 400 mosmol kg^{-1} depending on the species and degree of water deprivation (Willoughby and Peaker, 1979).

Venous blood was taken from a non-water deprived starling and immediately centrifuged at 0 °C for 10 minutes at 5,000 RPM. Following sacrifice, aqueous humour was removed from the anterior chamber of both eyes, using a 25 gauge hypodermic needle and 1 ml syringe, and centrifuged at 20 °C for 5 minutes at 5,000 RPM. The osmolalities of 100 µl aliquots of the plasma supernatant and aqueous humour were determined to be 360 and 346 mosmol kg^{-1} respectively using a freezing point micro-osmometer (Hermann-Roebling, Berlin). The osmolalities of a dilution series of tabletised phosphate-buffered saline (PBS, Dulbecco 'A' tabletised PBS, Oxoid Ltd., Basingstoke, UK) were also determined in an identical fashion (see Figure 2.7). Trial and error established the optimum osmolality of PBS in which to dissect retinae, and dissolve dextran for use as a mountant, to be 340 mosmol kg^{-1}. This concentration of PBS was also used to dissolve glycerol for use as a mountant (section 2.4.4), although the addition of glycerol will dramatically alter the osmolality of the PBS solution.

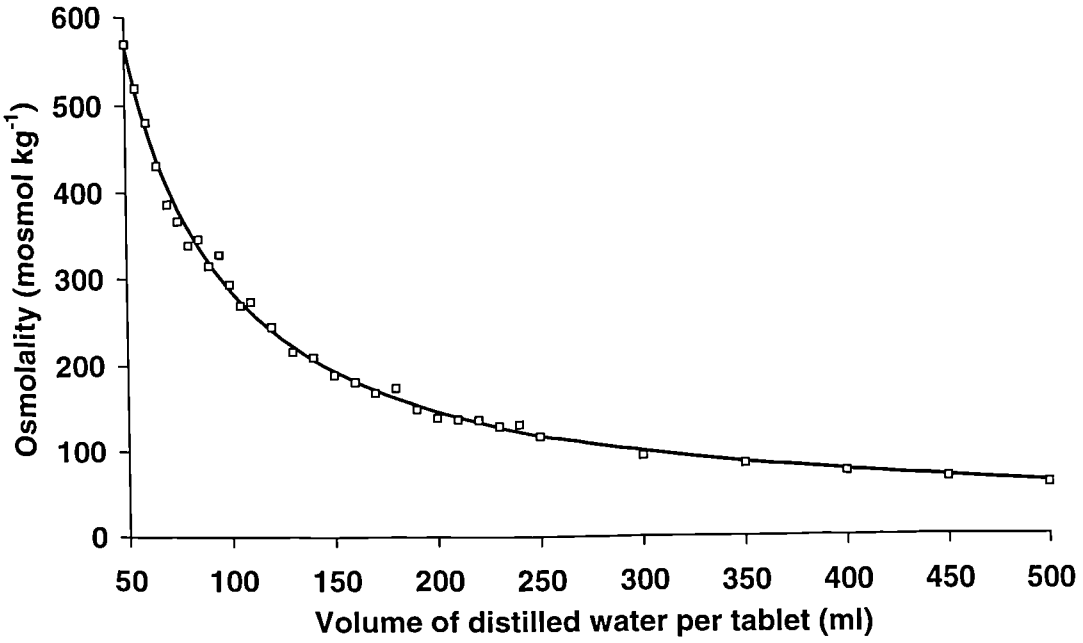

Figure 2.7 Osmolality of various dilutions of phosphate-buffered saline (PBS, Dulbecco 'A' tabletised PBS, Oxoid Ltd., UK) measured with a freezing point micro-osmometer. Symbols indicate measured dilutions. The line represents a best fit function:

$$y = ax^{b}$$

where x is the volume of distilled water in which the tablet was dissolved and y the measured osmolality. A non-linear regression, determined with the software package CurveExpert 1.2, yielded parameters: a = 25629.336 and b = -0.97516969. This equation can be rearranged as:

$$x = \left(\frac{y}{a}\right)^{\frac{1}{b}}$$

in order to determine the required volume of distilled water (x) in which to dissolve a single PBS tablet to give a solution of the required osmolality (y) (see section 2.4.2). The 'standard' Dulbecco 'A' solution (pH 7.1) specified by the manufacturer has an osmolality of 273 mosmol kg^{-1} and is obtained by dissolving one tablet in 100 ml of distilled water. The pH of the PBS buffer solution at different dilutions ranged from 6.93 (50 ml distilled water per tablet) to 7.21 (500 ml of distilled water per tablet).

2.4.3 Retinal dissection

Each eye was hemisected using a fine razor blade (Wilkinson sword double edged replaceable) and the posterior hemisphere placed immediately in a cold (3 °C) dissection medium (PBS made to a concentration of 340 mosmol kg^{-1} by dissolving one tablet in 84 ml of distilled water; pH 7.1). Small sections of retina, typically approximately 2 mm in diameter and often still attached to the pigmented epithelium, were cut away using fine scissors and transferred in a wide-bored Gilson pipette tip to a 22 x 64 mm No. 0 coverslip. Excess saline was blotted away and replaced with mountant solution (see section 2.4.4). Occasionally, the retina was dispersed with fine mounted needles or razor blades, although this was usually found to result in fewer intact photoreceptors. The preparation was then covered with a circular No. 0 coverslip (19 mm diameter) and pressed gently under filter paper to express excess mountant. The edges of the top coverslip were then sealed with clear nail varnish, using a fine paint-brush, to prevent dehydration and movement of the top coverslip.

2.4.4 Mountants

Different tissue mountants were used in the course of this study. Starling retinae, the first species studied, were mounted in a solution (pH 7.1) of 340 mosmol kg^{-1} PBS containing 7.5 % dextran (Sigma 242,000 RMM) to reduce cellular movement (after Mollon *et al.*, 1984; Partridge, 1986; Partridge *et al.*, 1988). Subsequent improvements to the MSP, mostly by virtue of a new photomultiplier tube, enabled the lower wavelength limit of recordings to be extended from 350 to 330 nm. However, a wavelength dependent artefact in the microspectrophotometric measurements became more noticeable with this adjustment, and necessitated the use of an alternative cell mountant.

Due to their high lipid content, outer segments typically have a high refractive index (RI, 1.39 cones, 1.41 rods, Sidman, 1957) relative to the surrounding medium. They also tend to take on a granular appearance as they deteriorate following enucleation (Levine and MacNichol, 1985). These properties are likely to cause Rayleigh and Mie scattering, both of which are wavelength-dependent and increase at short wavelengths (Born and Wolf, 1970). Rayleigh scattering occurs when the object is much smaller than the wavelength of the light it intercepts and scattering

occurs equally in both the forward and backward directions. As the radius of the object increases, however, more light is scattered forward of the object than backwards in the direction of the incident light. This is Mie scattering, and the phenomenon has been used to predict light intensification by cone oil droplets (Baylor and Fettiplace, 1975; Ives *et al.*, 1983; Young and Martin, 1984).

Much of the wavelength-dependent scattering of the measuring beam occurs at the interface between the outer segment limiting membrane and the surrounding medium. This undesirable optical behaviour can only be reduced by minimising the difference in RI between the outer segment and the mountant.

A high RI relative to the surrounding medium and a circular cross section causes the outer segment to act as a converging lens. Whilst potentially advantageous in refracting off-axis light into the cell, this phenomenon can also change the apparent absorbance by focusing the measuring beam onto the photomultiplier tube differently between baseline and sample scans. Alternatively, scattering and focusing effects by the outer segment may cause the transmitted beam to pass through different regions of the collecting objective optics which may vary significantly in their absorption of short wavelengths (Dr. Andrew Dorey, personal communication). Either way, it is possible to record an apparent 'negative absorbance' when the signal from the PMT is higher for the sample than the baseline. It was the manifestation of such an artefact that prompted the use of a solution of 340 mosmol kg^{-1} PBS containing 75 % glycerol (GPBS) in preference to the dextran-based mountant (DPBS).

The incorporation of additives into the external medium to increase its refractive index or viscosity must be approached with caution. Ideally, such additives should be osmotically insignificant (very large molecules), have insignificant absorption of their own and should not alter the absorption characteristics of either visual pigments or oil droplets. In practise it can prove difficult to satisfy all of these criteria whilst obtaining a suitable increase in mountant RI. A variety of substances used to reduce cell movements rarely increase the RI of the external medium beyond 1.35. For example, 10 % dextran (72,000 RMM) has a RI of 1.3481 (Wolf *et al.*, 1975) and this will be further reduced by dilution with the saline remaining on the retinal sample even if the excess has been blotted away during preparation.

Glycerol, however, has a high refractive index which can be modified by dilution (e.g. 75 % glycerol solution RI = 1.4340, Wolf *et al.*, 1975), absorbs less light than even low concentrations of dextran (Figure 2.8) and has the additional advantage of increasing mountant viscosity. Furthermore, it is has been used extensively in the measurement of oil droplet absorption spectra without apparent detriment to either structure or chemistry (Goldsmith *et al.*, 1984b; Partridge, 1989 and this study).

Nevertheless, the use of GPBS for outer segment preparations has several potential problems. Firstly, glycerol is a small molecule (RMM 92.09) and as such it has a very high osmolality (75 % glycerol $> 8.33 \times 10^3$ mosmol kg^{-1}). However, because it infiltrates outer segments so rapidly (coming to an osmotic equilibrium in 30 seconds or less, Liebman, 1975) damage by swelling and bursting cells is minimal. Secondly, glycerol does not act as a buffer, but dilution with PBS and adjustment to pH 7.1 with 1M NaOH maintained a suitable pH in the mountant for the duration of microspectrophotometric recordings. Lastly, GPBS contains a lower concentration of chloride ions (41 mM) than isosmotic DPBS (162 mM). Chloride depletion has been shown to cause hypsochromatic shifts in the λ_{max} of the long wavelength-sensitive cone visual pigment (iodopsin) in extracts from chicken retinae (Knowles, 1976; Shichida *et al.*, 1990). At the chloride ion concentration of GPBS, however, less than 2% of the total iodopsin in a digitonin extract would have been chloride depleted and the effect on the λ_{max} would have been insignificant (Shichida *et al.*, 1990).

The beneficial effects of incorporating glycerol into the external medium are illustrated using the absorbance spectra of retinal photoreceptors from the domestic turkey which were measured whilst mounted in both 75 % GPBS and 5 % DPBS (below). The success of a glycerol-based mountant prompted its use in the measurement of photoreceptors from the other species studied (blackbird, blue tit and peacock).

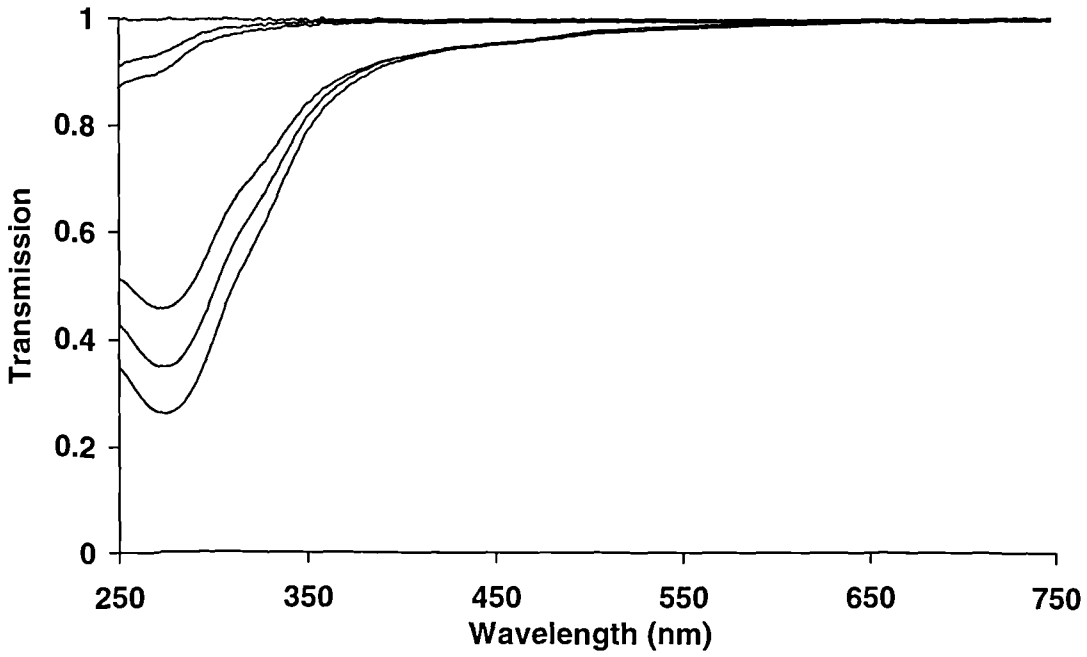

Figure 2.8 Spectral transmission of various tissue mountants investigated during the course of this study. These were measured, using a Shimadzu UV-2101PC UV-VIS scanning spectrophotometer, relative to distilled water and over a pathlength of 10 mm. The mountants, in order of increasing transmission at 250 nm, were: 10 % dextran (Sigma 242,000 RMM) in phosphate-buffered saline (PBS) made to a concentration of 340 mosmol kg^{-1} (10 % DPBS), 7.5 % DPBS, 5 % DPBS, 75 % glycerol in PBS (75 % GPBS), 50 % GPBS and PBS only.

2.4.5 Oil droplets

Microspectrophotometric measurements of oil droplets are also hampered by their high refractive index (Liebman and Granda, 1975; Lipetz, 1984a; Lipetz, 1984b). Retinae from all the species studied were mounted in 100 % glycerol (RI 1.4735, Wolf *et al.*, 1975) in an attempt to reduce the difference in refractive index between the oil droplets (RI approximately 1.48 to 1.69, Ives *et al.*, 1983) and the surrounding medium (RI of 100 % glycerol = 1.4735, Wolf *et al.*, 1975). Oil droplet diameter was determined with a graduated acetate sheet overlaid on the screen of the monochrome monitor used to view the specimen. The acetate scale was calibrated by viewing a stage graticule with the MSP set up optically as for normal use, and diameters were measured to the nearest 0.5 μm.

2.5 Data analysis

The primary objective in the analysis of absorption spectra is to obtain estimates of the spectral parameters which can conclusively identify or characterise the sample. With regards to visual pigment absorbance spectra, we are generally interested in the wavelength of maximum absorbance (λ_{max}) of the alpha band. In order to compare the λ_{max} values obtained in one individual with those in another individual or species, it is important to estimate this parameter with as much accuracy as possible.

2.5.1 Visual pigment absorbance spectra

Initially, MSP data files were read into the analysis program, a Microsoft Excel 5.0c macro, and the baseline and sample frequencies recorded from the V / F converter at 1 nm intervals were converted directly into absorbance values. Subsequent modelling of the effect of in-scan bleaching on the estimate of λ_{max} (see section 2.5.3) led to the upward and downward scans being averaged prior to conversion, a technique similar to that employed by Bowmaker *et al.* (1997). Analyses based on both analysis methods are presented here.

A variable-point 'box-car' running average was passed through the absorbance values and the peak value noted with its corresponding wavelength (the running average λ_{max}). MSP sample scans are frequently offset from the baseline

scans due to optical effects (e.g. scattering or focusing of the measuring beam by the sample, Lipetz (1984a); Young and Martin (1984); Levine and MacNichol (1985); Partridge (1986)), and it was therefore necessary to introduce an offset when normalizing the recorded absorbances. This was calculated at the long wavelength end of the spectrum where there is no detectable absorbance due to the visual pigment. Specifically, the long wavelength offset was defined as the value of the running average at the nearest wavelength to, or just longer than, the predicted wavelength at which the normalized absorbance of the visual pigment being measured was 0.005, plus the half-band width of the running average. The half-bandwidth is the number of points in the running average minus one, divided in half. Rhodopsin absorbance spectra with different λ_{max} are assumed to have an invariant shape when transformed as λ_{max}/λ (Mansfield, 1985; MacNichol, 1986). If true, it follows that for all rhodopsin spectra, there will be a consistent relationship between λ_{max} and any other wavelength of a given absorbance on the short and long wavelength limbs of the α-band. For the rhodopsin template used in this study, generated using the equation given by Stavenga *et al.* (1993), the wavelength corresponding to a normalized absorbance of 0.005 is equal to $\lambda_{max}/0.810373$ (calculated using a λ_{max}/λ transformation of a 500 nm λ_{max} template). Because the data must first be normalized before the λ_{max} can be estimated, the running average λ_{max} was used to calculate the long wavelength offset wavelength.

The maximum corrected absorbance was taken as the running average peak absorbance minus the long wavelength offset absorbance, and the data were normalized to this range for subsequent calculations and display. The bandwidths of absorbance spectra were calculated as the difference between the wavelength corresponding to half maximum absorbance on the long wavelength and short wavelength limbs of the running average absorbance spectrum.

In order to determine the λ_{max}, the analysis used the polynomial derived by Partridge and DeGrip (1991) to fit the data with a rhodopsin template spectrum. For display, the λ_{max}/λ transformed template of Stavenga *et al.* (1993) was used, but with the β-peak of the absorbance spectrum shifted linearly with respect to the α-peak as suggested by Palacios *et al.* (1996), and utilising the relative extinction coefficients

of the α- and β-peaks proposed by Stavenga *et al.* (1993). Each point on the long wavelength limb with an absorbance between 80 % and 20 % of the normalized maximum was used to estimate the λ_{max} (Partridge and DeGrip, 1991), the average of all these estimates being taken as the best estimate of the λ_{max} of the visual pigment. Only the long wavelength limb of a visual pigment absorbance spectrum was used to estimate the λ_{max} because this region of the curve is least affected by photoproduct build-up, short wavelength light scattering, and distortion due to high concentrations of visual pigment (Bowmaker *et al.*, 1975; Levine and MacNichol, 1985).

Ultraviolet-sensitive (UVS) visual pigments have absorbance spectra that are narrower than visual pigments with λ_{max} values in the human visible spectrum, even when transformed on a scale of λ_{max}/λ (Hawryshyn and Hárosi, 1994; Palacios *et al.*, 1996). It is evident that UVS visual pigments require their own template and Palacios *et al.* (1996) have produced coefficients to be used in conjunction with the visual pigment templates of Stavenga *et al.* (1993) for the analysis of UVS visual pigment data. A sixth-degree polynomial describing the relationship of absorbance between 80 % and 20 % long wavelength normalized absorbance and template λ_{max} was calculated from this modified model and used to fit UV templates to data from visual pigments with α-band absorbance in the near UV in preference to the polynomial of Partridge and DeGrip (1991). The polynomial relating normalized long wavelength absorbance (D) at a given wavelength (λ) to λ_{max} for UVS cones (for λ_{max} values between 340 and 380 nm) is:

$$\lambda_{max} = \lambda\left(0.8779 + 0.2317D - 0.5105D^2 + 0.9362D^3 - 1.005D^4 + 0.5744D^5 - 0.1192D^6\right)$$

Equation 6

Because the α-band of UV template is narrower than the original rhodopsin template, the wavelength corresponding to 0.005 maximum normalized absorbance will occur at a shorter wavelength. Thus, for finding the long wavelength offset absorbance, the wavelength corresponding to 0.005 maximum normalized

absorbance is equal to $\lambda_{max}/0.858164$ (calculated using a λ_{max}/λ transformation of a 360 nm λ_{max} UVS template).

Visual pigment absorbance spectra were subjected to an acceptance procedure, the justification of which has been explained by Levine and MacNichol (1985). Scans were accepted if: i) the template spectrum fell within the peak-to-peak noise of the data points between 80 % and 20 % normalized maximum absorbance on the short wavelength and long wavelength limbs of the data respectively; ii) the absorbance spectra were flat for 100 nm beyond the wavelength at which the long-wave limb first falls to an absorbance of zero; iii) were free from obvious distortions (Levine and MacNichol, 1985); and iv) were confirmed as photolabile by bleaching. Due to their rarity, criteria were relaxed for UVS cones, and all scans from cells which were shown to be photolabile were included. Accepted records for each photoreceptor cell type were averaged and re-analysed.

Difference spectra were calculated by deducting the average of the two post-bleach scans from the average of the two pre-bleach scans. These were then analysed, selected and averaged in the same way as the pre-bleach spectra.

2.5.2 Optimising the running average

Before comparison with a visual pigment template, the absorbance data must first be normalized, and it is easier to find the maxima and minima of data that have been smoothed (MacNichol, 1986) or noise-filtered (Hárosi, 1987). A 'box-car' or unweighted running average, which takes the average of a range of successive data points and assigns that value to the middle datum point, was used to smooth the data collected in this study.

The number of data points over which the running average is calculated will affect the normalization of the data (Kent, 1997). If too few points are used, the peak absorbance will be overestimated as the running average incorporates additional absorbance due to random noise. This will cause the maximum corrected absorbance to be overestimated and the data will be 'compressed' when normalized, thus reducing the gradient of the long wavelength limb of the α-band and shifting the estimate of λ_{max} to shorter wavelengths. Conversely, if too many data points are used, the peak absorbance will be underestimated as the running average includes

additional points either side of the peak on the descending short and long wavelength limbs. The maximum corrected absorbance will be underestimated and the data will be 'stretched' when normalized. This will increase the gradient of the long wavelength limb of the α-band and shift the estimate of λ_{max} to longer wavelengths.

The effect on the estimation of λ_{max} and maximum corrected absorbance of the number of data points over which the running average is calculated is displayed in Figure 2.9 (A and B, respectively). Normally distributed (Gaussian) noise with a S / N ratio at the λ_{max} of 10 was added to a rhodopsin template (generated using the equations given by Stavenga *et al.*, 1993) with a λ_{max} of 500 nm and a maximum corrected absorbance of unity. Estimates of λ_{max} (using the polynomial given by Partridge and DeGrip, 1991) and maximum corrected absorbance were obtained with an increasing number of points over which the running average was calculated. This procedure was repeated one hundred times to give a mean estimate of the λ_{max} and maximum corrected absorbance for each number of running average points.

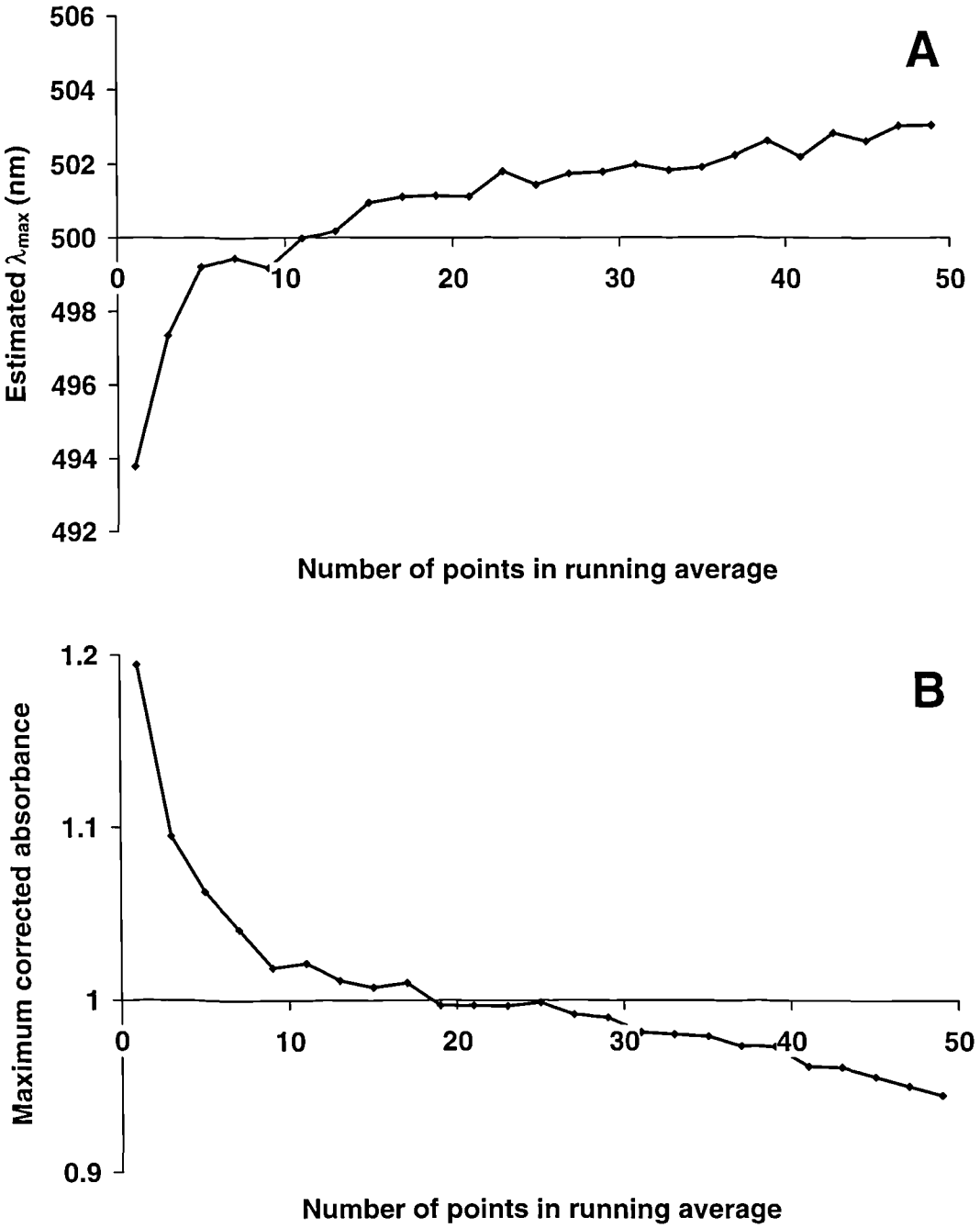

Figure 2.9 The effect on (**A**) the estimated λ_{max} and (**B**) the estimated maximum corrected absorbance of the number of running average points used to normalize visual pigment absorbance data. Normally distributed (Gaussian) noise with a S / N ratio at the λ_{max} of 10 (typical of an individual cone scan) was added to a 500 nm λ_{max} rhodopsin template generated using the equation given by Stavenga *et al.* (1993). Each of the datum points are the average of 100 iterations from which mean estimates of the λ_{max} and maximum corrected absorbance are derived. Note that the number of running average points can only be an odd number.

It is evident that the estimation of both visual pigment λ_{max} and maximum corrected absorbance is affected by the number of points over which the running average is calculated. Thus, it was important to ensure that absorbance spectra were analysed using the optimum number of points, and a mathematical model was constructed to this end.

A 500 nm λ_{max} rhodopsin template was generated using the equation given by Stavenga *et al.* (1993) and normally distributed (Gaussian) noise added to give a peak signal-to-noise ratio of 1000. The peak S / N ratio is described as the maximum corrected absorbance at the λ_{max} divided by the standard deviation of the deviations from the template. Because the data are normalized to unity at the λ_{max}, the peak S / N ratio is simply the reciprocal of this standard deviation. Running averages with increasing numbers of points were then passed through the data. The optimum number of points was chosen as that producing the least root mean-squared (RMS) deviation between the running average spectrum and the original template, for absorbance values between 80 % short wavelength absorbance and the long wavelength offset absorbance. The RMS deviation describes the 'fit' of the running average to the template. In this way, the optimum running average chosen is that which smoothes the data best whilst retaining the underlying shape of the data[1]. This process was repeated using new noise of the same level until a mean optimum number of points was determined with a 95 % confidence limits of less than ± 1, i.e. to the nearest integer. This in turn was repeated for decreasing signal-to-noise ratios. The data obtained were best-fitted with a quadratic equation using CurveExpert 1.2 to facilitate the estimation of signal-to-noise ratio ranges for which analysis using a given number of running average points was optimal. The results are displayed in Table 2.1.

The maximum number of points used in the running average was limited to 31. Above this value, the shift in λ_{max} induced by underestimation of peak

---

[1] Arguably, the accuracy in estimating either maximum corrected absorbance or λ_{max} could be used to determine the optimum number of running average points. However, both of these variables are affected by the amount of noise in the data and, consequently, were not used for this purpose. Furthermore, as shown in Figure 2.9, the optimum number of points giving the most accurate estimate of the maximum corrected absorbance is not necessarily the same as that which gives the most accurate estimate of the λ_{max}.

absorbance exceeded 1 nm, which was considered to be the wavelength accuracy of the MSP. In reality, the noise affecting visual pigment absorbance spectra recorded microspectrophotometrically is often wavelength dependent. Furthermore, distortions due to in-scan bleaching and photoproduct build up may increase the apparent deviation of the long wavelength limb from the template and thus overestimate the number of points required. However, the results of the model are seen as a reasonable attempt to maximise the accuracy with which the raw data are normalized.

Signal-to-Noise ratio at λ_{max}	**Optimum number of data points in the running average**
$413.22 > x \geq 123.00$	13
$122.85 > x \geq 70.52$	15
$70.47 > x \geq 48.47$	17
$48.45 > x \geq 36.25$	19
$36.23 > x \geq 28.43$	21
$28.42 > x \geq 22.92$	23
$22.92 > x \geq 18.76$	25
$18.76 > x \geq 15.39$	27
$15.39 > x \geq 12.36$	29
$12.36 > x$	31

Table 2.1 Optimum number of points in the running average employed to smooth data (to allow the accurate estimation of the peak and long wavelength offset absorbances) over the range of signal-to-noise ratios indicated. Peak signal-to-noise ratio is defined as the maximum corrected absorbance divided by the standard deviation of the deviations from the original template.

2.5.3 In-scan bleaching of visual pigments

Detectivity is quantitatively proportional to the S / N ratio. However, maximising the S / N ratio, either by enlarging the cross-sectional area of the measuring beam, increasing the photon flux density of the illumination, or lengthening the integration time at each wavelength, must be traded off with increased bleaching of the visual pigment during each scan. Whilst this is not a problem when measuring cone oil droplets, the carotenoid pigments of which are stable under moderate levels of illumination, in-scan bleaching of visual pigments can result in distortion of the recorded absorbance spectra. If the bleached molecules of pigment are replaced by photoproduct molecules which absorb little or no light over the range of wavelengths scanned, or if photoproducts are rapidly lost from the cell or the area of the outer segment in the immediate vicinity of the measuring beam, the effect on the recorded curve will be to shift its λ_{max} towards the end of the spectrum from which the scan originated.

The MSP utilised in the present study recorded baseline and sample data at 2 nm intervals on each odd wavelength of the downward (long wavelength to short wavelength) scan and on each of the interleaved even wavelengths during the upward (short wavelength to long wavelength) scan. A typical MSP recording comprised two long wavelength to short wavelength to long wavelength scans, during which the visual pigment was bleached continuously by the measuring beam. On the 'downward' long wavelength to short wavelength spectral pass, the amount of visual pigment remaining, and consequently the fraction of the incident light absorbed, decreases with decreasing wavelength. This results in the apparent λ_{max} of the visual pigment being shifted towards longer wavelengths relative to the true λ_{max}. Similarly, on the 'upward' short wavelength to long wavelength spectral pass, the apparent λ_{max} of the visual pigment is shifted towards shorter wavelengths. By scanning from both directions, and then combining the spectra obtained, it might be assumed that the shifts in apparent λ_{max} induced by in-scan bleaching should effectively cancel out.

However, there are a number of important considerations in this approach to reducing the effects of in-scan bleaching. Firstly, the shape of the absorbance

spectrum, and potentially the apparent λ_{max} of the visual pigment, may be affected if photoproducts which absorb light over the range of wavelengths scanned accumulate within the outer segment. Secondly, as the amount of in-scan bleaching is dependent on the intensity of the illumination, wavelength-dependent variations in photon flux from the MSP light source will alter the 'balance' of bleaching. The quartz halogen bulb use in this study is relatively deficient in short wavelengths. Accordingly, the magnitude of the shift in apparent λ_{max} towards longer wavelengths on the downward scan will be greater than the shift towards shorter wavelengths on the upward scan. Thirdly, even if the apparent λ_{max} of the 'averaged' up and down scans was identical to the true λ_{max} of the visual pigment, in-scan bleaching would increase the apparent bandwidth of the absorbance spectrum.

Nevertheless, bi-directional scanning has been employed frequently in the determination of visual pigment absorbance spectra (e.g. Bowmaker *et al.*, 1975; Sillman *et al.*, 1993; Ellingson *et al.*, 1995; Bowmaker *et al.*, 1997). An alternative approach is to use multiple scans with very little in-scan bleaching (MacNichol *et al.*, 1983; Partridge, 1986; Partridge and DeGrip, 1991). Attempts have also been made to correct mathematically visual pigment absorption spectra distorted by significant in-scan bleaching in measurements made with uni-directional spectral passes (Marks, 1965; Partridge, 1986).

The effects of in-scan bleaching on visual pigment absorbance spectra were modelled for the MSP used in this study. The rhodopsin template of Stavenga *et al.* (1993) was used to create an absorbance spectrum for visual pigment with a λ_{max} at 500 nm, and the amount of bleaching induced by the measuring beam calculated at each wavelength. For the purposes of the model, only the relative photon flux emitted from the monochromator at each wavelength was required. This was calculated from the 'gain file' produced by the microcomputer when flattening the baseline prior to measuring an absorption spectrum (see section 2.2.2). The hexadecimal gainbyte signal sent to the digital to analogue converter at each wavelength was converted into its equivalent voltage input to the analogue multiplier, which was inversely proportional to the relative photon flux. The amount of bleaching was proportional to the irradiance and the absorbance of the visual pigment at each wavelength. A wavelength-independent 'bleaching factor' was also

incorporated into the model to adjust the degree of bleaching at each wavelength. This was analogous to increasing the photon flux density of the measuring beam or lengthening the integration time at each wavelength step. The two downward scans were averaged together, as were the two upward scans. Because the amount of visual pigment remaining will differ between subsequent scans of a given direction, so will the magnitude of apparent shift in λ_{max}. However, the distortions induced by the scans will be in the same 'direction'.

The 'raw' data calculated were then treated in two different ways, analogous to the two different analysis methods detailed in section 2.5.1. On the one hand, the raw data were simply normalized to the maximum and minimum obtained by fitting an 11-point unweighted running average. Alternatively, the up and down scans were averaged mathematically by fitting a weighted three point running average to the data. Specifically, the two absorbance values either side of a given datum point were averaged together, and then averaged with the datum point. The 'up / down averaged' data were then normalized to their own maximum and minimum. Both the raw and up / down averaged scans thus calculated were used to estimate the λ_{max} of the visual pigment using the polynomial of Partridge and DeGrip (1991). The bleaching factor was then adjusted to investigate the error in apparent λ_{max} for different levels of bleaching. The results of the model are displayed in Figure 2.10 (A to D).

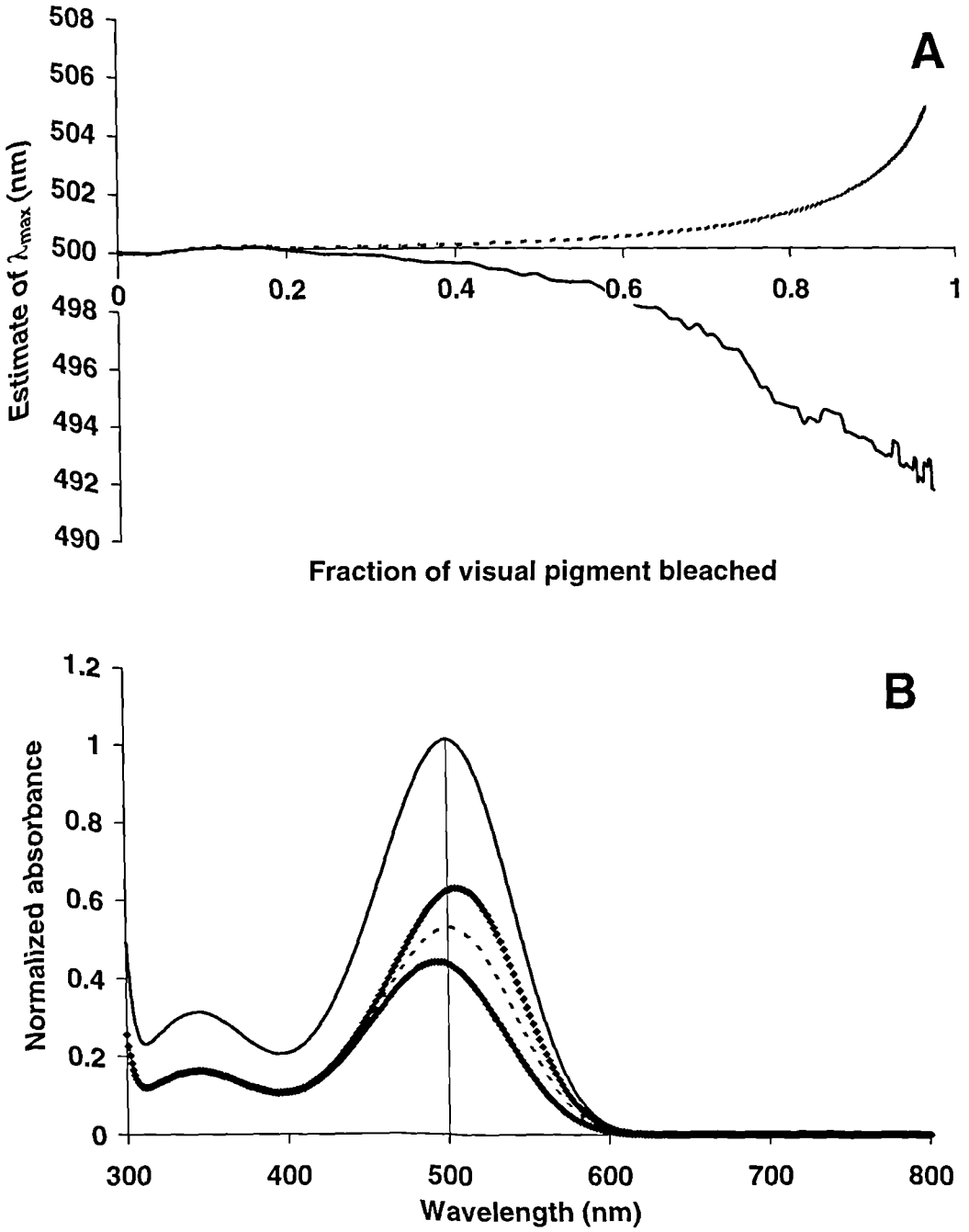

Figure 2.10 The effect of in-scan bleaching on the estimation of visual pigment λ_{max}. The original visual pigment template, generated using the equations given by Stavenga *et al.* (1993), had a λ_{max} of 500 nm. (**A**) The relationship between the amount of in-scan bleaching and the shift in apparent λ_{max}. The 'Fraction of visual pigment bleached' refers to the total amount of visual pigment lost at the end of both spectral scans (i.e. four spectral passes). Solid trace: raw data (upward and downward scans not averaged together) normalized to the maxima and minima obtained by fitting an unweighted 11-point running average. Dotted trace: Upward and downward scans (raw data) averaged together before normalization (no running average fitted). (continued over).

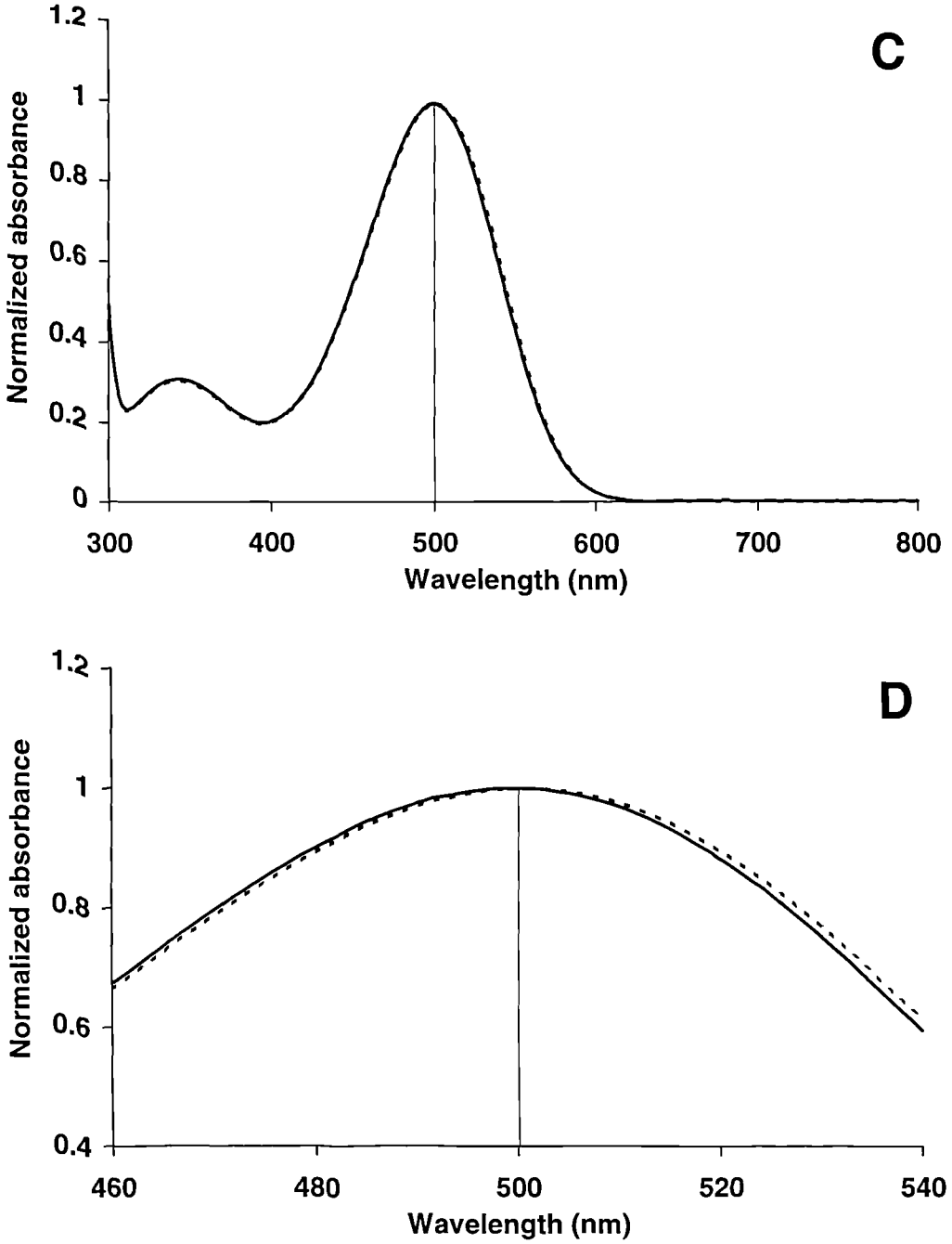

Figure 2.10 (continued). (**B**) Separation of up and down scans resulting from a level of in scan bleaching sufficient to cause a 1 nm shift in the apparent λ_{max} of the visual pigment (76 % of visual pigment bleached after four spectral passes). Solid trace: visual pigment prior to bleaching. Upper symbols: averaged downwards scans. Lower symbols: averaged upward scans. Dotted trace: averaged upward and averaged downward scans averaged together. (**C**) Normalized absorbance spectra of the original visual pigment (solid trace) and the averaged upwards and downwards scans (dotted trace). (**D**) Area around the λ_{max} depicted in **Figure 2.10 (C)** enlarged for clarity. Solid trace: original visual pigment prior to measurement. Dotted trace: upwards and downwards scans averaged together. The vertical line in each of the last three figures indicates a wavelength of 500 nm.

It is evident that bi-directional scanning compensated for the effects of in-scan bleaching on the estimate of λ_{max} even when the level of bleaching was relatively high. When the up and down scans (raw data) were averaged mathematically, the shift in apparent λ_{max} was towards longer wavelengths, as would be expected for an illuminant rich in long wavelength light. As noted in section 2.2.5, the wavelength accuracy of the monochromator was considered to be ±1 nm. Before the difference between true λ_{max} and apparent λ_{max} exceeded this value, the visual pigment could be bleached by 76 % in the course of two complete spectral scans (four spectral passes). At this level of bleaching, the FWHM bandwidth of the absorbance spectrum obtained was 102 nm, compared to the template bandwidth of 101 nm.

Conversely, when the raw data (normalized to the maxima and minima obtained by fitting the raw data with an 11-point running average) were analysed without averaging the up and down scans the shift in apparent λ_{max} was in the opposite direction. This shift in λ_{max} towards shorter wavelengths is an artefact of the analysis procedure. Because the upwards and downwards scans separated with bleaching, and because the scans commenced at long wavelengths, more of the absorbance values between 80 % and 20 % normalized long wavelength absorbance used to estimate the λ_{max} were taken from the upwards scan, and were therefore distorted towards shorter wavelengths. By, averaging the up and down scans both directions were represented equally in the absorbance values between 80 % and 20 % normalized long wavelength absorbance, and any shift in λ_{max} was due solely to the effects of bleaching.

It is concluded that averaging the up and down scans prior to analysis results in a more accurate estimate of the true λ_{max} and the spectral bandwidth, although peak absorbance will still be underestimated. This method also circumvents certain artefacts introduced by the use of a polynomial to estimate the λ_{max} from the long wavelength limb of normalized absorbance and permits an extensive amount of bleaching. Furthermore, averaging the up and down scans will reduce the apparent 'noise' of the data which is exaggerated by scan separation due to bleaching. Lower levels of noise permit the use of a fewer number of running average points in the

analysis, which results in a more accurate estimate of λ_{max} and peak absorbance (see section 2.5.2).

The amount of in-scan bleaching was estimated for the MSP used in this study by making sequential scans of the same region of a rod outer segment (blackbird). The results of this experiment are displayed in Figure 2.11. Each scan consisted of two long wavelength to short wavelength to long wavelength spectral passes. The mean change in maximum corrected absorbance at the λ_{max} between sequential scans (over four scans) was 9.7 % (s.d. ± 1.0 %, n = 4). The maximum corrected absorbance of the first scan was 0.06. From the results of the modelling (above), this level of in-scan bleaching should have a negligible effect (a shift of less than 0.1 nm) on the estimate of the λ_{max}. Indeed, the λ_{max} values of the first and last scans (which represented a change in the maximum corrected absorbance of 34 %) were 504.0 and 503.7 nm respectively.

However, it must also be remembered that bleaching may result in the production of stable photoproducts which absorb over the range of wavelengths routinely scanned by the MSP. If the photoproducts accumulate during a pre-bleach scan, the apparent λ_{max} of the absorbance spectrum may be shifted to shorter wavelengths depending on the spectral location of the visual pigment λ_{max} (Knowles and Dartnall, 1977). Absorption by photoproducts in the post-bleach scan may be reflected in a shift in the apparent λ_{max} of the difference spectrum towards longer wavelengths. Thus, although averaging the up and down scans may permit a greater amount of bleaching *per se*, it is still advisable to minimise in-scan bleaching as far as is practicably possible.

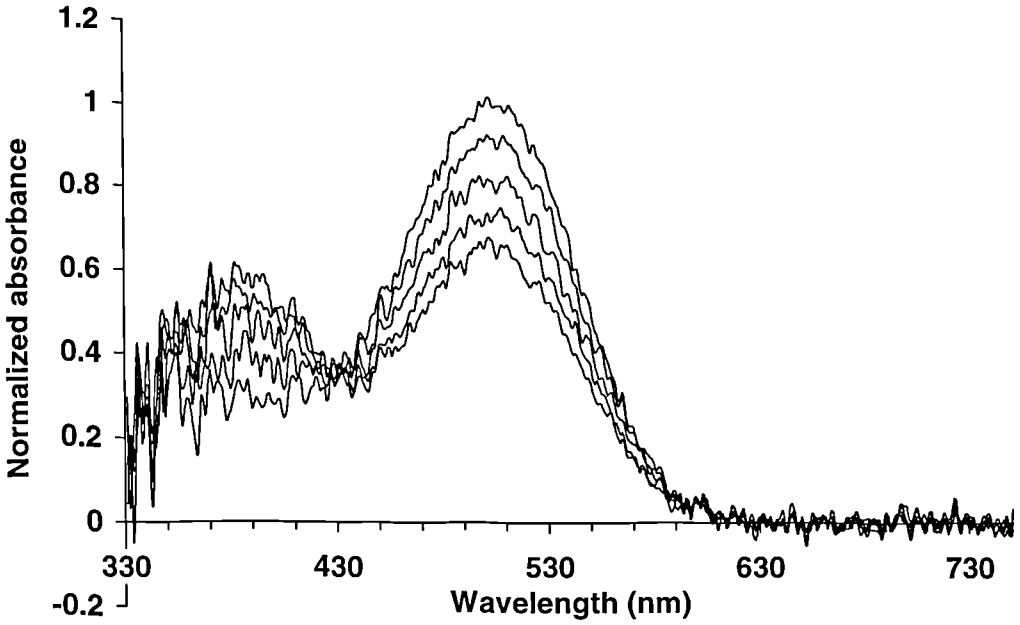

Figure 2.11 Sequential bleaches of a blackbird rod outer segment to illustrate the level of in-scan bleaching induced by the MSP used in this study. Traces represent long wavelength offset-corrected absorbance data (two long wavelength to short wavelength to long wavelength spectral passes; upwards and downwards scans averaged) and are normalized to the maximum corrected absorbance of the first scan. The mean change in maximum corrected absorbance between sequential scans was 9.7 %. The λ_{max} values of the first and last scans (which represented a change in the maximum corrected absorbance of 34 %) were 504.0 and 503.7 nm respectively. Note the accumulation of stable photoproduct, probably all-*trans* retinal, with maximum absorbance at 380 nm.

2.5.4 Oil droplet absorption spectra

MSP data files were read into the analysis program and baseline and sample frequencies converted into absorptance values. An eleven point running average was passed through the data and the peak value noted with its corresponding wavelength. Once again, a long wavelength offset was required to compensate for differences between the baseline and sample scans due to optical effects of the cell preparation. This was calculated as the average absorptance over the last 50 nm at the long wavelength end of the spectrum where there was no absorption due to the carotenoid pigment. The maximum corrected absorptance was calculated as the peak absorptance minus the long wavelength offset absorptance, and the data were normalized to this range for subsequent calculations and display.

Microspectrophotometric measurements of retinal oil droplets suffer from a number of artefacts. Small size, spherical shape, high refractive index and, frequently, high carotenoid concentration results in considerable 'leakage' of the measuring beam around the outside of the droplets (Liebman and Granda, 1975; Goldsmith *et al.*, 1984b). Microspectrophotometers can only make reliable measurements over a limited range of low absorbances, and the upper limit is reached when the light scattered around the sample becomes comparable to that passing through it (Lipetz, 1984a). Consequently, recorded oil droplet absorbance spectra tend to be limited to a maximum absorbance of approximately one, and display a 'flat-topped' cut-off character (Liebman and Granda, 1975). Furthermore, all evidence of carotenoid fine structure is lost, obscuring the identity of the compounds responsible.

Traditionally, oil droplet absorption spectra were described by the wavelength, $\lambda_{T50\%}$, at which measured transmission was 50 % (e.g. Liebman and Granda, 1975; Bowmaker, 1977). However, $\lambda_{T50\%}$ is dependent on the amount of by-passing light and is, therefore, not a reliable parameter for the characterisation of oil droplet absorption spectra (see chapter one).

Consequently, oil droplet absorptance spectra are characterised by their cut-off wavelength, λ_{cut}, which is the shortest wavelength at which there is any significant transmission on the long wavelength side of the oil droplet absorptance

peak and is independent of a constant by-passing light in the microspectrophotometer (Lipetz, 1984a). The λ_{cut} is defined as the intercept with the value of maximum apparent absorptance by the tangent to the curve at λ_{mid}, where λ_{mid} is the wavelength corresponding to 50 % maximum measured absorptance. In this study, absorptance values between 70 % and 30% of maximum measured absorptance on the long wavelength side of the absorptance peak were used to calculate the line tangent to λ_{mid}.

2.6 Microspectrophotometric results

The following figures and tables summarise the microspectrophotometric results from the starling, blackbird, blue tit, peacock and turkey. Visual pigment absorbance spectra were only made from outer segments that were still attached to the inner segment. In this way, absorption spectra of the associated oil droplets could be made in order to assist identification of the cone types, particularly with respect to the principal member of the double cones and the long wavelength-sensitive single cones which both contained a visual pigment with almost identical λ_{max} values. This was also necessary to confirm the reliable pairing of certain types of oil droplet with particular visual pigment, as reported previously (Bowmaker *et al.*, 1997).

Visual pigment data are presented as normalized mean pre- and post-bleach absorbance spectra, with their corresponding normalized difference spectra. Histograms of the distribution of visual pigment λ_{max} values are also provided, both for λ_{max} estimated from pre-bleach spectra and from difference spectra. Note that these values only represent records that were selected using the criteria specified in section 2.5.1. A much larger number of records were rejected due to measurement artefacts. Visual pigment specific absorbances were not calculated owing to uncertainty regarding transverse pathlength, cone outer segments often being distorted or folded over upon themselves. Instead, absorbances measured at the λ_{max} of the mean difference spectra are given.

In all tables, values are ± one standard deviation. Standard deviations for the λ_{max} values of mean visual pigment absorbance spectra refer to the error in estimating the λ_{max} using the polynomial of Partridge and DeGrip (1991) as described in section

2.5.1. Standard deviations for the mean λ_{max}, λ_{cut} and λ_{mid} values represent the variance of the individual records used to create the mean spectra.

Abbreviations: D, dorsal; V, ventral; UVS, ultraviolet-sensitive; VS, violet-sensitive; SWS, short wavelength-sensitive; MWS, medium wavelength-sensitive; LWS, long wavelength-sensitive; DPBS, 5 % dextran in phosphate-buffered saline; GPBS, 75 % glycerol in phosphate-buffered saline; λ_{max}, wavelength of maximum absorbance; λ_{cut}, cut-off wavelength, and λ_{mid}, wavelength corresponding to 50 % of maximum measured absorptance, as defined by Lipetz (1984a).

2.6.1 Original analysis method

2.6.1.1 European starling

Microspectrophotometric data for visual pigments and oil droplets in the European starling, *Sturnus vulgaris*, are displayed in Figure 2.12 to Figure 2.23 and summarised in Table 2.2 and Table 2.3. The starling retina contained five different types of vitamin A_1-based visual pigments (i.e. rhodopsins) in six different types of photoreceptor.

A single class of rod contained a medium wavelength-sensitive rhodopsin with a mean λ_{max} at 504 nm (n = 7). There were four different types of single cone, each of which was reliably associated with a different type of oil droplet. Oil droplets are referred to using the nomenclature of Jane and Bowmaker (1988). Single cones containing red (R-type) oil droplets, with a mean λ_{cut} at 573 nm (n = 27), were paired with a long wavelength-sensitive (LWS) visual pigment which had a mean pre-bleach λ_{max} of 563 nm (n = 10). Yellow (Y-type) oil droplets, having a mean λ_{cut} at 515 nm (n = 42), were paired with a medium wavelength-sensitive (MWS) visual pigment with a mean pre-bleach λ_{max} at 504 nm (n = 11). There were two short wavelength-sensitive cone classes. One had a short wavelength-sensitive (SWS) visual pigment (mean pre-bleach λ_{max} 450 nm, n = 7) which was paired with a 'colourless' (C-type) oil droplet of mean λ_{cut} 399 nm (n = 20). The other contained an ultraviolet-sensitive visual pigment (mean pre-bleach λ_{max} close to 369 nm, n = 2) and was paired with a transparent (T-type) droplet which showed no detectable absorbance over the range of wavelengths scanned (n = 6).

In addition, the retina was dominated by double cones, both members of which contained visual pigments resembling the LWS rhodopsin found in the single cones. The visual pigment in the larger, principal member of the double cone pair had a mean pre-bleach λ_{max} at 563 nm (n = 11) and was paired with a 'pale' (P-type) oil droplet of variable λ_{cut} between 407 and 472 nm depending on retinal location. Towards the anterior ventral region of the retina, the λ_{cut} occurred at longer wavelengths. Furthermore, a shoulder in the absorption spectrum at approximately 480 nm appeared in those P-type droplets taken from the ventral retina, and the relative absorption of this shoulder increased with increasing proximity to the peripheral region of the anterior ventral retina. No 480 nm shoulder was evident in the absorption spectra of P-type droplets taken from the dorsal retina. The smaller, accessory member of the double cone displayed a properly formed, spherical oil droplet (A-type) only in cells at the periphery of the ventral retina, and had a mean λ_{cut} at 479 nm (n = 5). The visual pigment measured in the outer segment of the accessory cone had a mean pre-bleach λ_{max} of 558 nm (n = 2).

The maximum corrected absorptance of the C-type (0.31) and A-type (0.20) droplets was relatively low and these droplets may not act as cut-off filters in the same way as the more highly pigmented oil droplets are thought to (see chapter one).

The measured transverse absorbance at the λ_{max} of the mean difference spectrum of the UVS cone pigment was higher than the other cone types, and even the rod. This was unexpected as UVS cones generally have the narrowest outer segments, but may have resulted from drift in the baseline, or optical effects of the bleached cell preparation, which caused the apparent negative absorbance at short wavelengths evident in the post-bleach scan. Such distortion might also affect the estimated λ_{max} of the pigment, and the UVS pigment λ_{max} values quoted in Table 2.2 should be interpreted with caution.

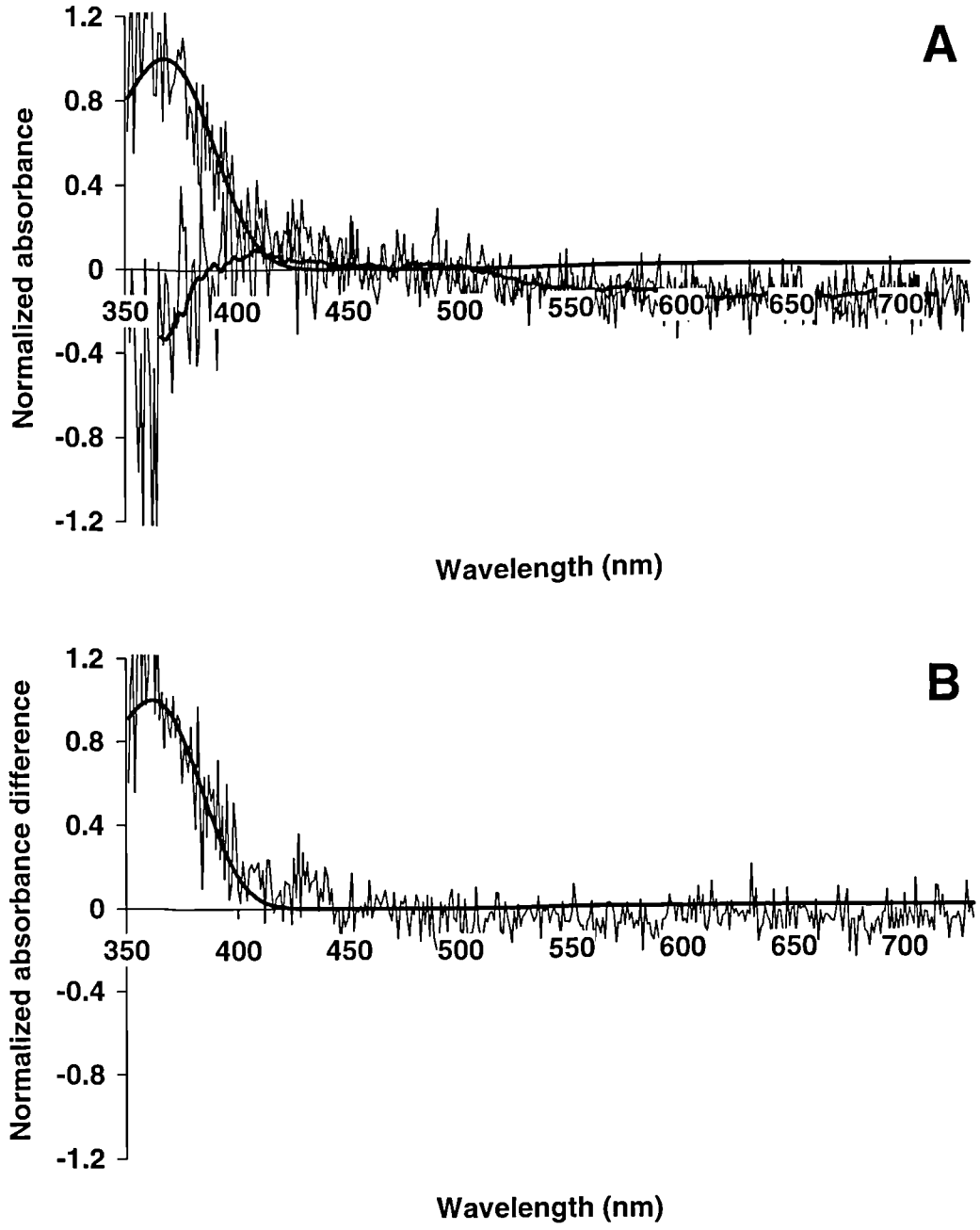

Figure 2.12 Microspectrophotometric results from 2 UVS single cones of the European starling, *Sturnus vulgaris*. (**A**) Mean pre-bleach absorbance spectrum (upper trace) with best-fitted visual pigment template (λ_{max} 368 nm, solid line) and mean post-bleach absorbance spectrum (lower trace) with running average (solid line). (**B**) Mean difference spectrum (trace) with best-fitted visual pigment template (λ_{max} 362 nm, solid line).

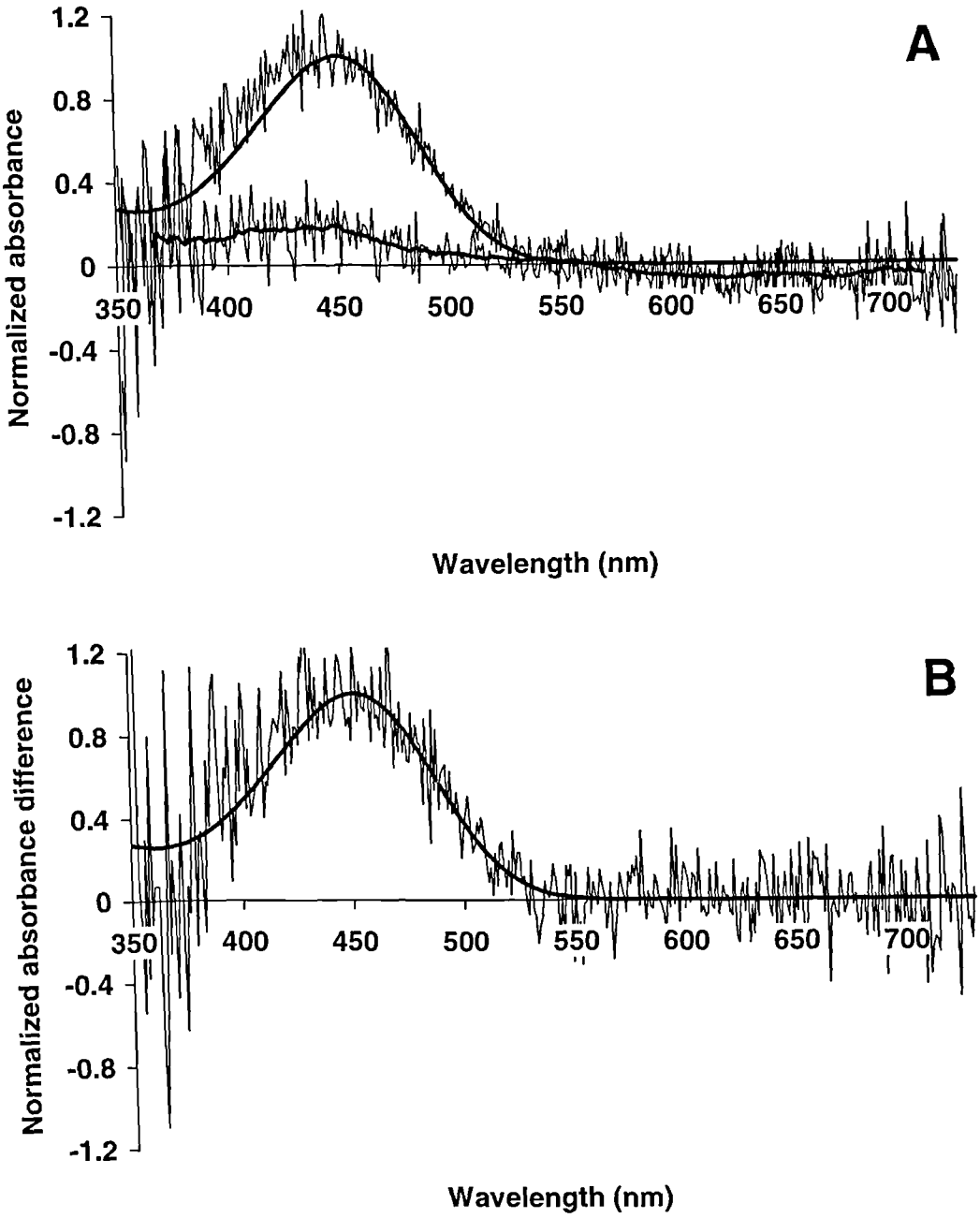

Figure 2.13 Microspectrophotometric results from 7 SWS single cones of the European starling, *Sturnus vulgaris*. (**A**) Mean pre-bleach absorbance spectrum (upper trace) with best-fitted visual pigment template (λ_{max} 450 nm, solid line) and mean post-bleach absorbance spectrum (lower trace) with running average (solid line). (**B**) Mean difference spectrum (trace) with best-fitted visual pigment template (λ_{max} 452 nm, solid line).

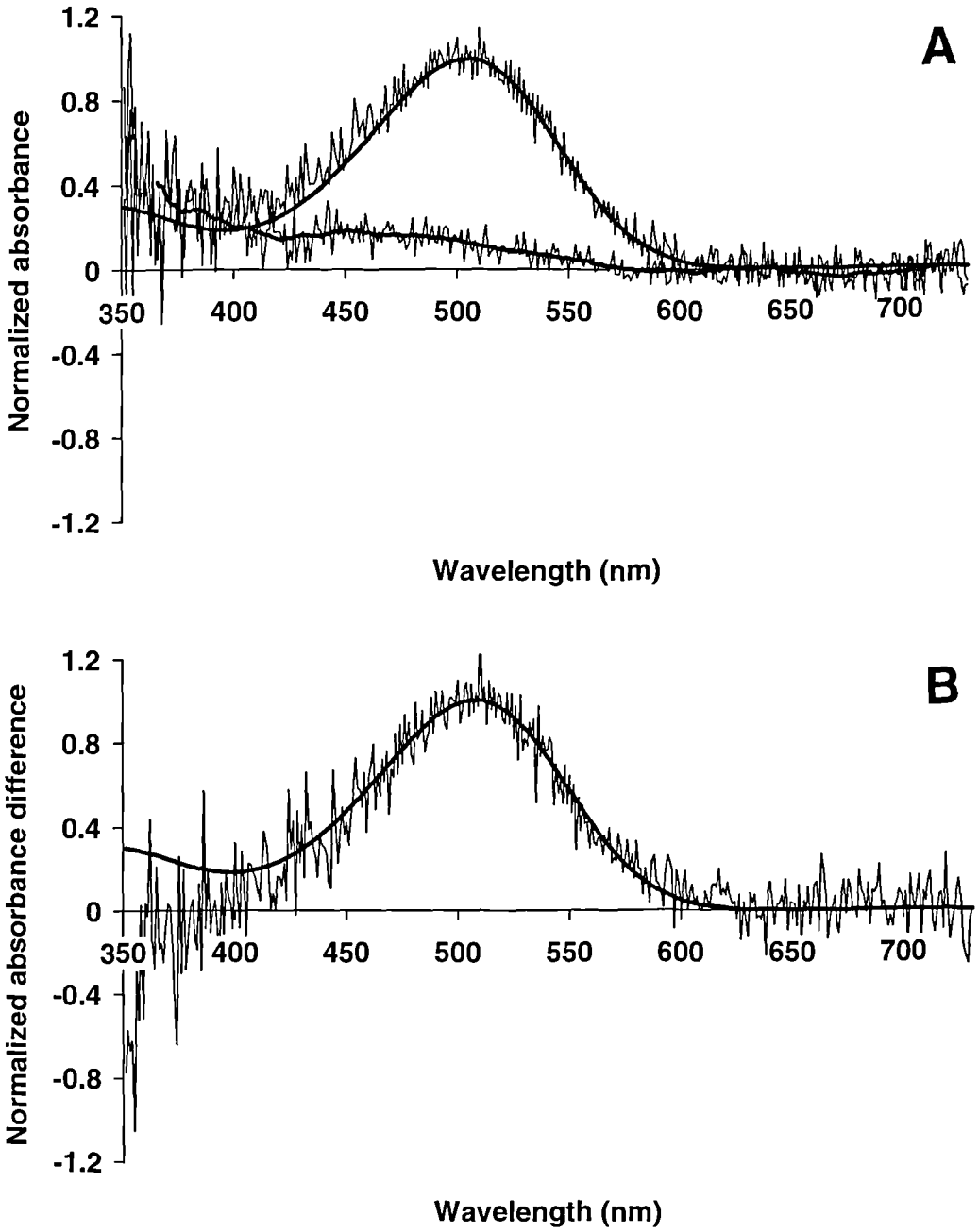

Figure 2.14 Microspectrophotometric results from 11 MWS single cones of the European starling, *Sturnus vulgaris*. (**A**) Mean pre-bleach absorbance spectrum (upper trace) with best-fitted visual pigment template (λ_{max} 505 nm, solid line) and mean post-bleach absorbance spectrum (lower trace) with running average (solid line). (**B**) Mean difference spectrum (trace) with best-fitted visual pigment template (λ_{max} 508 nm, solid line).

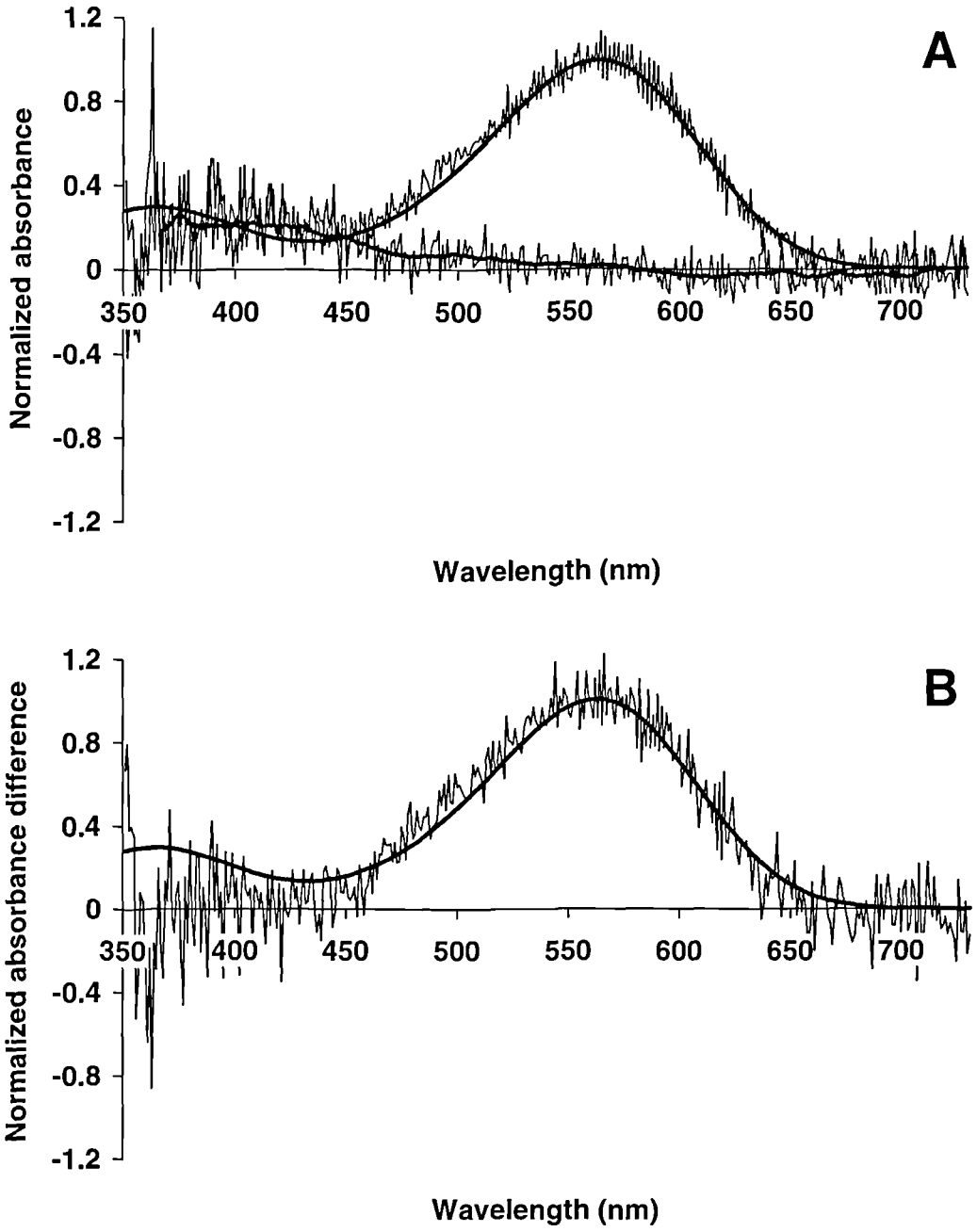

Figure 2.15 Microspectrophotometric results from 10 LWS single cones of the European starling, *Sturnus vulgaris*. (**A**) Mean pre-bleach absorbance spectrum (upper trace) with best-fitted visual pigment template (λ_{max} 563 nm, solid line) and mean post-bleach absorbance spectrum (lower trace) with running average (solid line). (**B**) Mean difference spectrum (trace) with best-fitted visual pigment template (λ_{max} 563 nm, solid line).

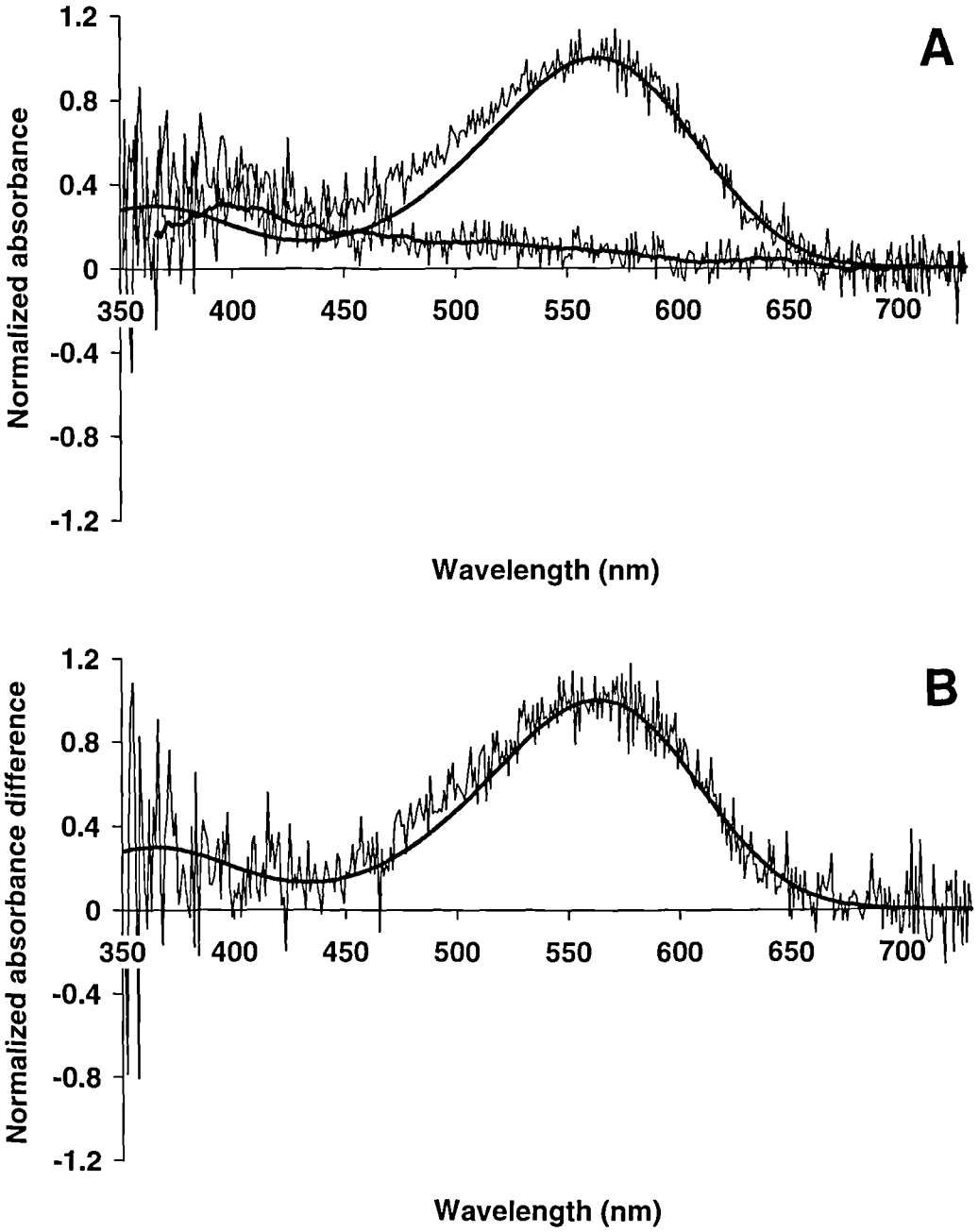

Figure 2.16 Microspectrophotometric results from 11 principal members of the double cone of the European starling, *Sturnus vulgaris*. (**A**) Mean pre-bleach absorbance spectrum (upper trace) with best-fitted visual pigment template (λ_{max} 564 nm, solid line) and mean post-bleach absorbance spectrum (lower trace) with running average (solid line). (**B**) Mean difference spectrum (trace) with best-fitted visual pigment template (λ_{max} 563 nm, solid line).

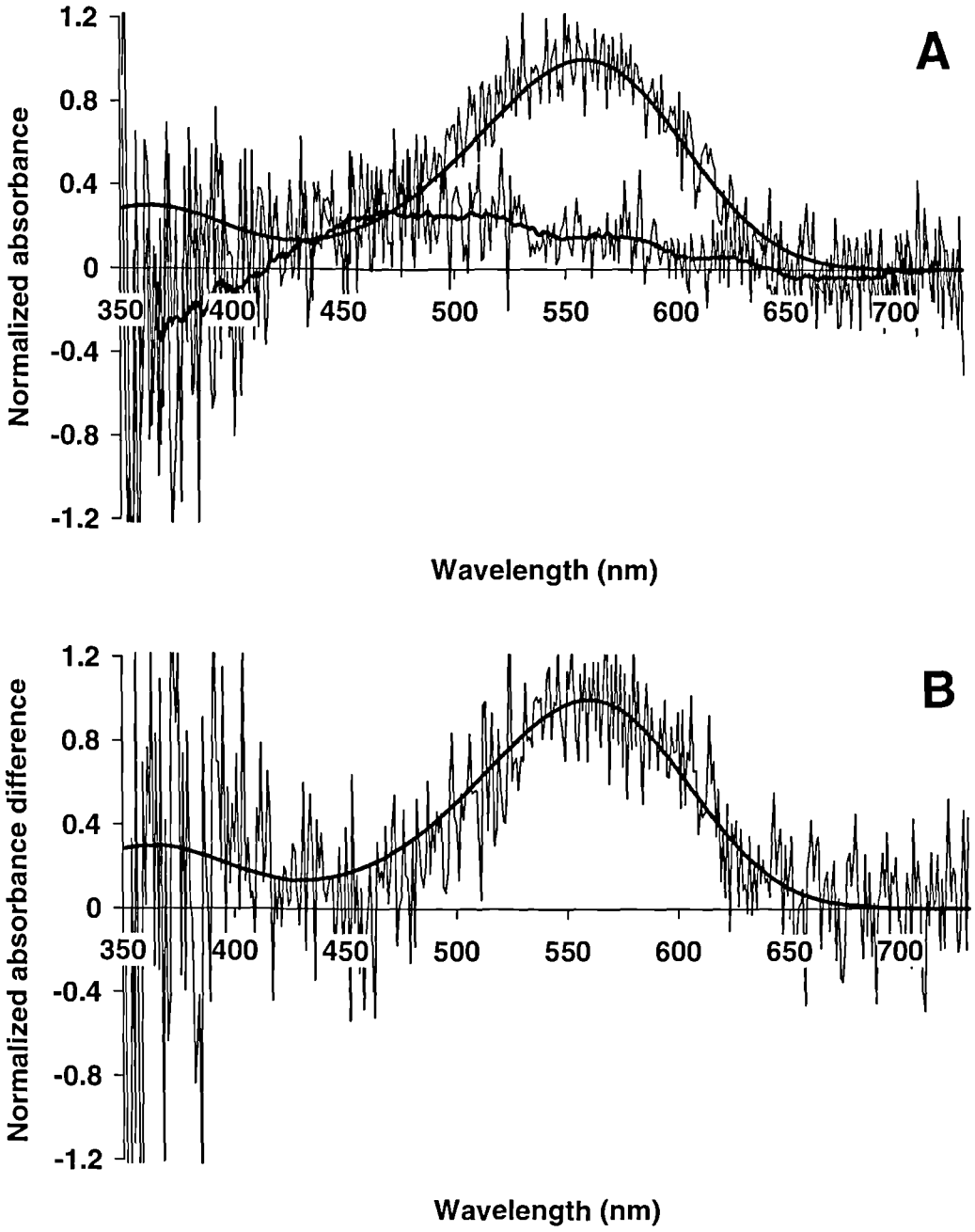

Figure 2.17 Microspectrophotometric results from 2 accessory members of the double cone of the European starling, *Sturnus vulgaris*. (**A**) Mean pre-bleach absorbance spectrum (upper trace) with best-fitted visual pigment template (λ_{max} 559 nm, solid line) and mean post-bleach absorbance spectrum (lower trace) with running average (solid line). (**B**) Mean difference spectrum (trace) with best-fitted visual pigment template (λ_{max} 560 nm, solid line).

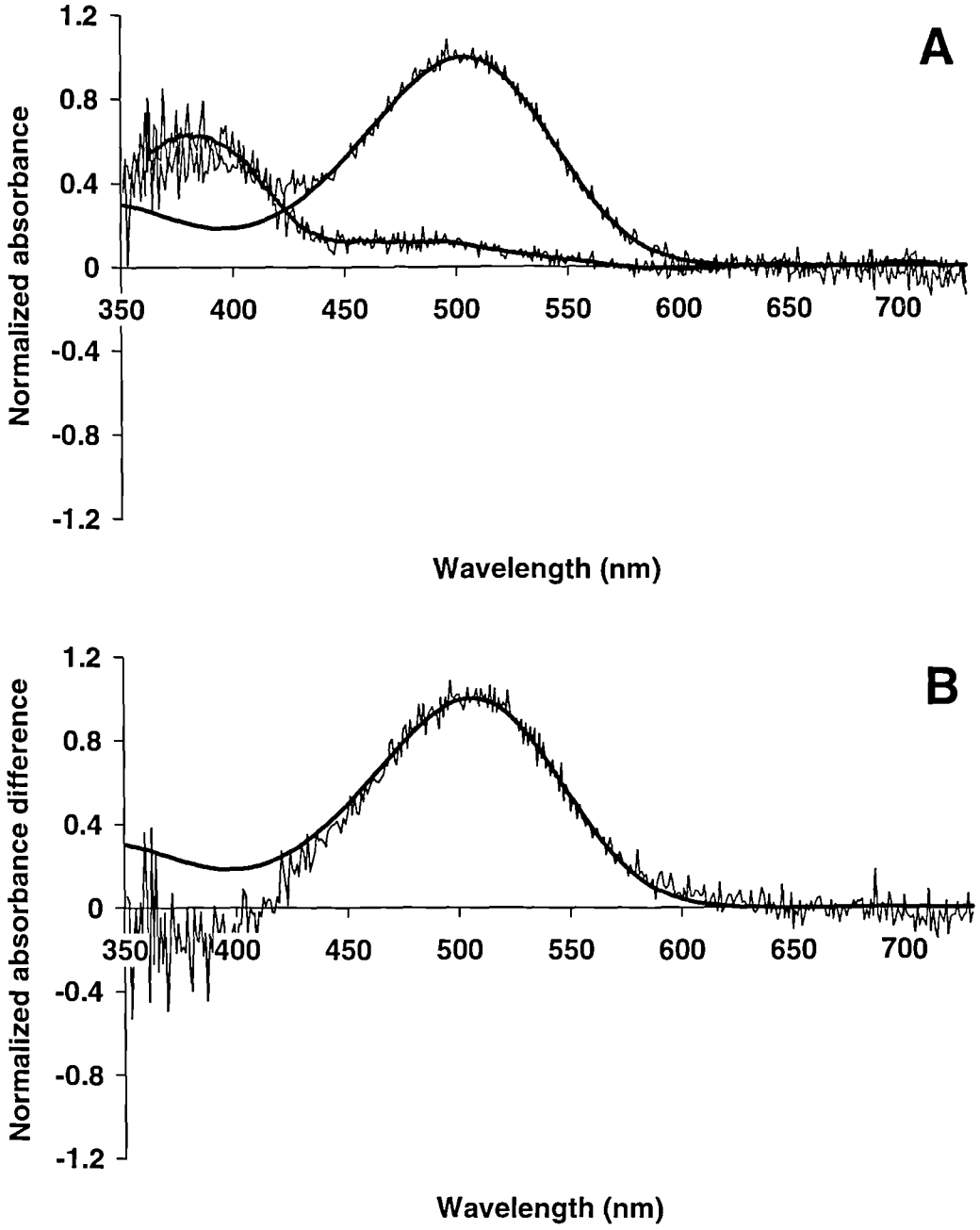

Figure 2.18 Microspectrophotometric results from 7 rods of the European starling, *Sturnus vulgaris*. (**A**) Mean pre-bleach absorbance spectrum (upper trace) with best-fitted visual pigment template (λ_{max} 503 nm, solid line) and mean post-bleach absorbance spectrum (lower trace) with running average (solid line). (**B**) Mean difference spectrum (trace) with best-fitted visual pigment template (λ_{max} 506 nm, solid line).

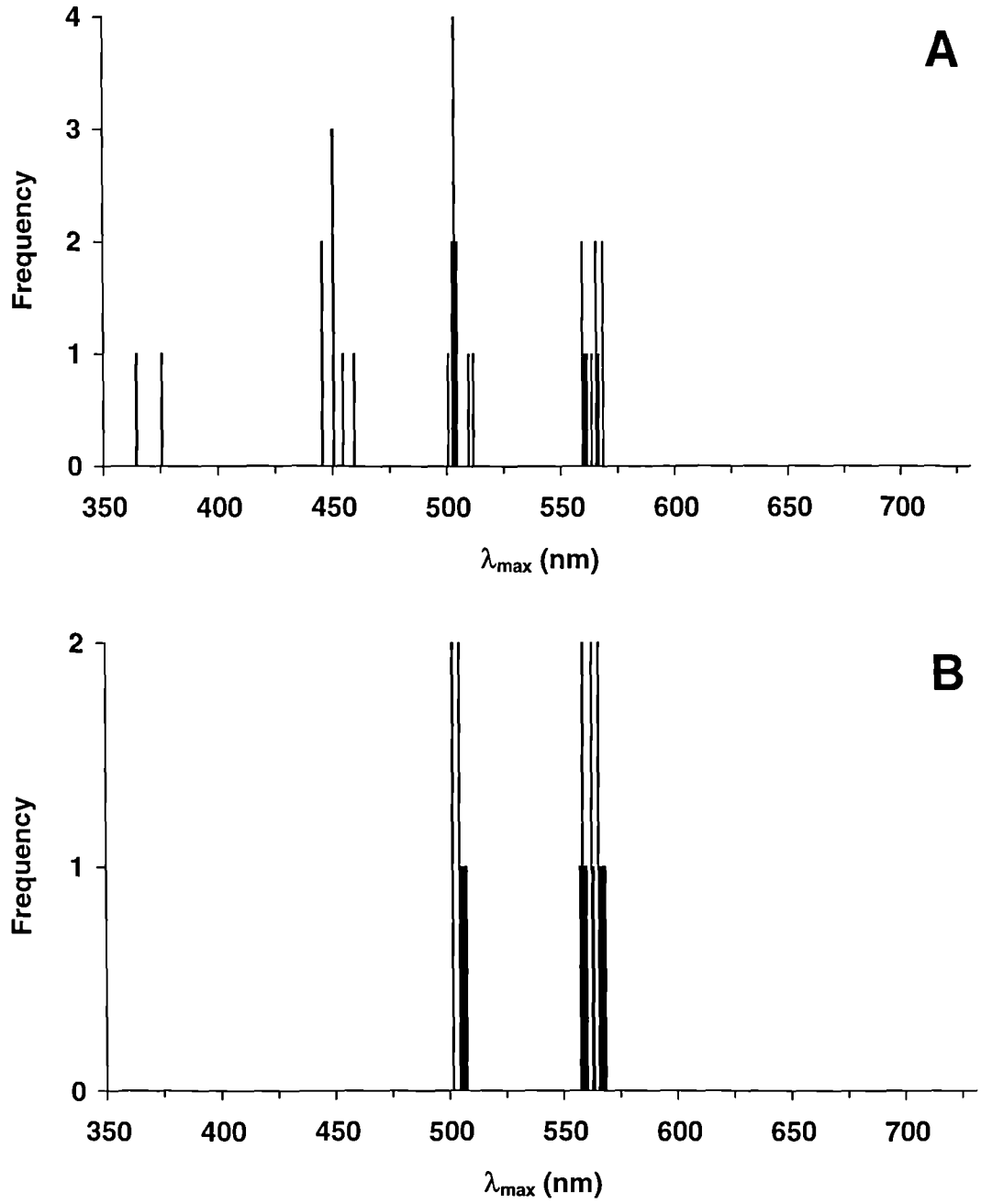

Figure 2.19 Histogram showing the distribution of estimated λ_{max} values obtained from pre-bleach absorbance spectra of visual pigments in the European starling, *Sturnus vulgaris*. (**A**) Single cones. λ_{max} values around 369, 450, 504 and 563 nm describe UVS, SWS, MWS and LWS visual pigments respectively. (**B**) Rods and double cones. λ_{max} values around 504 nm describe rod visual pigment, whilst λ_{max} values around 563 nm describe the LWS visual pigments found in the principal and accessory members of the double cones.

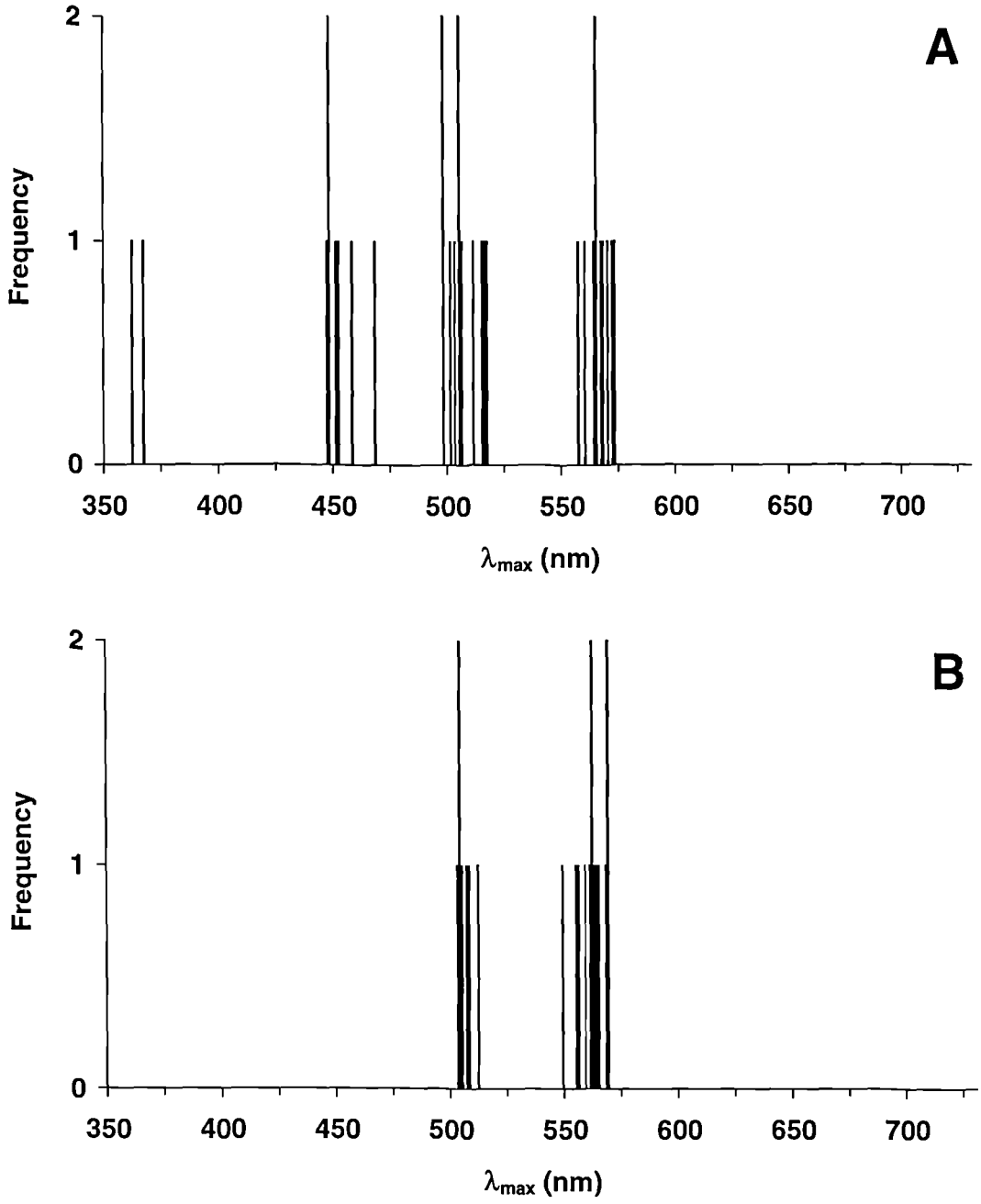

Figure 2.20 Histogram showing the distribution of estimated λ_{max} values obtained from difference spectra of visual pigments in the European starling, *Sturnus vulgaris*. (**A**) Single cones. λ_{max} values around 364, 453, 506 and 565 nm describe UVS, SWS, MWS and LWS visual pigments respectively. (**B**) Rods and double cones. λ_{max} values around 506 nm describe rod visual pigment, whilst λ_{max} values around 562 nm describe the LWS visual pigments found in the principal and accessory members of the double cones.

	Rod	Single Cones			Double cone	
		UVS	SWS	MWS	LWS	Principal	Accessory
Visual pigments							
λ_{max} of mean pre-bleach spectrum (nm)	503.2 ± 1.8	368.0 ± 6.8	450.2 ± 4.1	504.6 ± 3.7	563.4 ± 5.2	563.5 ± 4.3	559.2 ± 9.6
Mean of pre-bleach λ_{max} (nm)	503.5 ± 2.3	369.2 ± 7.7	450.0 ± 5.0	503.6 ± 3.1	562.9 ± 3.6	562.7 ± 3.5	557.5 ± 0.5
λ_{max} of mean difference spectrum (nm)	505.6 ± 2.7	362.0 ± 7.4	451.5 ± 7.7	507.8 ± 6.2	562.7 ± 7.5	563.4 ± 6.9	559.8 ± 17.4
Transverse absorbance at λ_{max} of mean difference spectrum	0.030	0.033	0.011	0.015	0.014	0.015	0.010
Mean of difference spectrum λ_{max} (nm)	505.8 ± 3.1	364.0 ± 3.7	452.8 ± 7.5	506.2 ± 6.9	565.3 ± 5.1	561.6 ± 6.1	558.9 ± 4.6
Number of cells	7	2	7	11	10	11	2

Table 2.2 Summary of the microspectrophotometric data obtained for the visual pigments of the European starling, *Sturnus vulgaris*.

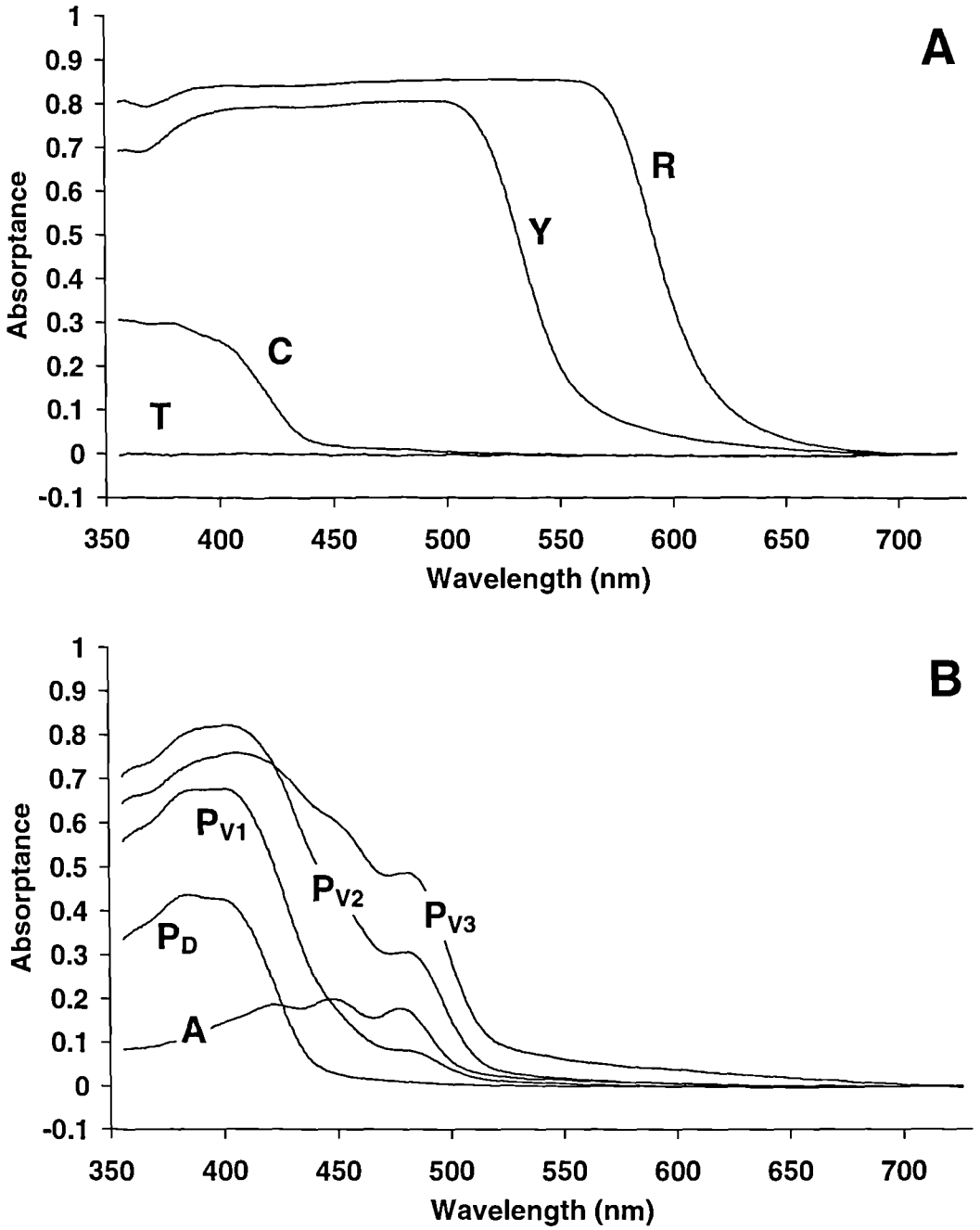

Figure 2.21 Mean absorptance spectra of oil droplets from the European starling, *Sturnus vulgaris*. (**A**) Oil droplets located in the single cones. T-, C-, Y- and R-type droplets were found in the UVS, SWS, MWS and LWS cones respectively. (**B**) Oil droplets located in the principal (P-type, solid lines) and accessory (A-type, dashed line) members of the double cones. The three absorption spectra displayed for the P-type droplets found in the principal member of the double cones in the ventral retina (P_V) are arbitrary categorisations based on the absorptance of the 480 nm shoulder relative to the peak absorptance. P_{V1}, P_{V2} and P_{V3} describe P-type droplets whose spectral absorption at 480 nm relative to the peak absorptance was (i) less than or equal to 25 %, (ii) more than 25 % but less than or equal to 50 %, and (iii) more than 50 %, respectively. P_D represents the P-type droplet found in the principal member of double cones located in the dorsal retina.

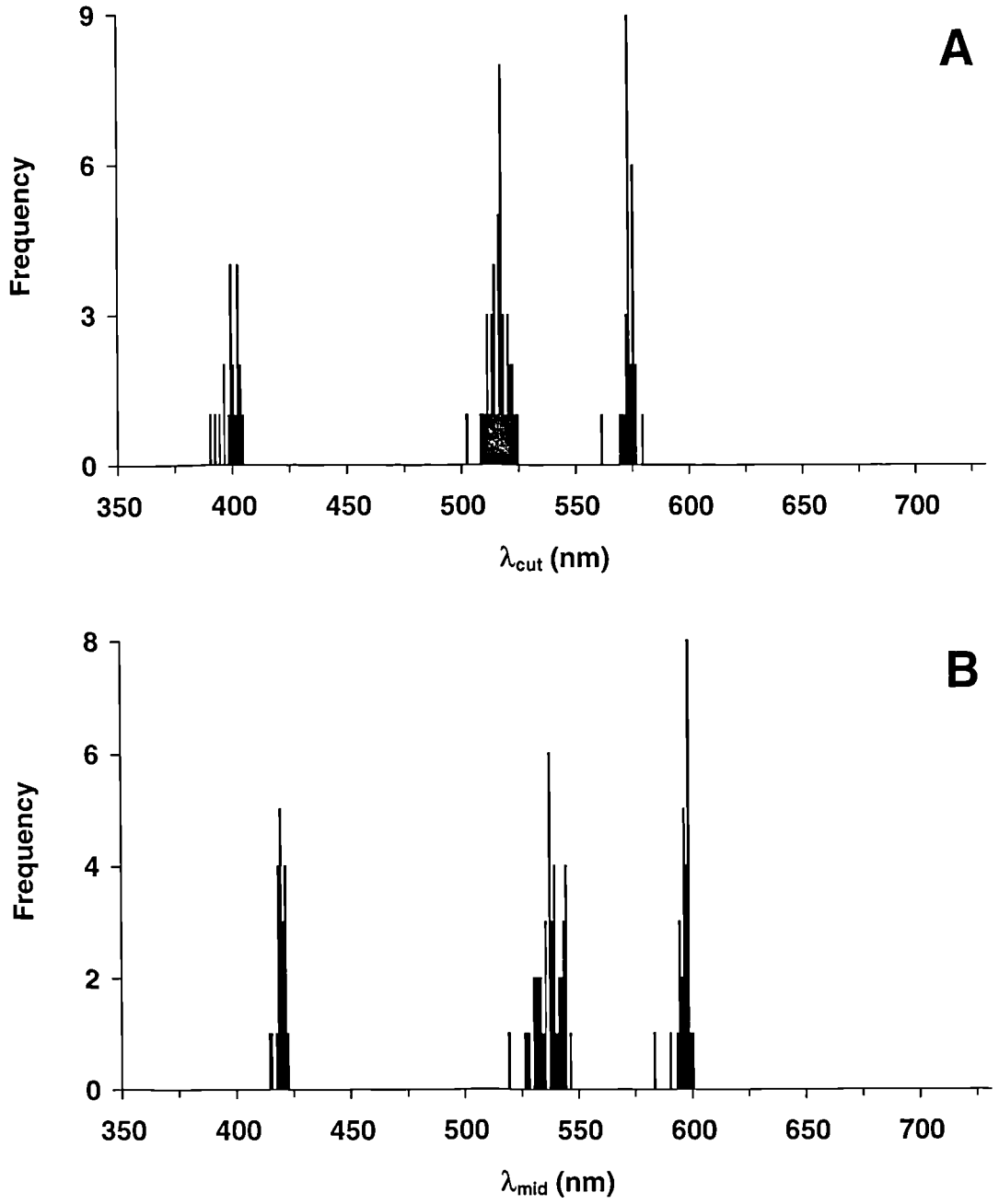

Figure 2.22 Histograms showing the spectral distribution of λ_{cut} and λ_{mid} values for single cone oil droplets measured in the European starling, *Sturnus vulgaris*. (**A**) λ_{cut} values around 399, 515 and 573 nm, and (**B**) λ_{mid} values around 419, 536 and 595 nm, describe C-type, Y-type and R-type oil droplets respectively.

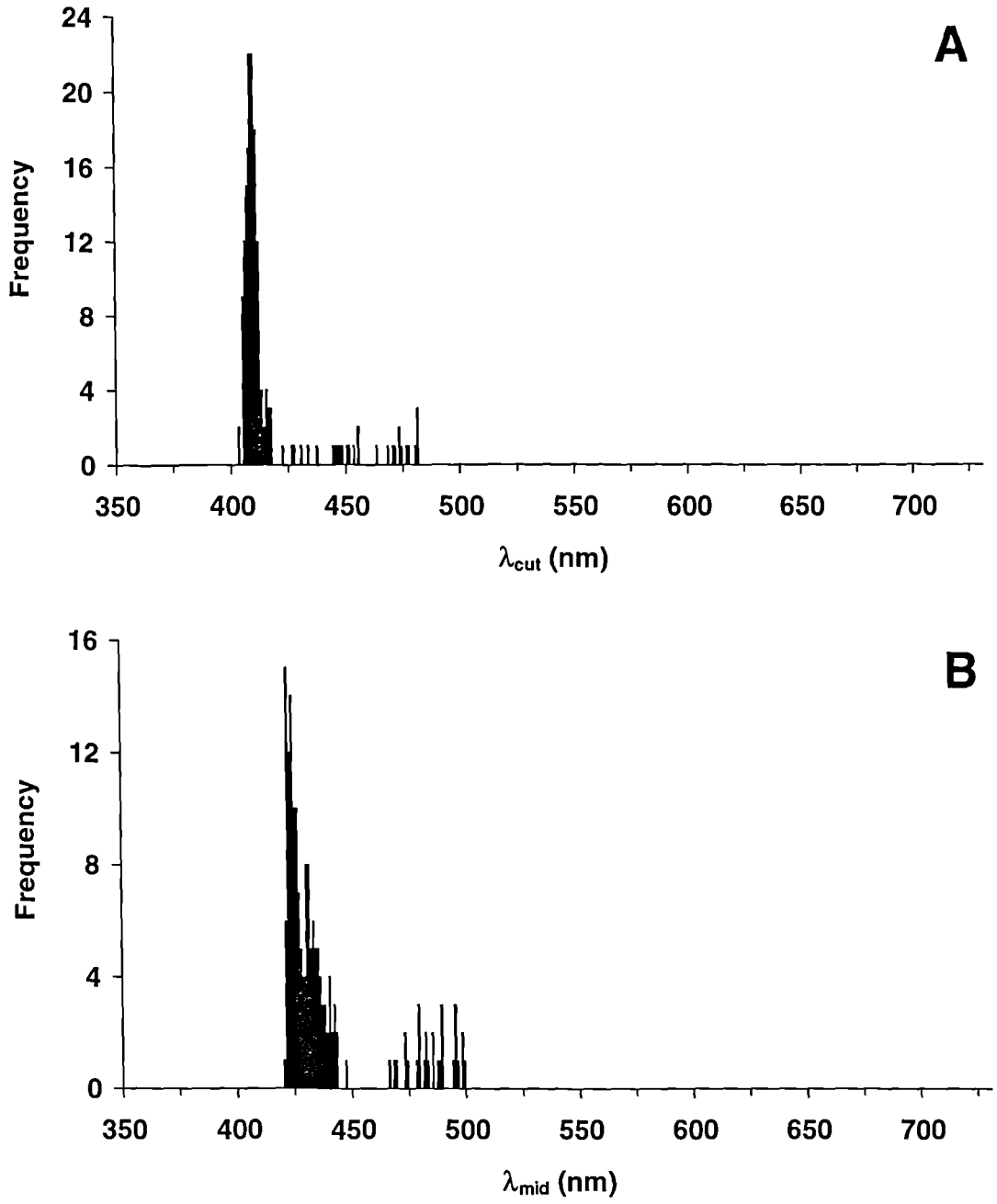

Figure 2.23 Histograms showing the spectral distribution of λ_{cut} and λ_{mid} values for the P-type oil droplets found in the principal member of the double cones in the European starling, *Sturnus vulgaris*. Both λ_{cut} value, and the relative absorptance of the 480 nm shoulder, increases as the location of the double cone approaches the anterior ventral retina. The apparent bimodal distribution in λ_{mid} is due to the 480 nm shoulder exceeding 50 % of maximum measured absorptance, which results in a sudden jump in its corresponding wavelength. Frequencies of oil droplets presented here are not directly representative of relative abundance

	Single cones				Double cone			
Cone type	UVS	SWS	MWS	LWS	Principal		Accessory	
Oil droplet type	T-type	C-type	Y-type	R-type	P-type		A-type	
					D	V1, V2, V3	D	V
λ_{cut} of mean absorption spectrum (nm)	<350	399.3	514.7	572.2	407.4	410.4 445.7 470.7	-	478.7
λ_{mid} of mean absorption spectrum (nm)	<350	418.9	536.5	595.4	423.1	432.9 478.9 494.4	-	493.0
Maximum corrected absorptance of mean absorption spectrum	<0.02	0.31	0.81	0.86	0.44	0.68 0.82 0.76	-	0.20
Mean λ_{cut} (nm)	<350	398.6 ± 3.9	515.3 ± 4.4	572.6 ± 3.2	407.3 ± 2.1	410.5 ± 2.5 442.5 ± 11.9 471.8 ± 3.0	-	479.0 ± 2.2
Mean λ_{mid} (nm)	<350	418.5 ± 2.0	536.2 ± 5.8	595.4 ± 3.3	423.2 ± 1.8	433.3 ± 4.8 477.4 ± 6.6 494.8 ± 3.0	-	491.0 ± 5.1
Mean diameter (μm)	1.6 ± 0.5	1.9 ± 0.3	2.2 ± 0.5	3.1 ± 0.4	2.5 ± 1.9	2.8 ± 0.5 2.7 ± 0.5 2.6 ± 0.5	-	1.5 ± 0.0
Number of oil droplets	6	20	42	27	70	75 17 7	-	5

Table 2.3 Summary of the microspectrophotometric data obtained for the cone oil droplets measured in the European starling, *Sturnus vulgaris*.

2.6.1.2 Domestic turkey

Microspectrophotometric examination revealed that, like the starling, the retina of the domestic turkey, *Meleagris gallopavo*, contained five different types of rhodopsin visual pigment, in six different types of photoreceptor.

The visual pigments of the turkey were initially measured whilst mounted in 5 % dextran in phosphate-buffered saline solution (DPBS). The results are displayed in Figure 2.24 to Figure 2.31 and summarised in Table 2.4. Due to excessive light scattering at short wavelengths in the MSP, it was decided to mount the photoreceptors in 75 % glycerol in phosphate-buffered saline solution (GPBS) to reduce the difference in refractive index between the outer segment and the surrounding medium. The results are displayed in Figure 2.32 to Figure 2.40 and summarised in Table 2.5.

Microspectrophotometric results obtained from the cone oil droplets in the turkey are displayed in Figure 2.41 to Figure 2.43 and summarised in Table 2.6. The oil droplet measurements displayed were made whilst the photoreceptors were mounted in 100 % glycerol, just as for the other species examined in this study.

Whilst it was evident from the following figures that the use of GPBS as a mountant reduced wavelength-dependent measurement artefacts in visual pigment absorbance spectra, the effect on λ_{max} was less obvious. Because there was no non-parametric alternative, λ_{max} values were normalized by rank transformation prior to the use of a two way analysis of variance to investigate the effect of cell mountant on λ_{max}. As such, the interaction term between mountant type and cell type (i.e. the spectral location of the λ_{max}) could not be used (Seamen *et al.*, 1994). Even though all of the λ_{max} values for photoreceptors measured whilst mounted in GPBS were at slightly longer wavelengths than those measured whilst mounted in DPBS, the effect of mountant on λ_{max} was found to be non-significant ($F_{1,69} = 2.02$, $p = 0.160$). Because the use of GPBS did not significantly affect the spectral location of the λ_{max}, and because it reduced wavelength-dependent light scatter in the MSP preparations, it was used subsequently as a mountant for the microspectrophotometric examination of the blackbird, blue tit and peacock visual pigments.

Glycerol was also noticed to have a mild preservative effect on MSP preparations. This was of great value in extending the period during which satisfactory records of outer segment absorbance could be obtained.

Although the mean absorbance spectra of visual pigments measured whilst mounted in both DPBS and GPBS are displayed in the ensuing figures, the following description uses the data obtained from GPBS-mounted outer segments.

A single class of rod contained a visual pigment with a mean pre-bleach λ_{max} at 505 nm (n = 6). There were four different types of single cone, each of which was reliably associated with a different type of oil droplet. Single cones containing R-type oil droplets (mean λ_{cut} 514 nm, n = 26) were paired with a LWS visual pigment which had a mean pre-bleach λ_{max} of 564 nm (n = 10).

Y-type oil droplets (mean λ_{cut} 490 nm, n = 36) were paired with a MWS visual pigment that had a mean pre-bleach λ_{max} of 505 nm (n = 10). Single cones containing a C-type droplet (mean λ_{cut} 437 nm, n = 10) were associated with a SWS visual pigment of mean pre-bleach λ_{max} 460 nm (n = 5). The fourth type of single cone contained an violet-sensitive (VS) visual pigment, of mean pre-bleach λ_{max} 419 nm (n = 4), and a T-type oil droplet which showed no detectable absorbance above 330 nm.

Both members of the double cone pair contained visual pigments resembling the LWS visual pigment measured in the single cones. The visual pigment in the principal member had a pre-bleach λ_{max} of 564 nm (n = 8) and was paired with a P-type oil droplet with a mean λ_{cut} at 436 nm (n = 12), which was independent of retinal location, and a shoulder in the absorptance spectrum at approximately 480 nm. The visual pigment in the accessory member of the double cone had a mean pre-bleach λ_{max} of 564 nm (n = 5). No A-type droplet was observed in the accessory cones, nor was any carotenoid detected at the distal end of their inner segments.

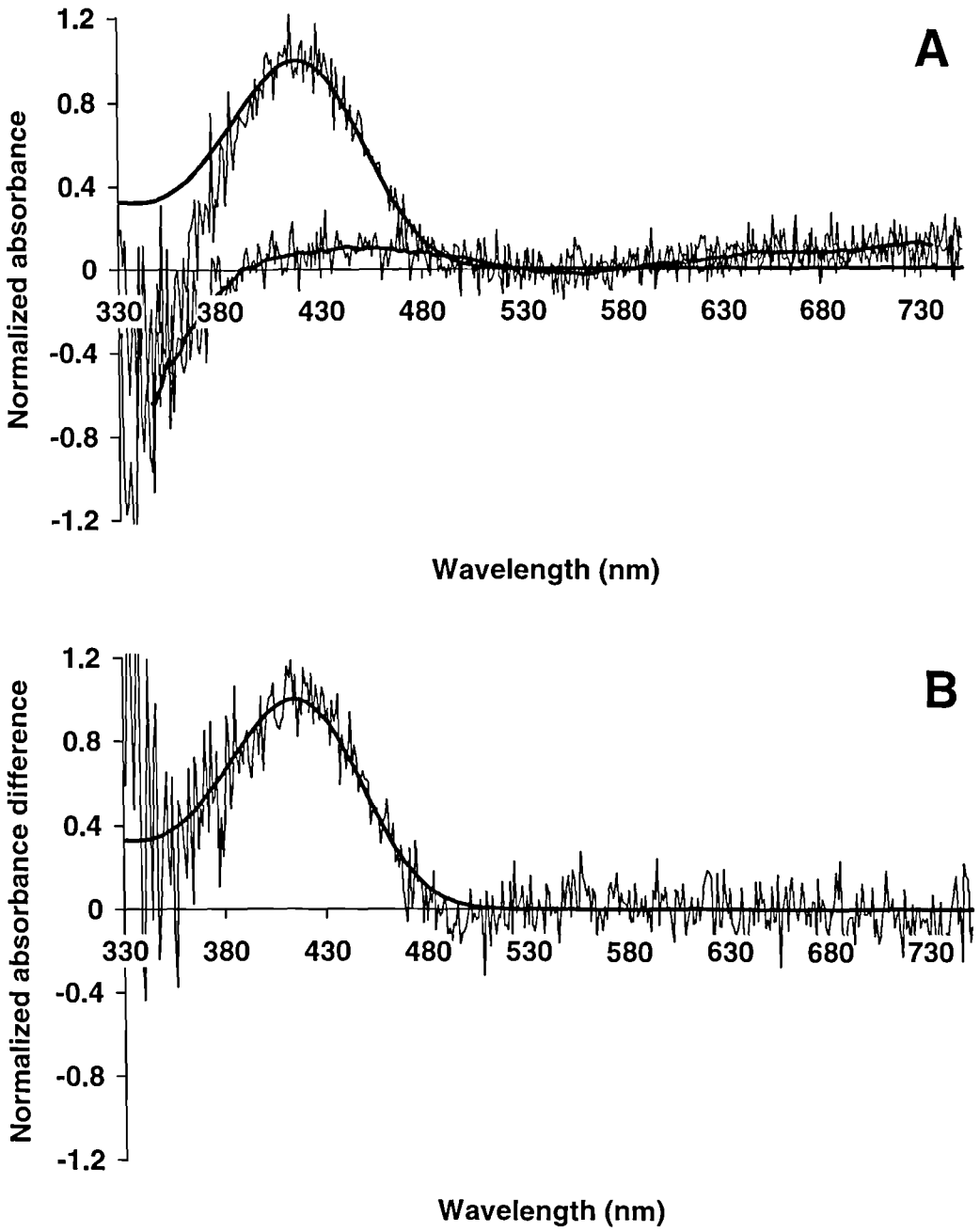

Figure 2.24 Microspectrophotometric results from 2 VS single cones of the domestic turkey, *Meleagris gallopavo*, measured whilst mounted in 5% DPBS. (**A**) Mean pre-bleach absorbance spectrum (upper trace) with best-fitted visual pigment template (λ_{max} 418 nm, solid line) and mean post-bleach absorbance spectrum (lower trace) with running average (solid line). (**B**) Mean difference spectrum (trace) with best-fitted visual pigment template (λ_{max} 415 nm, solid line).

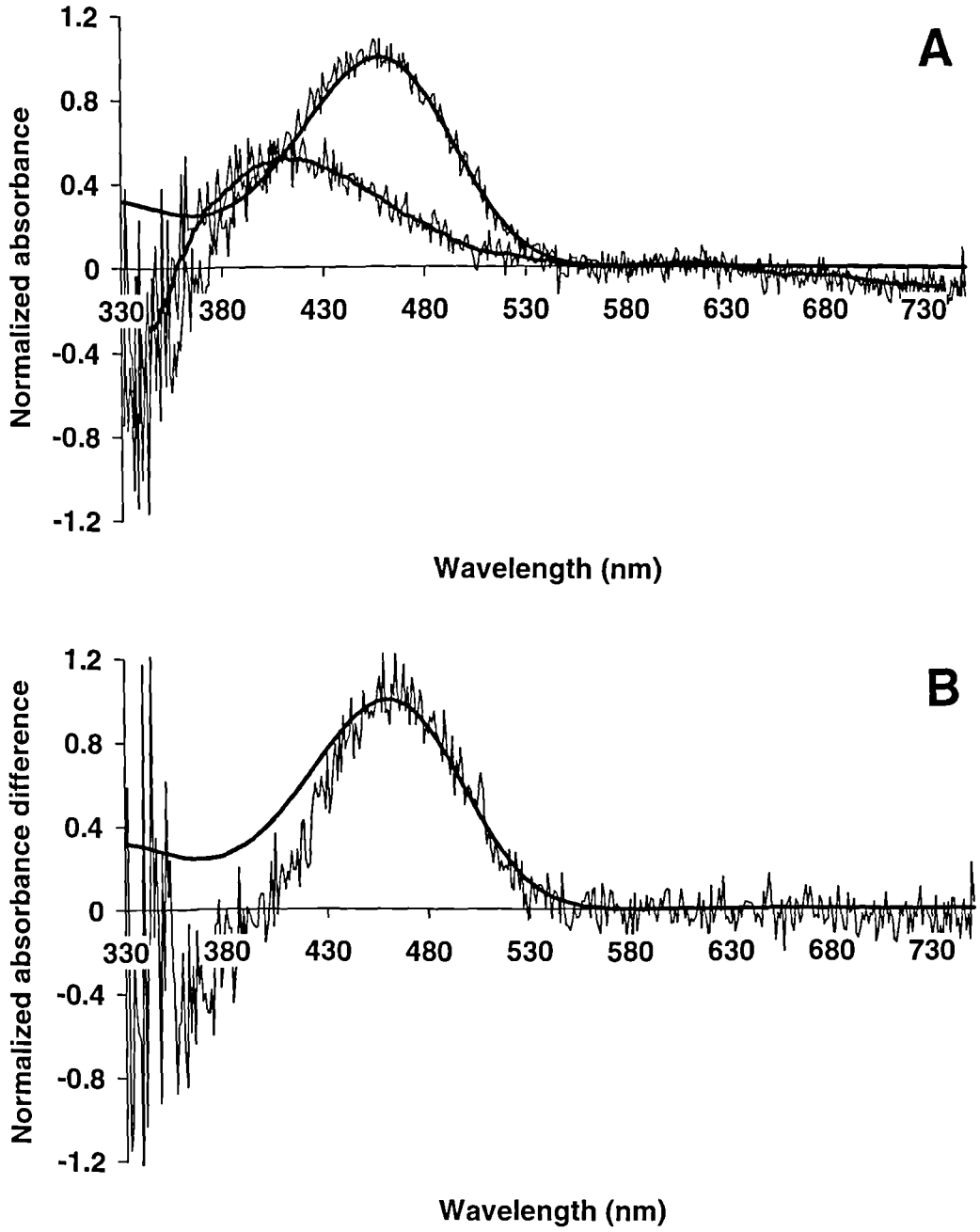

Figure 2.25 Microspectrophotometric results from 4 SWS single cones of the domestic turkey, *Meleagris gallopavo*, measured whilst mounted in 5% DPBS. (**A**) Mean pre-bleach absorbance spectrum (upper trace) with best-fitted visual pigment template (λ_{max} 458 nm, solid line) and mean post-bleach absorbance spectrum (lower trace) with running average (solid line). (**B**) Mean difference spectrum (trace) with best-fitted visual pigment template (λ_{max} 460 nm, solid line).

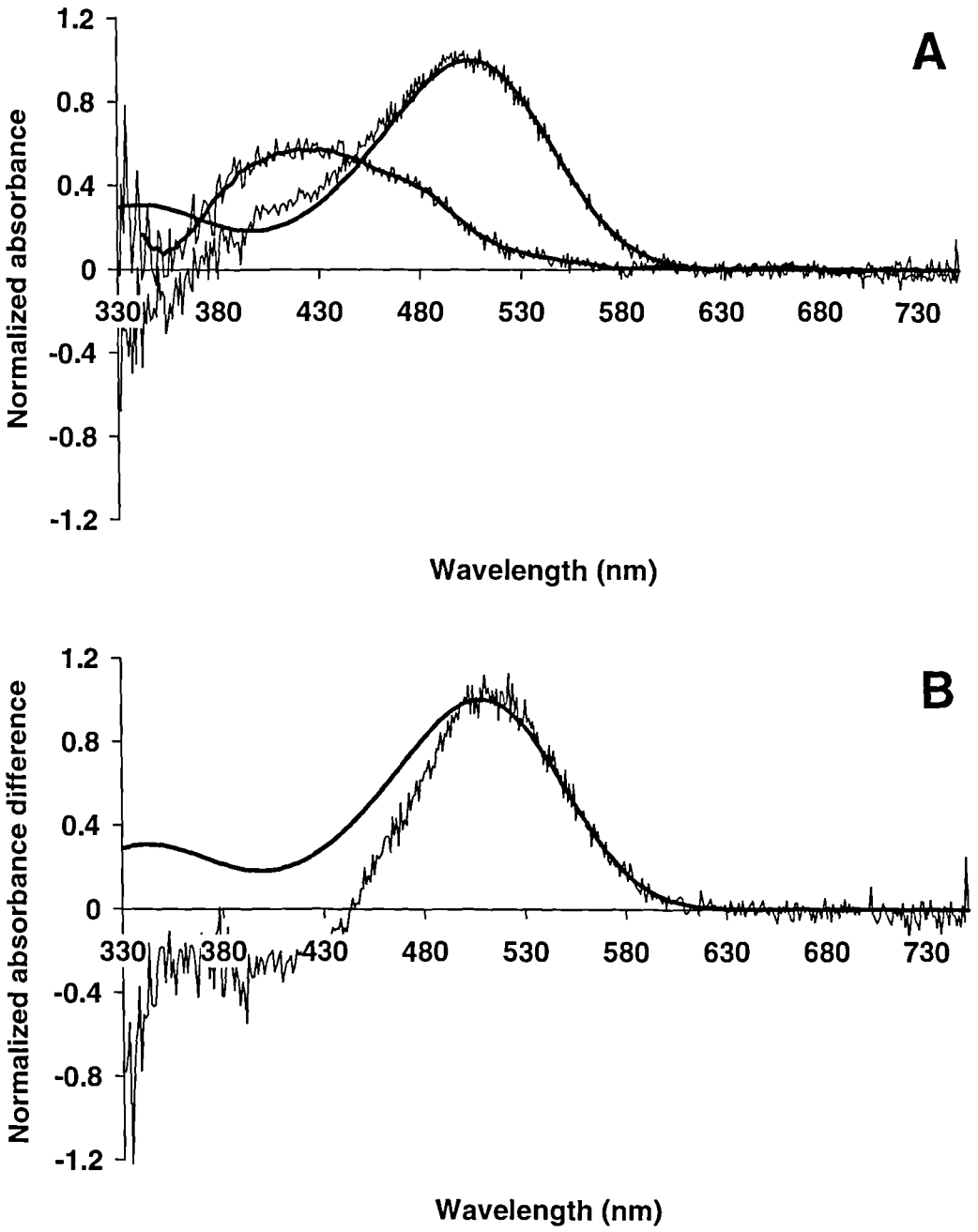

Figure 2.26 Microspectrophotometric results from 9 MWS single cones of the domestic turkey, *Meleagris gallopavo*, measured whilst mounted in 5% DPBS. (**A**) Mean pre-bleach absorbance spectrum (upper trace) with best-fitted visual pigment template (λ_{max} 505 nm, solid line) and mean post-bleach absorbance spectrum (lower trace) with running average (solid line). (**B**) Mean difference spectrum (trace) with best-fitted visual pigment template (λ_{max} 508 nm, solid line).

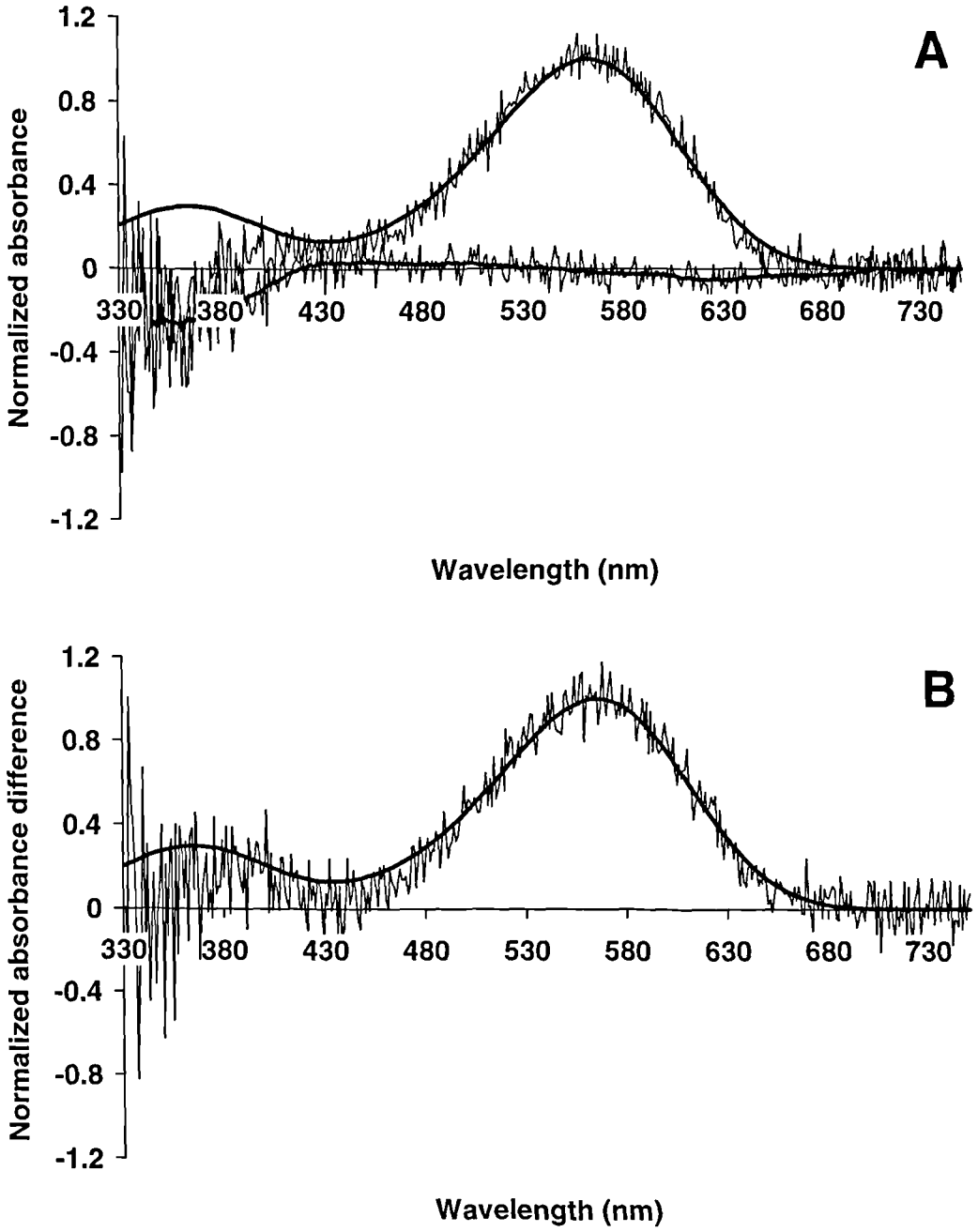

Figure 2.27 Microspectrophotometric results from 3 LWS single cones of the domestic turkey, *Meleagris gallopavo*, measured whilst mounted in 5% DPBS. (**A**) Mean pre-bleach absorbance spectrum (upper trace) with best-fitted visual pigment template (λ_{max} 563 nm, solid line) and mean post-bleach absorbance spectrum (lower trace) with running average (solid line). (**B**) Mean difference spectrum (trace) with best-fitted visual pigment template (λ_{max} 566 nm, solid line).

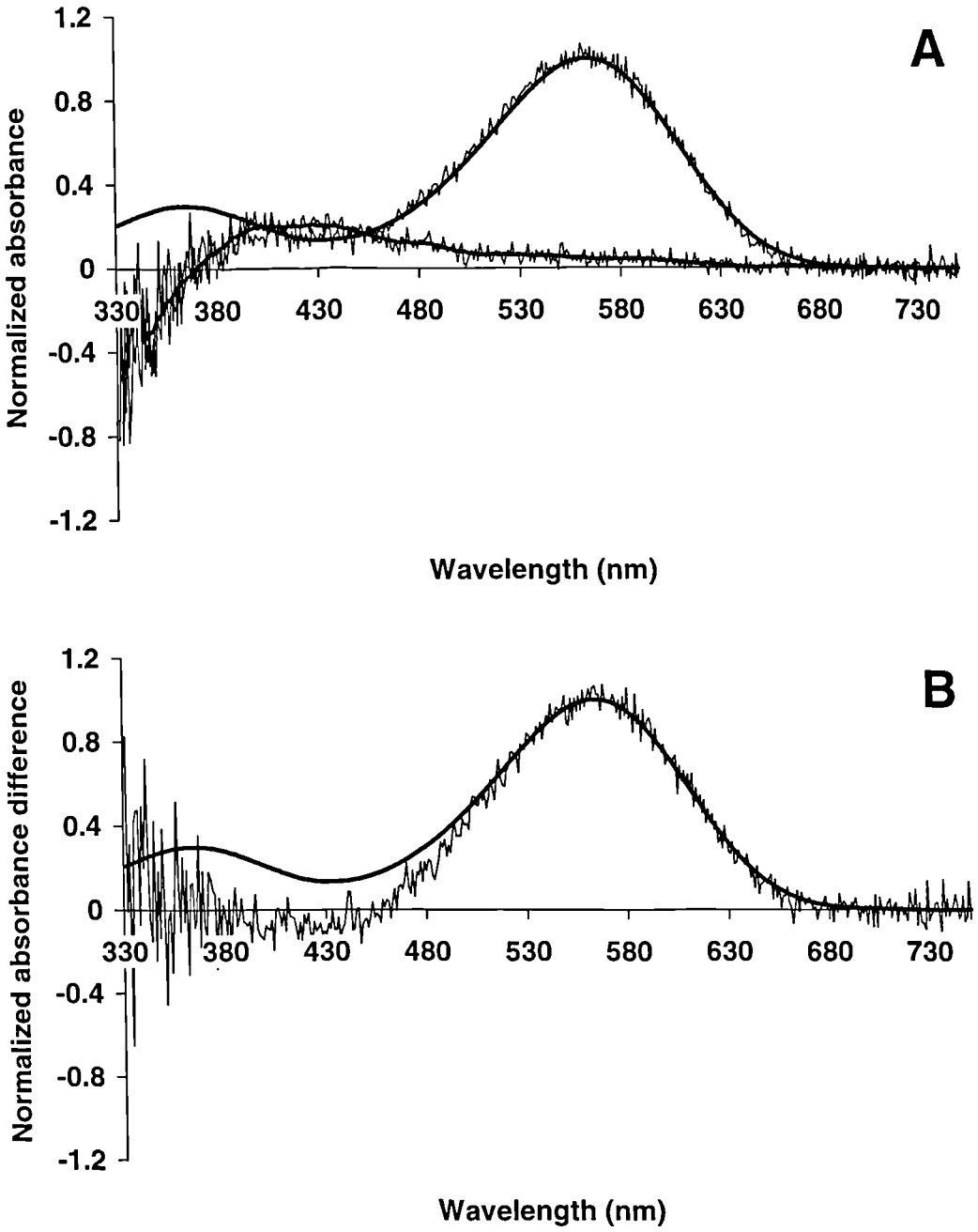

Figure 2.28 Microspectrophotometric results from 9 principal members of the double cone of the domestic turkey, *Meleagris gallopavo*, measured whilst mounted in 5% DPBS. (**A**) Mean pre-bleach absorbance spectrum (upper trace) with best-fitted visual pigment template (λ_{max} 564 nm, solid line) and mean post-bleach absorbance spectrum (lower trace) with running average (solid line). (**B**) Mean difference spectrum (trace) with best-fitted visual pigment template (λ_{max} 564 nm, solid line).

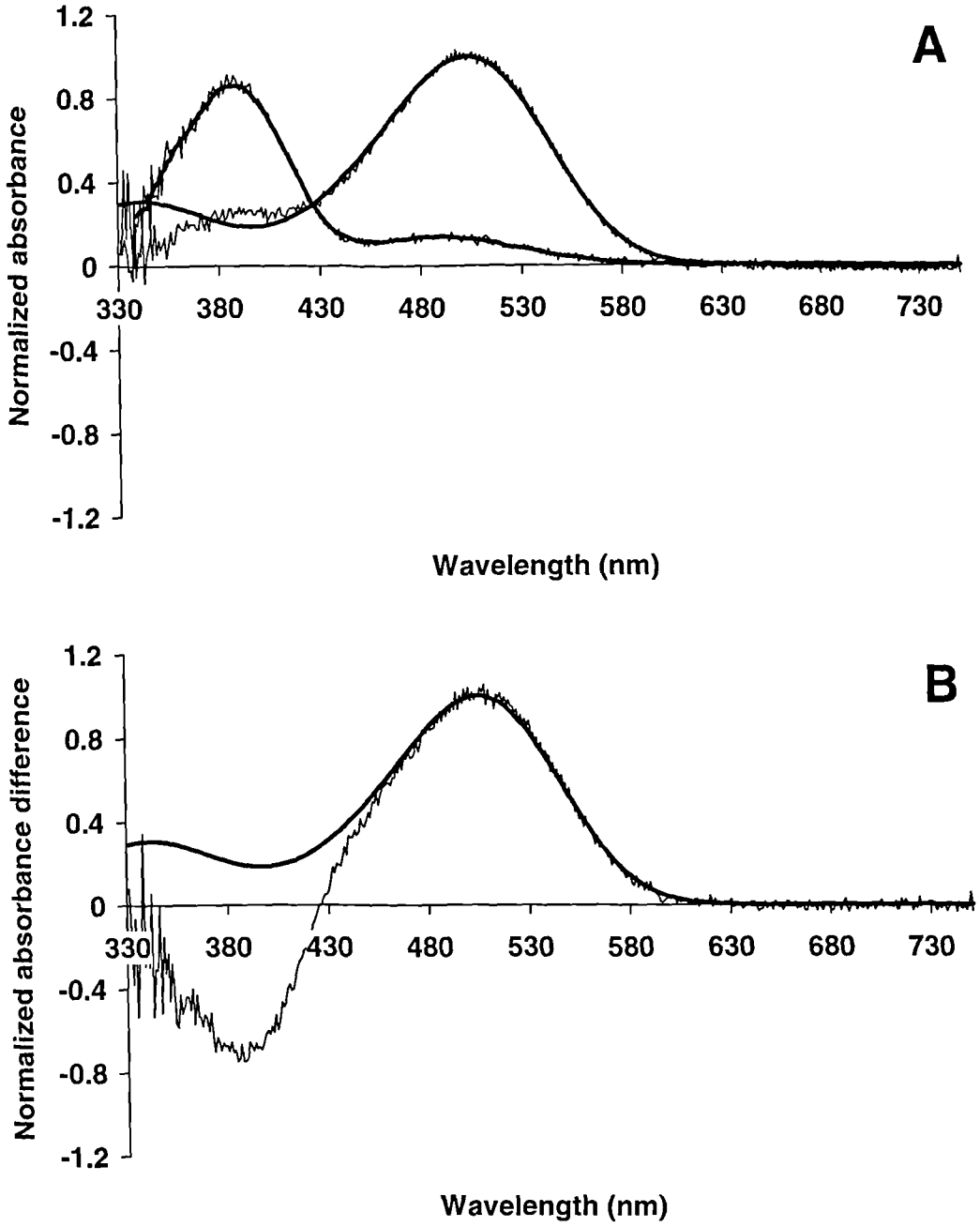

Figure 2.29 Microspectrophotometric results from 6 rods of the domestic turkey, *Meleagris gallopavo*, measured whilst mounted in 5% DPBS. (**A**) Mean pre-bleach absorbance spectrum (upper trace) with best-fitted visual pigment template (λ_{max} 504 nm, solid line) and mean post-bleach absorbance spectrum (lower trace) with running average (solid line). (**B**) Mean difference spectrum (trace) with best-fitted visual pigment template (λ_{max} 505 nm, solid line).

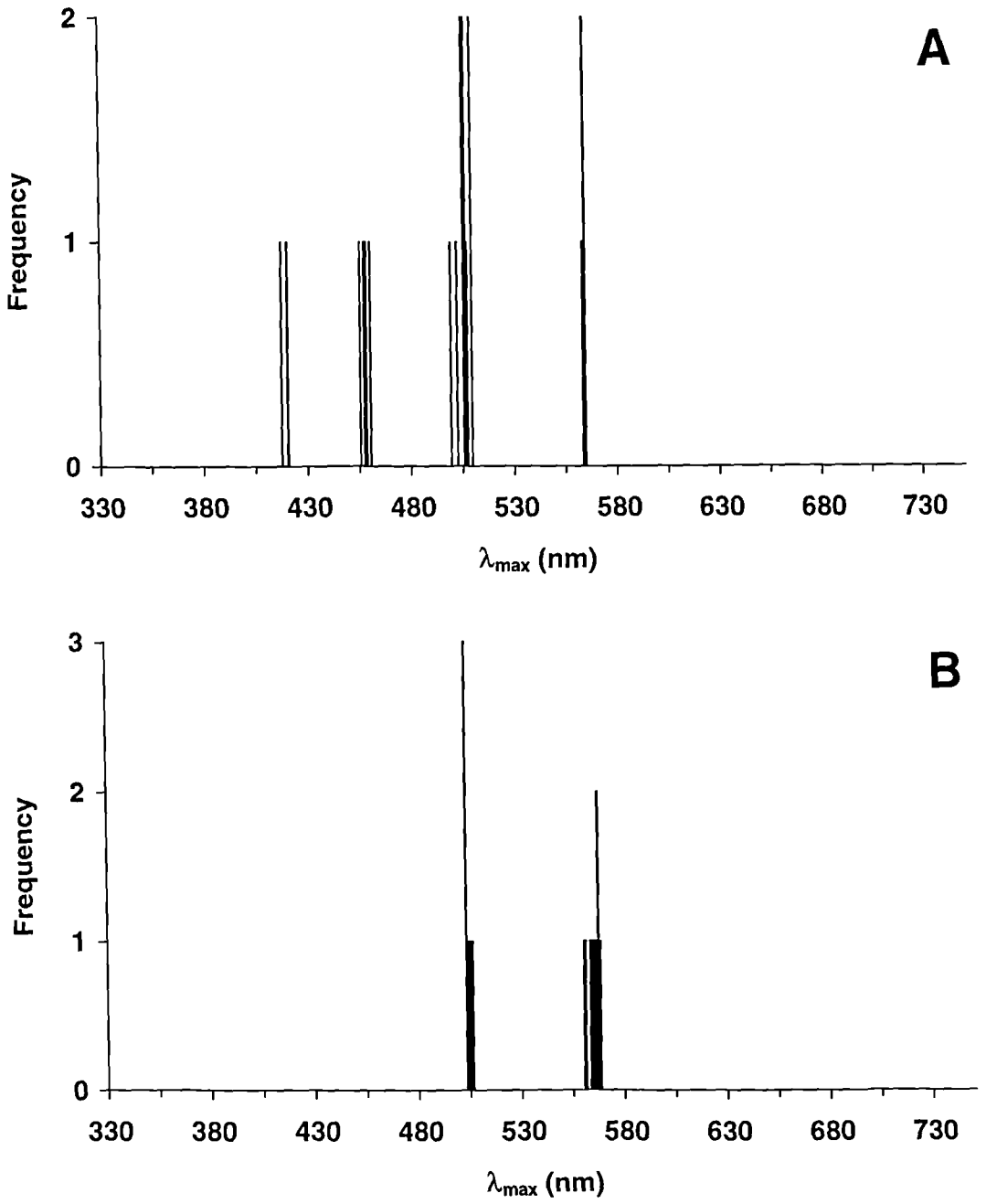

Figure 2.30 Histogram showing the distribution of estimated λ_{max} values obtained from pre-bleach absorbance spectra of visual pigments in the domestic turkey, *Meleagris gallopavo*, measured whilst mounted in 5 % DPBS. (**A**) Single cones. λ_{max} values around 418, 457, 505 and 563 nm describe VS, SWS, MWS and LWS visual pigments respectively. (**B**) Rods and double cones. λ_{max} values around 504 nm describe rod visual pigment, whilst λ_{max} values around 564 nm describe the LWS visual pigment found in the principal member of the double cones.

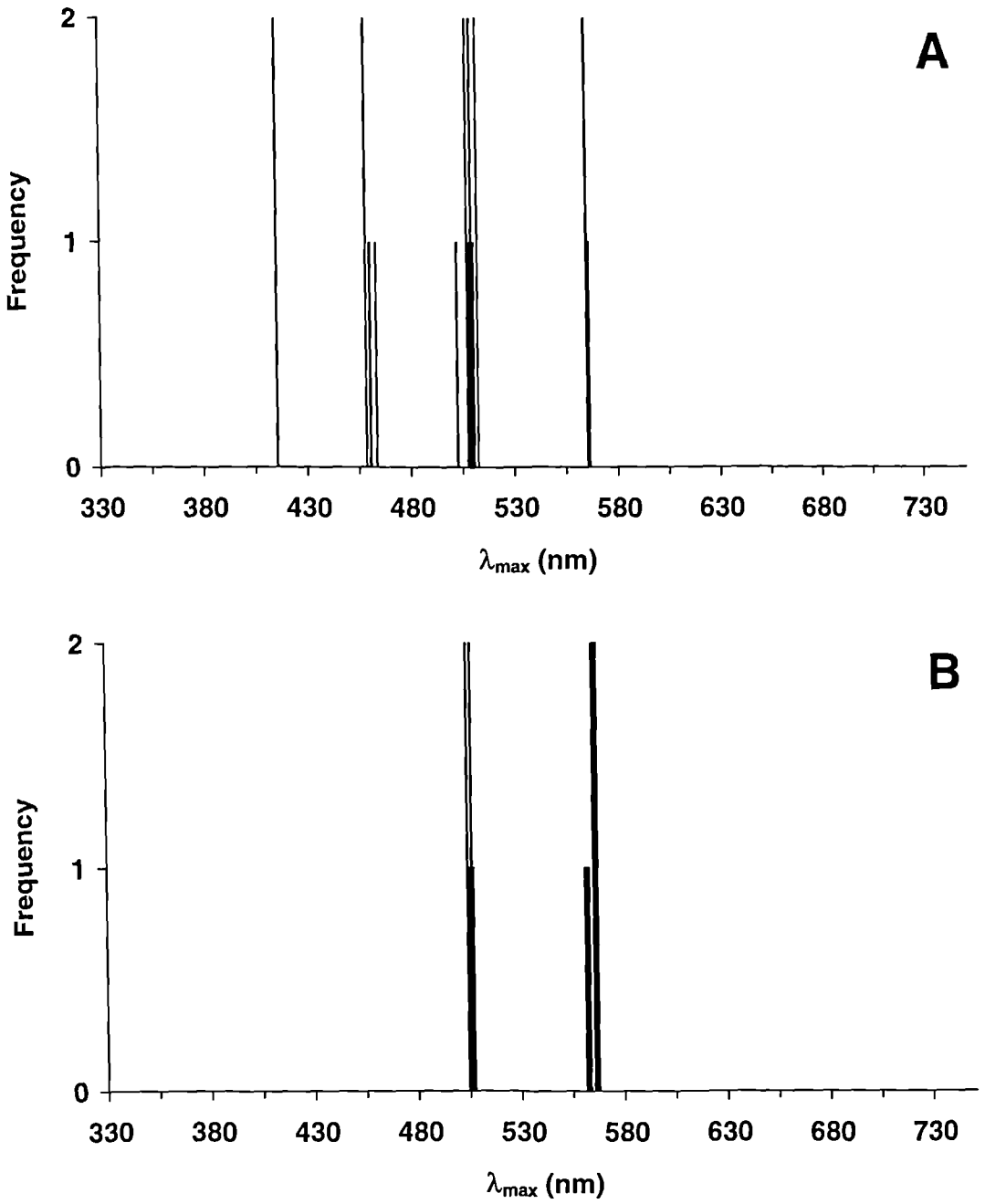

Figure 2.31 Histogram showing the distribution of estimated λ_{max} values obtained from difference spectra of visual pigments in the domestic turkey, *Meleagris gallopavo*, measured whilst mounted in 5 % DPBS. (**A**) Single cones. λ_{max} values around 415, 459, 508 and 563 nm describe VS, SWS, MWS and LWS visual pigments respectively. (**B**) Rods and double cones. λ_{max} values around 505 nm describe rod visual pigment, whilst λ_{max} values around 564 nm describe the LWS visual pigment found in the principal member of the double cones.

	Rod	Single Cones			Double cone	
DPBS		VS	SWS	MWS	LWS	Principal	Accessory
Visual pigments							
λ_{max} of mean pre-bleach spectrum (nm)	503.5 ± 0.9	418.2 ± 4.0	457.6 ± 2.7	504.6 ± 1.8	563.4 ± 4.5	564.2 ± 2.2	-
Mean of pre-bleach λ_{max} (nm)	503.7 ± 1.3	418.1 ± 2.2	457.0 ± 2.1	504.8 ± 3.2	563.2 ± 0.4	564.2 ± 2.7	-
λ_{max} of mean difference spectrum (nm)	504.8 ± 1.3	414.5 ± 5.5	460.1 ± 5.3	508.0 ± 2.6	565.5 ± 5.5	564.2 ± 2.8	-
Transverse absorbance at λ_{max} of mean difference spectrum	0.052	0.009	0.014	0.019	0.022	0.017	-
Mean of difference spectrum λ_{max} (nm)	504.9 ± 1.3	414.7 ± 0.2	459.4 ± 2.6	507.9 ± 3.2	565.3 ± 0.6	564.0 ± 2.1	-
Number of cells	6	2	4	9	3	9	-

Table 2.4 Summary of the microspectrophotometric results obtained for the visual pigments of the domestic turkey, *Meleagris gallopavo*, measured whilst mounted in 5 % dextran in phosphate-buffered saline (DPBS).

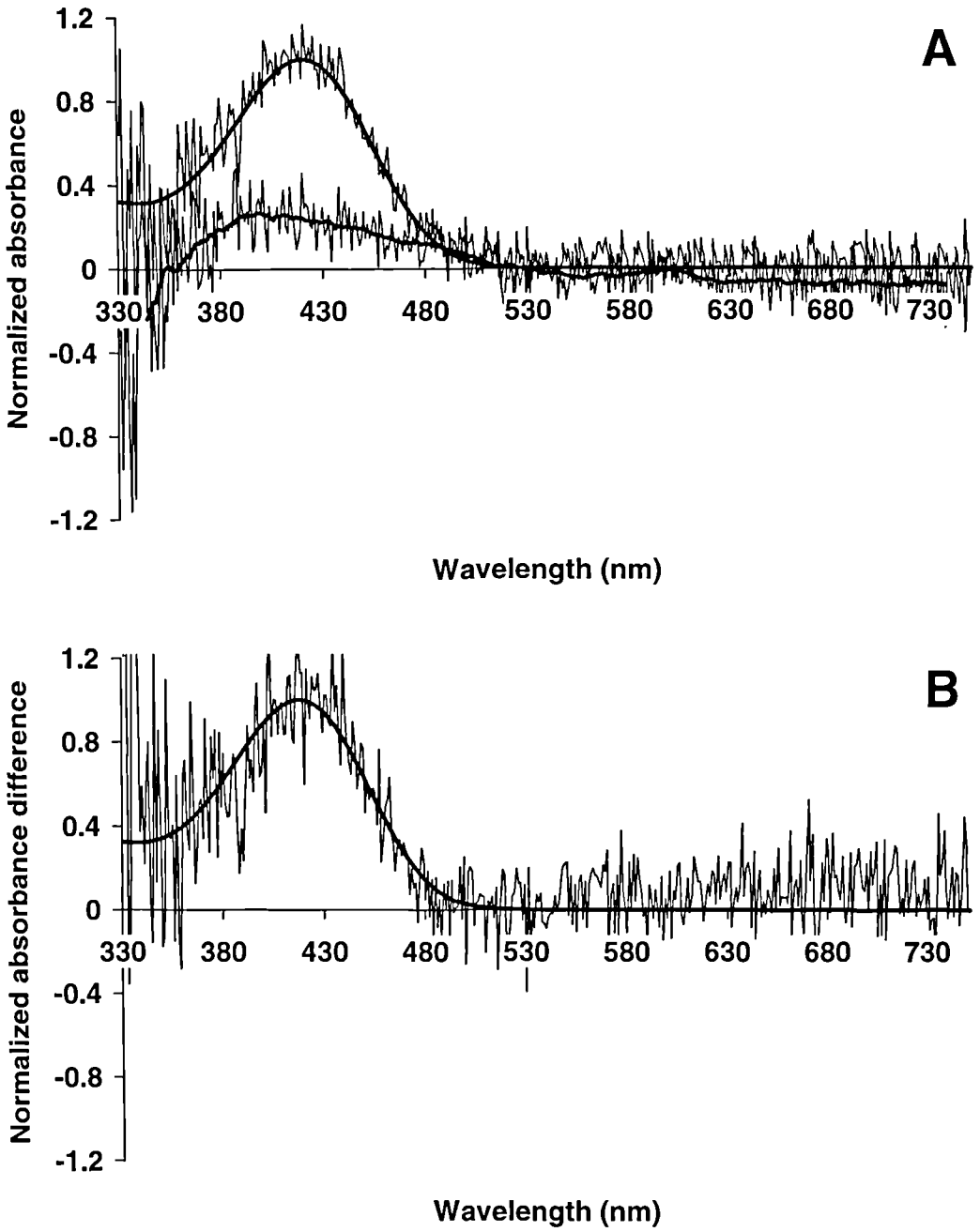

Figure 2.32 Microspectrophotometric results from 4 VS single cones of the domestic turkey, *Meleagris gallopavo*, measured whilst mounted in 75% GPBS. (**A**) Mean pre-bleach absorbance spectrum (upper trace) with best-fitted visual pigment template (λ_{max} 421 nm, solid line) and mean post-bleach absorbance spectrum (lower trace) with running average (solid line). (**B**) Mean difference spectrum (trace) with best-fitted visual pigment template (λ_{max} 418 nm, solid line).

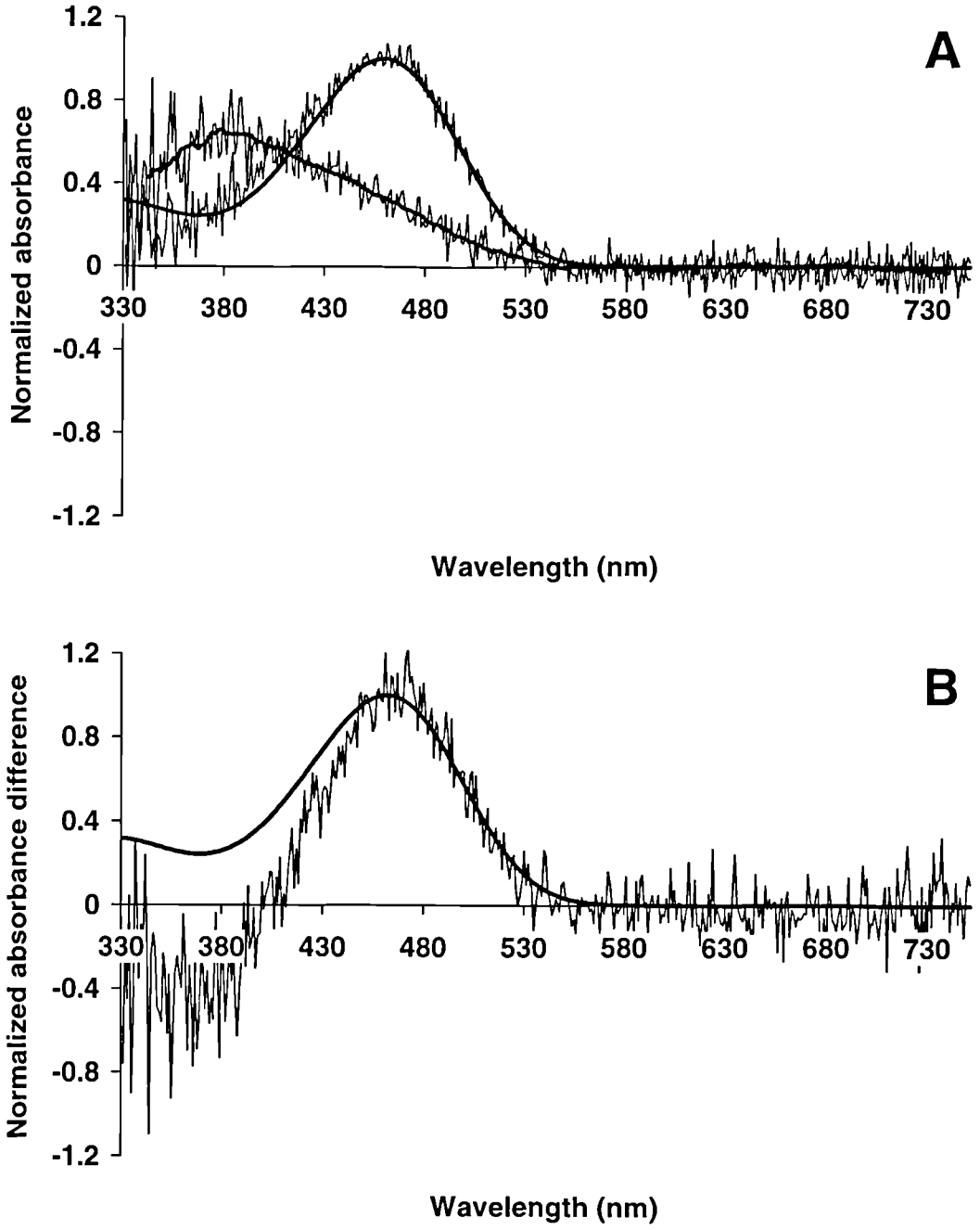

Figure 2.33 Microspectrophotometric results from 5 SWS single cones of the domestic turkey, *Meleagris gallopavo*, measured whilst mounted in 75% GPBS. (**A**) Mean pre-bleach absorbance spectrum (upper trace) with best-fitted visual pigment template (λ_{max} 460 nm, solid line) and mean post-bleach absorbance spectrum (lower trace) with running average (solid line). (**B**) Mean difference spectrum (trace) with best-fitted visual pigment template (λ_{max} 462 nm, solid line).

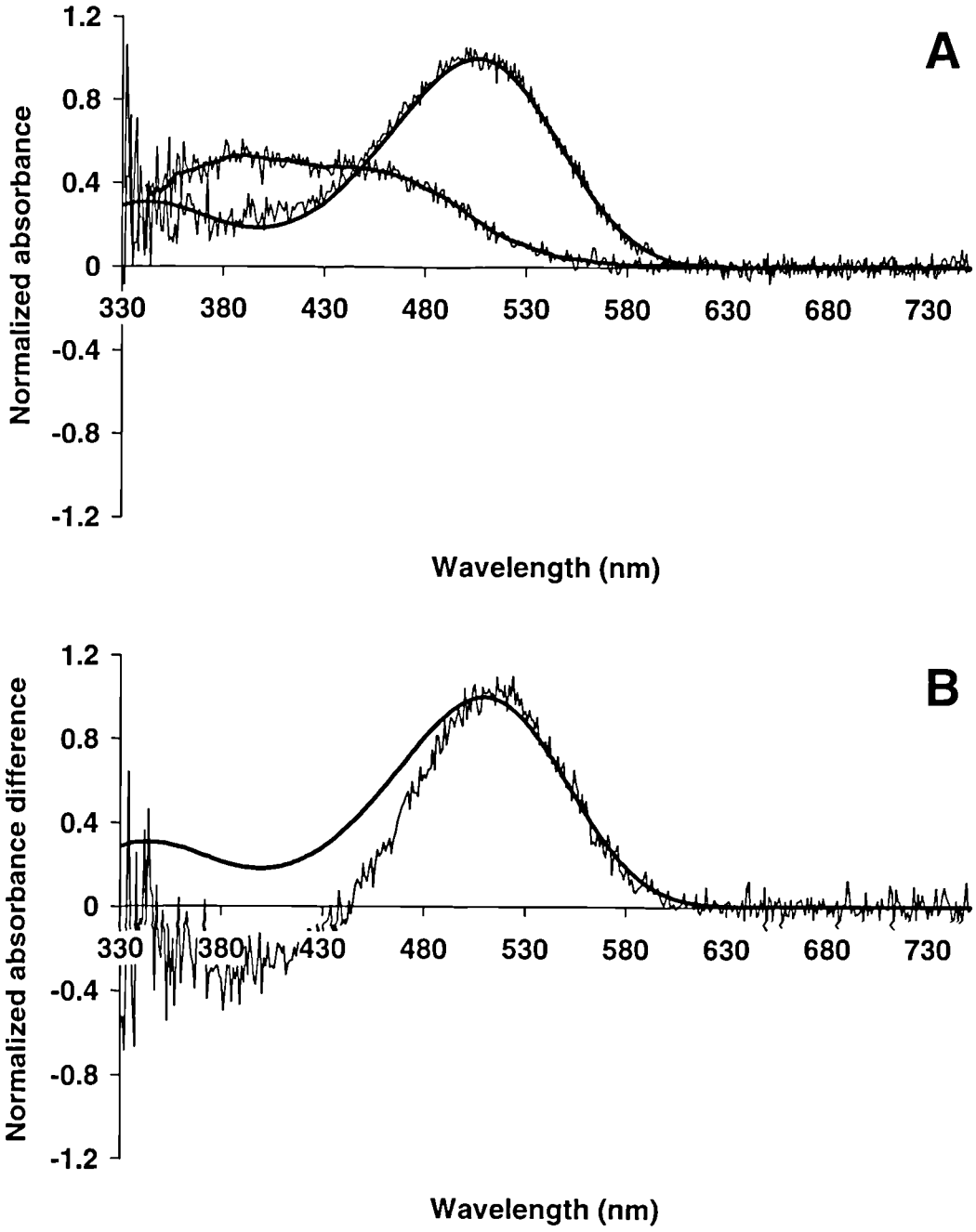

Figure 2.34 Microspectrophotometric results from 10 MWS single cones of the domestic turkey, *Meleagris gallopavo*, measured whilst mounted in 75% GPBS. (**A**) Mean pre-bleach absorbance spectrum (upper trace) with best-fitted visual pigment template (λ_{max} 506 nm, solid line) and mean post-bleach absorbance spectrum (lower trace) with running average (solid line). (**B**) Mean difference spectrum (trace) with best-fitted visual pigment template (λ_{max} 510 nm, solid line).

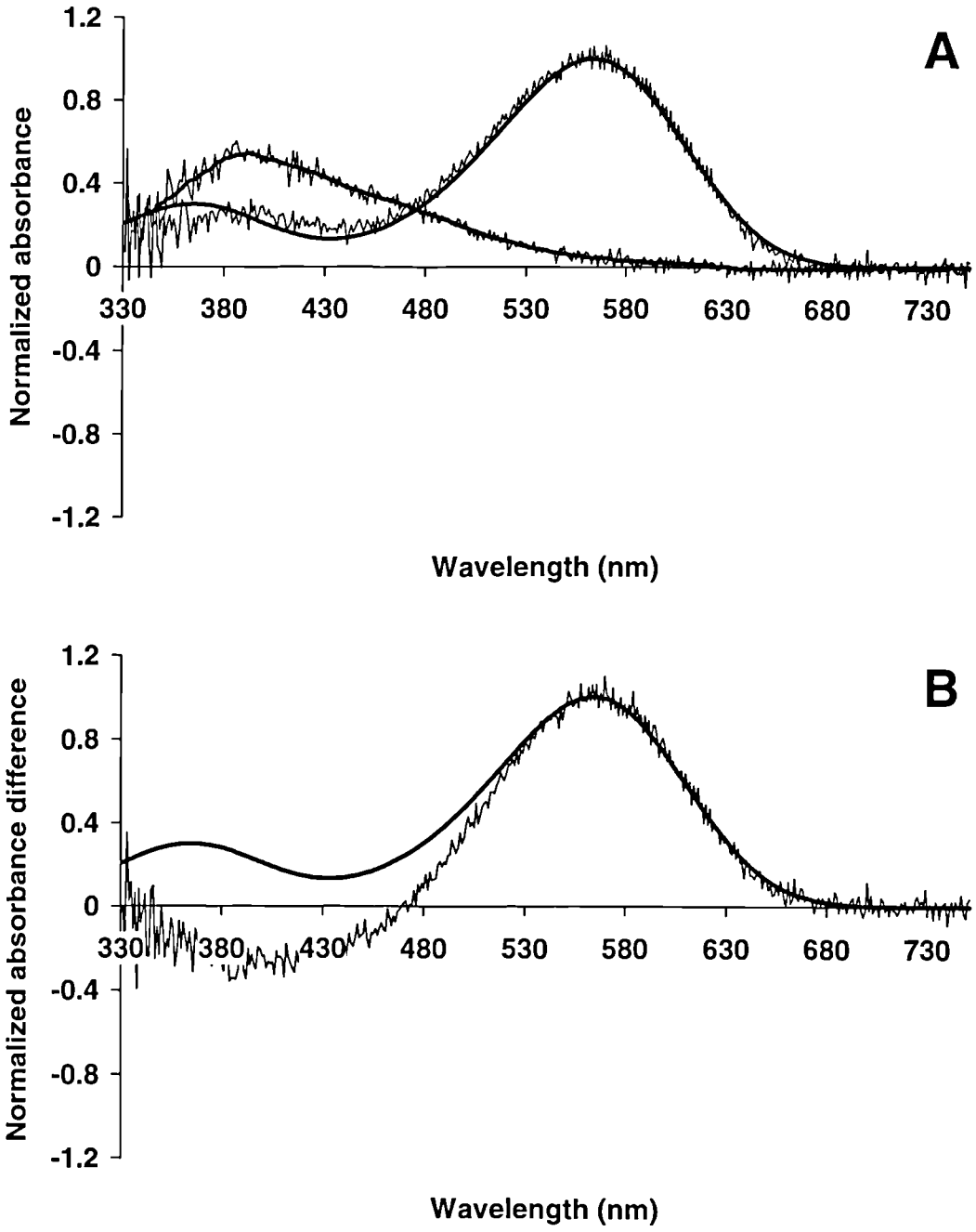

Figure 2.35 Microspectrophotometric results from 10 LWS single cones of the domestic turkey, *Meleagris gallopavo*, measured whilst mounted in 75% GPBS. (**A**) Mean pre-bleach absorbance spectrum (upper trace) with best-fitted visual pigment template (λ_{max} 564 nm, solid line) and mean post-bleach absorbance spectrum (lower trace) with running average (solid line). (**B**) Mean difference spectrum (trace) with best-fitted visual pigment template (λ_{max} 564 nm, solid line).

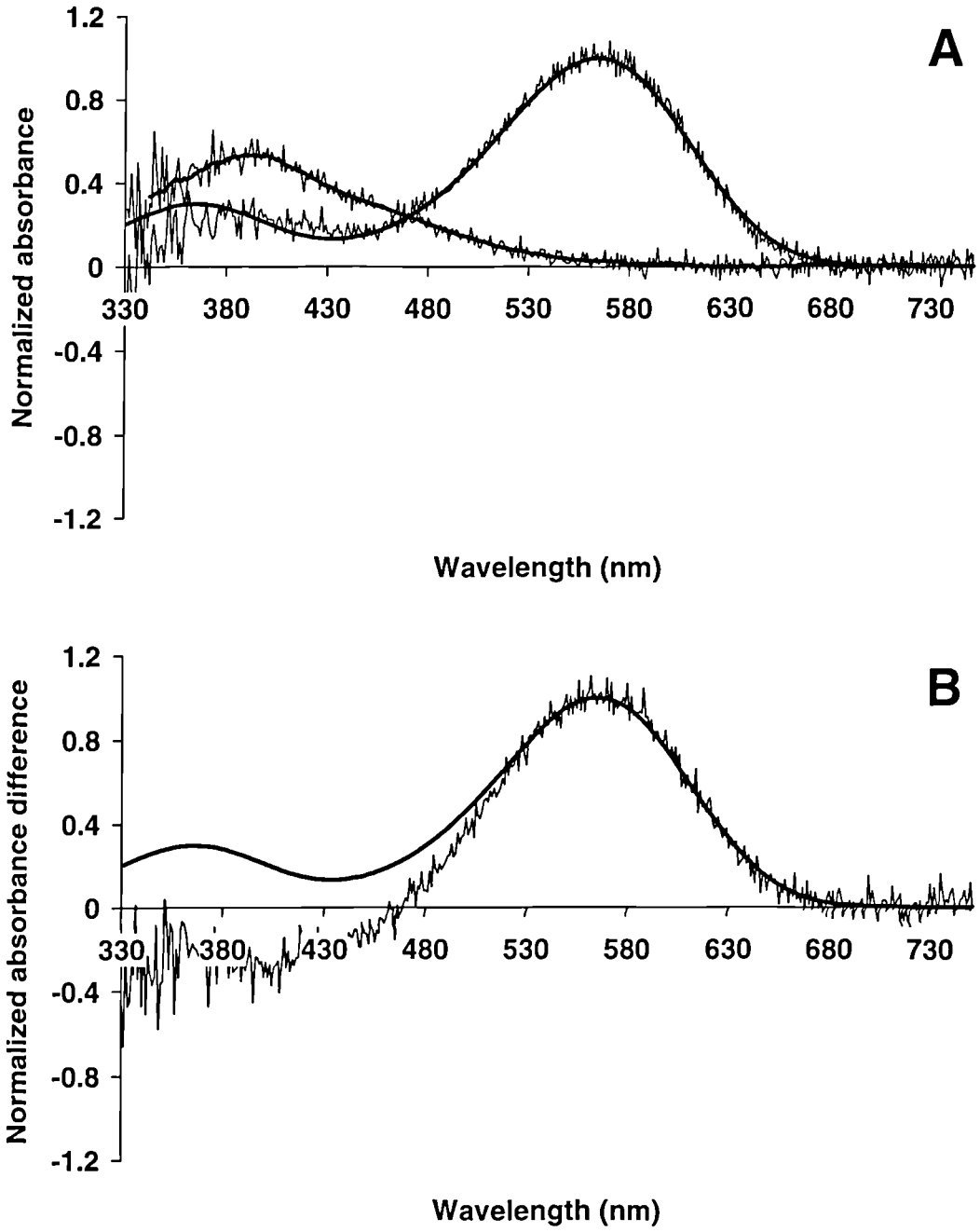

Figure 2.36 Microspectrophotometric results from 8 principal members of the double cone of the domestic turkey, *Meleagris gallopavo*, measured whilst mounted in 75% GPBS. (**A**) Mean pre-bleach absorbance spectrum (upper trace) with best-fitted visual pigment template (λ_{max} 564 nm, solid line) and mean post-bleach absorbance spectrum (lower trace) with running average (solid line). (**B**) Mean difference spectrum (trace) with best-fitted visual pigment template (λ_{max} 565 nm, solid line).

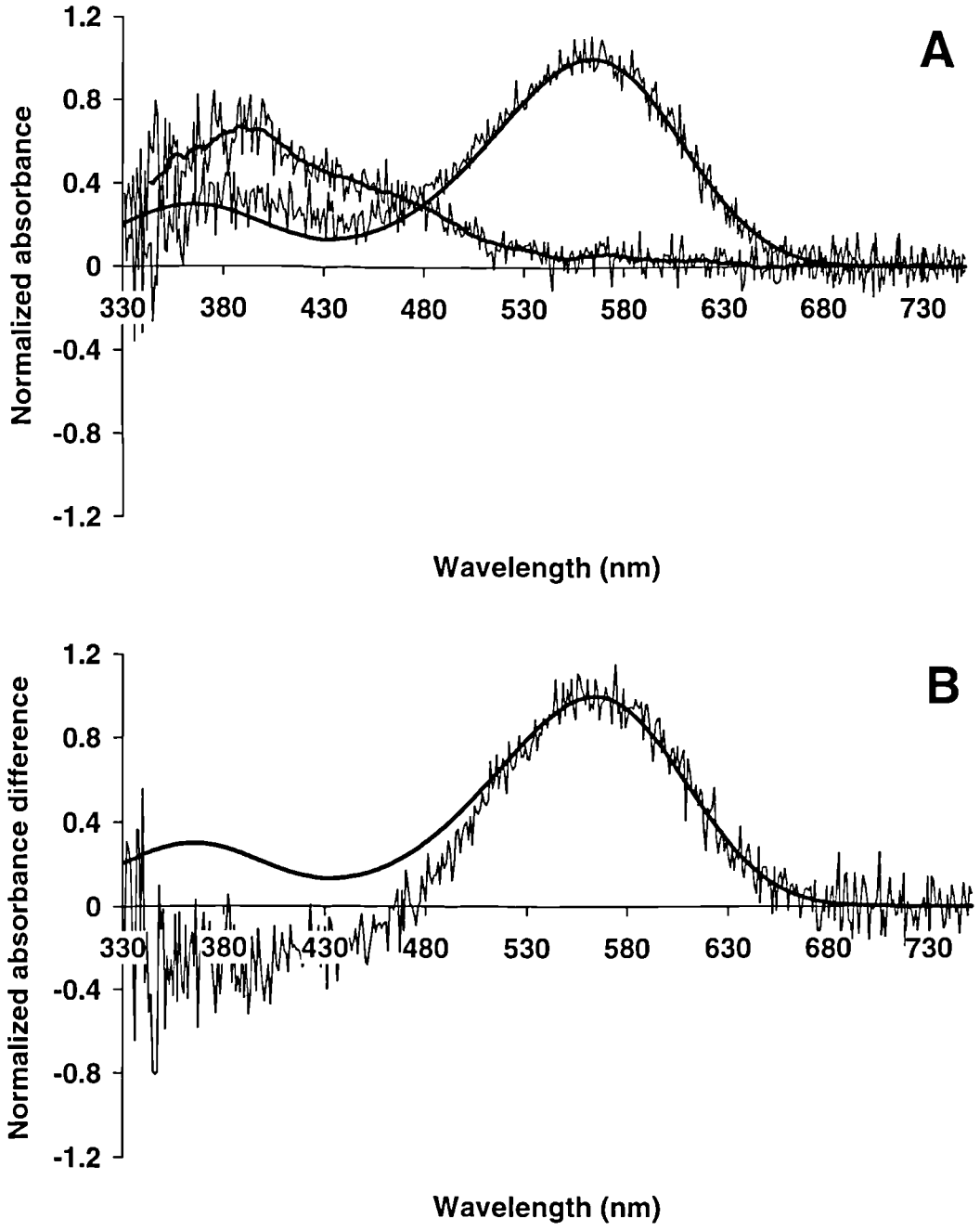

Figure 2.37 Microspectrophotometric results from 5 accessory members of the double cone of the domestic turkey, *Meleagris gallopavo*, measured whilst mounted in 75% GPBS. (**A**) Mean pre-bleach absorbance spectrum (upper trace) with best-fitted visual pigment template (λ_{max} 564 nm, solid line) and mean post-bleach absorbance spectrum (lower trace) with running average (solid line). (**B**) Mean difference spectrum (trace) with best-fitted visual pigment template (λ_{max} 564 nm, solid line).

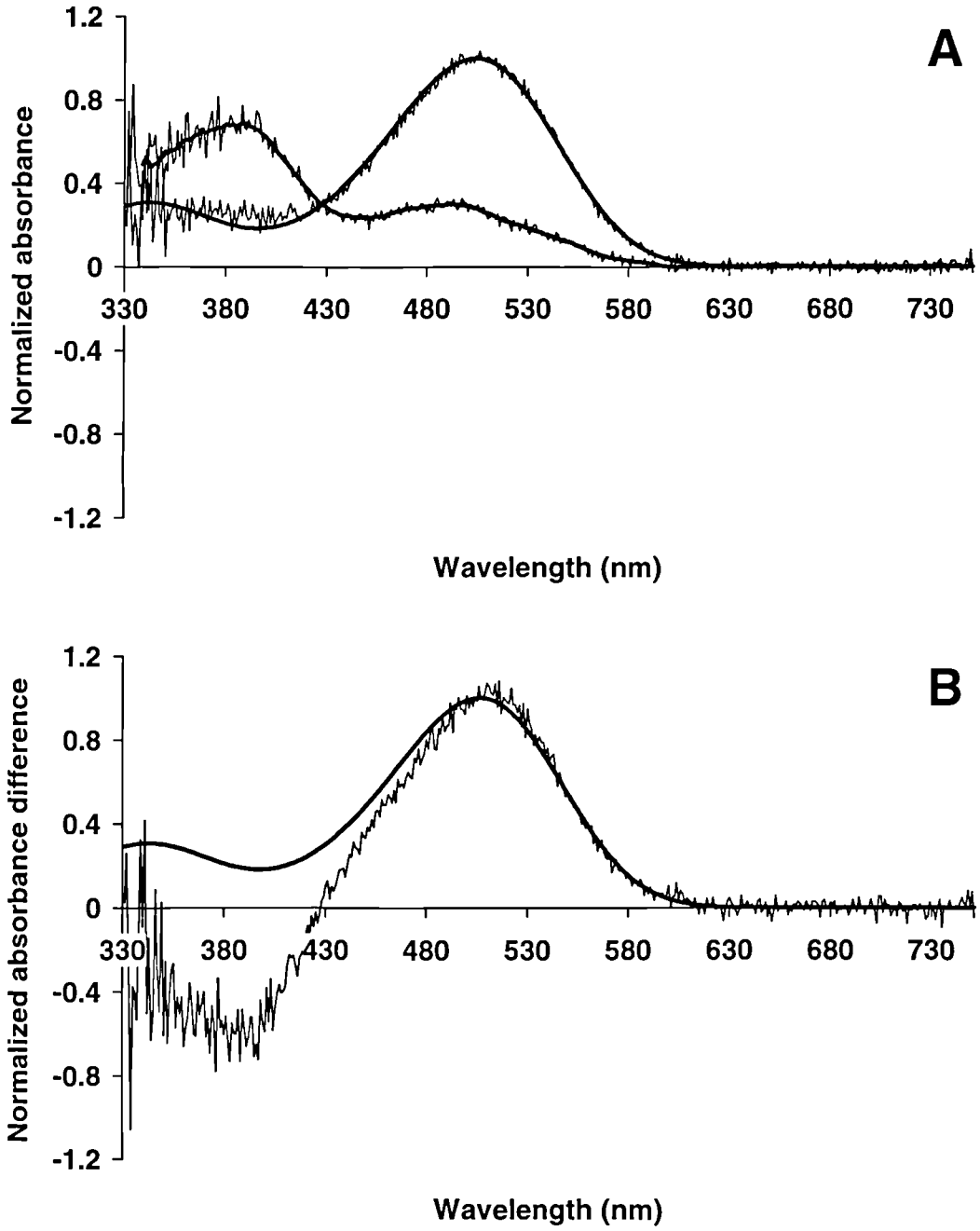

Figure 2.38 Microspectrophotometric results from 6 rods of the domestic turkey, *Meleagris gallopavo*, measured whilst mounted in 75% GPBS. (**A**) Mean pre-bleach absorbance spectrum (upper trace) with best-fitted visual pigment template (λ_{max} 504 nm, solid line) and mean post-bleach absorbance spectrum (lower trace) with running average (solid line). (**B**) Mean difference spectrum (trace) with best-fitted visual pigment template (λ_{max} 506 nm, solid line).

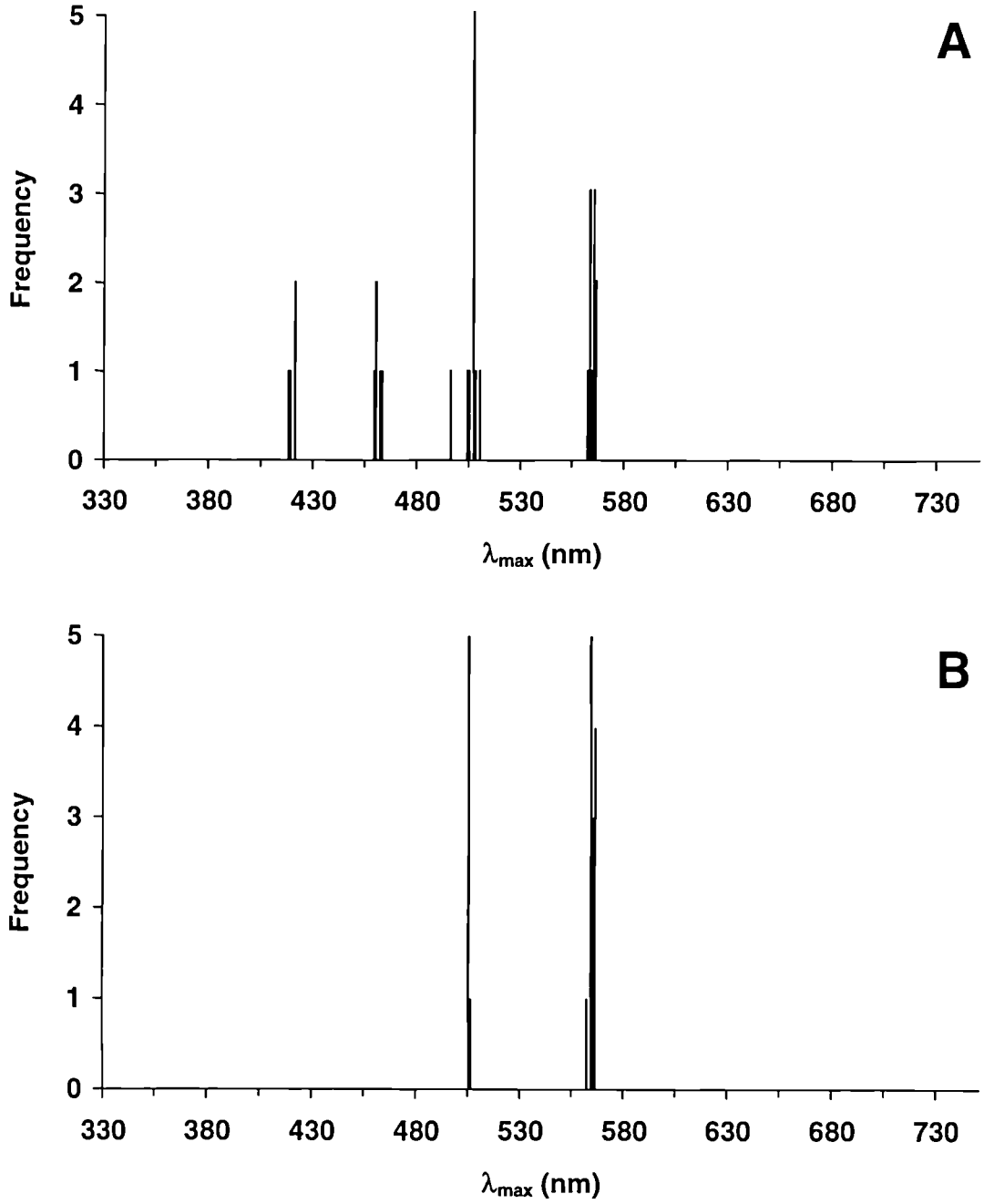

Figure 2.39 Histogram showing the distribution of estimated λ_{max} values obtained from pre-bleach absorbance spectra of visual pigments in the domestic turkey, *Meleagris gallopavo*, measured whilst mounted in 75 % GPBS. (**A**) Single cones. λ_{max} values around 419, 460, 505 and 564 nm describe VS, SWS, MWS and LWS visual pigments respectively. (**B**) Rods and double cones. λ_{max} values around 505 nm describe rod visual pigment, whilst λ_{max} values around 564 nm describe the LWS visual pigments found in the principal accessory members of the double cones.

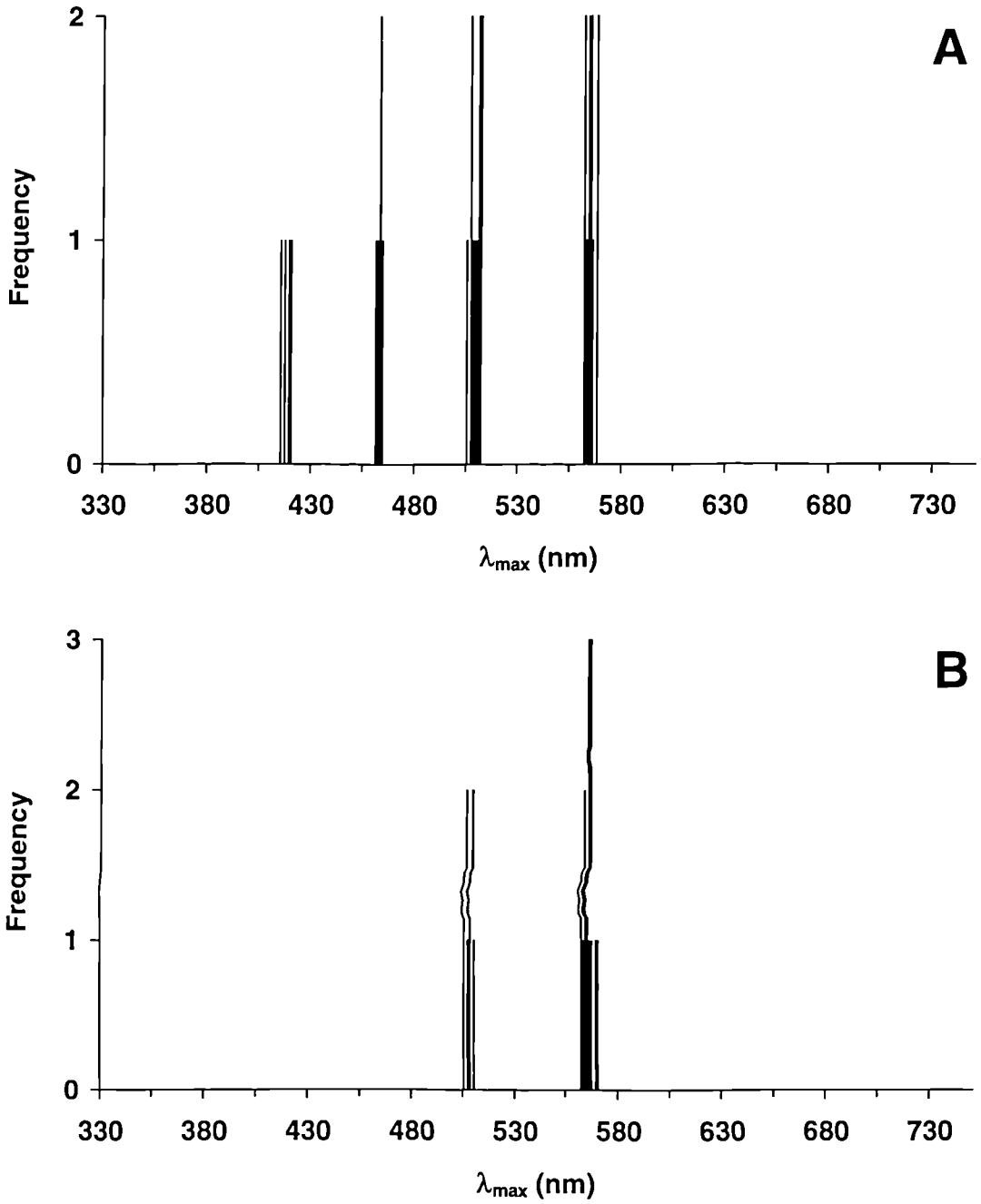

Figure 2.40 Histogram showing the distribution of estimated λ_{max} values obtained from difference spectra of visual pigments in the domestic turkey, *Meleagris gallopavo*, measured whilst mounted in 75 % GPBS. (**A**) Single cones. λ_{max} values around 417, 462, 509 and 564 nm describe VS, SWS, MWS and LWS visual pigments respectively. (**B**) Rods and double cones. λ_{max} values around 507 nm describe rod visual pigment, whilst λ_{max} values around 565 nm describe the LWS visual pigments found in the principal accessory members of the double cones.

	Rod	Single Cones			Double cone	
GPBS		VS	SWS	MWS	LWS	Principal	Accessory
Visual pigments							
λ_{max} of mean pre-bleach spectrum (nm)	504.2 ± 1.1	420.6 ± 3.4	459.5 ± 3.0	505.5 ± 2.0	563.6 ± 2.4	564.2 ± 2.9	563.9 ± 4.9
Mean of pre-bleach λ_{max} (nm)	504.5 ± 0.4	419.3 ± 1.3	460.1 ± 1.7	505.3 ± 3.7	563.7 ± 1.2	564.3 ± 1.3	563.9 ± 0.9
λ_{max} of mean difference spectrum (nm)	506.3 ± 2.0	417.7 ± 6.3	462.0 ± 5.4	509.5 ± 3.4	564.2 ± 2.6	565.4 ± 3.1	563.5 ± 5.9
Transverse absorbance at λ_{max} of mean difference spectrum	0.035	0.009	0.011	0.016	0.025	0.019	0.014
Mean of difference spectrum λ_{max} (nm)	506.5 ± 2.0	417.3 ± 2.1	462.2 ± 1.1	508.6 ± 2.3	564.3 ± 1.9	564.9 ± 1.7	564.3 ± 3.3
Number of cells	6	4	5	10	10	8	5

Table 2.5 Summary of the microspectrophotometric results obtained for the visual pigments of the domestic turkey, *Meleagris gallopavo*, measured whilst mounted in 75 % glycerol in phosphate-buffered saline (GPBS).

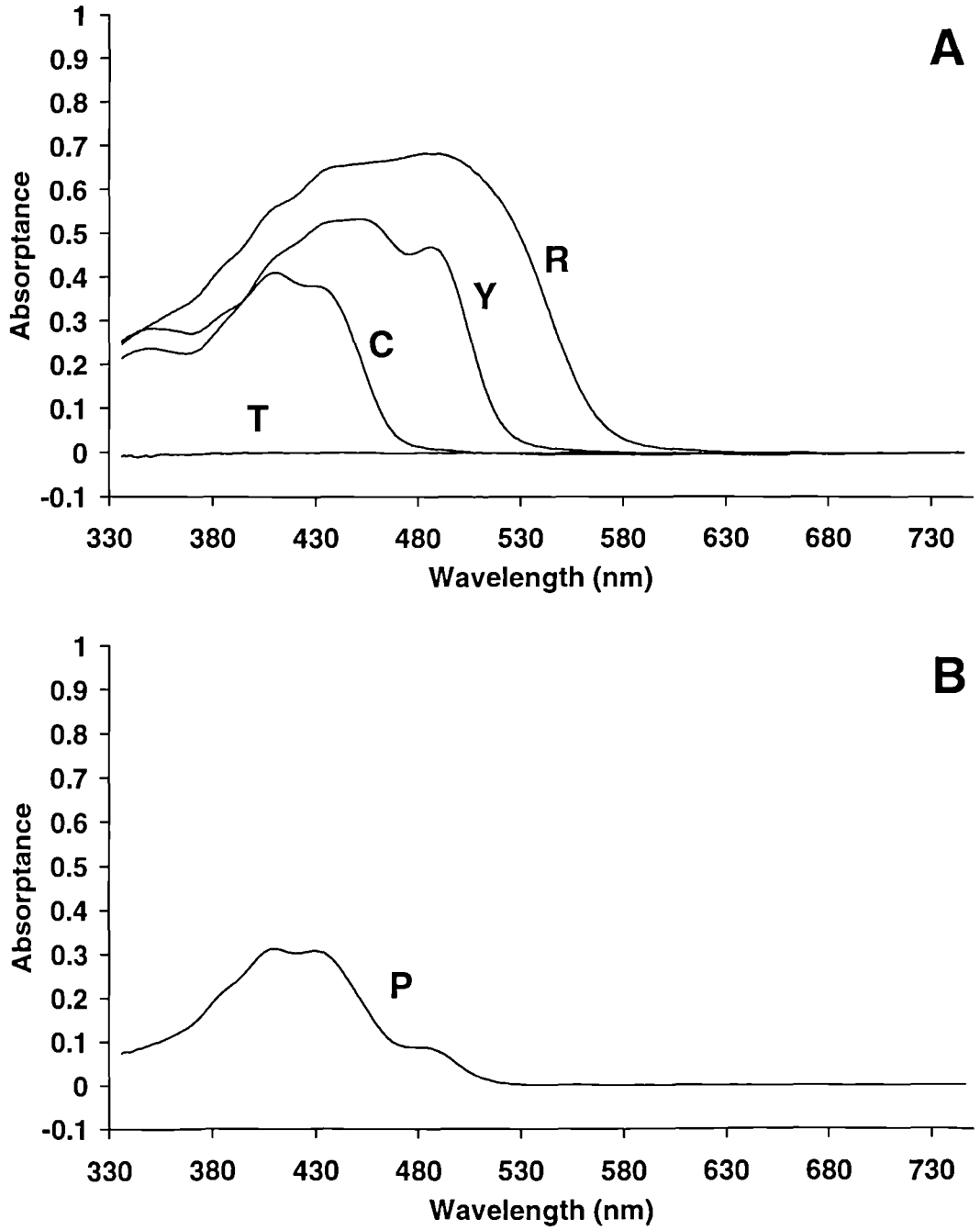

Figure 2.41 Mean absorptance spectra of oil droplets from the domestic turkey, *Meleagris gallopavo*. (**A**) Oil droplets located in the single cones. T-, C-, Y- and R-type droplets were found in the VS, SWS, MWS and LWS cones respectively. (**B**) Oil droplets located in the principal member of the double cones (P-type). No A-type droplet was measured in the accessory member.

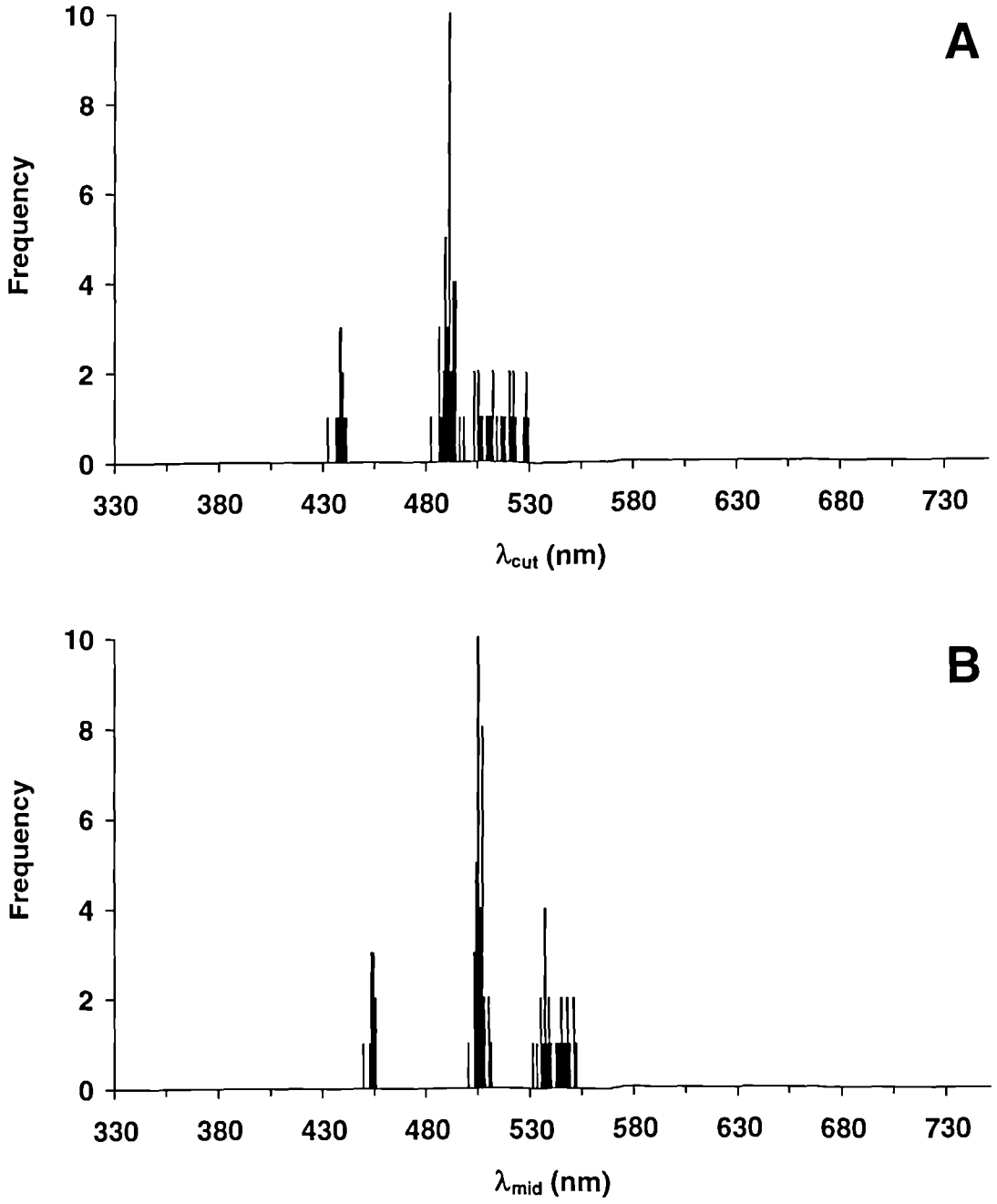

Figure 2.42 Histograms showing the spectral distribution of λ_{cut} and λ_{mid} values for single cone oil droplets measured in the domestic turkey, *Meleagris gallopavo*. (**A**) λ_{cut} values around 437, 490 and 514 nm, and (**B**) λ_{mid} values around 453, 505 and 541 nm, describe C-type, Y-type and R-type oil droplets respectively.

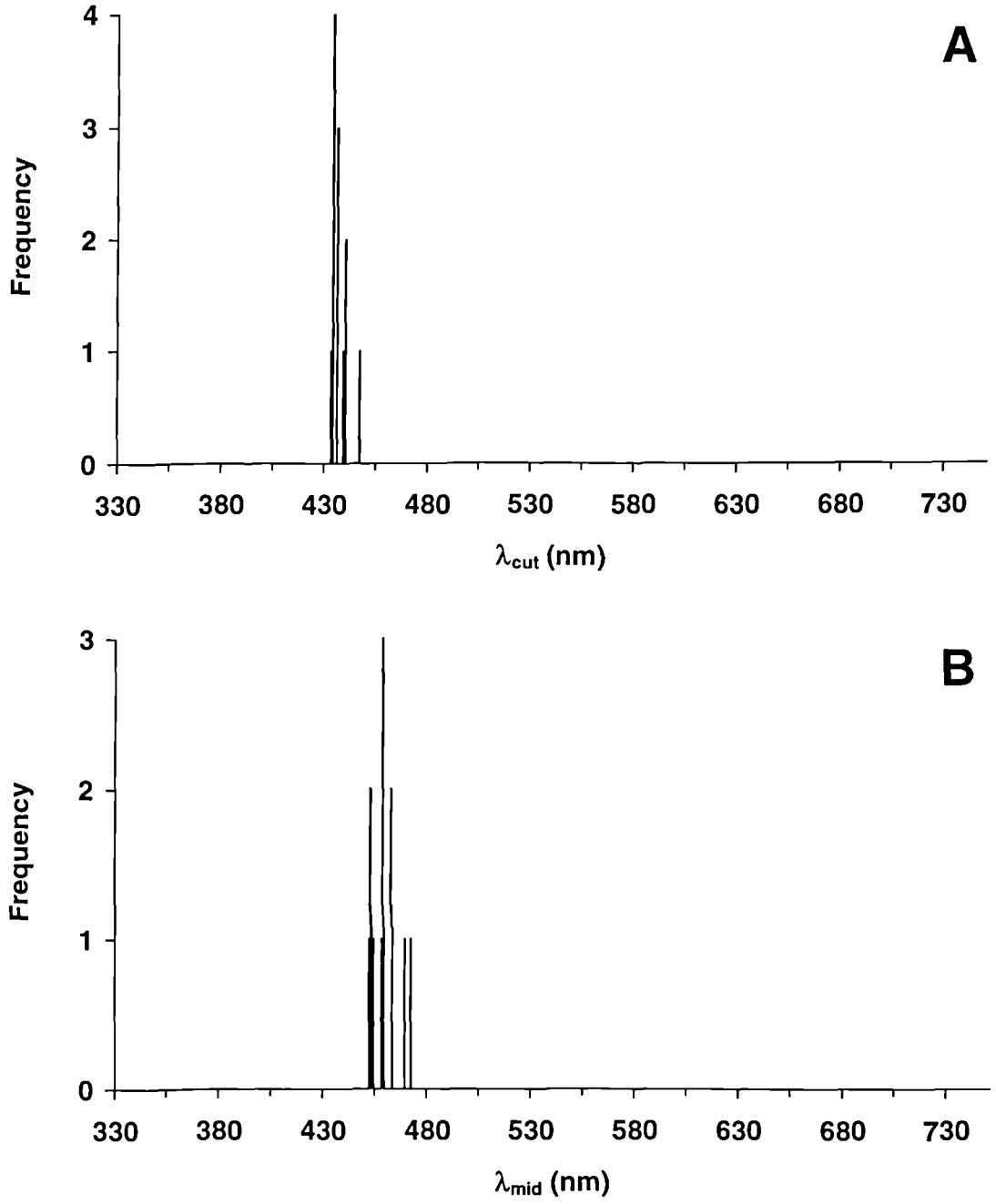

Figure 2.43 Histograms showing the spectral distribution of (**A**) λ_{cut} and (**B**) λ_{mid} values for the P-type droplets measured in the principal member of the double cones in the domestic turkey, *Meleagris gallopavo*. There were no dorsal-ventral variations in droplet pigmentation. The mean λ_{cut} and λ_{mid} values were 436 and 459 nm respectively.

	Single cones				Double cone	
Cone type	**VS**	**SWS**	**MWS**	**LWS**	**Principal**	**Accessory**
Oil droplet type	**T-type**	**C-type**	**Y-type**	**R-type**	**P-type**	**A-type**
λ_{cut} of mean absorption spectrum (nm)	<330	437.7	490.4	516.6	434.3	-
λ_{mid} of mean absorption spectrum (nm)	<330	452.5	505.4	542.7	457.7	-
Maximum corrected absorptance of mean absorption spectrum	<0.02	0.41	0.53	0.68	0.31	-
Mean λ_{cut} (nm)	<330	437.4 ± 2.5	490.1 ± 2.9	514.2 ± 9.2	436.4 ± 3.9	-
Mean λ_{mid} (nm)	<330	452.7 ± 1.9	505.2 ± 2.2	541.2 ± 6.1	459.0 ± 6.5	-
Mean diameter (μm)	1.9 ± 0.2	2.8 ± 0.3	2.8 ± 0.4	2.9 ± 0.2	3.0 ± 0.3	
Number of oil droplets	4	10	36	26	12	-

Table 2.6 Summary of the microspectrophotometric results obtained for the cone oil droplets of the domestic turkey, *Meleagris gallopavo*.

2.6.1.3 Blackbird

Microspectrophotometric data for visual pigments and oil droplets measured in the blackbird, *Turdus merula*, are displayed in Figure 2.44 to Figure 2.55 and summarised in Table 2.7 and Table 2.8. Like the starling, the blackbird retina contained five different types of rhodopsin visual pigment, in six different types of photoreceptor.

The single class of rod contained a visual pigment with a mean pre-bleach λ_{max} at 505 nm (n = 13). There were four different types of single cone, each of which was reliably associated with a different type of oil droplet. Single cones containing R-type oil droplets (mean λ_{cut} 570 nm, n = 61) were paired with a LWS visual pigment which had a mean pre-bleach λ_{max} of 557 nm (n = 9).

Y-type oil droplets (mean λ_{cut} 515 nm, n = 33) were paired with a MWS visual pigment that had a mean pre-bleach λ_{max} of 503 nm (n = 8). Single cones containing a C-type droplet (mean λ_{cut} 414 nm, n = 23) were associated with a SWS visual pigment of mean pre-bleach λ_{max} 453 nm (n = 12). The fourth type of single cone contained an UVS visual pigment, of mean pre-bleach λ_{max} 374 nm (n = 4), and a T-type oil droplet which showed no detectable absorbance above 330 nm.

Both members of the double cone pair contained visual pigments resembling the LWS visual pigment measured in the single cones. The visual pigment in the principal member had a pre-bleach λ_{max} at 557 nm (n = 23). Like the starling, the P-type oil droplet in the principal member had a variable λ_{cut} depending on retinal location. The λ_{cut} occurred at progressively longer wavelengths as the location varied from the dorsal to the ventral retina. A shoulder at approximately 480 nm was apparent in the absorptance spectra of P-type droplets taken from the central and ventral regions of the retina.

The visual pigment in the accessory member of the double cone had a mean pre-bleach λ_{max} of 556 nm (n = 7). No A-type droplet was observed in the accessory cones, nor was any carotenoid detected at the distal end of their inner segments.

The maximum corrected absorptance of the C-type oil droplet was relatively low (0.29). This suggests that, like the C- and A-type droplets of the starling, the C-type droplets in the blackbird SWS cones do not act as true cut-off filters.

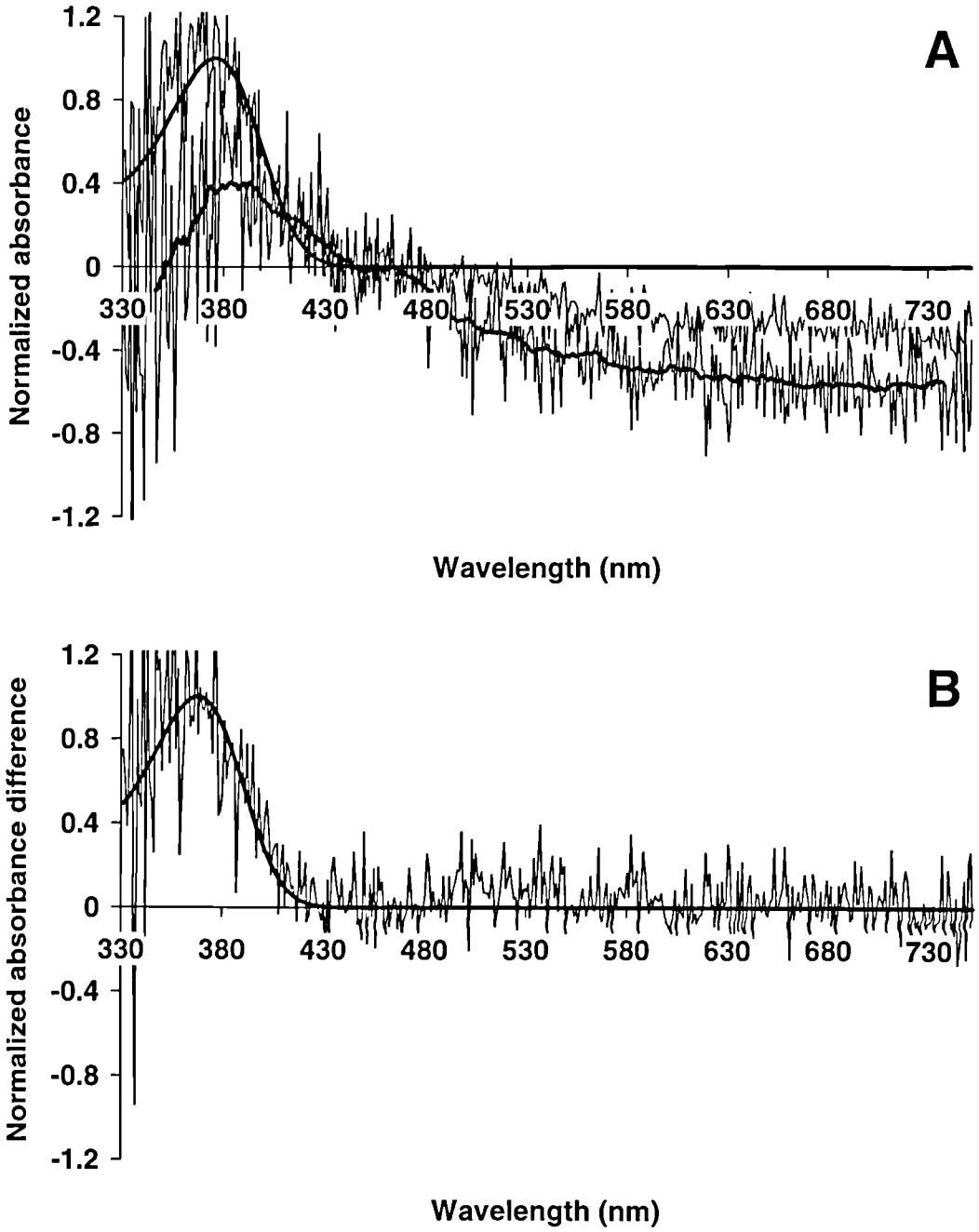

Figure 2.44 Microspectrophotometric results from 4 UVS single cones of the blackbird, *Turdus merula*. (**A**) Mean pre-bleach absorbance spectrum (upper trace) with best-fitted visual pigment template (λ_{max} 376 nm, solid line) and mean post-bleach absorbance spectrum (lower trace) with running average (solid line). (**B**) Mean difference spectrum (trace) with best-fitted visual pigment template (λ_{max} 368 nm, solid line).

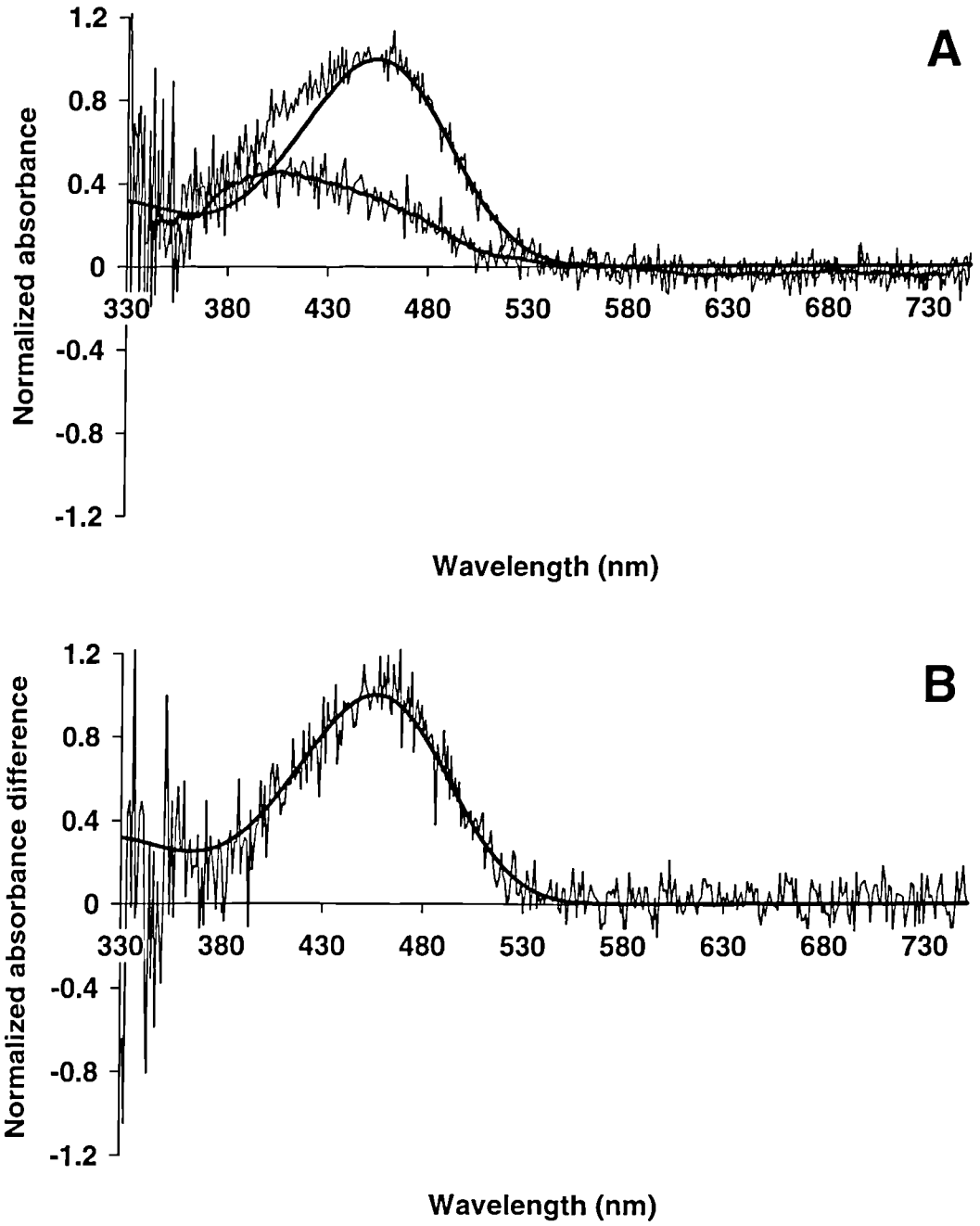

Figure 2.45 Microspectrophotometric results from 12 SWS single cones of the blackbird, *Turdus merula*. (**A**) Mean pre-bleach absorbance spectrum (upper trace) with best-fitted visual pigment template (λ_{max} 454 nm, solid line) and mean post-bleach absorbance spectrum (lower trace) with running average (solid line). (**B**) Mean difference spectrum (trace) with best-fitted visual pigment template (λ_{max} 456 nm, solid line).

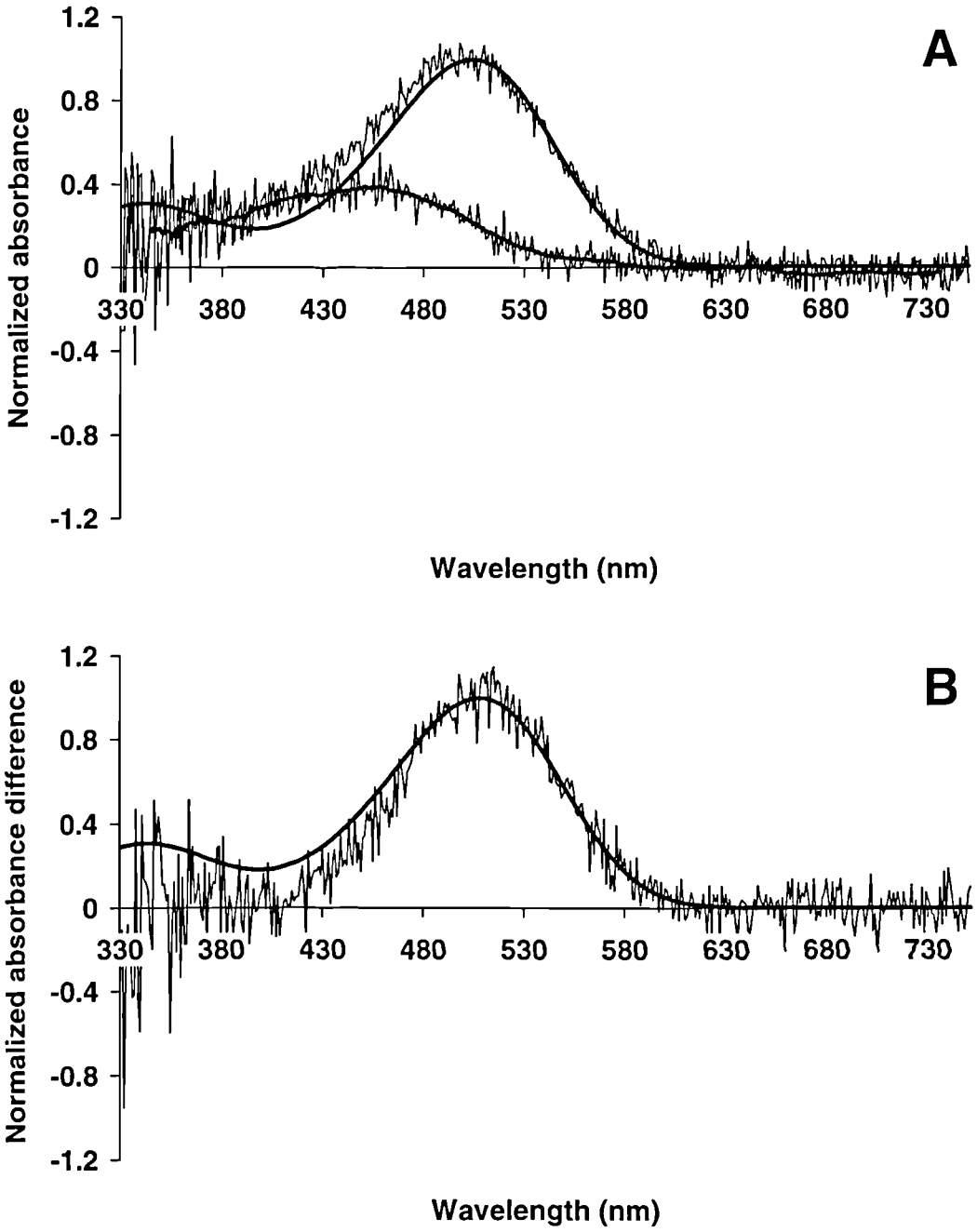

Figure 2.46 Microspectrophotometric results from 8 MWS single cones of the blackbird, *Turdus merula*. (**A**) Mean pre-bleach absorbance spectrum (upper trace) with best-fitted visual pigment template (λ_{max} 504 nm, solid line) and mean post-bleach absorbance spectrum (lower trace) with running average (solid line). (**B**) Mean difference spectrum (trace) with best-fitted visual pigment template (λ_{max} 508 nm, solid line).

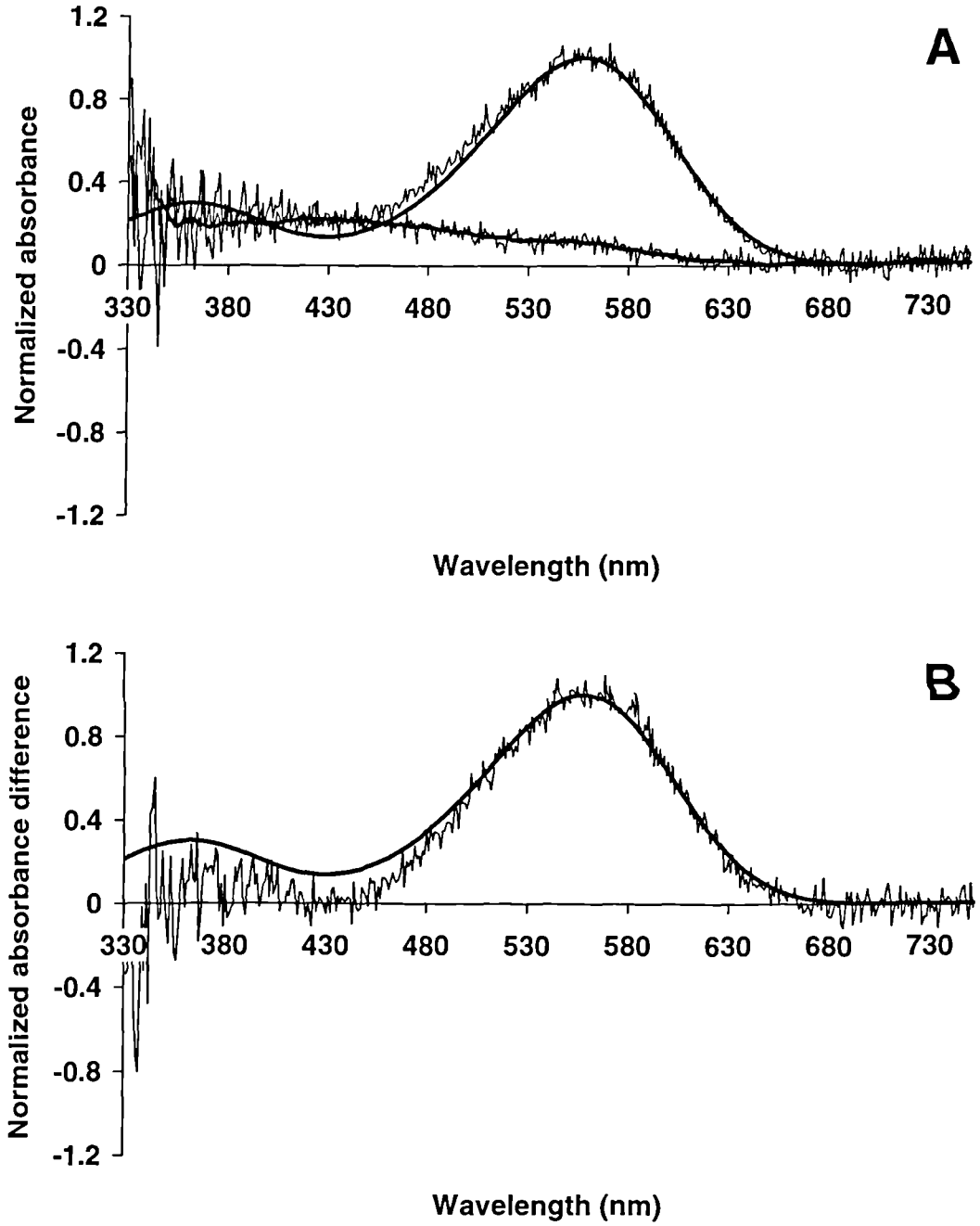

Figure 2.47 Microspectrophotometric results from 9 LWS single cones of the blackbird, *Turdus merula*. (**A**) Mean pre-bleach absorbance spectrum (upper trace) with best-fitted visual pigment template (λ_{max} 557 nm, solid line) and mean post-bleach absorbance spectrum (lower trace) with running average (solid line). (**B**) Mean difference spectrum (trace) with best-fitted visual pigment template (λ_{max} 558 nm, solid line).

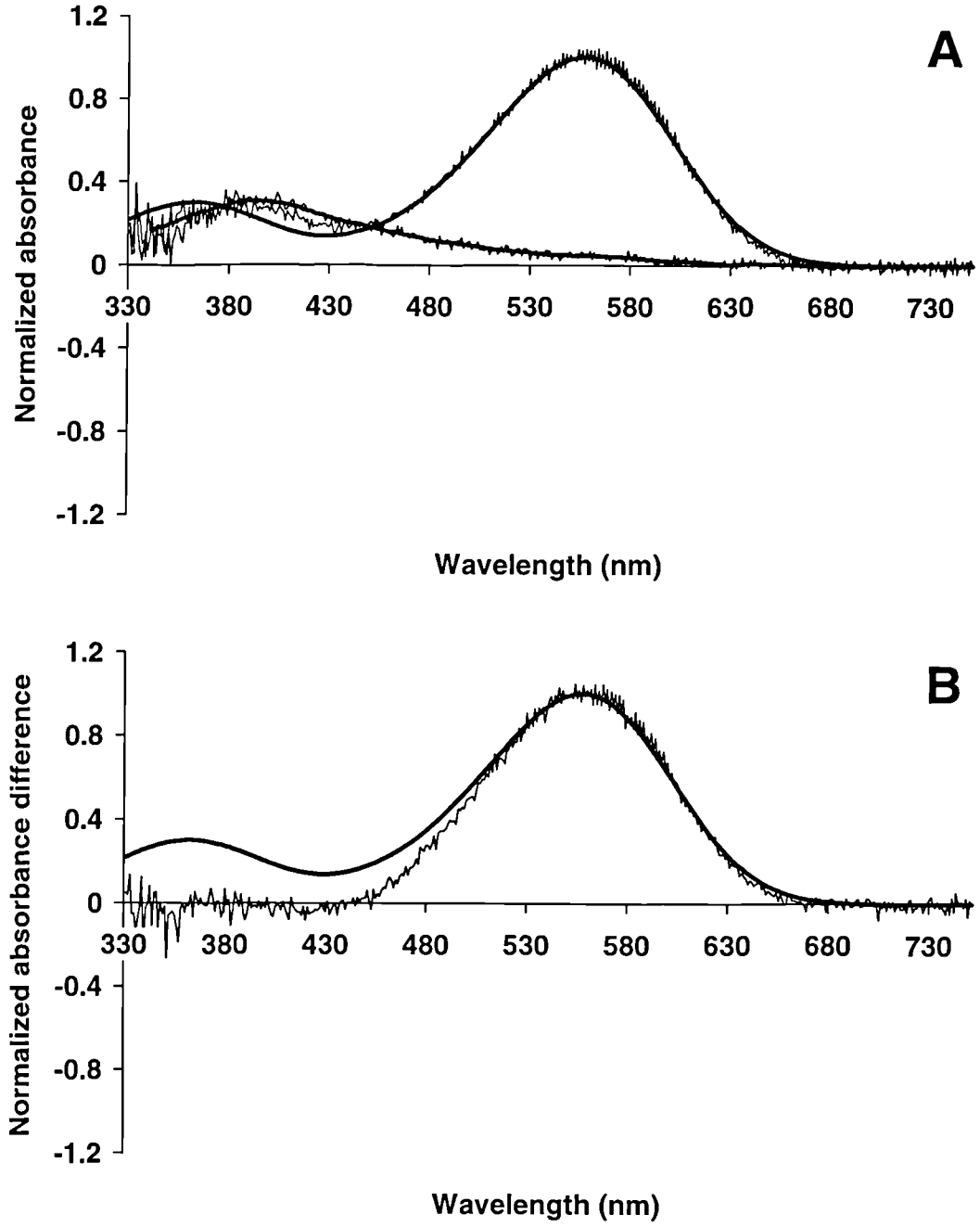

Figure 2.48 Microspectrophotometric results from 23 principal members of the double cone of the blackbird, *Turdus merula*. (**A**) Mean pre-bleach absorbance spectrum (upper trace) with best-fitted visual pigment template (λ_{max} 557 nm, solid line) and mean post-bleach absorbance spectrum (lower trace) with running average (solid line). (**B**) Mean difference spectrum (trace) with best-fitted visual pigment template (λ_{max} 557 nm, solid line).

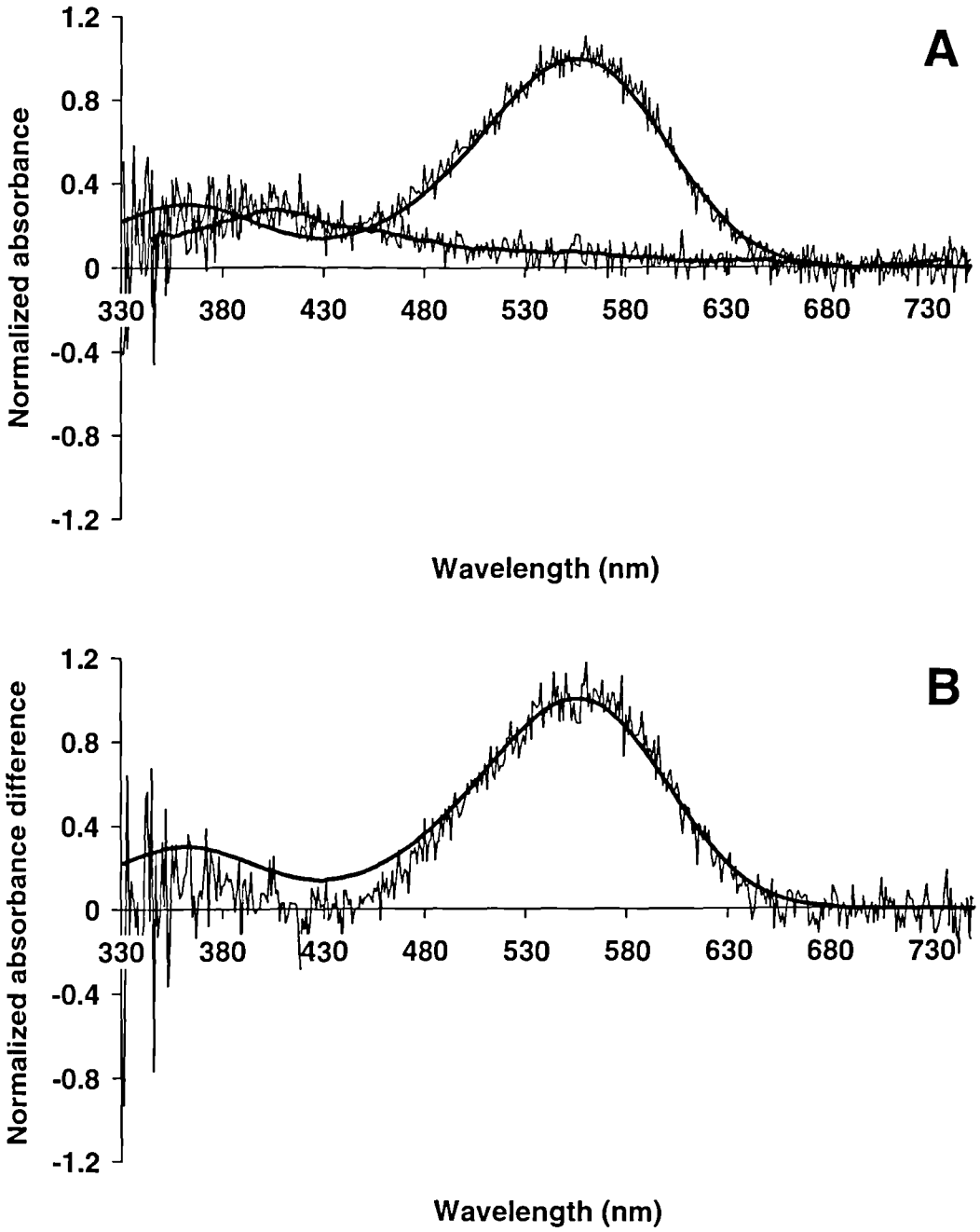

Figure 2.49 Microspectrophotometric results from 7 accessory members of the double cone of the blackbird, *Turdus merula*. (**A**) Mean pre-bleach absorbance spectrum (upper trace) with best-fitted visual pigment template (λ_{max} 556 nm, solid line) and mean post-bleach absorbance spectrum (lower trace) with running average (solid line). (**B**) Mean difference spectrum (trace) with best-fitted visual pigment template (λ_{max} 556 nm, solid line).

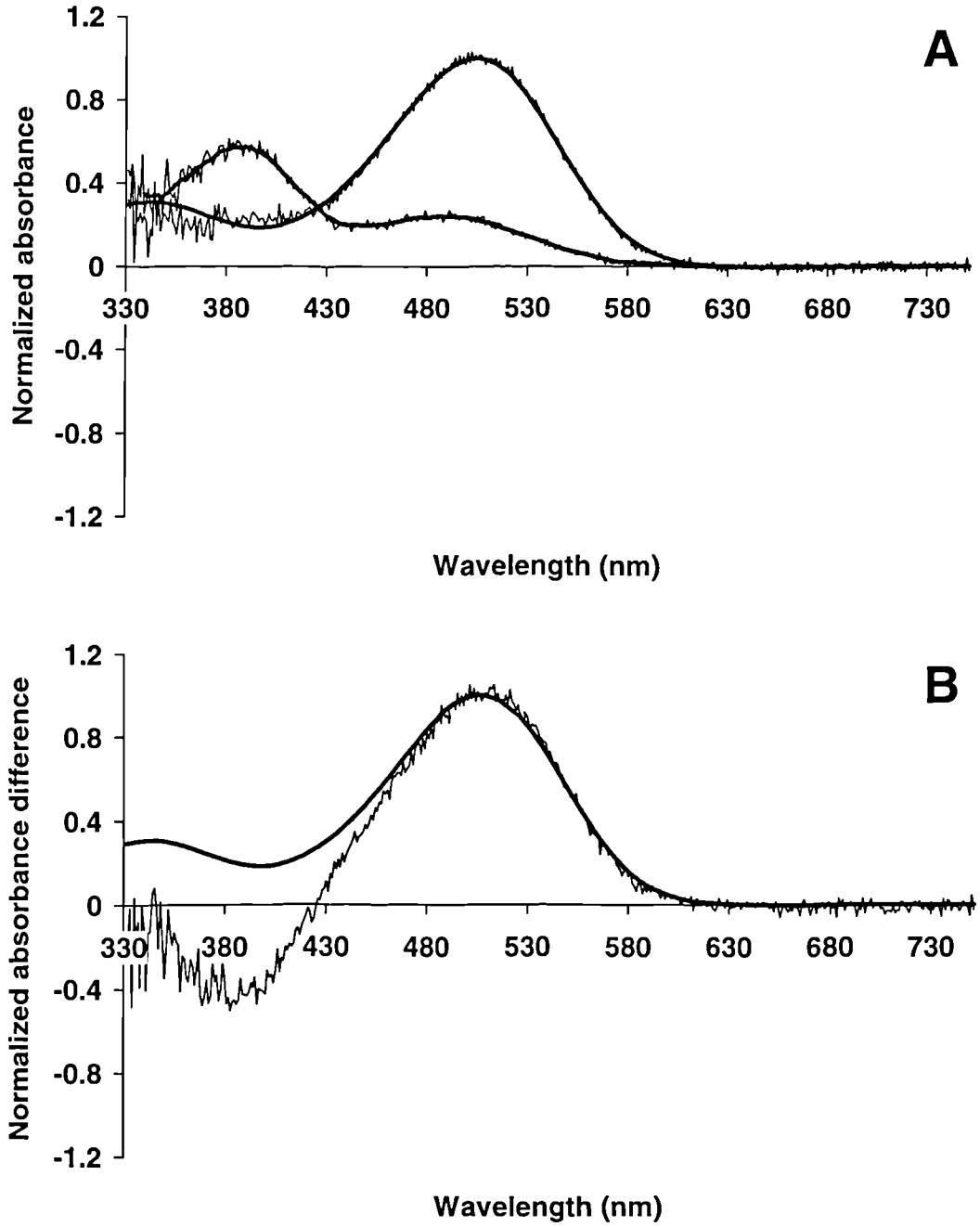

Figure 2.50 Microspectrophotometric results from 13 rods of the blackbird, *Turdus merula*. (**A**) Mean pre-bleach absorbance spectrum (upper trace) with best-fitted visual pigment template (λ_{max} 504 nm, solid line) and mean post-bleach absorbance spectrum (lower trace) with running average (solid line). (**B**) Mean difference spectrum (trace) with best-fitted visual pigment template (λ_{max} 507 nm, solid line).

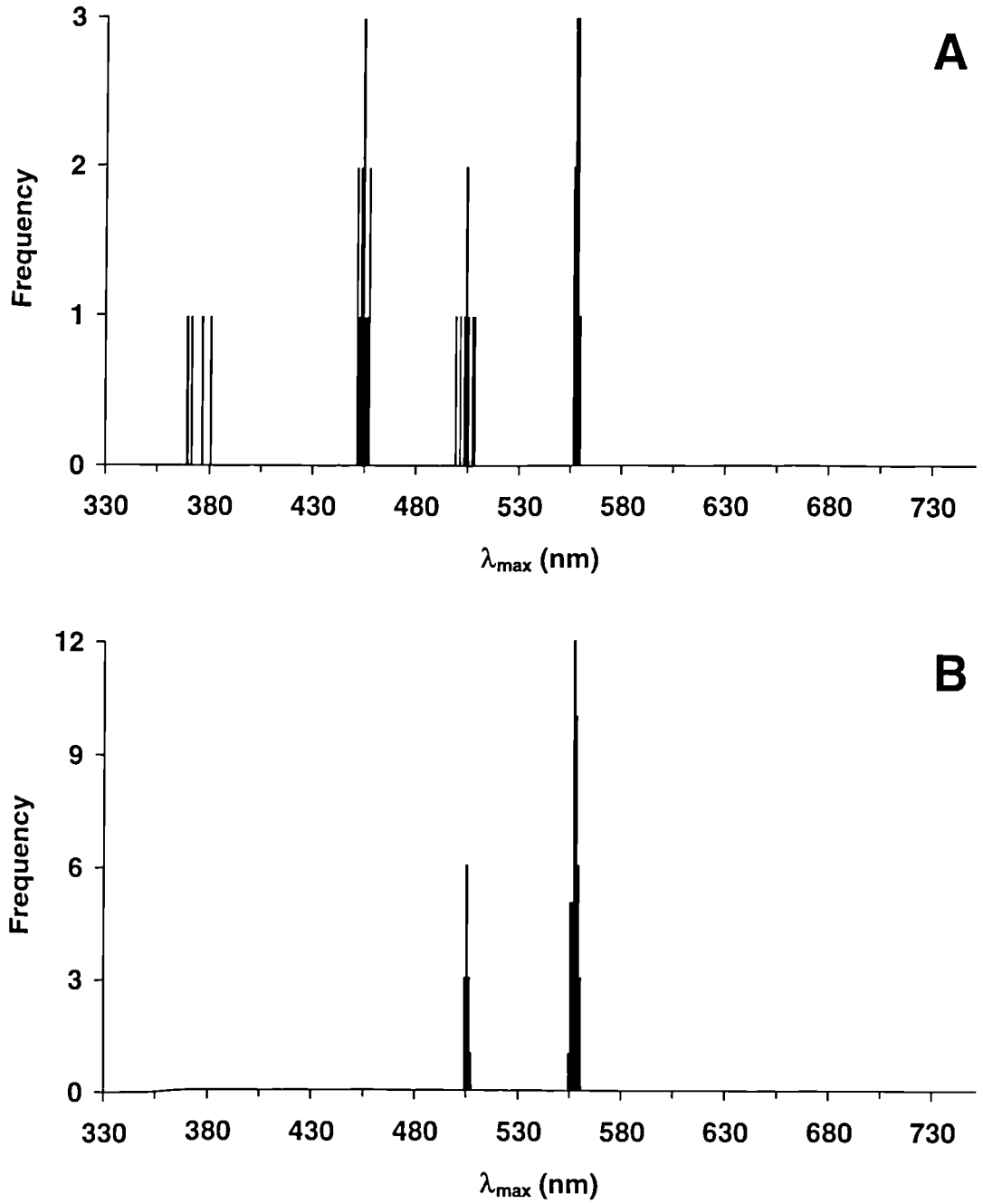

Figure 2.51 Histogram showing the distribution of estimated λ_{max} values obtained from pre-bleach absorbance spectra of visual pigments in the blackbird, *Turdus merula*. (**A**) Single cones. λ_{max} values around 374, 453, 503 and 557 nm describe UVS, SWS, MWS and LWS visual pigments respectively. (**B**) Rods and double cones. λ_{max} values around 505 nm describe rod visual pigment, whilst λ_{max} values around 557 nm describe the LWS visual pigments found in the principal and accessory members of the double cones.

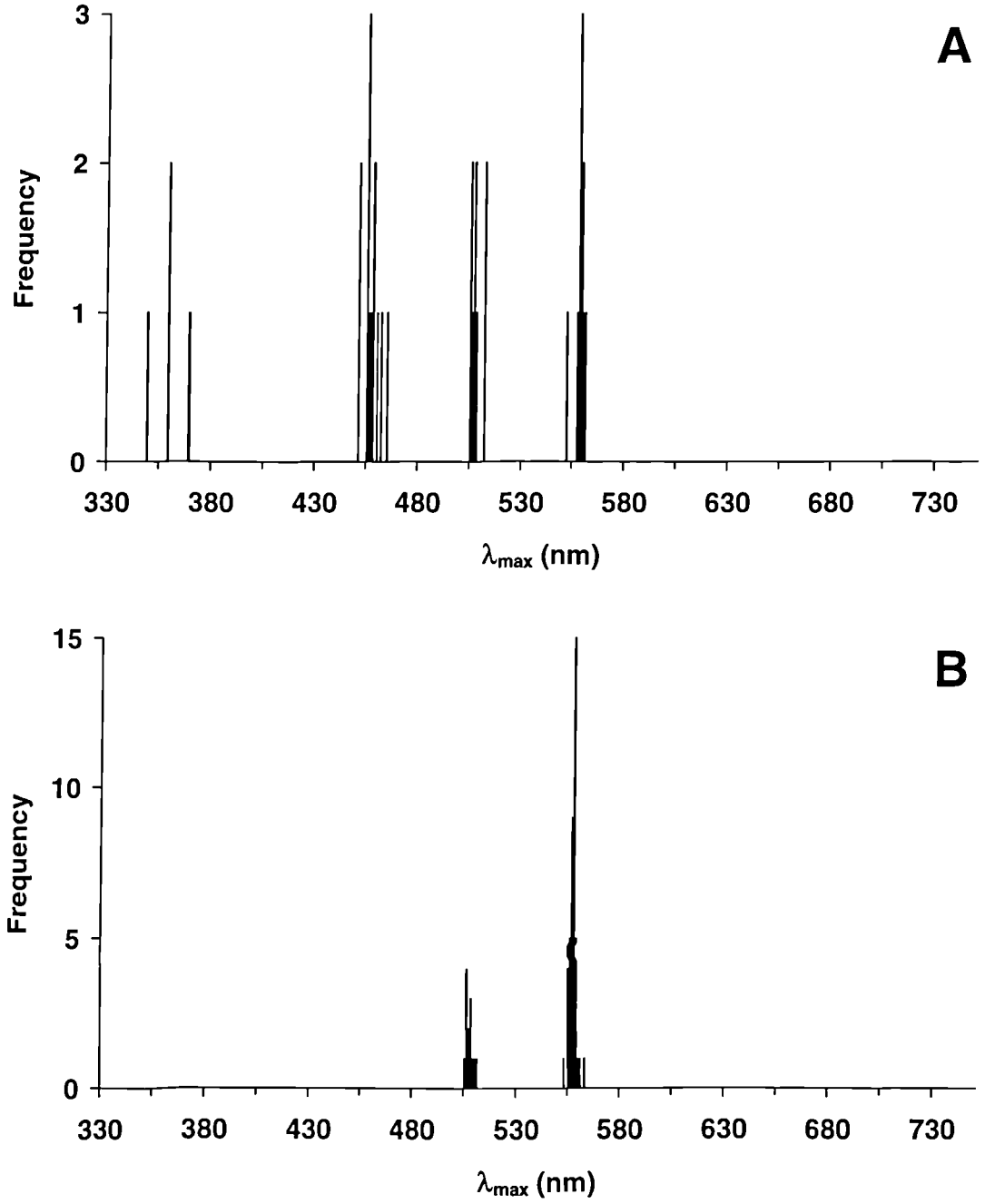

Figure 2.52 Histogram showing the distribution of estimated λ_{max} values obtained from difference spectra of visual pigments in the blackbird, *Turdus merula*. (**A**) Single cones. λ_{max} values around 359, 456, 507 and 558 nm describe UVS, SWS, MWS and LWS visual pigments respectively. (**B**) Rods and double cones. λ_{max} values around 507 nm describe rod visual pigment, whilst λ_{max} values around 557 nm describe the LWS visual pigments found in the principal and accessory members of the double cones.

	Rod	Single Cones				Double cone	
		UVS	SWS	MWS	LWS	Principal	Accessory
Visual pigments							
λ_{max} of mean pre-bleach spectrum (nm)	504.4 ± 0.9	375.6 ± 3.9	453.9 ± 2.6	504.1 ± 2.9	557.3 ± 2.5	557.0 ± 2.0	556.0 ± 3.9
Mean of pre-bleach λ_{max} (nm)	504.7 ± 0.9	373.5 ± 4.9	453.4 ± 2.1	503.4 ± 3.0	557.0 ± 0.9	557.0 ± 1.3	555.7 ± 1.9
λ_{max} of mean difference spectrum (nm)	506.6 ± 1.5	368.0 ± 7.5	455.9 ± 5.6	508.2 ± 6.3	557.9 ± 3.7	557.4 ± 2.0	555.8 ± 4.7
Transverse absorbance at λ_{max} of mean difference spectrum	0.038	0.007	0.008	0.011	0.018	0.023	0.016
Mean of difference spectrum λ_{max} (nm)	507.0 ± 1.6	358.7 ± 8.5	456.3 ± 4.1	507.44 ± 2.7	557.5 ± 2.6	557.3 ± 1.7	555.9 ± 1.3
Number of cells	13	4	12	8	9	23	7

Table 2.7 Summary of the microspectrophotometric data obtained for the visual pigments of the blackbird, *Turdus merula*.

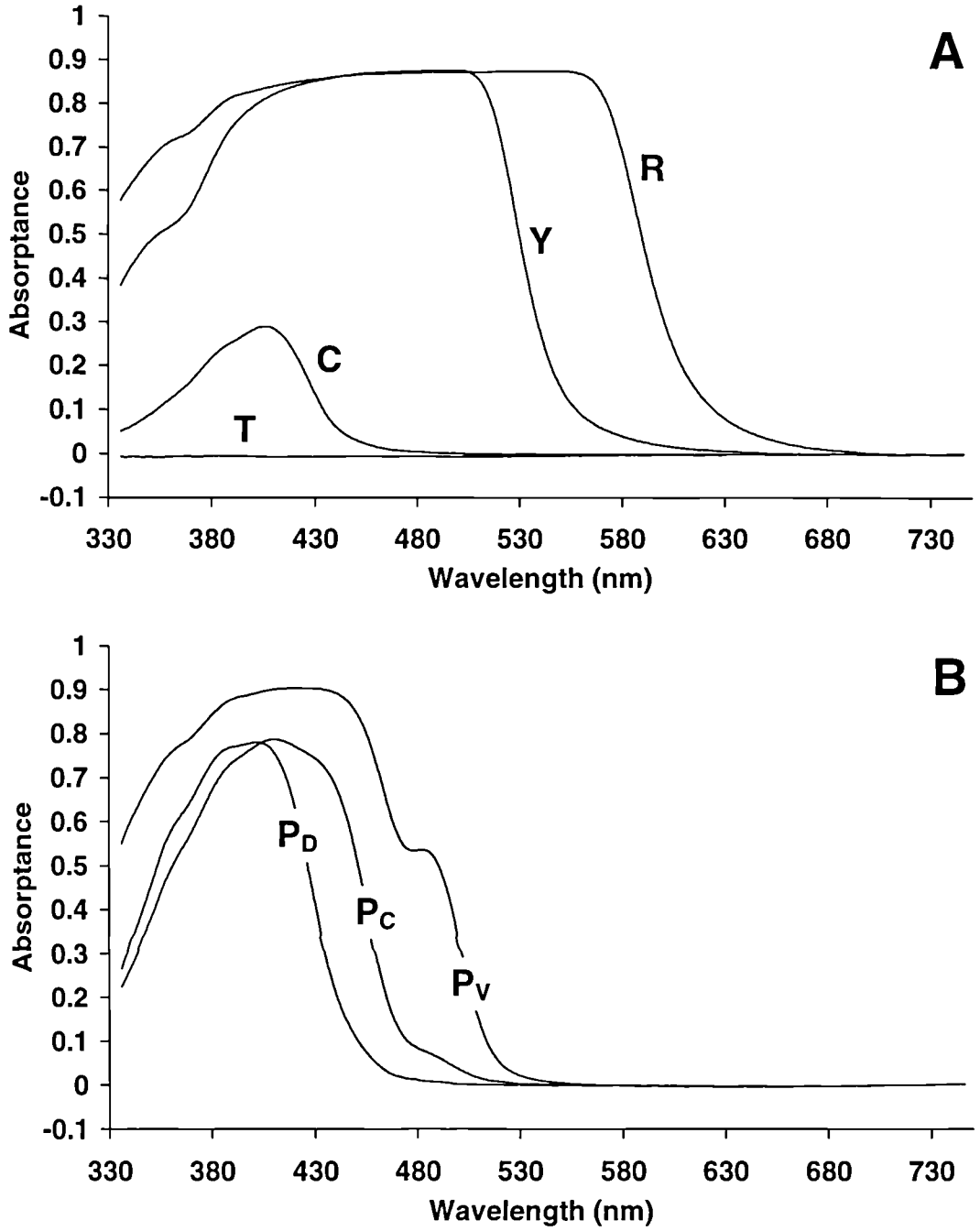

Figure 2.53 Mean absorptance spectra of oil droplets from the blackbird, *Turdus merula*. (**A**) Oil droplets located in the single cones. T-, C-, Y- and R-type droplets were found in the UVS, SWS, MWS and LWS cones respectively. (**B**) Oil droplets located in the principal member of the double cones (P-type). P-type droplets located in the ventral retina (P_V) had their λ_{cut} at longer wavelengths than those located in the central retina (P_C) which, in turn, had their λ_{cut} at longer wavelengths than those found in the dorsal retina (P_D). No A-type droplet was measured in the accessory member.

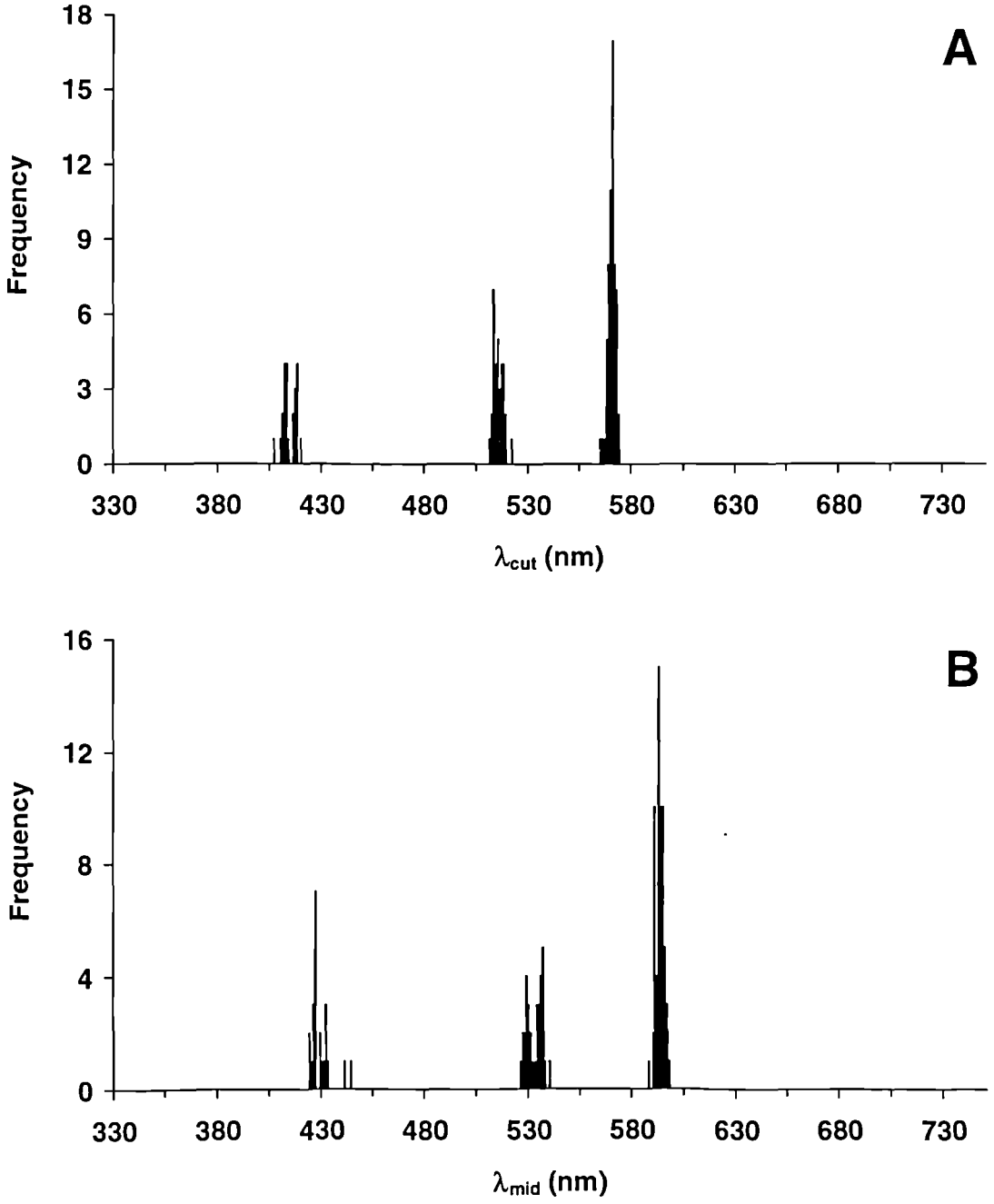

Figure 2.54 Histograms showing the spectral distribution of λ_{cut} and λ_{mid} values for single cone oil droplets measured in the blackbird, *Turdus merula*. (**A**) λ_{cut} values around 414, 515 and 570 nm, and (**B**) λ_{mid} values around 429, 532 and 593 nm, describe C-type, Y-type and R-type oil droplets respectively.

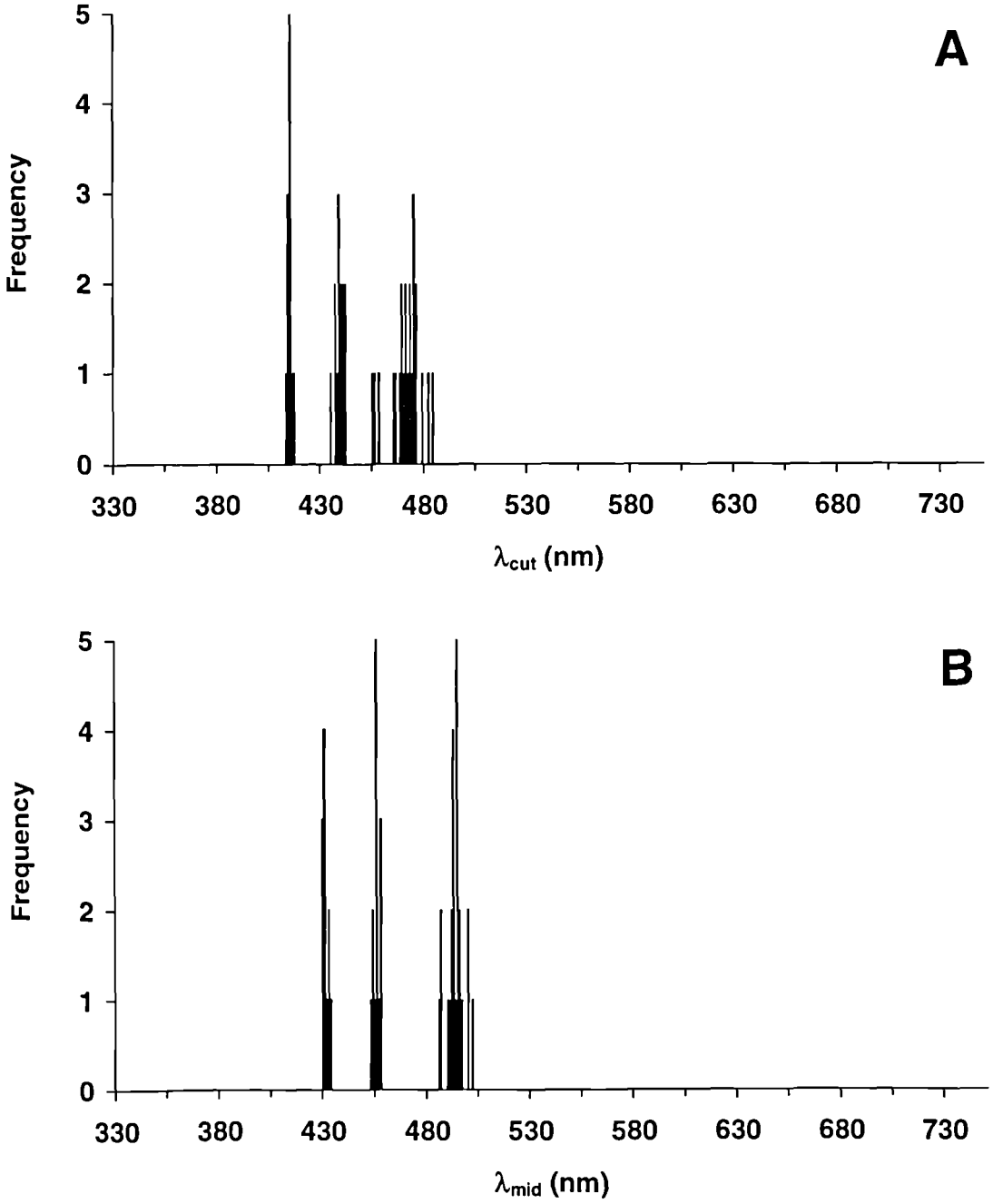

Figure 2.55 Histograms showing the spectral distribution of λ_{cut} and λ_{mid} values for P-type oil droplets measured in the principal member of the double cones of the blackbird, *Turdus merula*. (**A**) λ_{cut} values around 414, 439 and 470 nm, and (**B**) λ_{mid} values around 431, 456 and 493 nm, describe P-type oil droplets taken from the dorsal, central and ventral regions of the retina respectively.

	Single cones				Double cone			
Cone type	UVS	SWS	MWS	LWS	Principal			Accessory
Oil droplet type	T-type	C-type	Y-type	R-type	P-type			A type
					D	C	V	
λ_{cut} of mean absorption spectrum (nm)	<330	414.3	514.2	569.9	414.7	439.1	472.3	-
λ_{mid} of mean absorption spectrum (nm)	<330	429.1	532.5	593.0	431.0	455.5	494.2	-
Maximum corrected absorptance of mean absorption spectrum	<0.01	0.29	0.88	0.88	0.78	0.79	0.90	-
Mean λ_{cut} (nm)	<330	413.8 ± 3.2	514.8 ± 2.4	570.0 ± 1.8	414.3 ± 1.1	438.8 ± 2.1	470.4 ± 7.5	-
Mean λ_{mid} (nm)	<330	428.8 ± 5.1	532.3 ± 3.9	592.9 ± 2.0	431.0 ± 1.5	455.5 ± 1.5	493.4 ± 4.0	-
Mean diameter (μm)	2.25 ± 0.6	2.5 ± 0.6	3.2 ± 0.4	3.3 ± 0.4	4.0 ± 0.3	3.2 ± 0.2	3.9 ± 0.2	-
Number of oil droplets	5	23	33	61	11	13	23	-

Table 2.8 Summary of the microspectrophotometric data obtained for the cone oil droplets measured in the blackbird, *Turdus merula*.

2.6.1.4 Blue tit

Microspectrophotometric data for visual pigments and oil droplets measured in the blue tit, *Parus caeruleus*, are displayed in Figure 2.56 to Figure 2.67 and summarised in Table 2.9 and Table 2.10. Like the starling and blackbird, the blue tit retina contained five different types of rhodopsin visual pigment, in six different types of photoreceptor.

The single class of rod contained a visual pigment with a mean pre-bleach λ_{max} at 504 nm (n = 6). There were four different types of single cone, each of which was reliably associated with a different type of oil droplet. Single cones containing R-type oil droplets (mean λ_{cut} 573 nm, n = 14) were paired with a LWS visual pigment which had a mean pre-bleach λ_{max} of 563 nm (n = 7).

Y-type oil droplets (mean λ_{cut} 508 nm, n = 13) were paired with a MWS visual pigment that had a mean pre-bleach λ_{max} of 502 nm (n = 10). Single cones containing a C-type droplet (mean λ_{cut} 413 nm, n = 12) were associated with a SWS visual pigment of mean pre-bleach λ_{max} 448 nm (n = 5). The fourth type of single cone contained an UVS visual pigment, of mean pre-bleach λ_{max} 374 nm (n = 5), and a T-type oil droplet which showed no detectable absorbance above 330 nm.

Both members of the double cone pair contained visual pigments resembling the LWS visual pigment measured in the single cones. The visual pigment in the principal member had a pre-bleach λ_{max} at 565 nm (n = 14). The P-type oil droplets in the principal member of the double cones had a similar λ_{cut} regardless of retinal location. Nevertheless, a shoulder at approximately 480 nm was just visible in the absorptance spectra of P-type droplets taken from the ventral region of the retina, which distinguished these droplets from those located dorsally.

The visual pigment in the accessory member of the double cone had a mean pre-bleach λ_{max} of 563 nm (n = 4). No A-type droplet was observed in the accessory cones, nor was any carotenoid detected at the distal end of their inner segments.

The maximum corrected absorptance of the C-type oil droplet was relatively low (0.25). This suggests that, like the C- and A-type droplets of the starling and the C-type droplets in the blackbird, the C-type droplets in the blue tit SWS cones do not act as true cut-off filters.

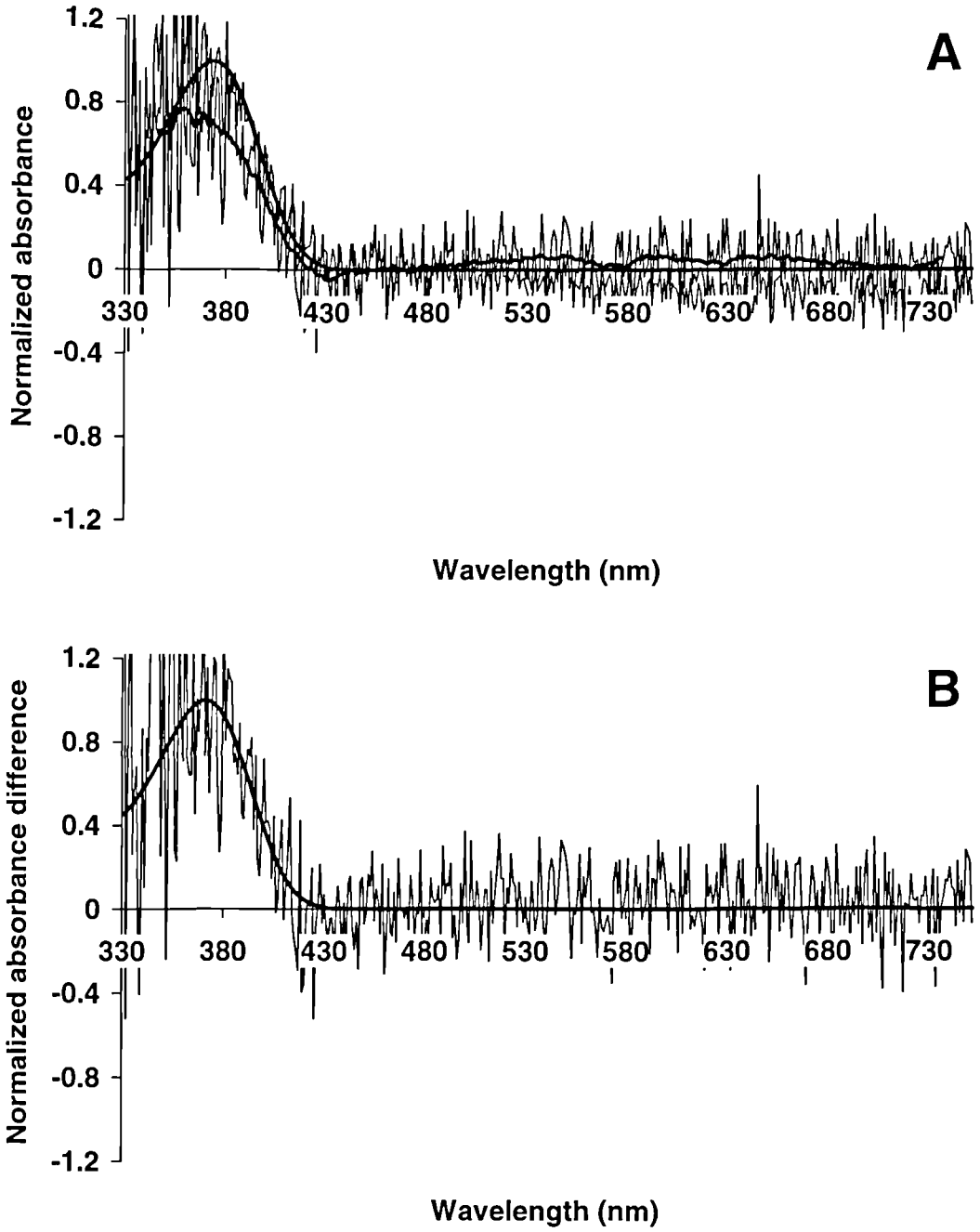

Figure 2.56 Microspectrophotometric results from 5 UVS single cones of the blue tit, *Parus caeruleus*. (**A**) Mean pre-bleach absorbance spectrum (upper trace) with best-fitted visual pigment template (λ_{max} 374 nm, solid line) and mean post-bleach absorbance spectrum (lower trace) with running average (solid line). (**B**) Mean difference spectrum (trace) with best-fitted visual pigment template (λ_{max} 371 nm, solid line).

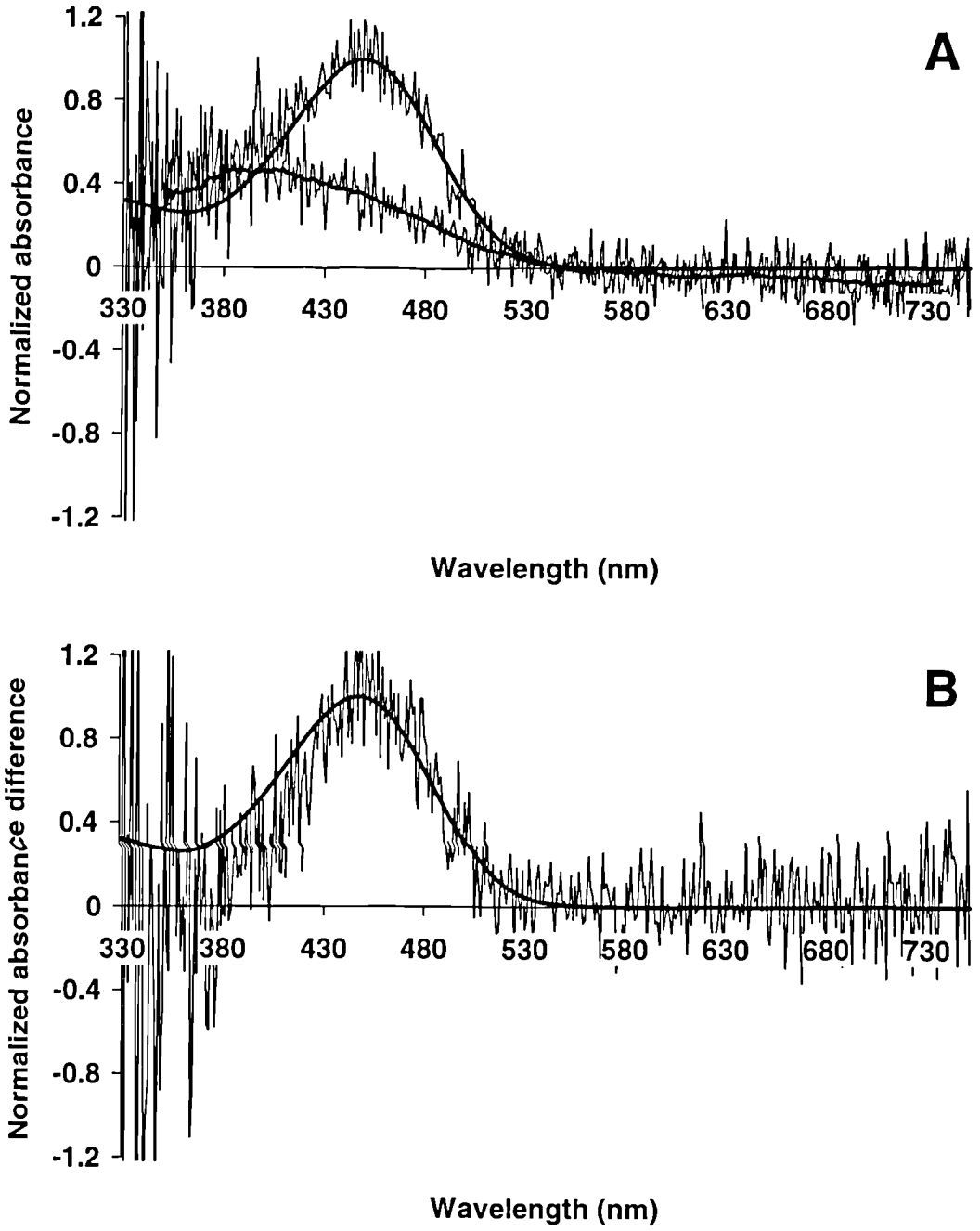

Figure 2.57 Microspectrophotometric results from 5 SWS single cones of the blue tit, *Parus caeruleus*. (**A**) Mean pre-bleach absorbance spectrum (upper trace) with best-fitted visual pigment template (λ_{max} 449 nm, solid line) and mean post-bleach absorbance spectrum (lower trace) with running average (solid line). (**B**) Mean difference spectrum (trace) with best-fitted visual pigment template (λ_{max} 448 nm, solid line).

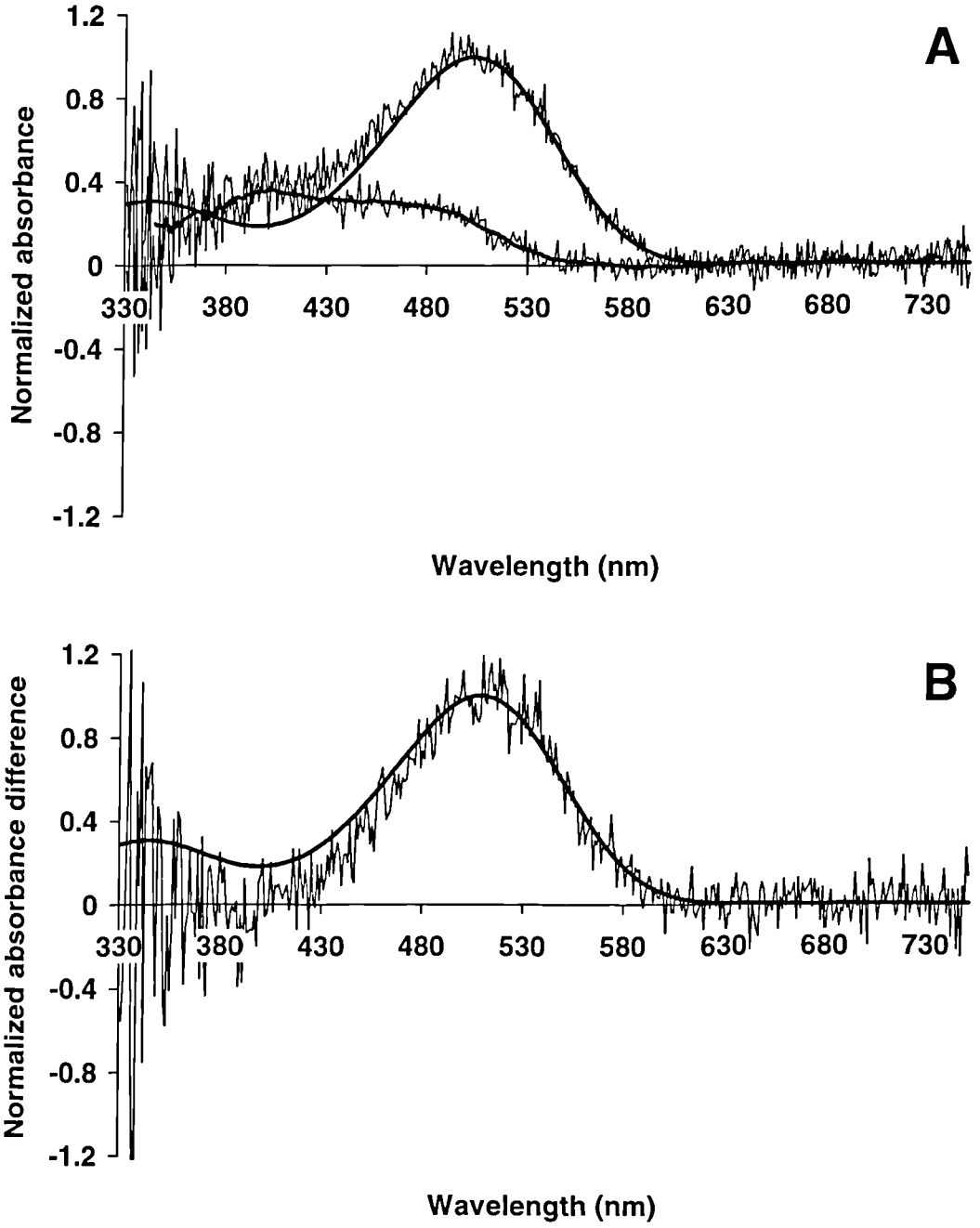

Figure 2.58 Microspectrophotometric results from 10 MWS single cones of the blue tit, *Parus caeruleus*. (**A**) Mean pre-bleach absorbance spectrum (upper trace) with best-fitted visual pigment template (λ_{max} 503 nm, solid line) and mean post-bleach absorbance spectrum (lower trace) with running average (solid line). (**B**) Mean difference spectrum (trace) with best-fitted visual pigment template (λ_{max} 509 nm, solid line).

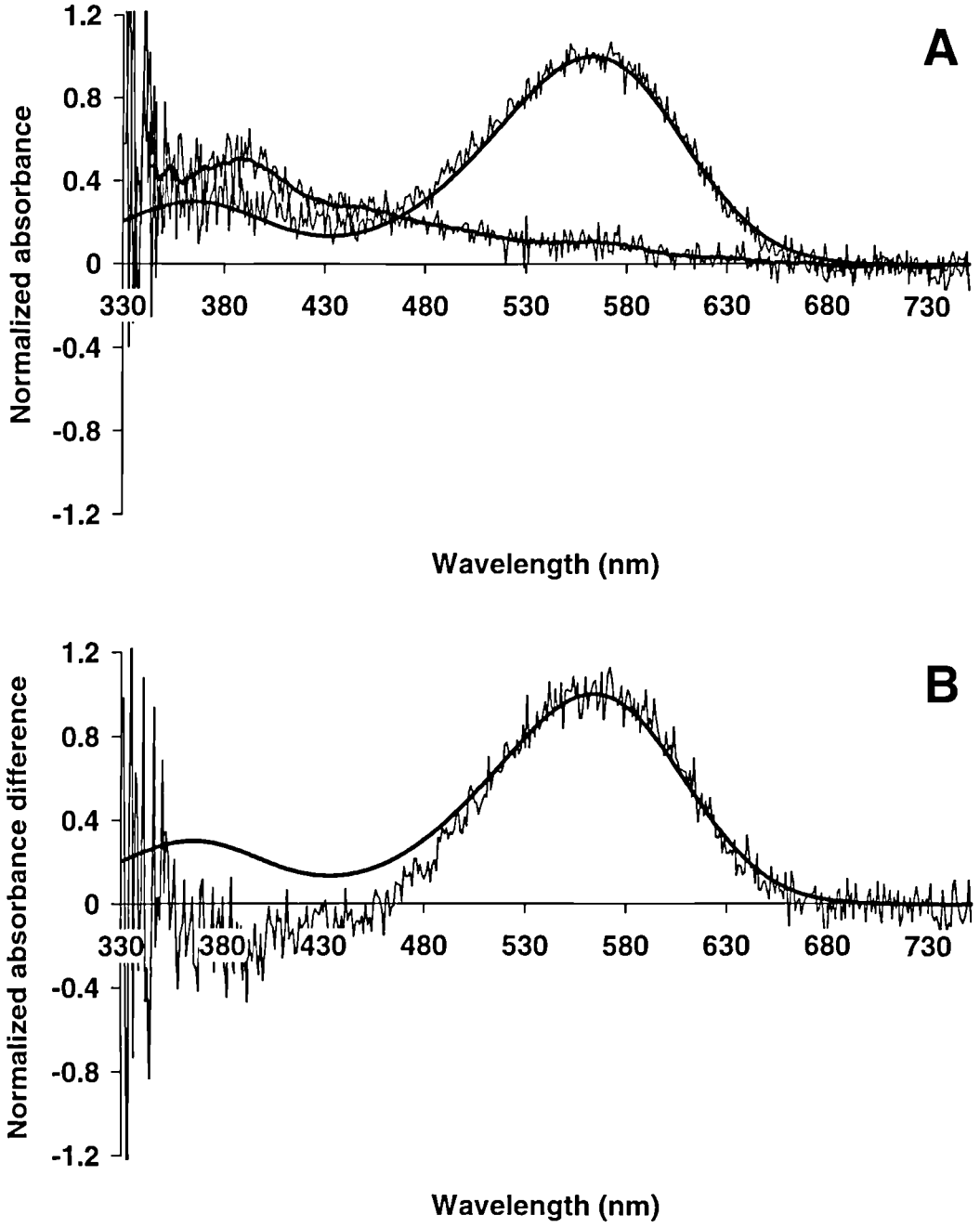

Figure 2.59 Microspectrophotometric results from 7 LWS single cones of the blue tit, *Parus caeruleus*. (**A**) Mean pre-bleach absorbance spectrum (upper trace) with best-fitted visual pigment template (λ_{max} 563 nm, solid line) and mean post-bleach absorbance spectrum (lower trace) with running average (solid line). (**B**) Mean difference spectrum (trace) with best-fitted visual pigment template (λ_{max} 564 nm, solid line).

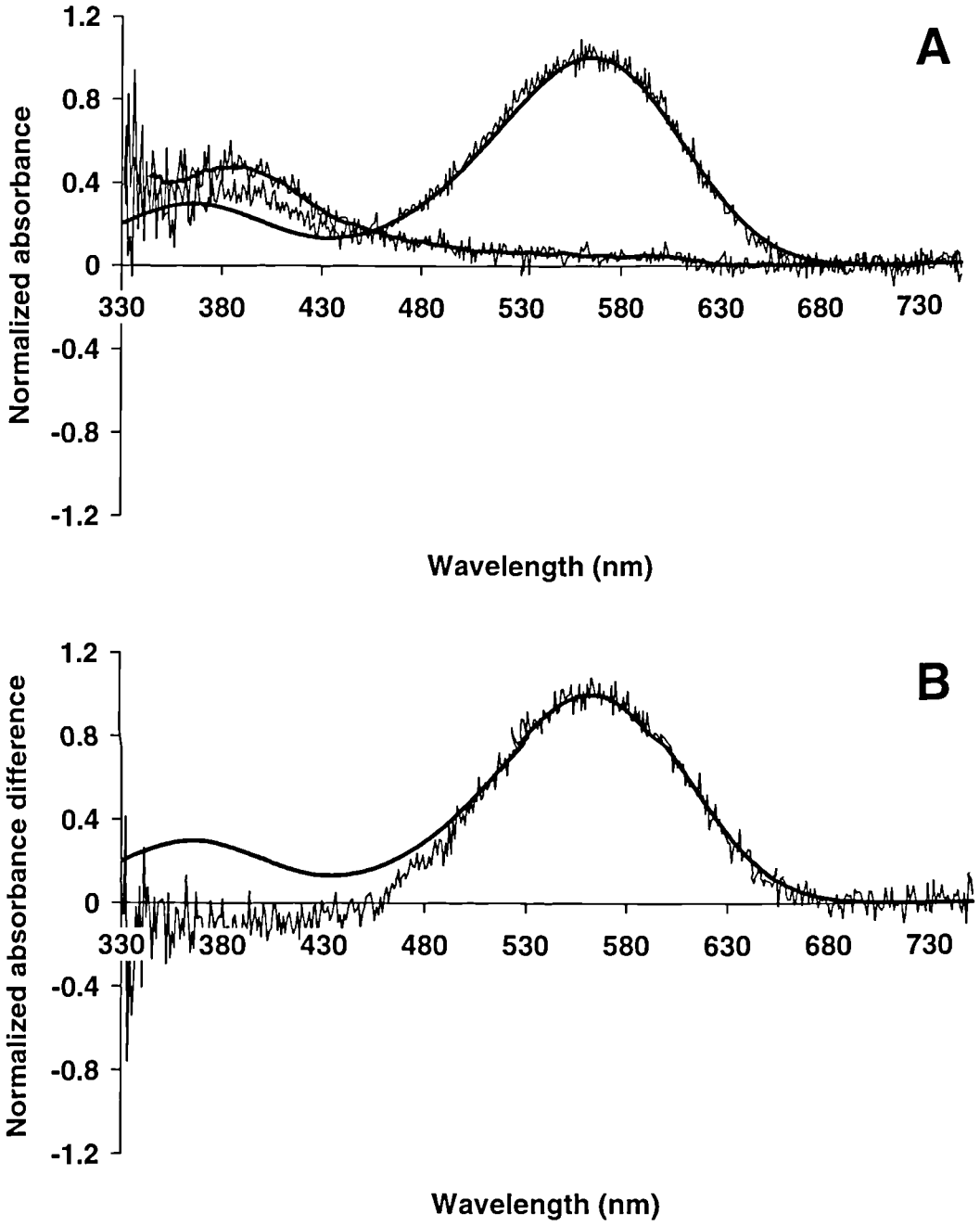

Figure 2.60 Microspectrophotometric results from 14 principal members of the double cone of the blue tit, *Parus caeruleus*. (**A**) Mean pre-bleach absorbance spectrum (upper trace) with best-fitted visual pigment template (λ_{max} 565 nm, solid line) and mean post-bleach absorbance spectrum (lower trace) with running average (solid line). (**B**) Mean difference spectrum (trace) with best-fitted visual pigment template (λ_{max} 566 nm, solid line).

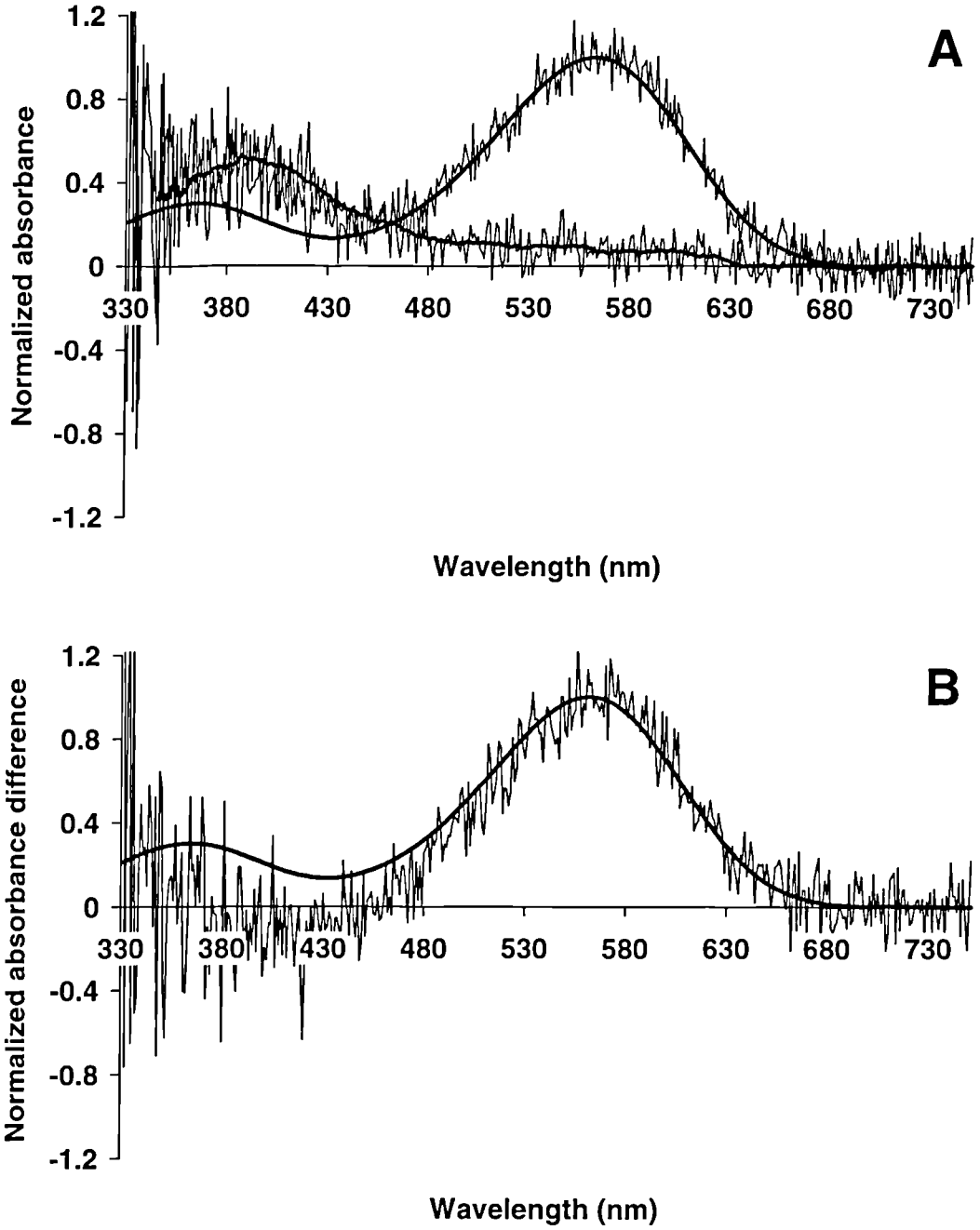

Figure 2.61 Microspectrophotometric results from 4 accessory members of the double cone of the blue tit, *Parus caeruleus*. (**A**) Mean pre-bleach absorbance spectrum (upper trace) with best-fitted visual pigment template (λ_{max} 563 nm, solid line) and mean post-bleach absorbance spectrum (lower trace) with running average (solid line). (**B**) Mean difference spectrum (trace) with best-fitted visual pigment template (λ_{max} 562 nm, solid line).

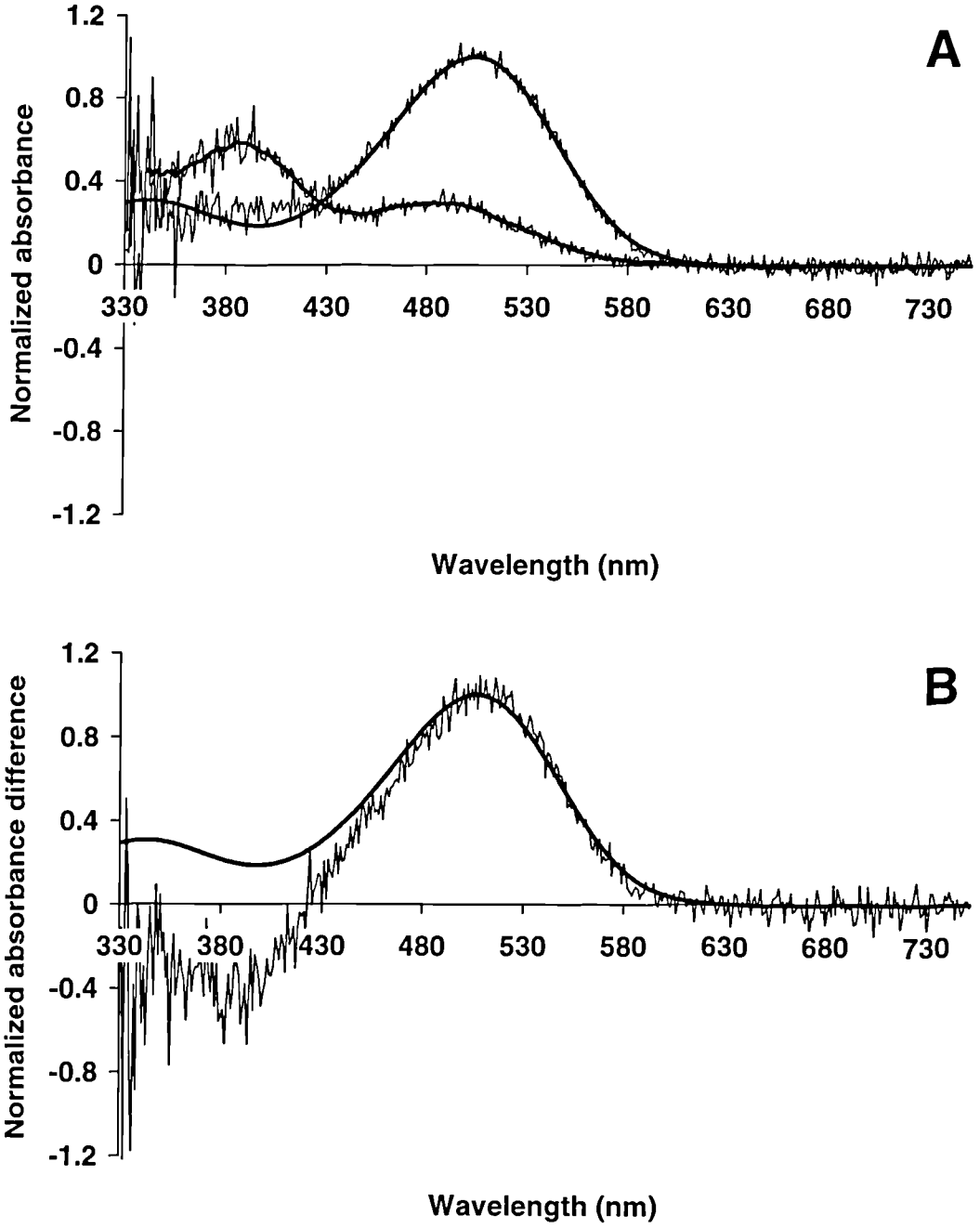

Figure 2.62 Microspectrophotometric results from 6 rods of the blue tit, *Parus caeruleus*. (**A**) Mean pre-bleach absorbance spectrum (upper trace) with best-fitted visual pigment template (λ_{max} 504 nm, solid line) and mean post-bleach absorbance spectrum (lower trace) with running average (solid line). (**B**) Mean difference spectrum (trace) with best-fitted visual pigment template (λ_{max} 507 nm, solid line).

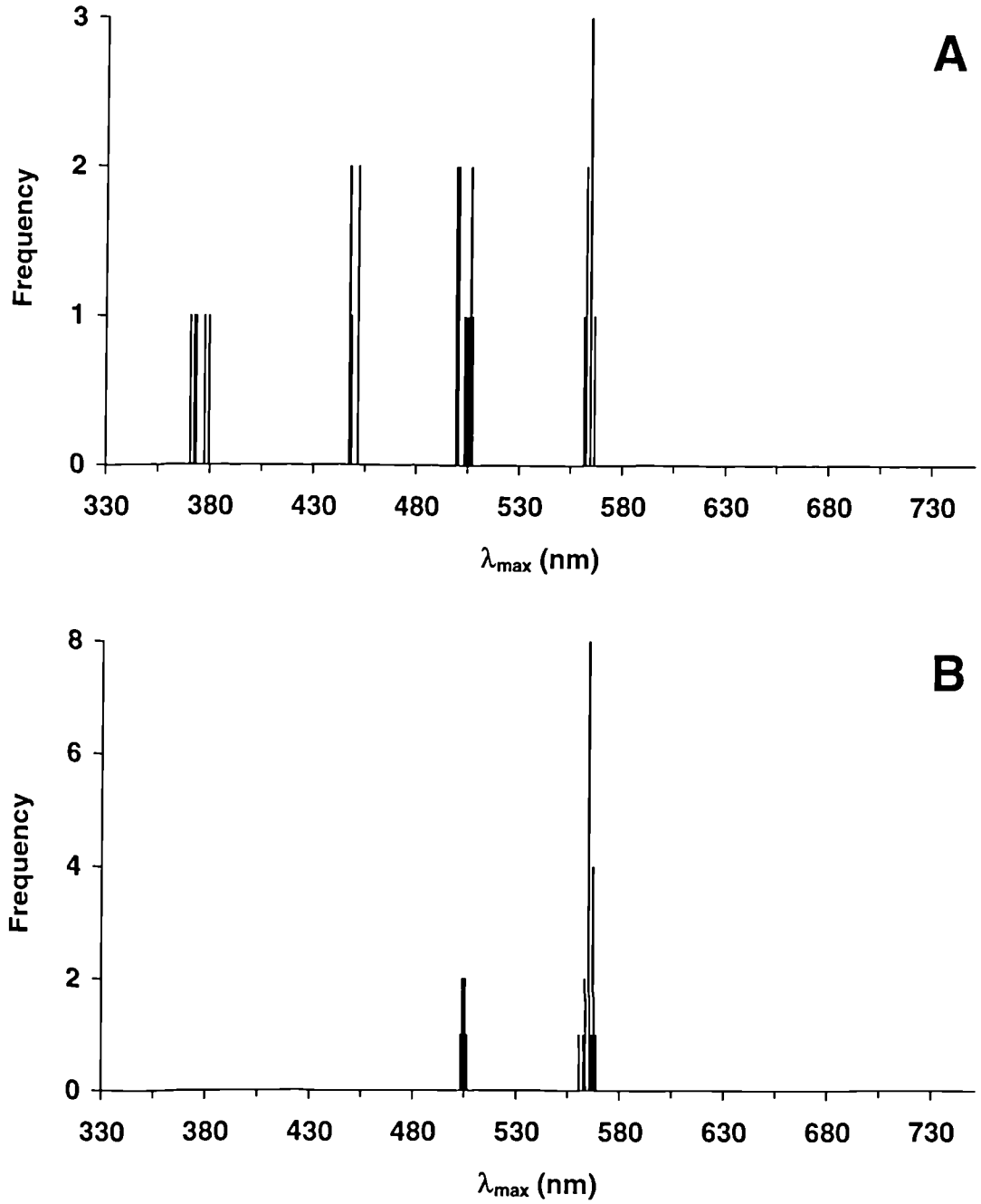

Figure 2.63 Histogram showing the distribution of estimated λ_{max} values obtained from pre-bleach absorbance spectra of visual pigments in the blue tit, *Parus caeruleus*. (**A**) Single cones. λ_{max} values around 374, 448, 502 and 563 nm describe UVS, SWS, MWS and LWS visual pigments respectively. (**B**) Rods and double cones. λ_{max} values around 504 nm describe rod visual pigment, whilst λ_{max} values around 565 nm describe the LWS visual pigments found in the principal and accessory members of the double cones.

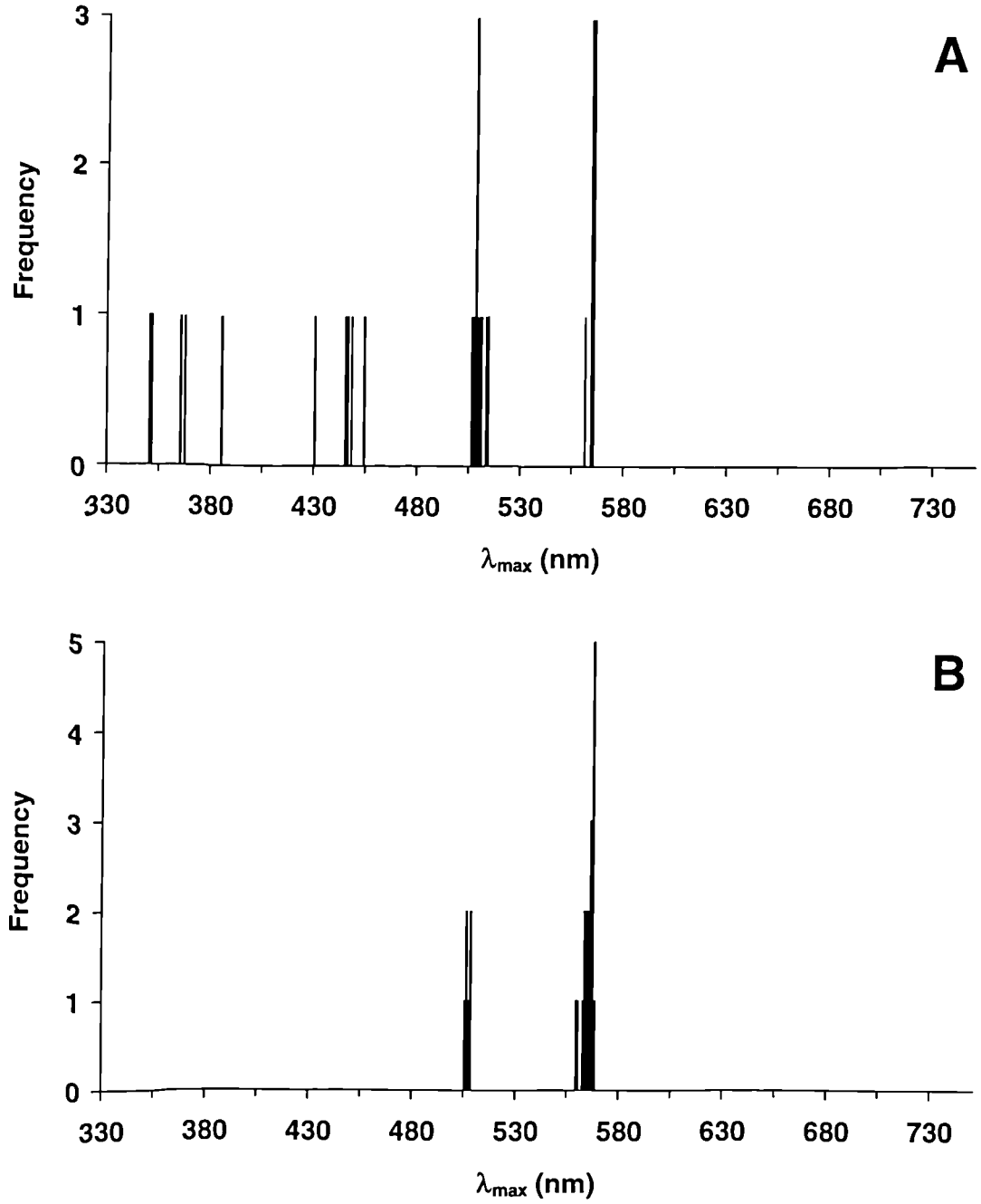

Figure 2.64 Histogram showing the distribution of estimated λ_{max} values obtained from difference spectra of visual pigments in the blue tit, *Parus caeruleus*. (**A**) Single cones. λ_{max} values around 363, 444, 509 and 564 nm describe UVS, SWS, MWS and LWS visual pigments respectively. (**B**) Rods and double cones. λ_{max} values around 507 nm describe rod visual pigment, whilst λ_{max} values around 565 nm describe the LWS visual pigments found in the principal and accessory members of the double cones.

	Rod	Single Cones			Double cone	
		UVS	SWS	MWS	LWS	Principal	Accessory
Visual pigments							
λ_{max} of mean pre-bleach spectrum (nm)	503.5 ± 1.8	373.7 ± 4.2	449.0 ± 5.1	503.3 ± 3.3	563.1 ± 3.0	565.4 ± 3.0	562.9 ± 5.4
Mean of pre-bleach λ_{max} (nm)	503.9 ± 1.0	373.7 ± 3.9	448.4 ± 2.3	502.3 ± 3.1	562.7 ± 1.8	564.9 ± 1.7	563.1 ± 2.7
λ_{max} of mean difference spectrum (nm)	506.7 ± 3.1	371.2 ± 7.9	448.1 ± 11.7	508.8 ± 6.5	563.9 ± 4.8	565.5 ± 3.2	561.9 ± 7.8
Transverse absorbance at λ_{max} of mean difference spectrum	0.023	0.005	0.007	0.010	0.018	0.017	0.012
Mean of difference spectrum λ_{max} (nm)	506.5 ± 1.3	363.3 ± 14.4	444.2 ± 9.2	508.9 ± 2.7	563.5 ± 1.3	565.0 ± 1.6	562.3 ± 4.0
Number of cells	6	5	5	10	7	14	4

Table 2.9 Summary of the microspectrophotometric data obtained for the visual pigments of the blue tit, *Parus caeruleus*.

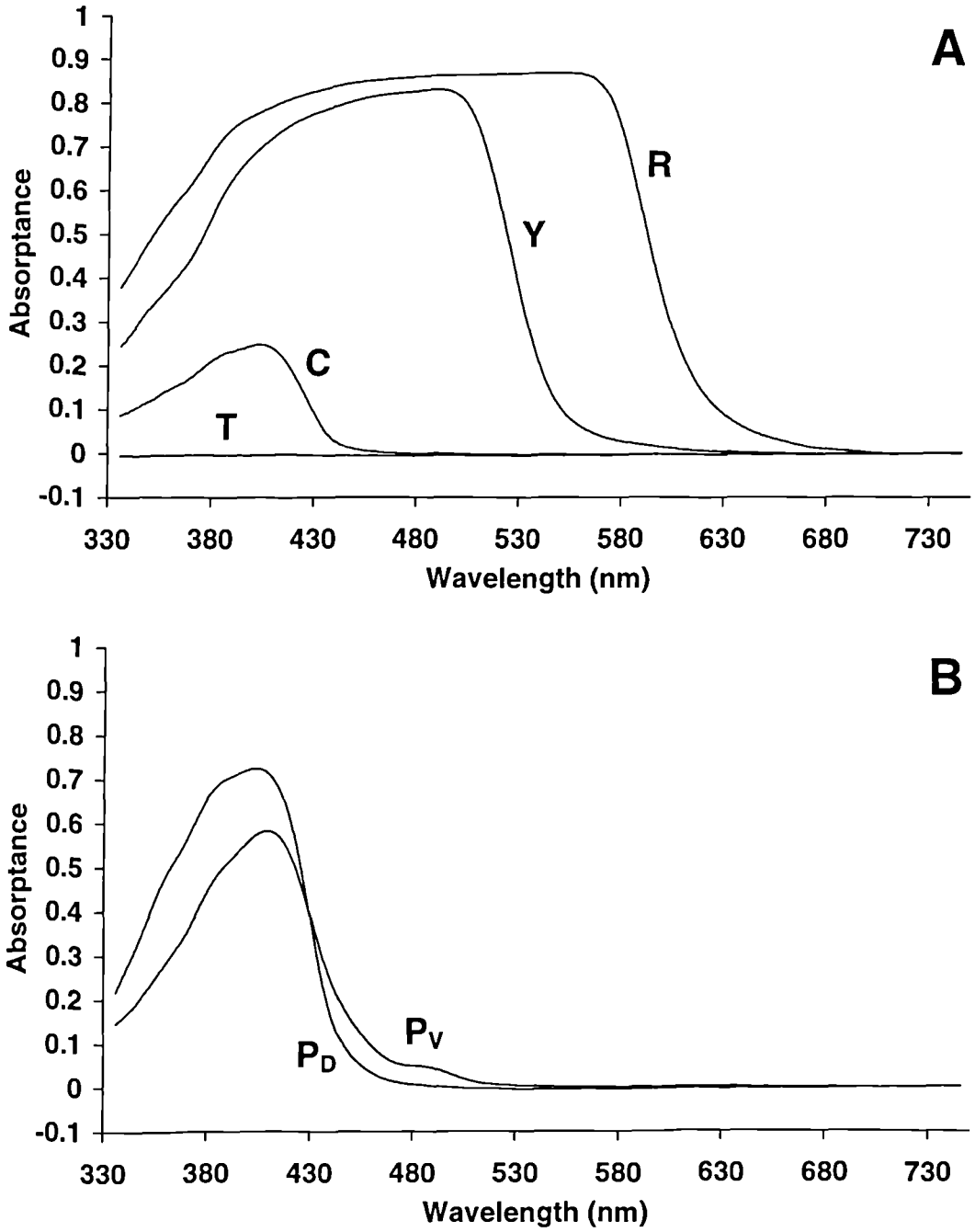

Figure 2.65 Mean absorptance spectra of oil droplets from the blue tit, *Parus caeruleus*. (**A**) Oil droplets located in the single cones. T-, C-, Y- and R-type droplets were found in the UVS, SWS, MWS and LWS cones respectively. (**B**) Oil droplets located in the principal member of the double cones (P-type). P-type droplets located in the ventral retina (P_V) had their λ_{cut} at marginally longer wavelengths than those located in the dorsal retina (P_D). No A-type droplet was measured in the accessory member.

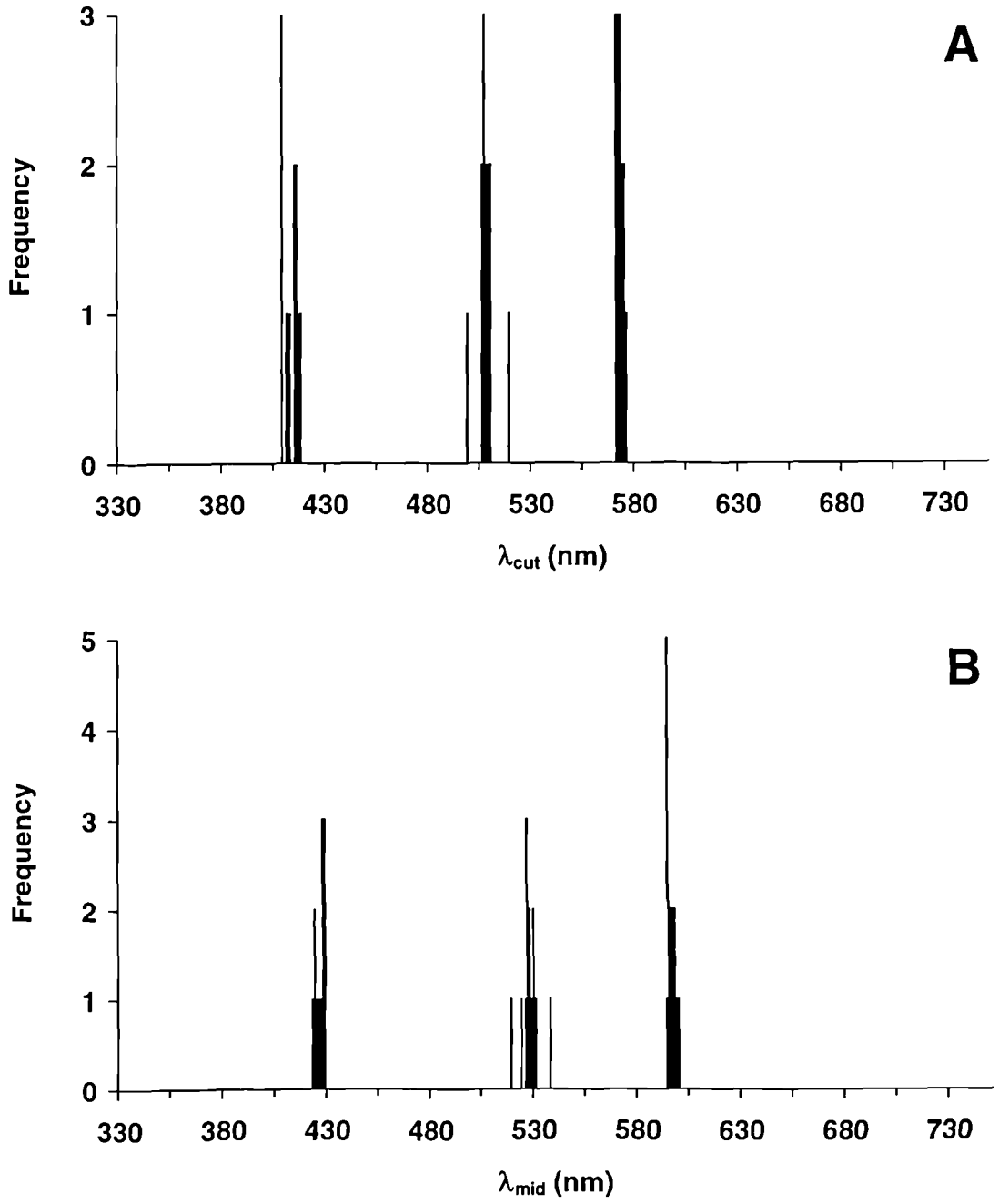

Figure 2.66 Histograms showing the spectral distribution of λ_{cut} and λ_{mid} values for single cone oil droplets measured in the blue tit, *Parus caeruleus*. (**A**) λ_{cut} values around 413, 508 and 573 nm, and (**B**) λ_{mid} values around 426, 528 and 596 nm, describe C-type, Y-type and R-type oil droplets respectively.

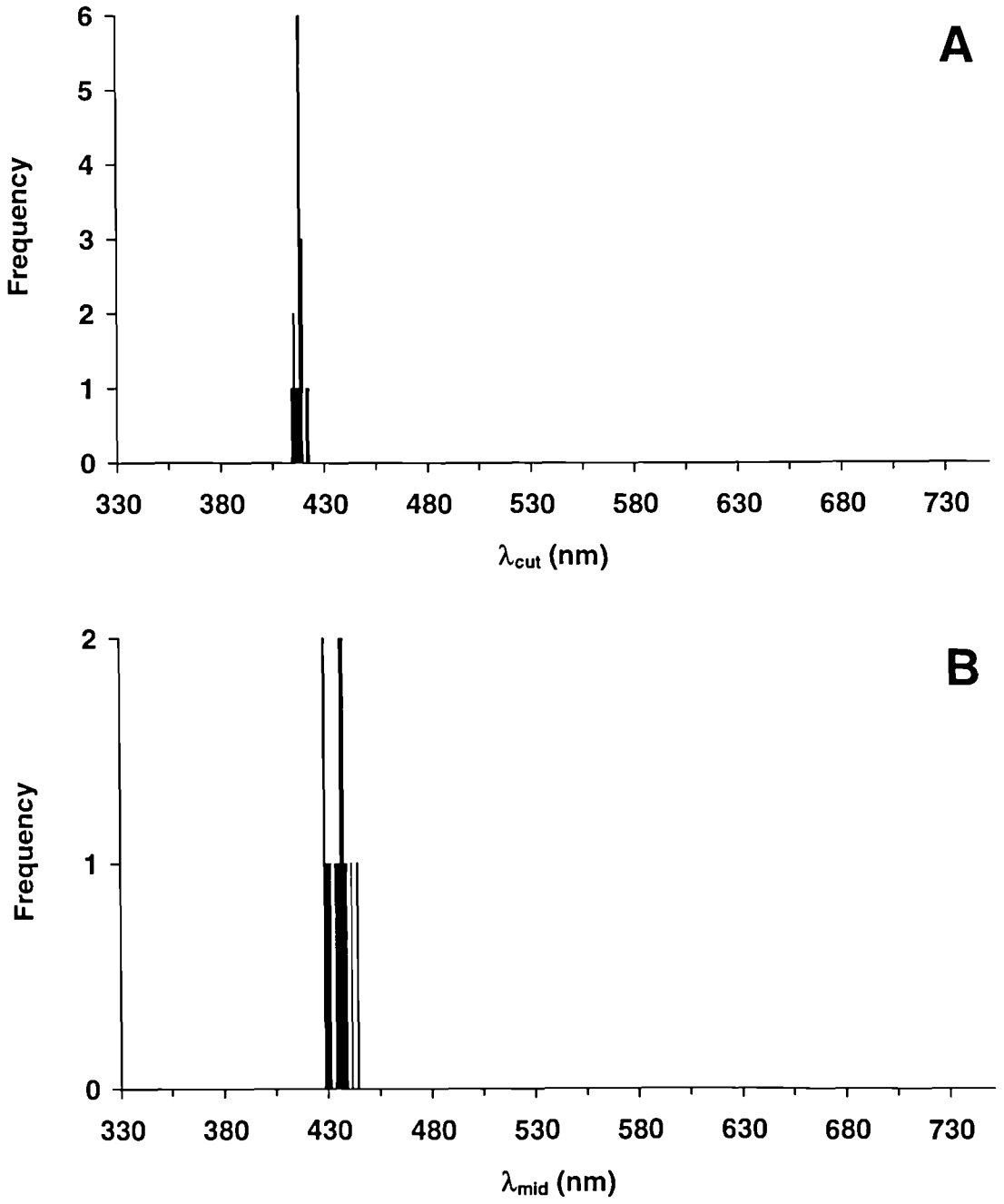

Figure 2.67 Histograms showing the spectral distribution of λ_{cut} and λ_{mid} values for P-type droplets measured in the principal member of the double cones of the blue tit, *Parus caeruleus*. There was little difference between droplets taken from the dorsal and ventral regions of the retina in (**A**) their mean λ_{cut} values (417 and 418 nm respectively) or (**B**) their mean λ_{mid} values (431 and 437 nm respectively).

	Single cones				Double cone		
Cone type	UVS	SWS	MWS	LWS	Principal		Accessory
Oil droplet type	T-type	C-type	Y-type	R-type	P-type		A-type
					D	V	
λ_{cut} of mean absorption spectrum (nm)	<330	413.5	507.7	572.6	417.4	417.9	-
λ_{mid} of mean absorption spectrum (nm)	<330	426.6	528.0	595.9	431.1	436.4	-
Maximum corrected absorptance of mean absorption spectrum	<0.01	0.25	0.83	0.87	0.72	0.58	-
Mean λ_{cut} (nm)	<330	412.9 ± 3.1	507.6 ± 4.3	572.5 ± 1.7	416.8 ± 3.2	417.9 ± 0.5	-
Mean λ_{mid} (nm)	<330	426.2 ± 2.2	527.5 ± 4.3	595.9 ± 1.8	430.6 ± 3.5	437.0 ± 3.4	-
Mean diameter (μm)	2.0 ± 0.5	2.2 ± 0.4	2.7 ± 0.3	3.1 ± 0.2	3.2 ± 0.2	3.0 ± 0.3	-
Number of oil droplets	8	12	13	14	7	9	-

Table 2.10 Summary of the microspectrophotometric data obtained for the cone oil droplets of the blue tit, *Parus caeruleus*.

2.6.1.5 Peacock

Microspectrophotometric data for visual pigments and oil droplets measured in the peacock, *Pavo cristatus*, are displayed in Figure 2.68 to Figure 2.79 and summarised in Table 2.11 and Table 2.12. Like the starling, turkey, blackbird and blue tit, the peacock retina contained five different types of rhodopsin visual pigment, in six different types of photoreceptor.

The single class of rod contained a visual pigment with a mean pre-bleach λ_{max} at 504 nm (n = 7). There were four different types of single cone, each of which was reliably associated with a different type of oil droplet. Single cones containing R-type oil droplets (mean λ_{cut} 569 nm, n = 29) were paired with a LWS visual pigment which had a mean pre-bleach λ_{max} of 566 nm (n = 4).

Y-type oil droplets (mean λ_{cut} 511 nm, n = 28) were paired with a MWS visual pigment that had a mean pre-bleach λ_{max} of 505 nm (n = 5). Single cones containing a C-type droplet (mean λ_{cut} 449 nm, n = 9) were associated with a SWS visual pigment of mean pre-bleach λ_{max} 458 nm (n = 14). The fourth type of single cone contained an violet-sensitive (VS) visual pigment, of mean pre-bleach λ_{max} 421 nm (n = 4), and a T-type oil droplet which showed no detectable absorbance above 330 nm.

Both members of the double cone pair contained visual pigments resembling the LWS visual pigment measured in the single cones. The visual pigment in the principal member had a pre-bleach λ_{max} at 567 nm (n = 9). The P-type oil droplets in the principal member had a variable λ_{cut} depending on retinal location. P-type droplets in the ventral retina and their λ_{cut} at longer wavelengths (mean λ_{cut} 500 nm, n = 22) compared to those found in the dorsal retina (mean λ_{cut} 479 nm, n = 9).

The visual pigment in the accessory member of the double cone had a mean pre-bleach λ_{max} of 565 nm (n = 4) and was associated with an A-type droplet with a mean λ_{cut} of 488 nm (n = 6).

The maximum corrected absorptance of the C-type oil droplets was relatively high (0.87), and of the same order of magnitude as the other pigmented droplet types. In fact, because of by-passing light in the MSP, this is almost certainly an

underestimation. This suggests that the C-type droplets in the peacock SWS cones act as cut-off filters in the same way as the R- and Y-type droplets. A-type droplets, however, had a much lower maximum corrected absorbance (0.40), suggesting that, like the A-type droplets of the starling, they do not act as cut-off filters.

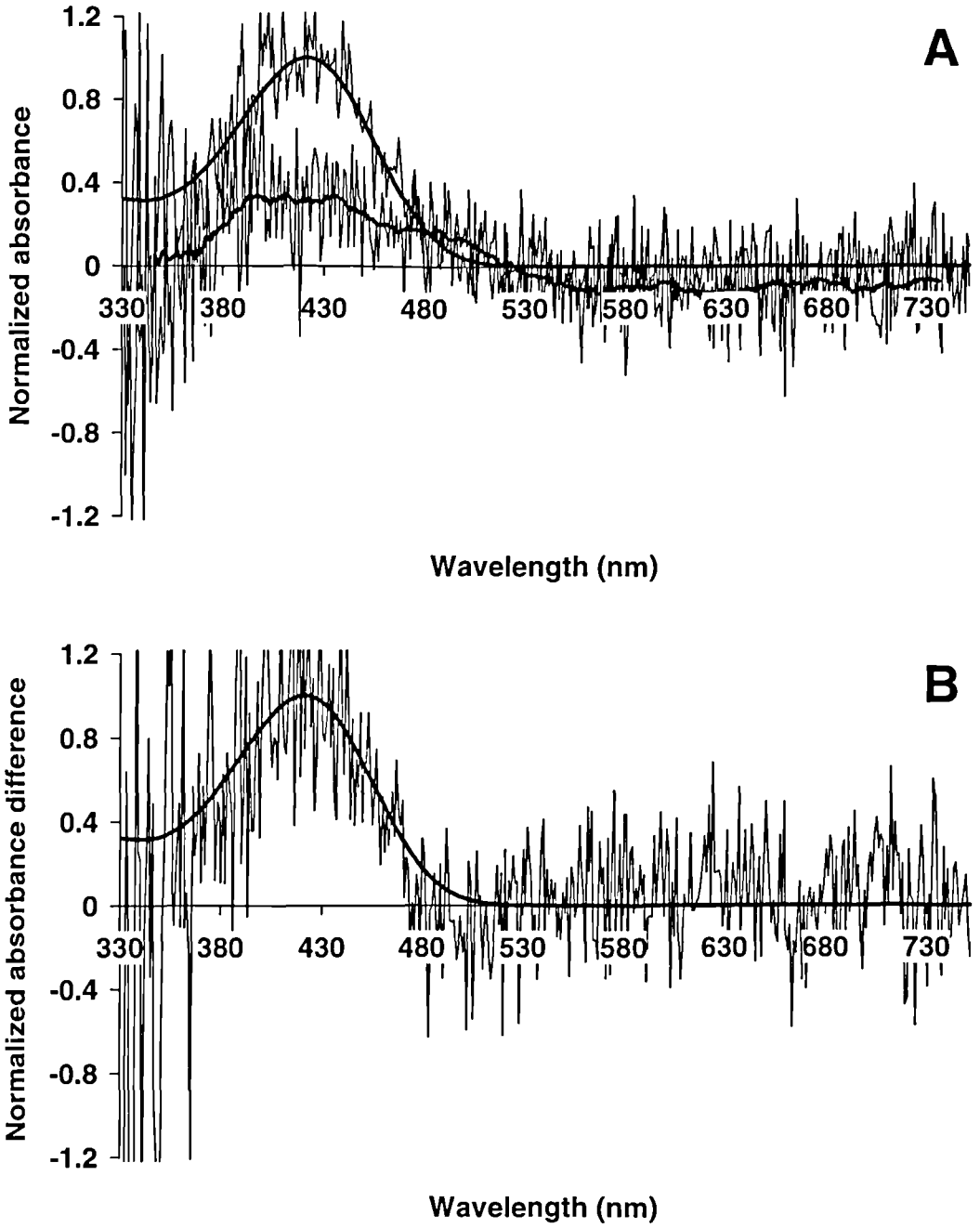

Figure 2.68 Microspectrophotometric results from 4 VS single cones of the peacock, *Pavo cristatus*. (**A**) Mean pre-bleach absorbance spectrum (upper trace) with best-fitted visual pigment template (λ_{max} 421 nm, solid line) and mean post-bleach absorbance spectrum (lower trace) with running average (solid line). (**B**) Mean difference spectrum (trace) with best-fitted visual pigment template (λ_{max} 421 nm, solid line).

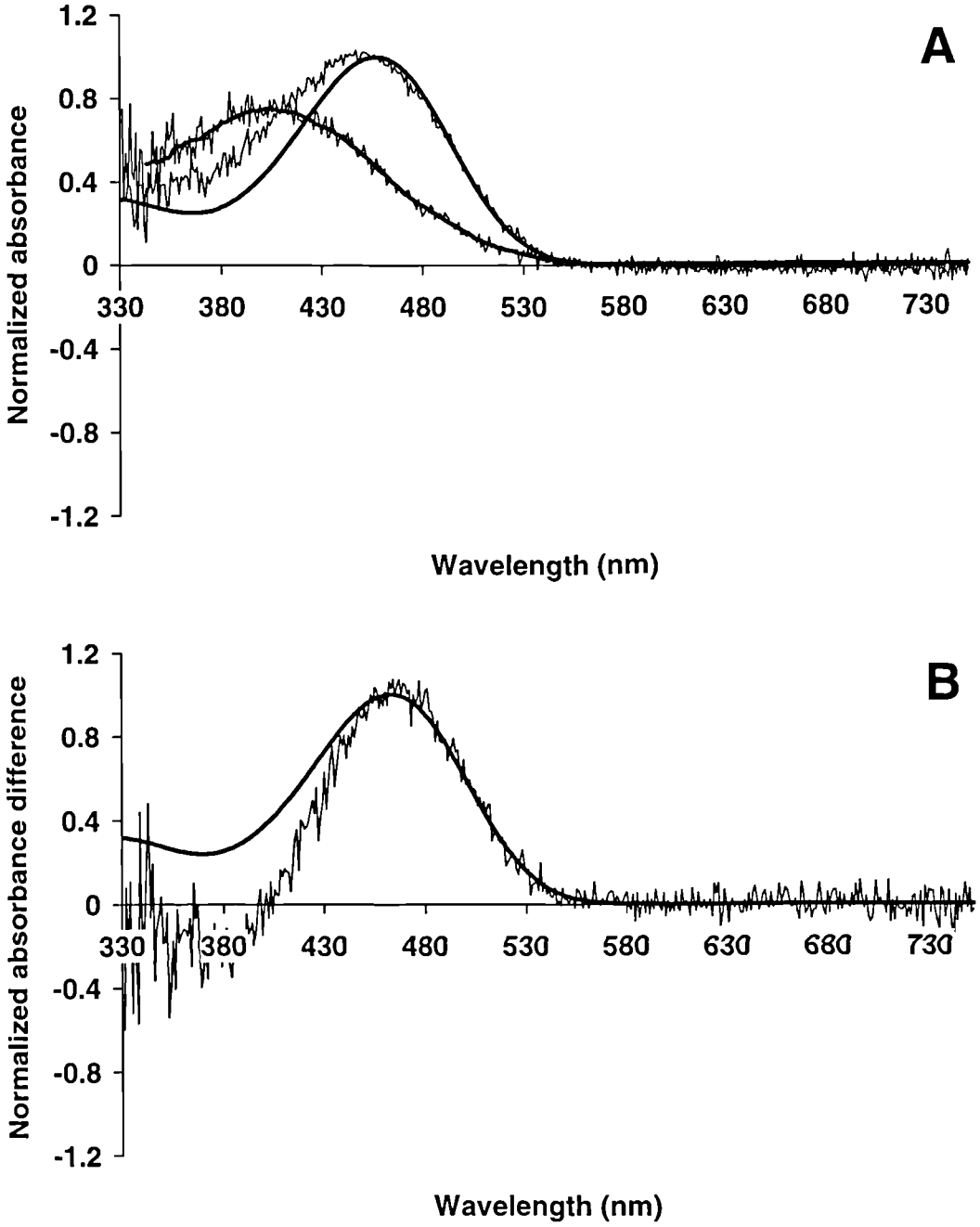

Figure 2.69 Microspectrophotometric results from 14 SWS single cones of the peacock, *Pavo cristatus*. (**A**) Mean pre-bleach absorbance spectrum (upper trace) with best-fitted visual pigment template (λ_{max} 457 nm, solid line) and mean post-bleach absorbance spectrum (lower trace) with running average (solid line). (**B**) Mean difference spectrum (trace) with best-fitted visual pigment template (λ_{max} 463 nm, solid line).

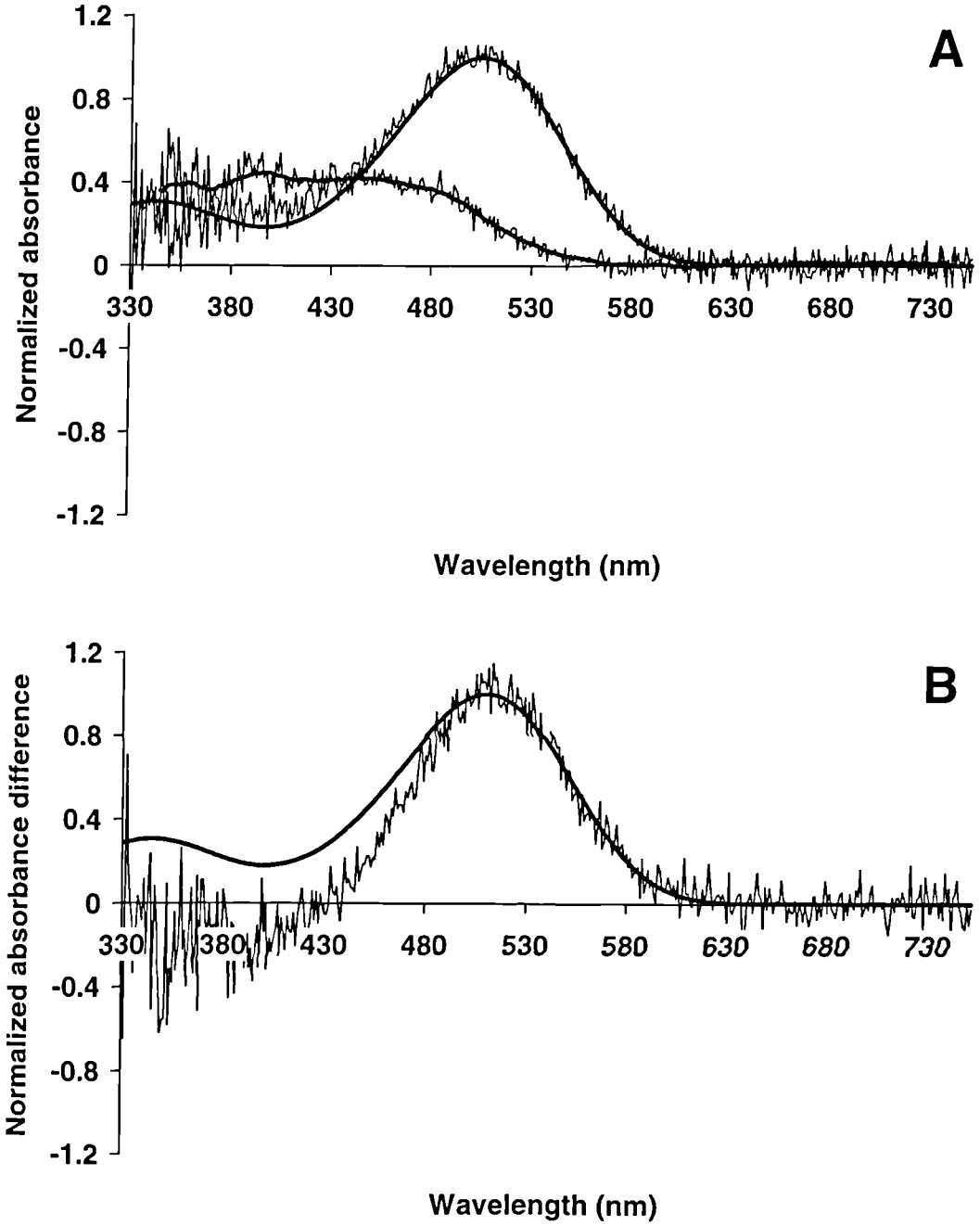

Figure 2.70 Microspectrophotometric results from 5 MWS single cones of the peacock, *Pavo cristatus*. (**A**) Mean pre-bleach absorbance spectrum (upper trace) with best-fitted visual pigment template (λ_{max} 505 nm, solid line) and mean post-bleach absorbance spectrum (lower trace) with running average (solid line). (**B**) Mean difference spectrum (trace) with best-fitted visual pigment template (λ_{max} 511 nm, solid line).

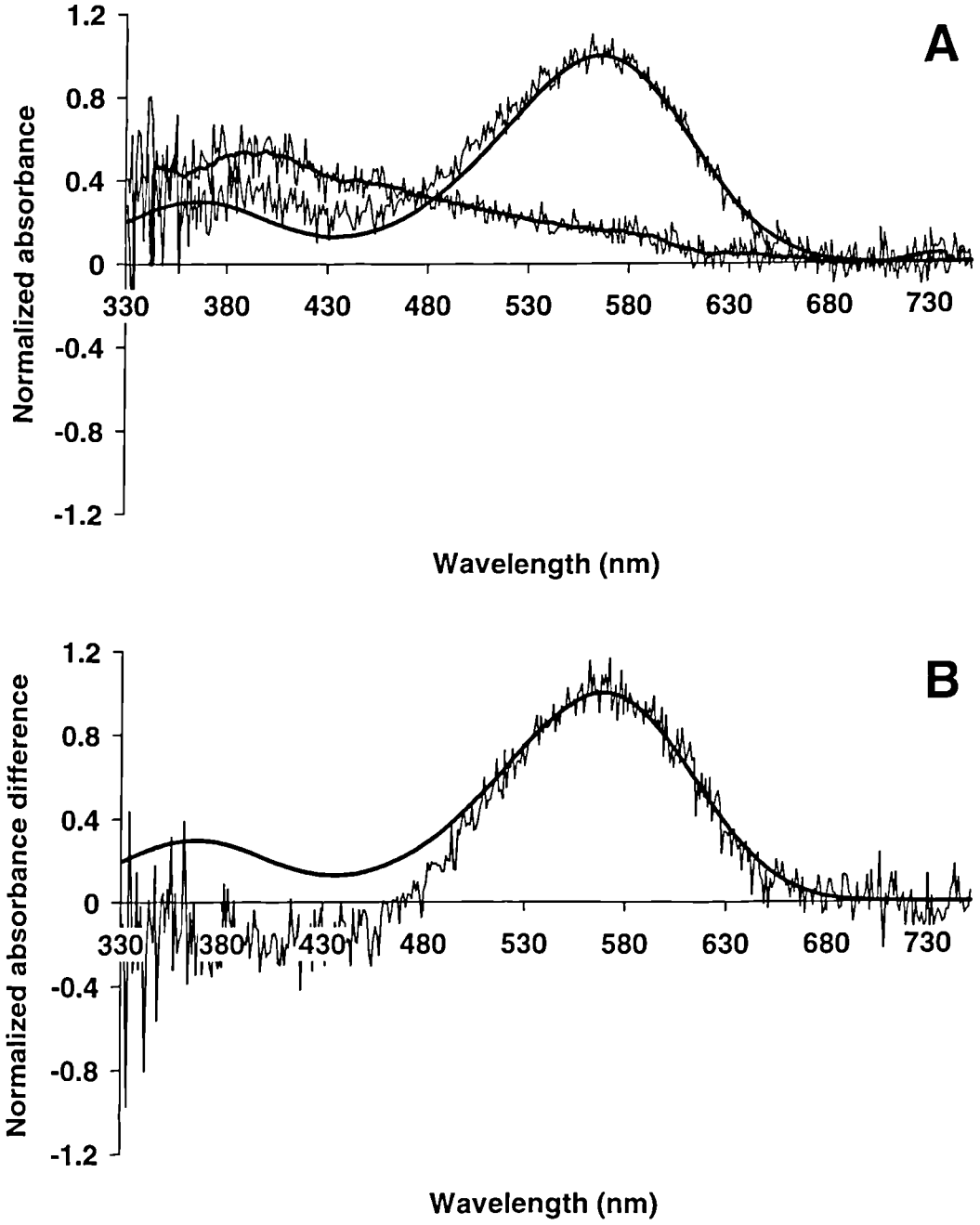

Figure 2.71 Microspectrophotometric results from 4 LWS single cones of the peacock, *Pavo cristatus*. (**A**) Mean pre-bleach absorbance spectrum (upper trace) with best-fitted visual pigment template (λ_{max} 566 nm, solid line) and mean post-bleach absorbance spectrum (lower trace) with running average (solid line). (**B**) Mean difference spectrum (trace) with best-fitted visual pigment template (λ_{max} 569 nm, solid line).

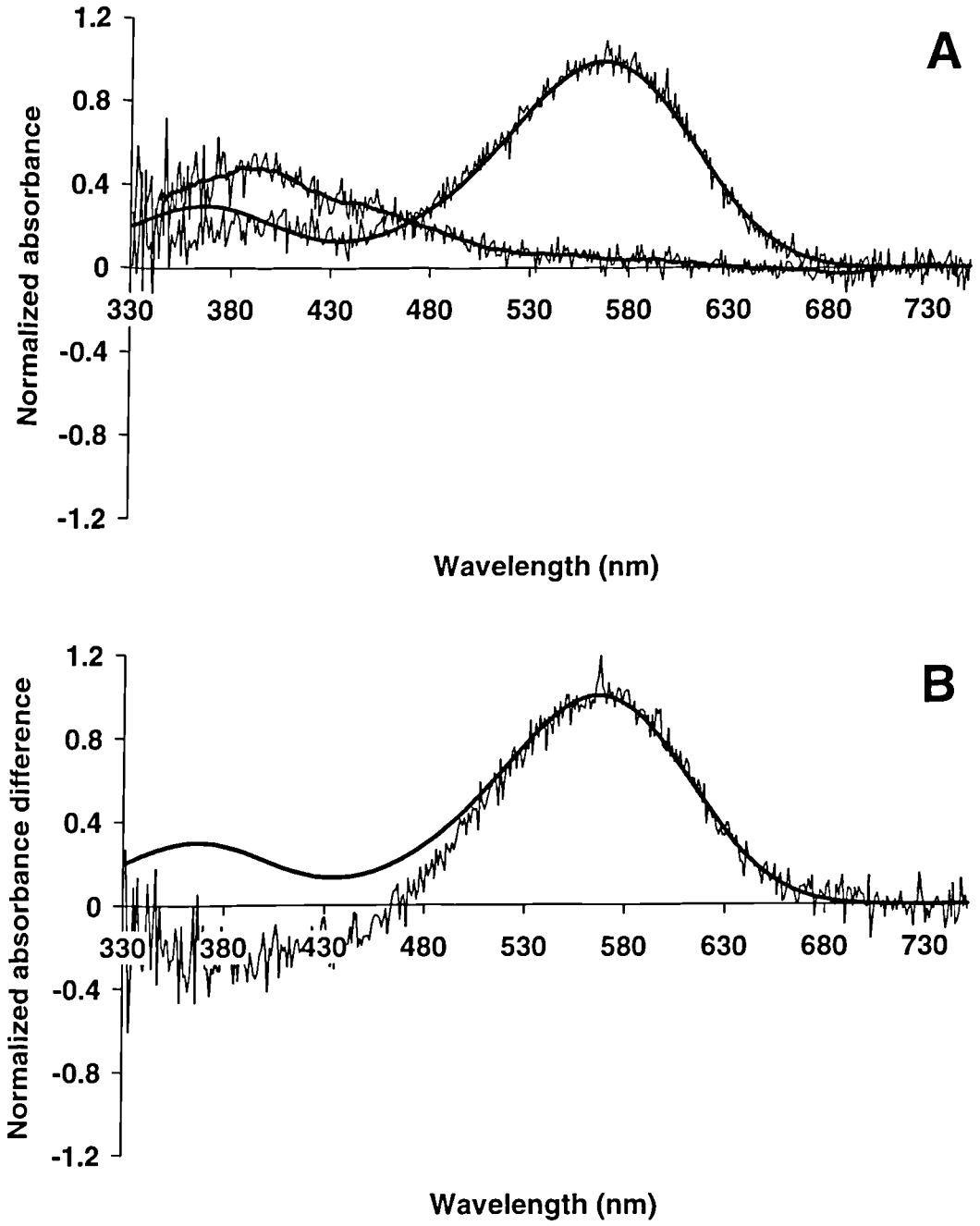

Figure 2.72 Microspectrophotometric results from 9 principal members of the double cone of the peacock, *Pavo cristatus*. (**A**) Mean pre-bleach absorbance spectrum (upper trace) with best-fitted visual pigment template (λ_{max} 567 nm, solid line) and mean post-bleach absorbance spectrum (lower trace) with running average (solid line). (**B**) Mean difference spectrum (trace) with best-fitted visual pigment template (λ_{max} 567 nm, solid line).

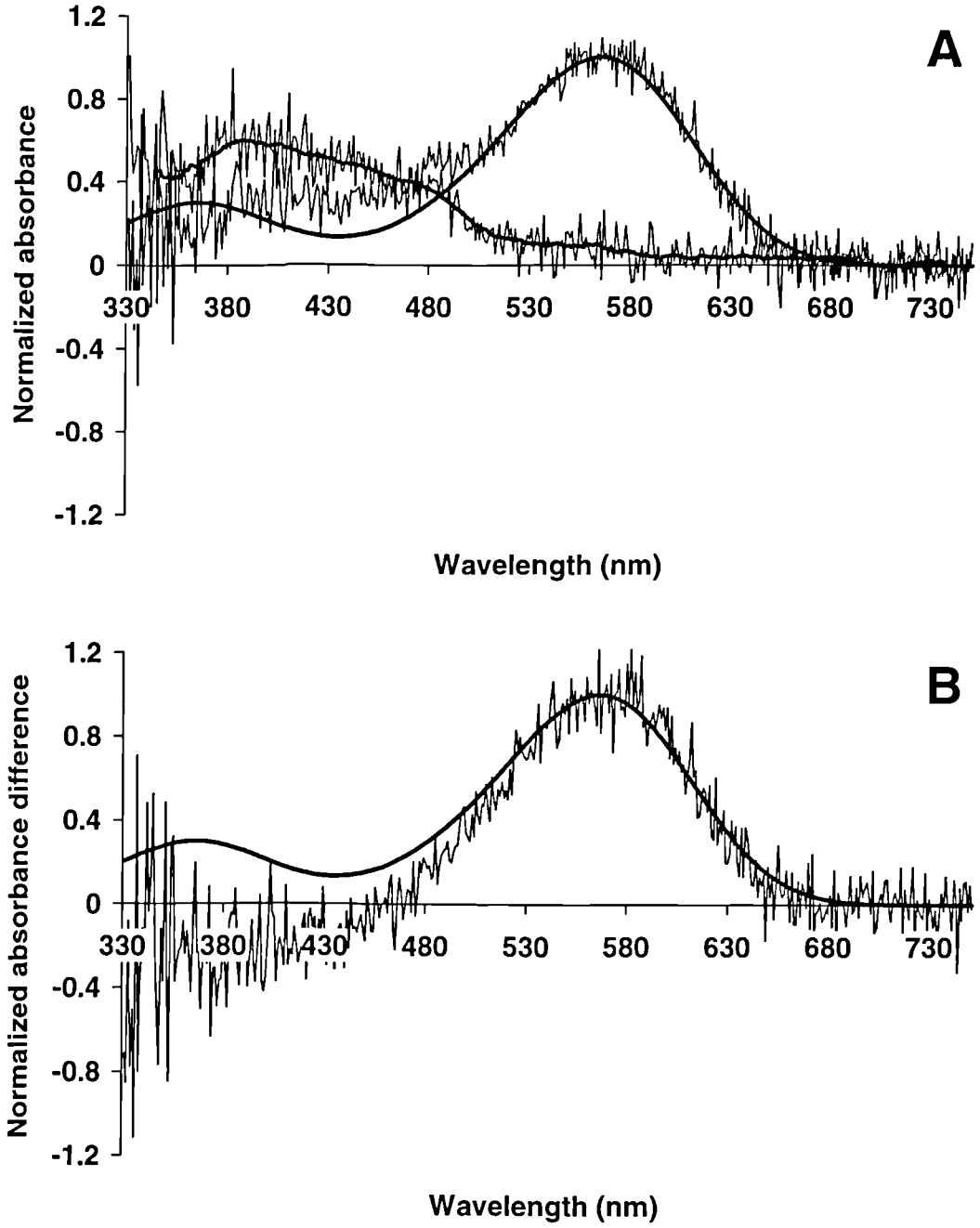

Figure 2.73 Microspectrophotometric results from 4 accessory members of the double cone of the peacock, *Pavo cristatus*. (**A**) Mean pre-bleach absorbance spectrum (upper trace) with best-fitted visual pigment template (λ_{max} 566 nm, solid line) and mean post-bleach absorbance spectrum (lower trace) with running average (solid line). (**B**) Mean difference spectrum (trace) with best-fitted visual pigment template (λ_{max} 566 nm, solid line).

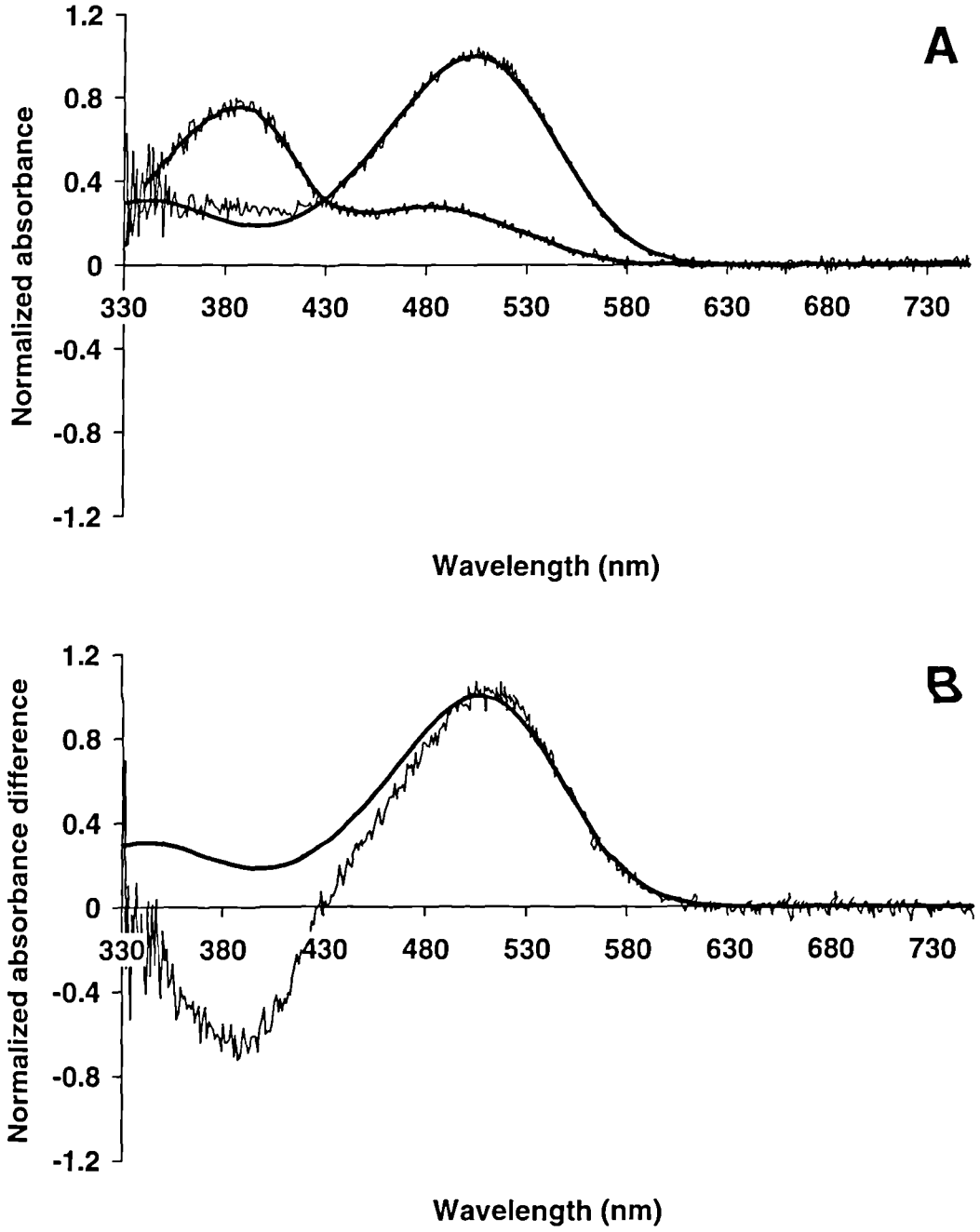

Figure 2.74 Microspectrophotometric results from 7 rods of the peacock, *Pavo cristatus*. (**A**) Mean pre-bleach absorbance spectrum (upper trace) with best-fitted visual pigment template (λ_{max} 504 nm, solid line) and mean post-bleach absorbance spectrum (lower trace) with running average (solid line). (**B**) Mean difference spectrum (trace) with best-fitted visual pigment template (λ_{max} 506 nm, solid line).

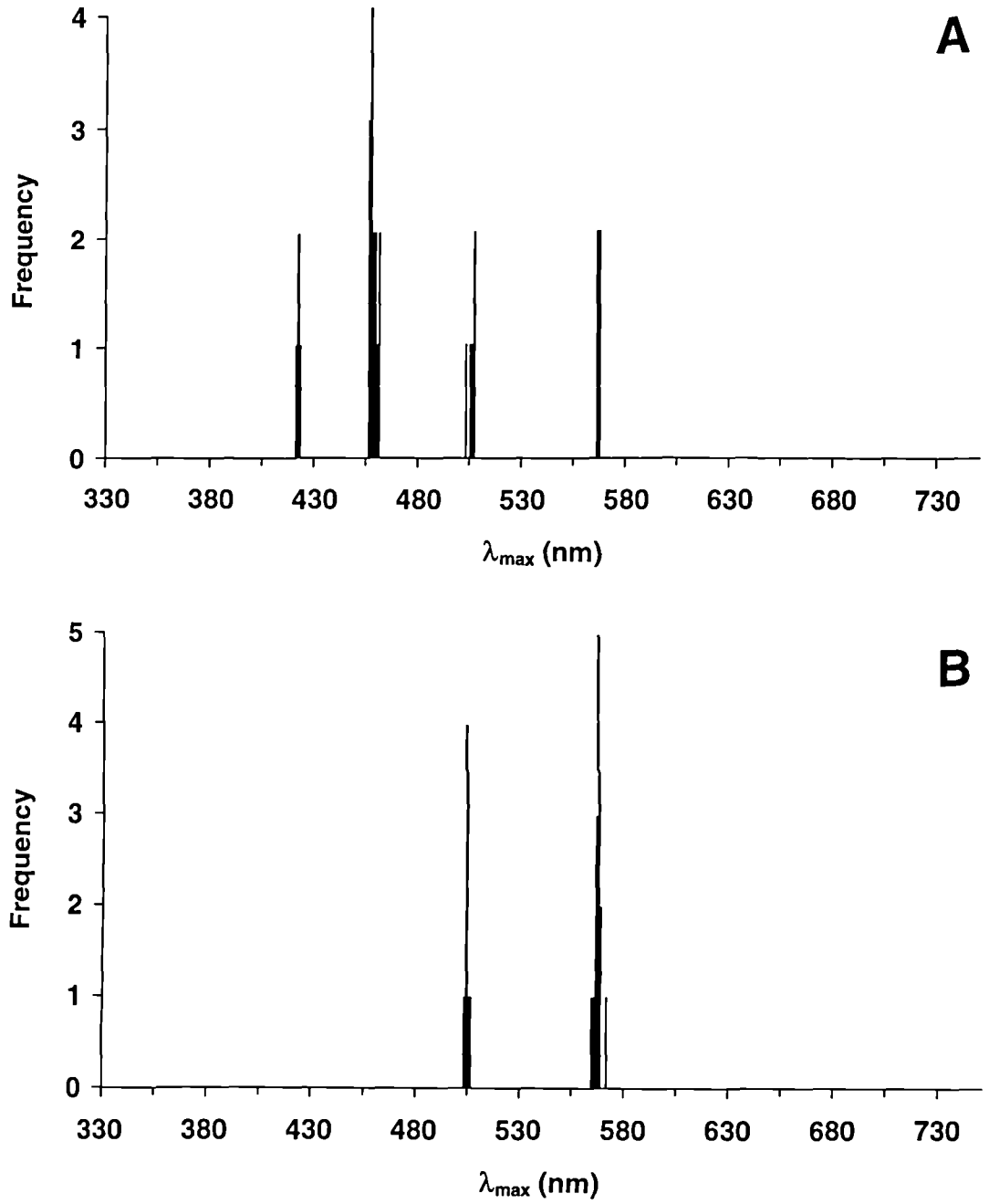

Figure 2.75 Histogram showing the distribution of estimated λ_{max} values obtained from pre-bleach absorbance spectra of visual pigments in the peacock, *Pavo cristatus*. (**A**) Single cones. λ_{max} values around 421, 458, 505 and 566 nm describe VS, SWS, MWS and LWS visual pigments respectively. (**B**) Rods and double cones. λ_{max} values around 504 nm describe rod visual pigment, whilst λ_{max} values around 566 nm describe the LWS visual pigments found in the principal and accessory members of the double cones.

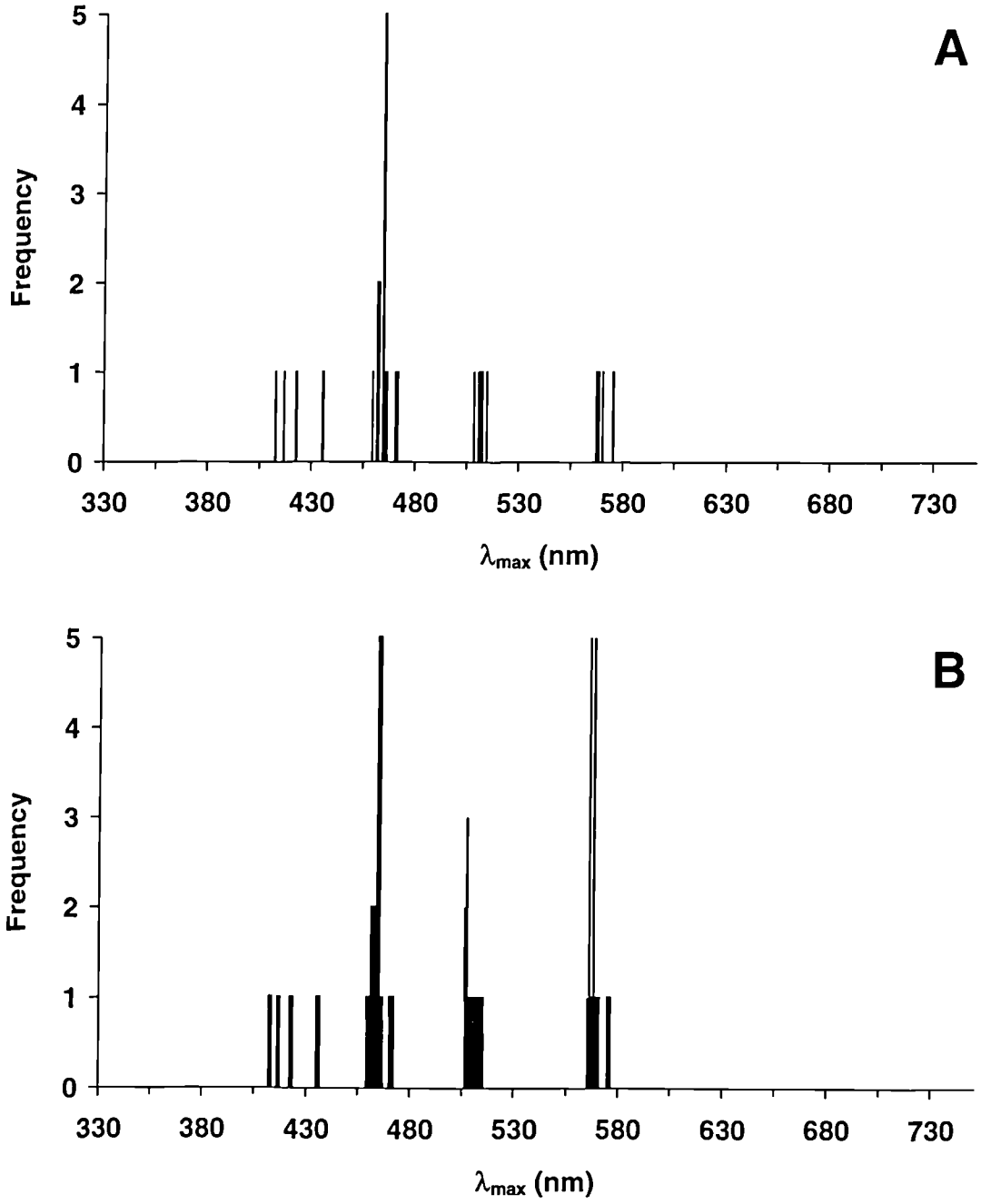

Figure 2.76 Histogram showing the distribution of estimated λ_{max} values obtained from difference spectra of visual pigments in the peacock, *Pavo cristatus*. (**A**) Single cones. λ_{max} values around 421, 464, 511 and 570 nm describe VS, SWS, MWS and LWS visual pigments respectively. (**B**) Rods and double cones. λ_{max} values around 507 nm describe rod visual pigment, whilst λ_{max} values around 568 nm describe the LWS visual pigments found in the principal and accessory members of the double cones.

	Rod	Single Cones			Double cone	
		VS	SWS	MWS	LWS	Principal	Accessory
Visual pigments							
λ_{max} of mean pre-bleach spectrum (nm)	503.7 ± 0.8	421.1 ± 5.4	457.1 ± 1.5	504.9 ± 2.6	566.4 ± 2.8	566.9 ± 3.1	565.7 ± 5.7
Mean of pre-bleach λ_{max} (nm)	503.8 ± 0.9	421.4 ± 0.9	457.5 ± 1.8	505.1 ± 1.9	566.2 ± 0.8	566.6 ± 1.7	565.1 ± 1.1
λ_{max} of mean difference spectrum (nm)	506.2 ± 1.8	421.0 ± 13.4	463.0 ± 2.6	511.2 ± 3.8	568.6 ± 5.6	567.3 ± 3.3	566.3 ± 7.9
Transverse absorbance at λ_{max} of mean difference spectrum	0.039	0.004	0.012	0.017	0.017	0.017	0.014
Mean of difference spectrum λ_{max} (nm)	506.6 ± 1.0	420.8 ± 10.1	463.5 ± 3.3	510.6 ± 2.1	569.6 ± 3.6	567.7 ± 3.1	565.7 ± 1.2
Number of cells	7	4	14	5	4	9	4

Table 2.11 Summary of the microspectrophotometric results obtained for the visual pigments of the peacock, *Pavo cristatus*.

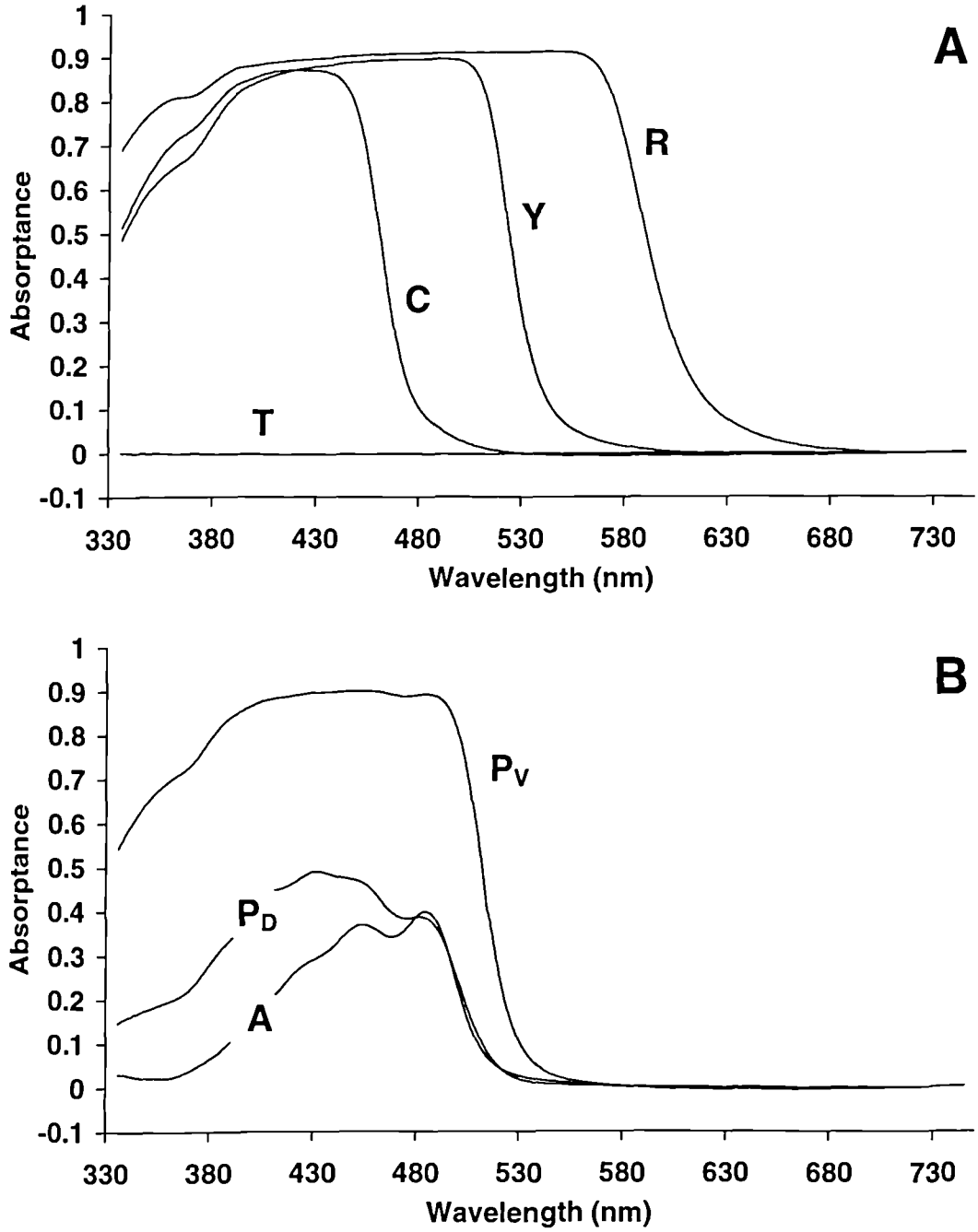

Figure 2.77 Mean absorptance spectra of oil droplets from the peacock, *Pavo cristatus*. (**A**) Oil droplets located in the single cones. T-, C-, Y- and R-type droplets were found in the VS, SWS, MWS and LWS cones respectively. (**B**) Oil droplets located in the principal (P-type, solid lines) and accessory (A-type, dashed line) members of the double cones . P-type droplets located in the ventral retina (P_V) had their λ_{cut} at longer wavelengths than those located in the dorsal retina (P_D).

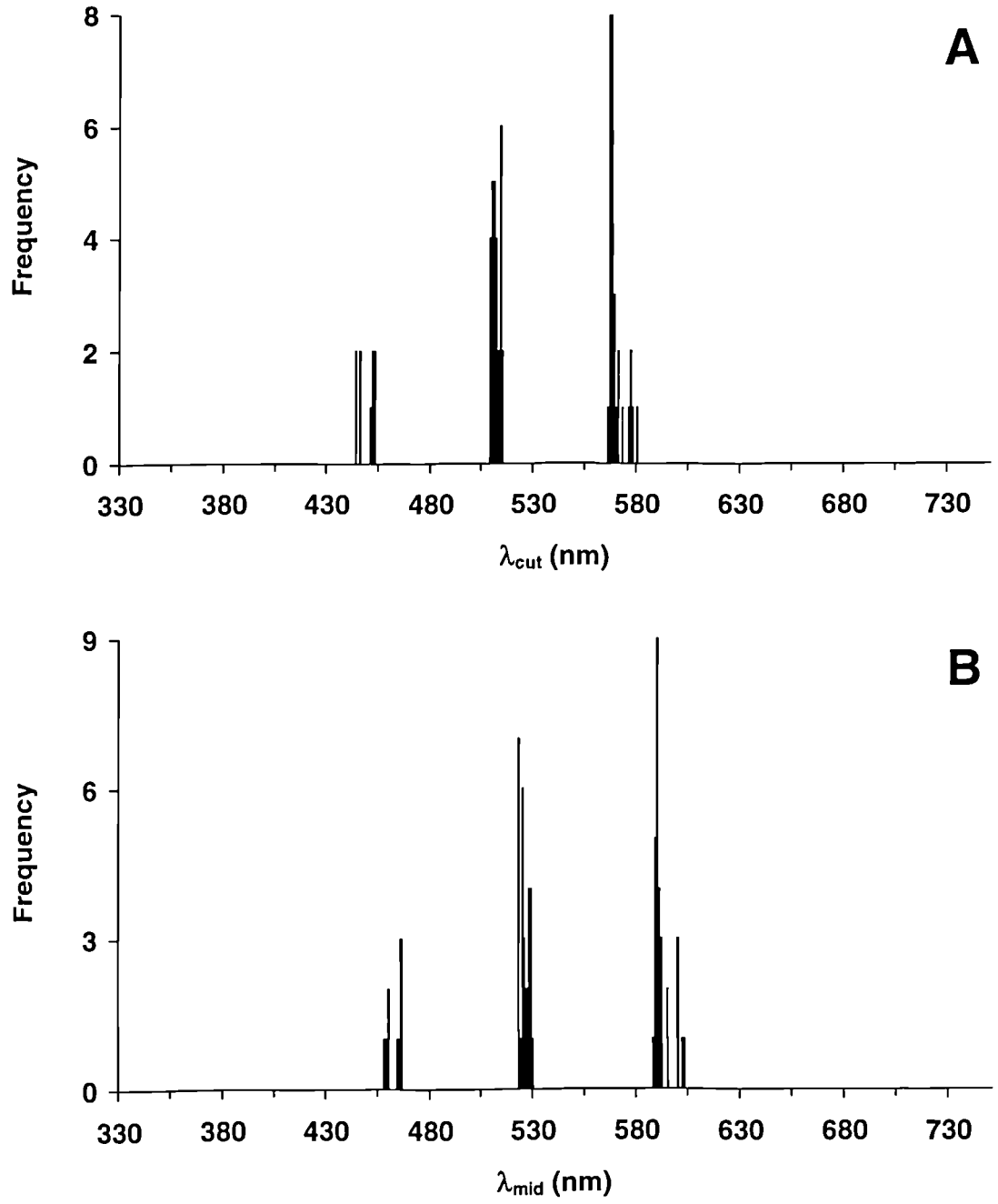

Figure 2.78 Histograms showing the spectral distribution of λ_{cut} and λ_{mid} values for single cone oil droplets measured in the peacock, *Pavo cristatus*. (**A**) λ_{cut} values around 449, 511 and 569 nm, and (**B**) λ_{mid} values around 462, 525 and 592 nm, describe C-type, Y-type and R-type oil droplets respectively.

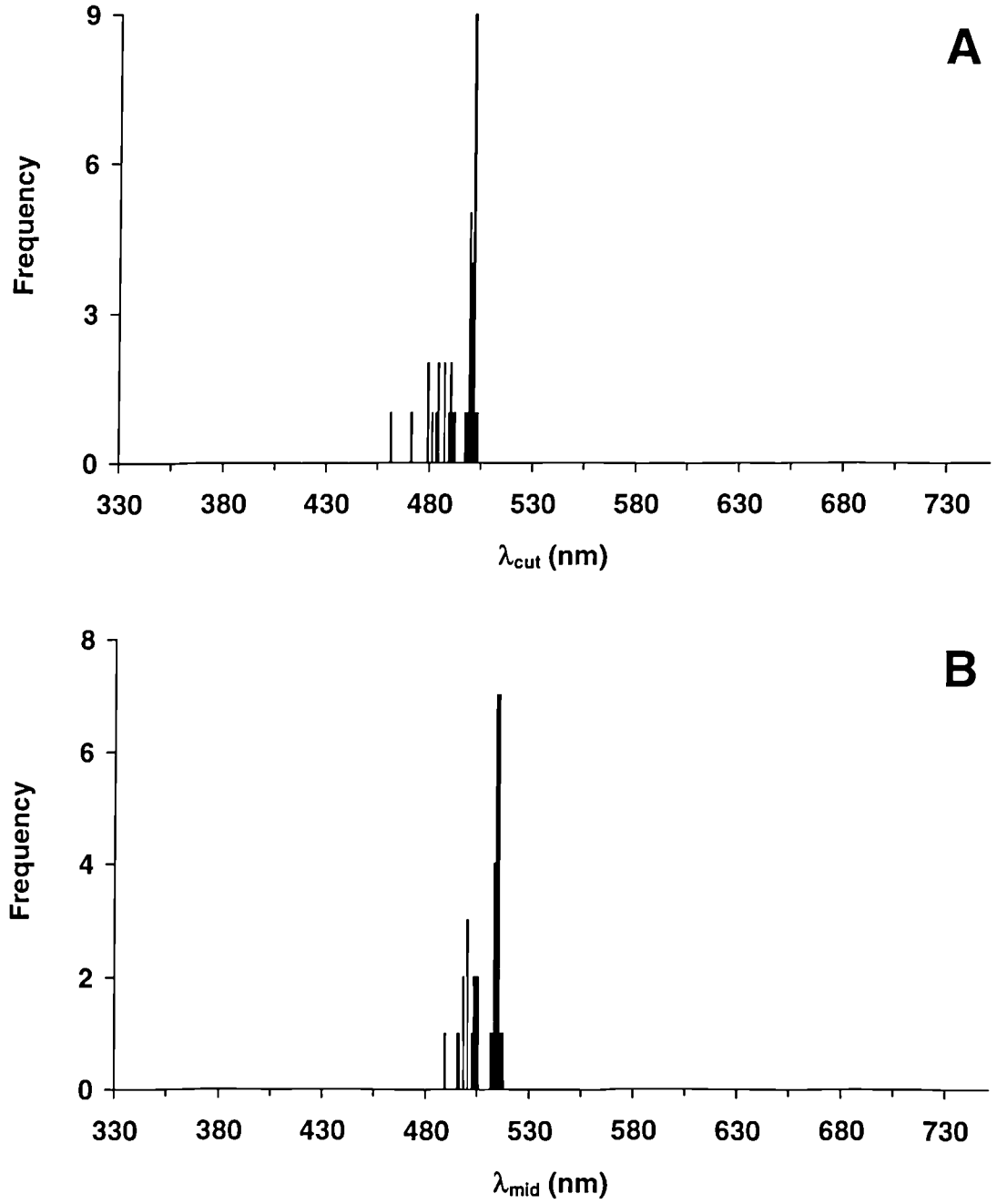

Figure 2.79 Histograms showing the spectral distribution of λ_{cut} and λ_{mid} values for the A-type and P-type oil droplets measured in the double cones of the peacock, *Pavo cristatus*. (**A**) λ_{cut} values around 488, 479 and 500 nm, and (**B**) λ_{mid} values around 501, 499 and 514 nm, describe A-type, dorsally located P-type and ventrally located P-type droplets respectively.

	Single cones				Double cone		
Cone type	**VS**	**SWS**	**MWS**	**LWS**	**Principal**		**Accessory**
Oil droplet type	**T-type**	**C-type**	**Y-type**	**R-type**	**P-type**		**A-type**
					D	**V**	
λ_{cut} of mean absorption spectrum (nm)	<330	449.5	511.4	569.6	482.5	499.6	489.9
λ_{mid} of mean absorption spectrum (nm)	<330	462.7	525.6	592.4	500.4	513.6	502.3
Maximum corrected absorptance of mean absorption spectrum	<0.01	0.87	0.90	0.92	0.49	0.90	0.40
Mean λ_{cut} (nm)	<330	448.5 ± 3.8	511.3 ± 1.9	569.4 ± 3.9	479.1 ± 9.0	499.6 ± 1.4	488.2 ± 3.7
Mean λ_{mid} (nm)	<330	462.1 ± 3.3	525.4 ± 2.3	591.9 ± 4.3	498.8 ± 5.0	513.6 ± 1.4	500.9 ± 3.4
Mean diameter (μm)	2.3 ± 1.0	3.6 ± 0.2	3.6 ± 0.3	3.8 ± 0.3	3.8 ± 0.4	4.0 ± 0.3	1.5 ± 0.5
Number of oil droplets	18	9	28	29	9	22	6

Table 2.12 Summary of the microspectrophotometric results obtained for the cone oil droplets of the peacock, *Pavo cristatus*.

2.6.2 Averaging the upward and downward scans prior to analysis

Following the results of the modelling in section 2.5.3, it was decided that averaging the upward and downward scans of visual pigment absorbance spectra prior to analysis resulted in a more accurate estimate of λ_{max}. Consequently, all of the averaged spectra were reanalysed using this alternative method. The new mean spectra for all species are displayed in Figure 2.80 to Figure 2.120 and the results summarised in Table 2.13. Averaging the up and down scans not only increases the accuracy of the λ_{max} estimate when there are significant distortions due to in-scan bleaching, but also reduces the apparent noise of the data (manifested as the deviation of the recorded spectra from the predicted template spectra). This permits the use of fewer points in the running average used to smooth the raw data prior to analysis and thus allows a more accurate estimate of the λ_{max} to be made (see section 2.5.2). Because the data obtained in this study suffered little from in-scan bleaching, the differences in λ_{max} estimates between the two analysis methods, for both pre-bleach and difference spectra, were small. Nevertheless, it is perhaps advisable to use the most robust analysis techniques available. Without re-analysing each of the individual records from which the mean spectra were calculated with the new up / down averaging method, no suitable statistical test could be performed to confirm whether or not there was a significant difference between the two methods. However, as the majority of differences in mean λ_{max} estimates were less than 1 nm, the calculated accuracy of the MSP used in this study, this was deemed unnecessary.

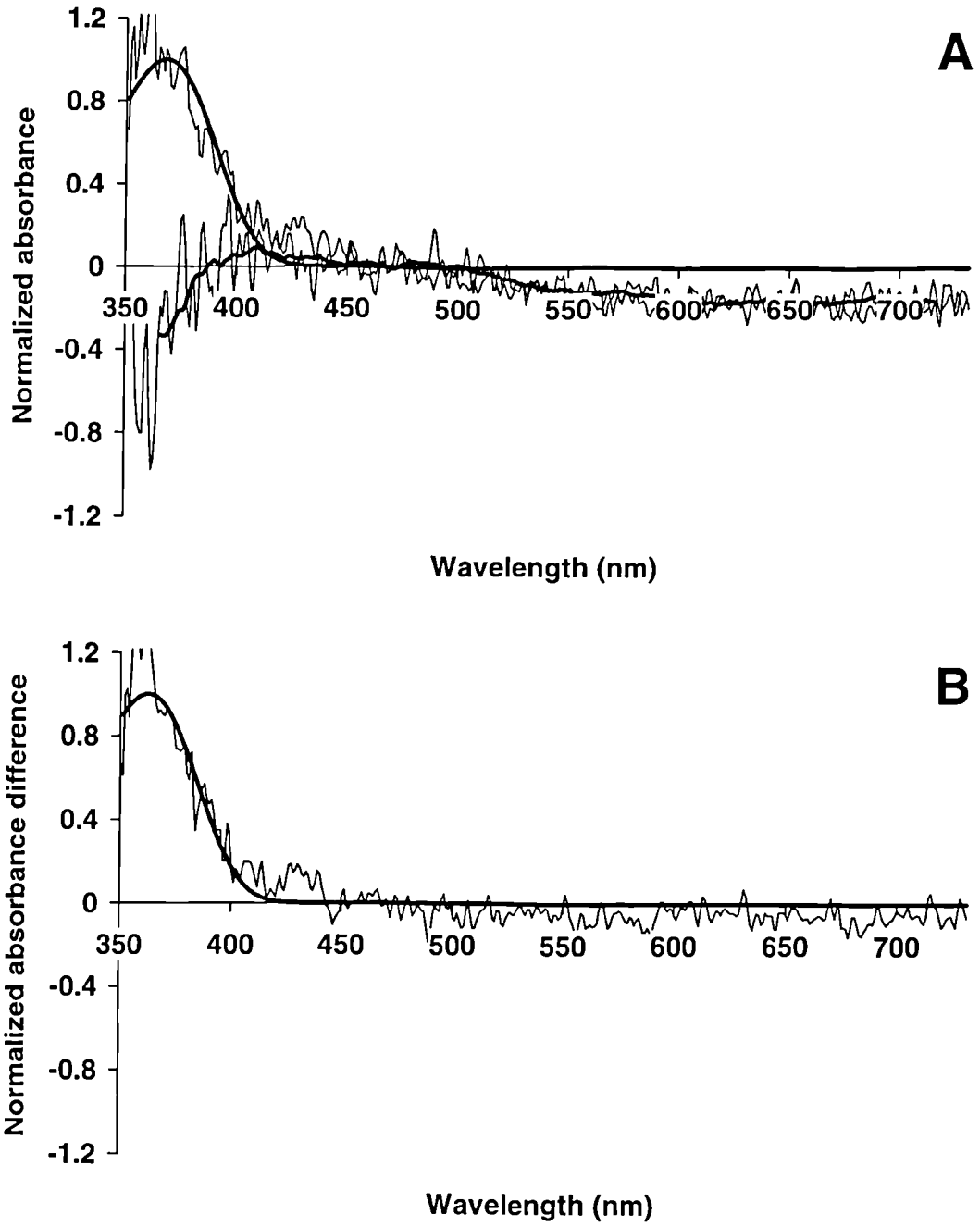

Figure 2.80 Microspectrophotometric results from 2 UVS single cones of the European starling, *Sturnus vulgaris*. Up and down scans were averaged prior to analysis and display. (**A**) Mean pre-bleach absorbance spectrum (upper trace) with best-fitted visual pigment template (λ_{max} 368 nm, solid line) and mean post-bleach absorbance spectrum (lower trace) with running average (solid line). (**B**) Mean difference spectrum (trace) with best-fitted visual pigment template (λ_{max} 363 nm, solid line).

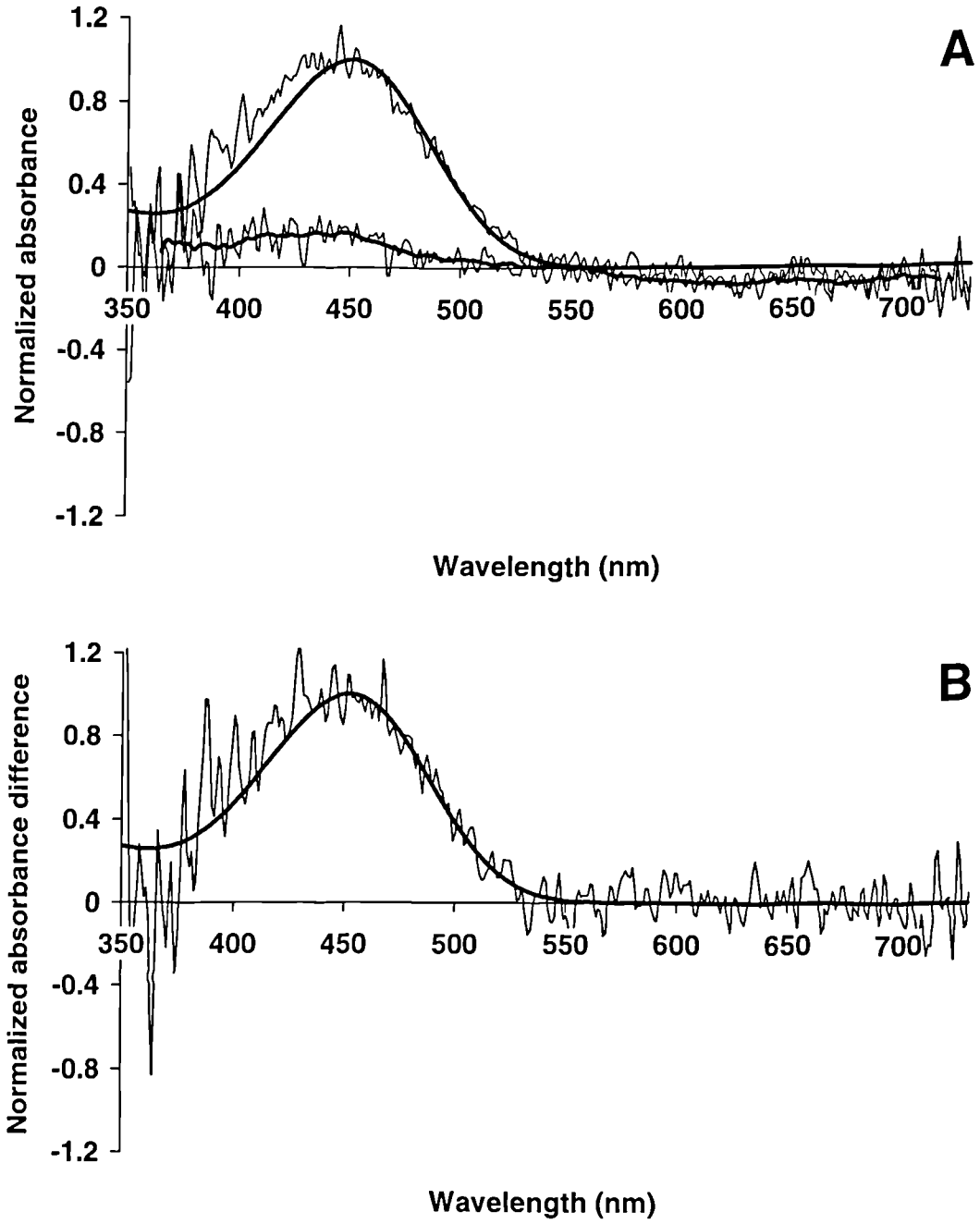

Figure 2.81 Microspectrophotometric results from 7 SWS single cones of the European starling, *Sturnus vulgaris*. Up and down scans were averaged prior to analysis and display. (**A**) Mean pre-bleach absorbance spectrum (upper trace) with best-fitted visual pigment template (λ_{max} 450 nm, solid line) and mean post-bleach absorbance spectrum (lower trace) with running average (solid line). (**B**) Mean difference spectrum (trace) with best-fitted visual pigment template (λ_{max} 452 nm, solid line).

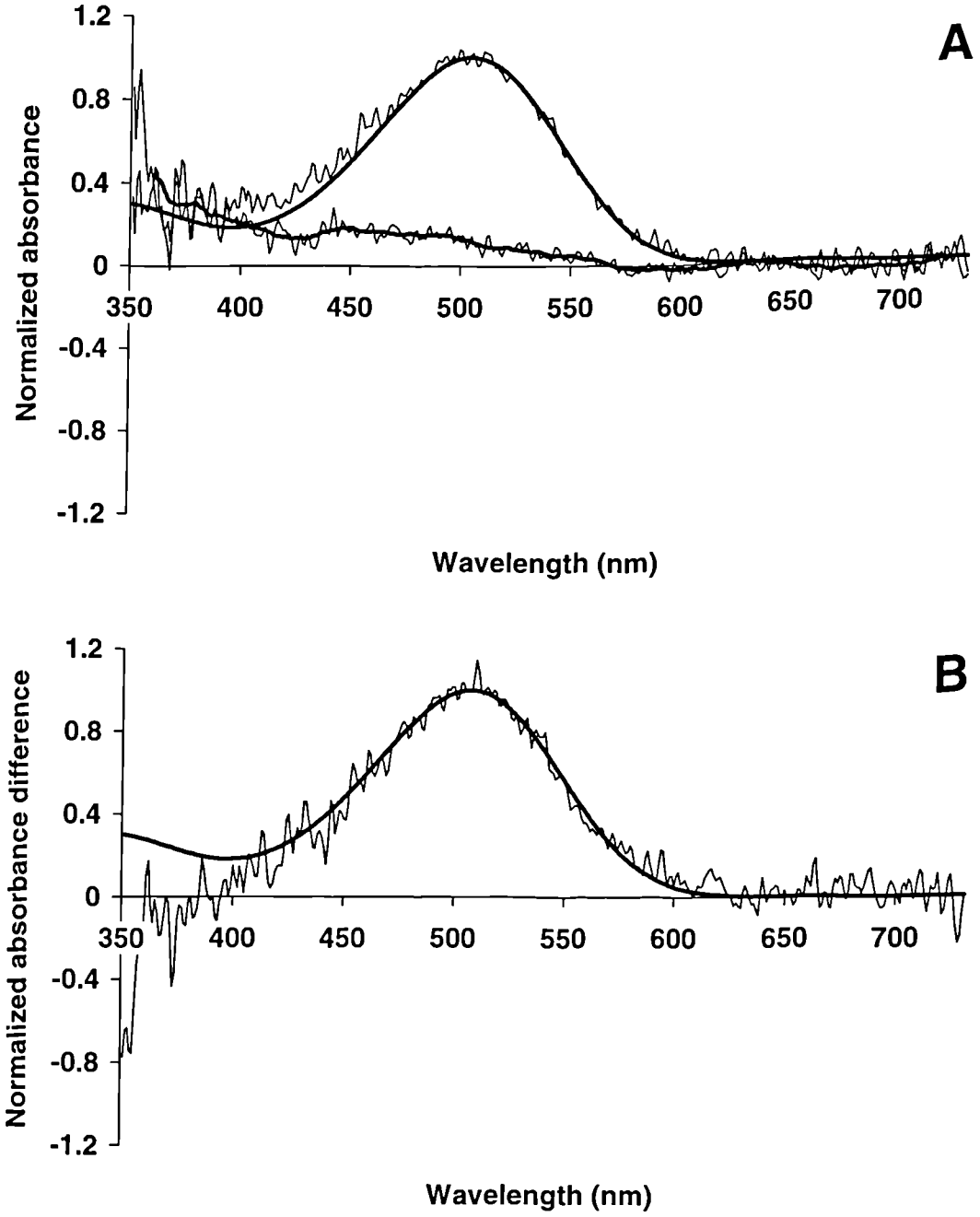

Figure 2.82 Microspectrophotometric results from 11 MWS single cones of the European starling, *Sturnus vulgaris*. Up and down scans were averaged prior to analysis and display. (**A**) Mean pre-bleach absorbance spectrum (upper trace) with best-fitted visual pigment template (λ_{max} 504 nm, solid line) and mean post-bleach absorbance spectrum (lower trace) with running average (solid line). (**B**) Mean difference spectrum (trace) with best-fitted visual pigment template (λ_{max} 508 nm, solid line).

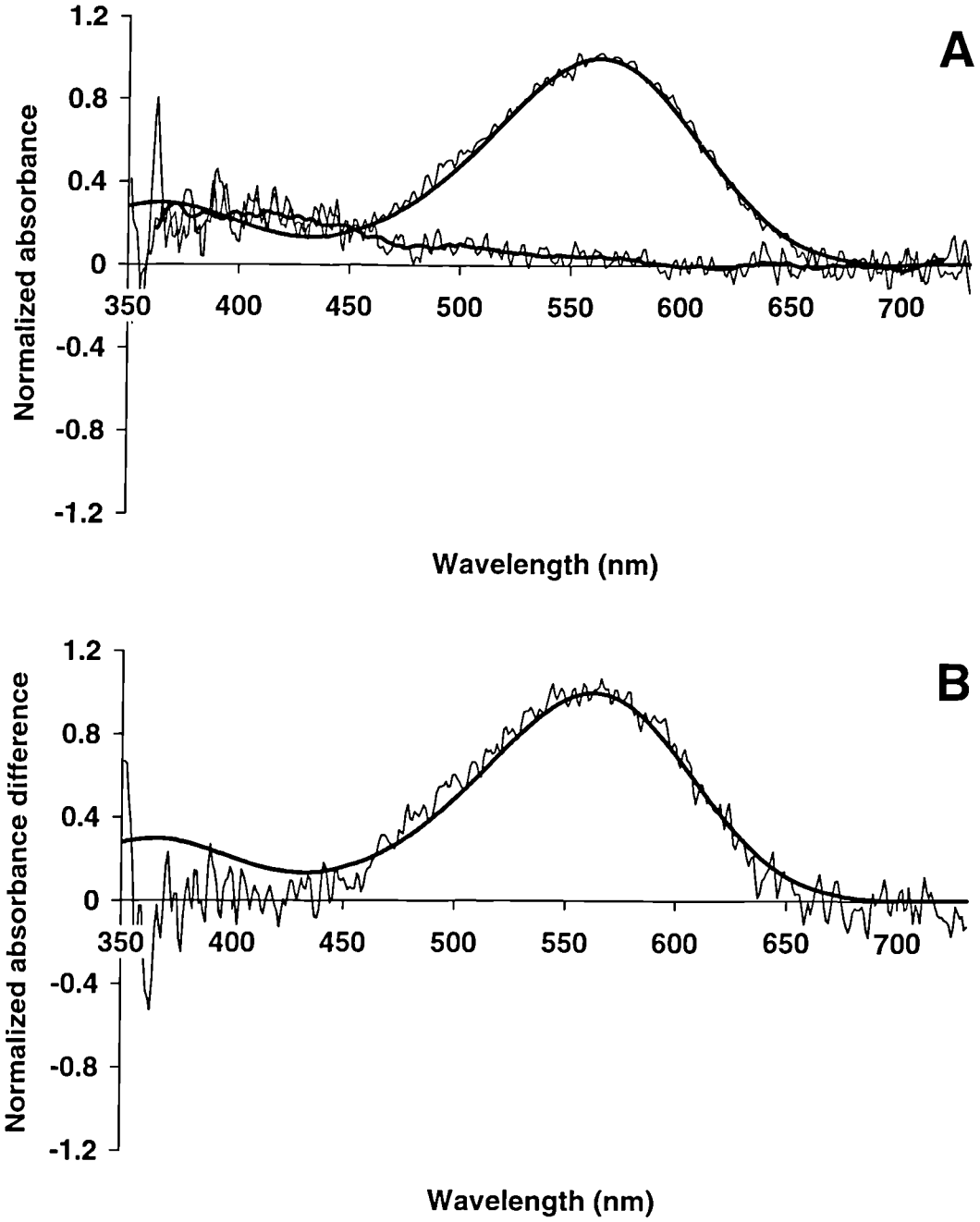

Figure 2.83 Microspectrophotometric results from 10 LWS single cones of the European starling, *Sturnus vulgaris*. Up and down scans were averaged prior to analysis and display. (**A**) Mean pre-bleach absorbance spectrum (upper trace) with best-fitted visual pigment template (λ_{max} 563 nm, solid line) and mean post-bleach absorbance spectrum (lower trace) with running average (solid line). (**B**) Mean difference spectrum (trace) with best-fitted visual pigment template (λ_{max} 562 nm, solid line).

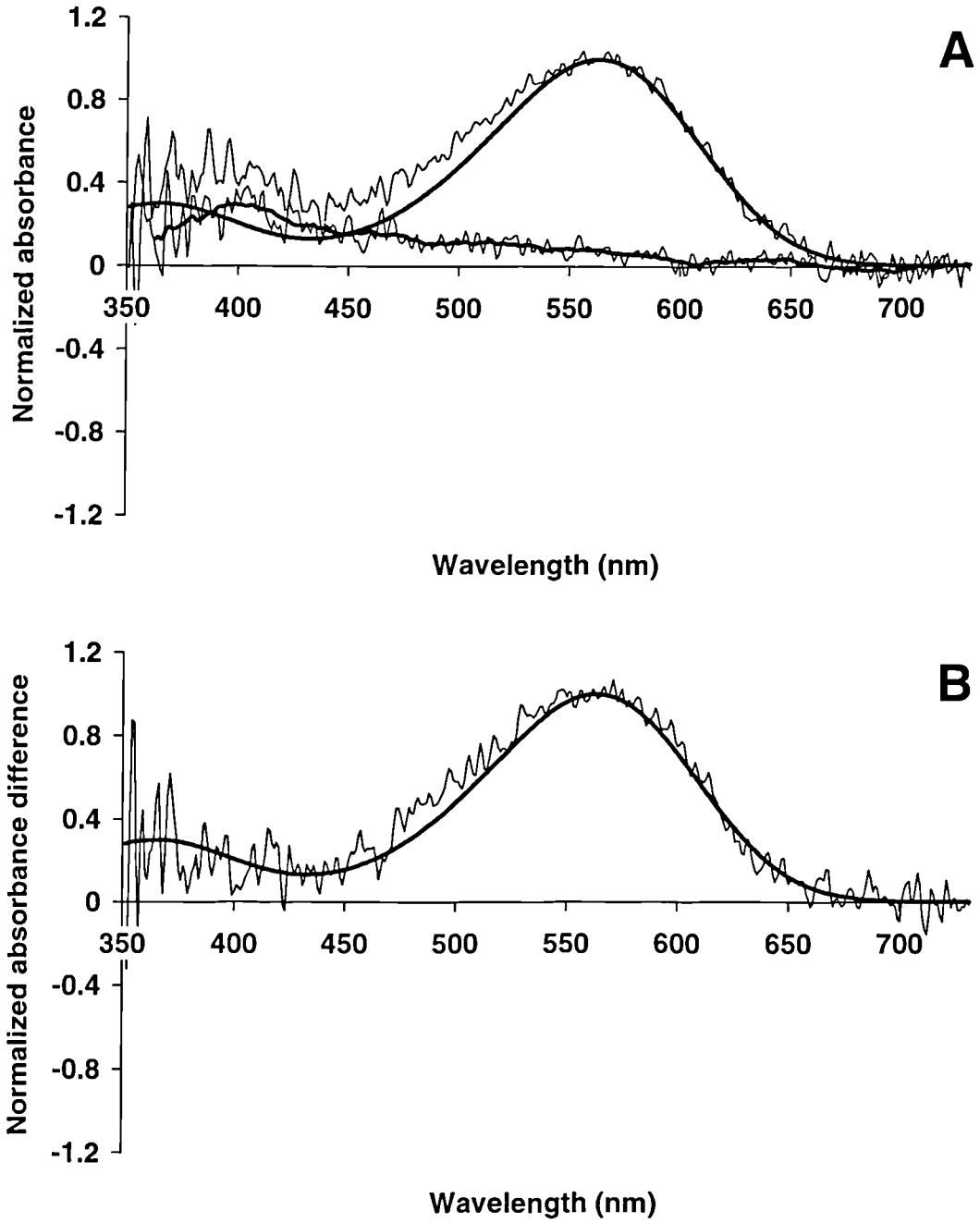

Figure 2.84 Microspectrophotometric results from 11 principal members of the double cone of the European starling, *Sturnus vulgaris*. Up and down scans were averaged prior to analysis and display. (**A**) Mean pre-bleach absorbance spectrum (upper trace) with best-fitted visual pigment template (λ_{max} 563 nm, solid line) and mean post-bleach absorbance spectrum (lower trace) with running average (solid line). (**B**) Mean difference spectrum (trace) with best-fitted visual pigment template (λ_{max} 563 nm, solid line).

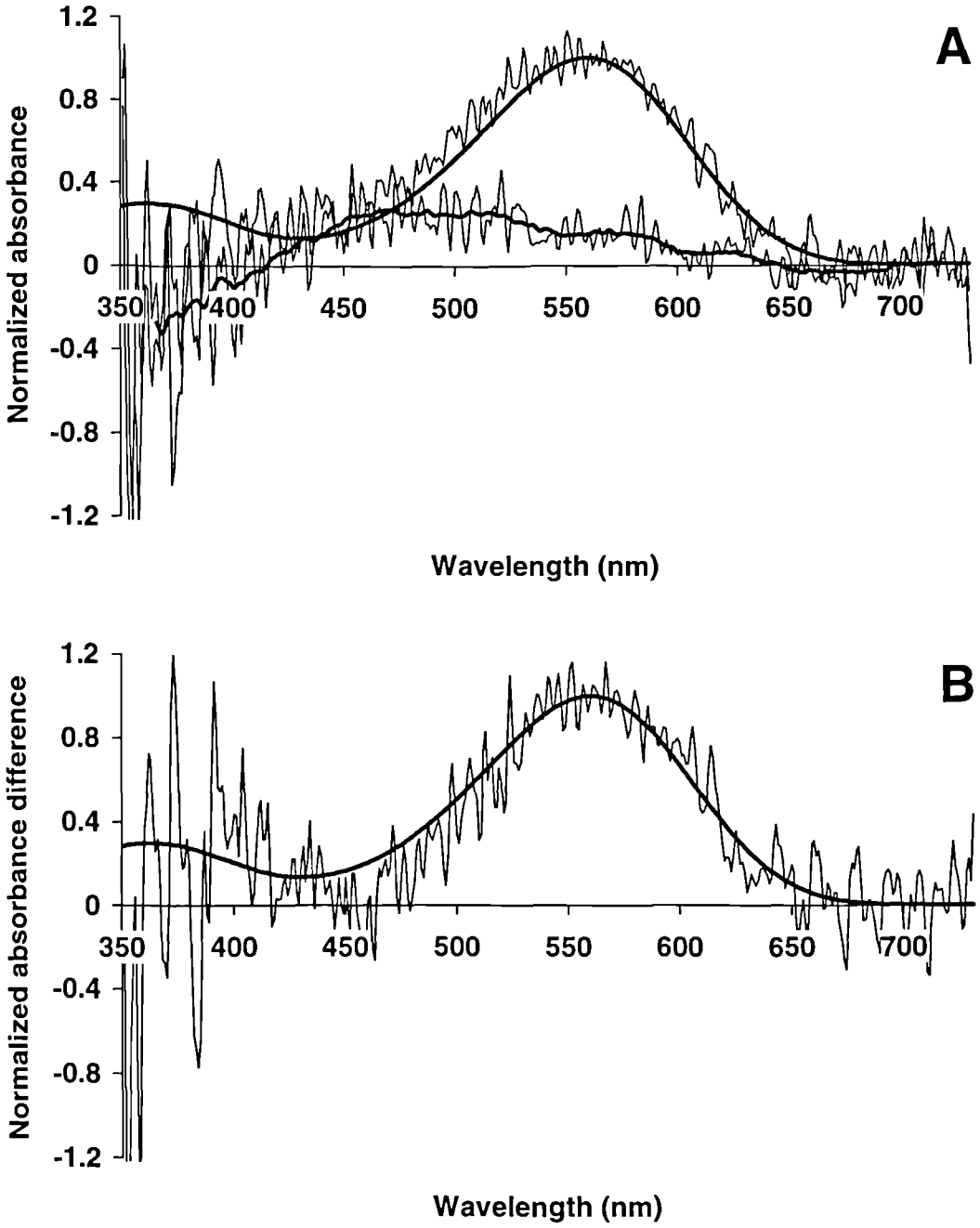

Figure 2.85 Microspectrophotometric results from 2 accessory members of the double cone of the European starling, *Sturnus vulgaris*. Up and down scans were averaged prior to analysis and display. (**A**) Mean pre-bleach absorbance spectrum (upper trace) with best-fitted visual pigment template (λ_{max} 560 nm, solid line) and mean post-bleach absorbance spectrum (lower trace) with running average (solid line). (**B**) Mean difference spectrum (trace) with best-fitted visual pigment template (λ_{max} 560 nm, solid line).

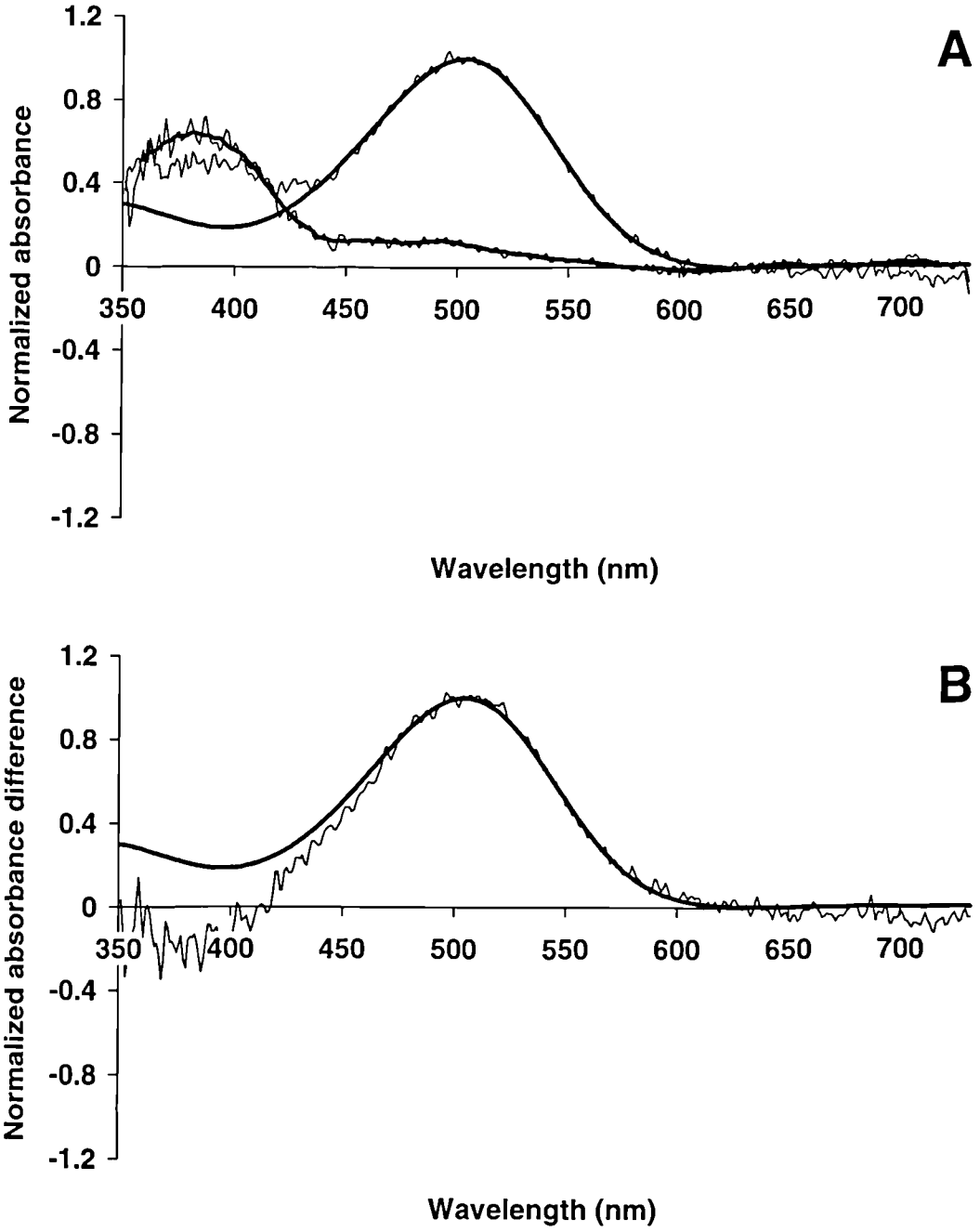

Figure 2.86 Microspectrophotometric results from 7 rods of the European starling, *Sturnus vulgaris*. Up and down scans were averaged prior to analysis and display. (**A**) Mean pre-bleach absorbance spectrum (upper trace) with best-fitted visual pigment template (λ_{max} 503 nm, solid line) and mean post-bleach absorbance spectrum (lower trace) with running average (solid line). (**B**) Mean difference spectrum (trace) with best-fitted visual pigment template (λ_{max} 505 nm, solid line).

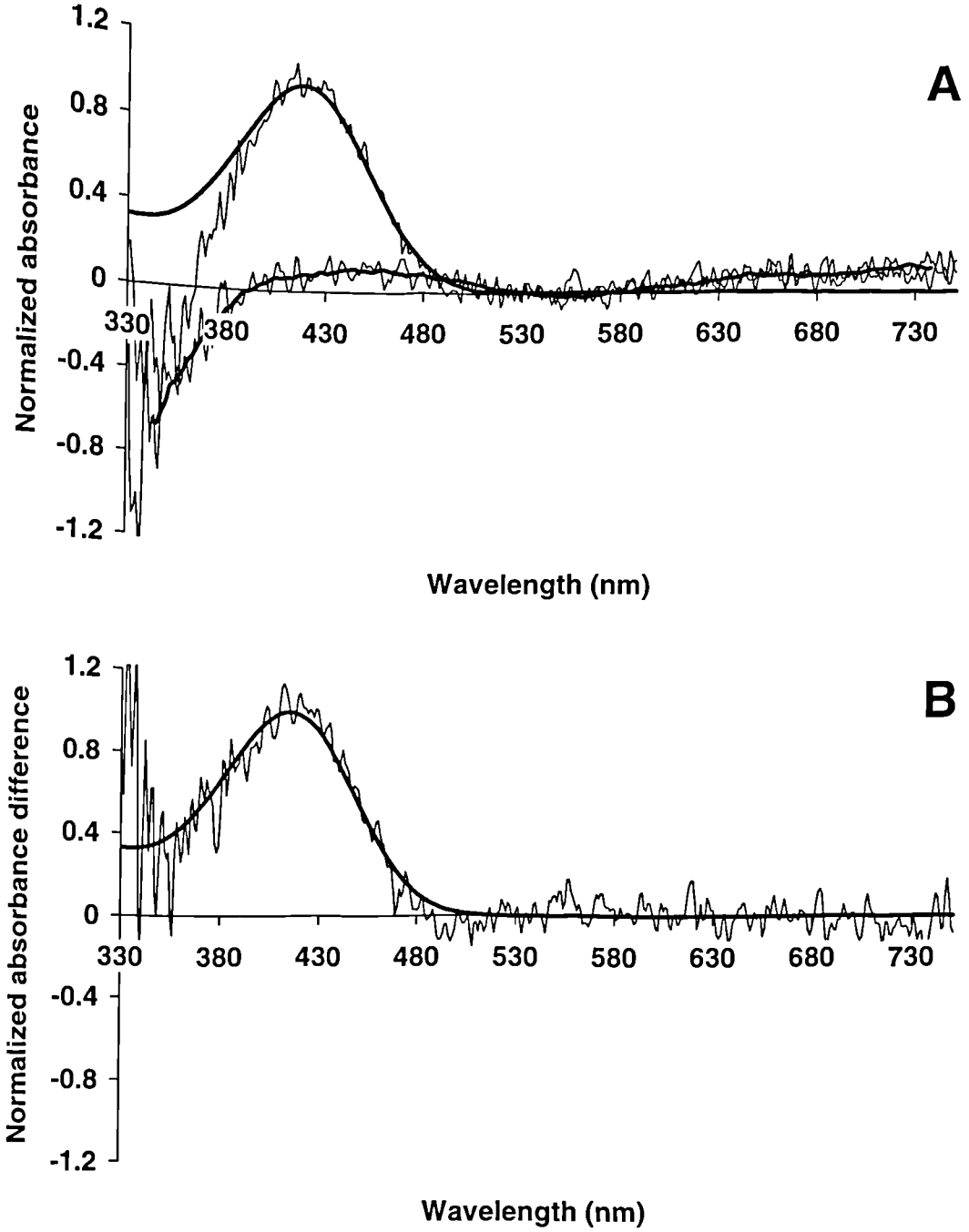

Figure 2.87 Microspectrophotometric results from 2 VS single cones of the domestic turkey, *Meleagris gallopavo*, measured whilst mounted in 5% DPBS. Up and down scans were averaged prior to analysis and display. (**A**) Mean pre-bleach absorbance spectrum (upper trace) with best-fitted visual pigment template (λ_{max} 418 nm, solid line) and mean post-bleach absorbance spectrum (lower trace) with running average (solid line). (**B**) Mean difference spectrum (trace) with best-fitted visual pigment template (λ_{max} 415 nm, solid line).

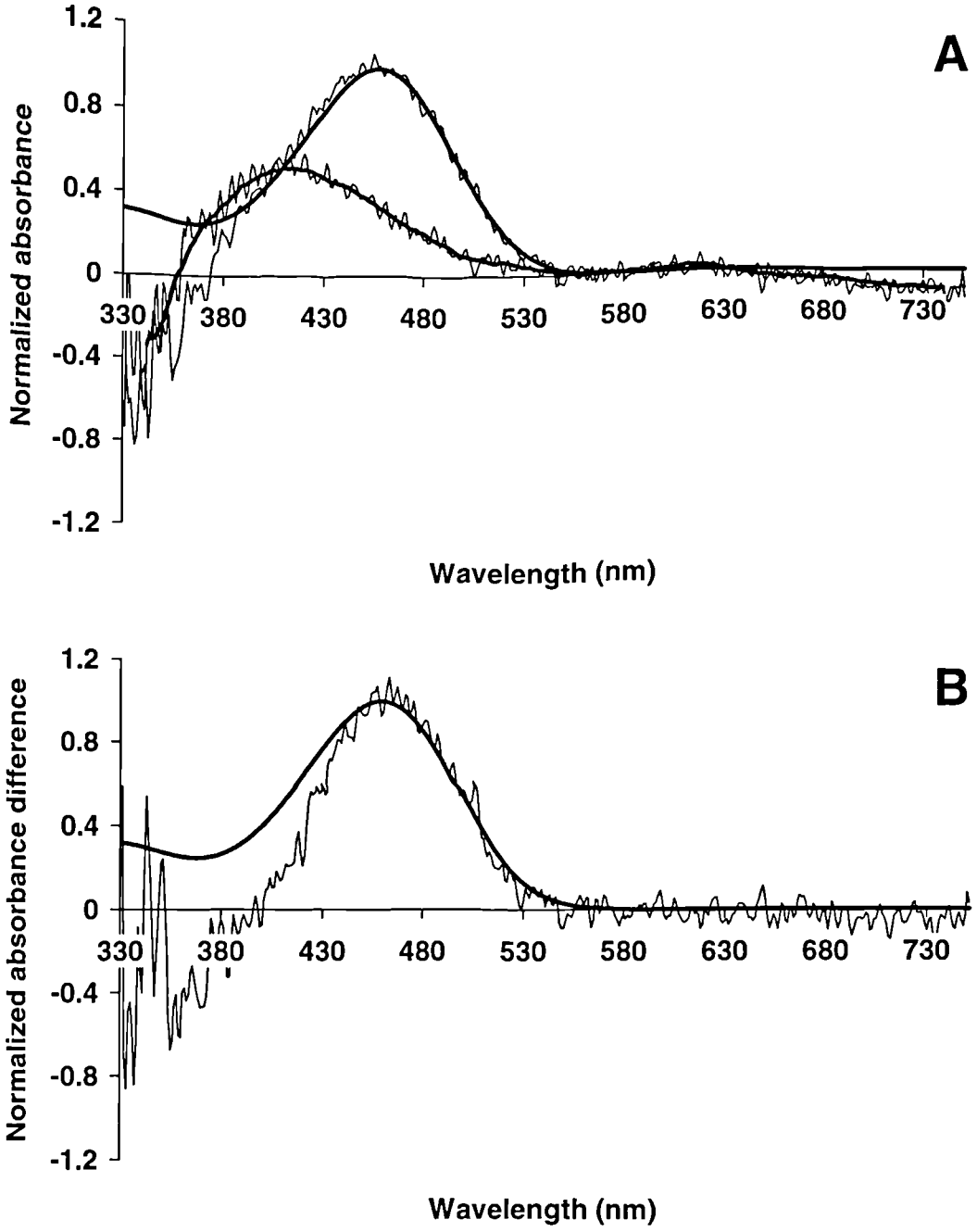

Figure 2.88 Microspectrophotometric results from 4 SWS single cones of the domestic turkey, *Meleagris gallopavo*, measured whilst mounted in 5% DPBS. Up and down scans were averaged prior to analysis and display. (**A**) Mean pre-bleach absorbance spectrum (upper trace) with best-fitted visual pigment template (λ_{max} 458 nm, solid line) and mean post-bleach absorbance spectrum (lower trace) with running average (solid line). (**B**) Mean difference spectrum (trace) with best-fitted visual pigment template (λ_{max} 460 nm, solid line).

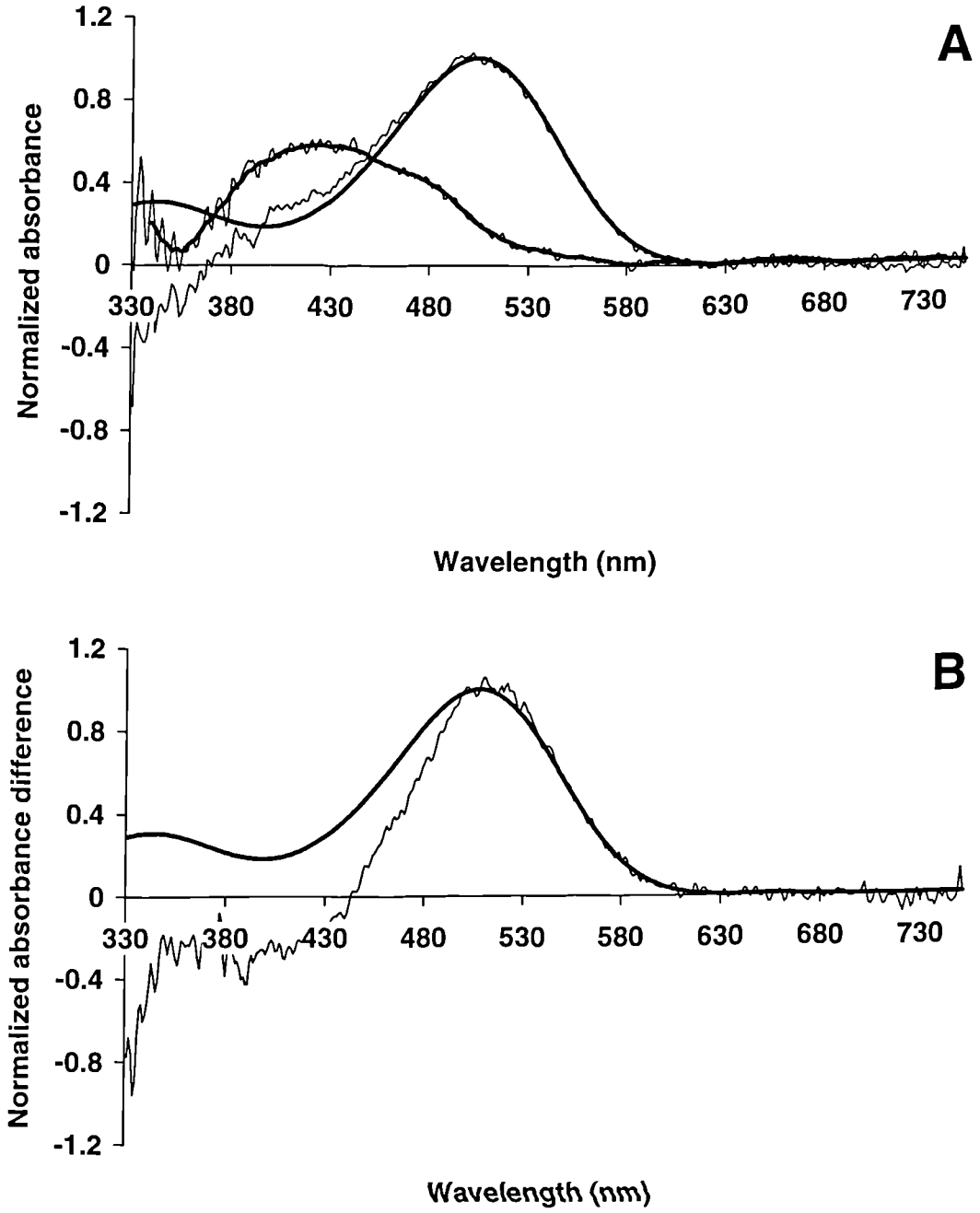

Figure 2.89 Microspectrophotometric results from 9 MWS single cones of the domestic turkey, *Meleagris gallopavo*, measured whilst mounted in 5% DPBS. Up and down scans were averaged prior to analysis and display. (**A**) Mean pre-bleach absorbance spectrum (upper trace) with best-fitted visual pigment template (λ_{max} 504 nm, solid line) and mean post-bleach absorbance spectrum (lower trace) with running average (solid line). (**B**) Mean difference spectrum (trace) with best-fitted visual pigment template (λ_{max} 508 nm, solid line).

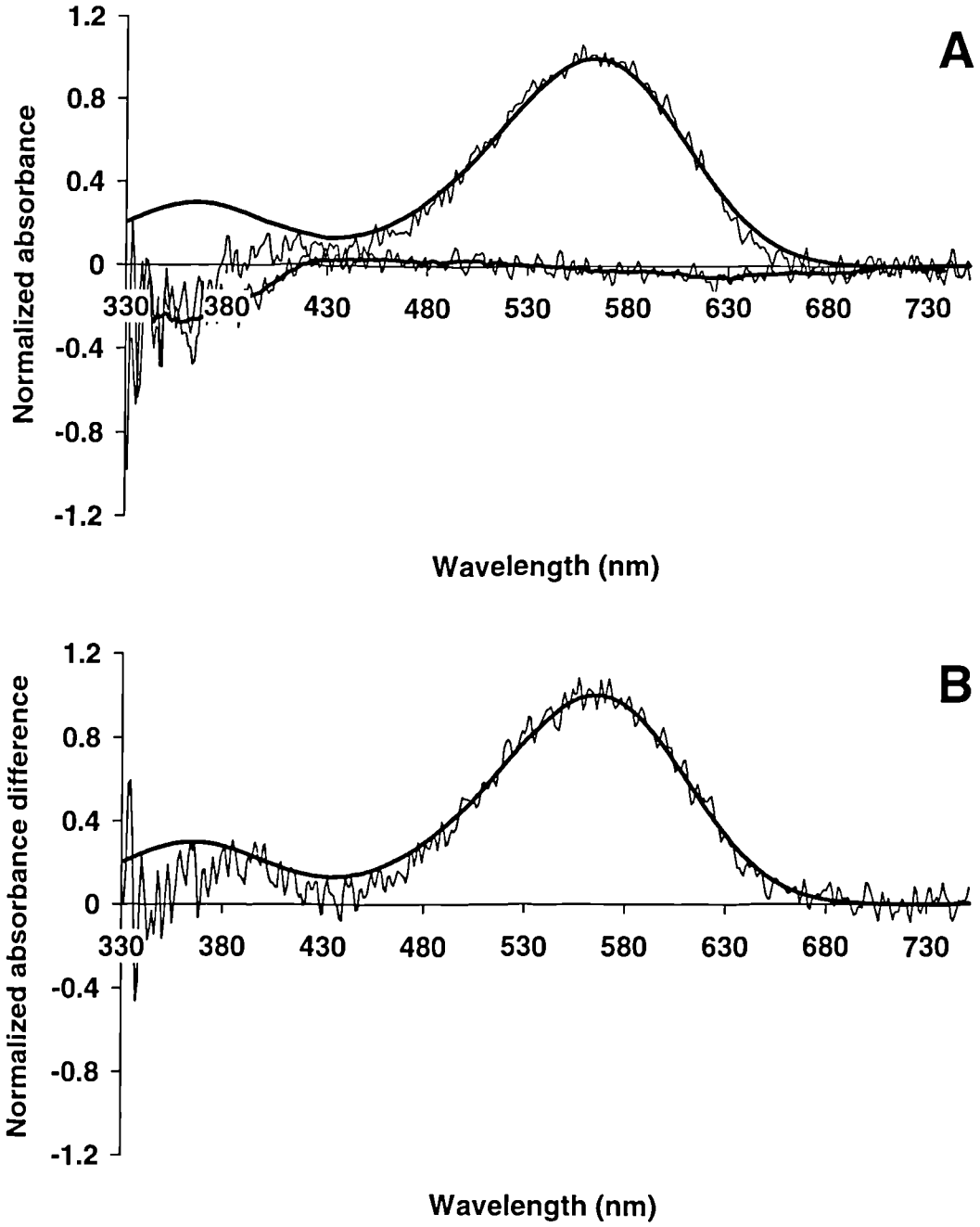

Figure 2.90 Microspectrophotometric results from 3 LWS single cones of the domestic turkey, *Meleagris gallopavo*, measured whilst mounted in 5% DPBS. Up and down scans were averaged prior to analysis and display. (**A**) Mean pre-bleach absorbance spectrum (upper trace) with best-fitted visual pigment template (λ_{max} 563 nm, solid line) and mean post-bleach absorbance spectrum (lower trace) with running average (solid line). (**B**) Mean difference spectrum (trace) with best-fitted visual pigment template (λ_{max} 566 nm, solid line).

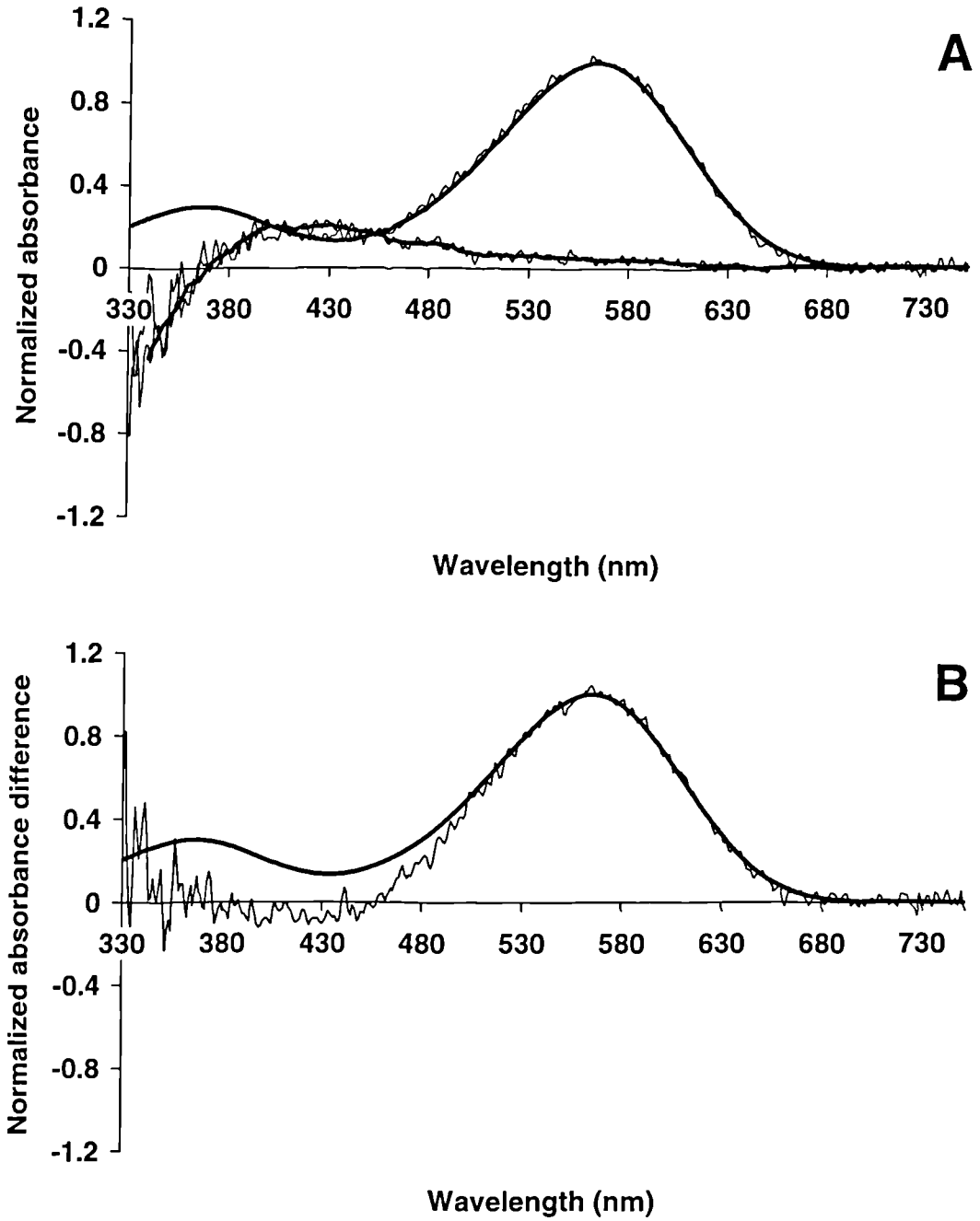

Figure 2.91 Microspectrophotometric results from 9 principal members of the double cone of the domestic turkey, *Meleagris gallopavo*, measured whilst mounted in 5% DPBS. Up and down scans were averaged prior to analysis and display. (**A**) Mean pre-bleach absorbance spectrum (upper trace) with best-fitted visual pigment template (λ_{max} 564 nm, solid line) and mean post-bleach absorbance spectrum (lower trace) with running average (solid line). (**B**) Mean difference spectrum (trace) with best-fitted visual pigment template (λ_{max} 564 nm, solid line).

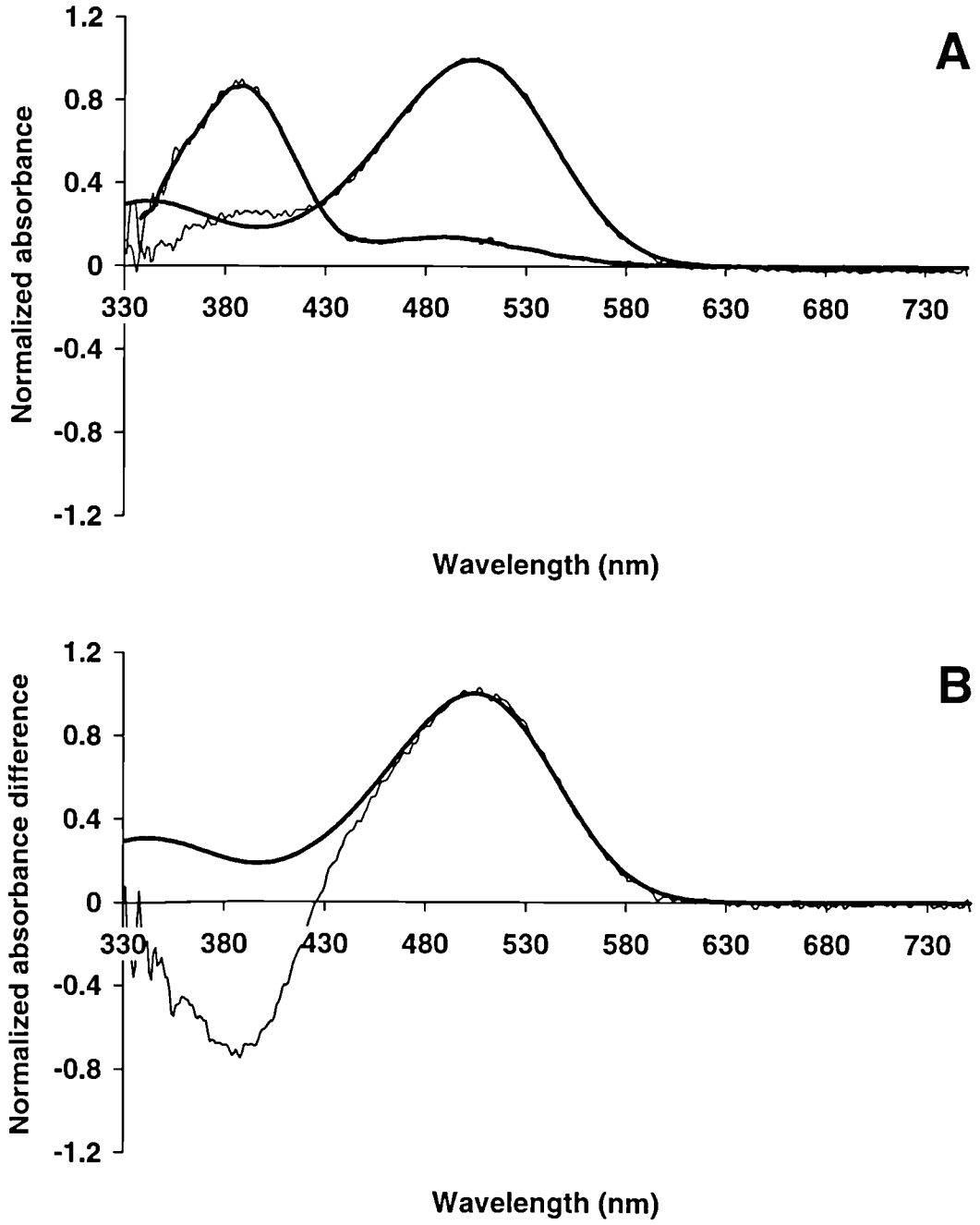

Figure 2.92 Microspectrophotometric results from 6 rods of the domestic turkey, *Meleagris gallopavo*, measured whilst mounted in 5% DPBS. Up and down scans were averaged prior to analysis and display. (**A**) Mean pre-bleach absorbance spectrum (upper trace) with best-fitted visual pigment template (λ_{max} 504 nm, solid line) and mean post-bleach absorbance spectrum (lower trace) with running average (solid line). (**B**) Mean difference spectrum (trace) with best-fitted visual pigment template (λ_{max} 505 nm, solid line).

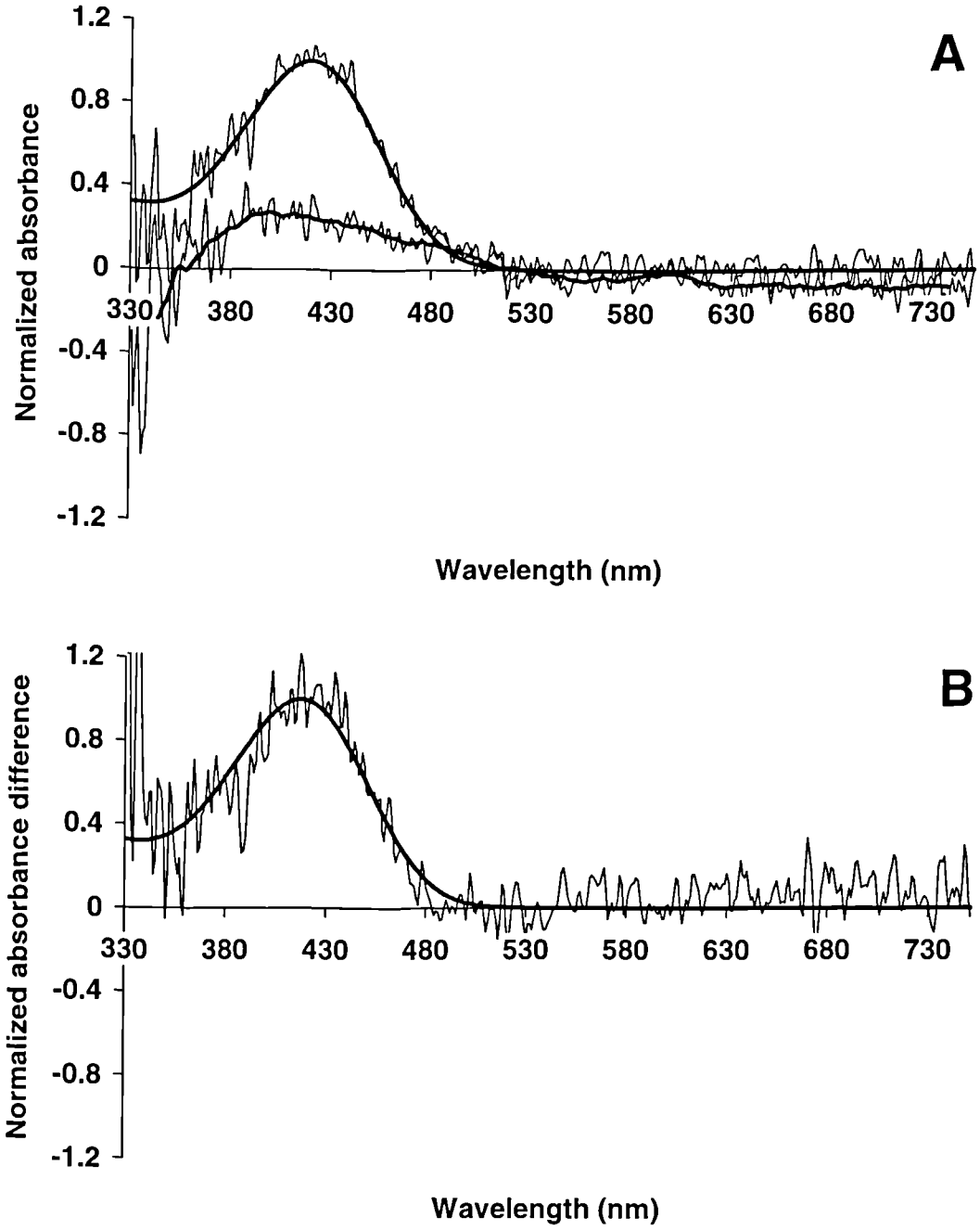

Figure 2.93 Microspectrophotometric results from 4 VS single cones of the domestic turkey, *Meleagris gallopavo*, measured whilst mounted in 75% GPBS. Up and down scans were averaged prior to analysis and display. (**A**) Mean pre-bleach absorbance spectrum (upper trace) with best-fitted visual pigment template (λ_{max} 420 nm, solid line) and mean post-bleach absorbance spectrum (lower trace) with running average (solid line). (**B**) Mean difference spectrum (trace) with best-fitted visual pigment template (λ_{max} 417 nm, solid line).

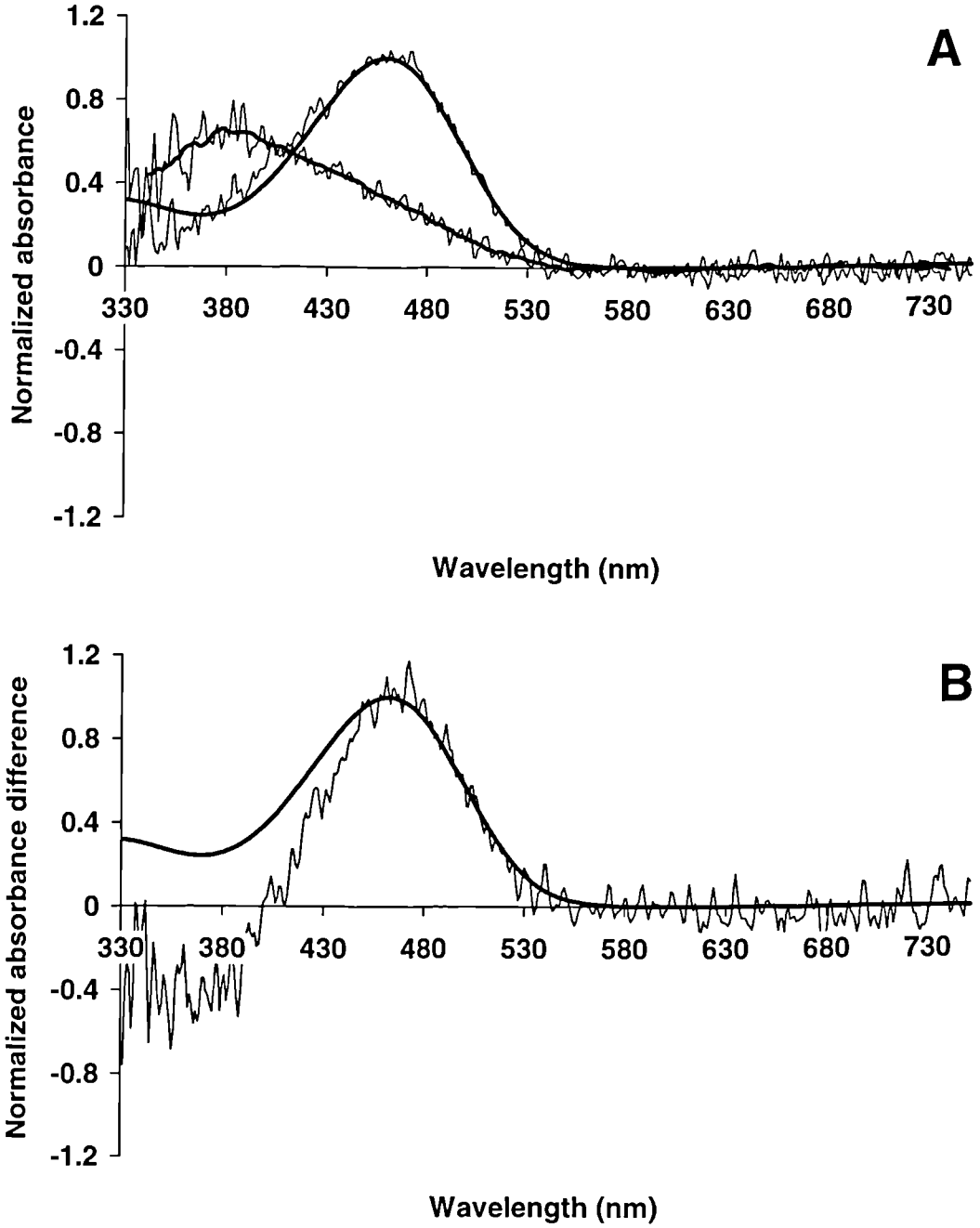

Figure 2.94 Microspectrophotometric results from 5 SWS single cones of the domestic turkey, *Meleagris gallopavo*, measured whilst mounted in 75% GPBS. Up and down scans were averaged prior to analysis and display. (**A**) Mean pre-bleach absorbance spectrum (upper trace) with best-fitted visual pigment template (λ_{max} 459 nm, solid line) and mean post-bleach absorbance spectrum (lower trace) with running average (solid line). (**B**) Mean difference spectrum (trace) with best-fitted visual pigment template (λ_{max} 462 nm, solid line).

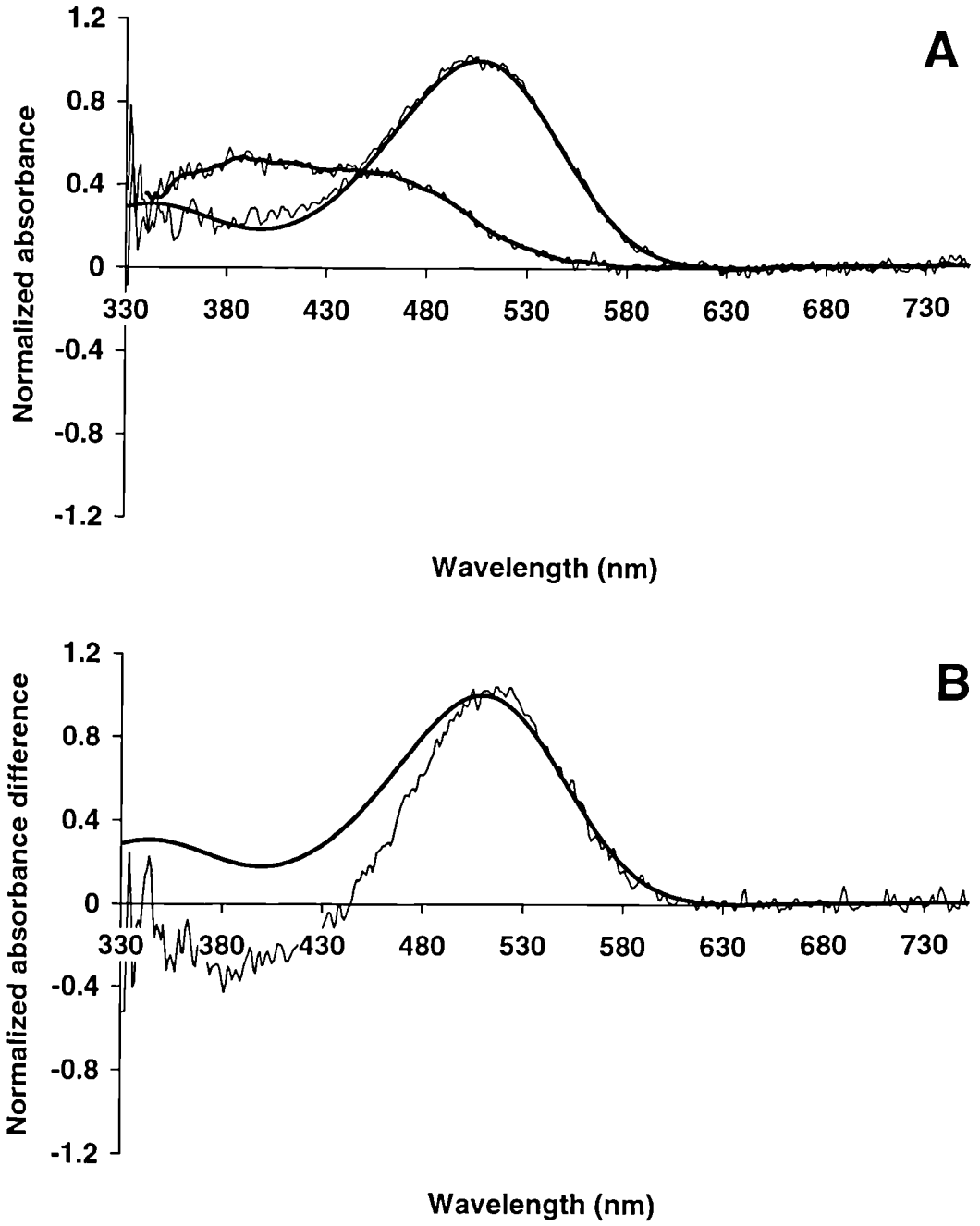

Figure 2.95 Microspectrophotometric results from 10 MWS single cones of the domestic turkey, *Meleagris gallopavo*, measured whilst mounted in 75% GPBS. Up and down scans were averaged prior to analysis and display. (**A**) Mean pre-bleach absorbance spectrum (upper trace) with best-fitted visual pigment template (λ_{max} 505 nm, solid line) and mean post-bleach absorbance spectrum (lower trace) with running average (solid line). (**B**) Mean difference spectrum (trace) with best-fitted visual pigment template (λ_{max} 510 nm, solid line).

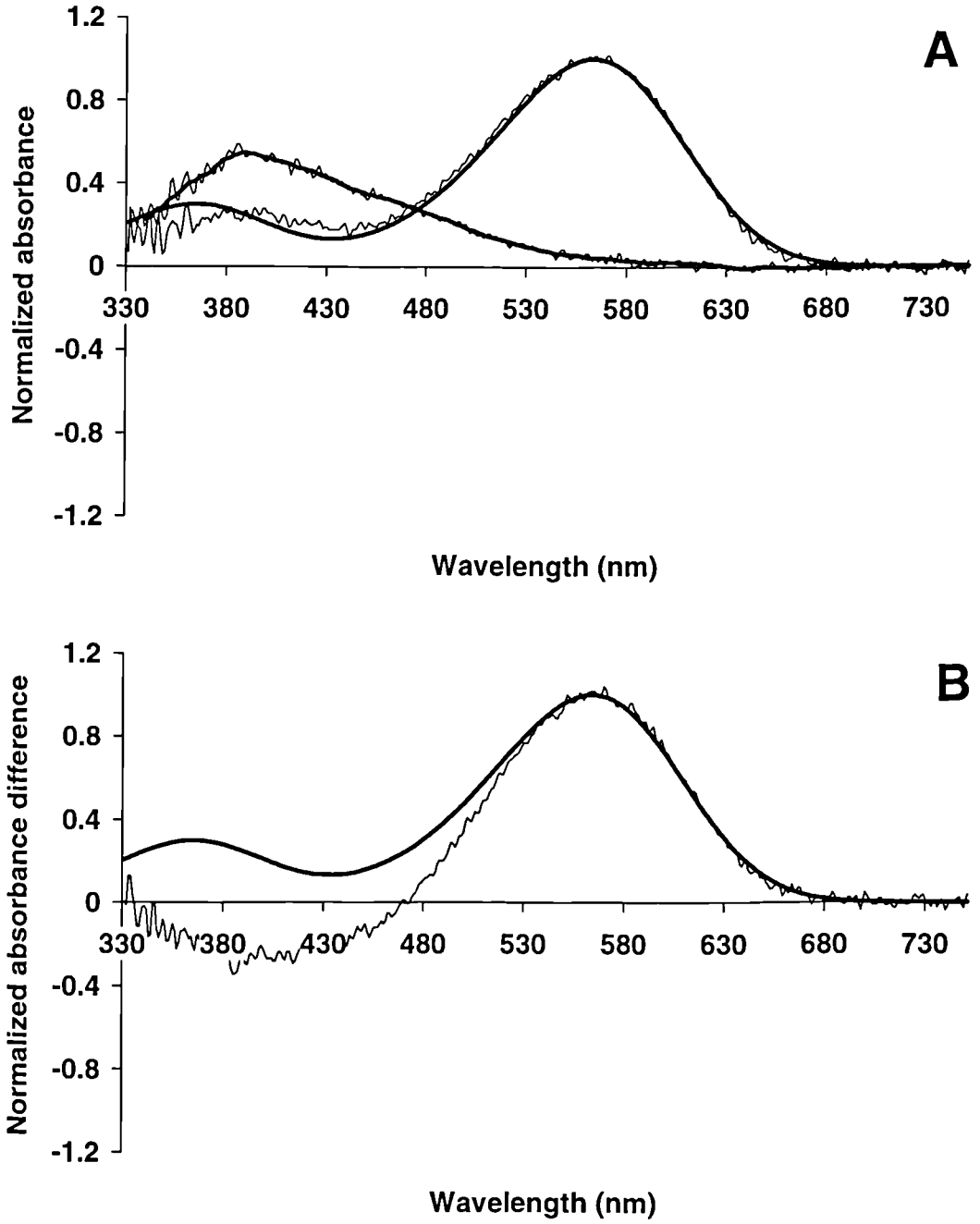

Figure 2.96 Microspectrophotometric results from 10 LWS single cones of the domestic turkey, *Meleagris gallopavo*, measured whilst mounted in 75% GPBS. Up and down scans were averaged prior to analysis and display. (**A**) Mean pre-bleach absorbance spectrum (upper trace) with best-fitted visual pigment template (λ_{max} 564 nm, solid line) and mean post-bleach absorbance spectrum (lower trace) with running average (solid line). (**B**) Mean difference spectrum (trace) with best-fitted visual pigment template (λ_{max} 564 nm, solid line).

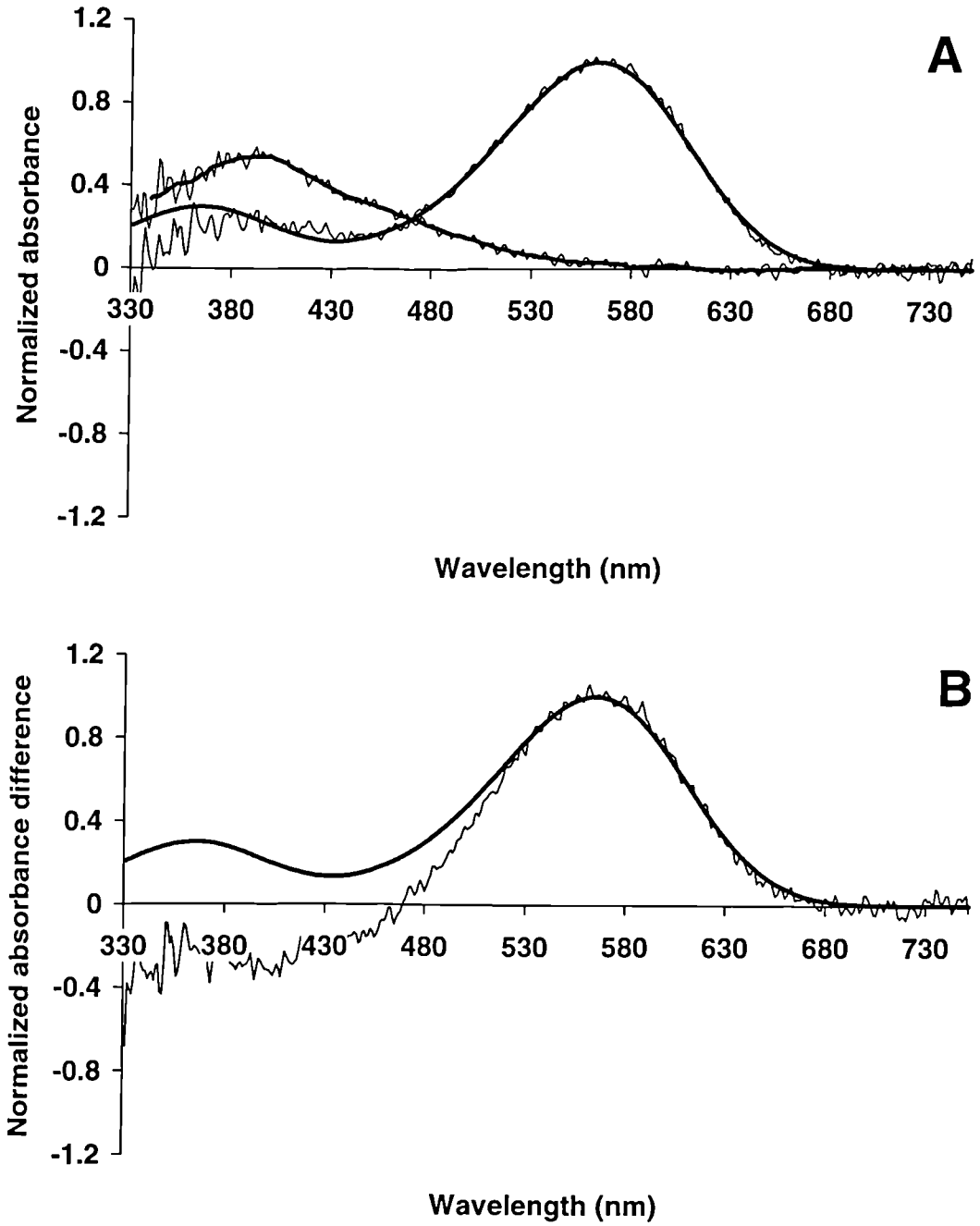

Figure 2.97 Microspectrophotometric results from 8 principal members of the double cone of the domestic turkey, *Meleagris gallopavo*, measured whilst mounted in 75% GPBS. Up and down scans were averaged prior to analysis and display. (**A**) Mean pre-bleach absorbance spectrum (upper trace) with best-fitted visual pigment template (λ_{max} 564 nm, solid line) and mean post-bleach absorbance spectrum (lower trace) with running average (solid line). (**B**) Mean difference spectrum (trace) with best-fitted visual pigment template (λ_{max} 565 nm, solid line).

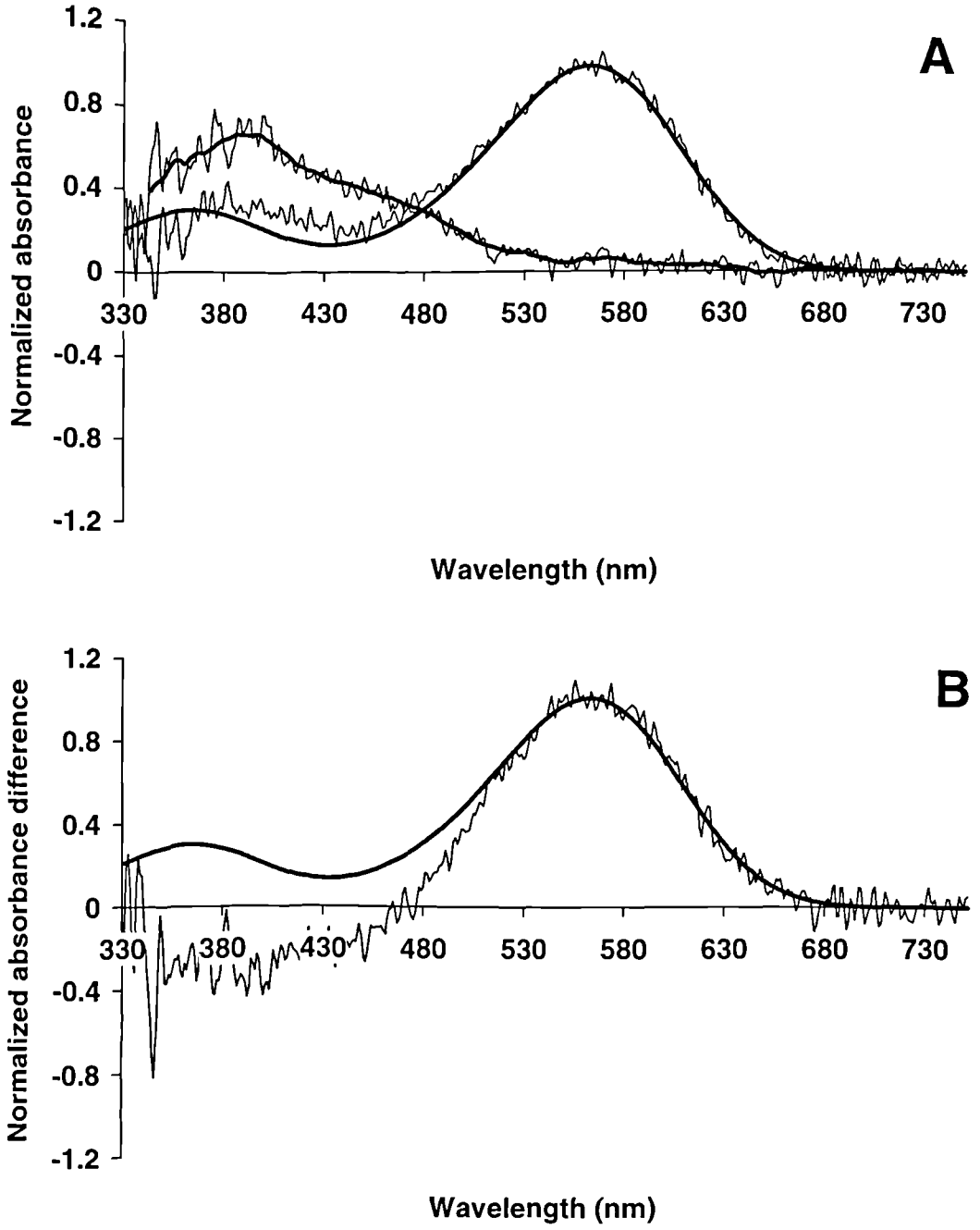

Figure 2.98 Microspectrophotometric results from 5 accessory members of the double cone of the domestic turkey, *Meleagris gallopavo*, measured whilst mounted in 75% GPBS. Up and down scans were averaged prior to analysis and display. (**A**) Mean pre-bleach absorbance spectrum (upper trace) with best-fitted visual pigment template (λ_{max} 563 nm, solid line) and mean post-bleach absorbance spectrum (lower trace) with running average (solid line). (**B**) Mean difference spectrum (trace) with best-fitted visual pigment template (λ_{max} 564 nm, solid line).

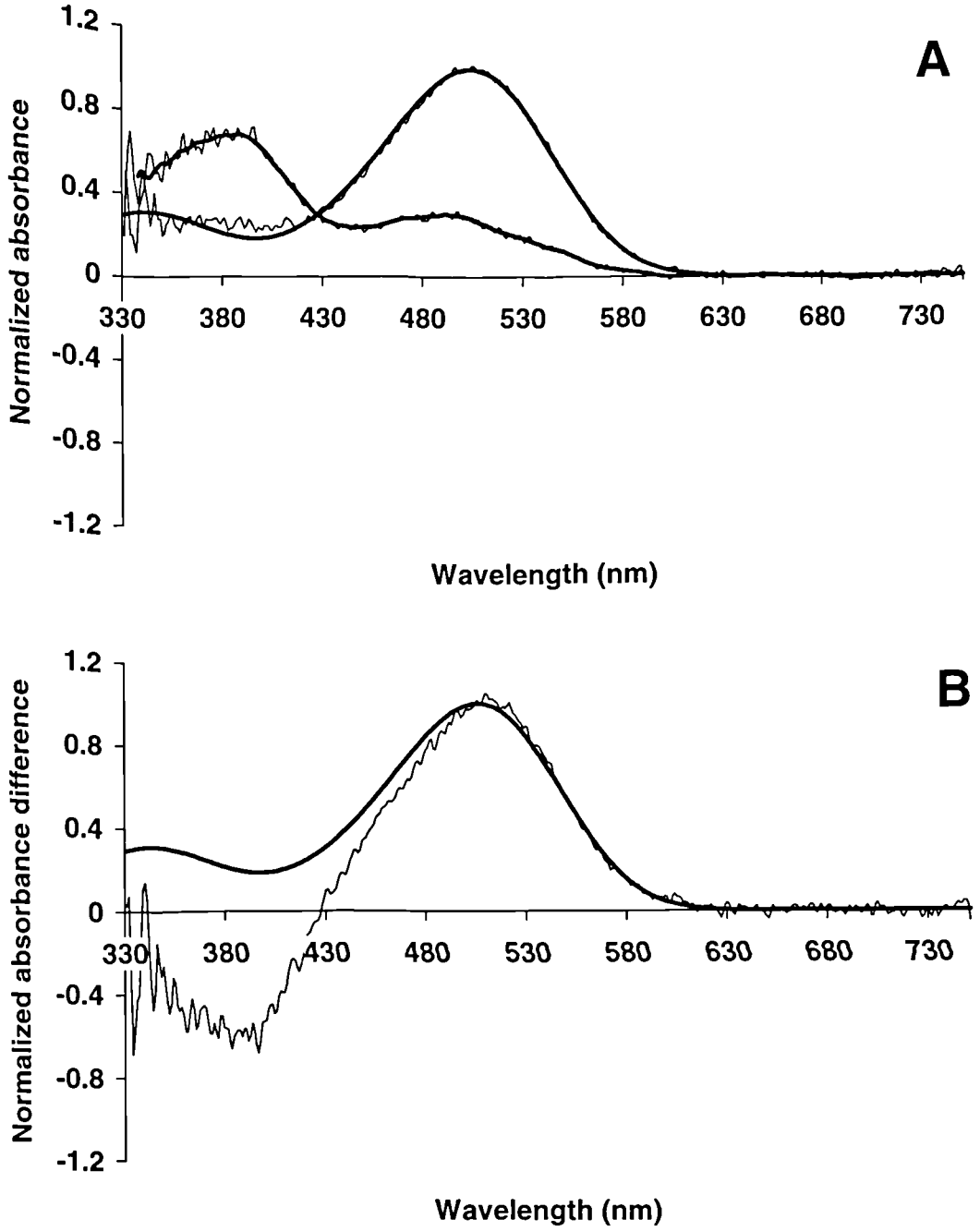

Figure 2.99 Microspectrophotometric results from 6 rods of the domestic turkey, *Meleagris gallopavo*, measured whilst mounted in 75% GPBS. Up and down scans were averaged prior to analysis and display. (**A**) Mean pre-bleach absorbance spectrum (upper trace) with best-fitted visual pigment template (λ_{max} 504 nm, solid line) and mean post-bleach absorbance spectrum (lower trace) with running average (solid line). (**B**) Mean difference spectrum (trace) with best-fitted visual pigment template (λ_{max} 506 nm, solid line).

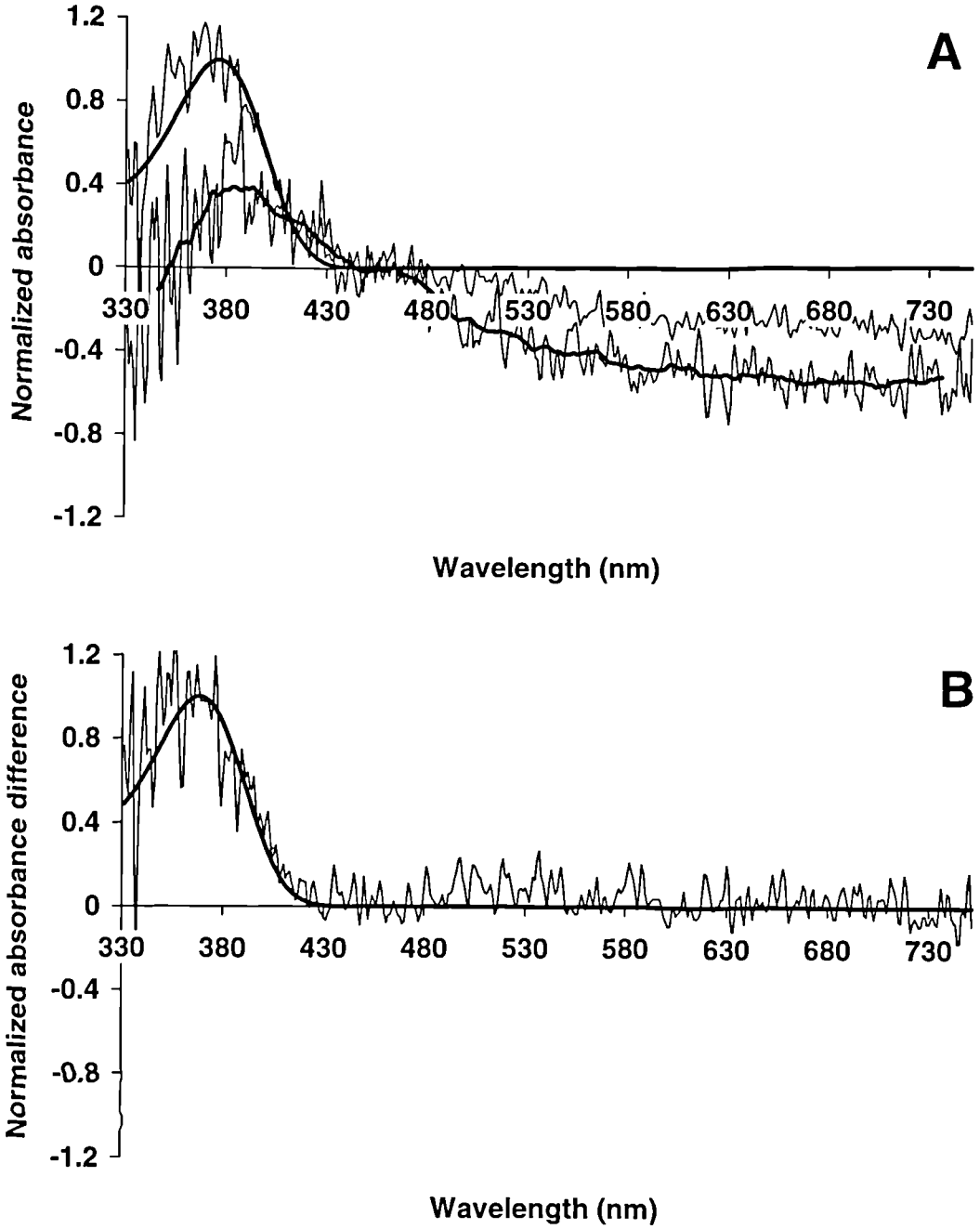

Figure 2.100 Microspectrophotometric results from 4 UVS single cones of the blackbird, *Turdus merula*. Up and down scans were averaged prior to analysis and display. (**A**) Mean pre-bleach absorbance spectrum (upper trace) with best-fitted visual pigment template (λ_{max} 376 nm, solid line) and mean post-bleach absorbance spectrum (lower trace) with running average (solid line). (**B**) Mean difference spectrum (trace) with best-fitted visual pigment template (λ_{max} 368 nm, solid line).

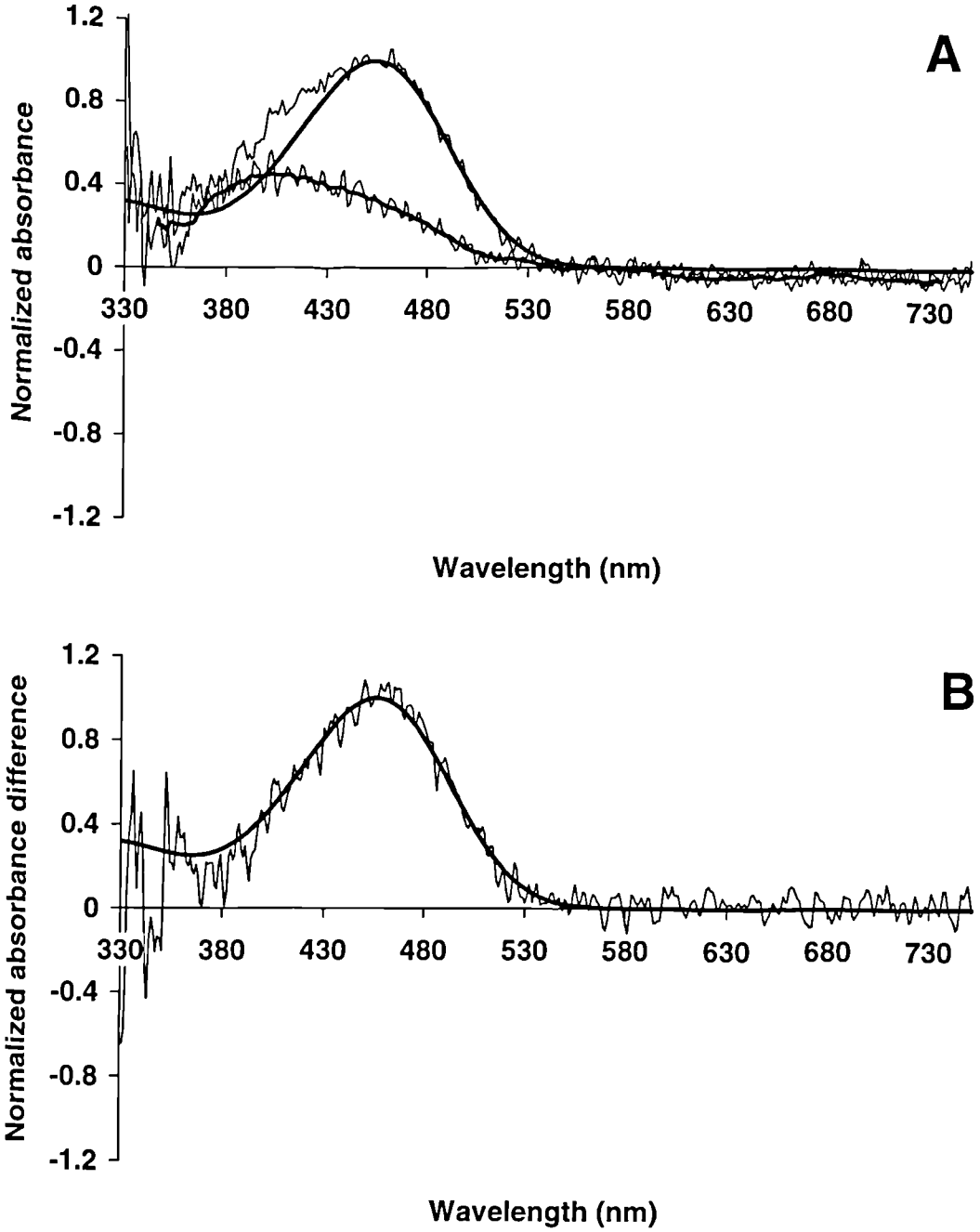

Figure 2.101 Microspectrophotometric results from 12 SWS single cones of the blackbird, *Turdus merula*. Up and down scans were averaged prior to analysis and display. (**A**) Mean pre-bleach absorbance spectrum (upper trace) with best-fitted visual pigment template (λ_{max} 454 nm, solid line) and mean post-bleach absorbance spectrum (lower trace) with running average (solid line). (**B**) Mean difference spectrum (trace) with best-fitted visual pigment template (λ_{max} 456 nm, solid line).

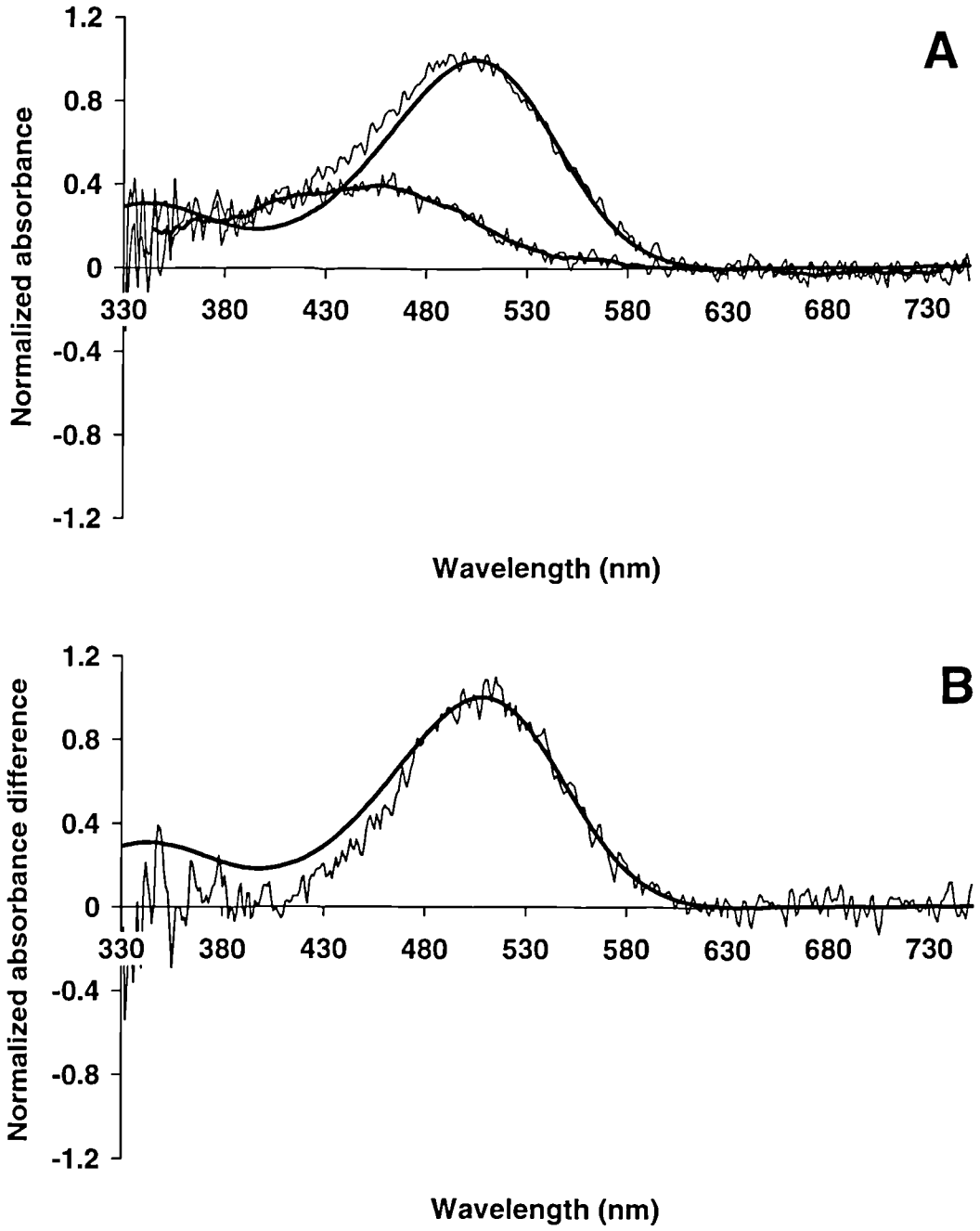

Figure 2.102 Microspectrophotometric results from 8 MWS single cones of the blackbird, *Turdus merula*. Up and down scans were averaged prior to analysis and display. (**A**) Mean pre-bleach absorbance spectrum (upper trace) with best-fitted visual pigment template (λ_{max} 504 nm, solid line) and mean post-bleach absorbance spectrum (lower trace) with running average (solid line). (**B**) Mean difference spectrum (trace) with best-fitted visual pigment template (λ_{max} 508 nm, solid line).

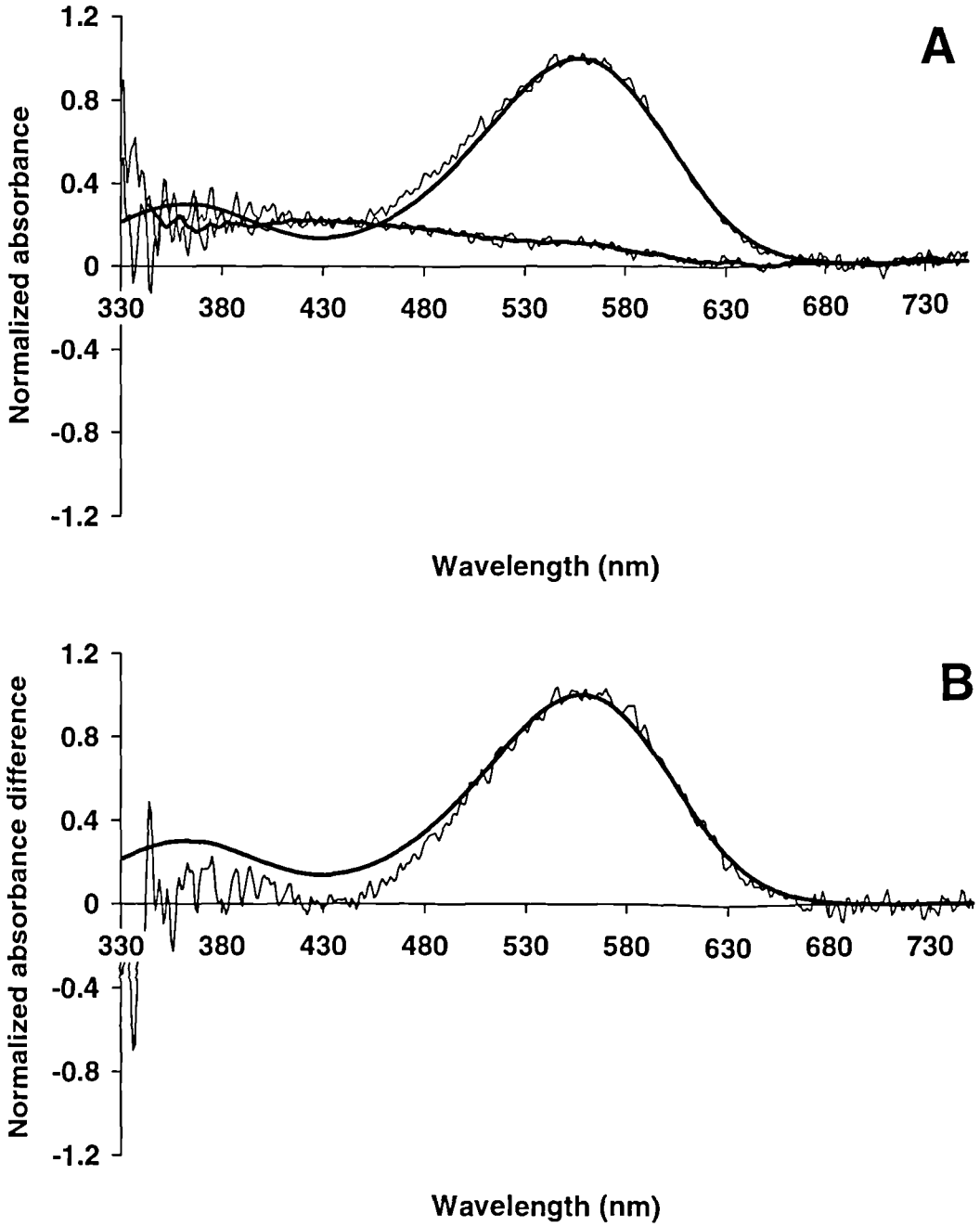

Figure 2.103 Microspectrophotometric results from 9 LWS single cones of the blackbird, *Turdus merula*. Up and down scans were averaged prior to analysis and display. (**A**) Mean pre-bleach absorbance spectrum (upper trace) with best-fitted visual pigment template (λ_{max} 557 nm, solid line) and mean post-bleach absorbance spectrum (lower trace) with running average (solid line). (**B**) Mean difference spectrum (trace) with best-fitted visual pigment template (λ_{max} 558 nm, solid line).

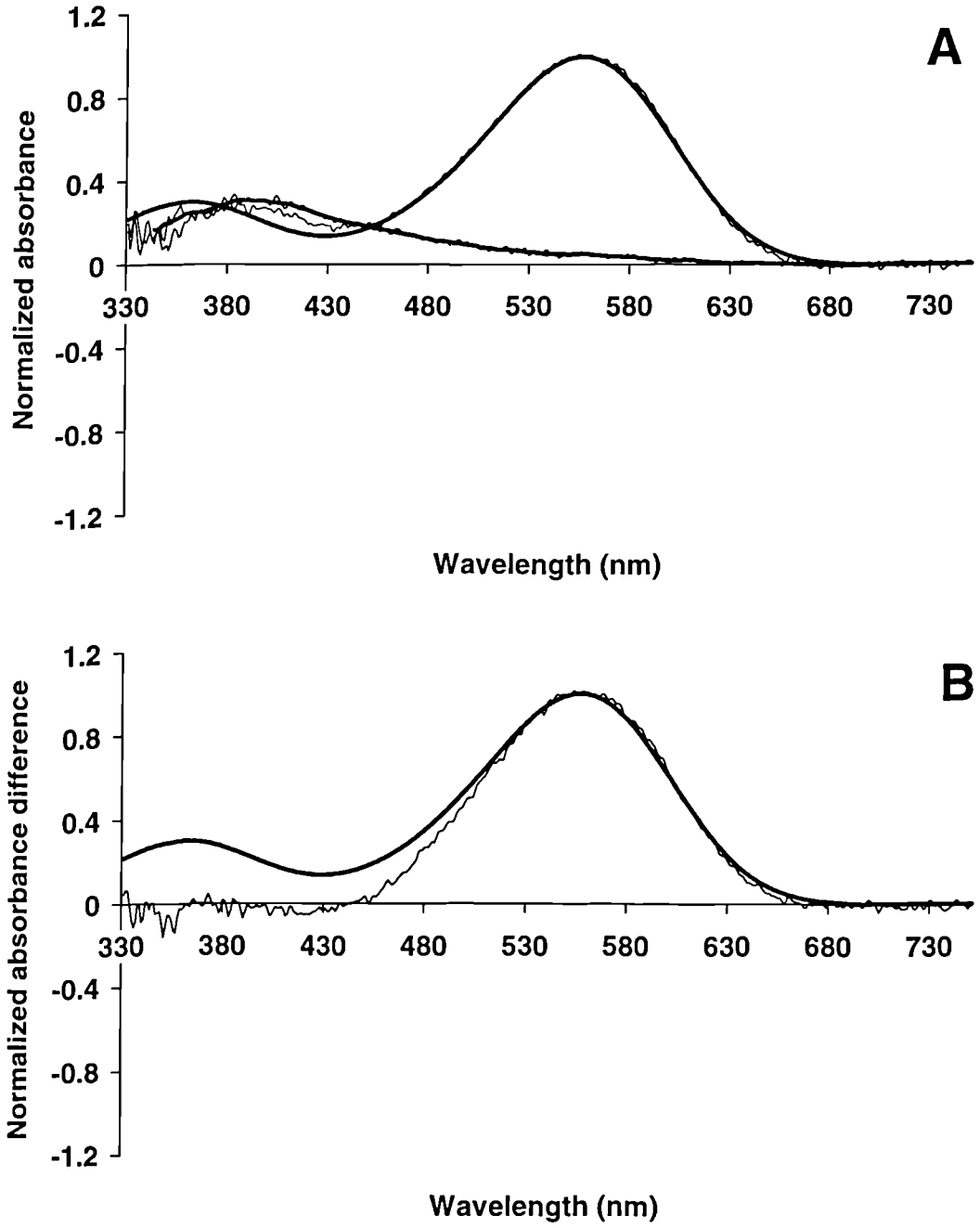

Figure 2.104 Microspectrophotometric results from 23 principal members of the double cone of the blackbird, *Turdus merula*. Up and down scans were averaged prior to analysis and display. (**A**) Mean pre-bleach absorbance spectrum (upper trace) with best-fitted visual pigment template (λ_{max} 557 nm, solid line) and mean post-bleach absorbance spectrum (lower trace) with running average (solid line). (**B**) Mean difference spectrum (trace) with best-fitted visual pigment template (λ_{max} 557 nm, solid line).

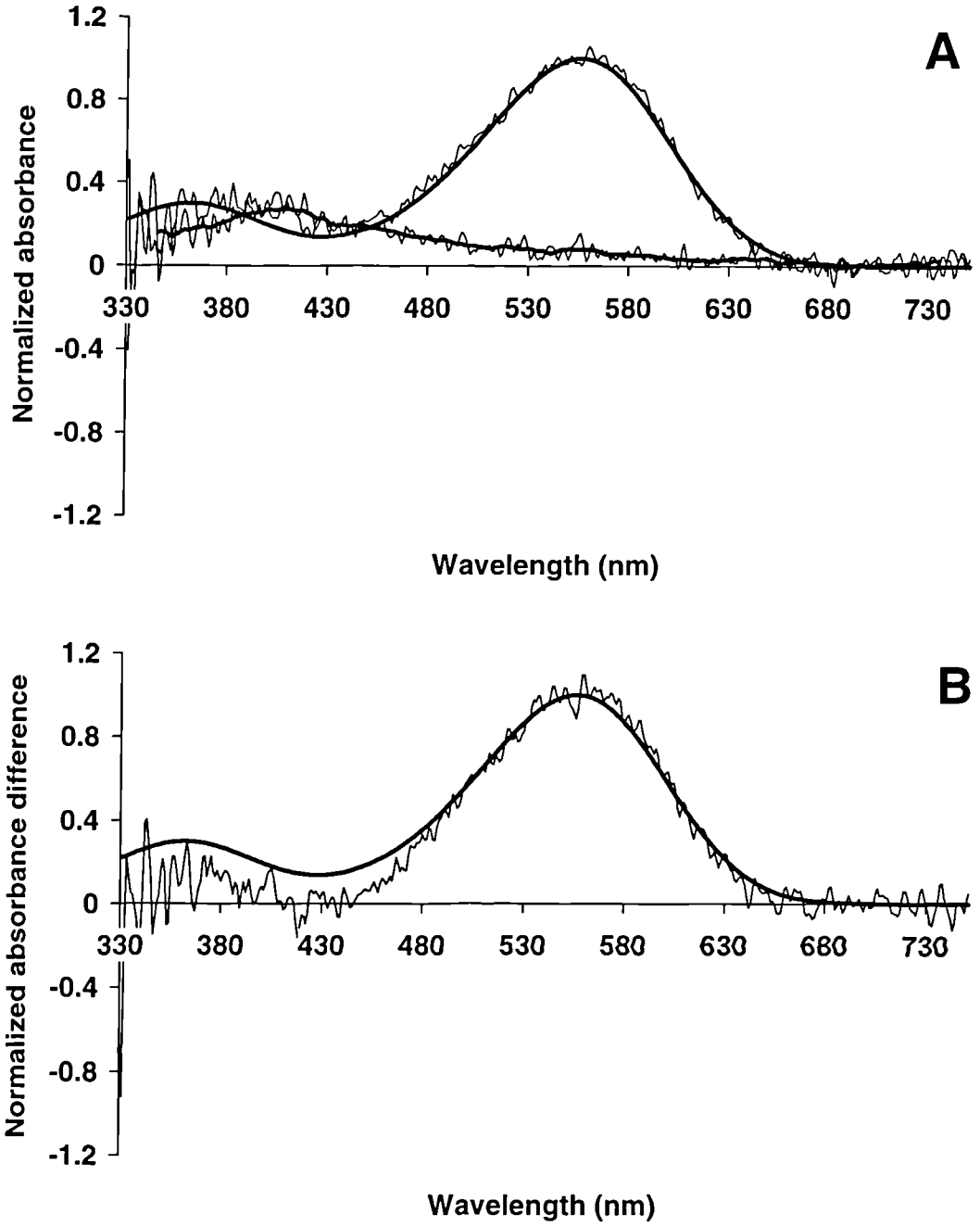

Figure 2.105 Microspectrophotometric results from 7 accessory members of the double cone of the blackbird, *Turdus merula*. Up and down scans were averaged prior to analysis and display. (**A**) Mean pre-bleach absorbance spectrum (upper trace) with best-fitted visual pigment template (λ_{max} 556 nm, solid line) and mean post-bleach absorbance spectrum (lower trace) with running average (solid line). (**B**) Mean difference spectrum (trace) with best-fitted visual pigment template (λ_{max} 556 nm, solid line).

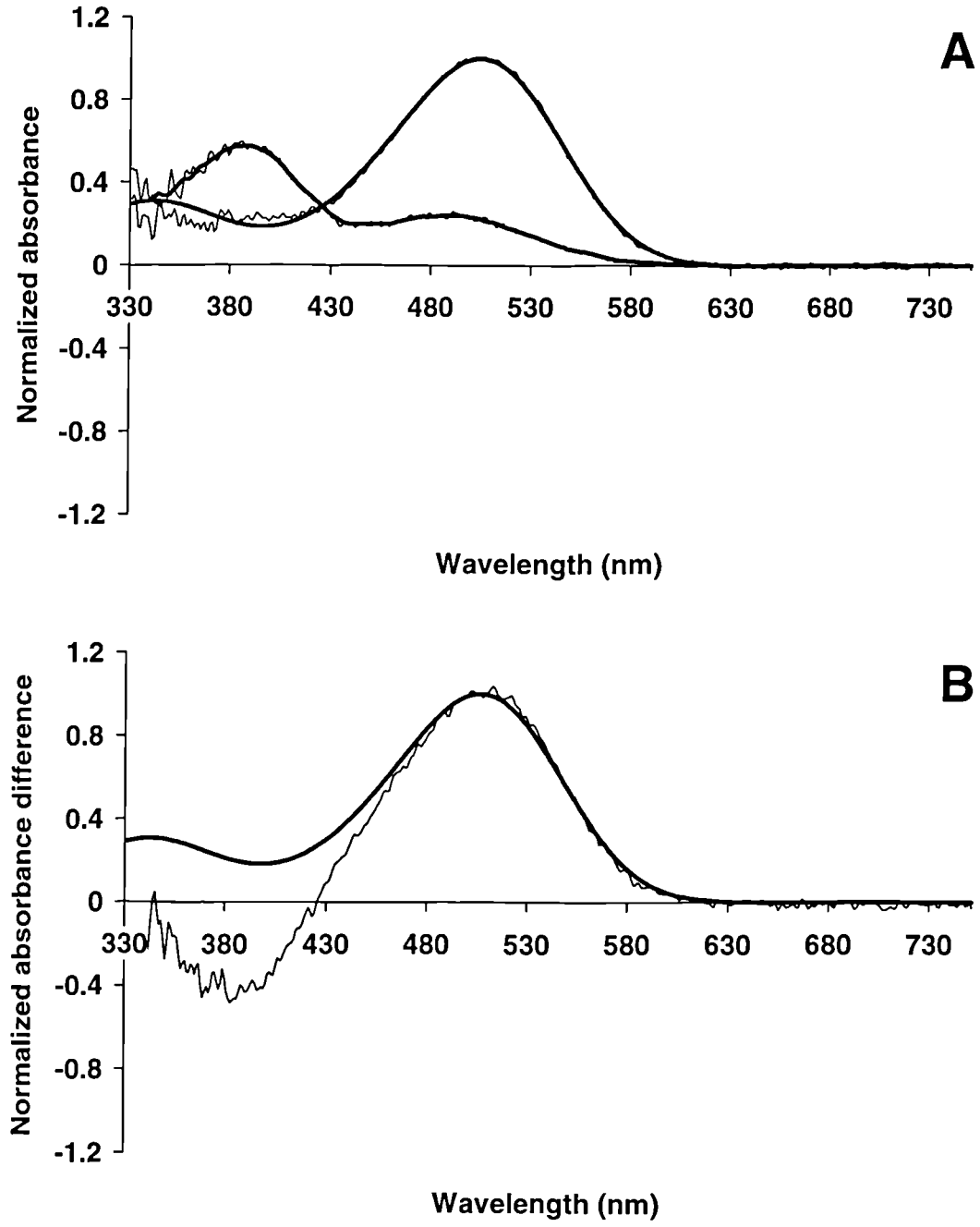

Figure 2.106 Microspectrophotometric results from 13 rods of the blackbird, *Turdus merula*. Up and down scans were averaged prior to analysis and display. (**A**) Mean pre-bleach absorbance spectrum (upper trace) with best-fitted visual pigment template (λ_{max} 505 nm, solid line) and mean post-bleach absorbance spectrum (lower trace) with running average (solid line). (**B**) Mean difference spectrum (trace) with best-fitted visual pigment template (λ_{max} 507 nm, solid line).

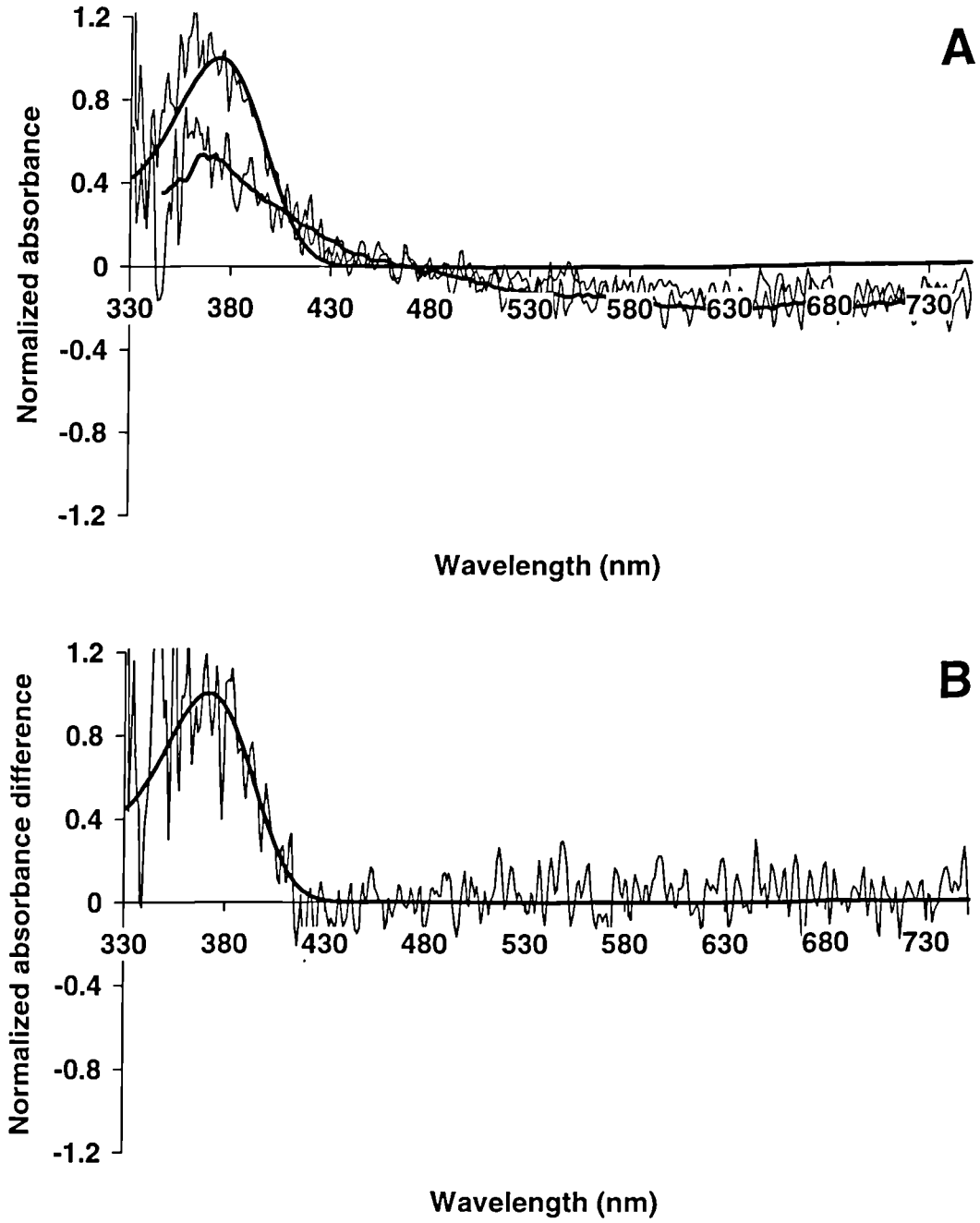

Figure 2.107 Microspectrophotometric results from 5 UVS single cones of the blue tit, *Parus caeruleus*. Up and down scans were averaged prior to analysis and display. (**A**) Mean pre-bleach absorbance spectrum (upper trace) with best-fitted visual pigment template (λ_{max} 374 nm, solid line) and mean post-bleach absorbance spectrum (lower trace) with running average (solid line). (**B**) Mean difference spectrum (trace) with best-fitted visual pigment template (λ_{max} 372 nm, solid line).

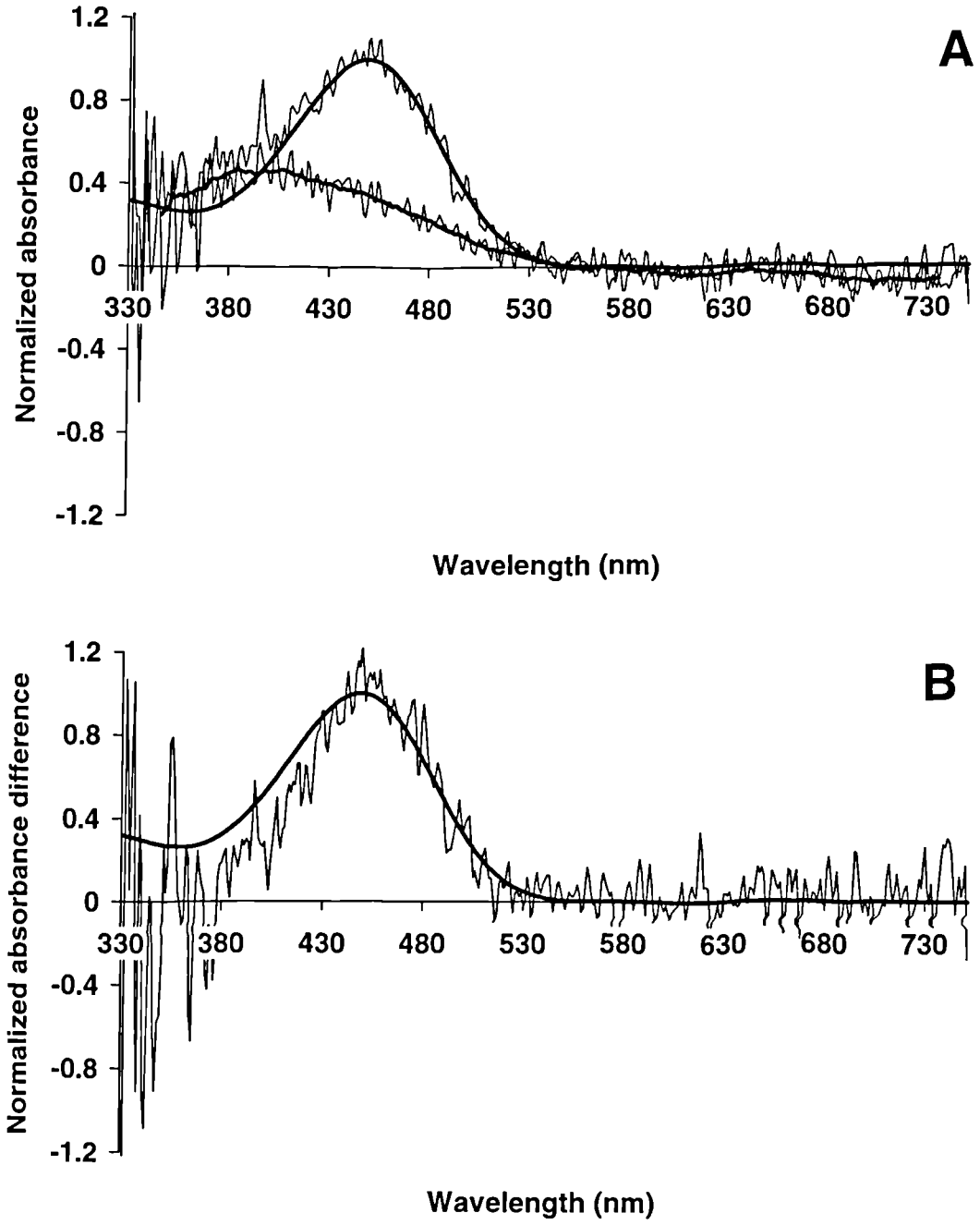

Figure 2.108 Microspectrophotometric results from 5 SWS single cones of the blue tit, *Parus caeruleus*. Up and down scans were averaged prior to analysis and display. (**A**) Mean pre-bleach absorbance spectrum (upper trace) with best-fitted visual pigment template (λ_{max} 449 nm, solid line) and mean post-bleach absorbance spectrum (lower trace) with running average (solid line). (**B**) Mean difference spectrum (trace) with best-fitted visual pigment template (λ_{max} 449 nm, solid line).

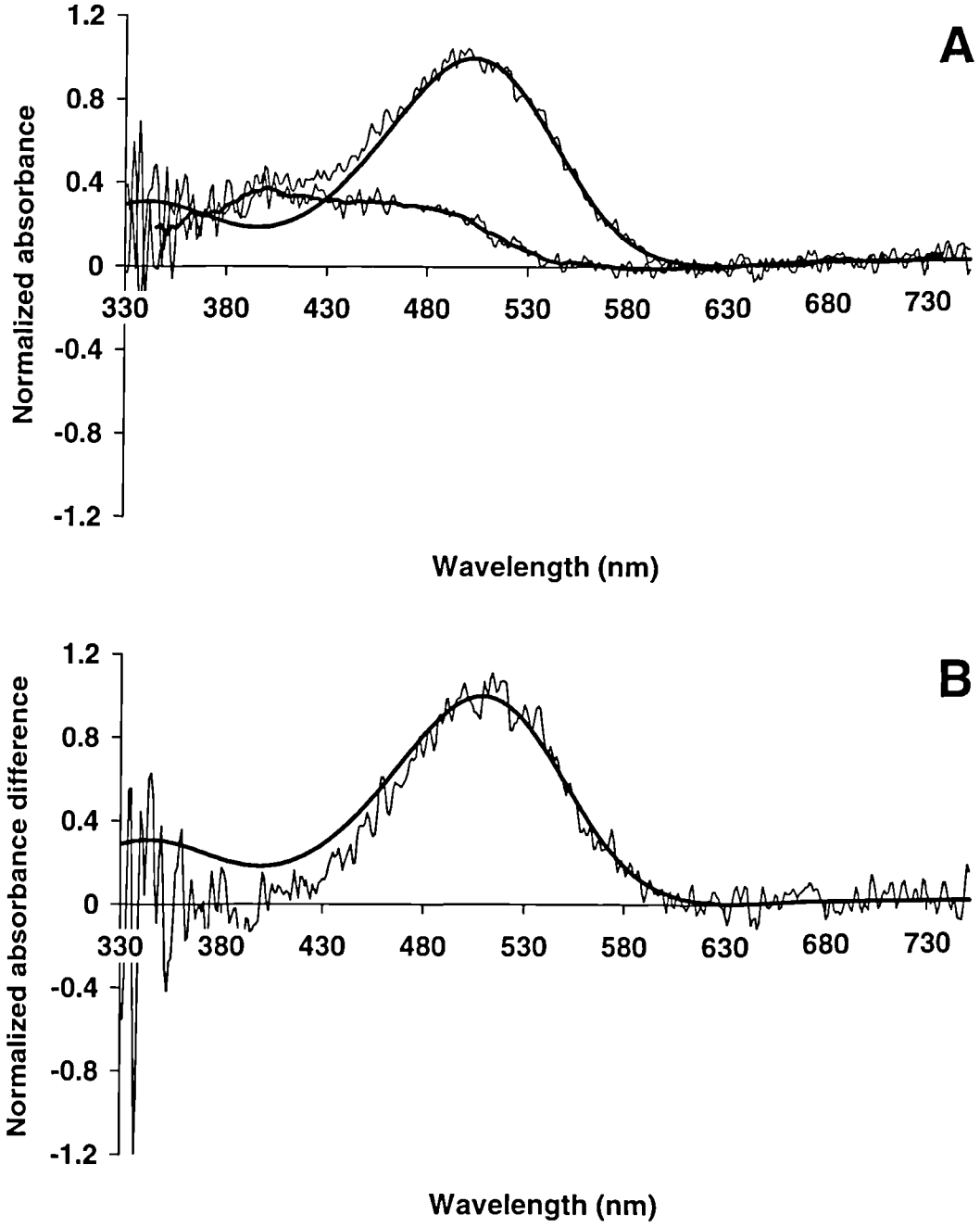

Figure 2.109 Microspectrophotometric results from 10 MWS single cones of the blue tit, *Parus caeruleus*. Up and down scans were averaged prior to analysis and display. (**A**) Mean pre-bleach absorbance spectrum (upper trace) with best-fitted visual pigment template (λ_{max} 503 nm, solid line) and mean post-bleach absorbance spectrum (lower trace) with running average (solid line). (**B**) Mean difference spectrum (trace) with best-fitted visual pigment template (λ_{max} 509 nm, solid line).

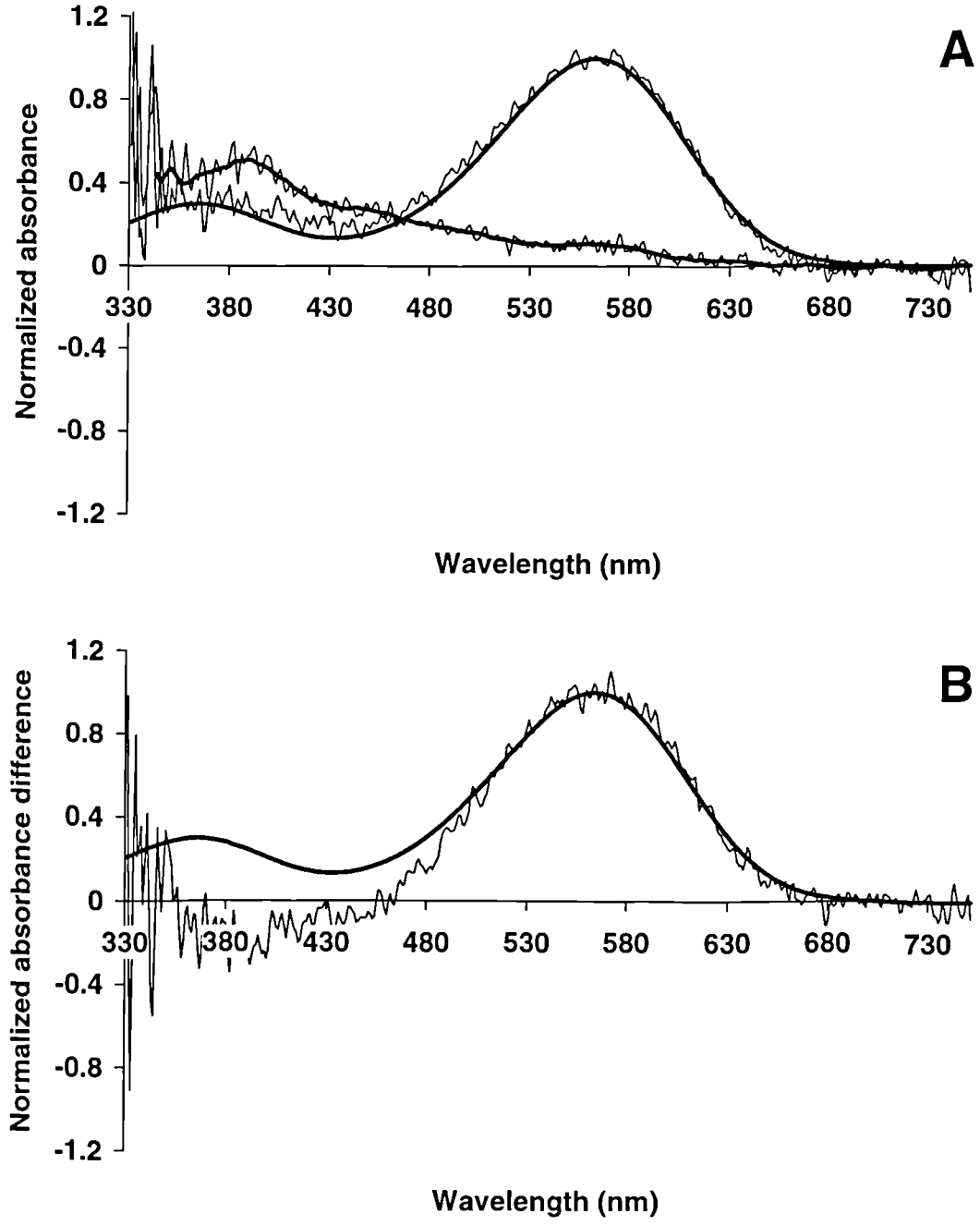

Figure 2.110 Microspectrophotometric results from 7 LWS single cones of the blue tit, *Parus caeruleus*. Up and down scans were averaged prior to analysis and display. (**A**) Mean pre-bleach absorbance spectrum (upper trace) with best-fitted visual pigment template (λ_{max} 563 nm, solid line) and mean post-bleach absorbance spectrum (lower trace) with running average (solid line). (**B**) Mean difference spectrum (trace) with best-fitted visual pigment template (λ_{max} 564 nm, solid line).

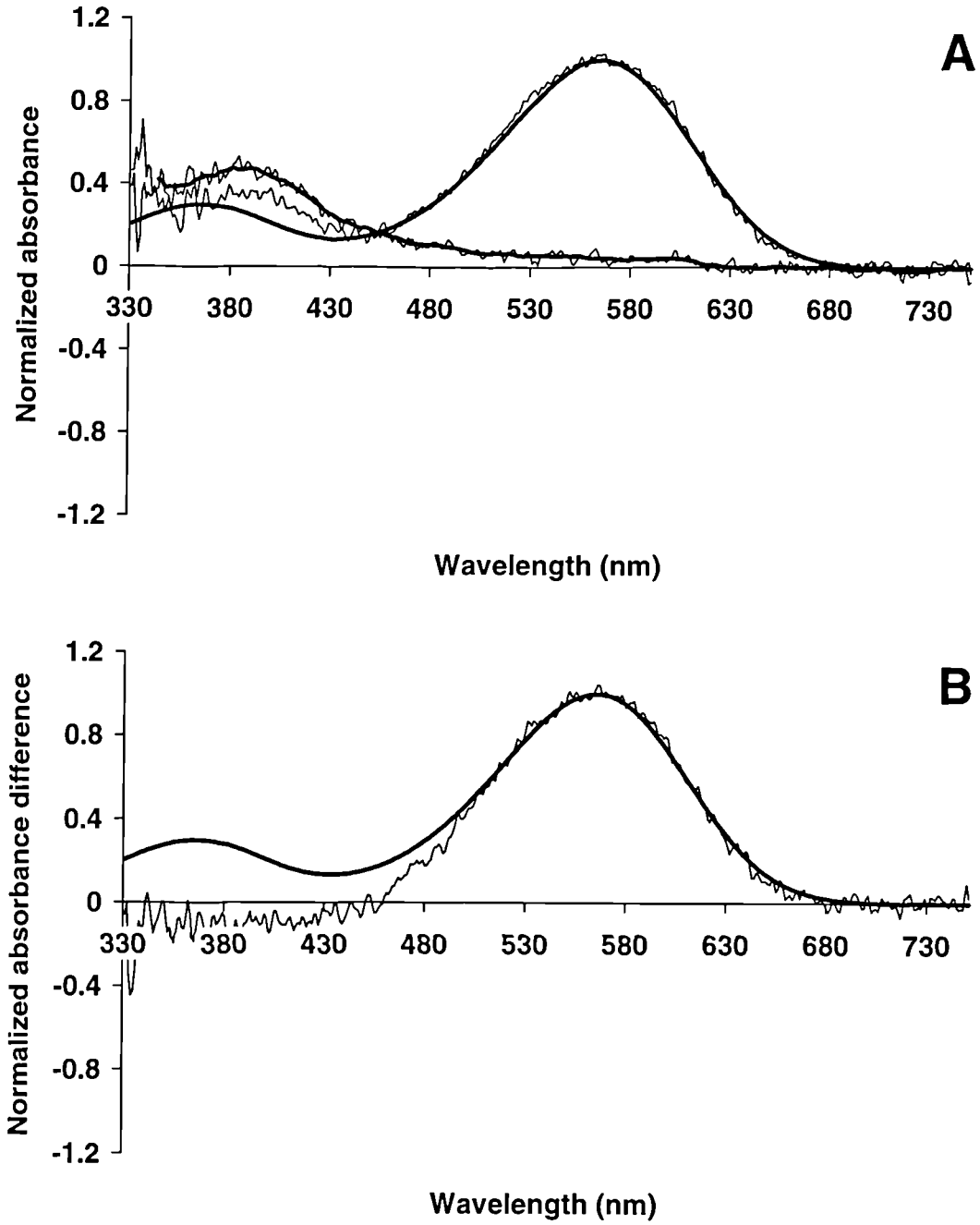

Figure 2.111 Microspectrophotometric results from 14 principal members of the double cone of the blue tit, *Parus caeruleus*. Up and down scans were averaged prior to analysis and display. (**A**) Mean pre-bleach absorbance spectrum (upper trace) with best-fitted visual pigment template (λ_{max} 565 nm, solid line) and mean post-bleach absorbance spectrum (lower trace) with running average (solid line). (**B**) Mean difference spectrum (trace) with best-fitted visual pigment template (λ_{max} 565 nm, solid line).

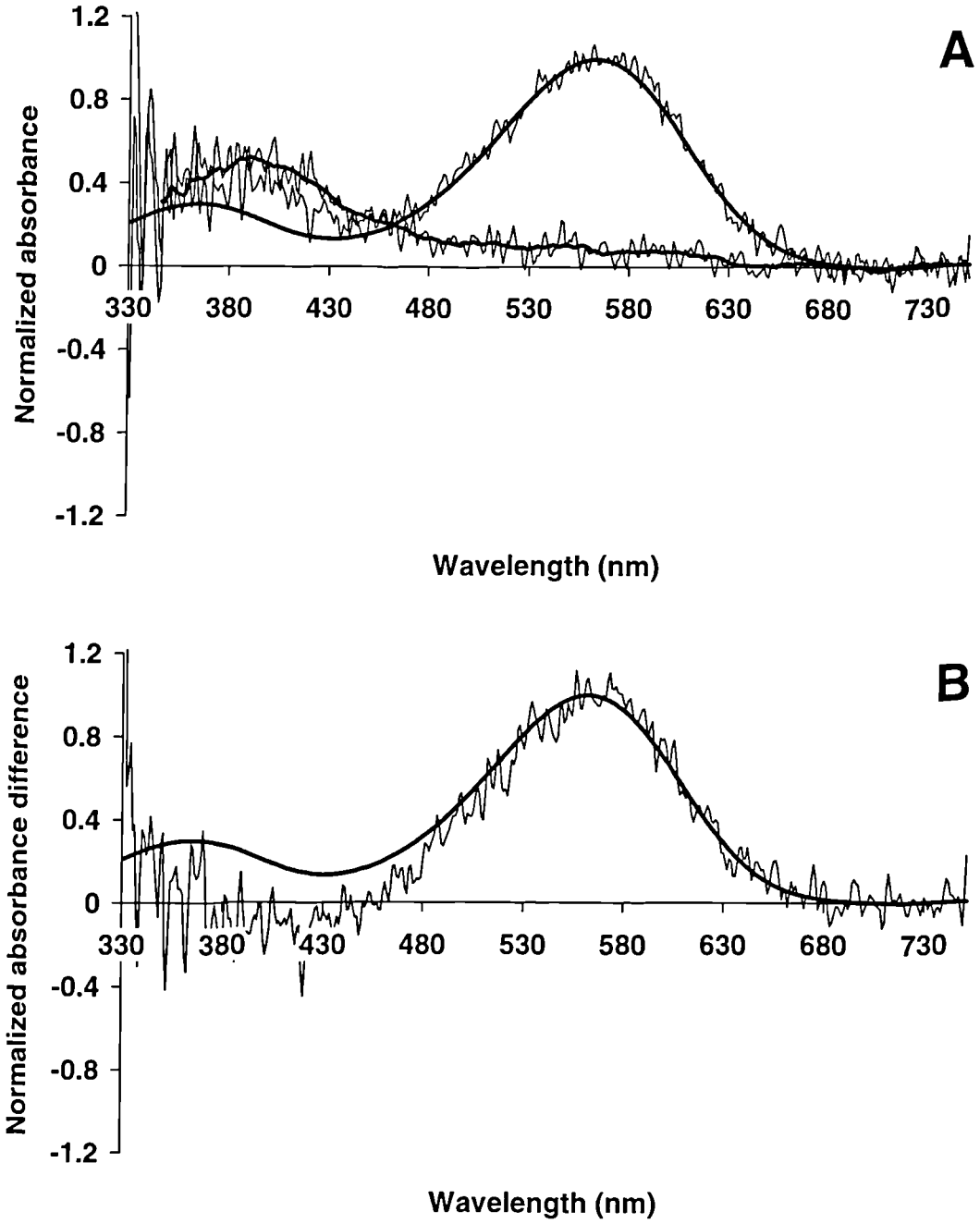

Figure 2.112 Microspectrophotometric results from 4 accessory members of the double cone of the blue tit, *Parus caeruleus*. Up and down scans were averaged prior to analysis and display. (**A**) Mean pre-bleach absorbance spectrum (upper trace) with best-fitted visual pigment template (λ_{max} 563 nm, solid line) and mean post-bleach absorbance spectrum (lower trace) with running average (solid line). (**B**) Mean difference spectrum (trace) with best-fitted visual pigment template (λ_{max} 562 nm, solid line).

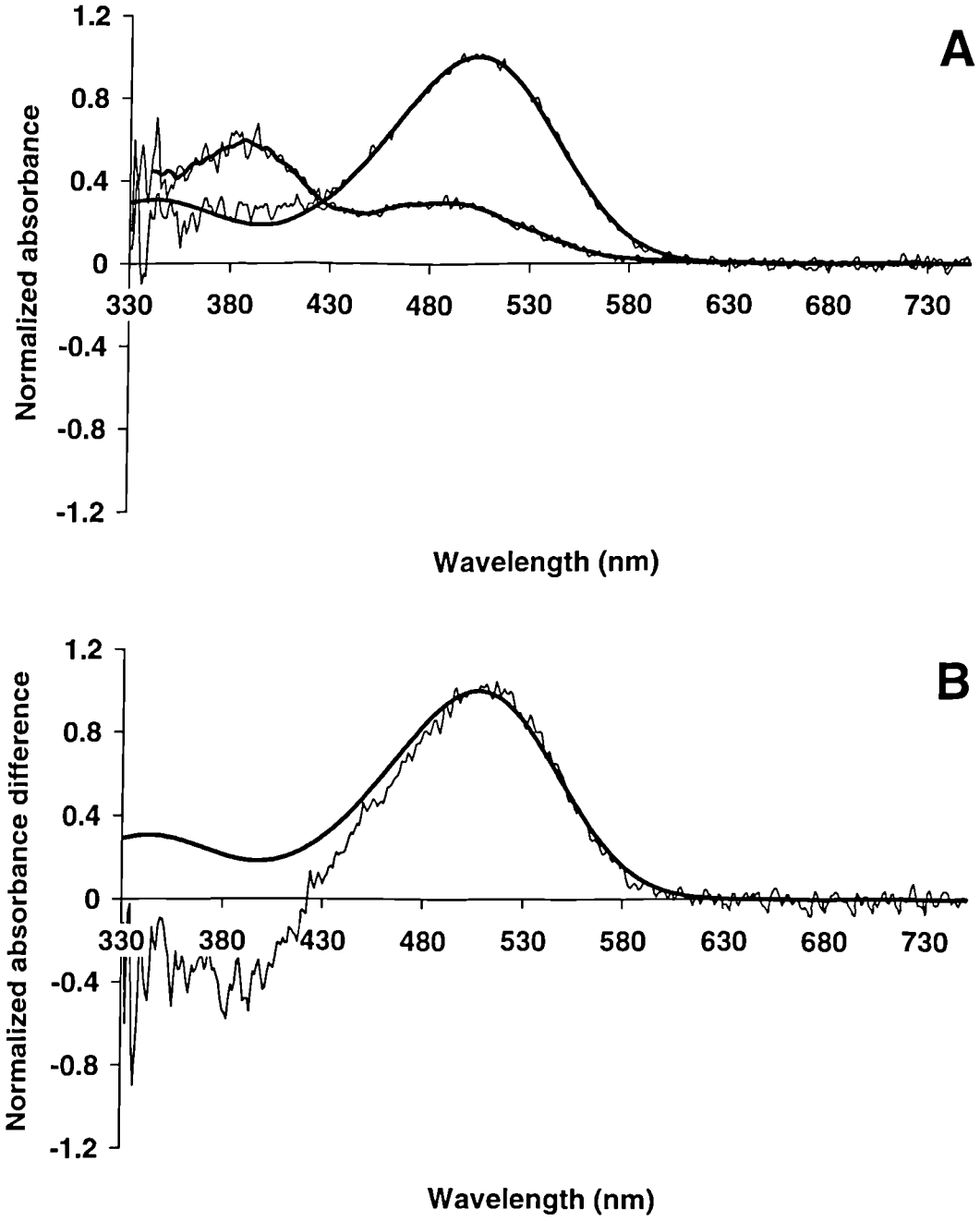

Figure 2.113 Microspectrophotometric results from 6 rods of the blue tit, *Parus caeruleus*. Up and down scans were averaged prior to analysis and display. (**A**) Mean pre-bleach absorbance spectrum (upper trace) with best-fitted visual pigment template (λ_{max} 503 nm, solid line) and mean post-bleach absorbance spectrum (lower trace) with running average (solid line). (**B**) Mean difference spectrum (trace) with best-fitted visual pigment template (λ_{max} 507 nm, solid line).

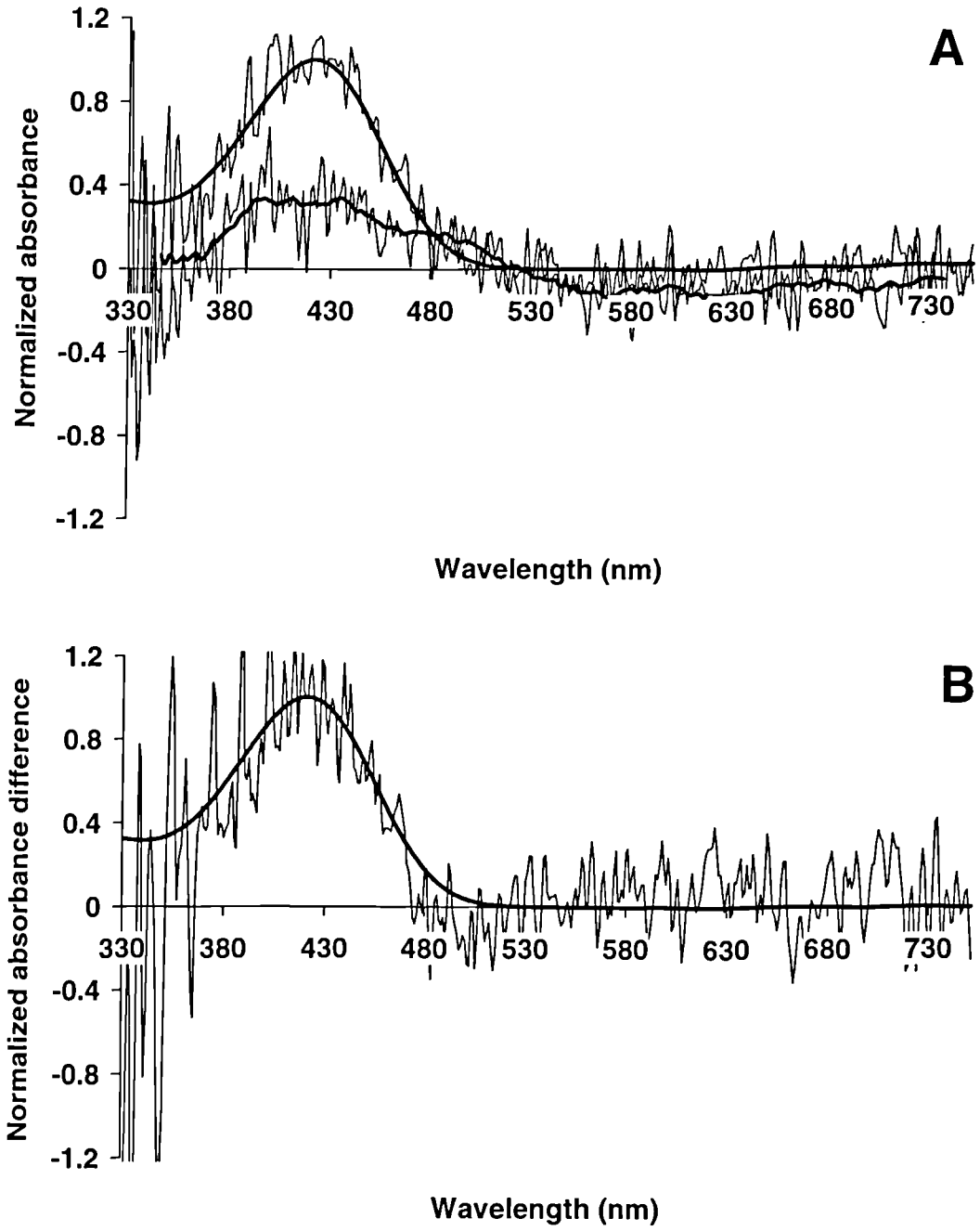

Figure 2.114 Microspectrophotometric results from 4 VS single cones of the peacock, *Pavo cristatus*. Up and down scans were averaged prior to analysis and display. (**A**) Mean pre-bleach absorbance spectrum (upper trace) with best-fitted visual pigment template (λ_{max} 421 nm, solid line) and mean post-bleach absorbance spectrum (lower trace) with running average (solid line). (**B**) Mean difference spectrum (trace) with best-fitted visual pigment template (λ_{max} 421 nm, solid line).

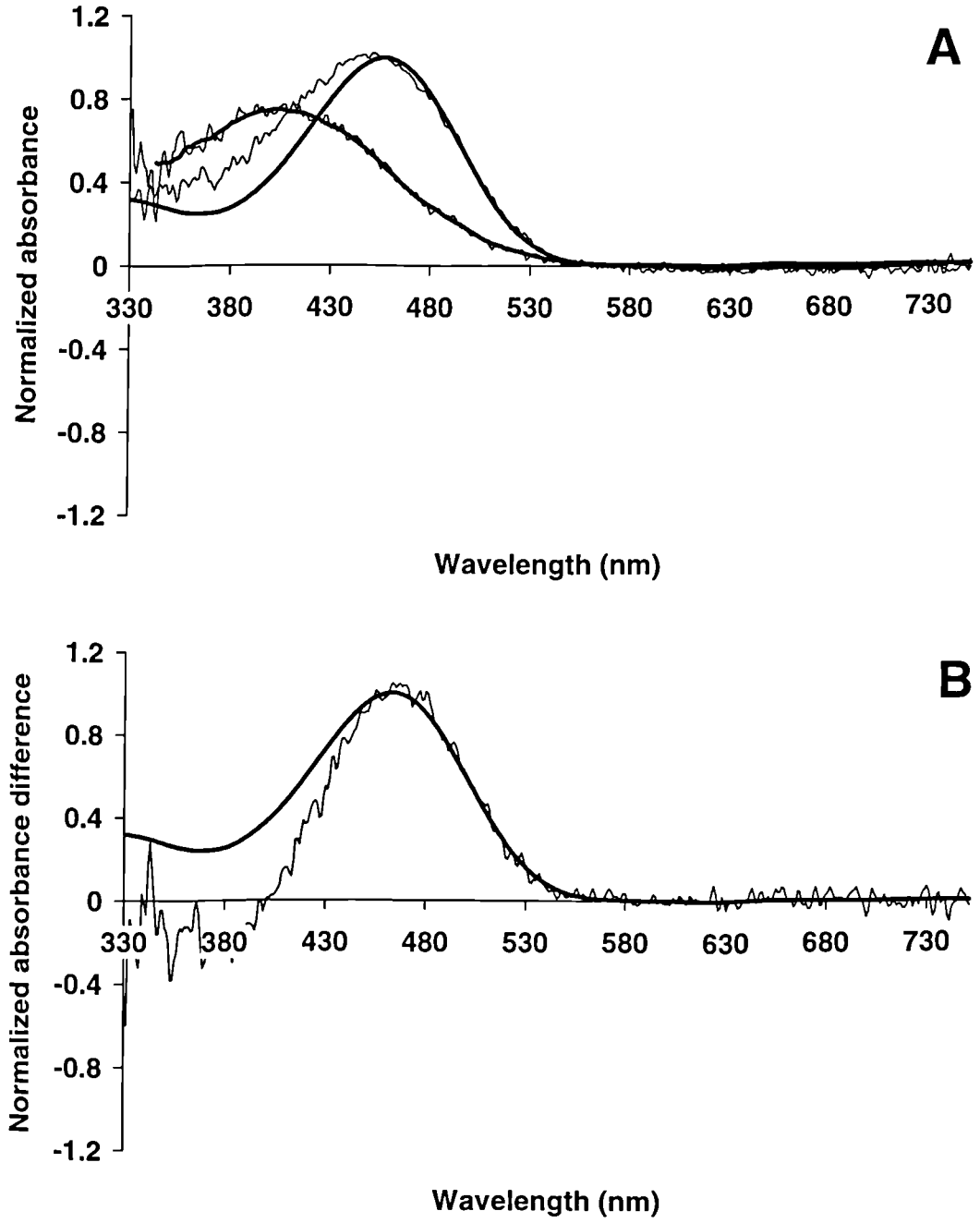

Figure 2.115 Microspectrophotometric results from 14 SWS single cones of the peacock, *Pavo cristatus*. Up and down scans were averaged prior to analysis and display. (**A**) Mean pre-bleach absorbance spectrum (upper trace) with best-fitted visual pigment template (λ_{max} 457 nm, solid line) and mean post-bleach absorbance spectrum (lower trace) with running average (solid line). (**B**) Mean difference spectrum (trace) with best-fitted visual pigment template (λ_{max} 463 nm, solid line).

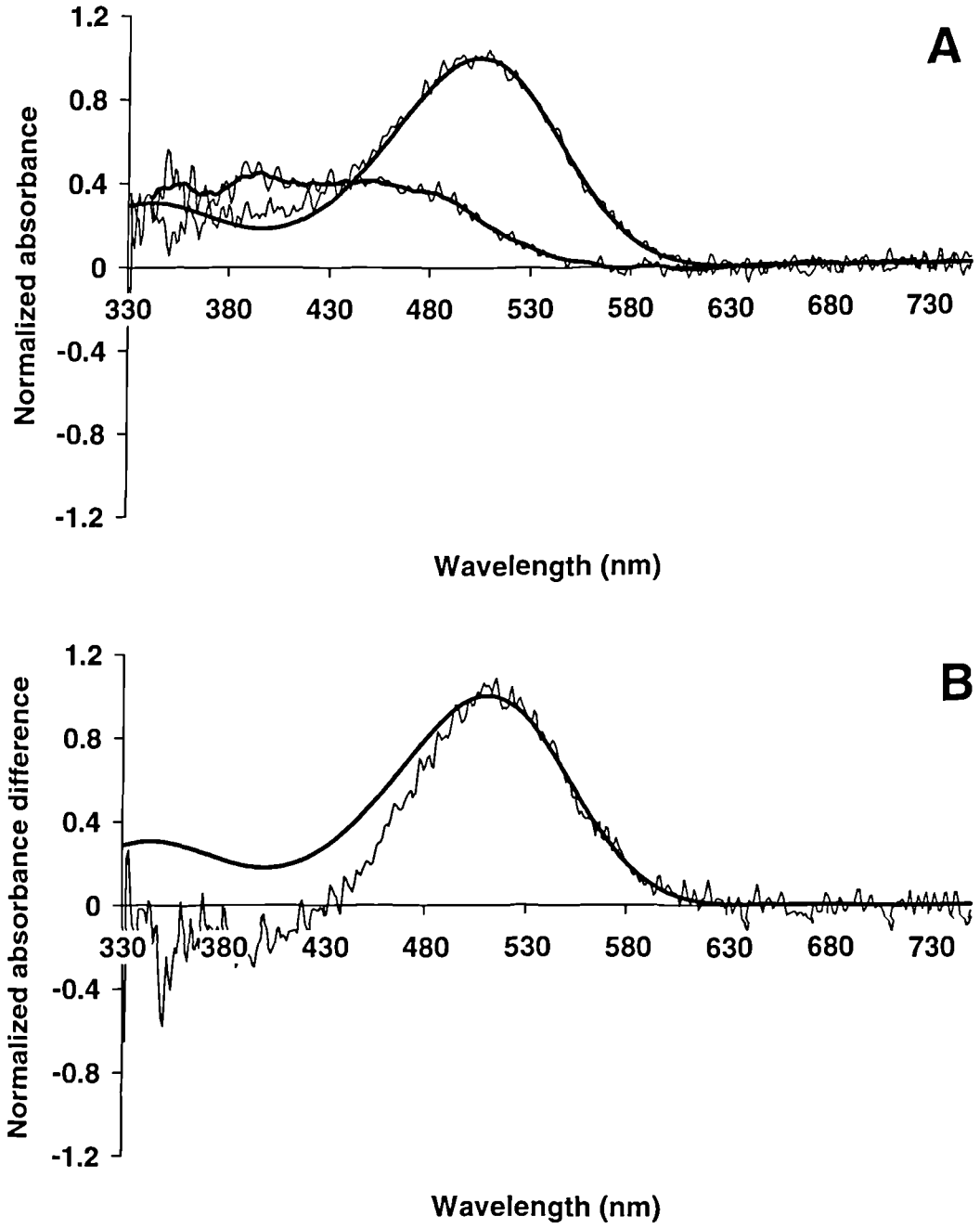

Figure 2.116 Microspectrophotometric results from 5 MWS single cones of the peacock, *Pavo cristatus*. Up and down scans were averaged prior to analysis and display. (**A**) Mean pre-bleach absorbance spectrum (upper trace) with best-fitted visual pigment template (λ_{max} 505 nm, solid line) and mean post-bleach absorbance spectrum (lower trace) with running average (solid line). (**B**) Mean difference spectrum (trace) with best-fitted visual pigment template (λ_{max} 511 nm, solid line).

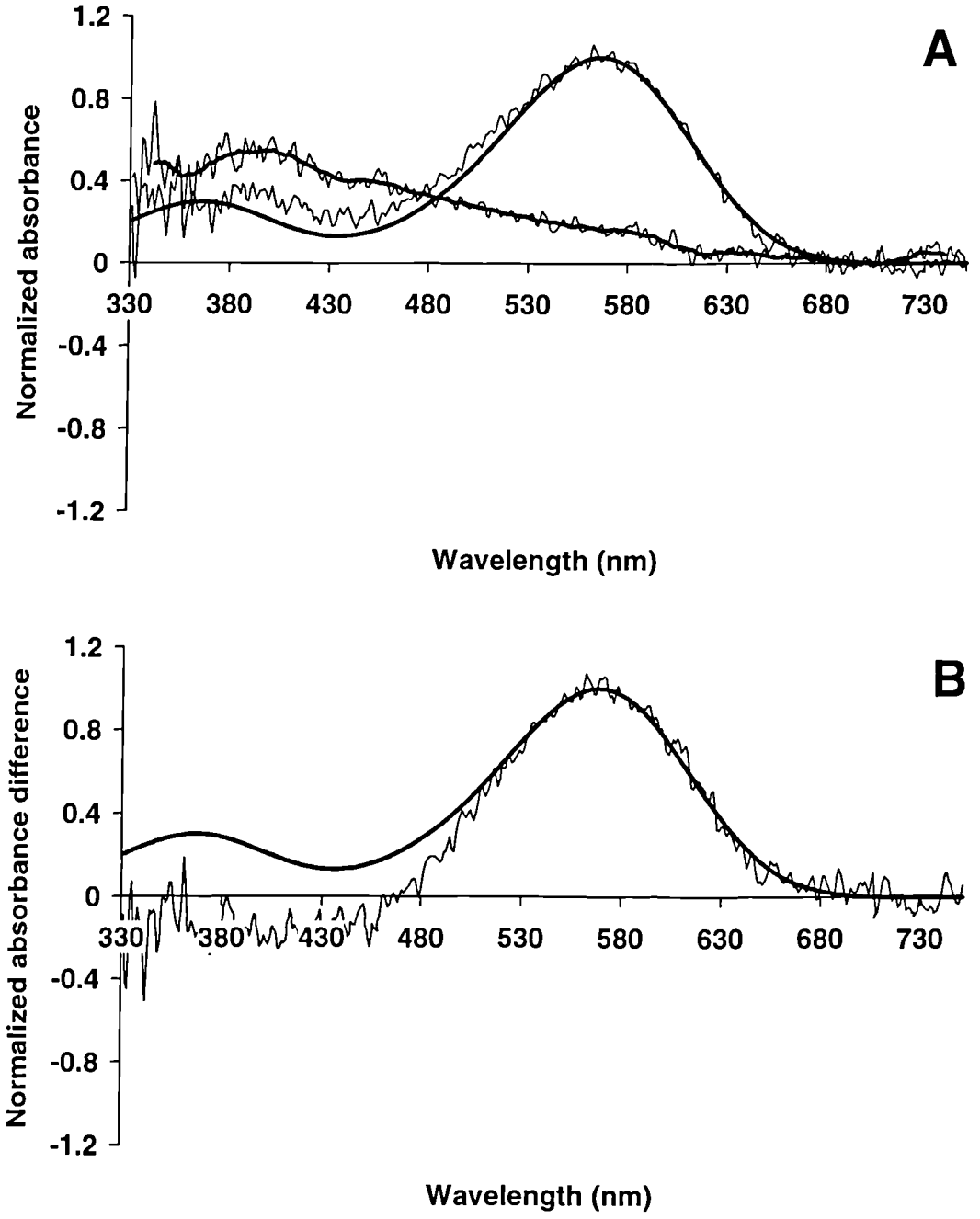

Figure 2.117 Microspectrophotometric results from 4 LWS single cones of the peacock, *Pavo cristatus*. Up and down scans were averaged prior to analysis and display. (**A**) Mean pre-bleach absorbance spectrum (upper trace) with best-fitted visual pigment template (λ_{max} 566 nm, solid line) and mean post-bleach absorbance spectrum (lower trace) with running average (solid line). (**B**) Mean difference spectrum (trace) with best-fitted visual pigment template (λ_{max} 569 nm, solid line).

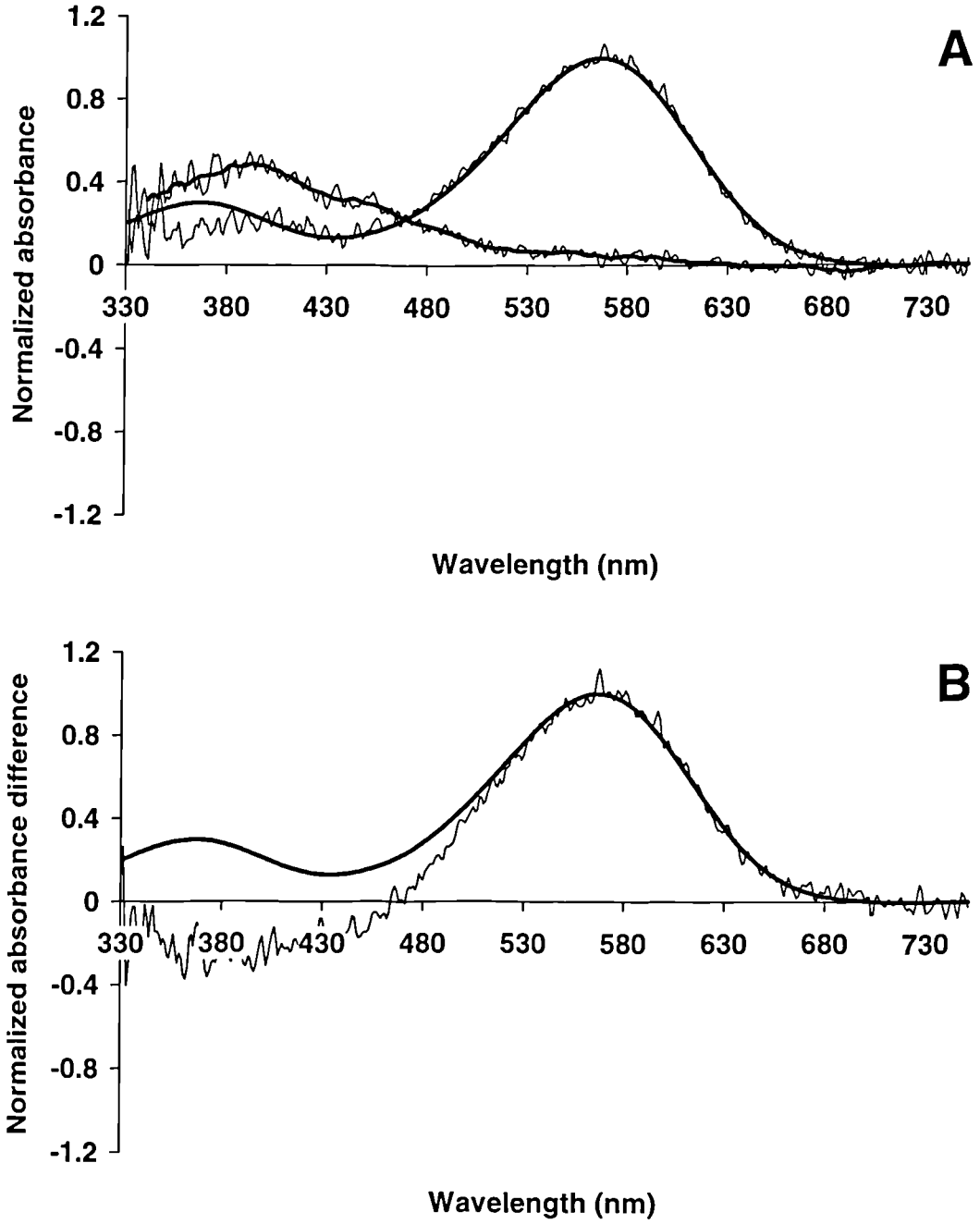

Figure 2.118 Microspectrophotometric results from 9 principal members of the double cone of the peacock, *Pavo cristatus*. Up and down scans were averaged prior to analysis and display. (**A**) Mean pre-bleach absorbance spectrum (upper trace) with best-fitted visual pigment template (λ_{max} 567 nm, solid line) and mean post-bleach absorbance spectrum (lower trace) with running average (solid line). (**B**) Mean difference spectrum (trace) with best-fitted visual pigment template (λ_{max} 567 nm, solid line).

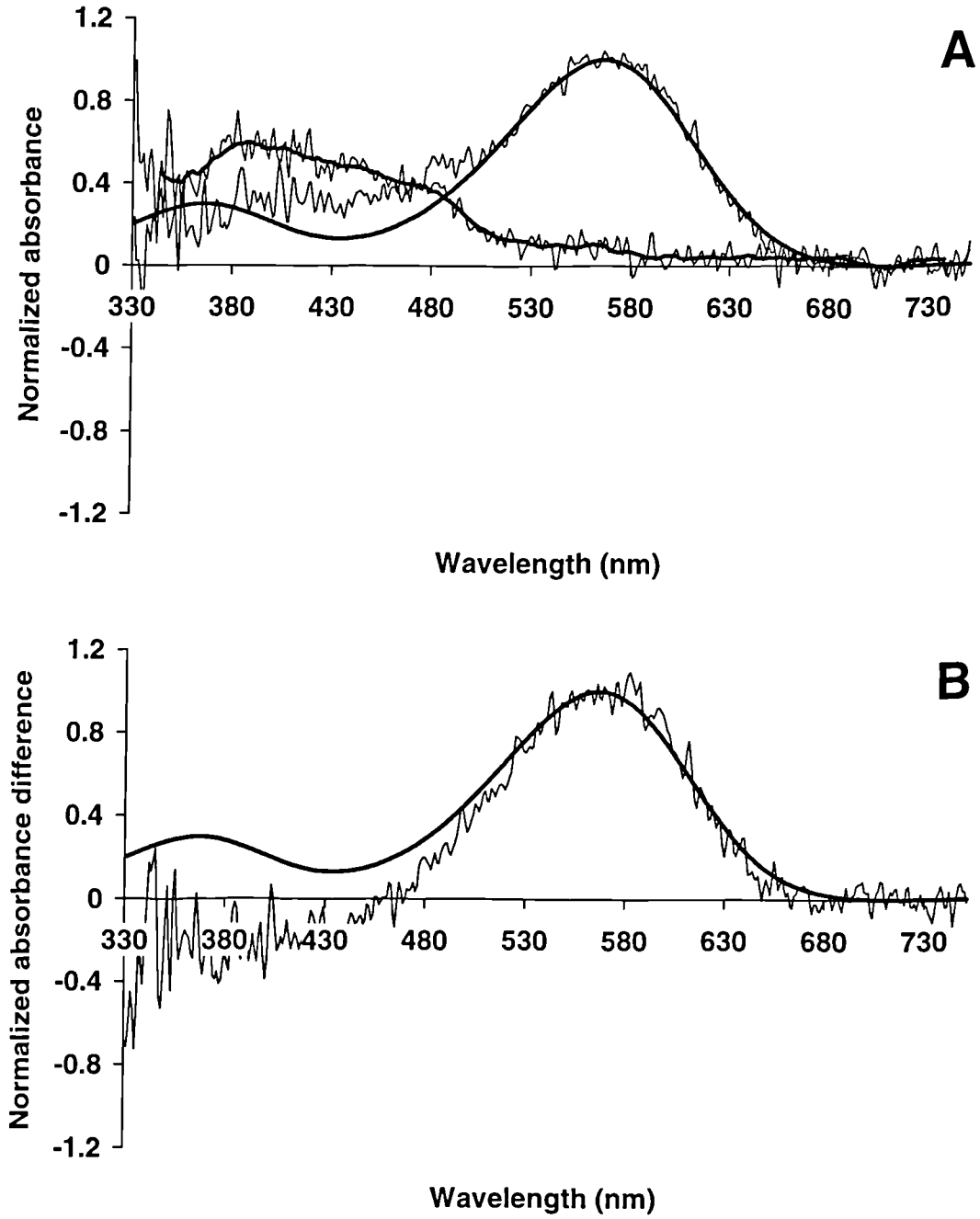

Figure 2.119 Microspectrophotometric results from 4 accessory members of the double cone of the peacock, *Pavo cristatus*. Up and down scans were averaged prior to analysis and display. (**A**) Mean pre-bleach absorbance spectrum (upper trace) with best-fitted visual pigment template (λ_{max} 566 nm, solid line) and mean post-bleach absorbance spectrum (lower trace) with running average (solid line). (**B**) Mean difference spectrum (trace) with best-fitted visual pigment template (λ_{max} 567 nm, solid line).

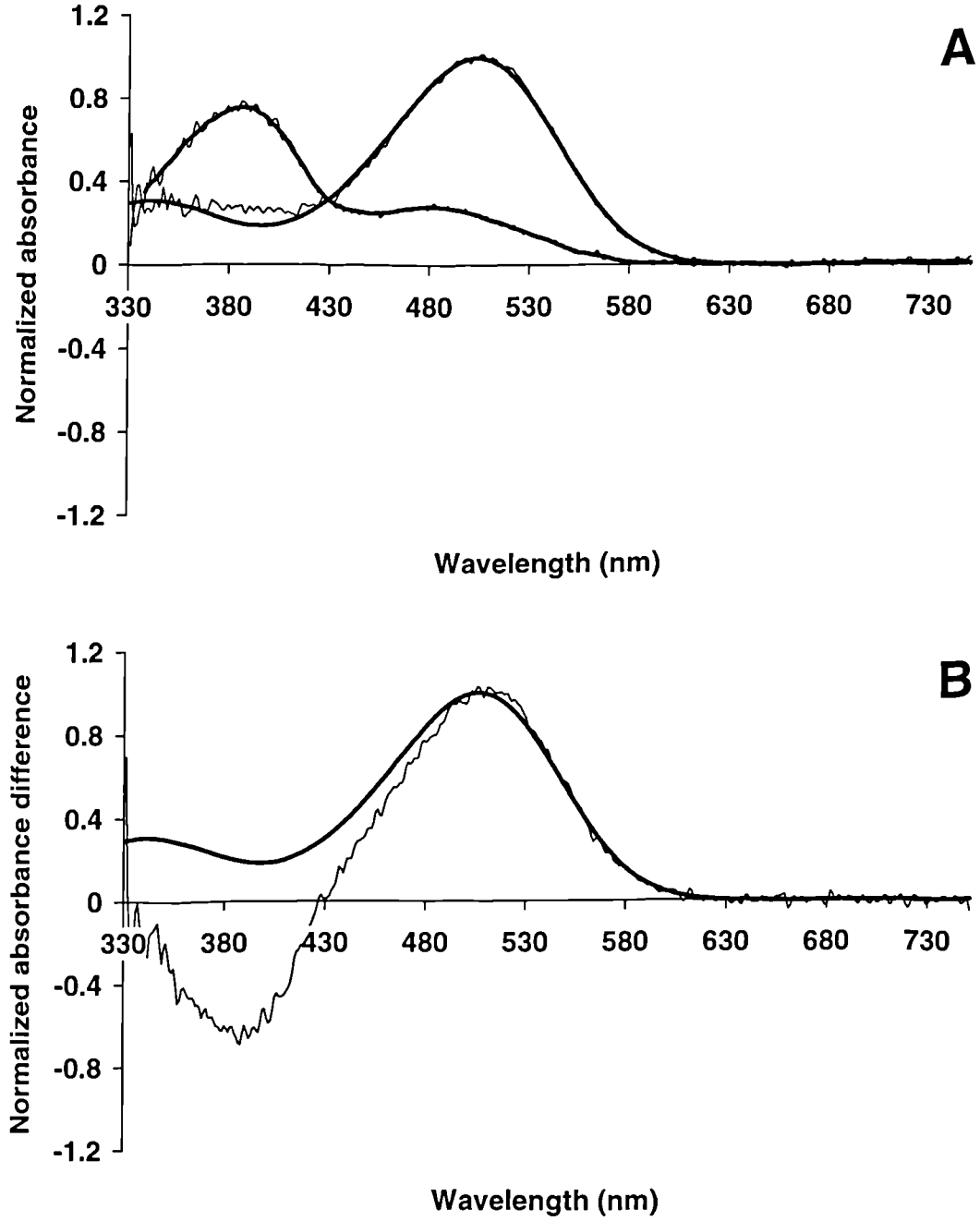

Figure 2.120 Microspectrophotometric results from 7 rods of the peacock, *Pavo cristatus*. Up and down scans were averaged prior to analysis and display. (**A**) Mean pre-bleach absorbance spectrum (upper trace) with best-fitted visual pigment template (λ_{max} 504 nm, solid line) and mean post-bleach absorbance spectrum (lower trace) with running average (solid line). (**B**) Mean difference spectrum (trace) with best-fitted visual pigment template (λ_{max} 506 nm, solid line).

	Starling	Blackbird	Blue tit	Peacock	Turkey	
Mountant	**DPBS**	**GPBS**	**GPBS**	**GPBS**	**DPBS**	**GPBS**
λ_{max} of mean pre-bleach spectrum (nm)						
UVS / VS	368.2 ± 4.9	376.0 ± 2.6	374.0 ± 2.6	421.3 ± 3.4	418.3 ± 1.9	419.7 ± 2.0
SWS	450.3 ± 2.6	453.7 ± 1.5	448.8 ± 3.3	457.1 ± 1.2	457.5 ± 1.6	459.4 ± 1.4
MWS	504.4 ± 1.5	504.2 ± 2.0	502.7 ± 1.7	504.6 ± 1.5	504.3 ± 0.7	505.4 ± 0.9
LWS	563.0 ± 2.0	557.2 ± 1.2	563.1 ± 2.0	566.0 ± 1.5	563.3 ± 3.0	563.5 ± 1.0
Double (principal)	563.3 ± 2.3	556.9 ± 1.1	565.3 ± 1.9	566.8 ± 1.7	564.2 ± 1.0	563.9 ± 1.4
Double (accessory)	559.7 ± 5.7	555.9 ± 2.1	563.1 ± 3.2	566.2 ± 2.9	-	563.4 ± 2.6
Rod	503.0 ± 0.8	504.5 ± 0.6	503.3 ± 1.0	503.6 ± 0.5	503.5 ± 0.5	504.2 ± 0.7
λ_{max} of mean difference spectrum (nm)						
UVS / VS	362.8 ± 3.1	368.4 ± 4.8	371.5 ± 5.0	420.7 ± 6.1	414.5 ± 4.1	417.1 ± 3.3
SWS	451.7 ± 3.9	456.0 ± 3.1	448.5 ± 7.7	463.1 ± 1.8	460.1 ± 3.6	462.2 ± 2.9
MWS	507.5 ± 3.3	508.2 ± 3.4	509.0 ± 4.4	510.7 ± 2.4	508.0 ± 1.1	509.5 ± 2.0
LWS	562.4 ± 4.0	557.9 ± 2.1	564.1 ± 3.1	568.6 ± 3.3	565.5 ± 3.8	564.1 ± 1.2
Double (principal)	563.4 ± 4.4	557.3 ± 1.4	565.2 ± 2.0	567.2 ± 2.0	564.2 ± 1.3	565.0 ± 1.8
Double (accessory)	560.3 ± 9.6	556.2 ± 2.9	562.0 ± 4.8	566.5 ± 4.3	-	563.5 ± 3.6
Rod	504.7 ± 1.0	506.6 ± 1.1	506.7 ± 2.0	506.3 ± 1.3	504.6 ± 0.7	506.2 ± 1.4

Table 2.13 Summary visual pigment λ_{max} values for the five species investigated in this study (legend continued on following page).

Table 2.13 (continued) Summary visual pigment λ_{max} values for the five species investigated in this study. All mean pre-bleach and difference spectra were re-analysed after averaging the up and down scans to remove the effects of in-scan photobleaching (see section 2.5.3). Values are ± standard deviations, which refer to the error in estimating the λ_{max} using the method described in the section 2.5.1. UVS, ultraviolet-sensitive single cones; VS, violet-sensitive single cones; SWS, short wavelength-sensitive single cones; MWS, medium wavelength-sensitive single cones; LWS, long wavelength-sensitive single cones; DPBS and GPBS refer to the type of cell mountant used (see section 2.4.4).

2.7 Discussion

The retinae of the five bird species surveyed microspectrophotometrically were shown to contain a single class of medium wavelength-sensitive rod, four types of single cone maximally sensitive to long, medium, short and either violet (turkey and peacock) or ultraviolet wavelengths (starling, blackbird, blue tit), and a single class of long wavelength-sensitive double cone.

2.7.1 Visual pigments

The spectral distribution of the visual pigments for all species examined by microspectrophotometry, including those in this study, are summarised in Figure 2.122. The cone visual pigments of avian retinae examined to date clearly fall into five main groups. It is likely that some of the variation observed is due to measurement artefacts and noise, particularly with respect to the visual pigments maximally sensitive to shorter wavelengths. A discriminant analysis (Minitab 10.51) was performed on the cone visual pigment λ_{max} values, for each of the species which have been shown microspectrophotometrically to possess four types of cone visual pigment. The groups into which each λ_{max} value was assigned were LWS (associated with R-type oil droplet), MWS (associated with Y-type oil droplet), SWS (associated with C-type oil droplet), VS (λ_{max} of visual pigment associated with T-type oil droplet > 400 nm) and UVS (λ_{max} of visual pigment associated with T-type oil droplet < 400 nm). The results are summarised in
Table 2.14. All of the λ_{max} values were predicted by the analysis to belong to the same group as they were assigned, with the exception of the SWS cone visual pigment of the zebra finch, which was reassigned to the VS group of cone visual pigments. Whilst the SWS cone visual pigment of the zebra finch is associated with a C-type oil droplet, the spectral absorption characteristics of which resemble those of other C-type droplets associated with SWS cone visual pigments in other species which were 'correctly' assigned, its λ_{max} value is unusually low.

Predicted cone class	Assigned cone class				
	UVS	VS	SWS	MWS	LWS
UVS	7	0	0	0	0
VS	0	8	1*	0	0
SWS	0	0	14	0	0
MWS	0	0	0	15	0
LWS	0	0	0	0	15
Number	**7**	**8**	**15**	**15**	**15**
Number correct	**7**	**8**	**14**	**15**	**15**
Percentage correct	**100**	**100**	**93.3**	**100**	**100**

Table 2.14 Discriminant analysis (Minitab 10.51) of the spectral location of the λ_{max} of visual pigments in different cone types, for all avian species which have been shown microspectrophotometrically to possess four spectrally distinct cone visual pigments. All of the λ_{max} values were predicted by the analysis to belong to the same group as they were assigned, with the exception of the SWS cone visual pigment of the zebra finch (asterisk) which was reassigned to the VS group of cone visual pigments.

Whilst the functional significance of a short wavelength-shifted SWS cone visual pigment in the zebra finch retina is unclear, there is an interesting relationship between the λ_{max} value of the cone visual pigment associated with the C-type oil droplet (SWS visual pigment) and the λ_{max} value of the cone visual pigment associated with the T-type oil droplet (i.e. VS or UVS visual pigment). A reduced major axis regression (Fowler and Cohen, 1990) was performed on the microspectrophotometric data from all avian species in which both types of visual pigment had been measured, with the exception of the zebra finch and the Pekin robin for which the estimates of UVS cone visual pigment λ_{max} were deemed insufficiently accurate (although including the data from these species does not affect the significance of the correlation observed). The λ_{max} value of the cone visual pigment associated with the C-type oil droplet was classed as the dependent variable. The results are displayed in Figure 2.121. Polynomial regression was performed on the data to test for a departure from linearity, but the squared term was found to be non-significant ($t_{14} = 1.18$; $p = 0.260$). The linear regression line calculated had a gradient of 0.1951 and an intercept of 373.4906. The correlation was found to be

statistically significant by calculating (Minitab 10.51) the Pearson product-moment correlation coefficient ($r = 0.680$; $n = 15$; $p < 0.01$).

The spectral absorption characteristics of the visual pigments of the turkey and peacock resemble most those measured in the chicken, duck and Japanese quail. The visual pigments of the blackbird, blue tit and starling are most similar to the Pekin robin, budgerigar, zebra finch and canary (see chapter one). These two groupings tend to reflect the degree of phylogenetic relatedness between the different species (Sibley and Ahlquist, 1990; Sibley and Monroe, 1990). Specifically, the majority of species which possess a UVS cone visual pigment are passerines (Passeriformes). The budgerigar, which also possesses a UVS cone visual pigment, is a member of the Psittaciformes, which are more closely related to the Passeriformes than the Galliformes (chicken, quail, peacock and turkey) and Anseriformes (duck), both of which possess a VS cone visual pigment instead of the UVS type. These data are most parsimoniously explained by a single evolutionary split at the divergence of the Passeriform / Psittaciform lineages from the Galliform / Anseriform lineages. To illustrate this separation, cluster analysis (Minitab 10.51) was performed on the cone visual pigment λ_{max} values for all species in which four cone visual pigment types have been measured microspectrophotometrically (see Tables 1.3 and 2.13). The results, which are largely independent of the linkage method or distance measure used, are displayed in Figure 2.123.

However, the Manx shearwater, Humboldt penguin (both Ciconiformes) and pigeon (Columbiformes), which have nominal VS cone visual pigments but with λ_{max} values at slightly shorter wavelengths than those found in the Galliform and Anseriform species studied (402, 403 and 409 nm respectively), are more closely related to the Passeriformes and Psittaciformes than the Galliformes and Anseriformes. Therefore, it is possible that the lineages which gave rise to the Passeriformes and Psittaciformes underwent a further division with regard to the spectral location of the λ_{max} of this cone visual pigment type. Phylogenetic relatedness, however, is often inextricably linked to ecology, and a great deal more comparative data on the absorption properties of avian retinal photoreceptors, and the characteristics of the visual environment which have driven the spectral tuning of the ancestral opsin genes, are required before further conclusions can be made.

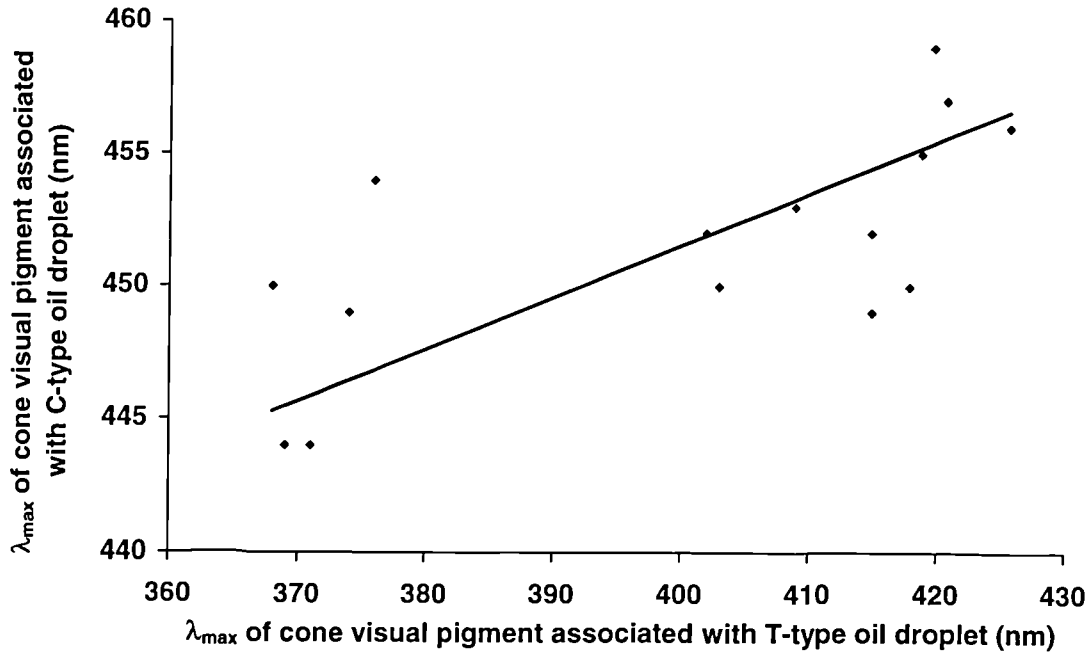

Figure 2.121 Results of a reduced major axis regression (Fowler and Cohen, 1990) which reveals that the λ_{max} value of the cone visual pigment associated with the C-type oil droplet (SWS visual pigment) is positively correlated with the λ_{max} value of the cone visual pigment associated with the T-type oil droplet (i.e. VS or UVS visual pigments). Polynomial regression was performed on the data to test for a departure from linearity, but the squared term was found to be non-significant ($t_{14} = 1.18$; $p = 0.260$). The linear regression line calculated had a gradient of 0.1951 and an intercept of 373.4906. The correlation was found to be statistically significant by calculating (Minitab 10.51) the Pearson product-moment correlation coefficient ($r = 0.680$; $n = 15$; $p < 0.01$).

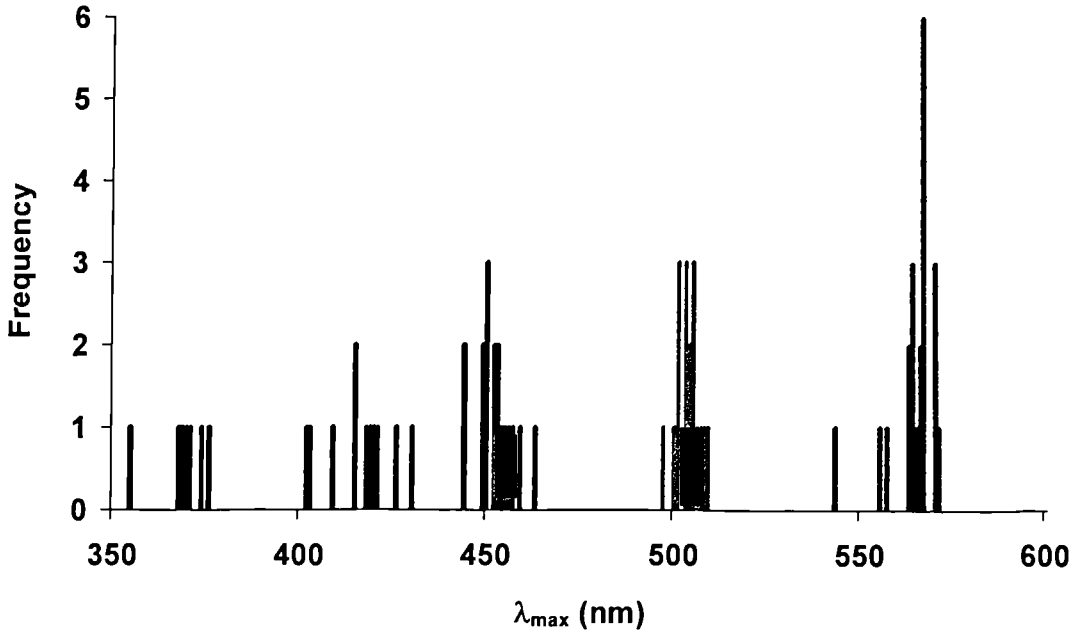

Figure 2.122 Distribution of avian cone visual pigment λ_{max} values for all species measured using microspectrophotometry. Values around 565 (red lines), 505 (green lines), 450 (blue lines), 420 (purple lines) and 370 nm (black lines) represent LWS, MWS, SWS, VS and UVS single cone visual pigments respectively. References for the data not obtained during this study are the same as for Table 1.3 (chapter one).

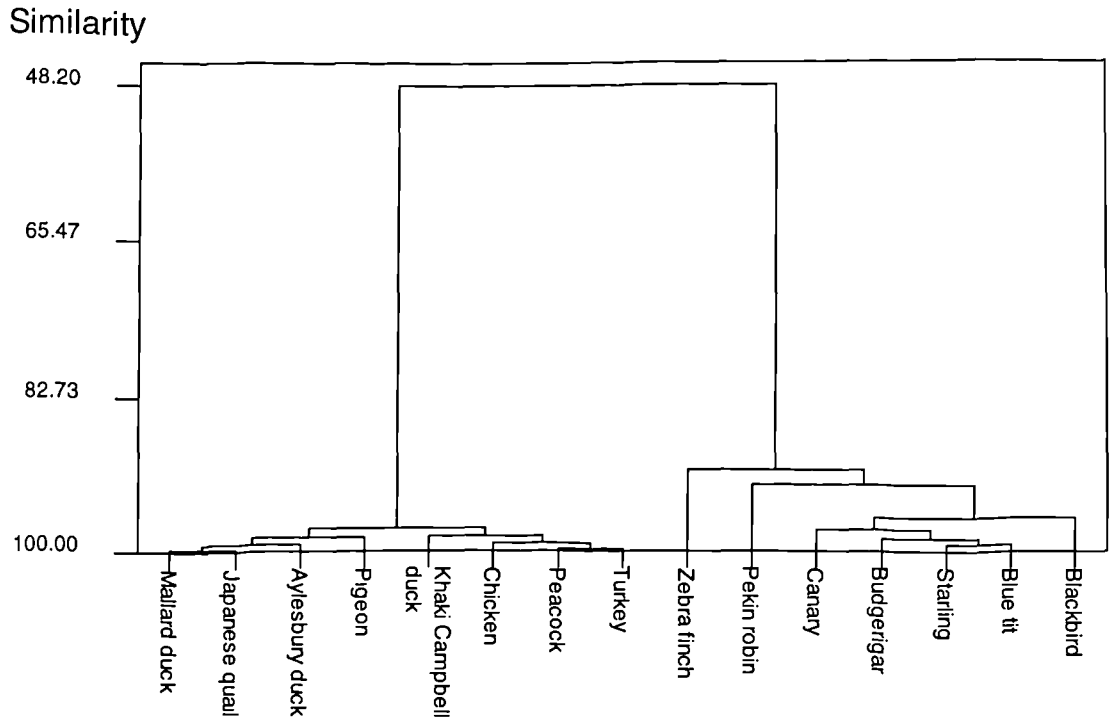

Figure 2.123 A dendrogram generated by a cluster analysis (Minitab 10.51, average linkage, squared Euclidean distance measure) of the cone visual pigment λ_{max} values for all species in which four cone visual pigment types have been measured microspectrophotometrically (see Tables 1.3 and 2.13). The species studied to date clearly fall into two principal groups, the main difference being the spectral location of the λ_{max} of the visual pigment which is associated with the T-type (transparent) oil droplet (i.e. either VS or UVS).

Two notable improvements were made over the course of this study with regard to the microspectrophotometric measurement of avian visual pigments. The first was the incorporation of glycerol into the medium used to mount the photoreceptors. This had the effect of reducing optical artefacts in the cell preparation which increased the quality of the data obtained. Furthermore, the use of a high concentration of glycerol in the mountant extended the time period over which acceptable measurements could be made. Glycerol at concentrations of up to 20 % are known to improve the thermal stability of both rod and cone pigments extracted from chicken retinae (Okano *et al.*, 1989) and it would seem that the preservative effect of glycerol extends to visual pigments *in situ.*

The second improvement involved the analysis protocol for visual pigment absorbance data. By averaging the up and down scans prior to fitting with a visual pigment template, the effects of in-scan bleaching were reduced. Although the visual pigment λ_{max} values of the spectra obtained during this study were affected little by in scan bleaching, mathematical modelling suggests that an appreciable degree of in-scan bleaching can be tolerated before the absorbance spectra are significantly distorted. This is a distinct advantage in the measurement of avian cone visual pigments as the outer segments are extremely small and therefore prone to significant in-scan bleaching.

A noticeable shift (2 to 3 nm) in apparent λ_{max} between the pre-bleach absorbance spectrum and the difference spectrum was observed in both the MWS cone pigment and the rod pigment. This was probably due to accumulation of a stable photoproduct which is visible in the post-bleach spectrum as a broad peak at around 480 to 490 nm. Because this peak was apparent in the rod, it is assumed that it was not a result of scattering of the measuring beam by the oil droplet. The photoproduct may have been metarhodopsin III (λ_{max} 470 nm), or acidic N-retinylidene-opsin (λ_{max} 440 nm, Rodieck, 1973). The similarity in the type of photoproducts accumulated by these two photoreceptor types, and the similarity of their λ_{max}, is perhaps indicative of their phylogenetic relatedness (Okano *et al.*, 1992).

Photoproduct absorption at approximately 380 to 390 nm was observed in the post-bleach absorbance spectra of all photoreceptor types, which was most likely due

to the accumulation of all-*trans* retinal (λ_{max} 440 nm, Knowles and Dartnall, 1977). Whilst absorption by all-*trans* retinal would probably not affect the difference spectrum λ_{max} for the MWS or LWS pigments, it would account for the shift in the difference spectra λ_{max} of the UVS and VS cone pigments towards shorter wavelengths, and the shift in the difference spectra λ_{max} of the SWS cone pigment towards longer wavelengths.

The pre-bleach absorbance spectra of SWS pigments in the starling, blackbird and peacock showed considerably higher absorbance on the short wavelength limb than would be predicted from the visual pigment template. This may have been due to rapid photoproduct accumulation or scattering of the measuring beam by the C-type oil droplet. The outer segments of SWS cones are generally smaller than those of the MWS and LWS single cones and the double cones. Consequently, the MSP measuring beam is positioned closer to the oil droplet when recording an absorbance spectrum from a SWS cone outer segment than when measuring outer segments associated with the other cone classes. This may have resulted in increased scattering or absorption of the measuring beam by the associated oil droplet in this cone class, particularly at shorter wavelengths.

Possibly the most interesting result of this limited survey of avian visual pigments is the discovery of a λ_{max} 557 nm LWS cone visual pigment in the LWS single cones and both members of the double cone in the blackbird retina. The λ_{max} values of the same visual pigment type in the starling, blue tit, peacock and turkey range from 563 to 566 nm.

Similar visual pigments (both with λ_{max} 555 nm) were measured microspectrophotometrically in the tawny owl (Bowmaker and Martin, 1978), and electrophysiologically in the great horned owl (Jacobs *et al.*, 1987), and another long wavelength-sensitive visual pigment with a slightly different peak sensitivity (λ_{max} 543 nm) was measured microspectrophotometrically in the Humboldt penguin (Bowmaker and Martin, 1985). Whilst any assumptions are made from very limited data sets, it is interesting to note that these three groups of λ_{max} values for avian LWS visual pigments (543, 555 / 557 and 563 to 570) are remarkably similar to those produced by the three different allelic forms of the single polymorphic middle- to

long wavelength-sensitive cone visual pigment opsin gene in marmosets, *Callithrix jacchus jacchus*, (543, 556 and 563 nm, Williams *et al.*, 1992). Four possible spectral tuning sites have been identified, which involve non-homologous substitutions between the different pigment types, at positions 285, 233 230 and 180 (which correspond to positions 269, 217, 214 and 164 in the bovine rhodopsin numbering system).

The most striking conclusion in the case of the avian LWS visual pigments is that the function of the double cones would seem to be responsible for the spectral location of the λ_{max} value. LWS single cones have their effective spectral sensitivity shifted towards longer wavelengths by approximately 40 nm due to the cut-off characteristics of the R-type oil droplet with which they are associated (Maier and Bowmaker, 1993). Consequently, the oil droplet determines the exact peak effective spectral sensitivity of the cone and not the visual pigment. However in the double cones, the LWS visual pigment is associated with an oil droplet which absorbs strongly at short wavelengths, but will not shift the peak sensitivity of the double cone away from the λ_{max} of the visual pigment. Therefore, it is conceivable that the visual pigment is spectrally tuned to optimise the visual function of the double cones rather than the LWS single cones, although the function of the double cones, and the reasons for variations in their visual pigment λ_{max}, are unknown.

The other more obvious differences between bird species lie in the short wavelength region of the spectrum. It appears that there are two main spectral locations for the λ_{max} of the UVS / VS visual pigments in birds, at about 360 to 380 or 415 to 426. The opsin proteins responsible for both visual pigment types are thought to be derived from the same ancestral UVS-type visual pigment gene (Okano *et al.*, 1992; Yokoyama *et al.*, 1998). There may also be a third spectral location for the UVS / VS cone visual pigment type, at around 402 to 409 nm, as measured microspectrophotometrically in the pigeon, Manx shearwater and Humboldt penguin.

Ultraviolet sensitivity is now realised to be an important component of avian visual ecology. Conspecific signals in Pekin robins (Maier, 1993), zebra finches (Bennett *et al.*, 1996; Hunt *et al.*, 1997), starlings (Bennett *et al.*, 1997), bluethroats *Luscinia svecica svecica* (Andersson and Amundsen, 1997) and blue tits (Hunt *et al.*, 1998) are affected if the UV component of plumage coloration is removed. The role

of UV in prey detection was predicted by Burkardt (1982) and has been demonstrated in hummingbirds *Archilochus alexandri*, *Lampornis clemenciae*, and *Eugenes fulgens* (Goldsmith, 1980), kestrels *Falco tinnunculus* (Viitala *et al.*, 1995) and blue tits (Church *et al.*, 1998). Ultraviolet light may also be used by birds as a 'sun-compass' for orientation, or as a cue to calibrate their circadian clocks (see Bennett and Cuthill, 1994 for review). Due to the large variation in λ_{max} of visual pigments in the UVS / VS single cone type, it is likely that there is considerable interspecific variation in the utility of ultraviolet wavelengths in visual ecology.

2.7.2 Oil droplets

C-type oil droplets had λ_{cut} at longer wavelengths and a higher measured absorptance when the two short wavelength-sensitive visual pigments were spectrally close, as in the peacock, but not when they were further apart, as in the starling, blue tit and blackbird. This confirms the observations made by Bowmaker *et al.* (1997) and suggests that one of the major functions of oil droplet pigmentation is to reduce the overlap between spectral classes. Whilst some overlap is essential, excessive overlap will lead to a reduction in hue discrimination ability. The lower density of carotenoid in the C-type oil droplets of birds possessing UVS pigments does not shift the λ_{max} significantly and may serve only to reduce absorption by the β-band of the visual pigment (Wolbarsht, 1976).

Intra-retinal variations in oil droplet carotenoid density were restricted to the P-type droplets of the double cones. In the peacock, starling, blackbird and blue tit, P-type droplets in the ventral retina had λ_{cut} at longer wavelengths than those in the dorsal retina. Increased pigmentation of oil droplets in the ventral retina, which observes the celestial visual hemifield, might be adaptive in improving visual acuity. Rayleigh scattering, by atmospheric particles smaller than the wavelength of light, is proportional to the reciprocal of the fourth power of the wavelength (Born and Wolf, 1970). Consequently, as short wavelengths are scattered more, longer wavelengths are more useful in the detection of distant objects. The dorsal retina in these species generally views the ground from close range and would have less need for acute distance vision.

Highly pigmented droplets would also absorb short wavelengths scattered within the eye and reduce the effects of chromatic aberration by the dioptric apparatus, thus 'sharpening' the retinal image (Lythgoe, 1979). Of relevance to this theory is the observation that, in the pigeon, SWS cones in the retina are located more vitread (closer to the lens) than the MWS and LWS cones (Mariani and Leure-DuPree, 1978). As discussed in section 2.2.6, longitudinal chromatic aberration results in short wavelengths coming to a point of focus closer to the back of a lens than longer wavelengths, and the stratification of the photoreceptors *in vivo* may be designed to compensate for this optical phenomenon.

An alternative hypothesis is that the oil droplets act as intraocular eye shades. Because the ventral retina observes the celestial visual field, it receives much more light (particularly of shorter wavelengths) than the dorsal retina. Perhaps a progressive decrease in short wavelength sensitivity is advantageous, either by protecting the eye from potentially damaging ultraviolet radiation (Kirschfeld, 1982), or by reducing luminance differences between the two visual hemifields to allow good vision of the ground whilst reducing excessive irradiance from the sky. In this respect, it is interesting to note that the jungle nightjar (*Caprimulgus indicus*) has been reported to possess a tapetum only in the dorsal half of the retina (Nicol and Arnott, 1974; Gondo and Ando, 1995). This may be an alternative or additional adaptation to increase photon capture by photoreceptors receiving light from the ventral visual hemifield. Similarly, in many diurnal teleosts, yellow pigmentation is much higher in the dorsal half of the lens and / or cornea than in the ventral region, thus reducing the amount of light from the celestial visual hemifield that reaches the ventral retina. By selectively filtering the light after it has passed through, and been inverted by, the dioptric apparatus, increased pigmentation in the oil droplets can control brightness but still permit short wavelength sensitivity in separate specialised receptors.

However, this cannot be the only reason for intraretinal variations in droplet pigmentation. In the retina of the pigeon, the P-type, Y-type, and possibly the R-type, oil droplets in the red field (PD quadrant of the retina) have λ_{cut} at longer wavelengths than those in the yellow field (Bowmaker, 1977; Bowmaker *et al.*, 1997). No such intraretinal variation in the spectral absorption characteristics of

single cone oil droplets was observed in any of the species investigated during this study. The functional significance of the pigeon's peculiar retinal organisation is unclear. The pigeon is a feral strain of the rock dove (*Columba livia*) which nests on cliff faces, particularly by the coast (Perrins, 1987). It is largely granivorous, feeding on the seeds of cereals, legumes and weeds, and its food is almost exclusively taken from the ground. With regards to its diet, the pigeon is little different from the chicken, turkey or peacock. However, one difference may be that, in the wild, these three Galliform species forage under forest shade and as such inhabit environments in which the visible spectrum is dominated by 'green' wavelengths (approximately 500 to 600 nm; Endler, 1993), whereas the pigeon forages mostly under an open sky.

The oil droplets of the turkey retina appeared to be considerably deficient in carotenoid when compared to P-, Y- and R-type oil droplets measured in the American bronze turkey (*Meleagris gallopavo gallopavo*), which were shown to cut off wavelengths below about 530, 540 and 570 nm respectively (Strother, 1963). It is unclear whether the reduction of oil droplet pigmentation observed in the turkeys used in this study was due to domestication of the BUT8 strain, a dietary deficiency, or the reduced light levels under which the turkeys are kept to prevent them fighting (Dr. Chris Sherwin, personal communication). A reduction in oil droplet carotenoid concentration was also observed in starlings which had been kept in captivity for more than one or two months, particularly in the P-type droplets of the ventral retina, which rapidly lost the 480 nm shoulder from their absorption spectra. This is possibly further evidence of a shading function for P-type droplets. These observations emphasise the importance of using freshly caught wild individuals when investigating avian visual physiology.

CHAPTER THREE

DETERMINATION OF CONE PHOTORECEPTOR ABUNDANCE

3. Determination of cone photoreceptor abundance

3.1 Previous studies and conclusions

Birds have four different classes of single cone and a single class of double cone (Bowmaker *et al.*, 1997; and see chapter two), but these are not equally represented in the retina (Muntz, 1972). It has been proposed that both the relative abundance and spectral absorption properties of cone oil droplets are explained more by species' visual ecology than phylogeny (Peiponen, 1964; Muntz, 1972; Partridge, 1989), and it is known that cones are distributed non-uniformly in the retinae a variety of avian species (Goldsmith *et al.*, 1984b; Gondo and Ando, 1995), although some maintain a largely isotropic distribution of cone types (e.g. Japanese quail, Budnik *et al.*, 1984).

Investigations of relative cone abundance and intraretinal distribution have suffered from the technical difficulties involved in discriminating between certain types of oil droplet (see below). Consequently, in counts of cone abundance, certain cone classes were pooled, most notably those types containing oil droplets which appeared 'colourless' to the human eye, resulting in a loss of potentially useful information (Peiponen, 1964; Mayr, 1972; Meyer and May, 1973; Budnik *et al.*, 1984; Begin and Handford, 1987). In addition, the subjective nature of many of these observations, which were made largely by light microscopy, may have affected their accuracy. The spectral absorption characteristics of some oil droplets vary across the retina (Bowmaker, 1977; Goldsmith *et al.*, 1984b, and this study) and this may have led to some oil droplets, which in fact belong to the same cone class, being classified differently depending on where they were located in the retina. Even in studies employing a microspectrophotometer to characterise the different droplet types objectively (Goldsmith *et al.*, 1984b; Partridge, 1989), a lack of information regarding which type of visual pigment was associated with which type of oil droplet may have confused the results.

Nevertheless, some general trends have emerged. In nocturnal birds, the number of coloured oil droplets is greatly reduced. Primarily, this is the result of a rod-dominated retina. Rods comprise approximately 90 % of the photoreceptor population in the great horned owl, *Bubo virginianus* (Fite, 1973; Braekevelt, 1993a),

and the barred owl, *Strix varia* (Braekevelt *et al.*, 1996), compared to less than 40 % in the diurnal species studied (Morris, 1970; Braekevelt, 1990; Braekevelt, 1994a). Microspectrophotometry has revealed the presence of at least four different cone types in the retina of the tawny owl, *Strix aluco* (Bowmaker and Martin, 1978). Furthermore, electrophysiological and behavioural measures of spectral sensitivity suggest that this species possesses a functional colour vision system (Martin, 1974; Martin and Gordon, 1974; Martin *et al.*, 1975). Thus it seems likely that, whilst retaining the ability to discriminate colours, the increased rod population reflects a largely nocturnal habit.

Erhard (1924, cited in Peiponen, 1964) stated that neither the tawny owl nor the barn owl, *Tyto alba*, possessed 'coloured' (i.e. red or yellow) oil droplets. Additionally, a recent investigation by two Japanese authors suggested that the Hondo Ural owl, *Strix uralensis*, and the snowy owl, *Nyctea scandiaca*, display only pale green oil droplets (Gondo and Ando, 1995). These anomalous results may be explained by the microspectrophotometric data of Bowmaker and Martin (1978), which revealed the presence of four spectrally distinct droplet types, but also demonstrated their low carotenoid concentration, which would render the majority of them pale green, pale yellow or colourless in appearance. Presumably the reduction in oil droplet pigmentation, which would otherwise reduce cone sensitivity, is adaptive to a nocturnal, crepuscular or arrhythmic existence.

Diurnal birds with retinae containing relatively few red and yellow oil droplets include the barn swallow, *Hirundo rustica*, swift, *Micropus apus*, sand martin, *Riparia riparia*, and house martin, *Delichon urbica*, (Peiponen, 1964; Goldsmith *et al.*, 1984b; Gondo and Ando, 1995). The pale green or colourless appearance of the majority of droplets in these retinae suggests that double cones are of more importance.

Species that fly above water and need to see through its surface have a relatively higher proportion of red oil droplets (Muntz, 1972). Red and yellow oil droplets comprise over 75 % of the cone population in the retinae of lesser black-backed gulls, *Larus fuscus*, common gulls, *L. canus*, and common terns, *Sterna hirundo*, (Peiponen, 1964), and in the European kingfisher, over 60 % of the droplets are red (Erhard, 1924, cited in Peiponen, 1964). This phenomenon has been

attributed to the function of reducing glare as the birds peer down at the water's surface, and it has been noted that birds which live on the water, but do not need to look through it from a distance, lack this development of red oil droplets (Muntz, 1972; Partridge, 1989).

Intra-retinal variations in cone abundance have been observed in a number of species. The pigeon is especially noteworthy in this respect. The retina is clearly demarcated into two disparate regions known as the 'red' and 'yellow' fields (Muntz, 1972). The red field, which constitutes most of the posterior dorsal retina, contains a higher proportion of red and orange oil droplets than the remaining retina, or yellow field (Waelchli, 1883). These two droplet types correspond to the LMW and MWS single cones respectively (Bowmaker, 1977). Such severe demarcation in the retina is rare in the species studied to date, but a similar distribution is found in the common tern, which again has much higher proportions of LWS and MWS cones in the dorsal retina (Goldsmith *et al.*, 1984b). Variations in cone abundance between the dorsal and ventral regions may be adaptations to differences in the amount and spectral composition of the light impinging on different areas of the retina, as is thought to be the case in some teleosts (Levine and MacNichol, 1982). The underwater light environment is notably asymmetrical in dorsal / ventral spectral distribution, but this is also true of many terrestrial habitats (Lythgoe, 1979).

Whilst some of these conclusions may be valid, it is wise to exercise some caution in their adoption. Oil droplets have rarely been characterised using objective measures such as cut-off wavelength (λ_{cut}), or correlated with visual pigment type. Furthermore, most of these conclusions are not supported by rigorous statistical analysis. Whilst the results of Pézard (1964, cited in Muntz, 1972), who suggested that oil droplet complement was affected by sex, hormonal status, sexual activity and even the time of year, have not been replicated (Mayr, 1972), the abundance of some cone types may be dependent upon age. Hodos *et al.* (1991) found that double cones gradually disappeared in ageing pigeons, whereas single cone densities remain unchanged. The relative proportions of single cones would therefore be seen to increase in older birds, thus complicating cross-species comparisons. In addition, intraretinal variation in the spectral absorption characteristics of a given class of droplet might lead to confusion between cone types. For example, when viewed

under the light microscope or even when measured microspectrophotometrically, P-type droplets of the LWS double cones can resemble very closely the C-type droplets of the SWS cones or, at the other extreme, the Y-type droplets of the MWS cones (Goldsmith *et al.*, 1984; Maier and Bowmaker, 1993).

Avian photoreceptors may be organised in mosaics, as are those of many fish (Marc and Sperling, 1976; Boehlert, 1978; Levine *et al.*, 1979) and some primates (Marc and Sperling, 1977; Mollon and Bowmaker, 1992). In the retina of the great tit, *Parus major*, each single cone is surrounded by four double cones, and these units are arranged in rows (Engström, 1958). The domestic chicken, however, has single and double cones arranged in a hexagonal lattice, which is regarded as the outcome of an evenly spaced distribution of the different cone types (Morris, 1970). An electron microscopic study of the photoreceptors of the great horned owl revealed no obvious patterning of arrangement or mosaic (Braekevelt, 1993a).

In general, the topographical distribution of the different types of photoreceptor in the avian retina has received little attention. Inter-specific and intra-retinal variation in total photoreceptor density, on the other hand, has been the subject of numerous studies on avian visual ecology. Improved visual acuity in birds is generally correlated with the presence of well-developed areae (often one or two) which house a higher density of photoreceptors, usually cones (Meyer, 1977). The visual cells found in the areae are characteristically longer and thinner and the concomitant increase in ganglion and bipolar cell density results in a thickening of the nervous layers of the retina.

Generally, a depression, or fovea, of variable depth and size is observed within an area. The fovea contains an even higher density of photoreceptors, and the convergence ratio (photoreceptors to ganglion cells) is usually 1:1 (Pumphrey, 1948). The fovea is caused by radial displacement of the more internal layers of the retina, resulting in a shallow saucer-shaped depression (concaviclivate) or deep funnel-shaped (convexiclivate) pit.

The size, shape and position of avian areae and foveae have been reviewed a number of times (Wood, 1917; Walls, 1942; Pumphrey, 1948; Meyer, 1977; Martin, 1985). The most common area, which is found in many birds (e.g. Stellar jay, *Cyanocitta stelleri*), is a circular region in the central fundus, slightly dorsal and

anterior to the optic nerve. It is thought that central areae, which often contain predominantly yellow oil droplets, are involved in monocular vision. Double cones are thought to be absent from the central foveae of blackbirds and starlings (Meyer, 1977), but have been observed in several members of the weaverbird family (Meyer, 1977).

A second type of area, often more oval than circular and located laterally towards the temporal periphery of the retina, is sometimes found in place of (e.g. barn owl, *Tyto alba*), or in addition to (e.g. bittern, *Botaurus lentigenosus*; kingfisher, *Alcedo ispida*), a central area. Lateral areae are situated in a location consistent with their use in binocular vision, and are reported to lack double cones (Walls, 1942; Meyer, 1977).

A number of species display a large linear or ribbon shaped area extending horizontally for a variable distance across the central retina. Some species display a linear area and no additional fovea (e.g. Manx shearwater, *Puffinis puffinis*; fulmar petrel, *Fulmaris glacialis*); a linear area incorporating a central area and fovea (e.g. American coot, *Fulica americana*); a linear area connecting a central and lateral fovea (e.g. sparrow hawk, *Falco sparverius*) or a linear area with an enclosed central fovea and a separate lateral fovea (e.g. tern, *Sterna hirundo*). Linear areae are thought to enhance movement detection, and give high visual acuity, in the horizontal visual field (Meyer, 1977). A large linear area in the mallard and concurrent increase in ganglion cell density (Dubbeldam and Tellegen, 1996), combined with a 360° cyclopean visual field (Martin, 1993), suggests that its visual attention is directed towards the horizon. A prominent linear area, also known as the visual streak, is often observed in the chelonian retina (Ives *et al.*, 1983), and in some mammals and amphibians (Walls, 1942; Rodieck, 1973).

A completely afoveate retina is known for only one species, the California valley quail (*Lophortyx californicus vallicola*). Another galliform species, the domestic chicken, exhibits only marginal thickening of the retina in the central region (Meyer, 1977), and a slight increase in cone density in the topographical region which corresponds to the site of the lateral fovea in some birds (Meyer and May, 1973).

Whilst the increased photoreceptor density should enhance visual acuity in all foveae (Martin, 1985), the function of deep foveal pits is disputed. Walls (1942) suggested that the increased refractive index of the retina relative to the vitreous would result in the edge of a convexiclivate fovea acting as a convex lens, thus magnifying the retinal image. Pumphrey (1948), however, considered that any advantage gained by magnification of the retinal image would be offset by optical aberrations induced by the steep sides of the fovea. More recently, Snyder and Miller (1978) suggested that the concave portion of retina at the base of the foveal pit functions as a negative lens which, together with the positive power of the cornea and lens, forms a telephoto optical system.

3.2 Methods of determining photoreceptor abundance

3.2.1 Light microscopy

The most straightforward method used to distinguish between different types of retinal photoreceptor, and thence identify any variations in their topographical distribution, is bright-field light microscopy. The identification of some cone types in the avian retina is very simple due to the brightly coloured oil droplets they contain. All oil droplets, apart from the T-type droplets associated with VS or UVS visual pigments, contain carotenoids (Goldsmith *et al.*, 1984b). It is the spectral absorption properties of these 'coloured' compounds which are exploited in identifying certain droplet types. However, whereas red oil droplets are readily identified and unambiguously distinct, many of the other types of droplet vary in their spectral absorption characteristics and, therefore, their appearance to a human observer.

In some species, or depending on the retinal location within a given species, the usually pale green P-type droplets of the double cones may appear almost as yellow as the Y-type droplets of the MWS single cones. Alternatively, they may appear as colourless as the C-type droplets associated with the SWS cones. Thus it is sometimes impossible to distinguish between the P-, C- and T-type droplets using white-light bright field microscopy alone, and this has led to the pooling of two or more droplet types in most quantitative estimates of oil droplet (cone) abundance (Waelchli, 1883; Meyer and May, 1973; Budnik *et al.*, 1984; Begin and Handford,

1987; Jane and Bowmaker, 1988; Partridge, 1989; Bowmaker *et al.*, 1993; Gondo and Ando, 1995).

Narrow band interference filters or monochromators have been employed to control the wavelength of the illumination and exploit the cut-off nature of many droplets, thus enhancing discriminations between spectrally similar types (Goldsmith *et al.*, 1984b; Jane and Bowmaker, 1988; Bowmaker *et al.*, 1993). For example, red oil droplets with a λ_{cut} at approximately 570 nm will appear black when illuminated with 540 nm monochromatic light. However, the droplets which are most readily distinguished using this technique are those which are most obviously different to the human eye. The T-, C- and P-type droplets usually have lower carotenoid concentrations, thus reducing their ability to act as long-pass cut-off filters in retinal squashes. Furthermore, the highly refractile nature of all oil droplets means that much of the illumination is scattered around the outside of the droplets, making discriminations more subjective.

Microspectrophotometry can help to elucidate the nature of the different droplet types by correlating accurate measures of spectral absorption with droplet size and retinal location. Although microspectrophotometry is generally too slow and insufficiently random to generate reliable counts of droplet type and distribution, the knowledge gained from microspectrophotometric studies can help the investigator to discern better the droplets as they appear under the light microscope (Goldsmith *et al.*, 1984b; Partridge, 1989). Microspectrophotometry can also be used to confirm the association of certain droplet types with particular visual pigments.

3.2.2 Electron microscopy

Although a number of electron microscopic investigations of avian retinae have been conducted, the utility of the technique in discriminating between different cone types is limited. Furthermore, the laborious and time-consuming nature of the preparation techniques involved have hampered the use of electron microscopy to examine topographic variation in cone abundance. Nevertheless, electron microscopy has been used to estimate the ratios of rods : double cones : single cones in a number of bird species (Braekevelt, 1990; Braekevelt, 1993a; Braekevelt, 1993b; Braekevelt, 1994a; Braekevelt, 1994b; Braekevelt *et al.*, 1996), and even distinguish between different types of single cone in the chicken, although largely on the basis of

the oil droplet density, which could have been performed using the light microscope (Morris and Shorey, 1967).

3.2.3 Autofluorescence

Some of the carotenoids incorporated into retinal oil droplets autofluoresce on stimulation with near-UV light, and this inherent property has been used to distinguish different cone types in both turtles (Ohtsuka, 1984; Ohtsuka, 1985; Kolb and Jones, 1987) and birds (Goldsmith *et al.*, 1984b). It is the quickest and simplest way in which the 'colourless' oil droplets can be separated into their respective classes. T-type droplets contain no carotenoid and thus do not autofluoresce. P- and C-type droplets contain different mixtures of carotenoids and vary accordingly in the apparent 'colour' and duration of their autofluorescence.

However, as encountered in the present investigation with starlings, the oil droplets of birds which have been kept in captivity for a prolonged period become depleted in oil droplet carotenoids, and it is thus more difficult to distinguish the different types on the basis of their differential autofluorescence.

3.2.4 Cytochemical staining

Both rods and cones have stores of glycogen in their inner segments which are thought to constitute an energy source for cell metabolism (Meyer, 1977). In rods and the accessory member of the double cones these glycogen stores form large, discrete organelles known as the hyperboloid and paraboloid respectively.

The rod hyperboloid is smaller and situated more sclerad than the accessory cone paraboloid and, if the glycogen in each is stained by the periodic acid-Schiff (PAS) reaction, they are readily distinguished by their size and location in transverse retinal sections. This technique has been used to estimate the ratio of rods to double cones in adult chickens (Meyer and May, 1973).

3.2.5 Immunofluorescence

In order to discriminate between different types of single cones, more subtle cytochemical techniques are required. Antibodies raised to visual pigment antigens can be used to identify the nature and retinal location of different photoreceptor types. Cserháti *et al.* (1989) used two monoclonal antibodies (mAb), OS-2 and COS-

1, in conjunction with a polyclonal anti-opsin antibody (PAO) to distinguish the four different types of single cone in the pigeon retina. mAb COS-1 bound selectively to pigeon LWS visual pigment in both single and double cones. MWS visual pigment bound both mAb OS-2 and PAO, whereas SWS visual pigment bound only mAb OS-2. The fourth, putatively VS pigment class did not bind to any of the antibodies.

In their experiment, the bound antibodies were detected by secondary antibodies conjugated with an avidin-biotinylated peroxidase complex which reacts chromogenically with diaminobenzidine. Alternatively, antibodies may be conjugated with fluorescent moieties which are disclosed upon examination with a confocal or fluorescence microscope (Matsumoto and Hale, 1993). The technique has been refined to investigate the temporal and spatial expression of different visual pigments in mammals (Szél *et al.*, 1996; Bumstead *et al.*, 1997) and reptiles (Loew *et al.*, 1996).

3.2.6 NBT staining

An alternative method to distinguish between different photoreceptor types was developed by Enoch (1963; 1964). The transduction cascade initiated by the visual pigment on absorption of a photon causes increased oxidative metabolism in photoreceptor mitochondria, which can be detected using a redox probe such as Nitroblue tetrazolium chloride (NBT). NBT is a soluble yellow ditetrazole which can be locally reduced to an insoluble blue diformazan by increased mitochondrial succinic acid dehydrogenase activity, thus identifying which photoreceptors have been exposed to light and which have not.

Originally, Enoch (1964) used this histochemical technique to investigate the gross spectral sensitivity of the rod-dominated rat retina. However, the concept was refined to identify spectrally distinct cone classes in fish (Marc and Sperling, 1976; Levine *et al.*, 1979; Archer, 1988) and primate retinae (Marc and Sperling, 1977).

A protocol broadly similar to that employed by Archer (1988), but with some modifications, was used in the present study to distinguish the UVS and SWS single cones of the starling retina from each other, and from the double cones.

3.2.7 *In situ* hybridisation

In situ hybridisation is a tool for localising cellular RNAs and DNAs at the site of synthesis (Giaid *et al.*, 1990; Flannery *et al.*, 1993), and has been used gainfully in the determination of UVS cone abundance and distribution in the retina of the budgerigar (Wilkie *et al.*, 1998).

Since the technique was established (Gall and Pardue, 1969), a variety of nucleic acid probes have been used for *in situ* hybridisation: double-stranded DNA, single-stranded DNA, and complementary RNA probes and oligonucleotides. The primary criterion for a probe is the degree of complementarity with the target sequence. The stability of the duplex formed on hybridisation, and hence the specificity of the probe, depends on the extent of the complementarity (Southern, 1988).

The early development of *in situ* hybridisation relied on the use of radioisotopes and autoradiography for the visualisation of specifically hybridised gene probes. However, non-radioactive methods are now routinely used and fall into two main categories. Nucleic acids, which are subsequently incorporated into the synthetic probe, can be directly coupled with 'reporter' molecules, such as fluorochromes that are observed using a fluorescence or confocal microscope, colloidal gold for visualisation using electron microscopy, or enzymes which react to form a visible product. *Alternatively, nucleic acids can be conjugated with a hapten*, such as biotin or digoxygenin (DIG), which is detected by immunocytochemical techniques (Raap *et al.*, 1990).

Wilkie *et al.* (1998) employed the digoxygenin hapten method to localise the mRNA coding for UVS visual pigment opsin in the inner segments of retinal cones in the budgerigar. *In situ* hybridisation was performed on both radial sections and whole-mounted retinae, revealing a semi-regular distribution of presumptive UVS cones, which accounted for approximately 9 % of the cone population.

During the course of this study, initial difficulties in finding UVS cones in the starling retina led the author to enlist the help of Dr. Sue Wilkie and Prof. David Hunt of the Institute of Ophthalmology in London, who kindly performed *in situ* hybridisation, using the budgerigar UVS opsin probe, on starling retina prepared with

their guidance. The methods used, and the results obtained, are described in the following sections.

3.2.8 Other methods

Kawamuro *et al.* (1997) measured the gross spectral sensitivity of isolated Japanese quail retinae electroretinographically and attempted to deduce the relative contribution of the different photoreceptor types whose spectral sensitivity was known from microspectrophotometric studies (Bowmaker *et al.*, 1993). Yoshizawa and Fukada (1993) estimated photoreceptor abundance from the size of each visual pigment fraction separated chromatographically from visual pigment extracts of chicken retinae.

The estimates of photoreceptor abundance obtained using these two methods differ considerably from those derived from direct counts of individual photoreceptors (Meyer and May, 1973; Bowmaker *et al.*, 1993). This may be due to differences in overall sensitivity between cone classes, opponent interactions at a retinal level or disparities in visual pigment lability under extract conditions. Whilst electroretinograms can be performed on small sections of retina, visual pigment extraction usually requires the pooling of many entire retinae, thus masking subtle topographic variations in photoreceptor abundance, which are known to exist (e.g. Meyer and May, 1973).

3.3 Materials and methods

3.3.1 NBT

Counts were made from the retinae of male and female adult starlings to determine the relative abundance and distribution of the different classes of cone photoreceptor. MSP measurements confirmed the consistent associations of different types of oil droplets with visual pigments of different λ_{max} as previously reported (see Bowmaker *et al.*, 1997 for review). However, although the red and yellow oil droplets associated with the LWS and MWS visual pigments are readily distinguished using bright-field light microscopy, the oil droplets found in combination with the SWS and UVS visual pigments, and the long wavelength-sensitive double cones, all appear colourless to the human eye.

Because of difficulties in differentiating the three types of 'colourless' oil droplet using either autofluorescence or interference filters, largely due to carotenoid depletion of the C- and P-type droplets as a result of lengthy captivity, a state-dependent histochemical technique was used to identify selectively stimulated SWS and UVS cone photoreceptors. Increased oxidative metabolism in cone photoreceptors was detected using the redox probe nitro-blue tetrazolium chloride (NBT) (Enoch, 1963; 1964).

Subjects were dark adapted for at least 16 hours overnight before sacrifice. Under infra-red illumination eyes were removed, hemisected, and placed in a dissection medium comprising 340 mOsm kg^{-1} PBS and 11 mM D-glucose to sustain mitochondrial activity. After removing the lens and most of the vitreous, the eye cups were immediately placed in an illumination medium consisting of Ham F10 nutrient mixture (Sigma) corrected to 340 mOsm kg^{-1} by the addition of 1.75 g l^{-1} NaCl and adjusted to pH 7.4 using 1 M NaOH. The addition of 3.4 mM NADP and 4.9 mM glucose-6-phosphate (Boehringer Mannheim) to the illumination medium, which have been shown to enhance succinate oxidation by rat liver cells (Butcher, 1972), increased the density of diformazan in stained ellipsoids.

Retinae were then irradiated simultaneously for 10 minutes with either 386 nm or 434 nm monochromatic light, these wavelengths being close to the maximum spectral sensitivities of either the UVS or SWS cone types. Stimulation of only the targeted cell types was optimised by the careful selection of illumination conditions (wavelength of monochromatic illumination and length of exposure), and only darkly stained cone inner segments were counted. Illumination was provided by a 150 W tungsten-halogen lamp and an appropriate interference filter (Balzer B40; 10 nm FWHM bandwidth) in combination with a heat filter (Oriel 59875). Irradiances at the point of exposure, measured with a portable spectrometer (SPEX 1681, Glen Spectra Ltd.), were 2.1×10^{18} and 2.4×10^{18} photons s^{-1} m^{-2} for the UVS and SWS illumination conditions respectively.

After illumination, eye cups were transferred to an incubation medium consisting of the Ham F10 mixture plus 6 mM NBT (ICN) and 50 mM disodium succinate (Sigma) for 45 minutes at room temperature, after which they were washed briefly in cold PBS and fixed for 2 minutes in 10 % paraformaldehyde in 0.1 M

sodium phosphate buffer. Each retina was then removed from the eye cup into PBS and, using the pecten and optic nerve for orientation, divided into four parts corresponding to posterior dorsal (PD), posterior ventral (PV), anterior dorsal (AD) and anterior ventral (AV) quadrants. Any remaining attached pigment epithelium was removed gently using a fine paint brush and the retina mounted on a glass slide, receptor side up, in PBS. The preparation was covered with a No. 0 coverslip (22 × 32 mm) and the edges sealed with acrylic nail varnish to prevent dehydration of the sample.

Observations were made using an Olympus BHS microscope (Olympus, Japan), fitted with a reflected light fluorescence attachment (mercury lines isolated at 334 and 365 nm) which, following the method of Goldsmith *et al.* (1984b), was used in preliminary trials to confirm that the oil droplets associated with putative UVS cones did not autofluoresce, and that those associated with the putative SWS cones did. The retinal photoreceptors of five birds of each sex (confirmed by laparotomy *post mortem*) were labelled separately for UVS and SWS cones. Counts were made of the blue-stained inner segments of the labelled cone type, which were distinguished from labelled rod inner segments by size and the presence of a colourless oil droplet, from twenty fields of view from each of the four quadrants in both eyes. Counts of red, yellow, and the remaining colourless oil droplets without stained inner segments were also made from the same samples. Colourless oil droplets which were not associated with a labelled inner segment were assumed to be either in the non-labelled short wavelength-sensitive cone class or the principal member of the double cones. At a magnification of ×1250 each field of view represented an area of 0.02 mm^2. Thus, only an estimated 1 % of each retina was actually surveyed (approximately 26,000 cones per bird), and probably less as the retina spreads out on mounting, although this is minimised by prior fixation of the tissue. Nevertheless, having counted approximately 0.5 million cones in the retinae of 20 birds, this represented the most thorough survey of an avian retina to date.

A single male blackbird was also used to estimate the reliability of the NBT technique for labelling UVS cones. The procedure was identical to that used for the starling, except that retinae were illuminated with 366 nm monochromatic light (Balzer B40 interference filter; 10 nm FWHM bandwidth) for 12 minutes. Total

irradiance was measured as 1.8×10^{18} photons s^{-1} m^{-2}. Retinae from both left and right eyes were divided into the four quadrants and 10 fields of view counted from each quadrant.

3.3.2 Autofluorescence

Determination of cone class distribution in the blackbird, blue tit and peacock was more straightforward. Specimens available for study had been in captivity for a shorter period of time or, as in the case of the peacock, had more distinct C-type oil droplets, and were thus amenable to the use of autofluorescence to distinguish the different 'colourless' oil droplet types. Prolonged captivity had reduced the concentration of carotenoid in the oil droplets of starling retinae and, consequently, diminished the intensity of fluorescence exhibited by the C- and P-type oil droplets under ultraviolet illumination.

Subjects were dark adapted for at least one hour prior to sacrifice by approved humane methods. Eyes were removed under infra-red illumination, hemisected and left to soak in 340 mOsm kg^{1} PBS for one hour to encourage detachment of the pigment epithelium from the neural retina. Retinae were subsequently fixed for 1 to 2 minutes in 10 % paraformaldehyde in 0.1M phosphate buffer and divided into the four quadrants. Counts from ten fields of view from each quadrant were made from both the left and right eyes of the blackbird and blue tit. Only one (left) eye was available from the peacock as the other was used to determine the transmission of the pre-retinal media (see chapter four). Consequently, 25 counts were made from each quadrant of the peacock retina. Observations were made using an Olympus BHS microscope, fitted with a reflected light fluorescence attachment and a long-pass filter for viewing wavelengths longer than 435 nm.

LWS and MWS single cones were readily identified by their red and yellow oil droplets respectively. Transparent (T-type) oil droplets were the smallest observed and did not fluoresce on stimulation with ultraviolet light (mercury lines isolated at 334 and 365 nm). The principal oil droplets associated with the double cones were generally largest and displayed a long-lasting, faint greenish fluorescence. By contrast, the C-type oil droplets associated with SWS single cones were generally

smaller in diameter than all but the T-type droplets and displayed a brighter, more transient bluish fluorescence.

No direct measurements of the spectral absorption characteristics of the oil droplets displaying these different optical behaviours under UV illumination were conducted. Instead, the relative size and estimated abundance deduced from microspectrophotometric investigations was used to correlate fluorescence characteristics with photoreceptor type. Furthermore, ultraviolet illumination of some post-fix NBT-labelled starling retinae had revealed the characteristic greenish fluorescence of the principal oil droplet of the double cones, whose inner segments had not been labelled during the NBT procedure to isolate either UVS or SWS single cones. Similarly, the oil droplets associated with blue-stained inner segments in starling retinae NBT-labelled for SWS cones (434 nm monochromatic illumination) emitted a characteristic bluish fluorescence; those associated with blue-stained inner segments in starling retinae NBT-labelled for UVS cones (386 nm monochromatic illumination) did not fluoresce at all.

3.3.3 *In situ* hybridisation

In situ hybridisation was performed on both radially sectioned and flat whole-mounted starling retinae, which were prepared in Bristol and subsequently transported to the Institute of Ophthalmology in London.

Radial sections were made using a cryostat and following a protocol similar to that of Barthel and Raymond (1990). A single eye was hemisected and the lens and vitreous removed from the posterior half. The retina was fixed *in situ* in the eye cup for 1 hour, at room temperature (23 °C), in 4 % paraformaldehyde, 5 % sucrose, 0.1 M phosphate buffer (pH 7.4), after which it was rinsed three times in 0.1 M phosphate buffer (pH 7.4) containing 5 % sucrose. Fixation of the retina, particularly before freezing, inhibits the ubiquitous degradative RNAse enzymes. However, whilst reducing nucleic acid loss, fixation with cross-linking reagents such as paraformaldehyde reduces tissue permeability (Coulton, 1990). The retina was then cryoprotected with increasing concentrations of 20 % sucrose, prepared by mixing 5 % sucrose and 20 % sucrose in 0.1 M phosphate buffer in ratios of 2:1, 1:1 and 1:2. The retina was infiltrated for 30 minutes in each of the ascending series of sucrose

solutions at room temperature, and finally placed in 20 % sucrose solution overnight at 4 °C.

The following day, the retina was further infiltrated for 30 minutes at room temperature with a 2:1 mixture of 20 % sucrose in 0.1 M phosphate buffer (pH 7.4):OCT embedding medium. OCT (BDH), a commercially available product, is a mixture of polyethylene glycol and polyvinyl alcohol. Infiltration with OCT and sucrose reduces the water content of the tissue. This not only protects against tissue damage from water expansion on freezing, but improves the cutting consistency of the tissue block, allowing thinner cryosections to be made (Barthel and Raymond, 1990).

The eyecup was then transferred to an embedding mould (approximately 2 × 1.5 × 1.5 cm) made from aluminium foil, and orientated with the cut surface facing the bottom of the mould. The mould was filled with fresh 20 % sucrose in 0.1 M phosphate buffered saline : OCT compound (2:1) solution and frozen rapidly by submersion in isopentane cooled with liquid nitrogen. Rapid freezing helps to reduce the formation of ice crystals which can easily rupture cells. Radial sections of the eyecup approximately 8 µm thick were cut on a cryostat with a motor driven microtome. A maximum of three sections were mounted on Superfrost Plus microscope slides (BDH), which had been chemically treated to degrade RNAse enzymes and 'subbed' with poly-L-lysine to enhance tissue adhesion (Coulton, 1990), and allowed to air dry at room temperature. The slides were stored at -80 °C until the following day when they were transported to the Institute of Ophthalmology in London packed in dry ice. All subsequent operations were performed with Dr. Sue Wilkie in the Laboratory of Prof. David Hunt.

The other eye from the same bird was used to prepare the retinal whole-mounts. The globe was hemisected and the retina fixed *in situ* (overnight at 4 °C) using a solution of 0.1 M phosphate buffer (pH 7.4) containing 10 % paraformaldehyde and 0.1 % Triton X-100. Triton X-100 (iso-octylphenoxypolyethoxyethanol) is a non-ionic detergent used to permeabilise tissue. At the laboratory in London, the fixed retina was washed three times in phosphate buffered saline containing 0.1 % Tween detergent. Small sections of retina (approximately 5 × 5 mm) which had separated spontaneously from the pigment

epithelium, were transferred to Superfrost Plus microscope slides and allowed to dry for 5 minutes at room temperature.

Digoxygenin-labelled RNA probes (riboprobes) were constructed for hybridisation with photoreceptor opsin mRNA. Riboprobes are more sensitive and show lower background reaction than double-stranded DNA because they do not suffer from reannealing (Coulton, 1990). 350 base pair fragments from budgerigar UV and rod opsin were amplified from single-stranded budgerigar retinal cDNA and inserted in the sense orientation into the *Eco*RI and *Kpn*I sites of pBS KS+ (Stratagene). A similar sized fragment from budgerigar SWS opsin was also obtained, but was cloned into the *Bam*HI and *Eco*RI sites of pBS KS+ instead. The plasmids were linearised using *Eco*RI (*Bam*HI in the case of the SWS riboprobe) and *Kpn*I for the construction of anti-sense and sense probes respectively. Anti-sense probes contain the complementary sequence of nucleic acids to the mRNA of interest. Sense probes are included as a control. Using a digoxygenin (DIG) RNA labelling kit (Boehringer Mannheim), anti-sense and sense cRNA riboprobes were synthesised by run-off transcription from the T3 and T7 RNA polymerase promoters respectively, with digoxygenin-labelled uridine-triphosphate (DIG-UTP) as a substrate (Wilkie *et al.*, 1998). All of the probes were shown to have similar activity in an RNA dot-blot analysis, and showed no cross-hybridisation.

The hybridisation procedure was performed using probe clips, 500 µl and 200 µl in volume respectively for the whole-mounts and the cryosections, to create incubation chambers on the slides. The whole-mounts, but not the cryosections, were permeabilised with 10 µg ml^{-1} proteinase K for 25 minutes at 37 °C. Permeabilisation works in opposition to fixation and is necessary to allow penetration of the riboprobe in thicker tissue samples (Coulton, 1990). Both types of retinal preparation were then subject to an identical protocol, adapted from Stenkamp *et al.* (1996).

Samples were pre-hybridised for 1 hour at 68 °C in a hybridisation buffer containing 50 % formamide (a duplex stabiliser / stringency determinant), 5× SSC[1], 2 % blocking agent (dried milk powder), 0.1 % (w/v) *N*-lauryl sarcosine (a detergent)

[1] SSC, standard sodium citrate. 1× SSC contains 0.15 M sodium chloride and 0.015 M sodium citrate (pH 7.0).

and 0.2 % (w/v) sodium dodecyl sulphate (SDS, a powerful anionic detergent and denaturant) to decrease non-specific binding of the riboprobes.

Hybridisations were then conducted over night at 68 °C in hybridisation buffer containing 1 ng ml ^{1} probe (freshly denatured at 65 °C for 5 minutes). Only one type of probe was applied to a given slide of cryosectioned or whole-mounted retina. Two slides of cryosections were hybridised with UVS anti-sense probes, one with UV sense probes and one each with SWS and rod anti-sense probes. Slides were kept in a plastic box lined with moist tissues to prevent dehydration. Sense SWS and rod probes, and both anti-sense and sense UVS probes were used. The following day, probe clips were floated off in a Petri dish containing 2× SSC at room temperature. Slides were washed in a slide chamber to a high stringency: four 15 minute washes at 65 °C with 2× SSC and 50 % formamide, followed by two 30 minute washes at room temperature with 1× SSC. Post-hybridisation washes are crucial as some *in situ* hybridisations, especially those performed at a relatively low stringency, often display an appreciable degree of non-specific hybridisation (Coulton, 1990). Heterologous duplexes are less stable than homologous duplexes, and reducing the ionic strength of the interstitial medium reduces duplex stability. By using a series of decreasing salt (SSC) strength washes, non-specific (heterologous) duplexes are removed.

Hybrids were revealed using a DIG Nucleic Acid detection kit (Boehringer Mannheim). Slides were washed briefly (1 minute) in buffer 1[2] with the addition of 0.3 % (w/v) Tween and subsequently incubated for 30 minutes in buffer 2[3] (60 minutes for the whole-mounts), which contained a blocking reagent to prevent non-specific binding of the antibody. Slides were then incubated for 30 minutes in buffer 2 containing 150 mU ml^{-1} anti-digoxygenin Fab-alkaline phosphatase conjugate (anti-DIG-AP). Antibody conjugate which had not bound to the probe's digoxygenin hapten was removed by washing twice with buffer 1 for 15 minutes, and the samples stabilised in buffer 3[4] for 2 minutes. The colour-substrate solution[5] was added and

---

[2] Buffer 1 contains 0.1 M maleic acid, 0.15 M NaCl, pH 7.0 (20 °C).
[3] Buffer 2 contains 1 % (w/v) blocking reagent in buffer 1.
[4] Buffer 3 contains 100 mM Tris-HCl, 100 mM NaCl, 50 mM $MgCl_2$, pH 9.5 (20 °C).
[5] Colour-substrate solution consists of 200 µl Nitro Blue Tetrazolium (NBT) salt / 5-bromo-4-chloro-3-indolyl phosphate (BCPIP) diluted in 10 ml of buffer 3.

the slides incubated overnight in a light-tight moist chamber. During this stage of the procedure, the conjugated alkaline phosphatase enzyme hydrolysed the BCPIP substrate, which reduced the NBT salt to produce an insoluble purple blue precipitate at the site of hybridisation. The following day, colour precipitation was stopped by washing the slides in buffer 4[6] for 5 minutes. Slides were coverslipped under 100 % glycerol and examined using a Lietz Diaplan (Wild Leitz) microscope fitted with a Wild MPS46 Photoautomat camera attachment. Film stock was tungsten-corrected Kodak EPY64T.

3.3.4 Statistical analysis of NBT and autofluorescence count data

Because of potential variation in the degree to which the retina spreads out on mounting, percentages of each cell type were calculated and used in preference to actual cell densities. Consequently, percentages were converted to proportions and arcsine-square root transformed to normalize the data (Sokal and Rohlf, 1995). Significance was assessed using balanced repeated-measures multivariate analyses of variance (MANOVA, Minitab 10.51, Minitab Inc.), with the transformed proportions of all the measured cell types as the dependent variables.

Three separate MANOVAs were performed on the starling data: i) using pooled data from all twenty birds to investigate the abundance and distribution of the LWS and MWS cell types; ii) for the SWS cell types measured in half of those twenty birds; and iii) for the UVS cell types which were measured in the other half. In each case, the within-subject factors were 'quadrant' and 'left / right eye', with the between-subjects factor 'sex of bird'.

The blackbird and blue tit were analysed in a similar fashion, with 'quadrant' and 'left / right eye' as within-subject factors, but without a between-subjects factor as the data were from a single specimen only in each case. Any statistical significance and resultant inferences from the analysis were therefore limited to the individual studied rather than the species in general.

Only a single eye from one male peacock was analysed. A MANOVA was performed on the data to investigate any effect of retinal location (quadrant) on the

[6] Buffer 4 contains 10 mM Tris-HCl, 1 mM EDTA, pH 8.0 (20 °C).

observed distribution. The number of peacocks studied was limited largely by the cost of each individual.

3.4 Results

3.4.1 Starling NBT and *in situ* hybridisation

The analysis of the distribution of cone types in the starling was the most rigorous of all comparisons and, because a reasonably large number of birds from each sex were studied, the results are statistically reliable generalisations to the condition of the species, rather than just the individual. Pooling the results for all four quadrants from the left and right eyes of both sexes, the mean relative abundance of each type of cone are displayed in Table 3.1.

When the data from all 20 birds were pooled to compare the distribution of LWS and MWS single cones, results of the MANOVA revealed a significant effect of quadrant (Wilk's $F_{6,106} = 12.59$, $p < 0.001$) but this was only explained by the distribution of the LWS cones, which were significantly rarer in the PD quadrant of the retina (univariate $F_{3,54} = 29.20$, $p < 0.001$). Interestingly, there was also a significant difference in the distribution of these cone types between the left and right eyes. Both LWS (univariate $F_{1,18} = 8.28$, $p = 0.010$) and MWS cones (univariate $F_{1,18} = 6.32$, $p = 0.022$) were significantly more abundant, relative to the other cone types, in the left eye. There was no effect of sex on the observed distributions (Wilk's $F_{2,17} = 1.40$, $p = 0.275$).

SWS-labelled ($n = 10$) and UVS-labelled ($n = 10$) retinae were analysed separately in an identical fashion. Again, there was no significant effect of sex (Wilk's $F_{4,5} = 5.07$, $p = 0.052$), but there was a significant effect of quadrant on the distribution of SWS cones (Wilk's $F_{12,55} = 6.81$, $p < 0.001$; univariate $F_{3,24} = 27.10$, $p < 0.001$), which were more abundant in the dorsal half of the retina.

The distribution of UVS cones also varied significantly according to quadrant (Wilk's $F_{12,55} = 5.96$, $p < 0.001$; univariate $F_{3,24} = 20.17$, $p < 0.001$). These effects are due to the highest proportion of UVS cones being located in the PD region of the retina, probably replacing the LWS cones. There was no significant effect of sex on the observed distribution (Wilk's $F_{4,5} = 2.63$, $p = 0.158$).

As cone distribution was not significantly affected by sex, the data from males and females were pooled for each retinal quadrant, in both the left and right eyes, for display in Figure 3.4. Although no direct statistical analysis could be performed, calculated percentages indicated that double cones tended to be more abundant in the ventral retina, and notably deficient in the PD quadrant.

The results of the *in situ* hybridisation were partially successful, and were suggestive of the presence of a dedicated UVS pigment in the starling retina. Unfortunately, both cryosections and whole-mounts displayed a high level of background labelling, particularly in the outer and inner nuclear layers of the retina. In the case of the whole-mounts, the excessive labelling was sufficient to obscure any underlying pattern of labelling in the photoreceptor inner segments.

Although the rod anti-sense probe did not hybridise with any photoreceptors in the cryosections, both the anti-sense UVS (Figure 3.1) and anti-sense SWS probes did. As would be expected, the 'control' UVS sense probe did not hybridise (Figure 3.1). Because the majority of cone oil droplets had become fragmented, it was not possible to estimate reliably the proportion of UVS and SWS cones relative to any of the other cone types. However, both cell types appeared to be distributed regularly across the retina.

The fact that budgerigar rod anti-sense probes did not hybridise with the starling rods does not necessarily imply that the two pigments were different or that the technique had failed. The cryosections used were made sagitally, and it is known that the starling retina displays an 'unusually large' rod free area around its central fovea (Adler and Dalland, 1959; Dalland, 1958). Consequently, it is possible that there were no, or very few, rods within the cryosections used for hybridisation.

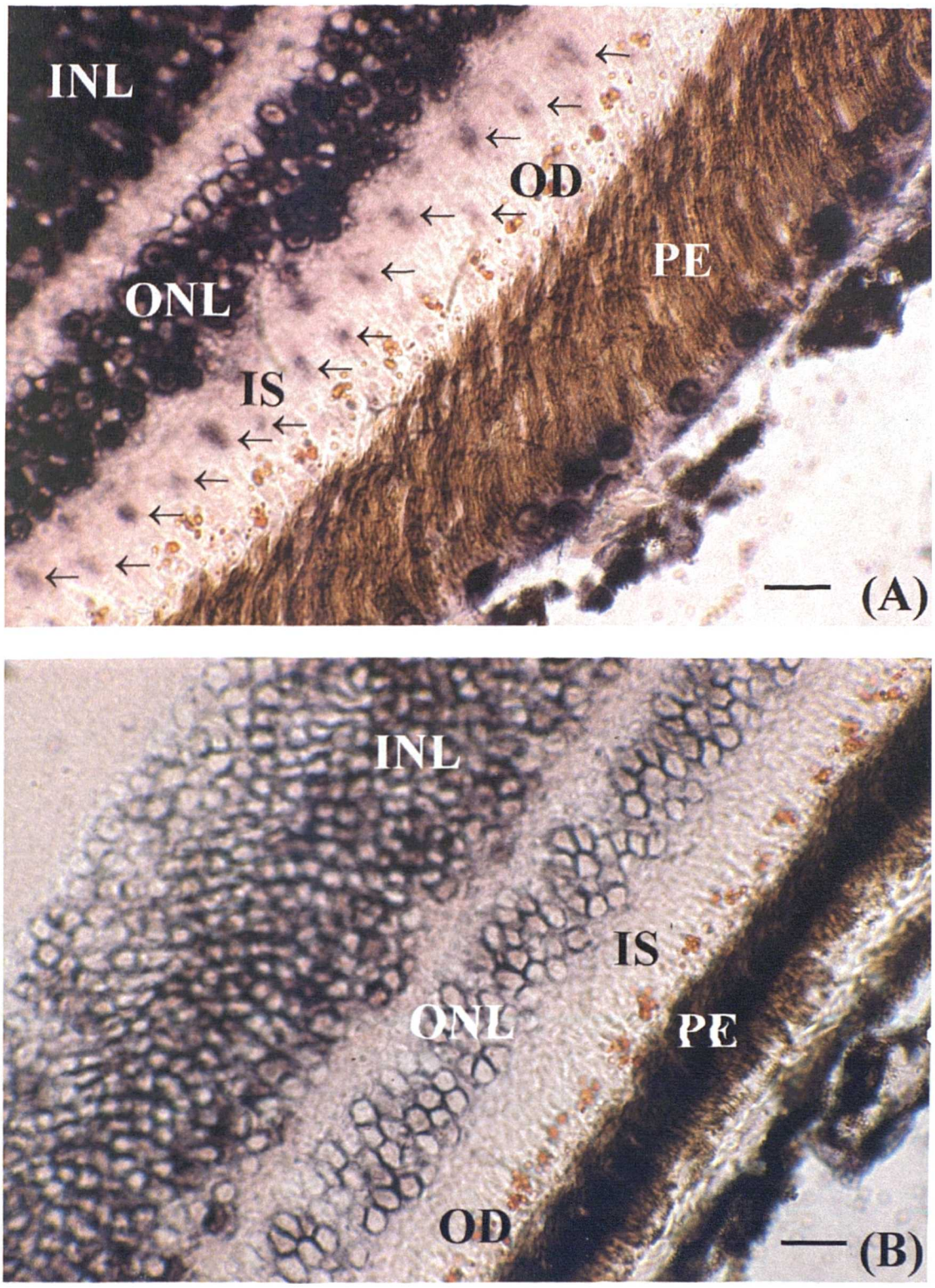

Figure 3.1 Radial cryosections of the retina of the European starling, *Sturnus vulgaris*, following *in situ* hybridisation with **(A)** budgerigar UVS opsin anti-sense riboprobe and **(B)** budgerigar UVS opsin sense (control) riboprobe. In **(A)**, arrows indicate the bluish purple labelled inner segments containing UVS opsin mRNA which has hybridised with the anti-sense riboprobe. The sense riboprobe did not hybridise with any inner segments. OD, oil droplet layer; IS, inner segment layer; PE, pigment epithelium; ONL, outer nuclear layer; INL, inner nuclear layer. Note the high degree of non-specific labelling in the INL and ONL. Scale bars: **(A)** 12.7 μm; **(B)** 17.6 μm.

The cause of the high level of background labelling was unknown. It is possible that endogenous phosphatases in the nuclear layers, which had not been inactivated by the fixation step, were responsible for reduction of the NBT chromogen. Diffusion of the blue NBT precipitate, which can be reduced by the incorporation of 5 % polyvinyl alcohol in the overnight colour development stage, was also a potential cause of background labelling. However, the marked localisation of the dye in the nuclear layers, and its absence from the intermediate outer plexiform layer, suggests that this is unlikely. A third explanation is that one of the blocking agents used failed to prevent non-specific hybridisation or non-specific conjugation with the anti-DIG antibody.

Nevertheless, the successful hybridisation of the UVS anti-sense probe implied the existence of a UVS cone opsin similar to that of the budgerigar. Microspectrophotometric results (chapter two) have subsequently confirmed that a UVS visual pigment is present in the starling retina, and is spectrally similar to the UVS visual pigment measured in the budgerigar (Bowmaker *et al.*, 1997; Wilkie *et al.*, 1998).

3.4.2 Blackbird autofluorescence and NBT

The analysis of the distribution of cone types in the blackbird, determined using autofluorescence, was restricted to the left and right eyes of a single male bird. Pooling the results for all four quadrants from both the left and right eye, the mean relative abundance of each cone type are displayed in Table 3.1. Results of the MANOVA indicated a significant effect of quadrant (Wilk's $F_{15,188} = 6.97$, $p < 0.001$) and left or right side (Wilk's $F_{5,68} = 4.77$, $p = 0.001$) on cone distribution. Furthermore, there was a significant interaction of quadrant and left / right side (Wilk's $F_{15,188} = 3.40$, $p < 0.001$) which suggests that the pattern of regional variations is different for left and right eyes.

The univariate tests revealed that the distribution of all of the different cone types differed depending on retinal location (LWS $F_{1,72} = 18.50$, $p < 0.001$; MWS $F_{1,72} = 7.63$, $p < 0.001$; SWS $F_{1,72} = 3.43$, $p = 0.021$; UVS $F_{1,72} = 11.72$, $p < 0.001$; Double cones $F_{1,72} = 7.12$, $p < 0.001$). The mean relative abundances of each cone type in each retinal quadrant of each eye are displayed in Figure 3.5. LWS single cones were most abundant in the PD quadrant, and least abundant in the PV

quadrant. MWS cones, like the LWS cones, were relatively more abundant in the PD quadrant. SWS cones were most abundant in the AV quadrant, whilst UVS cones were least abundant in this region. Double cones were most abundant in the PV quadrant and least abundant in the PD quadrant. Furthermore, these trends were identical for both the left and right eyes.

Although the results of the MANOVA revealed a significant difference between left and right eyes, none of the univariate tests were significant. It is possible that, whilst not significant on their own, some cumulative effect of the different cone types resulted in a significant multivariate test statistic. Variations in overall cone proportions between the two eyes are small. LWS single cones and double cones are slightly more abundant in the left eye, whereas the remaining single cone types are relatively more abundant in the right eye.

The significant interaction between quadrant and left / right side revealed by the MANOVA was explained only by the differing distribution of UVS (univariate: $F_{1,72} = 7.49$, $p < 0.001$) and LWS single cones (univariate: $F_{1,72} = 3.93$, $p = 0.012$) between the left and right eyes. The existence of such differences are difficult to interpret. With small sample sizes, the chances of committing a type one error are increased, and as such all results should be treated with caution.

A photomicrograph illustrating the NBT staining of UVS cones in the blackbird retina is provided in Figure 3.2. The mean proportion of UVS cones determined from the NBT-labelled blackbird retinae (5.2 %) was similar to that obtained using the autofluorescence method (6.6 %). No comparative statistical analysis was performed on the two data sets because of the small sample size - a significant difference between analysis methods might be confused with inherent variation between individual subjects. Nevertheless, the discrepancy between the two estimates obtained for the UVS cones was of a similar order of magnitude to the differences in estimates of the proportions of LWS and MWS cones (1.4 % and 3.5 % respectively). It is concluded that the NBT staining technique may be a reliable alternative to the autofluorescence method for determining relative photoreceptor abundances.

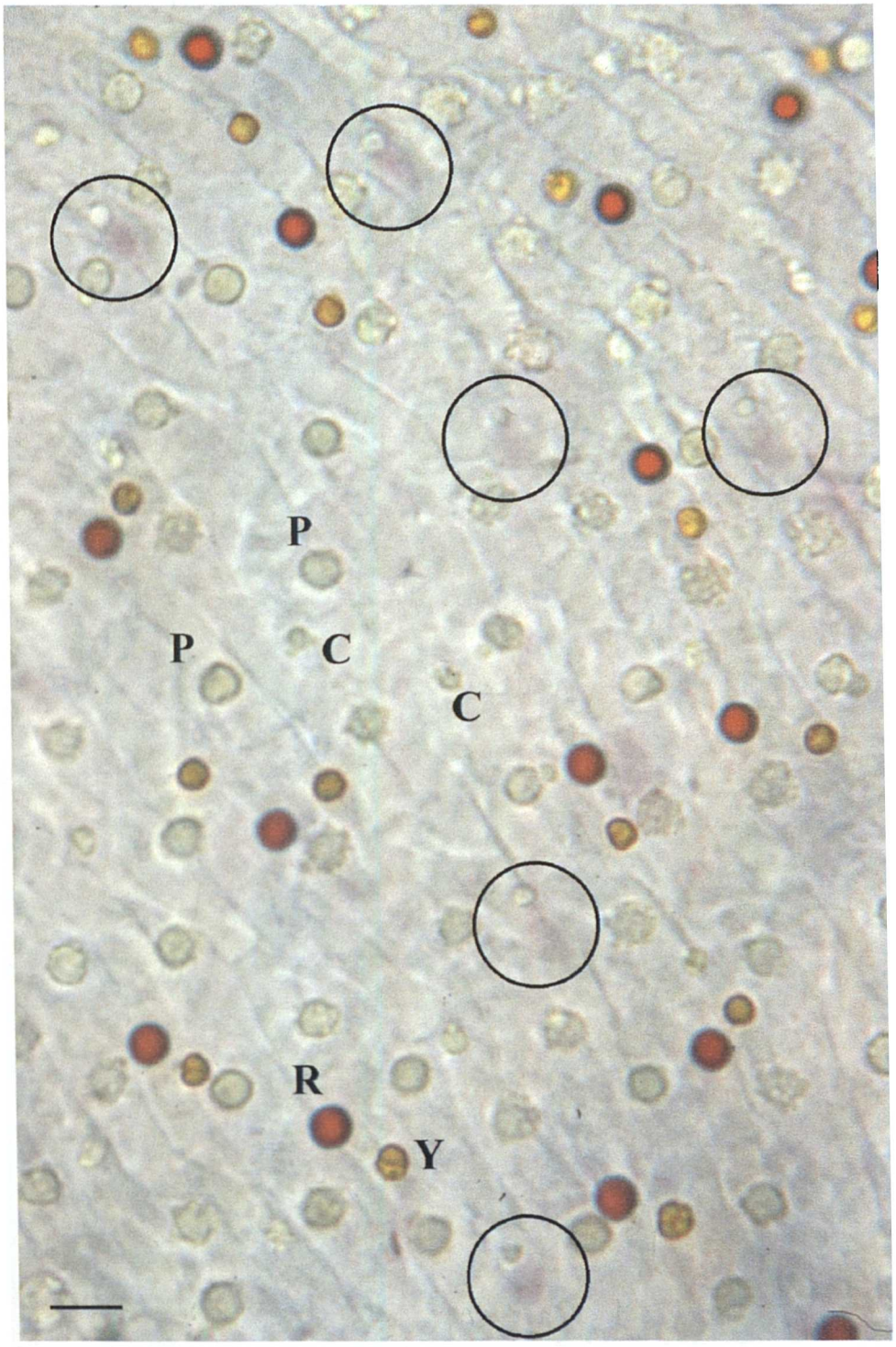

Figure 3.2 Nitroblue tetrazolium chloride (NBT) stained retina of the blackbird, *Turdus merula*, following illumination with 366 nm monochromatic light. UVS single cones, associated with T-type (transparent) oil droplets, are circled. Note the accumulation of purple stain (insoluble NBT diformazan) in the ellipsoid region of their inner segments. Examples of the oil droplets associated with the other cone types are also labelled: R, red or R-type oil droplets of the LWS single cones; Y, yellow or Y-type oil droplets of the MWS single cones; C, 'colourless' or C-type oil droplets of the SWS single cones; P, principal or P-type oil droplets found in the principal member of the double cone pair. Scale bar = 8 μm.

3.4.3 Blue tit autofluorescence

The analysis of the distribution of cone types in the blue tit was also restricted to a single (female) individual. Pooling the results for all four quadrants from both the left and right eye, the mean relative abundance of each cone type are summarised in Table 3.1.

Multivariate analysis revealed a significant effect of quadrant (Wilk's $F_{15,188} = 6.74$, $p < 0.001$) and left or right side (Wilk's $F_{5,68} = 12.28$, $p < 0.001$) on cone distribution. There was also a significant interaction of quadrant and left / right side (Wilk's $F_{15,188} = 4.69$, $p < 0.001$) which suggests that the distribution of cones across the retina differs between left and right eyes.

Inspection of the mean relative abundances of each cone type displayed in Figure 3.6 reveals that there are no consistent trends in retinal distribution, despite significant univariate test statistics for the effect of quadrant on LWS ($F_{1,72} = 16.82$, $p < 0.001$), MWS ($F_{1,72} = 22.03$, $p < 0.001$), UVS ($F_{1,72} = 6.89$, $p < 0.001$) and double cones ($F_{1,72} = 30.26$, $p < 0.001$). The lack of comparable retinal distributions between the two eyes explains the significant univariate test statistics for the quadrant*left / right eye interaction (LWS $F_{3,72} = 6.62$, $p = 0.001$; MWS $F_{3,72} = 11.52$, $p < 0.001$; UVS $F_{3,72} = 5.16$, $p = 0.003$; double cones $F_{3,72} = 18.96$, $p < 0.001$). It is conceivable that the small size of the blue tit eyes resulted in an uneven dissection of the left and right retinae. Errors of this type are exaggerated in smaller eyes, and will have a large influence with such a limited sample size.

In common with the starling, LWS and MWS single cones were significantly more abundant in the left eye (univariate: LWS $F_{1,72} = 10.30$, $p = 0.002$; MWS $F_{1,72} = 22.09$, $p < 0.001$), and double cones were significantly more abundant in the right eye (univariate: $F_{1,72} = 17.10$, $p < 0.001$).

3.4.4 Peacock autofluorescence

Representative photomicrographs illustrating the nature of cone oil droplet autofluorescence in the peacock are displayed in Figure 3.3. The analysis of the distribution of cones in the peacock was the least rigorous because, in addition to only studying one (male) bird, only one eye (left) was available for examination. Pooling the results for all four quadrants from the left eye, the mean relative

abundance of each type of cone are displayed in Table 3.1. Results of the MANOVA revealed a significant effect of quadrant on cone distribution (Wilk's $F_{15,254} = 17.17$, $p < 0.001$). Univariate tests showed that this result was due to all of the cone types varying significantly according to retinal location (LWS $F_{3,96} = 21.30$, $p < 0.001$; MWS $F_{3,96} = 33.38$, $p < 0.001$; SWS $F_{3,96} = 19.40$, $p < 0.001$; VS $F_{3,96} = 20.97$, $p < 0.001$; double cones $F_{3,96} =$, $p < 0.001$).

Inspection of the data from each quadrant, as displayed in Figure 3.7, revealed that LWS single cones were relatively more abundant in the PD quadrant and least abundant in the PV region. MWS single cones were also relatively more abundant in the PD quadrant, but had a relatively even distribution in the rest of the retina. The distribution of these two cone types is very similar to that observed in the blackbird. Both SWS and VS single cones were relatively more abundant in the PD quadrant and least abundant in the AV region, suggesting that the variation of these cone types across the retina takes the form of a posterior dorsal-anterior ventral gradient, rather than simply a dorsal-ventral trend. The distributions of SWS and VS cones in the peacock are similar to that observed for the SWS and UVS cones in the starling retina. Double cones were least abundant in the dorsal quadrants of the retina. The PD region was particularly deficient, although this is hardly surprising as all four single cone types are most abundant in this area.

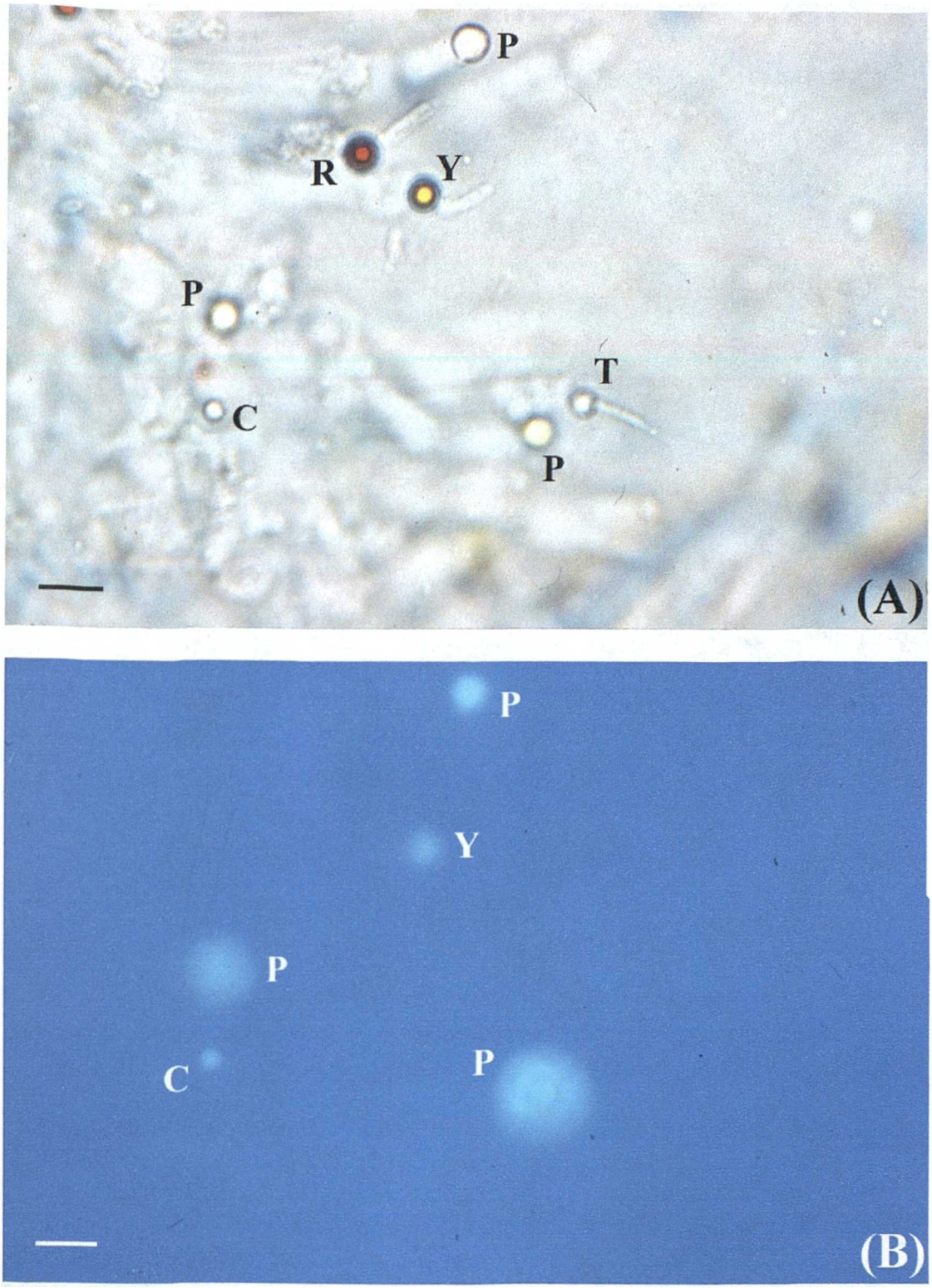

Figure 3.3 Whole-mounted retina of the peacock, *Pavo cristatus*. **(A)** Appearance under white light illumination. **(B)** The same field of view illuminated with ultraviolet light (mercury lines isolated at 334 and 365 nm), revealing autofluorescence of specific oil droplet types (only wavelengths above 435 nm were allowed to reach the photographic emulsion). Scale bar = 8 μm.

Species		Single cones				Double cones
		LWS	MWS	SWS	UVS / VS	
Starling	Mean (%)	17.7	17.4	6.4	4.7	53.8
	± s.d.	5.5	4.3	5.6	4.4	-
	n (birds)	20	20	10	10	20
Blackbird	Mean (%)	12.5	14.1	11.3	6.6	55.5
	± s.d.	2.1	2.1	2.1	2.3	5.5
	n (birds)	1	1	1	1	1
Blue tit	Mean (%)	20.3	20.3	14.4	7.6	37.5
	± s.d.	3.4	4.1	2.6	2.6	8.9
	n (birds)	1	1	1	1	1
Peacock	Mean (%)	15.6	16.3	13.9	7.4	46.9
	± s.d.	2.8	3.3	2.7	2.1	7.4
	n (birds)	1	1	1	1	1

Table 3.1 Relative abundance of the different cone classes in the retinae of starling, blackbird, blue tit and peacock. Data have been pooled across all regions of the retina and, where appropriate, left and right eyes and sex. Values are percentages. LWS long wavelength-sensitive; MWS medium wavelength-sensitive; SWS short wavelength-sensitive; UVS ultraviolet-sensitive; VS violet-sensitive; s.d. standard deviation. There is no standard deviation for double cones in the starling as these were not counted directly but calculated as described in the text.

Figure 3.4 to **Figure 3.7** Distribution of the different classes of cone photoreceptor in the retinae of starling, blackbird, blue tit and peacock. With the exception of the peacock, both left and right eyes were investigated. Because, there was no significant effect of sex on the distribution of cones in the starling, data from both sexes has been pooled. Each diagram represents the fundus of an eye as observed from the corneal aspect of the appropriate side of the birds head. The horizontal and vertical dashed lines represent dissection cuts which separated the retina into four quadrants. The oblique solid line indicates the position of the pecten. Values represent the mean percentage of each particular cone type relative to the mean total number of cones in each quadrant. AD, anterior dorsal; PD, posterior dorsal; AV, anterior ventral; PV, posterior ventral; LWS, long wavelength-sensitive; MWS, medium wavelength-sensitive; SWS, short wavelength-sensitive; UVS, ultraviolet-sensitive; VS, violet-sensitive.

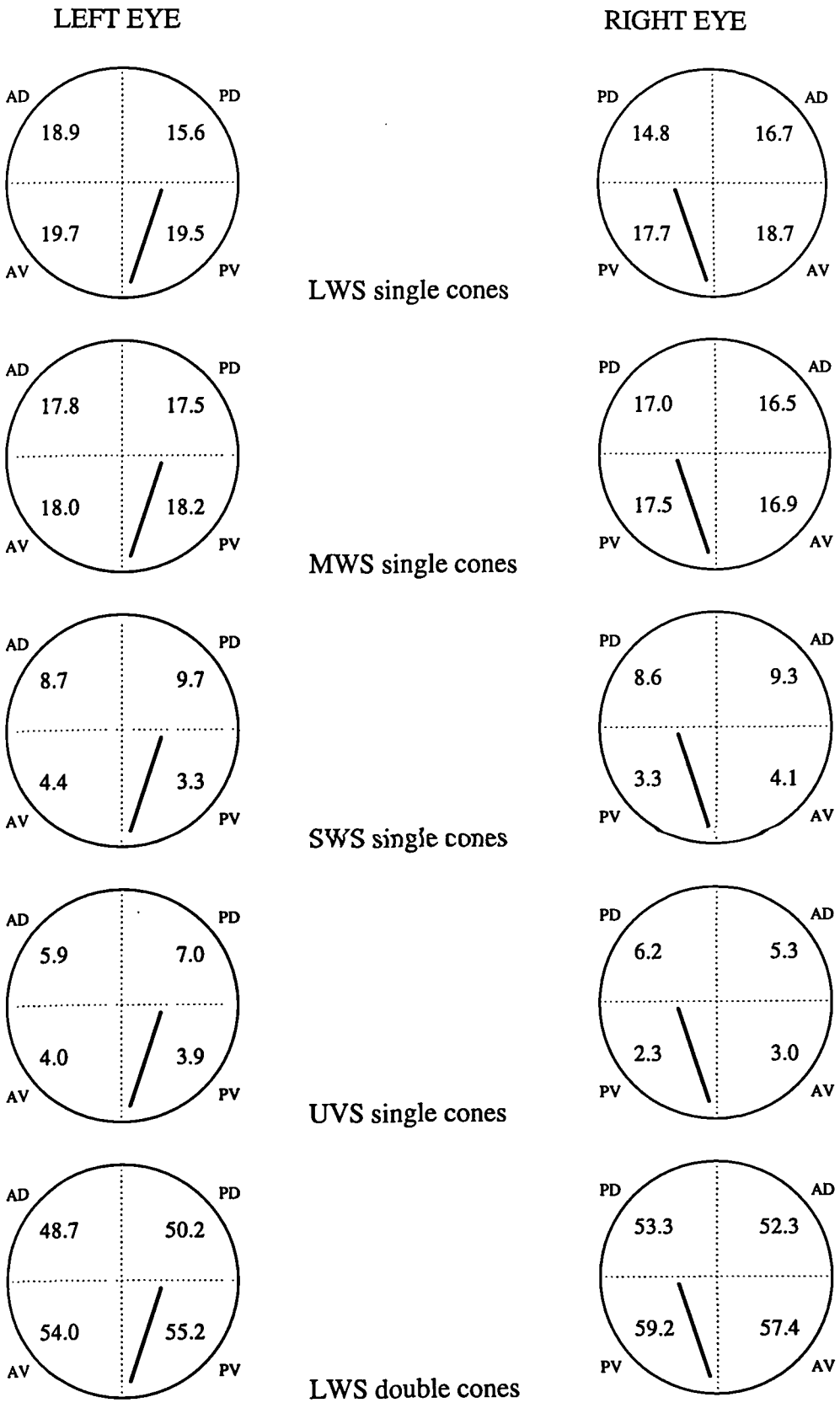

Figure 3.4 Distribution of cone photoreceptors in the starling (*Sturnus vulgaris*).

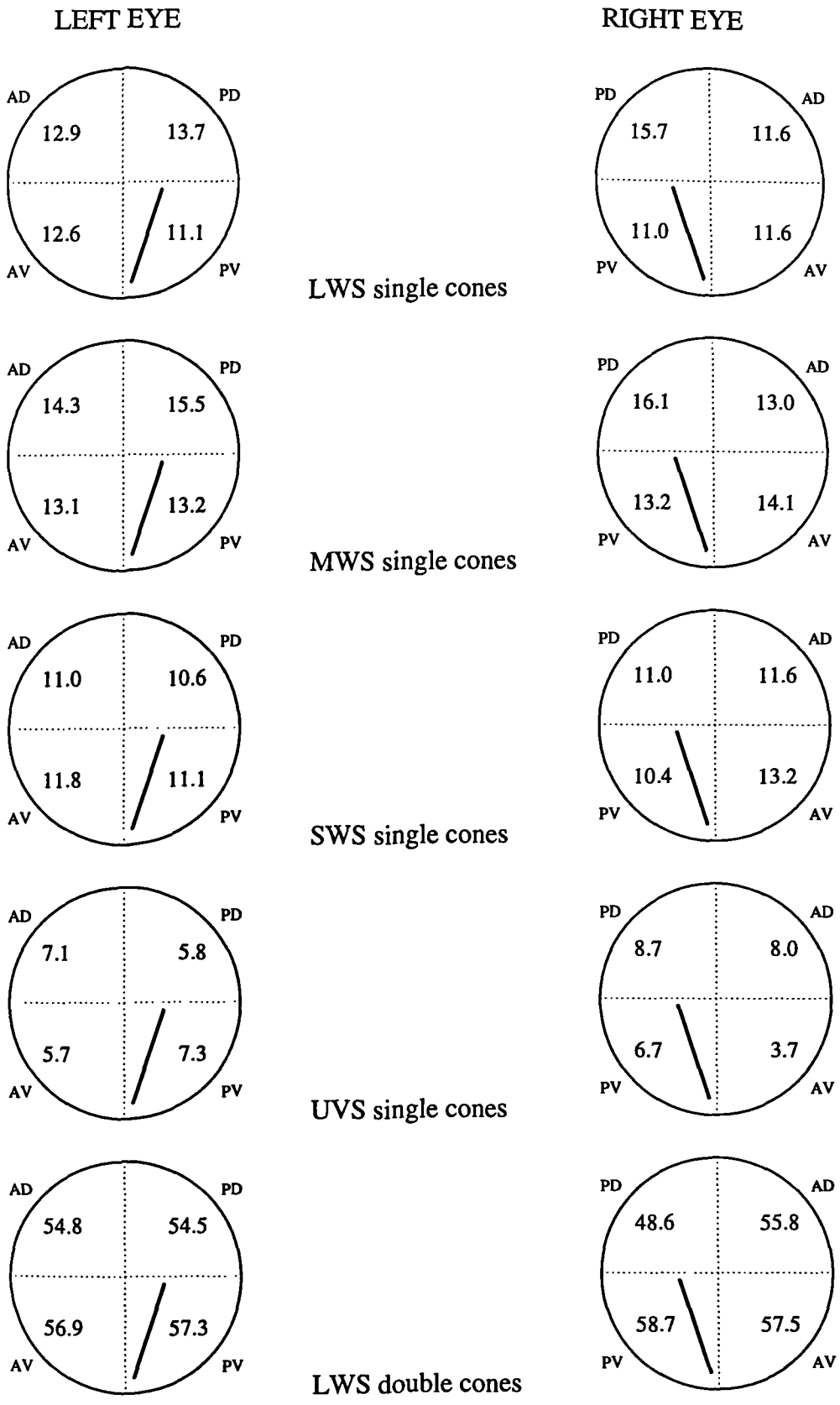

Figure 3.5 Distribution of cone photoreceptors in the blackbird (*Turdus merula*).

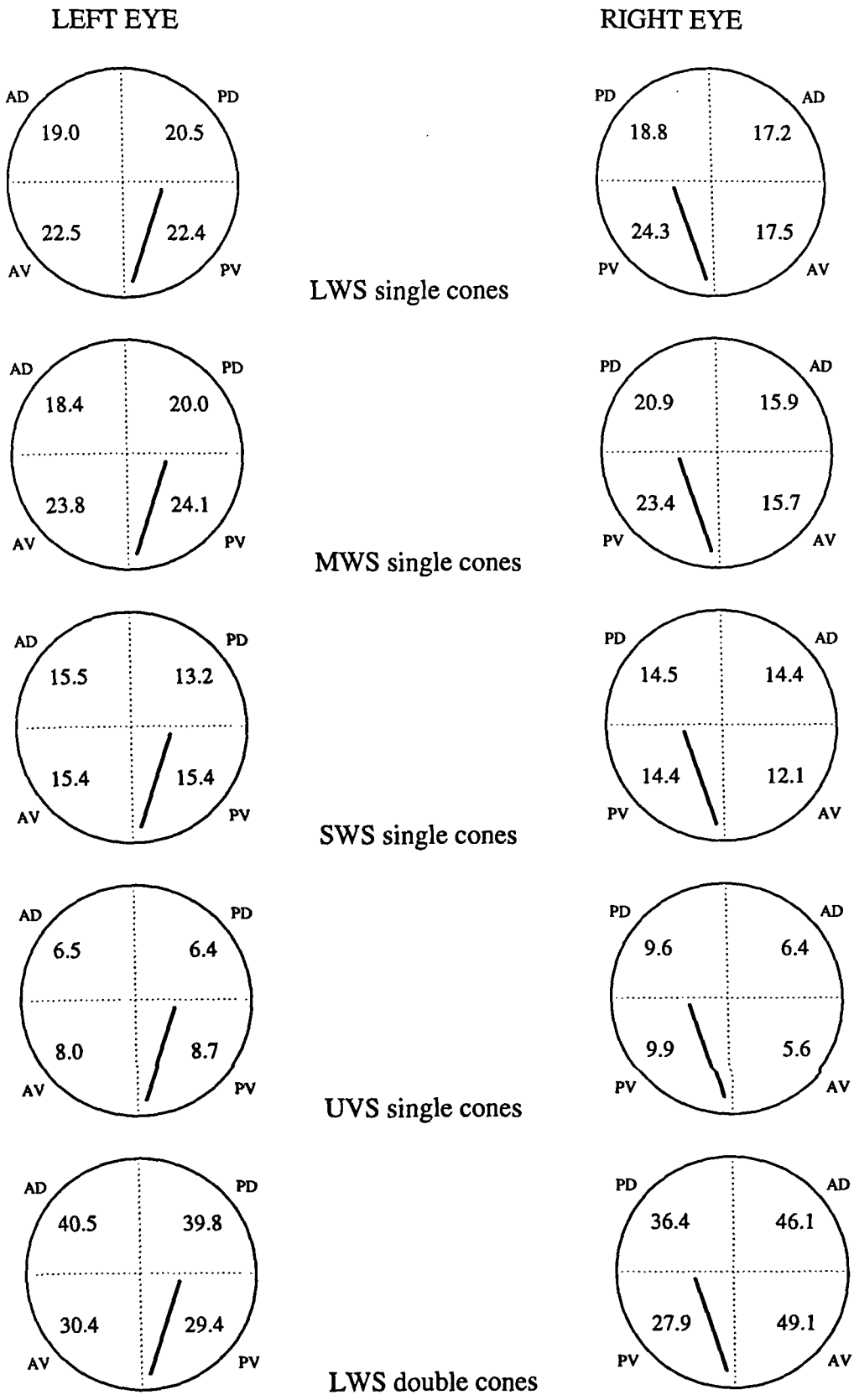

Figure 3.6 Distribution of cone photoreceptors in the blue tit (*Parus caeruleus*).

LEFT EYE

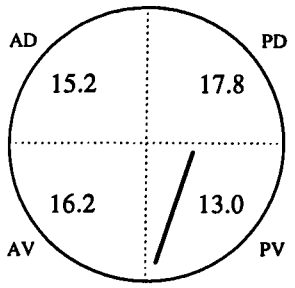

LWS single cones

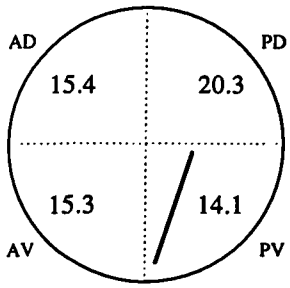

MWS single cones

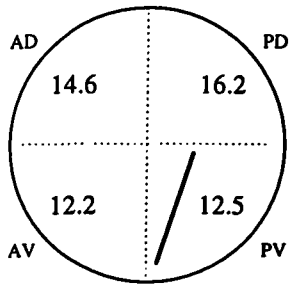

SWS single cones

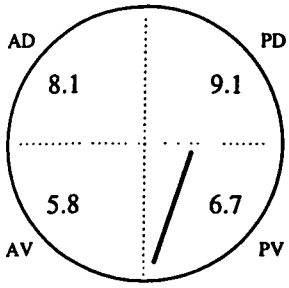

VS single cones

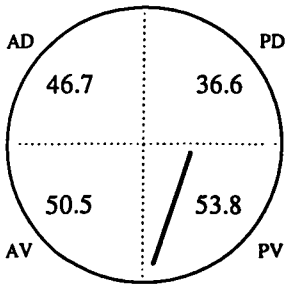

LWS double cones

Figure 3.7 Distribution of cone photoreceptors in the peacock (*Pavo cristatus*).

3.5 Discussion

The counts of photoreceptor distribution made in the course of this study were hampered by the availability of fresh, wild caught specimens. This would obviously need to be improved upon in a more rigorous investigation of intra-retinal cone variation for the purpose of cross-species comparisons. The starling was the only species to be studied in great detail and generalisations can only realistically be made about this species. However, the starlings available were long-term captives which necessitated the use of NBT staining to distinguish the cone types containing 'colourless' oil droplets. Whilst a comparison in the blackbird between the number of UVS cones determined using NBT or autofluorescence suggested that this method can be reliable, the NBT technique is considerably more difficult, is susceptible to the generation of false positives, and as such has a much higher potential for misclassification. The autofluorescence method would undoubtedly be the preferred technique for further studies as the properties of the different oil droplets are more stable and independent of the preparation methods used.

Left-right differences were noted in some of the species investigated. It is possible that these differences could be artefacts of the preparation techniques used. For example, it is possible that the eyes were dissected asymmetrically such that the four quadrants from each eye were not mirror-images of each other. Furthermore, manually removing residual pigmented epithelium from small areas of the retina, which were subsequently counted, might have removed some of the photoreceptors in an asymmetrical fashion and thus biased the results. With regard to the NBT-staining technique, the time between removal of the eye from the skull and illumination is quite critical and it is inevitable that one eye will be removed before the other. To avoid this eventuality, the eye removed first from a starling was alternated throughout the experiments.

Whilst the left-right differences noted in the blackbird and blue tit must be treated with caution, those noted in the starling are likely to be more robust in view of the larger sample size. Even if the trait was perfectly bilaterally symmetrical, some individuals would be expected to have more of a particular cone type in the right eye and some to have more in the left, due to fluctuating asymmetry. The only way of testing for directional asymmetries is to have a large sample size of

individuals. The observation that LWS and MWS single cones, the identification of which is the least ambiguous, were relatively more abundant in the left eye is very intriguing, although perhaps not entirely unexpected. In general, vertebrate sensory systems are based on bilaterally symmetrical sense organs. Nevertheless, it is evident that some birds use different eyes preferentially for certain visual tasks (Rogers, 1986; Güntürkün and Kesch, 1987; Dharmaretnam and Andrew, 1994; Güntürkün, 1997). Because of the nearly complete contralateral decussation of the optic nerve in birds (Cowan *et al.*, 1961), it has been assumed that this division of labour is solely due to cerebral hemispheric specialisation (Rogers, 1981; Andrew, 1991; Rogers, 1991). However, it is possible that the retinae are also morphologically asymmetrical.

Gross asymmetry in ocular morphology occurs in some invertebrates such as the squid *Histioteuthis spp.* (Wentworth and Muntz, 1989) but asymmetry in vertebrate eyes is usually restricted to independent eye movements (e.g. chameleons, *Chamaeleo dilepsis*, Ott and Schaeffel, 1995) or pupillary responses to light (e.g. barn owls, *Tyto alba*, Schaeffel and Wagner, 1992). Nevertheless, structurally asymmetric sense organs are known to be present in birds. In the barn owl, the ear flaps or operculi in front of the ears are positioned asymmetrically (Payne, 1971), as are the external ear openings of various other owl species (Bunn *et al.*, 1982). It is therefore reasonable to expect that subtle anatomical asymmetries may also exist in visual sense organs.

The development of structural and functional asymmetries in avian vision are thought to be dependent on uneven photostimulation of the eyes of the developing embryo during the last three to four days prior to hatching (Rogers and Bolden, 1991). During this period, the embryo is orientated in the egg such that the right eye is positioned next to the air sac whereas the left eye is occluded by the body. The right eye therefore receives much more light than the left which causes the thalamofugal visual projections connected to the right eye, in the left hemisphere, to develop in advance of those connected to the left eye, in the right hemisphere. This structural asymmetry is reversed if the embryo is manipulated *in vivo* so that the left eye receives more illumination than the right, and is absent in birds hatched from eggs incubated in the dark (Rogers and Bolden, 1991). Furthermore, some aspects of

this developmental response are thought to be wavelength-dependent (Rogers and Krebs, 1996), suggesting a role for the tectofugal pathway which, among other functions, mediates wavelength discrimination (Engelage and Bischof, 1993).

These structural asymmetries are thought to be reflected in the lateralization of visually-guided behaviours at an early age (Gaston and Gaston, 1984; Rogers, 1991; Dharmaretnam and Andrew, 1994). There is also evidence that behavioural lateralisation persists into adulthood, perhaps as a consequence of these early but transient asymmetries which may no longer be evident on examination of the visual projections (Rogers and Adret, 1993). Adult pigeons forced to undertake discrimination tasks (e.g. distinguishing edible grains from similar-sized pebbles), with one or other of their eyes occluded, perform more accurately when using their right eye (Güntürkün, 1985; 1987; 1992). Furthermore, adult male zebra finches tend to observe potential mates preferentially with their right eye (Workman, 1986). Despite the lateral position of the two eyes in many birds, both hemispheres are involved in analysing a visual stimulus by the rapid alternation of lateral fixation between the two eyes (Andrew and Dharmaretnam, 1993). This behaviour is obvious in passerine birds foraging for invertebrate prey on the ground, and presumably allows the different specialisations of both hemispheres, or any differences in retinal organisation between the two eyes, to be exploited in the identification of a potential prey item.

Behavioural lateralization as a result of hemispheric specialisation is widespread in other taxa. In man, the left hemisphere is dominant at the sensory and motor level, whilst spatial awareness is largely the domain of the right hemisphere (Bradshaw and Nettleton, 1981). Human and non-human primates also share a similar pattern of brain asymmetry for emotional expression and processing of species-typical vocal signals (Hauser, 1993).

It is conceivable that a developmental asymmetry has occurred in the starling retina. Although only the proportion of LWS and MWS cones was significantly higher in the left eyes, the SWS and UVS cones display a similar trend (Figure 3.4). These higher relative proportions of single cones in the left eye are balanced by a higher relative proportion of double cones in the right. Consequently, one would predict that, at least in the starling, the left eye should be superior in visual tasks

involving colour discrimination. In this respect, it is interesting to learn that, when foraging, starlings observe distant objects monocularly, first with one eye and then the other (Beecher, 1978). Presumably, the object of interest is focused onto the starling's large central fovea for detailed examination (Dalland, 1958). If the left / right differences in photoreceptor abundance observed (Figure 3.4) extend to the fovea, it is possible that the starling might compare or combine the different visual information provided by each eye. A detailed investigation of the distribution of photoreceptors in birds which have been shown to display visual lateralization would be required to investigate this phenomenon further.

From the data presented in Figure 3.4 to Figure 3.7 it is evident that in the starling, blackbird and peacock, there are often differences separating the PD region of the retina from the remaining quadrants. In the starling, this is manifested as a relative deficiency of LWS cones and a relative abundance of UVS cones in the PD quadrant. This region contains relatively more LWS and MWS cones in the blackbird retinae and more of all the single cone types in the peacock, at the expense of double cones.

The replacement of LWS cones by UVS cones in the posterior dorsal portion of the starling retina may be correlated with optical features of the eye and feeding behaviour. The PD quadrant of the starling eye becomes increasingly myopic with greater eccentricity as the scleral surface falls behind the focal plane of the image (Martin, 1986). It is proposed that this 'ramp retina' might be used as a static accommodatory device, enabling simultaneous focus of the posterior dorsal visual field (corresponding to the AV retina) at infinity to scan for aerial predators, as the anterior ventral visual field (PD retina) examines objects close to the bill while probing the ground for food. The starling is unusual in its reduction in LWS cones in the posterior dorsal retina. Most avian species studied show the opposite trend or a more uniform distribution of red oil droplets (Waelchli, 1883; Muntz, 1972; Bowmaker, 1977; Goldsmith *et al.*, 1984a; Partridge, 1989; this study). However, if the AV region of the starling retina is indeed designed for scanning the celestial hemisphere, the increased proportion of red oil droplets, and the increased pigmentation in the P-type oil droplets (see chapter two), in this region would seem adaptive for the detection of distant objects. The visual range is greater for long

wavelength light, which is scattered less by the atmosphere than light of shorter wavelengths (Muntz, 1972). In addition, red oil droplets will reduce the degradation of the visual image by filtering short wavelengths scattered within the eye by the ocular media, thus increasing visual acuity (Lythgoe, 1979). Conversely, starlings often forage using an open-bill probing technique (Feare, 1984), which means that they locate prey visually at a very short range. The PD region of the retina concerned with this task would have little need for the high acuity necessary for long distance vision, and this may explain the relative deficiency of LWS cones in the PD retina.

The blackbird and peacock are similar to the pigeon (*Columba livia*) in the distribution of cone photoreceptors across their retinae. The PD region, or 'red field', of the pigeon retina contains a higher proportion of LWS and MWS cones and a lower proportion of double cones than the remaining retinal area, known as the 'yellow field' (Waelchli, 1883). The disparity between these two retinal areas is greater in the pigeon than in any other species studied, but may represent the enhancement of a general trend. In birds with laterally placed eyes, the PD quadrant comprises the region of binocular overlap, and sometimes a temporal area or fovea, and would be involved in tasks such as pecking (Martin, 1985; Clarke *et al.*, 1996). This suggests that such variation in cone abundance may be of functional significance, most likely with regard to differences in the importance of single and double cones between the two areas.

The function of double cones, which occupy approximately four times the area of a single cone and dominate the retinae of diurnal birds (Meyer, 1977), is unclear. Behavioural measures of photopic spectral sensitivity appear to show no involvement of the double cones, only peaks in sensitivity corresponding to the corrected spectral sensitivities of the four single cone types (Maier and Bowmaker, 1993). Nevertheless, electroretinographically determined photopic spectral sensitivity functions are dominated by a broad peak at around 570 nm (e.g. Blough *et al.*, 1972; Chen and Goldsmith, 1986), which corresponds to the peak effective spectral sensitivity of the double cones. This mismatch suggests that the neural signal from the double cones is not involved in colour vision, at least under the conditions used for the behavioural test of photopic spectral sensitivity.

Results from behavioural experiments on zebra finches (*Taeniopygia guttata*) would be consistent with an enhanced role for double cones in movement detection, provided that they too display a higher proportion of double cones in the AV retina. The binocular field of the eye, subserved by the PD retina, has an upper threshold of movement detection at 540° s^{1}, whereas the upper threshold in the monocular or lateral visual field of the eye, subserved by the remaining retina, is 1100° s^{-1} (Bischof, 1988). Thus, the higher proportion of double cones observed in the AV retina of most birds, including the starling, blackbird and peacock, might be adaptive for the detection of aerial predators through movement or achromatic contrast.

Interestingly, the thalamofugal visual pathway of the pigeon receives so few afferents from the PD retina that it is functionally blind to the binocular visual field (Güntürkün *et al.*, 1993). Instead, visual information received by the PD retina is processed almost exclusively by the tectofugal pathway, which is known to be dominant over the thalamofugal pathway in visual discriminations involving colour, brightness, pattern or size (Engelage and Bischof, 1993). It is unlikely that this disparity is a result of the laterally placed eyes of pigeons, as the American kestrel (*Falco sparverius*), a diurnal raptor with laterally positioned eyes, has an over-representation of the frontal binocular field within the thalamofugal pathway (Pettigrew, 1978). It seems probable, therefore, that regional specialisation in the retina, and the division of labour between the two visual pathways, is correlated with visual ecology, and it would be of great interest to examine the distribution of the retinal photoreceptors in the kestrel.

Further support of a dominant role for double cones in movement detection comes from experiments investigating the spectral sensitivity of the neural structures controlling the optomotor response in birds. Pigeons display a wavelength-dependent sensitivity to moving stripe patterns which best approximates to the effective spectral sensitivity of their double cones (Campenhausen and Kirschfeld, 1998). The wavelength of peak sensitivity (approximately 560 nm) is unaffected by chromatic adaptation with 503 and 601 nm monochromatic illumination, which implies the involvement of only one type of cone.

Evidence from the chicken for a centrifugally-controlled circuit which might play a role in visual attention switching between the PD and AV regions of the avian

retina (Clarke *et al.*, 1996) may also be important in deducing a functional explanation. Efferents to the retina from the isthmo-optic nucleus (ION), a region of the midbrain which receives topographically organised retinal input *via* the optic tectum (Nalbach *et al.*, 1993), may excite amacrine and displaced ganglion cells locally in the AV retina but inhibit those in the PD region, thus mediating switches in attention between the PD retina, involved in feeding, and the AV retina, involved in scanning for predators. Centrifugal inputs have also been shown to increase the sensitivity of avian retinal ganglion cells to moving patterns (Uchiyama and Barlow, 1994). Intriguingly, ground-feeding species of bird (e.g. pigeon), which have most need to switch their visual attention between food and predators, have the largest and best developed IONs (Repérant *et al.*, 1989) and often display dorsal-ventral trends in cone distribution and oil droplet pigmentation (Goldsmith *et al.*, 1984b; Bowmaker *et al.*, 1997). Swallows (*Hirundo rustica*) and swifts (*Apus apus*), which feed on the wing and probably have less need to scan for predators whilst feeding, have few ION efferents (Clarke *et al.*, 1996) and display no topographic variation in photoreceptor type or oil droplet pigmentation (Goldsmith *et al.*, 1984b). By contrast, the blue tit, which is the only species investigated in this thesis which does not feed extensively on the ground, has relatively more double cones in the dorsal retina. It may be that, for this species, scanning the ground for predators is as, or more, important than aerial scanning.

CHAPTER FOUR

PREDICTING SPECTRAL SENSITIVITY FROM SPECTROPHOTOMETRIC, MICROSPECTROPHOTOMETRIC AND CONE DISTRIBUTION DATA

4. Predicting spectral sensitivity from spectrophotometric, microspectrophotometric and cone distribution data

4.1 Spectral sensitivity

Spectral sensitivity can be defined as the spectral variation of the reciprocal of the relative numbers of quanta in stimuli that evoke criterion responses (Muntz, 1972). Whilst most animals are sensitive over a range of luminances, their spectral sensitivity will vary greatly due to the number and spectral sensitivity of the photoreceptors mediating vision at the different light levels. At low light (scotopic) levels, signals from the more sensitive rods determine the animal's spectral sensitivity, whereas under bright light (photopic) conditions, the rods become saturated and, where present, one or more cone types dominate (Lythgoe, 1979). Because of the contribution of long wavelength-sensitive visual pigments, photopic spectral sensitivity often peaks at longer wavelengths than the scotopic (rod) function (λ_{max} around 500 nm in most terrestrial vertebrates). This shift in sensitivity to shorter wavelengths at low light intensities is known as the Purkinje shift (Wyszecki and Stiles, 1967) and is observed in both behavioural and electrophysiological determinations of avian spectral sensitivity (e.g. Armington and Thiede, 1956).

There will of course be intermediate light levels (mesopic illumination) at which both rods and cones would be functional and contributing to brightness assessment (Wyszecki and Stiles, 1967). Furthermore, at least in humans, rod signals under mesopic illumination affect the chromaticity (apparent saturation and hue) of a monochromatic light (Stabell and Stabell, 1996).

Spectral sensitivity is determined primarily by the wavelengths of light available for vision. For terrestrial vertebrates, including birds, the sun is the earth's main source of radiation, and has a spectral emission distribution resembling a perfect, or 'black body', radiator (Knowles and Dartnall, 1977). About 80 % of the energy reaching the earth's surface lies between 300 and 1000 nm. The maximum intensity lies a little below 500 nm. Wavelengths below 230 and 290 are absorbed by oxygen and ozone in the atmosphere respectively. At the long wavelength end, absorption by water vapour cuts out near infra-red radiation.

Within the eye, ultraviolet sensitivity is limited by absorption and scattering by the dioptric apparatus. The precise limit is largely dependent on the variable incorporation of short wavelength-absorbing pigments (generally carotenoids) into the lens and cornea (e.g. Walls and Judd, 1933; Walls, 1942; Wolbarsht, 1976; Heinermann, 1984). Short wavelengths are also subject to absorption by carotenoid pigments in the *macula lutea* (primates) and cone oil droplets (e.g. birds, reptiles and some amphibians). Because the energy of electromagnetic radiation decreases with increasing wavelength, the long wavelength limit to vision is largely determined by the minimum energy required to isomerise the chromophore and thus initiate the transduction cascade, although this threshold is dependent on temperature and the type of chromophore (Rodieck, 1973).

Finally, the number and spectral type of visual pigments employed by an animal to exploit the range of wavelengths reaching it's retina will depend on it's visual ecology (habitat, diet, activity, communication and even age) and evolutionary pedigree.

Whilst the presence of two or more photoreceptors containing spectrally distinct photopigments, and evidence that the nervous system compares the outputs of these receptors in spectrally opponent networks, is a prerequisite for colour vision, it does not constitute proof for its existence or use in a given species (Jacobs, 1993). Behavioural experiments must be performed to ascertain whether an organism can distinguish between different coloured stimuli on the basis of wavelength alone. The most important consideration in testing wavelength-specific visual ability is the elimination of brightness cues. In addition, when behavioural tests require the subject to perform an operant response, the results can be dependent on the visual task involved (Jacobs, 1993).

Evidence for colour vision in birds is derived from two main experimental paradigms: wavelength discrimination and colour mixing. Wavelength discrimination experiments test the ability of a subject to discriminate between spectrally similar monochromatic lights which are matched in intensity as perceived by the subject. Consequently, a behavioural measure of spectral sensitivity must usually be obtained prior to conducting the wavelength discrimination test. The number of minima in the wavelength discrimination function, i.e. regions of the

spectrum where the subject can discriminate very small differences in wavelength of two monochromatic stimuli, can reveal the dimensionality of the colour vision (Jacobs, 1993). Dichromats, such as the Western grey squirrel (*Sciurus griseus*), display only a single minimum, whilst trichromats, which include humans (*Homo sapiens sapiens*), display two.

Early determinations of wavelength discrimination ability in the pigeon discovered two minima in the function at about 500 and 580 nm in one experiment (Hamilton and Coleman, 1933) and 540 and 600 nm in another (Blough, 1972), both of which suggested trichromacy. Wright (1972; 1979) extended the range of wavelengths studied and observed three minima at about 500, 540 and 600 nm, suggestive of tetrachromacy. Further experiments, which extended the range of wavelengths studied into the near-ultraviolet, distinguished three definite minima at 460, 530 and 595-600 nm, and a possible minimum between 360 and 385 nm (Delius and Emmerton, 1979; Emmerton and Delius, 1980), suggesting the potential for pentachromatic colour vision. Two definite minima were observed in the wavelength discrimination function of the black-chinned hummingbird (*Archilochus alexandri*) at 555 and 585 nm (Goldsmith *et al.*, 1981). Wavelength discrimination performance deteriorated at longer wavelengths but not at the short wavelength end of the spectrum, suggesting that the colour dimensionality of this species might be more than trichromatic.

Most colour mixing experiments test an animal's ability to distinguish a mixture of two or more monochromatic lights from a monochromatic stimulus of identical intensity as perceived by the subject. Once again, the spectral sensitivity of the subject must be determined beforehand. To investigate the number of primary colour channels in the pigeon retina, Palacios *et al.* (1992) tested their ability to discriminate between a series of monochromatic stimuli, S^+ (390, 400, 450 and 520 nm) from a mixture (S^-) of two monochromatic lights on either side of each S^+. The relative contribution of the two components of S^- was varied until the dichromatic mixture was indistinguishable from S^+. In relating the observed colour matches to the effective spectral sensitivities of the pigeon's cones predicted from microspectrophotometric (Bowmaker, 1977) and electrophysiological data (Govardovskii and Zeuva, 1977; van Norren, 1975), the authors concluded that five

separate primary mechanisms, differentially active in the yellow and red fields, participated in colour discrimination. Interestingly, double cones were also treated as an additional chromatic channel.

In the middle wavelength range, all S^- combinations of 470 and 560 nm were distinguished from a 520 nm S^+, suggesting that the pigeon was more than dichromatic in this spectral region. As well as SWS and MWS single cones, the LWS double cones have their peak effective spectral sensitivity in this spectral region. Furthermore, colour mixtures in the long wavelength region (580 to 640 nm) were compatible with the involvement of double cones (peak sensitivity 575 or 589 nm, depending on the absorption of the P-type droplet) and LWS single cones filtered by an R-type droplet (peak cone effective sensitivity 619 nm). These results suggest that double cones might be used in colour vision, in addition to any other achromatic functions, raising the possibility that most birds have the potential for pentachromacy[1].

Colour mixtures in the short wavelength region of the spectrum indicated dichromatic matching by the VS (peak effective sensitivity 415 nm) and SWS (peak effective sensitivity 485 nm) cones. There was also evidence that colour discrimination was possible in the near-ultraviolet region. A S^- mixture of 350 and 430 nm could be made indistinguishable from a S^+ of 390 nm, although the contribution of the 350 nm S^- was relatively small (10 to 30 %). This suggested the involvement of an additional short wavelength mechanism, but did not exclude the possibility that it was due to absorption by the β-band of the LWS pigment in the double cones. If a dedicated UVS cone was present in addition to the VS cone, the possibility of hexachromatic colour vision in the pigeon would exist.

A similar procedure was used to establish tetrachromacy in the goldfish, *Carassius auratus* (Neumeyer and Arnold, 1989). Interestingly, goldfish were tetrachromatic under photopic illumination, but were reduced to trichromacy under mesopic conditions as the long wavelength-sensitive cone class was no longer used in colour discriminations. It is possible that such effects could also exist in birds.

---

[1] If the two members of the double cone pair ever function independently of one another, then hexachromacy is theoretically possible. However, as discussed in chapter one, there is evidence to suggest that the principal and accessory members are coupled both optically and electrically.

No behavioural tests of spectral sensitivity were performed on the species investigated during this study. However, a mathematical model, which relates receptor effective spectral sensitivity to discrimination thresholds, was used to predict the photopic spectral sensitivity of the starling, blue tit, blackbird and peacock. This approach has been used successfully with microspectrophotometric data from the pigeon and the Pekin robin to accurately replicate behavioural measures of photopic spectral sensitivity (Vorobyev and Osorio, 1998). Scotopic spectral sensitivity in the starling was also predicted from the absorption properties of the rod photoreceptors, and compared to a behaviourally-determined function (Adler and Dalland, 1959; Dalland, 1958). Data for the transmission properties of the ocular media, used in calculating receptor effective spectral sensitivity, are also presented.

4.2 Data

4.2.1 Proportions of cone photoreceptors

For the prediction of photopic spectral sensitivity using the model of Vorobyev and Osorio (1998), the relative proportions of the different classes of single cone photoreceptor used were those derived from topographic density measurements as described in chapter three. For the purposes of the model, cone abundances are expressed relative to the UVS / VS class (see Table 4.1).

Species	Cone class (single)			
	UVS / VS	SWS	MWS	LWS
Starling (*Sturnus vulgaris*)	1	1.36	3.70	3.77
Blackbird (*Turdus merula*)	1	1.71	2.14	1.89
Blue tit (*Parus caeruleus*)	1	1.90	2.67	2.67
Peacock (*Pavo cristatus*)	1	1.85	2.20	2.11

Table 4.1 Relative proportions (averages) of the different classes of single cone photoreceptor in the species for which photopic spectral sensitivity is modelled. The data are derived from topographical density measurements described in chapter three.

4.2.2 Oil droplets

For the purposes of predicting the effective spectral sensitivity of single cones in each of the species investigated, oil droplets were modelled as complete cut-off filters. This was perhaps the best compromise in modelling these organelles, the *in vivo* optical behaviour of which is largely unknown. The flat-topped character and increased apparent transmission at short wavelengths evident in many of the absorption spectra in chapter two can be attributed to 'leakage' of the measuring beam around the oil droplet (Liebman and Granda, 1975). Generally, the optical artefacts from which such measurements suffer arise when specimen absorbance exceeds the instrument's capability. Whilst most microspectrophotometers are designed to measure absorbances less than one, the absorbance of avian cone oil droplets is generally greater than this limit and can exceed 20 for the red droplets (Goldsmith *et al.*, 1984b).

At such high absorbances, it seems reasonable to assume that the red and yellow oil droplets act as complete cut off filters. The only possible exceptions are the 'colourless' or C-type oil droplets associated with SWS single cones of the three passeriform species studied. These droplets generally appeared to have lower absorptances then yellow or red droplets, or the C-type droplets of peacock SWS cones, but it is not clear whether these values represent true low concentrations of carotenoid or are simply the result of excessive light leakage (Bowmaker *et al.*, 1997). Whilst C-type droplets do contain relatively lower concentrations of carotenoid, calculated *in vivo* absorbances can be as high as 6 (Goldsmith *et al.*, 1984b). Furthermore, C-type oil droplets are generally smaller than the more densely pigmented types (chapter two) and apparent transmission of short wavelengths during microspectrophotometric measurement was more noticeable for smaller droplets of all types. Thus, it seems possible that C-type oil droplets in passerines could act as true cut-off filters, as they probably do in the peacock, especially if light leakage around them is reduced *in vivo* by the pigmented epithelium which extends to the level of the ellipsoid in the light-adapted retinae of many species (e.g. Braekevelt, 1990).

Consequently, the absorptance of oil droplets at a given wavelength shorter than the λ_{mid} was assumed to be equal to the value of the tangent to the absorptance

spectrum at λ_{mid} (which was fitted routinely for the estimation of λ_{cut}) at that wavelength, up to a maximum absorptance of 1. A similar approach was used by Vorobyev and Osorio (1998). The transparent oil droplets associated with either UVS or VS visual pigments were assumed to have no absorbance over the range of wavelengths investigated.

4.2.3 Transmission of the pre-retinal media and tissues

Before reaching the retina, electromagnetic radiation incident upon the eye must first pass through the ocular media. Spectral absorption by the cornea, aqueous humour, lens and vitreous humour must be accounted for in predicting both scotopic and photopic spectral sensitivity. In particular, absorption by the lens often determines the limits of short wavelength photosensitivity (Muntz, 1972). Short wavelength-absorbing pigments in the lens of the human eye preclude sensitivity to wavelengths below about 400 nm, which would otherwise be conferred by the short wavelength-sensitive cone pigment (Geeraets *et al.*, 1960; Wolbarsht, 1976; Griswold and Stark, 1992).

Improved sensitivity to ultraviolet wavelengths, as exhibited by birds, requires that the ocular media absorb less at short wavelengths. This is known to be the case for the pigeon (Emmerton *et al.*, 1980), Pekin robin (Maier, 1994) and domestic duck (Jane and Bowmaker, 1988). In this study, spectrophotometric measurements of the pre-retinal tissues and humours of the starling, blackbird, blue tit, peacock and turkey were made to determine the range of wavelengths likely to reach the retina.

4.2.3.1 Spectrophotometry

Absorbance measurements of the cornea, aqueous humour, lens and vitreous humour were made over the range 200 to 800 nm using a Shimadzu UV2101 PC UV-VIS scanning spectrophotometer fitted with a Shimadzu ISR-260 integrating sphere assembly to reduce the effects of light scattering by the tissue samples. Several approaches were used to determine the spectral absorption of the ocular media, the particular method primarily determined by the size of the eye. Although the ocular media of the turkey were measured, photopic spectral sensitivity was not calculated

for this species as its cone oil droplets were found to be appreciably depleted in carotenoid (cf. chapter two).

Spectral transmissions of eyes removed from the blue tit and blackbird were measured from entire eyes. A small circular 'window' was created in the posterior pole of the eye by removing a portion of the sclera opposite to, and of approximately the same size as, the cornea. Careful dissection ensured that a negligible amount of vitreous remained attached to the section of retina removed along with the sclera.

The intact eye of the blue tit was placed in a rectangular aluminium insert, designed to fit inside a standard (10 mm pathlength) quartz cuvette, in which a 6.8 mm diameter hole (the same diameter as the eye) had been drilled to coincide with the measuring beam of the spectrophotometer and in which the eye could be positioned in its normal orientation relative to the incident light. Thin plastic rings were lodged inside the insert hole in front of and behind the eye to prevent movement.

The eye of the blackbird was measured in a similar fashion, but using a modified 'cuvette'. This comprised a perspex cylinder of length 17.0 mm and internal diameter 15.8 mm, sealed at either end by glass coverslips (19 mm diameter, No. 0 thickness) held in place with silicone sealant. The internal diameter of the cylinder was reduced, using concentric rings of flexible plastic, to ensure that eyes were held perpendicular to the path of the measuring beam and did not move during measurement. Care was taken to avoid compression of the eye which would affect its pathlength.

Individual components of the ocular media were measured separately for the starling, turkey and peacock. In the case of the starling, pathlengths for the different components along the optic axis were already known (Martin, 1986). Lenses were dissected away from the anterior segment of the eye and measured using a rectangular aluminium insert identical to that used for measuring the intact blue tit eye, but with a 4.3 mm diameter hole. Corneas were excised from the sclera and measured whilst sandwiched between two stainless steel mesh inserts inside a standard cuvette. Both corneas and lenses were bathed in 340 mOsm kg^{-1} PBS, which was also placed in the identical inserts and cuvettes used as reference samples. Samples of aqueous humour were extracted from the anterior chambers of intact

eyes, using a 10 µl Hamilton syringe, and placed in a well created by sandwiching a sheet of aluminium (24 mm x 40 mm x 0.52 mm), in which a 5 mm diameter hole had been drilled to coincide with the measuring beam, between two No. 0 coverslips, using a thin ring of silicon grease as adhesive. The pathlength of this 'cuvette' was measured as 0.6 mm using precision Vernier callipers. Vitreous was removed from the vitreal body and measured in an identical fashion.

Eyes from the turkey (five week old) and peacock (one year old) were too big to measure entire, and pathlengths were easily determined from measurements of a radially sectioned eye (see section 4.2.3.2). Lenticular and corneal spectral transmissions were measured in an identical manner to the starling. The diameters of the holes in the aluminium cuvette inserts used to hold the lenses were 6.0 mm and 7.3 mm for the turkey and peacock respectively. Vitreous humour was removed from the vitreal body and placed in the hole (4.5 mm diameter) of an aluminium cuvette insert identical to that used to measure lenticular spectral transmission. The vitreous, which is a highly viscous gel, was trimmed in the insert to give a pathlength of exactly 10 mm. Aqueous humour was removed from the anterior chamber, using a hypodermic syringe, and measured in a 200 µl 10 mm pathlength quartz cuvette.

With the exception of the vitreous and aqueous humours from the starling eye and the aqueous humour from the peacock and turkey eyes, which were measured relative to distilled water, the eyes of all species, or ocular media components thereof, were bathed in, and measured relative to, 340 mOsm kg^{-1} PBS. In every case, identical inserts and cuvettes were placed in the reference channel of the spectrophotometer.

The spectrophotometer performed a single spectral pass from 800 nm to 200 nm, recording absorbance at 1 nm intervals. The spectral Full Width at Half Maximum (FWHM) bandwidth of the monochromator used by the spectrophotometer was set at 5 nm to maximise light transmission and signal-to-noise ratio which are otherwise low with the integrating sphere.

4.2.3.2 Determination of pathlengths

Eyes from blue tit and blackbird were measured entire, so no adjustment of measured pathlength was required. Absorbance measurements of both the aqueous

and vitreous humours for the starling, turkey and peacock had to be adjusted arithmetically to correspond to *in vivo* ocular pathlengths. These were already known in the starling as 1.03 mm and 3.81 mm for the aqueous and vitreous respectively, although the measurements were taken from a single bird only, (Martin, 1986).

For the peacock and turkey, these distances were determined from scaled photographs of a frozen eye, hemisected sagittally, taken from the same individual (turkey) that was used for spectrophotometry of the ocular media, or one of comparable age (peacock), sectioned using a cryostat. Eyes were frozen at -20 °C and attached to the chuck of a motor driven microtome using OCT embedding compound (BDH). The eye was orientated such that sections made by the cryostat were parallel to the optic axis, and 10 μm sections were made at -20 °C until the edge of the lens was visible. Photographs of the eye, and a scale ruler positioned adjacent to the cut face of the eyeball, were then taken after every 10 sections, approximately 0.1 mm intervals (Figure 4.1). The negatives obtained were projected with a magnification of approximately ×13 using a photographic enlarger and the pathlengths of the aqueous and vitreous calculated according to the scale ruler.

Expansion of the eye upon freezing should not have an appreciable effect on the calculated pathlengths. If the eye of the turkey is modelled as a cylinder 17 mm in height with a fixed diameter of 21 mm, and assuming that the thermal expansivity of the aqueous and vitreous humours is identical to that of water, the height of the cylinder (total pathlength along the optic axis of the eye) would increase by only 0.08 mm at a temperature of -20 °C relative to the same structure at +20 °C. This increase in pathlength due to freezing (approximately 0.5 %) was less than the likely error in estimating the pathlengths by measuring an enlarged photograph (±1.4 to 5.3 %). The pathlengths of the aqueous and vitreous humours were determined, respectively, to be 2.7 mm and 10.4 mm in the turkey, and 3.2 mm and 10.6 mm in the peacock. Measured absorbances for the aqueous and vitreous (pathlengths 0.6 mm for the starling and 10 mm for the turkey and peacock) were scaled appropriately, summed with the absorbance data for the cornea and lens, and the combined absorbances converted to transmission for display (see section 4.2.3.3).

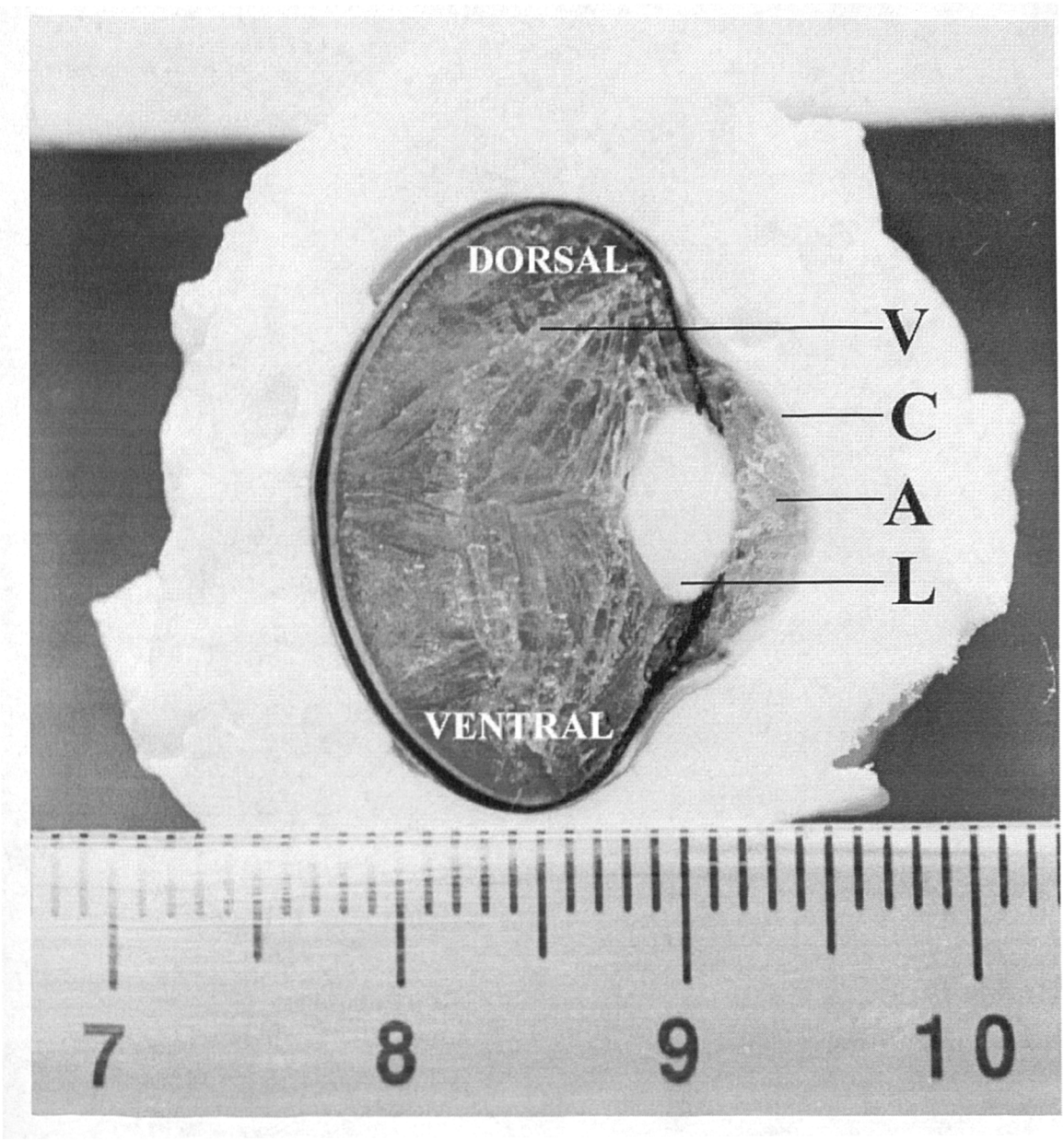

Figure 4.1 Photograph of an eye of a juvenile domestic turkey, *Meleagris gallopavo*, hemisected sagitally and parallel to the optic axis. C, cornea; A, aqueous humour; L, lens; V, vitreous humour. The calculated pathlengths of the aqueous and vitreous were 2.7 mm and 10.4 mm respectively. The graduations on the scale ruler are in mm.

4.2.3.3 Transmission spectra

Transmission spectra of the pre-retinal ocular media for the starling, blackbird, blue tit, peacock and turkey are displayed in Figure 4.2 to Figure 4.6. On the assumption that apparent absorbance by the combined ocular media at 800 nm was due only to light scattering (Geeraets *et al.*, 1960; van den Berg and Spekreijse, 1997), transmission was assumed to be unity at this wavelength, and all measurements were scaled relative to an absorbance of zero at 800 nm. All spectra were fitted with an 11-point unweighted running average to smooth random noise in the data. A number of smoothed spectra, obtained either from different individuals (starling) or multiple scans from the same individuals (all other species), were averaged together for display. All of the species investigated in this study have ocular media which transmit well into the near ultraviolet. Wavelengths of 50 % transmission were 338, 343, 317, 338 and 358 nm for the starling, blackbird, blue tit, peacock and turkey respectively.

Some of the differences in ocular media transmission apparent between species may be measurement artefacts. Transmission losses due to reflections at surfaces between the different ocular media cannot be quantified when the individual components are measured separately, but are incorporated when the transmission of the intact eye is measured, as was the case for the blue tit and blackbird. Furthermore, the degree of absorption and scattering by the retinal layers vitread to the photoreceptors is unknown for the species studied and thus not incorporated into the calculations of photoreceptor effective spectral sensitivity (Table 4.2). It is assumed that these losses are negligible compared to those imposed by the dioptric apparatus. Apart from the turkey and peacock, which were both one year old or less, the age of the other species was not determined. However, whilst age is known to affect the transmission properties of the human lens (Wolbarsht, 1976), no such correlation has been established for avian ocular media (Hodos *et al.*, 1991).

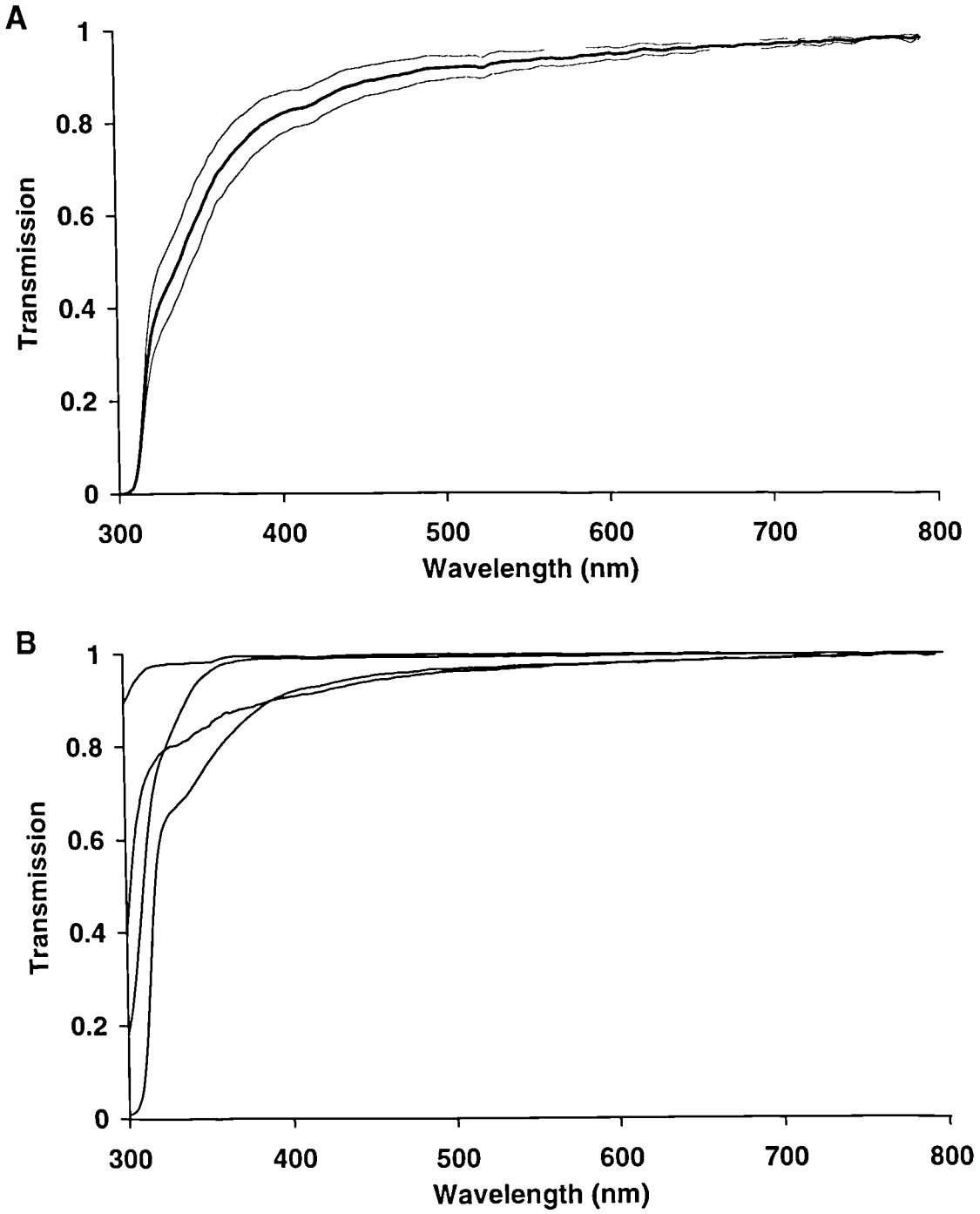

Figure 4.2 Ocular media of the European starling (*Sturnus vulgaris*) corrected for *in vivo* pathlengths as measured by Martin (1986). (**A**) Calculated transmission (thick line) ± standard deviation (thin lines) of the combined ocular media. The mean wavelength of 50 % transmission is 338 nm. (**B**) Mean transmission spectra (in order of increasing transmission at 300 nm) of the lens (n = 5 individuals), aqueous humour (n = 1), cornea (n = 4) and vitreous humour (n = 1).

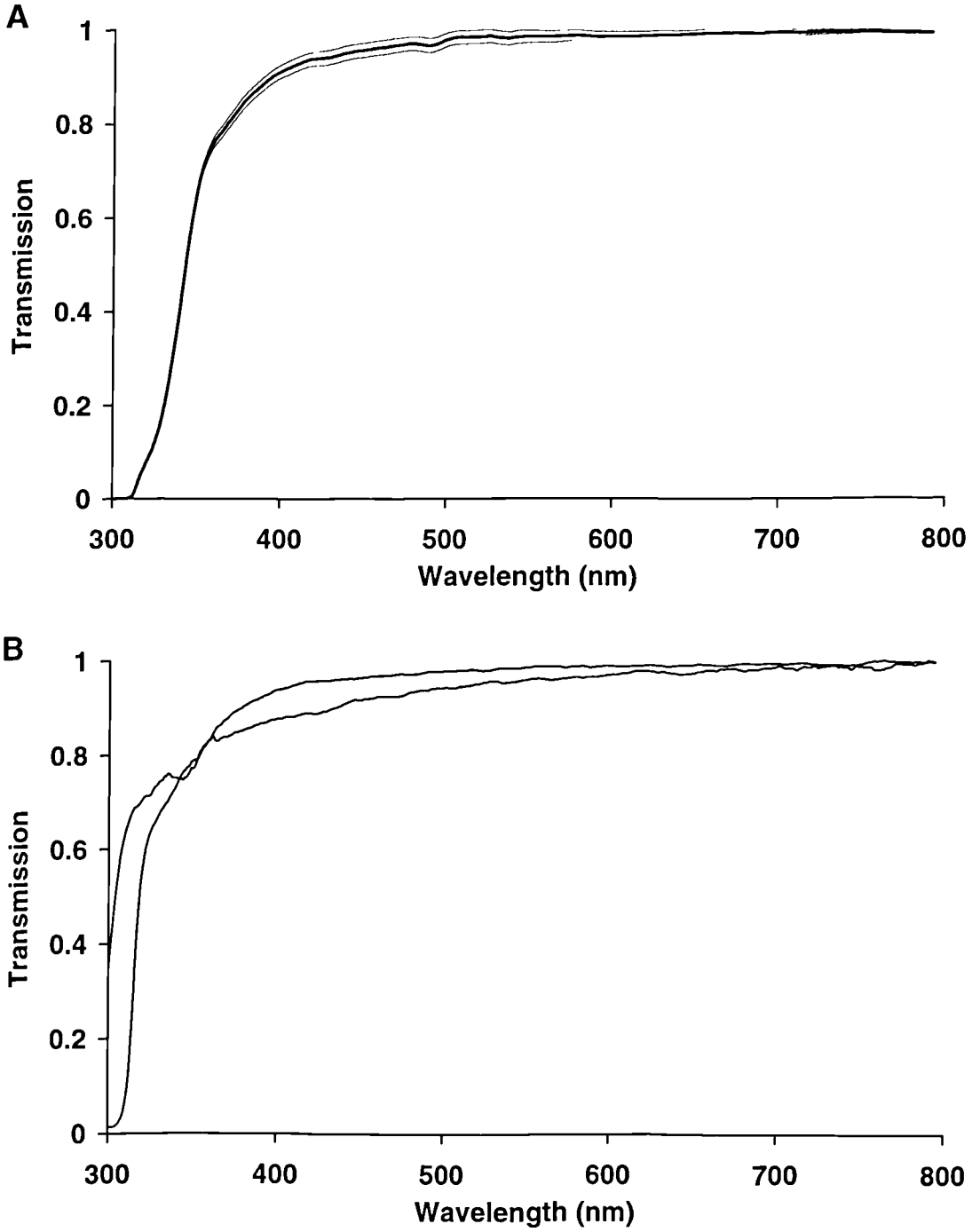

Figure 4.3 Ocular media of the blackbird (*Turdus merula*). (**A**) Mean transmission of the intact eye (thick line) ± standard deviation (thin lines) derived from three measurements of the same individual. The mean wavelength of 50 % transmission is 343 nm. (**B**) Transmission spectra (in order of increasing transmission at 300 nm) of the lens (n = 1 individual) and cornea (n = 1).

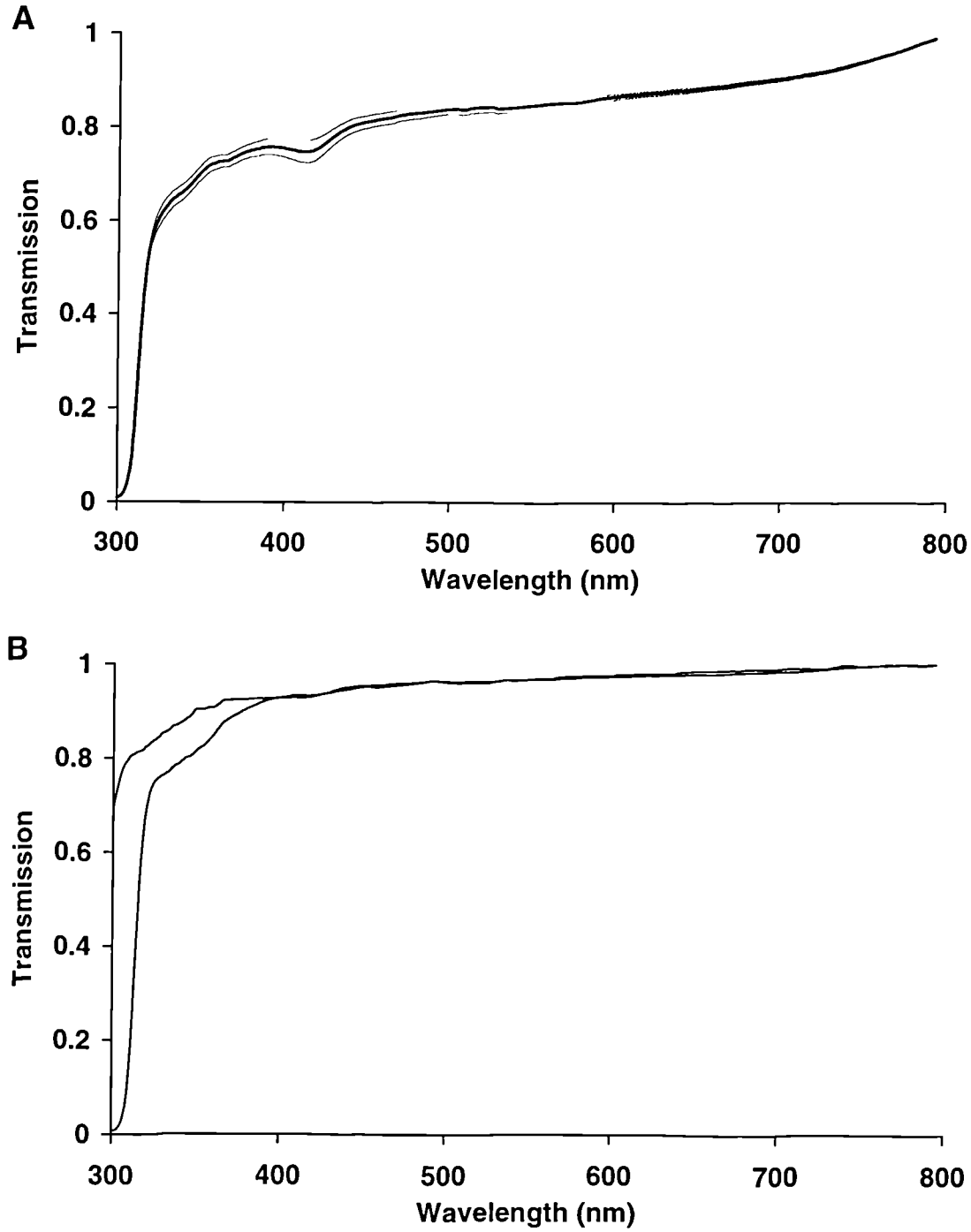

Figure 4.4 Ocular media of the blue tit (*Parus caeruleus*). (**A**) Mean transmission of the intact eye (thick line) ± standard deviation (thin lines) derived from four measurements of the same individual. The mean wavelength of 50 % transmission is 317 nm. (**B**) Transmission spectra (in order of increasing transmission at 300 nm) of the lens (n = 1 individual) and cornea (n = 1).

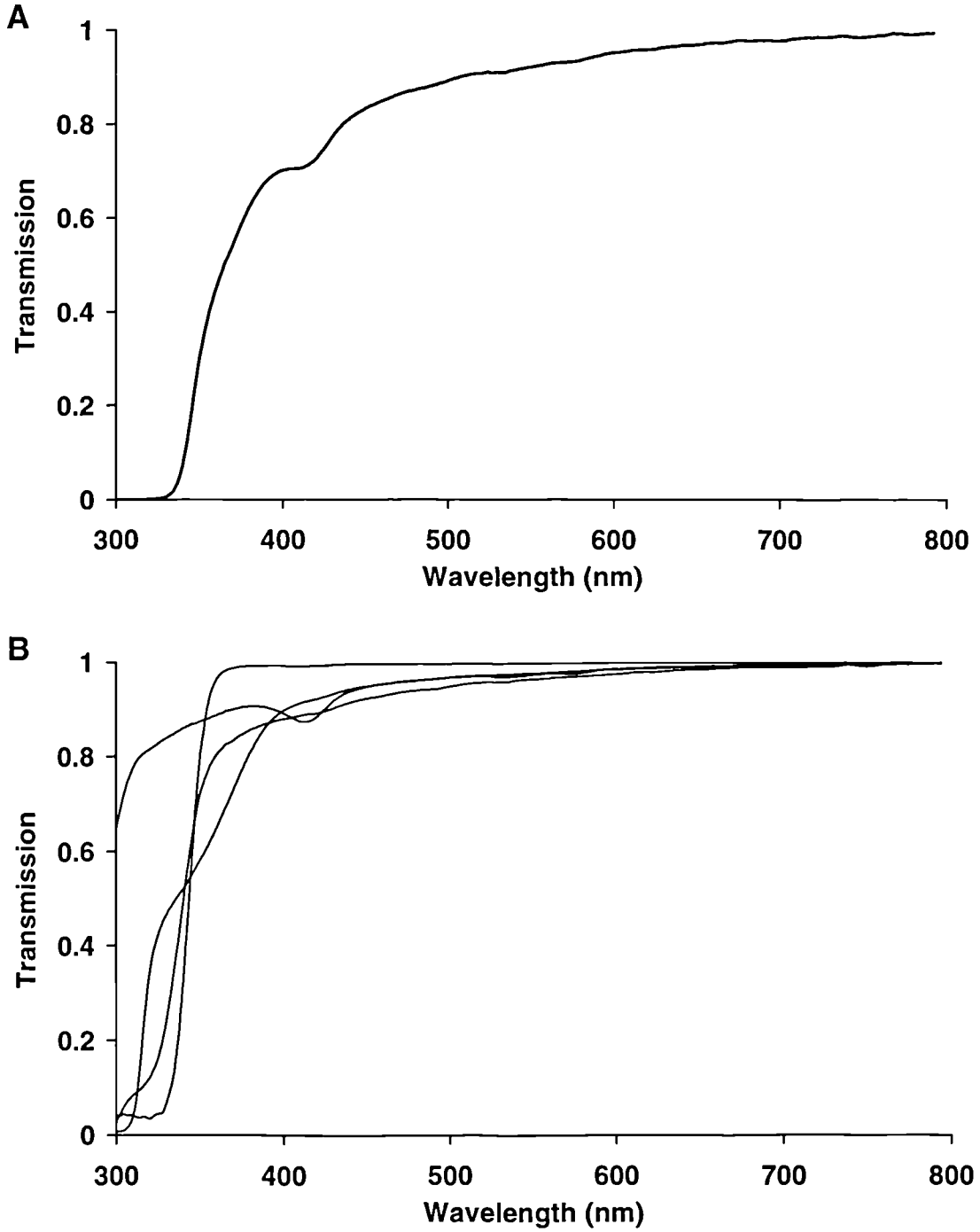

Figure 4.5 Ocular media of the peacock (*Pavo cristatus*) corrected for *in vivo* pathlengths as determined in section 4.2.3.2. (**A**) Calculated transmission, on the optic axis of the eye, of the combined ocular media. The wavelength of 50 % transmission is 338 nm. (**B**) Transmission spectra (in order of increasing transmission at 325 nm) of the aqueous humour (n = 1 individual), cornea (n = 1), lens (n = 1) and vitreous humour (n = 1).

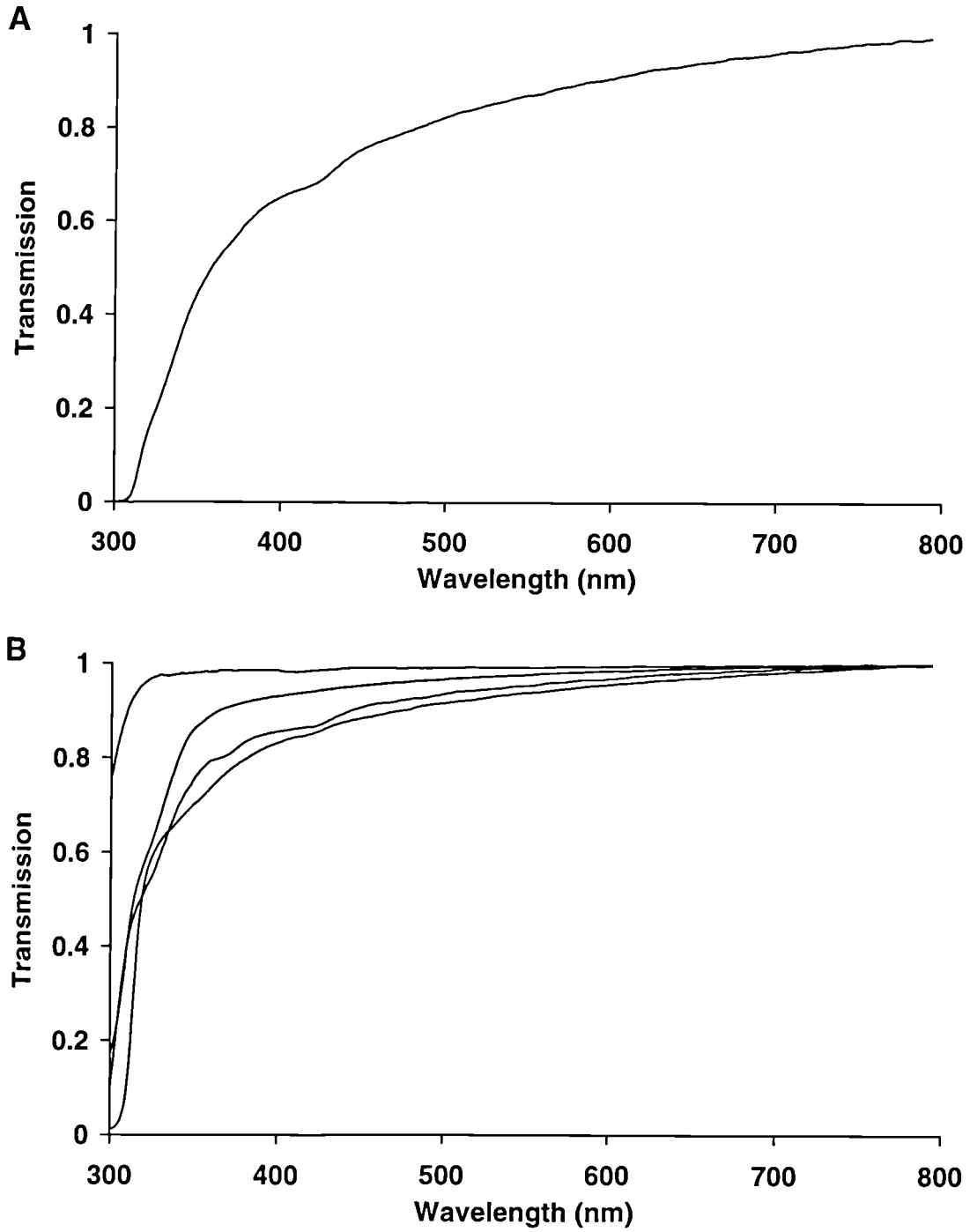

Figure 4.6 Ocular media of the turkey (*Meleagris gallopavo*) corrected for *in vivo* pathlengths as determined in section 4.2.3.2. (**A**) Calculated transmission, on the optic axis of the eye, of the combined ocular media. The wavelength of 50 % transmission is 358 nm. (**B**) Transmission spectra (in order of increasing transmission at 400 nm) of the lens (n = 1 individual), cornea (n = 1), aqueous humour (n = 1) and vitreous humour (n = 1).

4.2.4 Templates for visual pigment absorbance spectra

4.2.4.1 Why use a template?

For modelling spectral sensitivity, templates describing visual pigment absorbance spectra were used in preference to data obtained by microspectrophotometry. Primarily, this was because template absorbance spectra are created by mathematical functions and are free of both the intrinsic and extrinsic noise which pervades microspectrophotometric measurements. Templates can also provide absorbance data over a wider range of wavelengths than that routinely measured in microspectrophotometry. Furthermore, microspectrophotometers cannot measure accurately small absorbances by the visual pigment at long wavelengths; templates derived from behavioural or electrophysiological spectral sensitivity provide a better estimate of long wavelength sensitivity (e.g. Bernard, 1987; Lamb, 1995; Palacios *et al.*, 1996).

4.2.4.2 Templates and transformations

Dartnall (1953) proposed that the normalized absorbance spectrum of vitamin A_1-based visual pigments, when plotted on an abscissa of frequency rather than the customary wavelength scale, might have an invariant shape regardless of the spectral location of the λ_{max} of the α-band ($\lambda_{max,\alpha}$). The frequency, v of electromagnetic radiation is related to its wavelength, λ, measured *in vacuo*, by the expression:

$$v = \frac{c}{\lambda} \qquad \textbf{Equation 1}$$

where λ is in m, v is in Hertz and c is the velocity of light in a vacuum, i.e. 2.998×10^8 m s^{-1}. Frequency was traditionally expressed in wave numbers, $\bar{v}$ cm^{-1}, where:

$$\bar{v} = \frac{1}{\lambda} \qquad \textbf{Equation 2}$$

and wavelength is in cm. Dartnall transformed the wavelength abscissa to frequency such that wave number was expressed as a frequency difference, $\Delta\bar{v}$, relative to the frequency at the λ_{max}, thus:

$$\Delta\bar{\nu} = \frac{1}{\lambda} - \frac{1}{\lambda_{max}}$$ **Equation 3.**

He then created a visual pigment template relating the relative absorbance at a given wavelength to the absorbance at the α-peak λ_{max} and expressed this template in the form of a nomogram (alignment chart). However, the initial standard absorbance spectrum for frog rhodopsin (λ_{max} = 502 nm) used to create this original nomogram was later found to be contaminated by a second rod pigment (λ_{max} = 433 nm) present in the retina at much lower concentrations (Dartnall, 1967; Knowles and Dartnall, 1977). In addition, Dartnall's nomogram was only valid for visual pigments with λ_{max} values that were close to 500 nm and exhibited systematic deviations from visual pigment absorbance spectra with maximum sensitivity to shorter or longer wavelengths (Liebman and Entine, 1968; Ebrey and Honig, 1977).

Ebrey and Honig (1977) extended the concept of the template as new data became available. Using absorbance data from frog 'green' rods (λ_{max} 431 nm, Liebman and Entine, 1968), frog 'red' rods (λ_{max} 502 nm, Dartnall, 1953) and the long wavelength-sensitive cone pigment of the chicken (λ_{max} 562 nm, Wald *et al.*, 1955) they formulated three different templates (and associated nomograms) for visual pigments maximally sensitive to short, medium and long wavelengths, whilst retaining the Dartnall frequency transform.

Dawis (1981) refined the concept of visual pigment templates by deriving eighth-degree polynomials from published nomograms. This approach, however, did not obviate the constraints imposed by the Dartnall frequency transform. Three separate polynomials were recommended for visual pigments maximally sensitive to short (410 to 470 nm), medium (470 to 530 nm) and long (530 to 610 nm) wavelengths. An alternative method was used by Hárosi (1976) who derived the parameters for three Gaussian functions, sequentially fitted to frequency-transformed data, the sum of which accurately described the absorbance spectra of vitamin A_2-based visual pigments.

Analysing the microspectrophotometric data of Bowmaker *et al.* (1980), Barlow (1982) observed that the shapes of both short and long wavelength-sensitive visual pigments were rendered invariant when the wavelength abscissa was

transformed as the fourth root of wavelength, i.e. $\lambda^{0.25}$. Barlow's method, which replaced the triple nomogram of Ebrey and Honig (1977), superimposes normalized visual pigment absorbance spectra when the transform is expressed relative to the α-peak λ_{max}:

$$\lambda^{0.25} - \lambda_{max}^{0.25} \qquad \textbf{Equation 4.}$$

This abscissal transform was quickly superseded by a simpler solution proposed by Mansfield (1985) and MacNichol (1985; 1986). It followed the quantum mechanical considerations of Dartnall (1953) by expressing normalized absorbance spectra as functions of frequency, v, relative to peak frequency, v_{max}, i.e.

$$\frac{v}{v_{max}} \qquad \textbf{Equation 5.}$$

Because frequency is proportional to the reciprocal of the wavelength (equation 1) this corresponds to:

$$\frac{\lambda_{max}}{\lambda} \qquad \textbf{Equation 6}$$

and has become known as the Mansfield-MacNichol (MM) transform.

Partridge and DeGrip (1991) used the MM transform on the absorbance spectrum of purified bovine rhodopsin to create a new template for rhodopsin (vitamin A_1-based) visual pigments. The relationship between λ_{max} and the value of the normalized absorbance, D, at a wavelength, λ, on the long wavelength limb ($0.2 \leq D \leq 0.8$) was given by the following cubic function:

$$\lambda_{max} = \lambda\left(0.84628 + 0.20749D - 0.19932D^2 + 0.12486D^3\right) \qquad \textbf{Equation 7.}$$

The authors also calculated a Chebyshev polynomial which accurately described the template and could be used to generate visual pigment absorbance curves mathematically. However, the Chebyshev polynomial only described the alpha band of the absorbance spectrum.

The rhodopsin template used in this study is that derived by Stavenga *et al.* (1993) from the MM-transformed bovine rhodopsin absorbance data of Morton (1972) and Partridge and DeGrip (1991). Their approach characterised each of the

major absorption bands (α, β and γ) of the visual pigment by a modified lognormal function (Metzler and Harris, 1978):

$$D_{\lambda,i} = D_{max,i}\exp\left[-a_{0,i}x_i^2\left(1 + a_{1,i}x_i + a_{2,i}x_i^2\right)\right] \qquad \textbf{Equation 8}$$

where D_λ is absorbance at a given wavelength λ; the subscript i denotes the absorption band (α, β or γ); $A_{max,i}$ is the absorbance at the $\lambda_{max,i}$; $x_i = {}^{10}\log\left(\frac{\lambda}{\lambda_{max,i}}\right)$; $a_{0,i}$, $a_{1,i}$ and $a_{2,i}$ are coefficients characteristic of the *i*th absorption band, and $a_{2,i} = \frac{3a_{1,i}^2}{8}$. The absorbance of the visual pigment, D, is then the sum of the three individual functions:

$$D(\lambda) = \sum_i D_{\lambda,i}(\lambda) = D_{\lambda,\alpha}(\lambda) + D_{\lambda,\beta}(\lambda) + D_{\lambda,\gamma}(\lambda) \qquad \textbf{Equation 9.}$$

4.2.4.3 Shifting the β-band

The model of Stavenga *et al.* (1993) assumed that the spectral location, shape and relative absorbance of the β- and γ-bands were constant, irrespective of the position of the α-peak. This assumption would be adequate for visual pigments with maximum sensitivity to medium or long wavelengths where the visual pigment λ_{max} and the wavelength of maximum absorbance of the α-band ($\lambda_{max,\alpha}$) coincide (see Figure 4.7 A). However, with the spectral location of the β-peak fixed at 340 nm (Stavenga *et al.*, 1993), the effect of absorption by the β-band on visual pigments maximally sensitive to short wavelengths will be to shift the visual pigment λ_{max} to a shorter wavelength relative to the α-band $\lambda_{max,\alpha}$ and to increase the full width half maximum (FWHM) bandwidth and apparent absorbance of the short wavelength limb of the α-band (see Figure 4.7 B). This phenomenon would not only affect the fitting of templates to experimental visual pigment absorbance data using the polynomial of Partridge and DeGrip (1991) as described in chapter two, but would also over-estimate the sensitivity of short wavelength-sensitive visual pigments to short wavelengths.

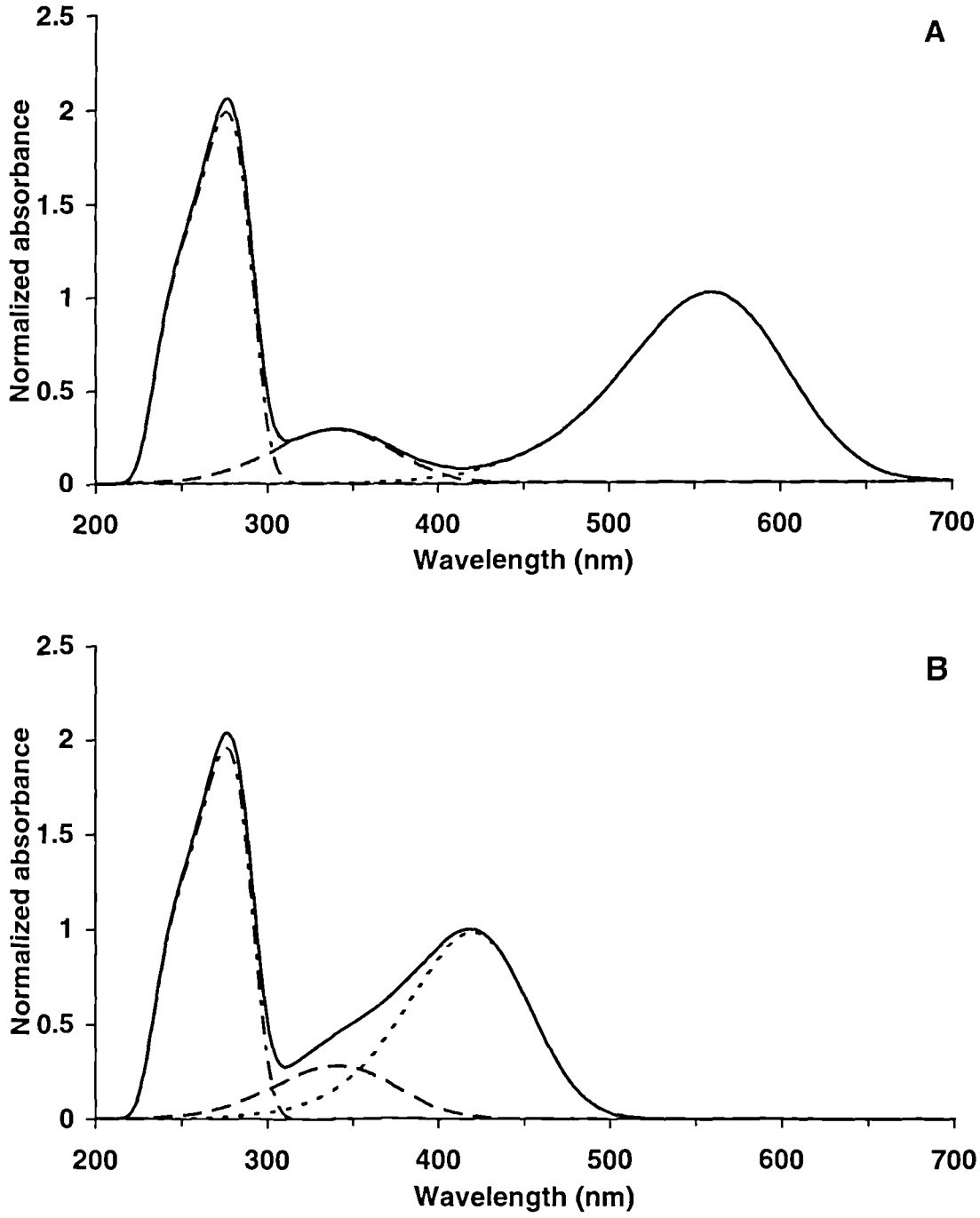

Figure 4.7 Examples of the rhodopsin (vitamin A_1-based) visual pigment template given by Stavenga *et al.* (1993). The rhodopsin absorbance spectrum (solid line) is the sum of the α-, β- and γ-bands, each derived from a lognormal function (dotted, dashed and dash-dot lines, respectively). With an alpha band $\lambda_{max,\alpha}$ of 560 nm (**A**) the λ_{max} of the template and the $\lambda_{max,\alpha}$ of the α-band coincide. At lower $\lambda_{max,\alpha}$ values, e.g. with an alpha band $\lambda_{max,\alpha}$ of 420 nm (**B**), and with the spectral location of the β-peak fixed at 340 nm, the template λ_{max} is shifted to shorter wavelengths than the α-band $\lambda_{max,\alpha}$ as overlap with the β-band becomes increasingly significant. Note also the resultant increase in template FWHM bandwidth relative to the α-band. The data have been normalized to the absorbance at the template λ_{max}.

Recent electrophysiological evidence suggests that the spectral location of the β-band is dependent upon the position of the α-peak in both vitamin A_1- and A_2-based visual pigments (Palacios *et al.*, 1996; Palacios *et al.*, 1998). In these studies, spectral sensitivity over the range 277 to 697 nm was determined in the fish *Danio aequipinnatus* (Cyprinidae) by recording photocurrents with suction pipette electrodes and revealed that the β-band of cone pigments is found at longer wavelengths as the α-band shifts towards the long wavelength end of the spectrum. Consequently, visual pigments with maximum sensitivity to short wavelengths will exhibit less overlap in spectral absorption by the α- and β-bands and the $\lambda_{max,\alpha}$ of the α-band will correspond to the λ_{max} of the visual pigment over a wider range of wavelengths extending towards the short wavelength end of the spectrum.

To quantify this trend, the spectral locations of the α- and β-peaks measured in the three longer-wave-sensitive visual pigments of *Danio* (Palacios *et al.*, 1996) were combined with the data for bovine rhodopsin (Morton, 1972; Stavenga *et al.*, 1993) and subjected to a reduced major axis regression (Fowler and Cohen, 1990). This analysis provided a function which predicts the λ_{max} of the β-band ($\lambda_{max,\beta}$) from the $\lambda_{max,\alpha}$ of the α-band for vitamin A_1-based visual pigments:

$$\lambda_{max,\beta} = 0.405269354\left(\lambda_{max,\alpha}\right) + 134.360016 \qquad \textbf{Equation 10.}$$

This relationship was introduced into the model of Stavenga *et al.* (1993) for creating visual pigment absorbance spectra templates. Spectral sensitivity data obtained from amphibian rod photoreceptors containing vitamin A_1-based visual pigment were not incorporated in the regression analysis because they appear to have a narrower full width half maximum (FWHM) spectral bandwidth than other vertebrate vitamin A_1-based visual pigments when transformed as λ_{max} / λ (Palacios *et al.*, 1998). The λ_{max} of the γ-band appears to be independent of the spectral location of the α-band $\lambda_{max,\alpha}$ (Palacios *et al.*, 1996) and its position is fixed at 276 nm (Stavenga *et al.*, 1993).

Palacios *et al.* (1996) also suggested that the photosensitivity of the β- and γ-bands relative to the α-band might be dependent on the spectral location of the α-band $\lambda_{max,\alpha}$. In the present thesis, their data were best-fitted with quadratic functions

using a non-linear regression software package (CurveExpert 1.2) such that the photosensitivity (K) of the β- and γ-bands relative to the α-band are related to the position of the α-band $\lambda_{max,\alpha}$ as follows:

$$K_\beta = -5.0268421 + 0.021121711(\lambda_{max,\alpha}) - 2.0970395 \times 10^{-5}(\lambda_{max,\alpha})^2$$

Equation 11

$$K_\gamma = -16.635088 + 0.070522661(\lambda_{max,\alpha}) - 7.0815058 \times 10^{-5}(\lambda_{max,\alpha})^2$$

Equation 12

where $407 < \lambda_{max,\alpha} < 587$ nm.

For the prediction of spectral sensitivity, photosensitivity data for the different photoreceptor types should be used in preference to template spectra, which are generally based on absorbance measurements (e.g. Stavenga *et al.*, 1993). Although limited evidence suggests that the photosensitivity of the α- and β-bands corresponds to their spectral absorption, photosensitivity in the γ-band is considerably less quantum efficient (Dartnall, 1972). Consequently, the relative photosensitivity coefficients (K_β and K_γ), adjusted for the spectral location of the α-band $\lambda_{max,\alpha}$ using equations 10 and 11, were used in preference to the relative extinction coefficients ($A_{max,\beta}$ and $A_{max,\gamma}$) for the prediction of spectral sensitivity. Nevertheless, $A_{max,\beta}$ and $A_{max,\gamma}$ were used at the values determined for bovine rhodopsin (Stavenga *et al.*, 1993) in the analysis of visual pigment absorbance data as described in chapter two.

It should be noted, however, that both of these alterations to the short wavelength region of visual pigment templates described by the model of Stavenga *et al.* (1993) will affect the prediction of spectral sensitivity very little after the effect of filtering by the ocular media and cone oil droplets is taken into consideration.

4.2.4.4 Long wavelength tails

Of more significance for the prediction of spectral sensitivity is the failure of the modified lognormal functions of Stavenga *et al.* (1993) to adequately describe long wavelength absorbance by the visual pigment. Absorbance in the far-red is very low and difficult to determine spectrophotometrically. It is better approximated from

sensitivity measurements and, aware of the shortcomings of their model, Stavenga *et al.* (1993) provided a log-linear function which described the photosensitivity, S, of the long wavelength limb of rods and cones based on electrophysiological measurements of primate photoreceptors, thus:

$$\log S = s\left(x_\alpha - x_0\right) \qquad \textbf{Equation 13}$$

where

$$x_\alpha = {}^{10}\log\left(\frac{\lambda}{\lambda_{max}}\right) \qquad \textbf{Equation 14}$$

and slope $s = -50.9$ and $x_0 = 0.047$ (cones); $s = -48.2$ and $x_0 = 0.046$ (rods). This long wavelength tail 'patch' was implemented above $x_\alpha = 0.080$ for cones and $x_\alpha = 0.078$ for rods, and very closely resembles the long wavelength region of the rhodopsin α-band template of Lamb (1995) which was derived from electrophysiological and psychophysical data (see Figure 4.8 A, B and C). The long wavelength tail patch was only used for the prediction of spectral sensitivity and not in the analysis of MSP data where the absorbance values in this range are less than the noise of individual recordings and, being below 20 % of maximum absorbance, are not used in estimating the λ_{max}.

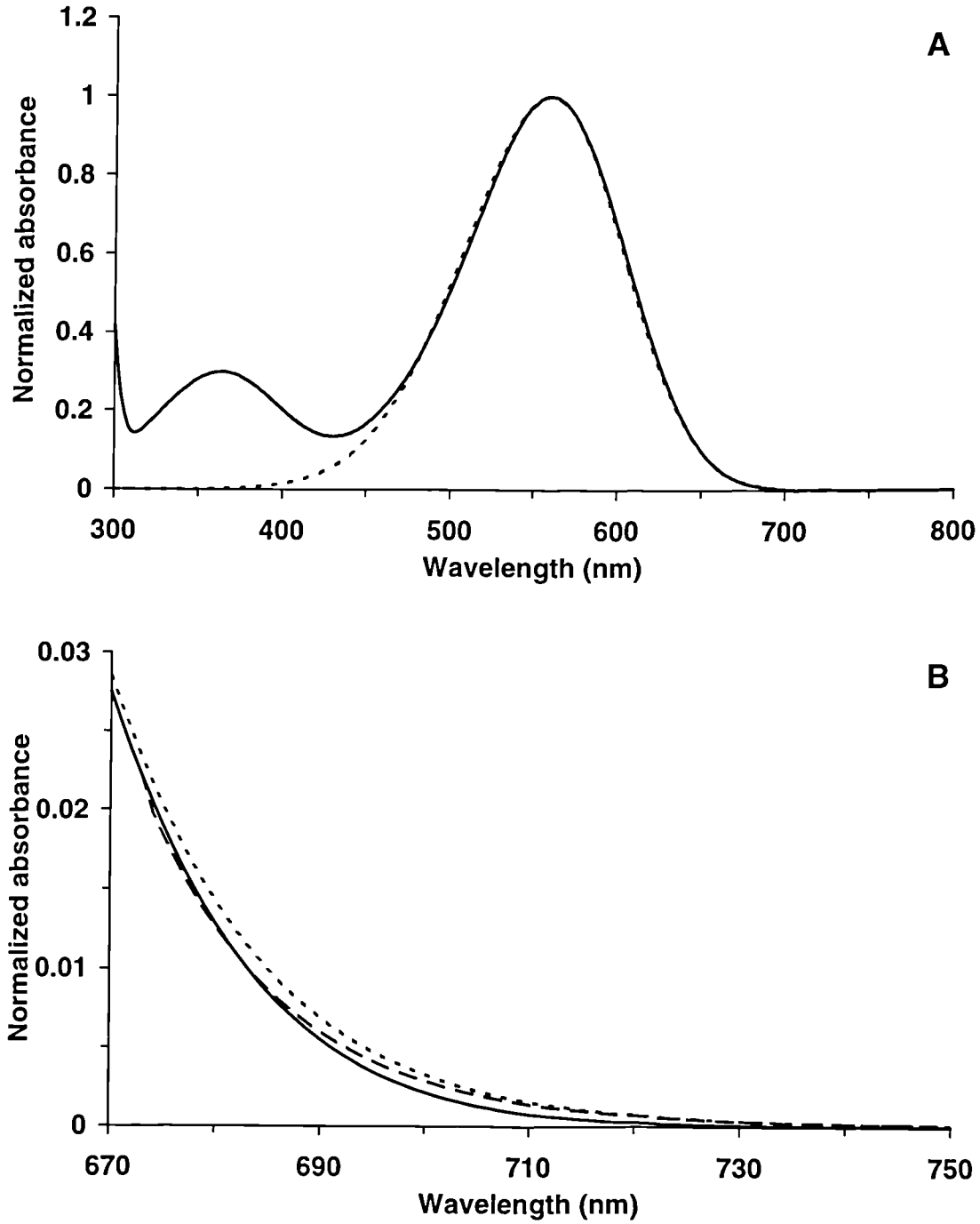

Figure 4.8 The rhodopsin template given by Stavenga *et al.* (1993) with (dashed line) and without (solid line) the long wavelength tail patch for cone visual pigment data (see section 4.2.4.4). Also displayed is the α-band only rhodopsin template given by Lamb (1995, dotted line). In (**A**) the added tail is not discernible, but the similarity between the α-bands described by Stavenga *et al.* (1993) and Lamb (1995) is clear. Under closer inspection of the long wavelength limb (**B**) the template incorporating the long wavelength tail patch is seen initially to have a lower absorbance than the original template it replaces (here it replaces the lognormal functions at 674 nm) but towards longer wavelengths the log-linear patch resembles the template given by Lamb (1995). All three templates have their λ_{max} at 560 nm and are normalized at this point.

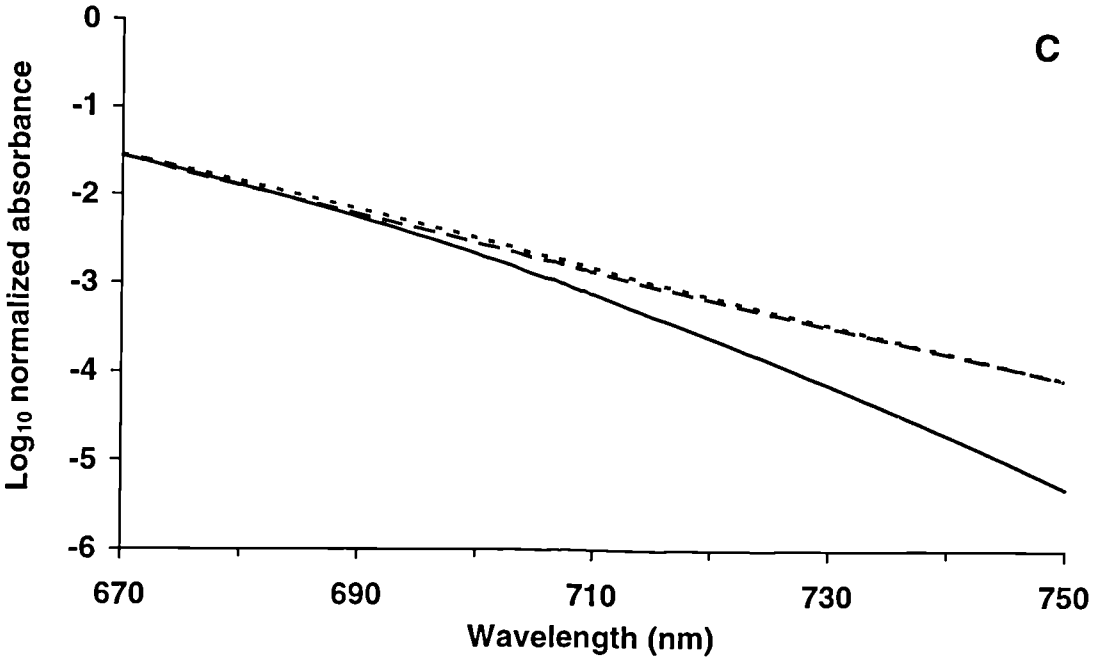

Figure 4.8 (continued) (**C**) The normalized absorbance values displayed in **Figure 4.8** (**B**) were transformed as $\log_{10}$ to express the difference between the long wavelength limbs on a photosensitivity basis. The rhodopsin template given by Stavenga *et al.* (1993) with (dashed line) and without (solid line) the long wavelength tail patch for cone visual pigment data (see section 4.2.4.4). Also displayed is the α-band only rhodopsin template given by Lamb (1995, dotted line).

4.2.4.5 Ultraviolet visual pigment templates

It is evident that the FWHM bandwidth, which displays a linear dependence on peak wavenumber $(\lambda_{max})^{-1}$ for visual pigments with λ_{max} values greater than at least 408 nm, is narrower than expected in the case of UVS visual pigments (λ_{max} 340-370 nm, Bowmaker *et al.*, 1980; Hárosi, 1987; Hárosi, 1994; Hawryshyn and Hárosi, 1991; Palacios *et al.*, 1996). Nevertheless, it appears that vitamin A_1-based UVS pigments from widely separated taxa have the same FWHM bandwidth when transformed as λ_{max} / λ. With this in mind, Palacios *et al.* (1996) provided new coefficients for the lognormal functions given by Stavenga *et al.* (1993) to describe the absorbance spectra of vitamin A_1-based UVS pigments.

Caution should be exercised in inferring visual pigment absorbance from photosensitivity data, even if measured from single cells. A constant quantum efficiency for the α-, β- and γ-bands must be assumed (Dartnall, 1972) and the effects of 'self-screening' by the visual pigment must be considered (Goldsmith, 1978). However, the new coefficients derived by Palacios *et al.* (1996) were based partly on the MSP absorbance data from zebrafish (*Brachydanio rerio*) UVS cones given by Robinson *et al.* (1993).

Adoption of these new coefficients in the present study necessitated the calculation of new parameters, for use with UVS visual pigments, for the long wavelength tail patch proposed by Stavenga *et al.* (1993). Palacios *et al.* (1996) provided the coefficients for an eighth degree polynomial (template) which fitted the invariant shape of normalized log spectral sensitivity data from various UVS photoreceptors when plotted on a frequency (λ_{max} / λ) scale. To obtain the new parameters, an 80 nm section (397 to 477 nm) of the linear region of the long wavelength limb given by the polynomial of Palacios *et al.* (1996) was fitted (CurveExpert 1.2) with the same linear function (equation 13, section 4.2.4.4) specified by Stavenga *et al.* (1993). Parameters for the new long wavelength tail patch were thus determined to be: slope, $s = -49.1$ and $x_0 = 0.027$. The patch was implemented above $x_\alpha = 0.047$ (equation 14, section 4.2.4.4) and was used, in conjunction with the function shifting the spectral location of the β-band (equation 10, section 4.2.4.3) to predict the spectral sensitivity of UVS cones. Relative

photosensitivities of the β- and γ-bands were set at those determined for the SWS visual pigment in each species (equations 11 and 12, section 4.2.4.3). The long wavelength tail patch greatly improves the 'fit' of the template to the spectral sensitivity data at longer wavelengths (see Figure 4.9).

4.2.4.6 Pathlengths and specific absorbance

Assuming a constant quantum efficiency, the spectral sensitivity of a photoreceptor is a function of the absorptance of its outer segment. This can be determined if the length of the outer segment (pathlength) and the concentration of the visual pigment (specific absorbance) are known. For the purposes of predicting spectral sensitivity, the lengths of avian cone and rod outer segments were assumed to be 10 μm and 20 μm respectively (Braekevelt, 1990; 1993b; 1994a; 1994b; Braekevelt *et al.*, 1996). Specific absorbance, i.e. the absorbance per micrometre length of the photoreceptor viewed end-on (Knowles and Dartnall, 1977), was taken to be 0.015 μm^{-1} for cones and 0.018 μm^{-1} for rods (Bowmaker, 1977; Bowmaker and Knowles, 1977).

Neither of these two parameters were calculated from the microspectrophotometric data obtained for each species. Cone outer segments were often folded over upon themselves or were otherwise misshapen, and thus dimensional measurements were unreliable. Consequently it was difficult to assess both the diameter (and hence approximate transverse pathlength) and the length of the outer segment. Rod outer segments were usually fragmented, but their diameter was almost invariably 3 μm. Inspection of the data in chapter two reveals that the absorbance change at the λ_{max} of the difference spectrum for rods in the four species varied from 0.023 to 0.039 (mean 0.033). This corresponds to a specific absorbance of 0.011 μm^{-1}, but it is possible that this figure was low due to incomplete bleaching of the rods. However, due to the relatively short pathlength of avian photoreceptors, self screening will be minimal (Warrant and Nilsson, 1998) and absolute values will affect the overall shape of the scotopic or photopic spectral sensitivity function relatively little.

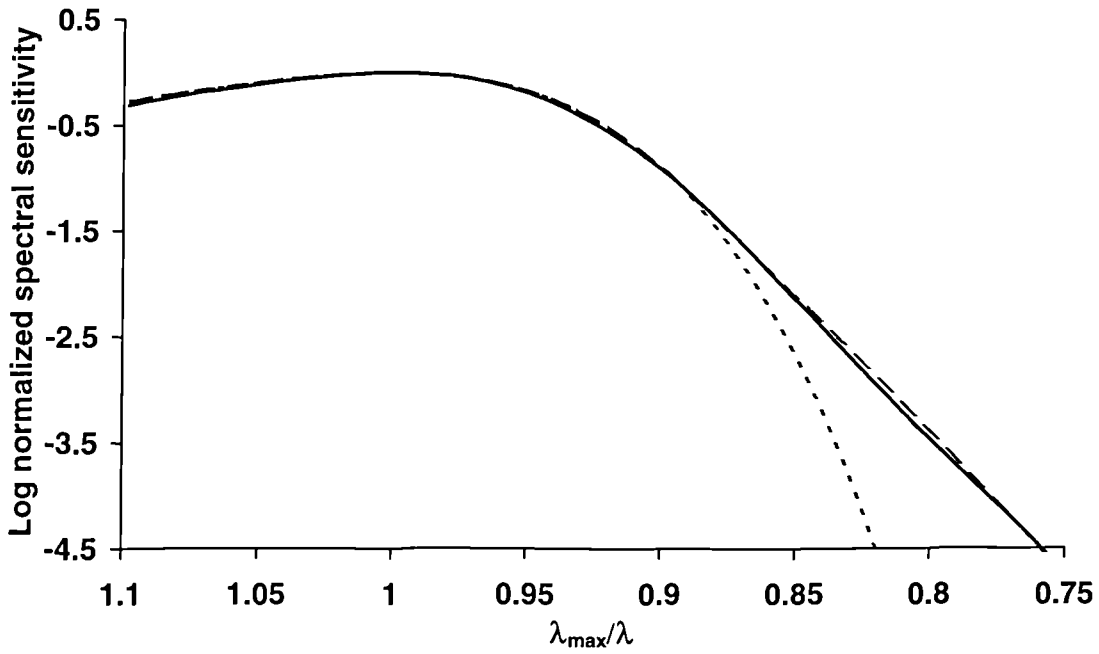

Figure 4.9 Predicted spectral sensitivity curves for UVS visual pigments using the rhodopsin template of Stavenga *et al.* (1993), modified using the α-band coefficients for UVS pigments given by Palacios *et al.* (1996), with (dashed line) and without (dotted line) the long wavelength tail patch for UVS cone pigments (see section 4.2.4.5). Also displayed is the polynomial given by Palacios *et al.* (1996) which describes the spectral sensitivity of UVS pigments determined from electrophysiological and microspectrophotometric data (solid line). Rhodopsin template spectra are based on a cone 5 μm long (Hárosi and Hashimoto, 1983) containing a UVS pigment (λ_{max} 358 nm) with a specific absorbance of 0.013 μm^{-1} (Hárosi, 1976) to resemble the UVS photoreceptors of *Danio* (Palacios *et al.*, 1996).

4.3 Scotopic spectral sensitivity in the European starling, *Sturnus vulgaris*

Because avian retinae contain a single class of rod photoreceptor, scotopic spectral sensitivity can be predicted from the absorptance of rod outer segments and the transmission of the ocular media (Palacios and Goldsmith, 1993). Firstly, a 503 nm λ_{max} rhodopsin absorbance spectrum template was created using the log normal functions given by Stavenga *et al.* (1993), including the long wavelength tail patch for rods, with appropriately determined spectral locations and relative absorbances for the β- and γ-bands (equations 9, 10 and 11). The absorbance spectrum was then corrected for a visual pigment specific absorbance of 0.018 μm^{-1} and a pathlength of 20 μm (section 4.2.4.6), converted into absorptance and multiplied by the transmission of the ocular media at each wavelength (section 4.2.3.3). The corrected template data (considered the dependent variable) was then regressed linearly against the behavioural data of Dalland (1958), expressed as relative quantal spectral sensitivity, over the range 440 to 560 nm and with the intercept of the regression line set at zero. The log of the value for the slope of the regression line obtained was then added to the log of the corrected template absorption so that it best fitted the behavioural log relative quantal spectral sensitivity data. The comparison between the scotopic spectral sensitivity of the starling predicted in this way and the behavioural scotopic spectral sensitivity determined using operant techniques (Dalland, 1958; Adler and Dalland, 1959) is displayed in Figure 4.10. The discrepancy between the predicted and behavioural measures of scotopic spectral sensitivity at longer wavelengths may be due to the inadequacy of the long wavelength tail patch to fully describe photosensitivity at long wavelengths (section 4.2.4.4). Alternatively, van Roessel *et al.* (1997) discovered that long wavelength-sensitive cones contributed to the scotopic spectral sensitivity function measured electroretinographically in *Danio aequipinnatus*. If the LWS visual pigment of the single or double cones in the starling retina were active under scotopic conditions, it would explain the failure of the model to adequately predict sensitivity to longer wavelengths.

The effective spectral sensitivities of the rod photoreceptors in the starling, blackbird, blue tit and peacock, expressed as effective absorptance, are displayed in

Figure 4.11 to Figure 4.14 for comparison with the effective spectral sensitivities of the cone photoreceptors and are all very similar to one another. There are no behavioural measures of scotopic, or photopic, spectral sensitivity for the blackbird, blue tit or peacock.

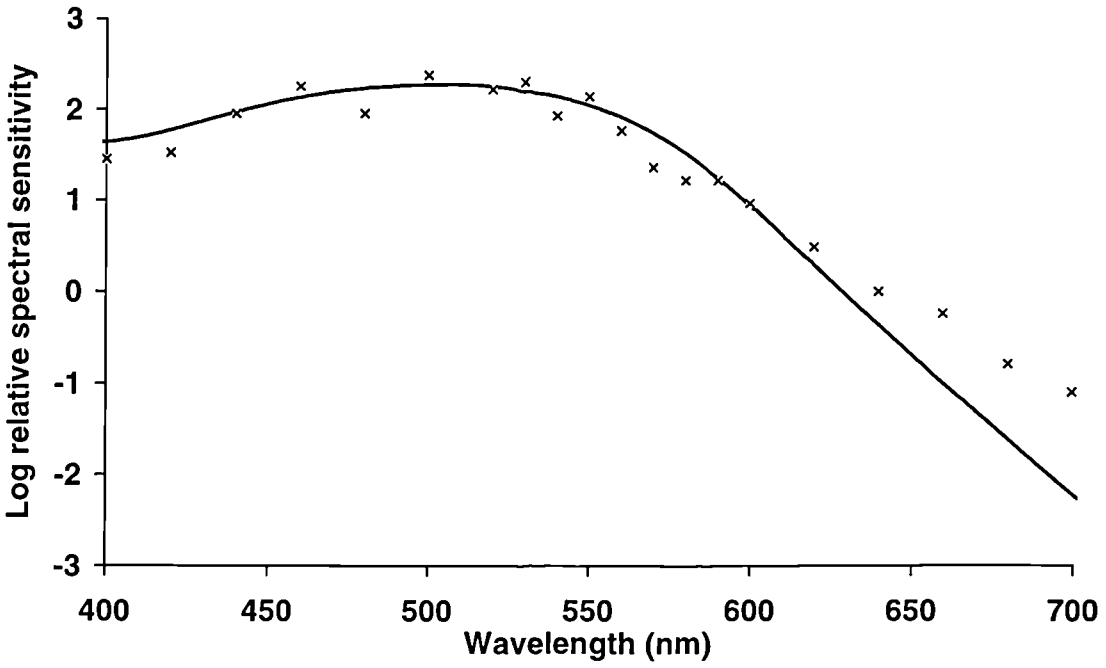

Figure 4.10 Scotopic spectral sensitivity of the European starling (*Sturnus vulgaris*) determined using an operant technique (Dalland, 1958, crosses) and predicted on the basis of a rod photoreceptor 20 μm long containing a λ_{max} 503 nm visual pigment of specific absorbance 0.018 μm^{-1} (solid line). Predicted sensitivity was shifted along the ordinate to best fit the behavioural data as described in section 4.3.

4.4 Photopic spectral sensitivity

Whereas the prediction of scotopic spectral sensitivity is relatively straightforward, inferences about photopic spectral sensitivity from physiological and anatomical data are complicated by assumptions regarding the performance and relative contributions of the different receptor mechanisms.

With the advent of single cell microspectrophotometry, it was possible to establish the existence of multiple cone pigments in vertebrates and correlate the direct electrical responses of single photoreceptors with the spectral absorbance characteristics of the photopigments contained within their outer segments (Marks, 1965; Tomita *et al.*, 1967). In addition, the filtering effect of cone oil droplets predicted by Shultze (1866, cited in Roaf, 1929) has been confirmed in both turtles and birds by behavioural (Neumeyer and Jäger, 1985) and electrophysiological means (Ohtsuka, 1985; Wortel and Nuboer, 1986; Kawamuro *et al.*, 1997).

However, even if the effective spectral sensitivity of each photoreceptor type can be predicted, the exact way in which the signals from each of the different types are combined to generate the sense of colour vision is still the subject of some debate. Whilst the presence of multiple, spectrally-distinct photoreceptors is essential for colour vision, it is the comparison of the outputs of these receptors, in spectrally opponent networks, that engenders the wavelength discrimination ability observed experimentally. It is unsurprising, therefore, that models of spectral sensitivity based on receptor properties alone predict psychophysical data less accurately than those assuming that colour is coded by opponent chromatic mechanisms and an achromatic mechanism (e.g. Sperling and Harwerth, 1971; Brandt and Vorobyev, 1997).

Measures of spectral sensitivity determine discrimination thresholds. These are set by noise which arises in the photoreceptors and at subsequent neural stages. Furthermore, where one noise source is dominant, threshold are set by the mechanism in which it originates. Most models have assumed that noise in the opponency mechanisms is statistically independent and that the probability of detection of a photon is given by the probability of its detection by the most sensitive post-receptoral mechanism (Vorobyev and Osorio, 1998). However, if thresholds are

dependent upon receptor noise and a single receptor type contributes to more than one opponent mechanism, noise in opponency channels will not be independent.

4.4.1 The model

Consequently, Vorobyev and Osorio (1998) have developed a receptor noise-limited colour opponent model for predicting the spectral sensitivity of di-, tri- and tetrachromatic eyes from a range of animals. Their approach is conditional on three main assumptions. Firstly, for a system with n receptor channels, colour is coded by n-1 unspecified colour opponent mechanisms. The achromatic signal is disregarded on the premise that under bright illumination for static targets subtending a large visual angle, sensitivity to the achromatic component of colour is low (Thornton and Pugh, 1983; Giurfa *et al.*, 1997). Accordingly, the model cannot predict thresholds where luminance mechanisms are important, as for small or moving targets, or in dim conditions. Secondly, colour opponent mechanisms give zero signal for stimuli that differ from the background in intensity only. Thirdly, thresholds are set by receptor noise, and not by opponent mechanisms.

Whilst these caveats are restrictive to the models generality, in particular the failure to account for thresholds measured under mesopic conditions (when the contribution of an achromatic channel is not suppressed by bright illumination), their approach has successfully predicted a variety of photopic psychophysical data (Brandt and Vorobyev, 1997; Vorobyev and Osorio, 1998). For the purposes of this study, the model of Vorobyev and Osorio (1998) is employed simply to compare the relative spectral sensitivities of the starling, blackbird, blue tit and peacock, on the assumption that photopic spectral sensitivity is determined only by the four single cone classes with no involvement of the double cone system (Maier and Bowmaker, 1993). Photopic spectral sensitivity is not modelled for the turkey as its cone oil droplets exhibited significant carotenoid deficiency (see chapter two). A simplified explanation of the model as applied to tetrachromatic colour vision is given below.

A colour stimulus with a reflectance spectrum $S(\lambda)$ is defined by receptor quantum catches:

$$Q_i = \int_{\min \lambda}^{\max \lambda} R_i(\lambda)S(\lambda)I(\lambda)d\lambda \qquad \textbf{Equation 15}$$

where i = 1, 2, ... n; Q_i is the quantum catch of receptor i; λ is the wavelength; $R_i(\lambda)$ is the spectral sensitivity of receptor i; $I(\lambda)$ is the spectrum of light entering the eye and integration is over the whole spectrum.

Relative cone spectral sensitivity, $R_i(\lambda)$, was obtained by multiplying the absorptance of the outer segment (using the adapted template spectra, specific absorbances and pathlengths described above), by the transmittance of its corresponding oil droplet and the ocular media at each wavelength. It was assumed that the proportion of incident photons transduced at the λ_{max} was independent of spectral class. The resulting effective spectral sensitivities for each of the four single cone types in each of the species for which photopic sensitivity was modelled are summarised in Table 4.2. In addition, the calculated effective spectral sensitivities of the rods and both single and double cones in each species are displayed in Figure 4.11 to Figure 4.14.

Species	**Effective cone λ_{max} (nm)**			
	UVS / VS	**SWS**	**MWS**	**LWS**
Starling (*Sturnus vulgaris*)	371	453	543	605
Blackbird (*Turdus merula*)	379	457	541	601
Blue tit (*Parus caeruleus*)	375	452	537	605
Peacock (*Pavo cristatus*)	430	477	537	605

Table 4.2 Single cone peak effective spectral sensitivities. The wavelength of maximum sensitivity (λ_{max}) of each single cone is determined from the pathlength and specific absorbance of the visual pigment contained in its outer segment and the transmission of its corresponding oil droplet and the pre-retinal media.

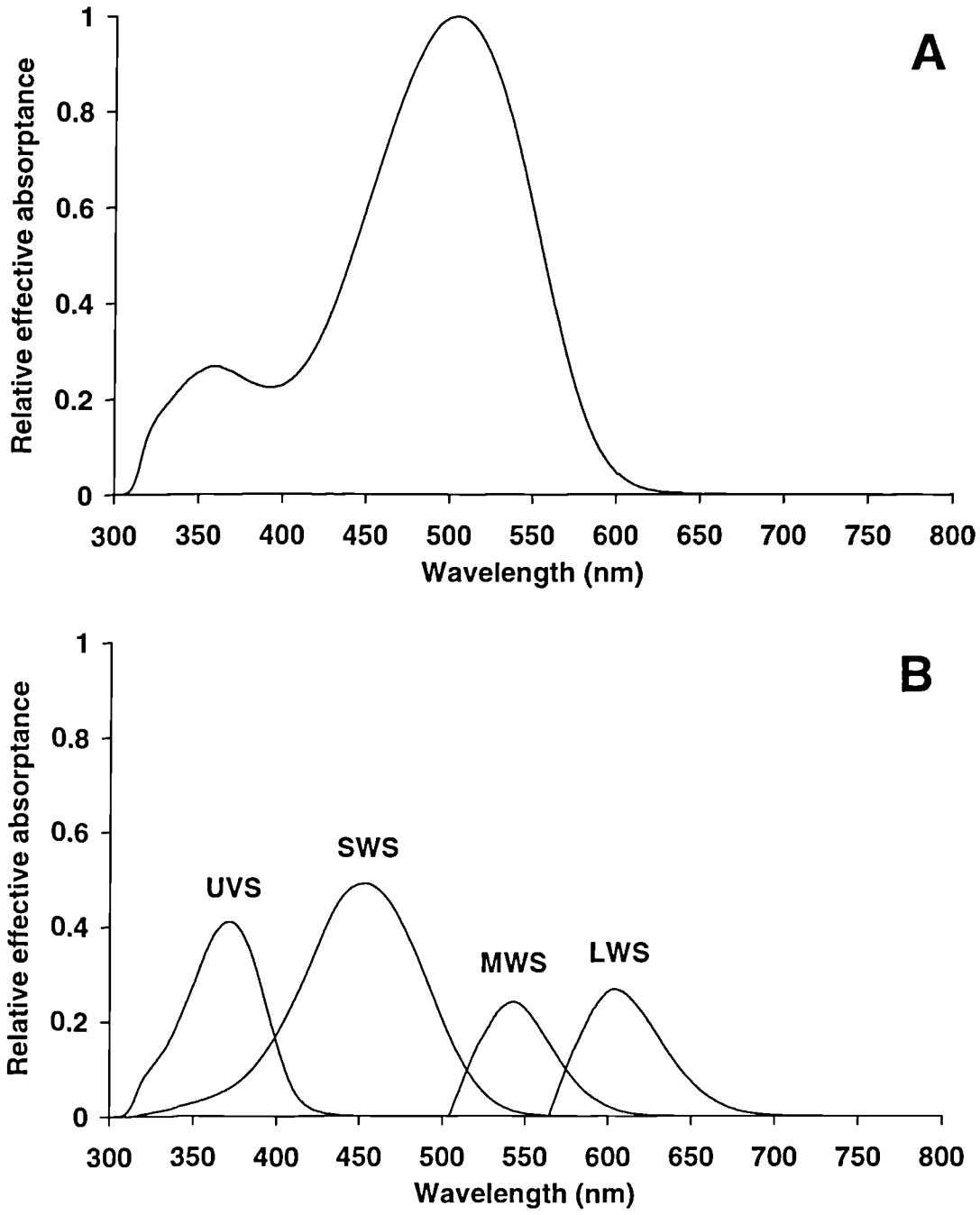

Figure 4.11 Effective spectral sensitivity of the rod (**A**) and single cones (**B**) of the European starling, *Sturnus vulgaris*, expressed as effective absorptance relative to the rod. UVS, ultraviolet-sensitive; SWS, short wavelength-sensitive; MWS, medium wavelength-sensitive; LWS, long wavelength-sensitive.

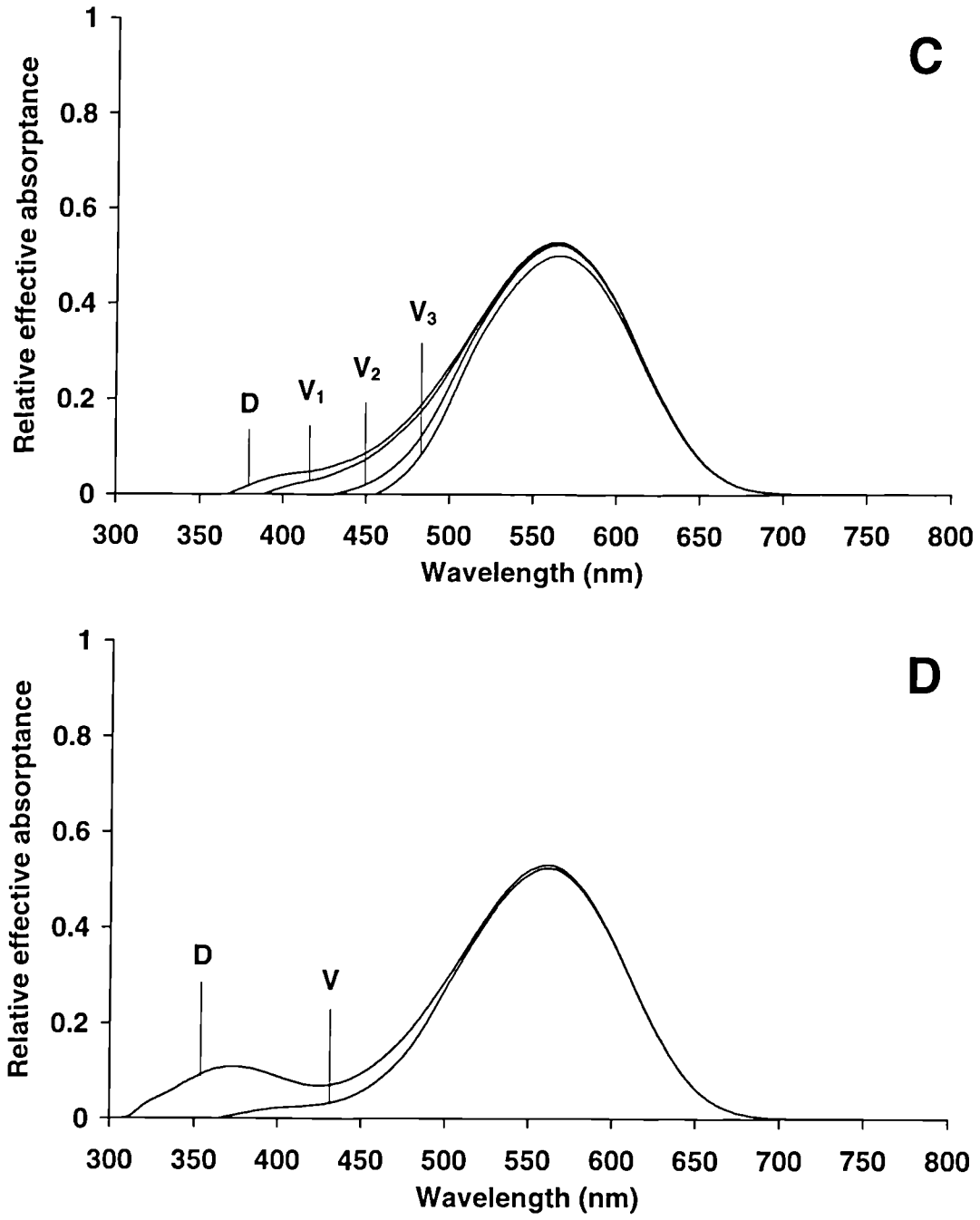

Figure 4.11 (continued) Effective spectral sensitivity of the principal (**C**) and accessory (**D**) members of the double cone pair of the European starling, *Sturnus vulgaris*, expressed as effective absorptance relative to the rod. D, dorsal retina; V, ventral retina. The subscripts V_1, V_2 and V_3 refer to three arbitrary categorisations of the P-type oil droplet in the principal member of the double cones located in the ventral retina (see chapter two). An oil droplet was observed in the accessory member only in double cones located in the ventral retina.

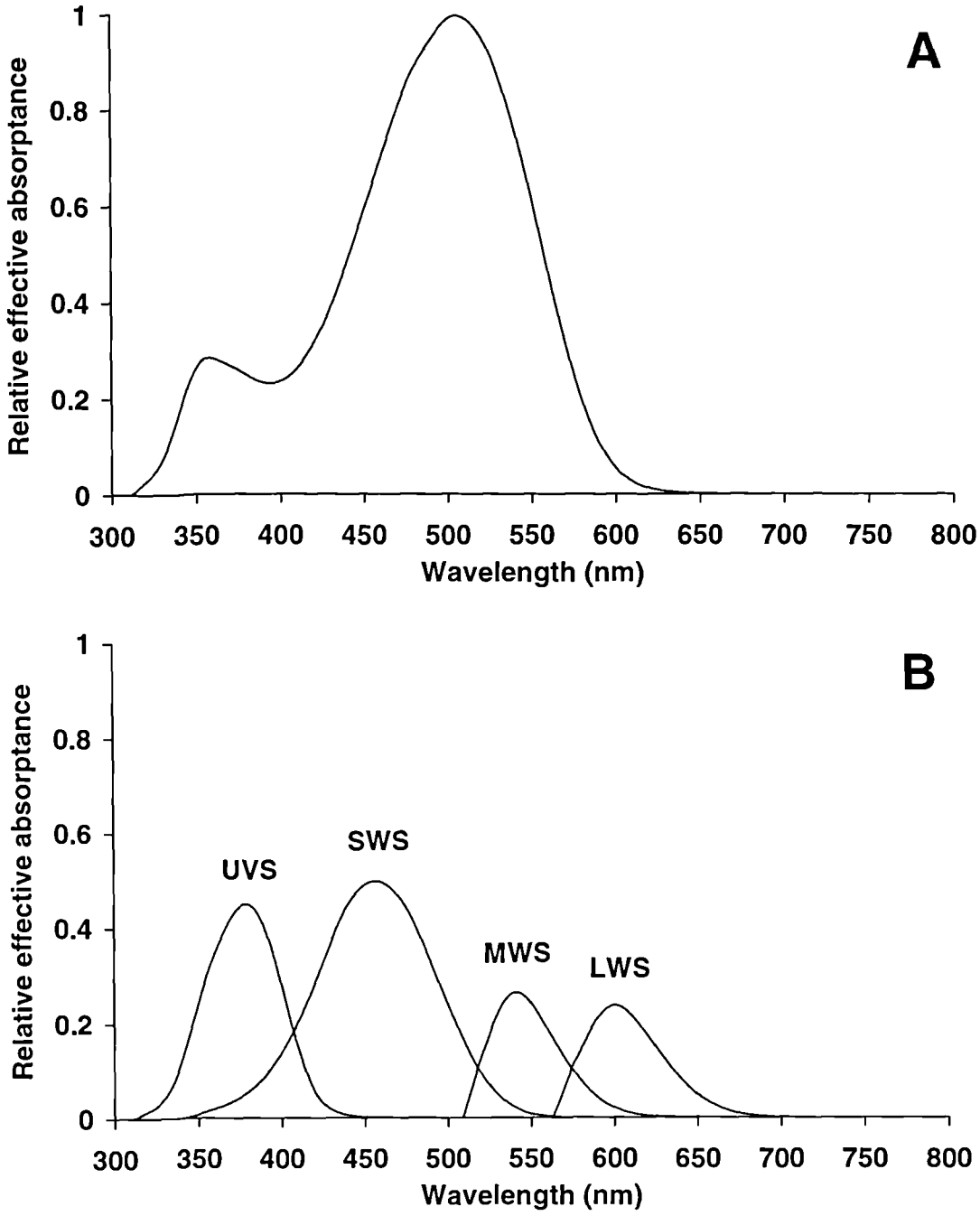

Figure 4.12 Effective spectral sensitivity of the rod (**A**) and single cones (**B**) of the blackbird, *Turdus merula*, expressed as effective absorptance relative to the rod. UVS, ultraviolet-sensitive; SWS, short wavelength-sensitive; MWS, medium wavelength-sensitive; LWS, long wavelength-sensitive.

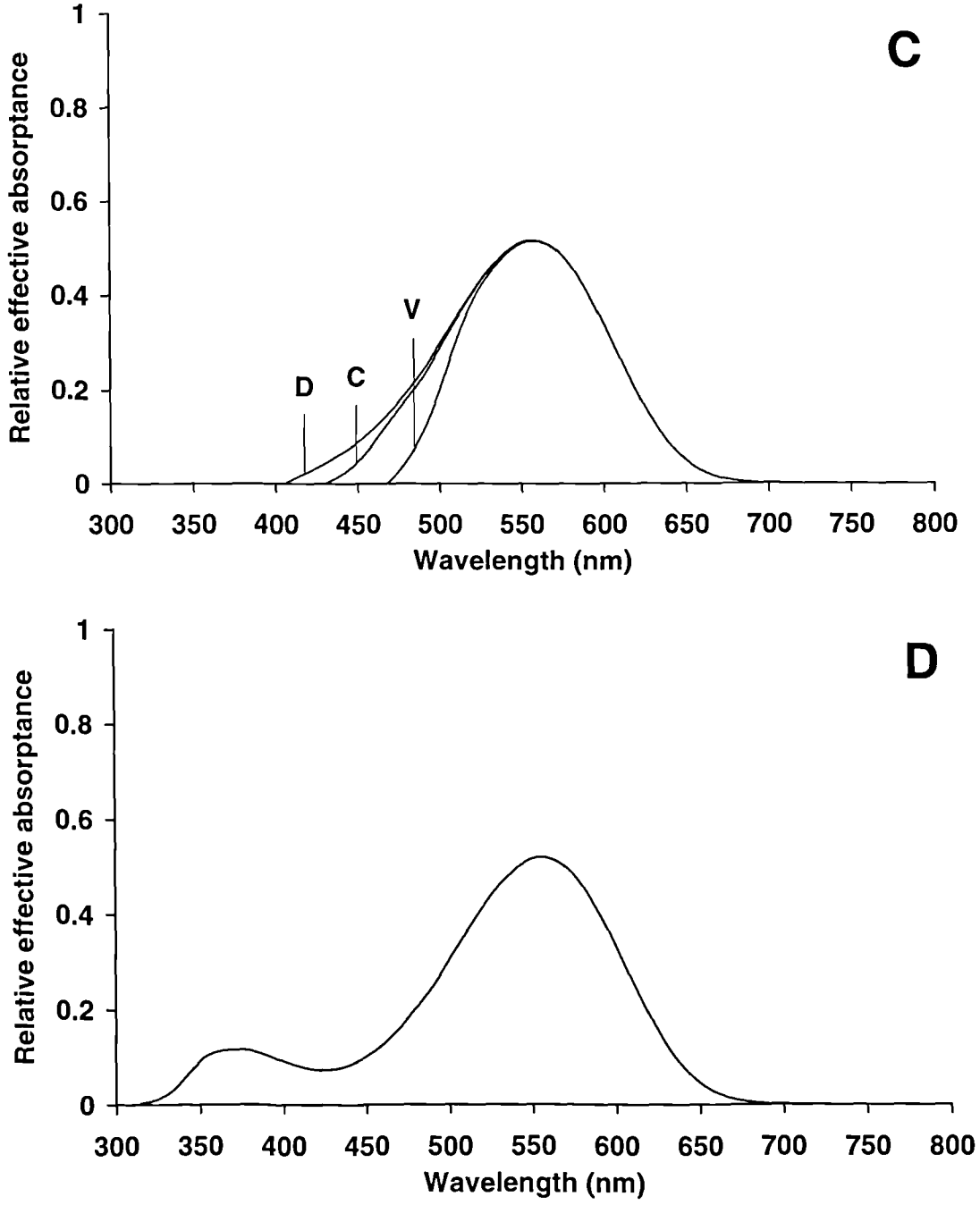

Figure 4.12 (continued) Effective spectral sensitivity of the principal (C) and accessory (D) members of the double cone pair of the blackbird, *Turdus merula*, expressed as effective absorptance relative to the rod. D, dorsal retina; C, central retina; V, ventral retina. No oil droplet was observed in the accessory member.

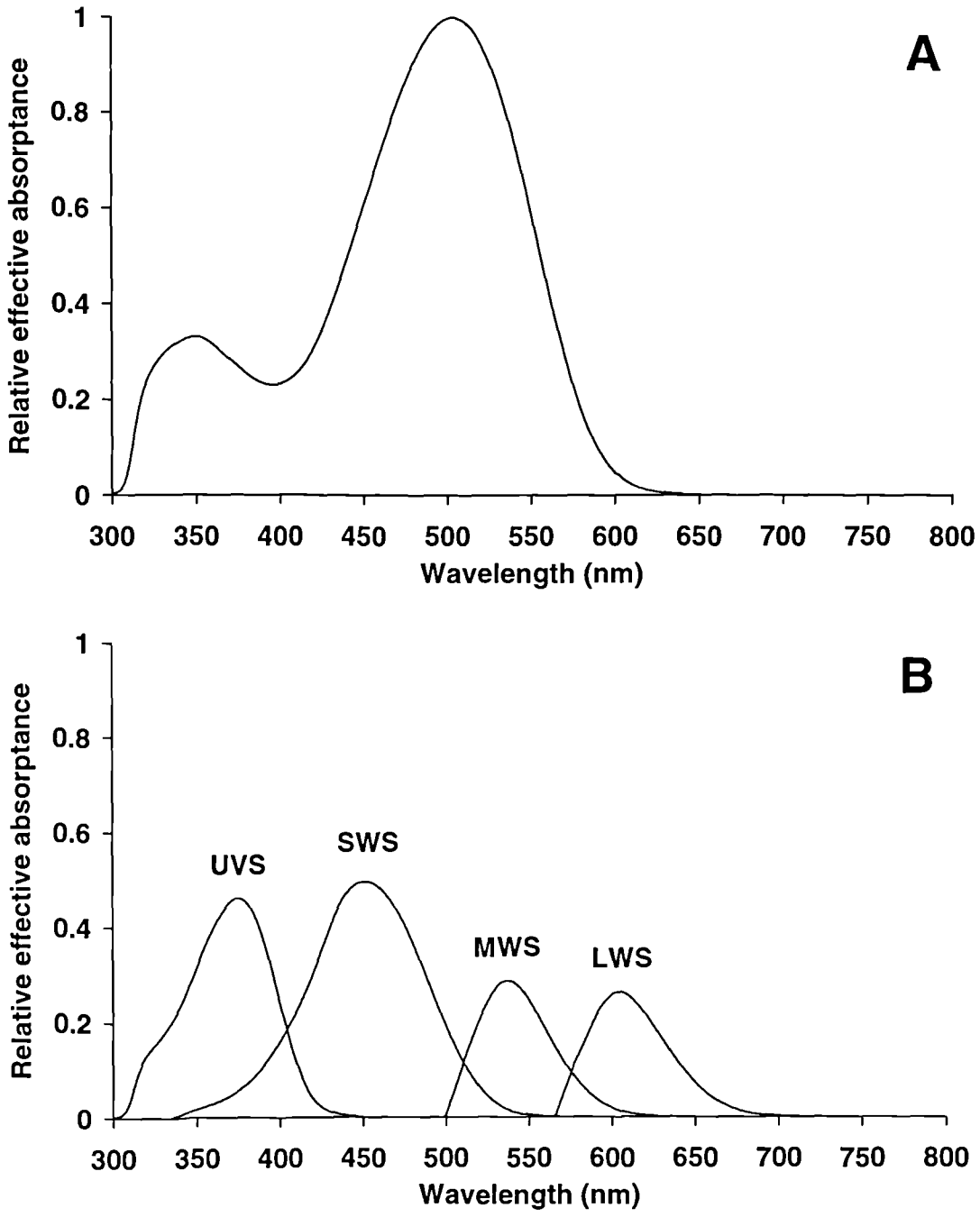

Figure 4.13 Effective spectral sensitivity of the rod (**A**) and single cones (**B**) of the blue tit, *Parus caeruleus*, expressed as effective absorptance relative to the rod. UVS, ultraviolet-sensitive; SWS, short wavelength-sensitive; MWS, medium wavelength-sensitive; LWS, long wavelength-sensitive.

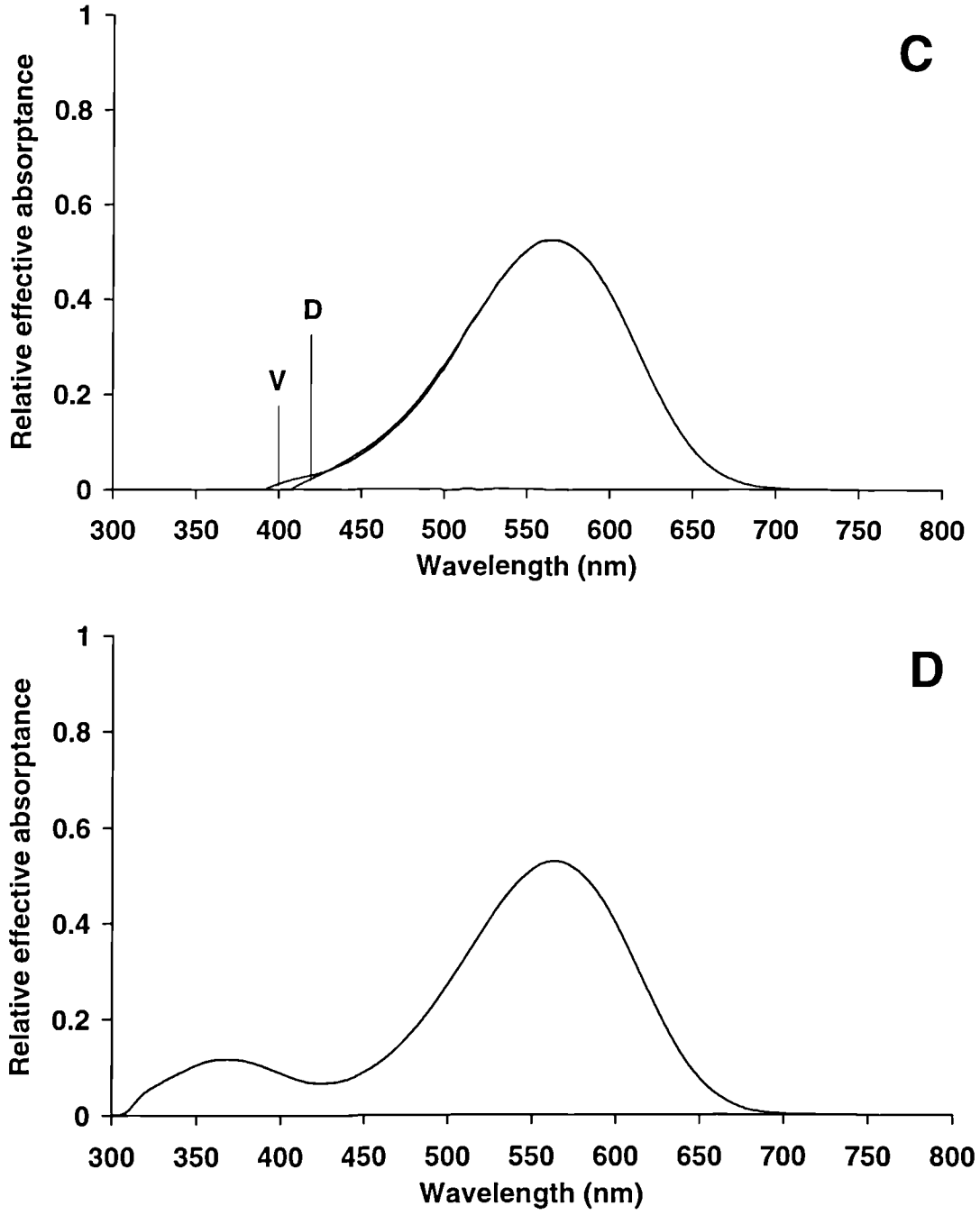

Figure 4.13 (continued) Effective spectral sensitivity of the principal (C) and accessory (D) members of the double cone pair of the blue tit, *Parus caeruleus*, expressed as effective absorptance relative to the rod. D, dorsal retina; V, ventral retina. No oil droplet was observed in the accessory member.

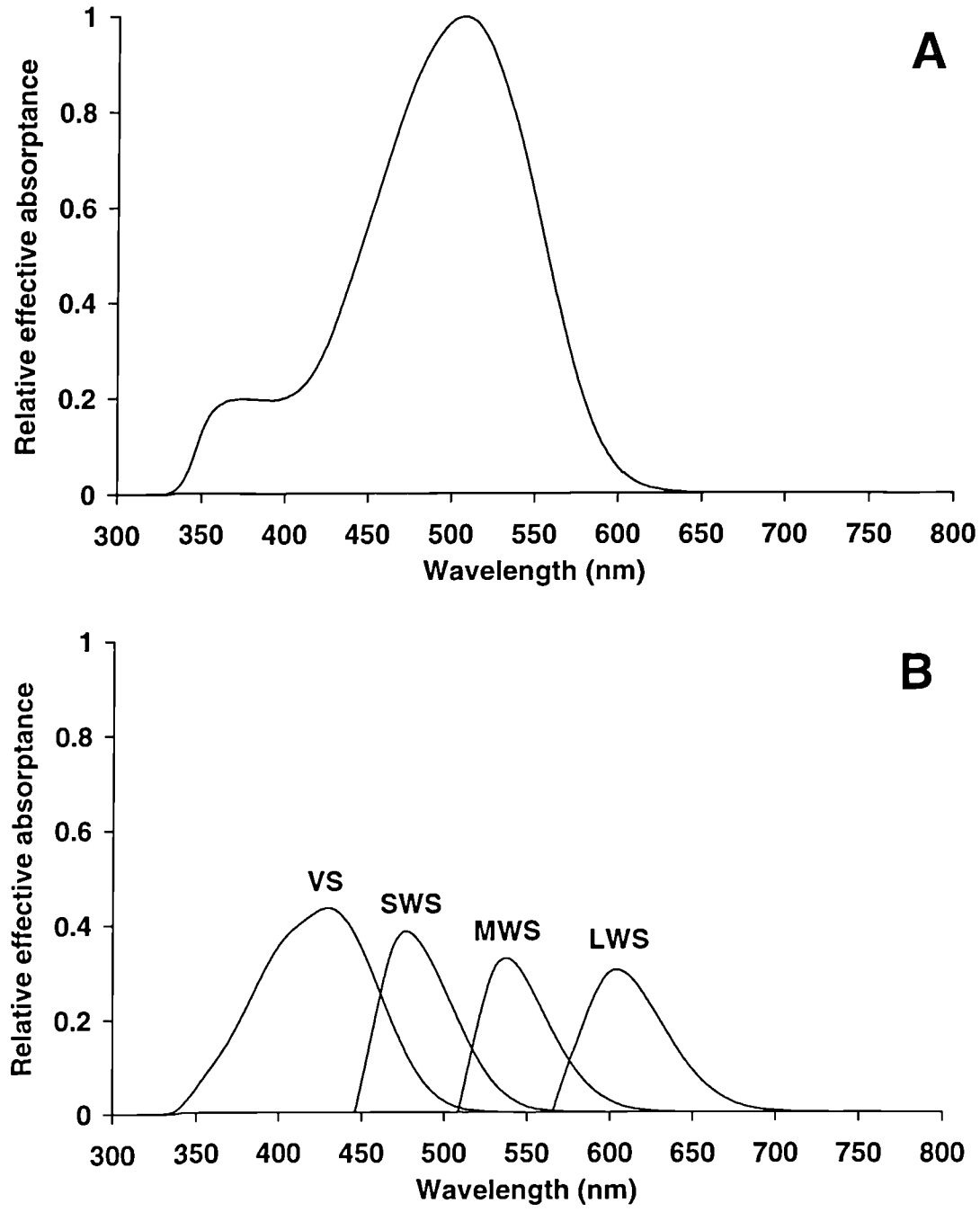

Figure 4.14 Effective spectral sensitivity of the rod (**A**) and single cones (**B**) of the peacock, *Pavo cristatus*, expressed as effective absorptance relative to the rod. VS, violet-sensitive; SWS, short wavelength-sensitive; MWS, medium wavelength-sensitive; LWS, long wavelength-sensitive.

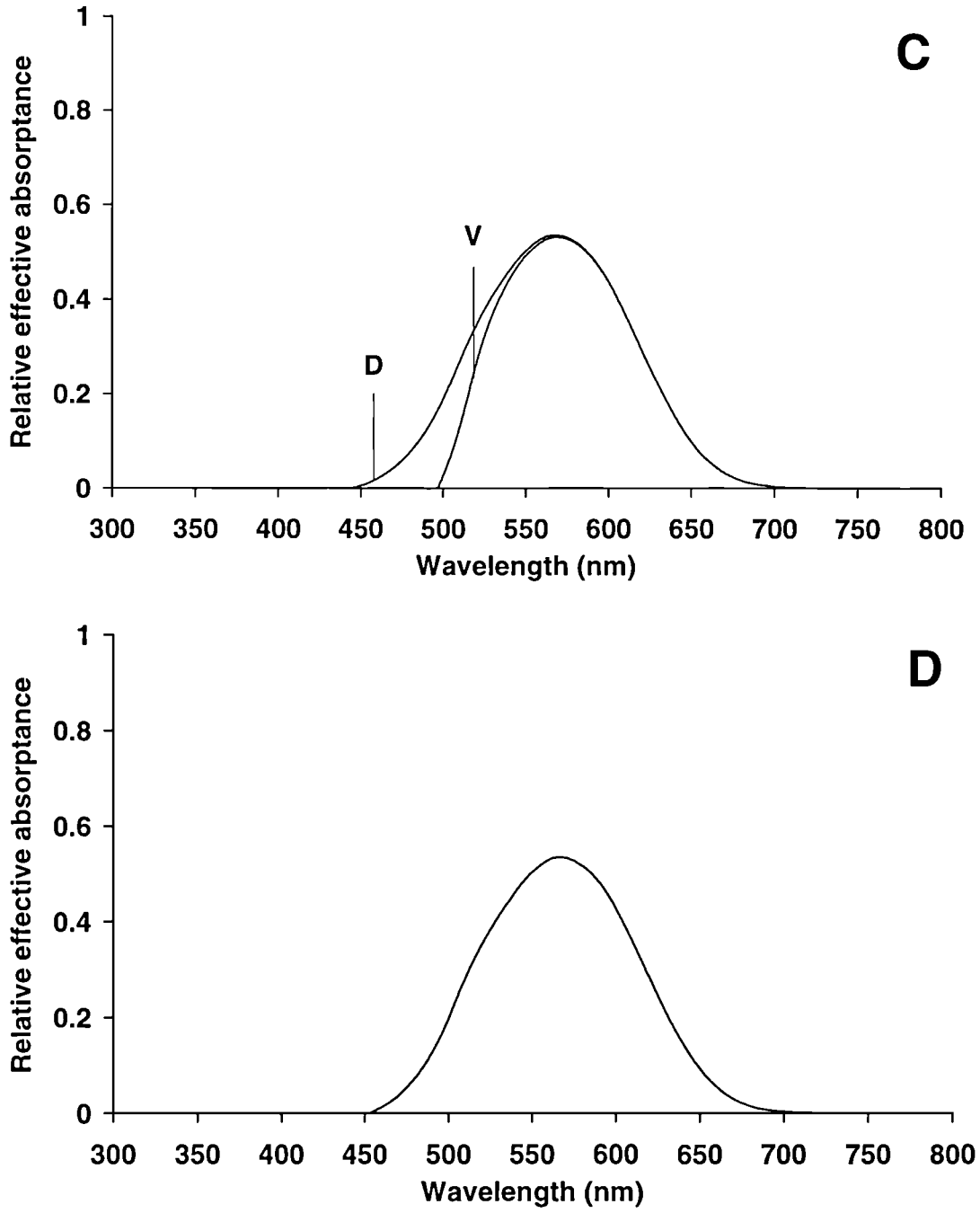

Figure 4.14 (continued) Effective spectral sensitivity of the principal (C) and accessory (D) members of the double cone pair of the peacock, *Pavo cristatus*, expressed as effective absorptance relative to the rod. D, dorsal retina; V, ventral retina.

To take account of receptor adaptation, receptor quantum catches, Q_i, were normalized to the background, such that:

$$q_i = k_i Q_i \qquad \textbf{Equation 16}$$

where the coefficients k_i describe the von Kries transformation (Vorobyev and Osorio, 1998), and are chosen so that the quantum catches for the adapting background are constant, i.e.

$$k_i = 1 \Big/ \int_{\min\lambda}^{\max\lambda} R_i(\lambda) S^b(\lambda) I(\lambda) d\lambda \qquad \textbf{Equation 17}$$

where S^b is the reflectance spectrum of the background.

If colour is defined as a point in a perceptual space with co-ordinate axes representing receptor quantum catches, and discriminability of any two colours is described by the 'distance', ΔS, between them, then stimuli are indistinguishable if ΔS is less than a 'threshold distance', ΔS^t. Weber's law states that relative rather than absolute values of the quantum catches are coded by a receptor channel (Wyszecki and Stiles, 1967), thus:

$$\Delta f_i = \frac{\Delta q_i}{q_i} \qquad \textbf{Equation 18}$$

where Δf_i is the difference of the signal, f_i, in receptor mechanism i between threshold stimuli and Δq_i denotes the difference in the quantum catch between the stimuli. Integration of equation 18 gives the Fechner law, that is, the signal of the receptor channel is proportional to the logarithm of the quantum catch:

$$f_i = \log(q_i). \qquad \textbf{Equation 19.}$$

However, because for the background $q_i = 1$ (see equation 16), the difference in the signals of receptor channels close to background is simply given by the difference of receptor quantum catches, i.e.

$$\Delta f_i \approx \Delta q_i. \qquad \textbf{Equation 20.}$$

The following equation is then valid for tetrachromatic vision when stimuli are close to background:

$$\left(\Delta S^{t}\right)^{2} = \Big(\left(e_1e_2\right)^2\left(\Delta q_4 - \Delta q_3\right)^2 + \left(e_1e_3\right)^2\left(\Delta q_4 - \Delta q_2\right)^2 + \left(e_1e_4\right)^2\left(\Delta q_3 - \Delta q_2\right)^2 + \left(e_2e_3\right)^2\left(\Delta q_4 - \Delta q_1\right)^2 + \left(e_2e_4\right)^2\left(\Delta q_3 - \Delta q_1\right)^2 + \left(e_3e_4\right)^2\left(\Delta q_2 - \Delta q_1\right)^2\Big) \div \left(\left(e_1e_2e_3\right)^2 + \left(e_1e_2e_4\right)^2 + \left(e_1e_3e_4\right)^2 + \left(e_2e_3e_4\right)^2\right)$$

Equation 21

where e_i is the standard deviation of the noise in receptor channel i, and the difference in the quantum catch of the receptor mechanism between background and stimulus is given (see equation 15) by:

$$\Delta q_i = k_i R_i(\lambda) I^{t}(\lambda) \qquad \textbf{Equation 22}$$

where $I^t(\lambda)$ is threshold intensity, i.e. the minimum intensity of monochromatic light of wavelength, λ, detectable over an adapting background. Substitution of equation 22 into equation 21 gives an expression for threshold intensity as a function of wavelength:

$$I^{t}(\lambda) = 1\Big/\sqrt{\Big(\left(e_1e_2\right)^2\left(k_4R_4 - k_3R_3\right)^2 + \left(e_1e_3\right)^2\left(k_4R_4 - k_2R_2\right)^2 + \left(e_1e_4\right)^2\left(k_3R_3 - k_2R_2\right)^2 + \left(e_2e_3\right)^2\left(k_4R_4 - k_1R_1\right)^2 + \left(e_2e_4\right)^2\left(k_3R_3 - k_1R_1\right)^2 + \left(e_3e_4\right)^2\left(k_2R_2 - k_1R_1\right)^2\Big) \div \left(\left(e_1e_2e_3\right)^2 + \left(e_1e_2e_4\right)^2 + \left(e_1e_3e_4\right)^2 + \left(e_2e_3e_4\right)^2\right)\Delta S^{t}}$$

Equation 23.

The value of ΔS^t depends on the specific threshold criterion of the sensitivity test (e.g. 75 % correct choices). However, because only relative spectral sensitivity was of interest, ΔS^t was ignored and spectral sensitivity was then proportional to $1/I^t(\lambda)$.

Noise in receptor channels, e_i, is defined as:

$$e_i = \frac{v_i}{\sqrt{\eta_i}} \qquad \textbf{Equation 24}$$

where v_i is the standard deviation of noise in a *single* receptor cell of type i, and η_i the number of cells of type i within a retinal integration area (e.g. a ganglion cell receptive field). Averaging the signal over η_i cells improves the signal to noise ratio as the square root of η_i. For simplicity, receptor noise was assumed to be independent of the number of absorbed quanta (i.e. the Weber fraction was independent of intensity). Furthermore, because measurements of the relative noise in different types of avian cone were unavailable, noise characteristics of the cones were deemed to be independent of spectral class. Thus, differences between receptor mechanisms were attributable only to differences in their density in the retinal array, i.e.

$$e_i \propto \frac{1}{\sqrt{\eta_i}} \qquad \textbf{Equation 25.}$$

Estimates of η_i for the four species under investigation were obtained as described in chapter three and are listed in Table 4.1 (above).

4.4.2 Spectral irradiance

Because threshold intensity is defined relative to background reflectance, spectral sensitivity is dependent upon illumination conditions. For instance, a deficiency of UV wavelengths in the ambient light will result in high UV sensitivity, and *vice versa*. However, the ambient spectral radiance of any natural environment is rarely, if ever, constant at each wavelength across the spectrum. Consequently, for the purposes of the model, the spectral composition of the illuminating light was chosen in attempt to reflect a more realistic situation. The illuminant used was the CIE (Commission Internationale de l'Eclairage) D65 standard daylight curve expressed as relative quantal radiance (see Figure 4.15). For simplicity, the background was assumed to be a perfect reflector at all wavelengths to which the birds were sensitive, i.e. 'bird white'.

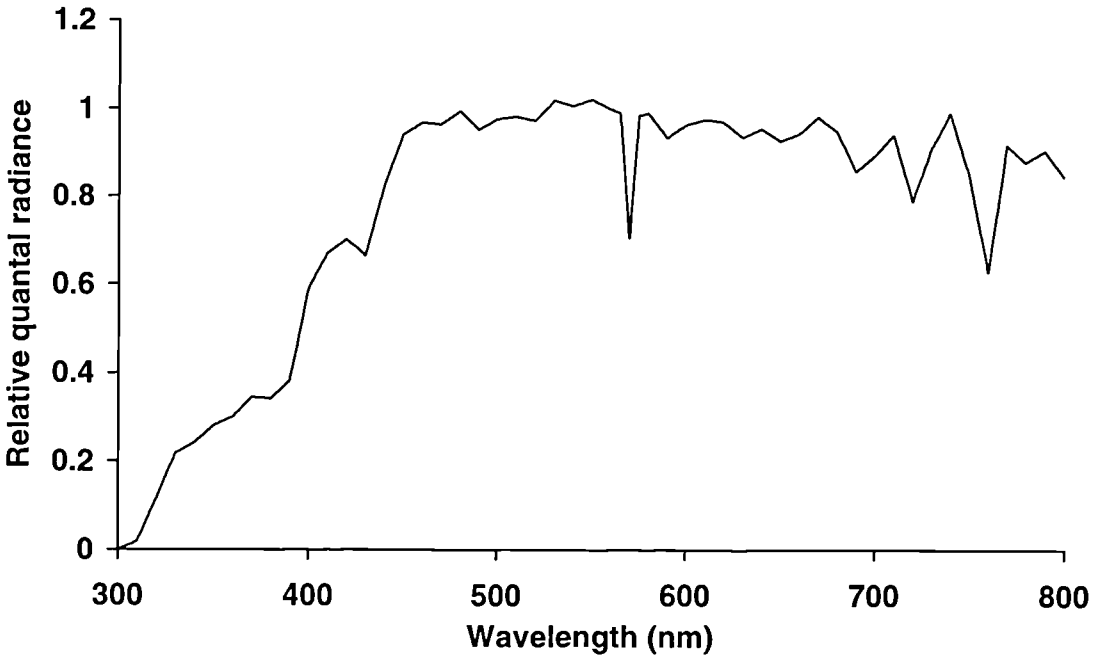

Figure 4.15 CIE standard daylight illuminant (D65). This radiance spectrum was used for the prediction of relative photopic spectral sensitivities. The relative spectral power distribution data of Hunt (1991) were interpolated to 1 nm intervals using a linear spline (CurveExpert 1.2) and converted into quantal radiance relative to 560 nm.

4.4.3 Predictions of photopic spectral sensitivity

The results from the model of Vorobyev and Osorio (1998), as applied to the starling, blackbird, blue tit and peacock, are displayed in Figure 4.16 to Figure 4.19. All four species display peaks in their photopic sensitivity functions close to the effective spectral sensitivities of their individual cone types. The relatively high sensitivity of the UVS / VS cone channel is due to the paucity of ultraviolet wavelengths in the illuminant.

The effect on spectral sensitivity of the difference in λ_{max} between the peacock VS pigment and the UVS pigments of the starling, blue tit and blackbird is evident in Figure 4.19. The peacock's VS colour channel has a broader sensitivity peak, but considerably less sensitivity to ultraviolet wavelengths than the passerine species which possess UVS pigments. The photopic sensitivity functions predicted for the three passerine species closely resemble that predicted for the Pekin robin (Vorobyev and Osorio, 1998), which correlated well with it's behaviourally-determined photopic spectral sensitivity (Maier, 1992; Maier and Bowmaker, 1993; Maier, 1994).

The photopic spectral sensitivity function determined behaviourally for the starling is not shown for comparison (Adler and Dalland, 1959; Dalland, 1958). It displayed a broad peak at around 550 nm, and probably represents the spectral sensitivity of the double cone rather than the single cones. Furthermore, the experimental conditions under which the behavioural test was conducted, particularly the spectral composition of the light source used for light adaptation, are unknown.

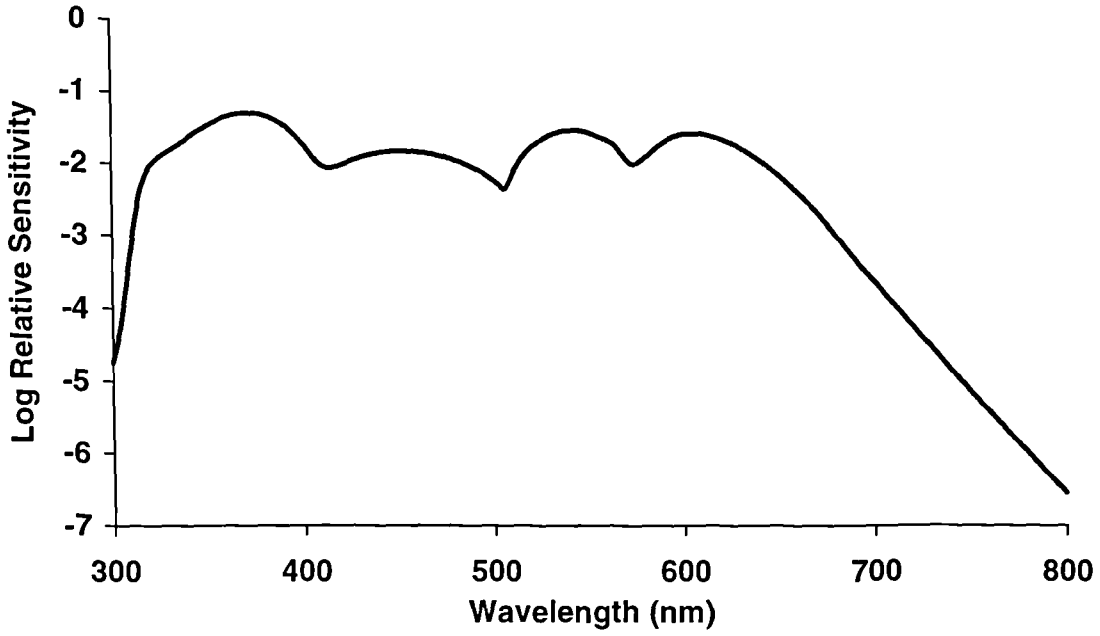

Figure 4.16 Predicted photopic spectral sensitivity of the European starling (*Sturnus vulgaris*). Peaks in sensitivity at about 371, 453, 543 and 605 nm represent the effective spectral sensitivity of the four single cone classes.

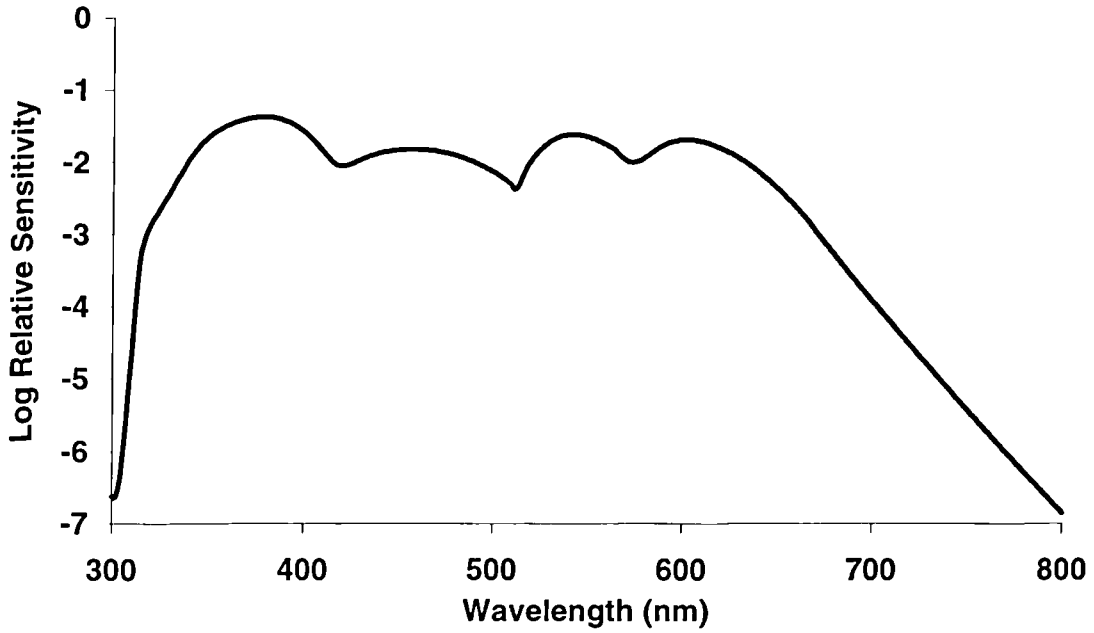

Figure 4.17 Predicted photopic spectral sensitivity of the blackbird (*Turdus merula*). Peaks in sensitivity at about 379, 457, 541 and 601 nm represent the effective spectral sensitivity of the four single cone classes.

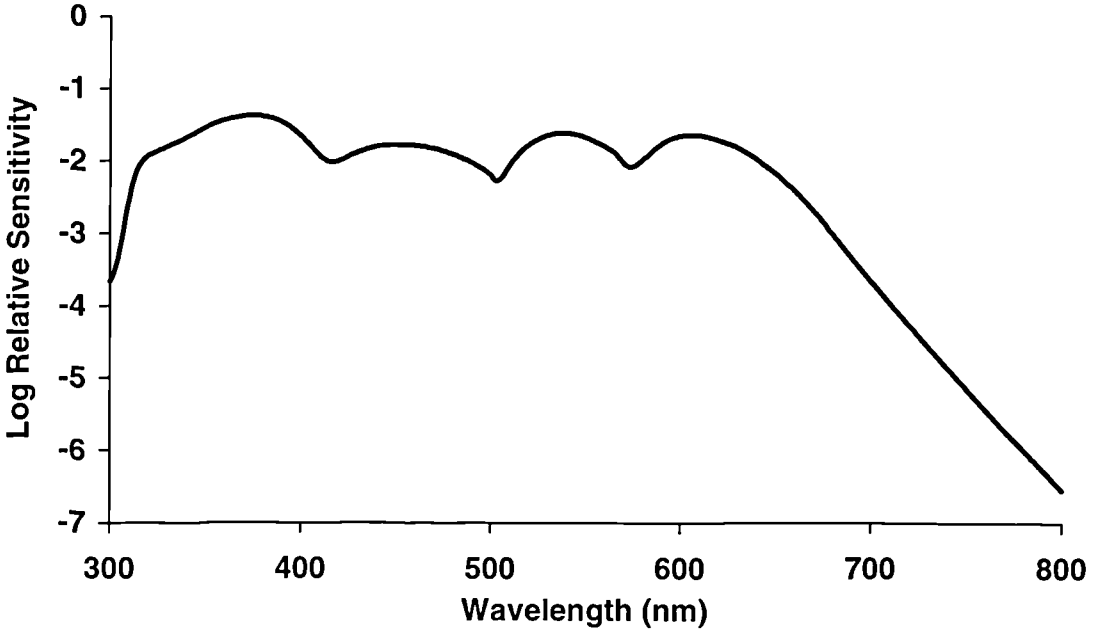

Figure 4.18 Predicted photopic spectral sensitivity of the blue tit (*Parus caeruleus*). Peaks in sensitivity at about 375, 452, 537 and 605 nm represent the effective spectral sensitivity of the four single cone classes.

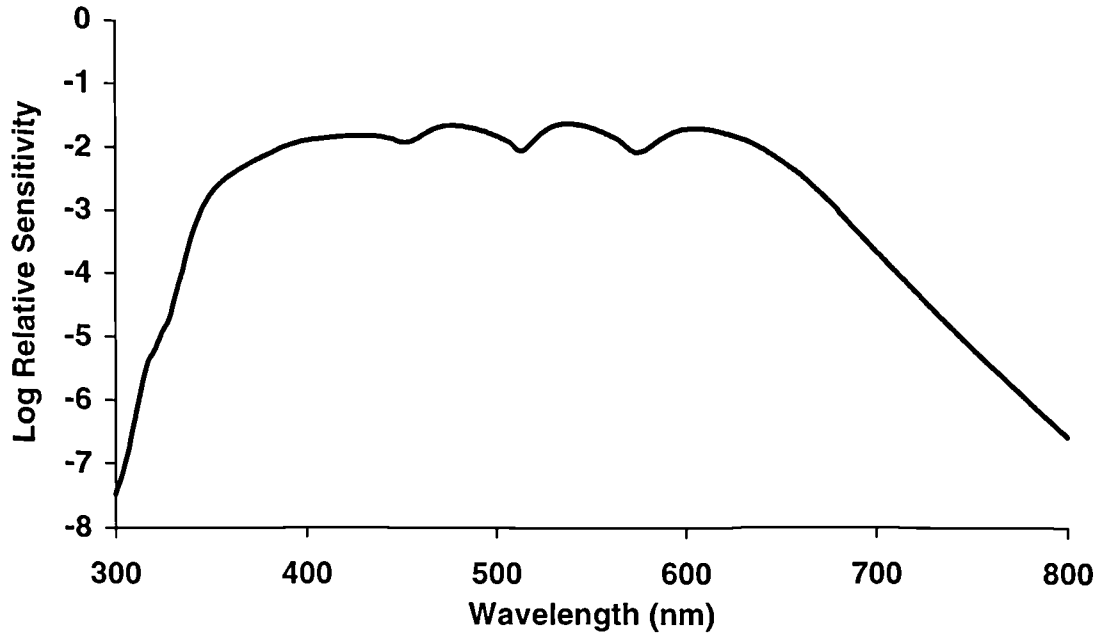

Figure 4.19 Predicted photopic spectral sensitivity of the peacock (*Pavo cristatus*). Peaks in sensitivity at about 430, 477, 537 and 605 nm represent the effective spectral sensitivity of the four single cone classes.

4.5 Discussion

Whilst the peak sensitivities of the photopic sensitivity function correspond to the effective spectral sensitivity of the cones, as predicted by Bowmaker (1977), the model of Vorobyev and Osorio (1998) has a number of advantages. Firstly, all potential opponent interactions between cone classes are taken into account, such that the sensitivity thresholds obtained represent receptor noise-limited performance of the visual system.

Secondly, the model can easily be adapted to investigate the effects of different illuminants, different stimulus reflectances, different adapting backgrounds and varying photoreceptor proportions or levels of summation. It is intended that the results of the model will be used to investigate the discriminability of bird relevant objects under natural irradiances.

This sort of model might also be extended to investigate the effects of intraretinal variations in cone photoreceptor abundance, which are observed in a number of species (chapter three). However, the model of Vorobyev and Osorio (1998) was relatively robust to changes in photoreceptor proportions at the magnitude observed in the species investigated during this study, and may not be sensitive enough to investigate such subtle differences. This may be because noise in the receptor channels was proportional to the square root of the proportions. For this reason the cone proportions used for each species in the model were an average for all quadrants and both left and right eyes. Intra-retinal variations in cone proportions are presumably adaptive for visual ecology (chapter three) and the effects on the colour vision ability of different retinal regions warrants further investigation.

The most striking feature of the photopic spectral sensitivity functions of the three passerine species is how similar they are to each other, and to the Pekin robin (another passerine). This is due to the similarity in the spectral absorption characteristics of the visual pigments and oil droplets of the single cones in their retinae. In view of the differences in plumage coloration, diet and habitat, the lack of variation in the spectral sensitivity of the single cones is surprising. The effective spectral sensitivity of the MWS and LWS cone classes in the peacock are almost identical to those calculated for the passerines. Perhaps the spectral sensitivity of

these two cone types is optimal for most terrestrial diurnal species, and differences in visual ecology are largely reflected in the nature of the SWS and VS / UVS cones.

CONCLUSIONS

5. Conclusions

The retinae of the European starling, blackbird, blue tit, peacock and domestic turkey contain five different types of vitamin A_1-based visual pigment (rhodopsins) in seven different types of photoreceptor cell. A single class of rod contained a medium wavelength-sensitive visual pigment (λ_{max} 503 to 505 nm). The four different types of single cone observed contained a visual pigment maximally sensitive to either long (LWS, λ_{max} 557 to 566 nm), medium (MWS, λ_{max} 503 to 505 nm), short (SWS, λ_{max} 449 to 459 nm) and either violet (VS, λ_{max} 420 to 421 nm) or ultraviolet (UVS, λ_{max} 368 to 376 nm) wavelengths. The LWS, MWS, SWS and VS / UVS visual pigments found in the single cones were associated with oil droplets designated as R-type (λ_{cut} 517 to 572 nm), Y-type (λ_{cut} 490 to 515 nm), C-type (λ_{cut} 399 to 450 nm) and T-type (transparent) respectively. The LWS cone visual pigment was also found in both the principal and accessory members of the double cone, associated with P-type (λ_{cut} 407 to 500 nm) and, occasionally, A-type (λ_{cut} 479 to 490 nm) oil droplets respectively. In this respect, these hitherto unstudied species are little different from the majority of other avian species which have been investigated microspectrophotometrically.

Nevertheless, it is apparent that there is variation in the exact spectral location of the λ_{max} of the visual pigment within certain photoreceptor types. Whereas most species studied to date have a LWS visual pigment maximally sensitive between 563 and 570 nm, the LWS visual pigment of the blackbird has, like the tawny owl (Bowmaker and Martin, 1978), a maximum sensitivity at shorter wavelengths (λ_{max} 557 and 555 nm respectively). Furthermore, because the λ_{cut} of the R-type oil droplet in the LWS single cone determines its exact peak effective spectral sensitivity to a greater extent than the visual pigment λ_{max}, the selective pressure affecting spectral tuning in the LWS visual pigments may act on the LWS double cones. Double cones contain oil droplets, but these do not shift the peak effective spectral sensitivity of the cone from that of the visual pigment. However, the function of the double cones is unknown. The fact that such variation in LWS visual pigment λ_{max} is observed within a closely related taxon (Passeriformes) might suggest that visual ecology

rather than phylogeny has driven the differentiation of the avian LWS visual pigment, although the environmental factors which might account for the difference between blackbirds and blue tits or starlings are not readily apparent. This result may also suggest that oil droplets, rather than visual pigments, are under the greatest selection pressure with regard to colour vision performance. Because most species of bird are diurnal, their vision is unlikely to be limited by the availability of photons, and the loss in sensitivity predicted when the light reaching the outer segment is filtered by a coloured oil droplet (Bowmaker, 1977) may be insignificant. Consequently, the precise spectral location of the visual pigment λ_{max} may be less important than the λ_{cut} of the oil droplet. Perhaps it is relatively easier to shift the peak effective spectral sensitivity of a cone to longer wavelengths by increasing the concentration of the carotenoid pigment in the oil droplet than by changing the λ_{max} of the visual pigment through alterations in the amino acid composition of the opsin. If true, it might explain why there is so little variation in the λ_{max} values of avian SWS, MWS and LWS cone visual pigments and why, in the case of the MWS and LWS visual pigments, the λ_{max} values are so different from the wavelength of peak effective sensitivity of the cone. By contrast, there is huge variation in the spectral location of the λ_{max} of the fourth type of cone visual pigment (UVS / VS), which is associated with a transparent oil droplet and may therefore be under greater selection pressure than the other visual pigment types.

Identifying the role of the double cones is of paramount importance in understanding the avian visual system. Double cones dominate the retinae of most diurnal species (Meyer, 1977), but we are only able to speculate about their purpose. The greater relative abundance of double cones in the ventral retina of ground foraging species, including the starling, blackbird and peacock, suggests that the visual information they are designed to transduce is more frequently derived from the dorsal visual field. Combined with the knowledge that the spectral sensitivity of the optomotor response in the pigeon corresponds to the spectral sensitivity of the double cones (Campenhausen and Kirschfeld, 1998), it is possible that one of their primary functions is motion detection. Nevertheless, despite the difficulties in separating the actions of one type of photoreceptor from another in both electrophysiological and behavioural measures of visual ability, further empirical investigations into the role

of double cones are essential in deducing whether or not they are able to detect the plane of polarised light (Young and Martin, 1984; Cameron and Pugh, 1991), or whether they are incorporated into spectrally opponent networks for wavelength discrimination (Palacios *et al.*, 1992).

The spectral locations of the rod visual pigment and the MWS cone visual pigment are not only almost identical within a given species, but show the least variation between species. There is, however, some hint of variation in the SWS cone visual pigment. Most species studied have an SWS visual pigment with a λ_{max} value between 450 and 460 nm. The budgerigar and canary, however, have SWS visual pigments maximally sensitive to slightly shorter wavelengths (λ_{max} 444 nm), as does the zebra finch (430 nm). Furthermore, as described in chapter two, there is a significant correlation between the spectral location of the UVS / VS-type visual pigment λ_{max} and the λ_{max} of the SWS-type visual pigment. Birds that have a UVS visual pigment have a SWS visual pigment with a λ_{max} value at shorter wavelengths than those species which possess a VS visual pigment. Whilst microspectrophotometric measurements of SWS and VS / UVS visual pigments are generally noisier than measurements from the other visual pigment types, and as such are susceptible to greater error in estimating the λ_{max} than other cone types, it is interesting that these three species all inhabit open, arid environments in, or near, the tropics (Goodwin, 1982; Blakers *et al.*, 1984; Snow and Perrins, 1998b). The ambient irradiance in such habitats will generally have a relatively high proportion of short and ultraviolet wavelengths (Endler, 1993). For species which possess a VS visual pigment, shifting the λ_{max} of the SWS visual pigment towards longer wavelengths will help to reduce overlap between these two spectral classes, as does the evolution of a C-type oil droplet with a longer λ_{cut}, which is thought to increase colour constancy and perceived colour contrast (Govardovskii, 1983; Vorobyev *et al.*, in press).

The largest variations in λ_{max} occur with the visual pigment associated with T-type oil droplets. As discussed in chapter two, the visual pigments measured in this class of cone fall into two broad categories. Galliformes (chicken, Japanese quail, peacock and turkey) and Anseriformes (duck) possess a VS visual pigment

(λ_{max} 415 to 426 nm). Passeriformes (zebra finch, Pekin robin, canary, starling, blackbird and blue tit) and the Psittaciformes (budgerigar) all possess a UVS visual pigment (λ_{max} approximately 355 to 376 nm). There may also be a third group (λ_{max} 402 to 409 nm) represented by the Manx shearwater, Humboldt penguin (both Ciconiformes) and pigeon (Columbiformes). Whilst these groupings appear to reflect phylogeny, they are undoubtedly influenced to some extent by visual ecology and, before firm conclusions can be made, more data are needed.

However, in order to estimate the importance of ecological influences on the spectral tuning of all classes of visual pigment, over and above the constraints imposed by historical legacy, comparisons between species must be phylogenetically independent (Harvey and Pagel, 1991). Broadly speaking, closely related species are likely to be more similar to each other than more distant relatives (Felsenstein, 1985). Accordingly, the analysis of phylogenetically independent contrasts, sometimes called the 'comparative method' (Harvey and Pagel, 1991), requires information about phylogenetic relatedness and time since divergence for all species investigated (Richman and Price, 1992). These data are now available for many birds (e.g. Sibley and Ahlquist, 1990; Sibley and Monroe, 1990) and, whilst beyond the scope of this thesis, it is envisaged that such an approach may soon be viable, especially if visual pigment data from more species are obtained.

With regard to future microspectrophotometric investigations, the desire to study as wide a range of avian species as possible is hampered by the time-consuming nature of the technique, and the difficulty in obtaining measurable outer segments. Nevertheless, certain species may be earmarked for priority selection. For example, other Columbiformes and Ciconiformes should be examined to determine whether there is indeed a third major spectral location (λ_{max} between about 400 and 410 nm) for the visual pigment associated with a T-type oil droplet. Furthermore, in light of recent work by Viitala *et al.* (1995), which revealed that the kestrel can detect voles using the ultraviolet reflectance of their scent marks, diurnal birds of prey may prove to be useful study species. Alternatively, phylogenetically closely related species which inhabit different light environments, or have markedly different diets or plumage coloration, may provide useful comparative information. In these

respects, the Sturnidae, a family of passerines to which the European starling belongs, would be a suitable candidate (cf. Beecher, 1978; Feare, 1984).

An alternative approach to the technique of microspectrophotometry is the molecular genetic study of visual pigment opsin genes. The amino acid composition of the opsin proteins produced by these genes determines the spectral absorption properties of the visual pigments they become. Many spectral tuning sites in opsin proteins have been identified, and it is conceivable that, before long, the genome of a given species can be screened for opsin genes and the λ_{max} values of the species' visual pigments predicted from their nucleotide sequences. Furthermore, *in situ* hybridisation with anti-opsin probes, as described in chapter three, will be able to show that a particular opsin gene is being expressed in specific photoreceptors (Wilkie *et al.*, 1998). This approach may prove to be more efficient then microspectrophotometry in surveying a large number of species and, by studying the genetic sequence, may provide more information about the evolution of opsin genes.

In addition to interspecific variations in visual pigment λ_{max}, there is also considerable variation in the topographical distribution of the different cone types within the retina, and the spectral absorption characteristics of the P-type oil droplets found in the principal member of the double cones. Whilst the patterns observed cannot always be correlated with particular aspects of visual ecology, they generally describe differences between the posterior dorsal region of the eye, which is thought to subserve binocular vision, and the remaining retinal area. However, some species, such as the mallard duck (Jane and Bowmaker, 1988), have a more homogeneous distribution of the different photoreceptor types across their retinae. In clarifying the factors which influence retinal organisation, it is essential that all cone types are distinguished. As described in chapter three, this has not been the case for many of the species studied to date and the available data is of limited use. Nevertheless, using the techniques described in this thesis, this is entirely possible and a more thorough survey of the relative proportions and topographic distribution of cone photoreceptors in a range of species, together with rigorous statistical analysis, is overdue.

In conclusion, despite well over a century of work in bird vision, few firm statements can be made about the relationship between visual physiology and visual

ecology. The varied anatomical structures of the avian eye and visual nervous system are a combination of functional adaptation and phylogenetic ancestry, which complicates the identification of task- or environment-specific specialisations. Nevertheless, it is hoped that this thesis contributes usefully to the growing body of knowledge regarding avian vision such that more reliable conclusions may one day be made.

REFERENCES

6. References

Adler, H. E. and Dalland, J. I. (1959). Spectral thresholds in the starling (*Sturnus vulgaris*). *Journal of Comparative and Physiological Psychology* **52,** 438-445.

Ammermüller, J., Itzhaki, A., Weiler, R. and Perlman, I. (1998). UV-sensitive input to horizontal cells in the turtle retina. *European Journal of Neuroscience* **10,** 1544-1552.

Andersson, S. and Amundsen, T. (1997). Ultraviolet colour vision and ornamentation in bluethroats. *Proceedings of the Royal Society of London B Biological Sciences* **264,** 1587-1591.

Andersson, S., Örnborg, J. and Andersson, M. (1998). Ultraviolet sexual dimorphism and assortative mating in blue tits. *Proceedings of the Royal Society of London B Biological Sciences* **265,** 445-450.

Andrew, R. J. (1991). The nature of behavioural lateralization in the chick. In *Neural and behavioural plasticity: the use of the domestic chick as a model* (Ed. R. J. Andrew). Oxford, New York, Tokyo: Oxford University Press.

Andrew, R. J. and Dharmaretnam, M. (1993). Lateralization and strategies of viewing in the domestic chick. In *Vision, brain and behavior in birds.* (Eds. H. P. Zeigler and H.-J. Bischoff), pp. 319-332. Cambridge, Massachussets; London, England: MIT press.

Applebury, M. L. and Hargrave, P. A. (1986). Molecular biology of the visual pigments. *Vision Research* **26,** 1881-1895.

Archer, S. N. (1988). A microspectrophotometric study of visual pigment polymorphism in the guppy, *Poecilia reticulata.* PhD Thesis. University of Bristol.

Armengol, J. A., Prada, F. and Genis-Galvez, J. M. (1981). Oil droplets in the chameleon (*Chamaleo chamaleo*) retina. *Acta Anatomica* **110,** 35-39.

Armington, J. C. and Thiede, F. C. (1956). Electroretinal demonstration of a purkinje shift in the chicken eye. *American Journal of Physiology* **186,** 258-262.

Avery, J. A. and Bowmaker, J. K. (1982). Visual pigments in the four eyed fish, *Anableps anableps. Nature (London)* **298,** 62-64.

Baird, S. F., Brewer, T. M. and Ridgway, R. (1875). *North American birds. Land Birds. Volume 3.* Boston: Little, Brown and company.

Barlow, H. B. (1982). What causes trichromacy? A theoretical analysis using comb-filtered spectra. *Vision Research* **22,** 635-643.

Barthel, L. K. and Raymond, P. A. (1990). Improved method for obtaining 3-μm cryosections for immunocytochemistry. *Journal of Histochemistry and Cytochemistry* **38,** 1383-1388.

Baylor, D. A. and Fettiplace, R. (1975). Light path and photon capture in turtle photoreceptors. *Journal of Physiology (London)* **248,** 433-464.

Baylor, D. A. and Hodgkin, A. L. (1973). Detection and resolution of visual stimuli by turtle photoreceptors. *Journal of Physiology (London)* **234,** 163-198.

Beecher, W. J. (1978). Feeding adaptations and evolution in the starlings. *Bulletin of the Chicago Academy of Sciences* **11,** 269-298.

Begin, M. T. and Handford, P. (1987). Comparative study of retinal oil droplets in grebes and coots. *Canadian Journal of Zoology* **65,** 2105-2110.

Bendire, C. (1892). *Life histories of North American birds. Volume 1.* Washington: Government Printing Office.

Bennett, A. T. D. and Cuthill, I. C. (1994). Ultraviolet vision in birds: What is its function? *Vision Research* **34,** 1471-1478.

Bennett, A. T. D., Cuthill, I. C., Partridge, J. C. and Lunau, K. (1997). Ultraviolet plumage colors predict mate preferences in starlings. *Proceedings of the National Academy of Sciences of the United States of America* **94,** 8618-8621.

Bennett, A. T. D., Cuthill, I. C., Partridge, J. C. and Maier, E. J. (1996). Ultraviolet vision and mate choice in zebra finches. *Nature (London)* **380,** 433-435.

Berger, E. R. (1966). On the mitochondrial origin of oil drops in the retinal double cone inner segments. *Journal of Ultrastructure Research* **14,** 143-157.

Bernard, G. D. (1987). Spectral characterization of butterfly *L*-receptors using extended Dartnall/MacNichol template functions. *Journal of the Optical Society of America Series A* **4,** P123.

Bischof, H.-J. (1988). The visual field and visually guided behaviour in the zebra finch (*Taeniopygia guttata*). *Journal of Comparative Physiology A Sensory, Neural and Behavioural Physiology* **163,** 329-337.

Blakers, M., Davies, S. J. J. F. and Reilly, P. N. (1984). *The atlas of Australian birds.* Victoria: Melbourne University Press.

Bliss, A. F. (1946). The chemistry of daylight vision. *Journal of General Physiology* **29,** 277-297.

Blough, P. M. (1972). Wavelength generalisation and discrimination in the pigeon. *Perception and Psychophysics* **12,** 342-348.

Blough, P. M., Riggs, L. A. and Schafer, K. L. (1972). Photopic spectral sensitivity determined electroretinographically for the pigeon eye. *Vision Research* **12,** 477-485.

Boehlert, G. W. (1978). Intraspecific evidence for the function of single and double cones in the teleost retina. *Science (Washington D.C.)* **202,** 309-311.

Bone, R. A. and Landrum, J. T. (1992). Distribution of macular pigment components, zeaxanthin and lutein, in human retina. *Methods in Enzymology* **213,** 360-366.

Born, M. and Wolf, E. (1970). *Principles of optics.* Oxford: Pergammon Press Ltd.

Bowmaker, J. K. (1973). Spectral sensitivity and visual pigment absorbance. *Vision Research* **13,** 783-792.

Bowmaker, J. K. (1977). The visual pigments, oil droplets and spectral sensitivity of the pigeon. *Vision Research* **17,** 1129-1138.

Bowmaker, J. K. (1979). Visual pigments and oil droplets in the pigeon retina, as measured by microspectrophotometry, and their relation to spectral sensitivity. In *Neural mechanisms of behaviour in the pigeon.* (Eds. A. M. Granda and J. H. Maxwell), pp. 287-305. New York, London: Plenum Press.

Bowmaker, J. K. (1984). Microspectrophotometry of vertebrate photoreceptors. *Vision Research* **24,** 1641-1650.

Bowmaker, J. K. (1991a). Visual pigments, oil droplets and photoreceptors. In *Vision and visual dysfunction. Volume 6. The perception of colour.* (Ed. P. Gouras), pp. 108-127. Boston: CRC Press, Inc.

Bowmaker, J.K. (1991b). Visual pigments: absorbance spectra and photoproducts. In *Photobiological techniques.* (Eds. Valenzeno, D. P., Pottier, R. H., Mathis, P. and R. H. Douglas), pp. 197-212. New York, London: Plenum Press.

Bowmaker, J. K., Astell, S., Hunt, D. M. and Mollon, J. D. (1991). Photosensitive and photostable pigments in the retinae of old world monkeys. *Journal of Experimental Biology* **156,** 1-19.

Bowmaker, J. K., Dartnall, H. J. A. and Mollon, J. D. (1980). Microspectrophotometric demonstration of four classes of photoreceptor in an Old World primate *Macaca fascicularis*. *Journal of Physiology (London)* **298,** 131-143.

Bowmaker, J. K., Heath, L. A., Wilkie, S. E. and Hunt, D. M. (1997). Visual pigments and oil droplets from six classes of photoreceptor in the retinas of birds. *Vision Research* **37,** 2183-2194.

Bowmaker, J. K. and Knowles, A. (1977). The visual pigments and oil droplets of the chicken retina. *Vision Research* **17,** 755-764.

Bowmaker, J. K., Kovach, J. K., Whitmore, A. V. and Loew, E. R. (1993). Visual pigments and oil droplets in genetically manipulated and carotenoid deprived quail: a microspectrophotometric study. *Vision Research* **33,** 571-578.

Bowmaker, J. K. and Kunz, Y. W. (1987). Ultraviolet receptors, tetrachromatic colour vision and retinal mosaics in the brown trout (*Salmo trutta*): Age-dependent changes. *Vision Research* **27,** 2101-2108.

Bowmaker, J. K., Loew, E. R. and Liebman, P. A. (1975). Variation in the λ_{max} of rhodopsin from individual frogs. *Vision Research* **15,** 997-1003.

Bowmaker, J. K. and Martin, G. R. (1978). Visual pigments and colour vision in a nocturnal bird, *Strix aluco* (tawny owl). *Vision Research* **18,** 1125-1130.

Bowmaker, J. K. and Martin, G. R. (1984). Colour vision in the penguin, *Spheniscus humboldti*: a microspectrophotometric study. *Vision Research* **24,** 1702.

Bowmaker, J. K. and Martin, G. R. (1985). Visual pigments and oil droplets in the penguin, *Spheniscus humboldti*. *Journal of Comparative Physiology A Sensory, Neural and Behavioural Physiology* **156,** 71-77.

Bownds, D. (1967). Site of attachment of retinal in rhodopsin. *Nature (London)* **216,** 1178-1181.

Bradbury, S. (1989). An introduction to the optical microscope. In *Royal microscopical society microscopy handbooks*. New York: Oxford University Press.

Bradshaw, J. L. and Nettleton, N. C. (1981). The nature of hemispheric specialization in man. *Behavioral and Brain Sciences* **4,** 51-91.

Braekevelt, C. R. (1990). Retinal photoreceptor fine structure in the mallard duck (*Anas platyrhynchos*). *Histology and Histopathology* **5,** 123-131.

Braekevelt, C. R. (1993a). Fine structure of the retinal photoreceptors of the great horned owl (*Bubo virginianus*). *Histology and Histopathology* **8,** 25-34.

Braekevelt, C. R. (1993b). Retinal photoreceptor fine structure in the red-tailed hawk. *Anatomia Histologia Embryologia* **22,** 222-232.

Braekevelt, C. R. (1994a). Retinal photoreceptor fine structure in the American crow (*Corvus brachyrhynchos*). *Anatomia Histologia Embryologia* **23,** 376-387.

Braekevelt, C. R. (1994b). Retinal photoreceptor fine structure in the great blue heron (*Ardea herodias*). *Anatomia Histologia Embryologia* **23,** 281-292.

Braekevelt, C. R., Smith, S. A. and Smith, B. J. (1996). Fine structure of the retinal photoreceptors of the barred owl (*Strix varia*). *Histology and Histopathology* **11,** 79-88.

Brandt, R. and Vorobyev, M. (1997). Metric analysis of threshold spectral sensitivity in the honeybee. *Vision Research* **37,** 425-439.

Bridges, C. D. B. (1962). Visual pigments of the pigeon (*Columba livia*). *Vision Research* **2,** 125-137.

Brines, M. L. and Gould, J. L. (1982). Skylight polarization patterns and animal orientation. *Journal of Experimental Biology* **96,** 69-91.

Brown, P. K. (1961). A system for microspectrophotometry employing a commercial recording spectrophotometer. *Journal of the Optical Society of America* **51,** 1000-1008.

Budnik, V., Mpodozis, J., Varela, F. J. and Maturana, H. R. (1984). Regional specialization of the quail retina: ganglion cell density and oil droplet distribution. *Neuroscience Letters* **51,** 145-150.

Bumstead, K., Jasoni, C., Szél, A. and Hendrikson, A. (1997). Spatial and temporal expression of cone opsins during monkey retinal development. *Journal of Comparative Neurology* **378,** 117-134.

Bunn, D. S., Warburton, A. B. and Wilson, R. D. S. (1982). *The barn owl.* Calton: T. and A.D. Poyser.

Burkhardt, D. (1982). Birds, berries and UV. *Naturwissenschaften* **69,** 153-157.

Butcher, R. G. (1972). Succinate oxidation in intact tissue sections: The effect of oxidation in the cytoplasm. *Histochemie* **32,** 369-378.

Cameron, D. A. and Pugh, E. N., Jr. (1991). Double cones as a basis for a new type of polarization vision in vertebrates. *Nature (London)* **353,** 161-164.

Campenhausen, M. v. and Kirschfeld, K. (1998). Spectral sensitivity of the accessory optic system of the pigeon. *Journal of Comparative Physiology A Sensory, Neural and Behavioural Physiology* **183,** 1-6.

Chan, T., Lee, M. and Sakmar, T. P. (1992). Introduction of hydroxyl-bearing amino acids causes bathochromic spectral shifts in rhodopsin. *Journal of Biological Chemistry* **267,** 9478-9480.

Chance, B., Perry, R., Åkerman, L. and Thorell, B. (1959). Highly sensitive recording microspectrophotometer. *The Review of Scientific Instruments* **30,** 735-741.

Chen, D.-M., Collins, J. S. and Goldsmith, T. H. (1984). The ultraviolet receptor of bird retinas. *Science (Washington D.C.)* **225,** 337-340.

Chen, D.-M. and Goldsmith, T. H. (1986). Four spectral classes of cone in the retinas of birds. *Journal of Comparative Physiology A Sensory, Neural and Behavioural Physiology* **159,** 473-479.

Church, S. C., Bennett, A. T. D., Cuthill, I. C. and Partridge, J. C. (1998). Ultraviolet cues affect the foraging behaviour of blue tits. *Proceedings of the Royal Society of London B Biological Sciences* **265,** 1509-1514.

Clarke, P. G. H., Gyger, M. and Catsicas, S. (1996). A centrifugally controlled circuit in the avian retina and its possible role in visual attention switching. *Visual Neuroscience* **13,** 1043-1048.

Coemans, M. A. J. M., Vos Hzn, J. J. and Nuboer, J. F. W. (1994). The orientation of the e-vector of linearly polarized light does not affect the behaviour of the pigeon *Columba livia*. *Journal of Experimental Biology* **191,** 107-123.

Cohen, A. I. (1963). The fine structure of the visual receptors in the pigeon. *Experimental Eye Research* **2,** 88-97.

Collier, R. J., Waldron, W. R. and Zigman, S. (1989). Temporal sequence to changes to the Gray squirrel retina after near-UV exposure. *Investigative Ophthalmology and Visual Science* **30,** 631-637.

Coulton, G. (1990). Non-radioisotopic labels for *in situ* hybridisation histochemistry: a histochemist's view. In *In situ hybridisation: application to developmental biology and medicine.* (Eds. N. Harris and D. G. Wilkinson), pp. 1-32. Cambridge, New York, Port Chester, Melbourne, Sydney: Cambridge University Press.

Cowan, W. M., Adamson, L. and Powell, T. P. S. (1961). An experimental study of the avian visual system. *Journal of Anatomy* **95,** 545-562.

Crescitelli, F. (1958). The natural history of visual pigments. *Annals of the New York Academy of Sciences* **74,** 230-255.

Crescitelli, F. (1977). The visual pigments of geckos and other vertebrates: an essay in comparative biology. In *The visual sytem in vertebrates.* (Ed. F. Crescitelli), pp. 391-449. Berlin, Heidelberg, New York: Springer-Verlag.

Crescitelli, F., Wilson, B. W. and Lilyblade, A. L. (1964). The visual pigments of birds. I. The turkey. *Vision Research* **4,** 275-280.

Crescitelli, F. a. K., B. (1991). The gecko visual pigment: the anion hypsochromic effect. *Vision Research* **31,** 945-950.

Cserháti, P., Szél, A. and Röhlich, P. (1989). Four cone types characterized by anti-visual pigment antibodies in the pigeon retina. *Investigative Ophthalmology and Visual Science* **30,** 74-81.

Cuthill, I. C., Bennett, A. T. D., Partridge, J. C. and Maier, E. J. (in press). Ultraviolet reflectance and the objective assessment of avian sexual dichromatism. *American Naturalist.*

Dalland, J. I. (1958). Spectral Thresholds in the Starling (*Sturnus vulgaris*). PhD thesis. University of Columbia.

Dartnall, H. J. A. (1953). The interpretation of spectral sensitivity curves. *British Medical Bulletin* **9,** 24-30.

Dartnall, H. J. A. (1967). The visual pigment of the green rods. *Vision Research* **7,** 1-16.

Dartnall, H. J. A. (1972). Photosensitivity. In *Photochemistry of vision.* (Ed. H. J. A. Dartnall), pp. 122-145. Berlin, Heidelberg, New York: Springer-Verlag.

Das, D. (1997). Visual pigments, oil droplets and opsin sequences from the canary, Serinus canaria. PhD Thesis. University of London.

Davies, B. H. (1976). Carotenoids. In *Chemistry and biochemistry of plant pigments. Volume 2.* (Ed. T. W. Goodwin). New York, London: Academic press.

Davies, B. H. (1979). Solved and unsolved problems of carotenoid formation. *Pure and Applied Chemistry* **51,** 623-630.

Davies, B. H. (1985). Carotenoid metabolism in animals: a biochemist's view. *Pure and Applied Chemistry* **57,** 679-684.

Dawis, S. M. (1981). Polynomial expressions of pigment nomograms. *Vision Research* **21,** 1427-1430.

Delius, J. D. and Emmerton, J. (1979). Visual performance of pigeons. In *Neural mechanisms of behaviour in the pigeon.* (Eds. A. M. Granda and J. H. Maxwell), pp. 51-69. New York, London: Plenum Press.

Dharmaretnam, M. and Andrew, R. J. (1994). Age- and stimulus-specific use of right and left eyes by the domestic chick. *Animal Behaviour* **48,** 1395-1406.

Donner, K. O. (1958). On the effect of the coloured oil droplets on the spectral sensitivity of the avian retina. In *Proceedings of the XIIth International Ornithological Congress*, pp. 167-172. Helsinki.

Dratz, E. A. and Hargrave, P. A. (1983). The structure of rhodopsin and the rod outer segment disk membrane. *Trends in Biological Sciences* **8,** 128-131.

Dubbeldam, J. L. and Tellegen, A. J. (1996). The role of the visual system in the mallard, *Anas platyrhynchos* L. In *Third Benelux Congress of Zoology*. Namur, Belgium.

Duecker, G. and Schultz, I. (1977). Color vision and color preference in japanese quail (*Coturnix coturnix japonica*) with colourless oil droplets. *Journal of Comparative and Physiological Psychology* **91,** 1110-1117.

Ebrey, T. G. and Honig, B. (1977). New wavelength dependant visual pigment nomograms. *Vision Research* **17,** 147-151.

Edmonds, D. T. (1996). A sensitive optically detected magnetic compass for animals. *Proceedings of the Royal Society of London B Biological Sciences* **263,** 295-298.

Ehrlich, P. R., Dobkin, D. S., Wheye, D. and Pimm, S. L. (1994). *The birdwatcher's handbook: a guide to the natural history of the birds of Britain and Europe.* Oxford, New York, Tokyo: Oxford University Press.

Ellingson, J. M., Fleishman, L. J. and Loew, E. R. (1995). Visual pigments and spectral sensitivity of the diurnal gecko *Gonatodes albogularis*. *Journal of Comparative Physiology A Sensory, Neural and Behavioural Physiology* **177,** 559-567.

Emmerton, J. and Delius, J. D. (1980). Wavelength discrimination in the 'visible' and ultraviolet spectrum by pigeons. *Journal of Comparative Physiology* **141,** 47-52.

Emmerton, J., Schwemer, J., Muth, J. and Schlecht, P. (1980). Spectral transmission of the ocular media of the pigeon (*Columba livia*). *Investigative Ophthalmology and Visual Science* **19,** 1382-1387.

Endler, J. A. (1993). The color of light in forests and its implications. *Ecological Monographs* **63,** 1-27.

Engelage, J. and Bischof, H.-J. (1993). The organization of the tectofugal pathway in birds: a comparative review. In *Vision, brain and behavior in birds.* (Eds. H. P. Zeigler and H.-J. Bischof), pp. 137-158. Cambridge, Massachusetts; London, England: MIT press.

Engström, K. (1958). On the cone mosaic in the retina of *Parus major*. *Acta Zoologica (Stockholm)* **39,** 65-69.

Enoch, J. M. (1963). The use of tetrazolium to distinguish between retinal receptors exposed and not exposed to light. *Investigative Ophthalmology* **2,** 16-23.

Enoch, J. M. (1964). Validation of an indicator of mammalian retinal receptor response: Action spectrum. *Journal of the Optical Society of America* **54,** 368-374.

Fager, L. Y. and Fager, R. S. (1981). Chicken blue and chicken violet, short wavelength visual pigments. *Vision Research* **21,** 581-586.

Fager, L. Y. and Fager, R. S. (1982). Chromatographic separation of rod and cone pigments from chicken retinas. *Methods in Enzymology* **81,** 160-167.

Falk, G. and Fatt, P. (1972). Physical changes induced by light in the rod outer segments of vertebrates. In *Photochemistry of vision.* (Ed. H. J. A. Dartnall), pp. 200-244. Berlin, Heidelberg, New York: Springer-Verlag.

Feare, C. (1984). *The starling*. Oxford, New York: Oxford University Press.

Fein, A. and Szuts, E. Z. (1982). *Photoreceptors: their role in vision.* Cambrdge: Cambridge University Press.

Felsenstein, J. (1985). Phylogenies and the comparative method. *American Naturalist* **125,** 1-15.

Fite, K. V. (1973). Anatomical and behavioural correlates of visual acuity in the great horned owl. *Vision Research* **13,** 219-230.

Flannery, J. G., Dinehart, W. J., Street, C. and Hauswirth, W. W. (1993). *In situ* hybridization of retinal messenger RNA using nonradioactive synthetic probes. In *Photoreceptor Cells.* (Ed. P. A. Hargrave), pp. 357-376. New York, London: Academic Press, Inc.

Fowler, J. and Cohen, L. (1990). *Practical statistics for field biology.* Chichester, New York, Brisbane, Toronto, Singapore: John Wiley and Sons, Ltd.

Fujimoto, K., Yanase, T. and Hanaoka, T. (1957). Spectral transmittance of retinal coloured oil globules re-examined with microspectrophotometer. *Japanese Journal of Physiology* **7,** 339-346.

Gall, J. C. and Pardue, M. L. (1969). Formation and detection of RNA-DNA hybrid molecules in cytological preparations. *Proceedings of the National Academy of Sciences of the United States of America* **63,** 378-383.

Gaston, K. E. and Gaston, M. G. (1984). Unilateral memory after binocular discrimination training: left hemisphere dominance in the chick? *Brain Research* **303,** 190-193.

Geeraets, W. J., Williams, R. C., Chan, G., Ham, W. T., Jr., Gerry, D., III and Schmidt, F. H. (1960). The loss of light energy in retina and choroid. *Archives of Ophthalmology* **64,** 606-615.

Giaid, A., Gibson, S. J., Steel, J. H., Facer, P. and Polak, J. M. (1990). The use of complementary RNA probes for the identification and localisation of peptide messenger RNA in the diffuse neuroendocrine system. In *In situ hybridisation: application to developmental biology and medicine.* (Eds. N. Harris and D. G. Wilkinson), pp. 43-67. Cambridge, New York, Port Chester, Melbourne, Sydney: Cambridge University Press.

Giurfa, M., Vorobyev, M., Brandt, R., Posner, B. and Menzel, R. (1997). Discrimination of coloured stimuli by honeybees: alternative use of achromatic

and chromatic signals. *Journal of Comparative Physiology A Sensory, Neural and Behavioural Physiology* **180,** 235-243.

Glasser, A. and Howland, H. C. (1996). A history of studies of visual accommodation in birds. *Quarterly Review of Biology* **71,** 475-509.

Goldsmith, T. H. (1978). The effects of screening pigments on the spectral sensitivity of some crustacea with scotopic (superposition) eyes. *Vision Research* **18,** 475-482.

Goldsmith, T. H. (1980). Hummingbirds see near ultraviolet light. *Science (Washington D.C.)* **207,** 786-788.

Goldsmith, T. H. (1990). Optimization, constraint and history in the evolution of eyes. *Quarterly Review of Biology* **65,** 281-321.

Goldsmith, T. H., Chen, D.-M. and Collins, J. S. (1984a). The ultraviolet receptors of bird retinas. *Investigative Ophthalmology and Visual Science* **25,** 287.

Goldsmith, T. H., Collins, J. S. and Licht, S. (1984b). The cone oil droplets of avian retinas. *Vision Research* **24,** 1661-1671.

Goldsmith, T. H., Collins, J. S. and Pearlman, D. L. (1981). A wavelength discrimination function for the hummingbird *Archilochus alexandri. Journal of Comparative Physiology* **143,** 103-110.

Gondo, M. and Ando, H. (1995). Comparative histophysiological study of oil droplets in the avian retina. *Japanese Journal of Ornithology* **44,** 81-91.

Goodwin, D. (1982). *Estrildid finches of the world.* Oxford: Oxford University Press.

Govardovskii, V. I. (1983). On the role of oil drops in colour vision. *Vision Research* **23,** 1739-1740.

Govardovskii, V. I. and Zeuva, L. V. (1977). Visual pigments of chicken and pigeon. *Vision Research* **17,** 537-543.

Graf, V. and Norren, D. V. (1974). A blue sensitive mechanism in the pigeon retina: λ_{max} 400nm. *Vision Research* **14,** 1203-1209.

Graf, V. A. (1969). A spectral luminosity function in the pigeon determined by flicker photometry. *Psychon. Sci.* **17,** 282-283.

Graf, V. A. (1979). Four spectral mechanisms in the pigeon (*Columba livia*). In *Neural mechanisms of behaviour in the pigeon.* (Eds. A. M. Granda and J. H. Maxwell), pp. 129-144. New York, London: Plenum Press.

Griswold, M. S. and Stark, W. S. (1992). Scotopic spectral sensitivity of phakic and aphakic observers extending into the near ultraviolet. *Vision Research* **32,** 1739-1743.

Guilford, T. and Dawkins, M. S. (1991). Receiver psychology and the evolution of animal signals. *Animal Behaviour* **42,** 1-14.

Güntürkün, O. (1985). Lateralization of visually controlled behavior in pigeons. *Physiology and Behavior* **34,** 575-577.

Güntürkün, O. (1997). Avian visual lateralization: a review. *NeuroReport* **8,** R3-R11.

Güntürkün, O. and Kesch, S. (1987). Visual lateralization during feeding in pigeons. *Behavioral Neuroscience* **101,** 433-435.

Güntürkün, O. and Kischkel, K.-F. (1992). Is visual lateralization in pigeons sex-dependent? *Behavioural Brain Research* **47,** 83-87.

Güntürkün, O., Miceli, D. and Watanabe, M. (1993). Anatomy of the avian thalamofugal pathway. In *Vision, brain and behavior in birds.* (Eds. H. P. Zeigler and H.-J. Bischof). Cambridge, Massachussets, London, England: MIT press.

Hailman, J. P. (1976). Oil droplets in the eyes of adult anuran amphibians: a comparative survey. *Journal of Morphology* **148,** 453-468.

Ham, W. T., Mueller, H. A. and Sliney, D. H. (1976). Retinal sensitivity to damage from short wavelength light. *Nature (London)* **260,** 153-155.

Ham, W. T., Ruffolo, J. J., Mueller, H. A., Clarke, A. M. and Moon, M. E. (1978). Histologic analysis of photochemical lesions produced in rhesus retina by short-wavelength light. *Investigative Ophthalmology and Visual Science* **17,** 1029-1035.

Hamilton, W. F. and Coleman, T. B. (1933). Trichromatic vision in the pigeon as illustrated by the spectral hue discrimination curve. *Journal of Comparative Psychology* **15,** 183-191.

Hanaoka, T. and Fujimoto, K. (1957). Absorption spectrum of a single cone in carp retina. *Japanese Journal of Physiology* **7,** 276-285.

Handelman, G. J., Snodderly, D. M., Adler, A. J., Russett, M. D. and Dratz, E. A. (1992). Measurement of carotenoids in human and monkey retinas. *Methods in Enzymology* **213,** 220-230.

Hárosi, F. I. (1971). Frog rhodopsin *in situ*: orientational and spectral changes in the chromophores of isolated retinal rod cells. PhD Thesis. The John Hopkins University, Baltimore, Maryland.

Hárosi, F. I. (1975). Absorption spectra and linear dichroism of some amphibian photoreceptors. *Journal of General Physiology* **66,** 357-382.

Hárosi, F. I. (1976). Spectral relations of cone pigments in goldfish. *Journal of General Physiology* **68,** 65-80.

Hárosi, F. I. (1985). Ultraviolet- and violet-absorbing vertebrate visual pigments: dichroic and bleaching properties. In *The Visual System.* (Eds. A. Fein and J. S. Levine), pp. 41-55. New York: Liss.

Hárosi, F. I. (1987). Cynomolgus and Rhesus monkey visual pigments: application of Fourier transform smoothing and statistical techniques to the determination of spectral parameters. *Journal of General Physiology* **89,** 717-743.

Hárosi, F. I. (1994). An analysis of two spectral properties of vertebrate visual pigments. *Vision Research* **34,** 1359-1367.

Hárosi, F. I. and Hashimoto, Y. (1983). Ultraviolet pigments in a vertebrate: a tetrachromatic cone system in the dace. *Science (Washington D.C.)* **222,** 1021-1023.

Hárosi, F. I. and MacNichol, E. F., Jr. (1974). Dichroic microspectrophotometer: a computer-assisted, rapid, wavelength-scanning photometer for measuring linear dichroism in single cells. *Journal of the Optical Society of America* **64,** 903-918.

Hárosi, F. I. and Malerba, F. E. (1975). Plane-polarized light in microspectrophotometry. *Vision Research* **15,** 379-388.

Hárosi, F. I. and Sandorfy, C. (1995). Retinylidene-opsin Schiff base chromophores and their accessibility to water. *Photochemistry and Photobiology* **61,** 510-517.

Harvey, P. H. and Pagel, M. D. (1991). *The comparative method in evolutionary biology.* Oxford: Oxford University Press.

Hauser, M. D. (1993). Right hemisphere dominance for the production of facial expression in monkeys. *Science (Washington D.C.)* **261,** 475-477.

Hawryshyn, C. W., Arnold, M. G., Bowering, E. and Cole, R. L. (1990). Spatial orientation of rainbow trout to plane-polarized light: the ontogeny of E-vector

discrimination and spectral sensitivity characteristics. *Journal of Comparative Physiology A Sensory, Neural and Behavioural Physiology* **166,** 565-574.

Hawryshyn, C. W. and Harosi, F. I. (1991). Ultraviolet photoreception in carp: microspectrophotometry and behaviourally determined action spectra. *Vision Research* **31,** 567-576.

Hawryshyn, C. W. and Hárosi, F. I. (1994). Spectral characteristics of visual pigments in Rainbow Trout (*Oncorhynchus mykiss*). *Vision Research* **34,** 1385-1392.

Hazlett, L. D., Meyer, D. B. and Susan, S. R. (1974). Visual cell ultrastructure in the Japanese Quail (*Coturnix coturnix japonica*). *Anatomical Record* **178,** 371-372.

Heath, L. A., Wilkie, S. E., Bowmaker, J. K. and Hunt, D. M. (1997). The rod and green cone opsins of two avian species, the budgerigar, *Melopsittacus undulatus*, and the mallard duck, *Anas platyrhynchus*. *Gene* **204,** 121-126.

Heinermann, P. H. (1984). Yellow intraocular filters in fishes. *Experimental Biology* **43,** 127-147.

Hillstead, A. F. C. (1944). *The blackbird.* London: Faber and Faber Ltd.

Hodos, W., Miller, R. F. and Fite, K. V. (1991). Age-dependent changes in visual acuity and retinal morphology in pigeons. *Vision Research* **31,** 669-677.

Hudon, J. and Muir, A. D. (1996). Characterization of the reflective materials and organelles in the bright irides of the North-American blackbirds (Icterinae). *Pigment Cell Research* **9,** 96-104.

Hudon, J. and Oliphant, L. W. (1995). Reflective organelles in the anterior pigment-epithelium of the iris of the European starling *Sturnus vulgaris*. *Cell and Tissue Research* **280,** 383-389.

Hunt, R. W. G. (1991). *Measuring Colour.* New York: Ellis Horwood.

Hunt, S., Bennett, A. T. D., Cuthill, I. C. and Griffiths, R. (1998). Blue tits are ultraviolet tits. *Proceedings of the Royal Society of London B Biological Sciences* **265,** 451-455.

Hunt, S., Cuthill, I. C., Swaddle, J. P. and Bennett, A. T. D. (1997). Ultraviolet vision and band-colour preferences in female zebra finches, *Taeniopygia guttata*. *Animal Behaviour* **54,** 1383-1392.

Huth, H. H. and Burkhardt, D. (1972). Der spektrale Sehbereich eines Violettohr-Kolibris. *Naturwissenschaften* **59,** 650.

Ikeda, H. (1965). The spectral sensitivity of the pigeon (*Columba livia*). *Vision Research* **5,** 19-36.

Imai, H., Kojima, D., Oura, T., Tachibanaki, S., Terakita, A. and Shichida, Y. (1997). Single amino acid residue as a functional determinant of rod and cone visual pigments. *Proceedings of the National Academy of Sciences of the United States of America* **94,** 2322-2326.

Isler, O. (1971). Carotenoids. Basle: Birkhäuser.

Ives, J., Barber, P. and Normann, R. (1982). Light intensification mediated by cone oil droplets. *Investigative Ophthalmology and Visual Science* **22,** 276A.

Ives, J. T., Normann, R. A. and Barber, P. W. (1983). Light intensification by cone oil droplets: electromagnetic considerations. *Journal of the Optical Society of America Series A* **73,** 1725-1731.

Jacobs, G. H. (1981). *Comparative color vision.* New York, London: Academic Press.

Jacobs, G. H. (1993). The distribution and nature of colour vision among the mammals. *Biological Reviews* **68,** 413-471.

Jacobs, G. H., Crognale, M. and Fenwick, J. (1987). Cone pigment of the great horned owl. *Condor* **89,** 434-436.

Jagger, W. S. and Liebman, P. A. (1976). Anomalous dispersion of rhodopsin in rod outer segments of the frog. *Journal of the Optical Society of America* **66,** 56-59.

Jane, S. D. and Bowmaker, J. K. (1988). Tetrachromatic colour vision in the duck (*Anas platyrhynchos* L.): microspectrophotometry of visual pigments and oil droplets. *Journal of Comparative Physiology A Sensory, Neural and Behavioural Physiology* **162,** 225-235.

Johnston, D. and Hudson, R. A. (1974). Phospholipids of the cone-rich chicken retina and its photoreceptor outer segment membranes. *Biochimica et Biophysica Acta* **369,** 269-277.

Johnston, D. and Hudson, R. A. (1976). Isolation and composition of the carotenoid-containing oil droplets from cone photoreceptors. *Biochimica et Biophysica Acta* **424,** 235-245.

Karnik, S. S., Sakmar, T. P., Chen, H. B. and Khorana, H. G. (1988). Csyteine residue-110 and residue-187 are essential for the formation of correct structure in bovine rhodopsin. *Proceedings of the National Academy of Sciences of the United States of America* **85,** 8459-8463.

Katzir, G. (1993). Visual mechanisms of prey capture in water birds. In *Vision, brain and behavior in birds.* (Eds. H. P. Zeigler and H.-J. Bischof). Cambridge, Massachusetts; London, England: MIT press.

Kawamuro, K., Irie, T. and Nakamura, T. (1997). Filtering effect of cone oil droplets detected in the P-III response spectra of Japanese Quail. *Vision Research* **37,** 2829-2834.

Kent, J. (1997). The visual pigments of deep-sea crustaceans. PhD Thesis. University of Bristol.

King-Smith, P. E. (1969). Absorption spectra and function of the coloured oil drops in the pigeon retina. *Vision Research* **9,** 1391-1399.

Kirsch, M., Wagner, H.-J. and Douglas, R. H. (1989). Rods trigger light adaptive retinomotor movements in all spectral cone types of a teleost fish. *Vision Research* **29,** 389-396.

Kirschfeld, K. (1982). Carotenoid pigments: their possible role in protecting against photooxidation in eyes and photoreceptor cells. *Proceedings of the Royal Society of London B Biological Sciences* **216,** 71-85.

Kleinschmidt, J. and Hárosi, F. (1992). Anion sensitivity and spectral tuning of cone visual pigments *in situ. Proceedings of the National Academy of Sciences of the United States of America* **89,** 9181-9185.

Knabe, W., Skatchkov, S. and Kuhn, H.-J. (1997). "Lens mitochondria" in the retinal cones of the tree-shrew *Tupaia belangeri. Vision Research* **37,** 267-271.

Knowles, A. (1976). The effects of chloride ion upon chicken visual pigments. *Biochemical and Biophysical Research Communications* **73,** 56-62.

Knowles, A. and Dartnall, H. J. A. (1977). *The photobiology of vision.* New York: Academic Press, Inc.

Kolb, H. and Jones, J. (1987). The distinction by light and electron microscopy of two types of cone containing colourless oil droplets in the retina of the turtle. *Vision Research* **27,** 1445-1458.

Kreithen, M. L. (1979). The sensory world of the homing pigeon. In *Neural mechanisms of behaviour in the pigeon.* (Eds. A. M. Granda and J. H. Maxwell), pp. 21-33. New York, London: Plenum Press.

Kreithen, M. L. and Eisner, T. (1978). Ultraviolet light detection by the homing pigeon. *Nature (London)* **272,** 347-348.

Kreithen, M. L. and Keeton, W. T. (1974). Detection of polarized light by the homing pigeon, *Columba livia. Journal of Comparative Physiology* **89,** 83-92.

Lamb, T. D. (1995). Photoreceptor spectral sensitivities: common shape in the longwave region. *Vision Research* **35,** 3083-3091.

Leask, M. J. M. (1977). A physicochemical mechanism for magnetic field detection by migratory birds and homing pigeons. *Nature (London)* **267,** 144-145.

Levine, J. S. and MacNichol, E. F., Jr. (1982). Color vision in fishes. *Scientific American* **246,** 108-117.

Levine, J. S. and MacNichol, E. F., Jr. (1985). Microspectrophotometry of primate photoreceptors: art, artefact and analysis. In *The visual system.* (Eds. A. Fein and J. S. Levine), pp. 73-87. New York: Liss.

Levine, J. S., MacNichol, E. F., Jr., Kraft, T. and Collins, B. A. (1979). Intraretinal distribution of cone pigments in certain teleost fishes. *Science (Washington D.C.)* **204,** 523-526.

Liebman, P. A. (1962). *In situ* microspectrophotometric studies on the pigments of single retinal rods. *Biophysics Journal* **2,** 161-178.

Liebman, P. A. (1972). Microspectrophotometry of photoreceptors. In *Photochemistry of vision.* (Ed. H. J. A. Dartnall), pp. 481-528. Berlin, Heidelberg, New York: Springer-Verlag.

Liebman, P. A. (1975). Birefringence, dichroism and rod outer segment structure. In *Photoreceptor optics.* (Eds. A. W. Snyder and R. Menzel), pp. 199-214. Berlin, Heidelberg, New York: Springer-Verlag.

Liebman, P. A. and Entine, G. (1964). Sensitive low-light-level microspectrophotometer: detection of photosensitive pigments of retinal cones. *Journal of the Optical Society of America* **54,** 1451-1459.

Liebman, P. A. and Entine, G. (1968). Visual pigments of frog and tadpole (*Rana pipiens*). *Vision Research* **8,** 761-775.

Liebman, P. A. and Granda, A. M. (1971). Microspectrophotometric measurements of visual pigments in two species of turtle *Pseudemys scripta* and *Chelonia mydas*. *Vision Research* **11,** 105-114.

Liebman, P. A. and Granda, A. M. (1975). Super dense carotenoid spectra resolved in single cone oil droplets. *Nature (London)* **253,** 370-372.

Lipetz, L. E. (1984a). A new method for determining peak absorbance of dense pigment samples and its application to the cone oil droplets of *Emydoidea blandingii*. *Vision Research* **24,** 597-604.

Lipetz, L. E. (1984b). Pigment types, densities and concentrations in cone oil droplets of *Emydoidea blandingii*. *Vision Research* **24,** 605-612.

Loew, E. R., Govardovskii, V. I., Röhlich, P. and Szél, A. (1996). Microspectrophotometric and immunocytochemical identification of ultraviolet photoreceptors in geckos. *Visual Neuroscience* **13,** 247-256.

Loew, E. R. and Wahl, C. M. (1991). A short-wavelength sensitive cone mechanism in juvenile yellow perch, *Perca flavescens*. *Vision Research* **31,** 353-360.

Lythgoe, J. N. (1979). The ecology of vision. Oxford: Oxford University Press.

MacNichol, E. F., Jr. (1978). A photon-counting microspectrophotometer for the study of single vertebrate photoreceptor cells. In *Frontiers of visual science.* (Eds. S. J. Cool and E. L. Smith), pp. 194-208. New York: Springer.

MacNichol, E. F., Jr. (1985). Predicting the entire spectral absorbance curve of any visual pigment from measurement on two template pigments. *Biological Bulletin* **169,** 555.

MacNichol, E. F., Jr. (1986). A unifying presentation of photopigment spectra. *Vision Research* **26,** 1543-1556.

MacNichol, E. F., Jr., Kunz, Y. W., Levine, J. S., Hárosi, F. I. and Collins, B. A. (1978). Elliposomes: organelles containing a cytochrome-like pigment in retinal cones of certain fishes. *Science (Washington D.C.)* **200,** 549-552.

MacNichol, E. F., Jr., Levine, J. S., Manfield, R. J. W., Lipetz, L. E. and Collins, B. A. (1983). Microspectrophotometry of visual pigments in primate photoreceptors. In *Colour vision: physiology and psychophysics.* (Eds. J. D. Mollon and L. T. Sharpe), pp. 13-38. London: Academic Press.

Maier, E. J. (1992). Spectral sensitivities including the ultraviolet of the passeriform bird *Leothrix lutea. Journal of Comparative Physiology A Sensory, Neural and Behavioural Physiology* **170,** 709-714.

Maier, E. J. (1993). To deal with the 'invisible'. On the biological significance of ultraviolet sensitivity in birds. *Naturwissenschaften* **80,** 476-478.

Maier, E. J. (1994). Ultraviolet vision in a passeriform bird: from receptor spectral sensitivity to overall spectral sensitivity in *Leothrix lutea. Vision Research* **34,** 1415-1418.

Maier, E. J. and Bowmaker, J. K. (1993). Colour vision in the passerifrom bird, *Leothrix lutea*: correlation of visual pigment absorbance and oil droplet transmission with spectral sensitivity. *Journal of Comparative Physiology A Sensory, Neural and Behavioural Physiology* **172,** 295-301.

Mansfield, R. J. W. (1985). Primate photopigments and cone mechanisms. In *The visual system.* (Eds. A. Fein and J. S. Levine), pp. 89-106. New York: Liss.

Marc, R. E. and Sperling, H. G. (1976). Colour receptor identities of goldfish cones. *Science (Washington D.C.)* **191,** 487-488.

Marc, R. E. and Sperling, H. G. (1977). Chromatic organization of primate cones. *Science (Washington D.C.)* **196,** 454-456.

Mariani, A. P. and Leure-DuPree, A. E. (1978). Photoreceptors and oil droplet colours in the red area of the pigeon retina. *Journal of Comparative Neurology* **182,** 821-838.

Marks, W. B. (1965). Visual pigments of single goldfish cones. *Journal of Physiology (London)* **178,** 14-32.

Marks, W. B., Dobelle, W. H. and MacNichol, E. F., Jr. (1964). Visual pigments of single primate cones. *Science (Washington D.C.)* **143,** 1181-1183.

Martin, G. R. (1974). Colour vision in the Tawny owl (*Strix aluco*). *Journal of Comparative and Physiological Psychology* **86,** 133-141.

Martin, G. R. (1982). An owl's eye: schematic optics and visual performance in *Strix aluco* L. *Journal of Comparative Physiology* **145,** 341-349.

Martin, G. R. (1985). Eye. In *Form and function in birds. Volume 3.* (Eds. A. S. King and J. McLelland), pp. 311-373. London: Academic Press.

Martin, G. R. (1986). The eye of a passeriform bird, the European starling (*Sturnus vulgaris*): eye movement amplitude, visual fields and schematic optics. *Journal of Comparative Physiology A Sensory, Neural and Behavioural Physiology* **159,** 545-557.

Martin, G. R. (1987). The world through a starling's eye. *New Scientist* **1562,** 49-51.

Martin, G.R. (1993). Producing the image. In *Vision, brain and behavior in birds.* (Eds. H. P. Zeigler and H.-J. Bischof), pp. 8-24. Cambridge, Massachussets; London, England: MIT press.

Martin, G. R. and Gordon, I. E. (1974). Increment-threshold spectral sensitivity in the tawny owl (*Strix aluco*). *Vision Research* **14,** 615-621.

Martin, G. R., Gordon, I. E. and Cadle, D. R. (1975). Electroretinographically determined spectral sensitivity in the tawny owl (*Strix aluco*). *Journal of Comparative and Physiological Psychology* **89,** 72-78.

Martin, G. R. and Muntz, W. R. A. (1978). Spectral sensitivity of the red and yellow oil droplet fields of the pigeon (*Columba livia*). *Nature (London)* **274,** 620-621.

Martin, G. R. and Muntz, W. R. A. (1979). Retinal oil droplets and vision in the pigeon (*Columba livia*). In *Neural mechanisms of behaviour in the pigeon.* (Eds. A. M. Granda and J. H. Maxwell), pp. 307-326. New York, London: Plenum Press.

Martin, G. R. and Young, S. R. (1984). The eye of the Humboldt penguin (*Spheniscus humboldti*): visual fields and schematic optics. *Proceedings of the Royal Society of London B Biological Sciences* **223,** 197-222.

Matsumoto, B. and Hale, I. L. (1993). Preparation of retinas for studying photoreceptors with confocal microscopy. In *Photoreceptor Cells.* (Ed. P. A. Hargrave), pp. 57-74. New York: Academic Press, Inc.

Mayr, I. (1972). Verteilung, Lokalisation und Absorption der Zapfenölkugeln bei Vögeln (Ploceidae). *Vision Research* **12,** 1477-1484.

Metzler, D. E. and Harris, C. M. (1978). Shapes of spectral bands of visual pigments. *Vision Research* **18,** 1417-1420.

Meyer, D. B. (1971). The effect of dietary carotenoid deprivation on avian retinal oil droplets. *Ophthalmic Research* **2,** 104-109.

Meyer, D. B. (1977). The avian eye and its adaptations. In *The visual system in vertebrates.* (Ed. F. Crescitelli), pp. 549-611. Berlin, Heidelberg, New York: Springer-Verlag.

Meyer, D. B., Cooper, T. G. and Gernez, C. (1965). Retinal oil droplets. In *The structure of the eye: II Symposium.* (Ed. J. W. Rohen), pp. 521-533. Stuttgart: Schattauer-Verlag.

Meyer, D. B. and May, H. C., Jr. (1973). The topographical distribution of rods and cones in the adult chicken retina. *Exp. Eye Res.* **17,** 347-355.

Meyer, D. B., Stuckey, S. R. and Hudson, R. A. (1971). Oil droplet carotenoids of avian cones - I. Dietary exclusion: models for biochemical and physiological studies. *Comparative Biochemistry and Physiology B* **40,** 61-70.

Miki, W. (1991). Biological functions and activities of animal carotenoids. *Pure and Applied Chemistry* **63,** 141-146.

Mollon, J. D. and Bowmaker, J. K. (1992). The spatial arrangement of cones in the primate fovea. *Nature (London)* **360,** 677-679.

Mollon, J. D., Bowmaker, J. K. and Jacobs, G. H. (1984). Variations of colour vision in a new world primate can be explained by polymorphism of retinal photopigments. *Proceedings of the Royal Society of London B Biological Sciences* **322,** 373-399.

Morris, V. B. (1970). Symmetry in a receptor mosaic demonstrated in the chick from the frequencies, spacing and arrangement of the types of retinal receptor. *Journal of Comparative Neurology* **140,** 359-398.

Morris, V. B. and Shorey, C. D. (1967). An electron microscope study of types of receptor in the chick retina. *Journal of Comparative Neurology* **129,** 313-340.

Morton, R. A. (1972). The chemistry of visual pigments. In *Photochemistry of vision.* (Ed. H. J. A. Dartnall), pp. 33-68. Berlin, Heidelberg, New York: Springer-Verlag.

Munro, U., Munro, J. A., Phillips, J. B. and Wiltschko, W. (1997). Effect of wavelength of light and pulse magnetism on different magnetoreception systems in a migratory bird. *Australian Journal of Zoology* **45,** 189-198.

Muntz, W. R. A. (1972). Inert absorbing and reflecting pigments. In *Photochemistry of Vision.* (Ed. H. J. A. Dartnall), pp. 529-565. Berlin, Heidelberg, New York: Springer-Verlag.

Nakanishi, K. (1991). 11-cis-retinal, a molecule uniquely suited for vision. *Pure and Applied Chemistry* **63,** 161-170.

Nakayama, T. A. and Khorana, H. G. (1990). Orientation of retinal in bovine rhodopsin determined by cross-linking using a photoactivatable analog of 11-cis-retinal. *Journal of Biological Chemistry* **265,** 15762-15769.

Nalbach, H.-O., Wolf-Oberhollenzer, F. and Remy, M. (1993). Exploring the image. In *Vision, brain and behavior in birds.* (Eds. H. P. Zeigler and H.-J. Bischof), pp. 25-46. Cambridge, Massachussets; London, England: MIT press.

Nelson, J. S. (1994). *Fishes of the world.* New York, Chichester, Brisbane, Toronto, Singapore: John Wiley and Sons, Inc.

Neumeyer, C. and Arnold, K. (1989). Tetrachromatic colour vision in the goldfish becomes trichromatic under white adaptation light of moderate intensity. *Vision Research* **29,** 1719-1727.

Neumeyer, C. and Jäger, J. (1985). Spectral sensitivity of the freshwater turtle *Pseudemys scripta elegans*: evidence for the filter-effect of colored oil droplets. *Vision Research* **25,** 833-838.

Nicol, J. A. C. and Arnott, H. J. (1974). Tapeta lucida in the eyes of goatsuckers (Caprimulgidae). *Proceedings of the Royal Society of London B Biological Sciences* **187,** 349-352.

Novales Flamarique, I. and Hawryshyn, C. W. (1997). No evidence of polarization sensitivity in freshwater Sunfish from multi-unit optic nerve recordings. *Vision Research* **37,** 967-973.

Novales Flamarique, I. and Hawryshyn, C. W. (1998). The common white sucker (*Catostomus commersoni*): a fish with ultraviolet sensitivity that lacks polarization sensitivity. *Journal of Comparative Physiology A Sensory, Neural and Behavioural Physiology* **182,** 331-341.

O'Day, K. (1935). A preliminary note on the presence of double cones and oil droplets in the retina of marsupials. *Journal of Anatomy* **70,** 465-467.

Ohtsuka, T. (1984). Fluorescence from colorless oil droplets: a new criterion for identification of cone photoreceptors. *Neuroscience Letters* **52,** 241-245.

Ohtsuka, T. (1985). Relation of spectral types to oil droplets in cones of turtle retina. *Science (Washington D.C.)* **229,** 874-877.

Okano, T., Fukada, Y., Artamonov, I. D. and Yoshizawa, T. (1989). Purification of cone visual pigment from chicken retina. *Biochemistry* **28,** 8848-8856.

Okano, T., Kojima, D., Fukada, Y., Shichida, Y. and Yoshizawa, T. (1992). Primary structures of chicken cone visual pigments: vertebrate rhodopsins have evolved out of cone visual pigments. *Proceedings of the National Academy of Sciences of the United States of America* **89,** 5932-5936.

Osorio, D. and Vorobyev, M. (1996). Colour vision as an adaptation to frugivory in primates. *Proceedings of the Royal Society of London B Biological Sciences* **263,** 593-599.

Ott, M. and Schaeffel, F. (1995). A negatively powered lens in the chameleon. *Nature (London)* **373,** 692-694.

Ovchinnikov, Y. A., Abdulaev, N. G. and Bogachuk, A. S. (1988). Two adjacent cysteine residues in the C-terminal cytoplasmic fragment of bovine rhodopsin are palmitoylated. *FEBS Letters* **230,** 1-5.

Palacios, A. G. and Goldsmith, T. H. (1993). Photocurrents in retinal rods of pigeons (*Columba livia*): kinetics and spectral sensitivity. *Journal of Physiology (London)* **471,** 817-829.

Palacios, A. G., Goldsmith, T. H. and Bernard, G. D. (1996). Sensitivity of cones from a cyprinid fish (*Danio aequipinnatus*) to ultraviolet and visible light. *Visual Neuroscience* **13,** 411-421.

Palacios, A. G., Srivastava, R. and Goldsmith, T. H. (1998). Spectral and polarization sensitivity of photocurrents of amphibian rods in the visible and ultraviolet. *Visual Neuroscience* **15,** 319-331.

Palacios, A. G. and Varela, F. J. (1992). Color mixing in the pigeon (*Columba livia*) II: A psychophysical determination in the middle, short and near-UV wavelength range. *Vision Research* **32,** 1947-1953.

Parrish, J., Benjamin, R. and Smith, R. (1981). Near-ultraviolet light reception in the mallard. *Auk* **98,** 627-628.

Parrish, J. W., Ptacek, J. A. and Will, K. L. (1984). The detection of near-ultraviolet light by non-migratory and migratory birds. *Auk* **101,** 53-58.

Partridge, J. C. (1986). Microspectrophotometry of vertebrate photoreceptors. PhD Thesis. Bristol University.

Partridge, J. C. (1989). The visual ecology of avian cone oil droplets. *Journal of Comparative Physiology A Sensory, Neural and Behavioural Physiology* **165,** 415-426.

Partridge, J. C., Archer, S. N. and Lythgoe, J. N. (1988). Visual pigments in the individual rods of deep-sea fishes. *Journal of Comparative Physiology A Sensory, Neural and Behavioural Physiology* **162,** 543-550.

Partridge, J. C. and DeGrip, W. J. (1991). A new template for rhodopsin (vitamin A_1 based) visual pigments. *Vision Research* **31,** 619-630.

Partridge, J. c., Speare, P., Shand, J., Muntz, W. R. A. and Williams, D. M. B. (1992). Microspectrophotometric determinations of rod visual pigments in some adult and larval Australian amphibians. *Visual Neuroscience* **9,** 137-142.

Pautler, E. L. (1967). Directional sensitivity of isolated turtle retinas. *Journal of the Optical Society of America* **57,** 1267-1269.

Payne, R. (1971). Acoustic location of prey by Barn Owls (*Tyto alba*). *Journal of Experimental Biology* **54,** 535-573.

Pedler, C. and Boyle, M. (1969). Multiple oil droplets in the photoreceptors of the pigeon. *Vision Research* **9,** 525-528.

Pedler, C. and Tansley, K. (1963). The fine structure of the cone of a diurnal gecko (*Phelsuma inunguis*). *Experimental Eye Research* **2,** 39-47.

Peiponen, V. A. (1964). Zur Bedeutung der Ölkugeln im Farbensehen der Sauropsiden. *Annales Zoologici Fennici* **1,** 281-302.

Perrins, C. (1987). *Collins new generation guide to the birds of Britain and Europe.* London: Collins.

Petrie, M. (1994). Improved growth and survival of offspring of peacocks with more elaborate trains. *Nature (London)* **371,** 598-599.

Petrie, M., Cotgreave, P. and Stewert, I. (1996). Variation in the train morphology of peacocks (*Pavo cristatus*). *Journal of Zoology (London)* **238,** 365-371.

Pettigrew, J. D. (1978). Comparison of the retinotopic organization of the visual Wulst in nocturnal and diurnal raptors, with a note on the evolution of frontal vision. In *Frontiers of visual science.* (Eds. S. J. Cool and E. L. Smith), pp. 328-335. New York: Springer.

Pettigrew, J. D. (1983). A note on the eye of the letter-winged kite *Elanus scriptus. Emu* **82,** 305-308.

Phillips, J. B. and Borland, S. C. (1992). Behavioural evidence for use of a light-dependent magnetoreception mechanism by a vertebrate. *Nature (London)* **359,** 142-144.

Phillips, J. B. and Sayeed, O. (1993). Wavelength-dependent effects of light on magnetic compass orientation in *Drosophila melanogaster. Journal of Comparative Physiology A Sensory, Neural and Behavioural Physiology* **172,** 303-308.

Prayitno, D. S. and Phillips, C. J. C. (1997). Equating the perceived intensity of coloured lights to hens. *British Poultry Science* **38,** 136-141.

Prayitno, D. S., Phillips, C. J. C., Omed, H. M. and Piggins, D. (1994). Effect of colour of lighting on the performance and behaviour of broilers. *British Poultry Science* **35,** 173-175.

Provencio, I., Loew, E. R. and Foster, R. G. (1992). Vitamin-A_2-based visual pigments in terrestrial vertebrates. *Vision Research* **32,** 2201-2208.

Pumphrey, R. J. (1948). The sense organs of birds. *Ibis* **90,** 171-199.

Raap, A. K., Nederlof, P. M., Dirks, R. W., Wiegant, J. C. A. G. and van der Ploeg, M. (1990). Use of haptenised nucleic acid probes in fluorescent *in situ* hybridisation. In *In situ hybridisation: application to developmental biology and medicine.* (Eds. N. Harris and D. G. Wilkinson), pp. 33-41. Cambridge, New York, Port Chester, Melbourne, Sydney: Cambridge University Press.

Repérant, J., Miceli, D., Vesselkin, N. P. and Molotchnikoff, S. (1989). The centrifugal visual system of vertebrates: A century-old search reviewed. *International Review of Cytology* **118,** 115-171.

Richman, A. D. and Price, T. (1992). Evolution of ecological differences in the Old World leaf warblers. *Nature (London)* **355,** 817-821.

Roaf, H. E. (1929). The absorption of light by the coloured globules in the retina of the domestic hen. *Proceedings of the Royal Society of London B Biological Sciences* **105,** 371-374.

Robinson, J., Schmitt, E. A., Hárosi, F. I., Reece, R. J. and Dowling, J. E. (1993). Zebrafish ultraviolet visual pigment: absorption spectrum, sequence and localization. *Proceedings of the National Academy of Sciences of the United States of America* **90,** 6009-6012.

Rodieck, R. W. (1973). *The vertebrate retina. Principals of structure and function.* San Francisco: W. H. Freeman and Company.

Rodieck, R.W. (1998). *The first steps in seeing*. Sunderland, Massachusetts: Sinauer Associates, Inc.

Rogers, L. J. (1981). Environmental influences on brain lateralization. *Behavioral and Brain Sciences* **4,** 35-36.

Rogers, L. J. (1986). Lateralization of learning in chicks. *Advances in the study of behavior* **16,** 147-189.

Rogers, L. J. (1991). Development of lateralization. In *Neural and behavioural plasticity: the use of the domestic chick as a model* (Ed. R. J. Andrew). Oxford, NewYork, Tokyo: Oxford University Press.

Rogers, L. J. and Adret, P. (1993). Developmental mechanisms of lateralization. In *Vision, brain and behavior in birds.* (Eds. H. P. Zeigler and H.-J. Bischof), pp. 227-242. Cambridge, Massachussets; London, England: MIT press.

Rogers, L. J. and Bolden, S. W. (1991). Light-dependent development and asymmetry of visual projections. *Neuroscience Letters* **121,** 63-67.

Rogers, L. J. and Krebs, G. A. (1996). Exposure to different wavelengths of light and the development of structural and functional asymmetries in the chicken. *Behavioural Brain Research* **80,** 65-73.

Röhler, R. and Fischer, W. (1971). Influence of waveguide modes on the light absorption in photoreceptors. *Vision Research* **11,** 97-101.

Romeskie, M. and Yager, D. (1976a). Psychophysical studies of pigeon colour vision - I. Photopic spectral sensitivity. *Vision Research* **16,** 501-505.

Romeskie, M. and Yager, D. (1976b). Psychophysical studies of pigeon colour vision - II. The spectral photochromatic interval function. *Vision Research* **16,** 507-512.

Saibil, H. R. (1986). From photon to receptor potential: the biochemistry of vision. *News in Physiological Sciences* **1,** 122-125.

Sakmar, T. P., Franke, R. R. and Khorana, G. H. (1989). Glutamic acid-113 serves as the retinylidene Schiff base counterion in bovine rhodopsin. *Proceedings of the National Academy of Sciences of the United States of America* **86,** 8309-8313.

Schaeffel, F. and Wagner, H. (1992). Barn owls have symmetrical accomodation in both eyes, but independent pupillary responses to light. *Vision Research* **32,** 1149-1155.

Schiedt, K., Bischof, S. and Glinz, E. (1991). Recent progress on carotenoid metabolism in animals. *Pure and Applied Chemistry* **63,** 89-100.

Seamen, J. W., Jr., Walls, S. C., Wise, S. E. and Jaeger, R. G. (1994). Caveat emptor: rank transform methods and interaction. *Trends in Ecology and Evolution* **9,** 261-263.

Seliger, H. H., Lall, A. B. and Biggley, W. H. (1994). Blue through UV polarization sensitivities in insects. *Journal of Comparative Physiology A Sensory, Neural and Behavioural Physiology* **175,** 475-486.

Shepherd, G. M. (1988). *Neurobiology*. New York, Oxford: Oxford University Press.

Sherwin, C. M. (1998). Light intensity preferences of domestic male turkeys. *Applied Animal Behaviour Science* **58,** 121-130.

Shichida, Y., Imai, H., Imamoto, Y., Fukada, Y. and Yoshizawa, T. (1994). Is chicken green-sensitive cone visual pigment a rhodopsin-like pigment? A comparative study of the molecular properties between chicken green and rhodopsin. *Biochemistry* **33,** 9040-9044.

Shichida, Y., Kato, T., Sasayama, S., Fukada, Y. and Yoshizawa, T. (1990). Effects of chloride on chicken iodopsin and the chromophore transfer reactions from iodopsin to scotopsin and B-photopsin. *Biochemistry* **29,** 5843-5848.

Sibley, C. G. and Ahlquist, J. E. (1990). *Phylogeny and classification of birds: A study in molecular evolution*. New Haven, London: Yale University Press.

Sibley, C. G. and Monroe, B. L. (1990). *Distribution and taxonomy of birds of the world.* New Haven and London: Yale University Press.

Sidman, R. L. (1957). The structure and concentration of solids in photoreceptive cells studied by refractometry and interference microscopy. *Journal of Biophysical and Biochemical Cytology* **3,** 15-30.

Sillman, A. J. (1969). The visual pigments of several species of birds. *Vision Research* **9,** 1063-1077.

Sillman, A. J. (1973). Avian vision. In *Avian biology. Volume 3.* (Eds. D. S. Farner and J. R. King), pp. 349-387. New York: Academic Press.

Sillman, A. J., Bolnick, D. A., Haynes, L. W., Walter, A. E. and Loew, E. R. (1981). Microspectrophotometry of the photoreceptors of palaeognathous birds - the emu and tinamou. *Journal of Comparative Physiology* **144,** 271-276.

Sillman, A. J., Ronan, S. J. and Loew, E. R. (1993). Scanning electron microscopy and microspectrophotometry of the photoreceptors of ictalurid catfishes. *Journal of Comparative Physiology A Sensory, Neural and Behavioural Physiology* **173,** 801-807.

Siopes, T. D., Timmons, M. B., Baughman, G. R. and Parkhurst, C. R. (1984). The effects of light intensity on turkey poult performance, eye morphology, and adrenal weight. *Poultry Science* **63,** 904-909.

Sivak, J. G. (1976). The role of the flat cornea in the amphibious behaviour of the black-footed penguin, *Spheniscus demersus*. *Canadian Journal of Zoology* **54,** 1341-1345.

Sivak, J. G., Lincer, J. L. and Bobier, W. (1977). Amphibious visual optics of the eyes of the double-crested cormorant (*Phalacrocorax auritus*) and the brown pelican (*Pelecanus occidentalis*). *Canadian Journal of Zoology* **55,** 782-788.

Slonaker, J. R. (1918). A physiological study of the anatomy of the eye and its accessory parts of the English sparrow (*Passer domesticus*). *Journal of Morphology* **31,** 351-460.

Smith, B. L., McDaniel, R., Skotko, D. and Owen, W. (1989). Color preference and discrimination in the wild turkey. *Psychological Record* **39,** 387-395.

Smith, R. L., Nishimura, Y. and Raviola, G. (1985). Interreceptor junction in the double cone of the chicken retina. *J. Submicrosc. Cytol.* **17,** 183-186.

Snow, D. W. and Perrins, C. M. (1998a). *The birds of the western palearctic. Volume 1. Non-passerines.* Oxford, New York: Oxford University Press.

Snow, D. W. and Perrins, C. M. (1998b). *The birds of the western palearctic. Volume 2. Passerines.* Oxford, New York: Oxford University Press.

Snyder, A. W. (1975). Photoreceptor optics - theoretical principles. In *Photoreceptor optics.* (Eds. A. W. Snyder and R. Menzel), pp. 38-55. Berlin, Heidelberg, New York: Springer-Verlag.

Snyder, A. W. and Hamer, M. (1972). The light capture area of a photoreceptor. *Vision Research* **12,** 1749-1753.

Snyder, A.W. and Miller, W.H. (1978). Telephoto lens system of falconiform eyes. *Nature (London)* **275,** 127-129.

Snyder, A. W. and Richmond, P. (1972). Anomalous dispersion in visual photoreceptors. *Vision Research* **13,** 511-515.

Sokal, R. R. and Rohlf, F. J. (1995). *Biometry.* New York: W. H. Freeman and Company.

Southern, E. M. (1988). Introduction. In *Nucleic acid hybridisation: a practical approach.* (Eds. B. D. Hames and S. J. Higgins), pp. 1-2. Oxford, Washington DC: IRL Press.

Sperling, H. G. and Harwerth, R. S. (1971). Red-green cone interactions in the increment-threshold spectral sensitivity of primates. *Science (Washington D.C.)* **172,** 180-184.

Stabell, B. and Stabell, U. (1996). Peripheral colour vision: Effects of rod intrusion at different eccentricities. *Vision Research* **36,** 3407-3414.

Stavenga, D. G., Smits, R. P. and Hoenders, B. J. (1993). Simple exponential functions describing the absorbance bands of visual pigment spectra. *Vision Research* **33,** 1011-1017.

Stenkamp, D. L., Hisatomi, O., Barthel, L. K., Tokunaga, F. and Raymond, P. A. (1996). Temporal expression of rod and cone opsins in embryonic goldfish retina predicts the spatial organization of the cone mosaic. *Investigative Ophthalmology and Visual Science* **37,** 363-376.

Strother, G. K. (1963). Absorption spectra of retinal oil globules in turkey, turtle and pigeon. *Experimental Cell Research* **29,** 349-355.

Strother, G. K. and Wolken, J. J. (1959). A simplified microspectrophotometer. *Science (Washington D.C.)* **130,** 1084-1088.

Strother, G. K. and Wolken, J. J. (1960). Microspectrophotometry. 1. Absorption spectra of coloured oil globules in the chicken retina. *Experimental Cell Research* **21,** 504-512.

Stryer, L. (1987). The molecules of visual excitation. *Scientific American* **257,** 32-40.

Suthers, R. A. (1978). Sensory ecology of birds. In *Sensory ecology: reviews and perspectives.* (Ed. M. A. Ali), pp. 217-251. New York, London: Plenum Press.

Szél, A., Röhlich, P., Caffe, A. R. and vanVeen, T. (1996). Distribution of cone photoreceptors in the mammalian retina. *Microscopy Research and Technique* **35,** 445-462.

Takao, M., Yasui, A. and Tokunaga, F. (1988). Isolation and determination of the chicken rhodopsin gene. *Vision Research* **28,** 471-480.

Thompson, P. and Findlay, J. B. C. (1984). Phosphorylation of ovine rhodopsin. Identification of the phosphorylated sites. *Biochemistry Journal* **221,** 773-780.

Thornton, J. E. and Pugh, E. N. (1983). Red-green color opponency at detection threshold. *Science (Washington D.C.)* **219,** 191-193.

Tomita, T., Kaneko, A., Murakami, M. and Pautler, E. L. (1967). Spectral response curves of single cones in the carp. *Vision Research* **7,** 519-531.

Uchiyama, H. and Barlow, R. B. (1994). Centrifugal inputs enhance responses of retinal ganglion cells in the japanese quail without changing their spatial coding properties. *Vision Research* **34,** 2189-2194.

van den Berg, T. J. T. P. and Spekreijse, H. (1997). Near infrared light absorption in the human eye media. *Vision Research* **37,** 249-253.

van Hateren, J. H. (1989). Photoreceptor optics, theory and practise. In *Facets of vision.* (Eds. D. G. Stavenga and R. C. Hardie), pp. 74-89. Berlin, Heidelberg, New York: Springer-Verlag.

van Norren, D. (1975). Two short wavelength sensitive cone systems in pigeon, chicken and daw. *Vision Research* **15,** 1164-1166.

van Roessel, P., Palacios, A. G. and Goldsmith, T. H. (1997). Activity of long-wavelength cones under scotopic conditions in the cyprinid fish *Danio*

aequipinnatus. Journal of Comparative Physiology A Sensory, Neural and Behavioural Physiology **181,** 493-500.

Varela, F. J., Palacios, A. G. and Goldsmith, T. H. (1993). Color vision of birds. In *Vision, brain and behavior in birds.* (Eds. H. P. Zeigler and H.-J. Bischoff), pp. 77-98. Cambridge, Massachusetts; London, England: MIT press.

Viitala, J., Korpimaki, E., Palokangas, P. and Koivula, M. (1995). Attraction of kestrels to vole scent marks visible in ultraviolet light. *Nature (London)* **373,** 425-427.

Vorobyev, M. and Osorio, D. (1998). Receptor noise as a determinant of colour thresholds. *Proceedings of the Royal Society of London B Biological Sciences* **265,** 351-358.

Vorobyev, M., Osorio, D., Bennett, A. T. D., Marshall, N. J. and Cuthill, I. C. (1998). Tetrachromacy, oil droplets and bird plumage colours. *Journal of Comparative Physiology A Sensory, Neural and Behavioural Physiology* **183,** 621-633.

Vos Hzn, J. J., Coemans, M. A. J. M. and Nuboer, J. F. W. (1994). The photopic sensitivity of the yellow field of the pigeon's retina to ultraviolet light. *Vision Research* **34,** 1419-1425.

Vos Hzn, J. J., Coemans, M. A. J. M. and Nuboer, J. F. W. (1995). No evidence for polarization sensitivity in the pigeon electroretinogram. *Journal of Experimental Biology* **198,** 325-335.

Waelchli, G. (1883). Zur Topographie der gefärbten Kugeln der Vogelnetzhaut. *Archiv fur Ophthalmologie* **29,** 205-223.

Wald, G. (1935). Carotenoids and the visual cycle. *Journal of General Physiology* **19,** 351-371.

Wald, G. (1937). Photo-labile pigments of the chicken retina. *Nature (London)* **140,** 545-546.

Wald, G., Brown, P. K. and Smith, P. H. (1955). Iodopsin. *Journal of General Physiology* **38,** 623-681.

Wald, G. and Zussman, H. (1937). Carotenoids of the chicken retina. *Nature (London)* **140,** 197.

Wallman, J. (1979). Role of the retinal oil droplets in the colour vision of japanese quail. In *Neural mechanisms of behaviour in the pigeon.* (Eds. A. M. Granda and J. H. Maxwell), pp. 327-351. New York, London: Plenum Press.

Walls, G. L. (1942). The vertebrate eye and its adaptive radiation. New York: Hafner.

Walls, G. L. and Judd, H. D. (1933). The intra-ocular colour-filters of vertebrates. *British Journal of Ophthalmology* **17,** 641-675/705-725.

Wang, J. K., McDowell, J. H. and Hargrave, P. A. (1980). Site of attachment of 11-*cis*-retinal in bovine rhodopsin. *Biochemistry* **19,** 5111-5117.

Wang, S. Z., Adler, R. and Nathans, J. (1992a). A putative green visual pigment from chicken that resembles rhodopsin: sequence, gene structure and functional expression. *Investigative Ophthalmology and Visual Science* **33,** 1003A.

Wang, S.-Z., Adler, R. and Nathans, J. (1992b). A visual pigment from chicken that resembles rhodopsin: amino acid sequence, gene structure, and functional expression. *Biochemistry* **31,** 3309-3315.

Wang, Z., Asenjo, A. B. and Oprian, D. D. (1993). Identification of the Cl^--binding site in the human red and green colour vision pigments. *Biochemistry* **32,** 2125-2130.

Warrant, E. J. and Nilsson, D.-E. (1998). Absorption of white light in photoreceptors. *Vision Research* **38,** 195-207.

Weitz, C. J. and Nathans, J. (1993). Rhodopsin activation: effects on the metarhodopsin I - metarhodopsin II equilibrum of neutralization or introduction of charged amino acids within putative transmembrane segments. *Biochemistry* **32,** 14176-14182.

Wentworth, S. L. and Muntz, W. R. A. (1989). Asymmetries in the sense organs and central nervous system of the squid *Histioteuthis. Journal of Zoology (London)* **219,** 607-619.

Whistler, H. (1935). *Popular handbook of Indian birds.* London, Edinburgh: Gurney and Jackson.

Wilkie, S. E., Vissers, P. M. A. M., Das, D., DeGrip, W. J., Bowmaker, J. K. and Hunt, D. M. (1998). The molecular basis for UV vision in birds: spectral characteristics, cDNA sequence and retinal localization of the UV-sensitive

visual pigment of the budgerigar (*Melopsittacus undulatus). Biochemical Journal* **330,** 541-547.

Williams, J. W., Hunt, D. M., Bowmaker, J. K. and Mollon, J. D. (1992). The polymorphic photopigments of the marmoset: spectral tuning and genetic basis. *EMBO Journal* **11,** 2039-2045.

Willoughby, E. J. and Peaker, M. (1979). Birds. In *Comparative physiology of osmoregulation in animals. Volume 2.* (Ed. G. M. O. Maloiy), pp. 1-55. London, New York, San Francisco: Academic Press.

Wiltschko, W., Munro, U., Ford, H. and Wiltschko, R. (1993). Red light disrupts orientation of migratory birds. *Nature (London)* **364,** 525-527.

Wolbarsht, M. L. (1976). The function of intraocular color filters. *Federation Proceedings* **35,** 44-50.

Wolf, A. V., Brown, M. G. and Prentiss, P. G. (1975). Concentrative properties of aqueous solutions: conversion tables. In *Handbook of chemistry and physics: a ready-reference book of chemical and physical data.* (Ed. R. C. Weast), pp. D230-231. Ohio: CRC Press, Inc.

Wolken, J. J., Forsberg, R., Gallik, G. and Florida, R. (1968). Rapid recording microspectrophotometer. *The Review of Scientific Instruments* **39,** 1734-1740.

Wood, C. A. (1917). *The fundus oculi of birds especially as viewed by the ophthalmoscope.* Chicago: Lakeside Press.

Workman, L. and Andrew, R.J. (1986). Asymmetries of eye use in birds. *Animal Behaviour* **34,** 1582-1584.

Wortel, J. F. and Nuboer, J. F. W. (1986). The spectral sensitivity of blue-sensitive pigeon cones: evidence for complete screening of the visual pigment by the oil droplets. *Vision Research* **26,** 885-886.

Wortel, J. F., Rugenbrink, H. and Nuboer, J. F. W. (1987). The photopic spectral sensitivity of the dorsal and ventral retinae of the chicken. *Journal of Comparative Physiology A Sensory, Neural and Behavioural Physiology* **160,** 151-154.

Wortel, J. F., Wubbels, R. J. and Nuboer, J. F. W. (1984). Photopic spectral sensitivities of the red and yellow fields of the pigeon retina. *Vision Research* **24,** 1107-1113.

Wright, A. A. (1972). Psychometric and psychophysical hue discrimination functions for the pigeon. *Vision Research* **12,** 1447-1464.

Wright, A. A. (1979). Color-vision psychophysics: a comparison of pigeon and human. In *Neural mechanisms of behaviour in the pigeon.* (Eds. A. M. Granda and J. H. Maxwell), pp. 89-127. New York, London: Plenum Press.

Wyszecki, G. and Stiles, W. S. (1967). *Color science. Concepts and methods, quantitative data and formulas.* New York, London, Sydney: John Wiley and Sons, Inc.

Yau, K.-W. (1994). Phototransduction mechanism in retinal rods and cones. *Investigative Ophthalmology and Visual Science* **35,** 9-32.

Yen, L. and Fager, R. S. (1984). Chromatographic resolution of the rod pigment from the four cone pigments of the chicken retina. *Vision Research* **24,** 1555-1562.

Yeum, K.-Y., Taylor, A., Tang, G. and Russell, R. M. (1995). Measurement of carotenoids, retinoids and tocopherols in human lens. *Investigative Ophthalmology and Visual Science* **36,** 2756-2761.

Yokoyama, S., Radlwimmer, F. B. and Kawamura, S. (1998). Regeneration of ultraviolet pigments of vertebrates. *FEBS Letters* **423,** 155-158.

Yoshizawa, T. and Fukada, Y. (1993). Preparation and characterisation of chicken rod and cone pigments. In *Photoreceptor cells.* (Ed. P. A. Hargrave), pp. 161-179. New York: Academic Press, Inc.

Yoshizawa, T., Shichida, Y. and Fukada, Y. (1991). Biochemical and photochemical analyses of retinal proteins in chicken cone cells. *Pure and Applied Chemistry* **63,** 171-176.

Young, H. M. and Pettigrew, J. D. (1991). Cone photoreceptors lacking oil droplets in the retina of the echidna, *Tachyglossus aculeatus* (monotremata). *Visual Neuroscience* **6,** 409-420.

Young, R. W. (1976). Visual cells and the concept of renewal. *Investigative Ophthalmology* **15.**

Young, S. R. and Martin, G. R. (1984). Optics of retinal oil droplets: a model of light collection and polarisation detection in the avian retina. *Vision Research* **24,** 129-137.